Subcooled Flow Boiling Heat Transfer and Critical Heat Flux in Water-Based Nanofluids at Low Pressure

by
Sung Joong Kim
B.S. Nuclear Engineering, Hanyang University, Seoul, Korea, 2001
M.S. Nuclear Engineering, Seoul National University, Seoul, Korea, 2003
S.M. Nuclear Science and Engineering, Massachusetts Institute of Technology, 2007

SUBMITTED TO THE DEPARTMENT OF NUCLEAR SCIENCE AND ENGINEERING
IN PARTIAL FULFILLMENT OF THE REQUIREMENTS FOR THE DEGREE OF

DOCTOR OF PHILOSOPHY IN NUCLEAR SCIENCE AND ENGINEERING
AT THE
MASSACHUSETTS INSTITUTE OF TECHNOLOGY
[June]
MARCH 2009

Signature of Author

Department of Nuclear Science and Engineering
March 2, 2009

Certified by

Jacopo Buongiorno - Thesis Supervisor
Associate Professor of Nuclear Science and Engineering

Certified by

Lin-wen Hu - Thesis Co-Supervisor
Principal Research Scientist

Certified by

Mujid Kazimi - Thesis Reader
Professor of Nuclear Science and Engineering

Accepted by

Dr. Jacquelyn C. Yanch
Professor of Nuclear Science and Engineering
Chair, Department Committee for Graduate Students

Subcooled Flow Boiling Heat Transfer and Critical Heat Flux in Water-Based Nanofluids at Low Pressure

By
Sung Joong Kim

Submitted to the Department of Nuclear Science and Engineering in partial fulfillment of the requirements for the degree of Doctor of Philosophy in Nuclear Science and Engineering

Abstract

A nanofluid is a colloidal suspension of nano-scale particles in water, or other base fluids. Previous pool boiling studies have shown that nanofluids can improve the critical heat flux (CHF) by as much as 200%. In this study, subcooled flow boiling heat transfer and CHF experiments were performed with low concentrations of alumina, zinc oxide, and diamond nanoparticles in water (≤ 0.1 % by volume) at atmospheric pressure. It was found that for comparable test conditions the values of the nanofluid and water heat transfer coefficient (HTC) are similar (within ±20%). The HTC increased with mass flux and heat flux for water and nanofluids alike, as expected in flow boiling. The CHF tests were conducted at 0.1 MPa and at three different mass fluxes (1500, 2000, 2500 kg/m^{2}s) under subcooled conditions. The maximum CHF enhancement was 53%, 53% and 38% for alumina, zinc oxide and diamond, respectively, always obtained at the highest mass flux. The measurement uncertainty of the CHF was less than 6.2%.

A post-mortem analysis of the boiling surface reveals that its morphology is altered by deposition of the particles during nanofluids boiling. A confocal-microscopy-based examination of the test section revealed nanoparticles deposition not only changes the number of micro-cavities on the surface, but also the surface wettability. A simple model was used to estimate the ensuing nucleation site density changes, but no definitive correlation between the nucleation site density and the heat transfer coefficient data could be found.

Wettability of the surface was substantially increased for heater coupons boiled in alumina and zinc oxide nanofluids, and such wettability increase seems to correlate reasonably well with the observed marked CHF enhancement for the respective nanofluids.

Interpretation of the experimental data was conducted in light of the governing surface parameters and existing models. It was found that no single parameter could explain the observed HTC or CHF phenomena. The existing models were limited in studying the surface effects, suggesting that more accurate models incorporating surface effects need to be developed. Finally, the research activities performed in this thesis help identify the research gaps and indicate future research directions.

Thesis Supervisor: Dr. Jacopo Buongiorno
Title: Associate Professor of Nuclear Science and Engineering, Carl R. Soderberg Professor of Power Engineering

Thesis Co-Supervisor: Dr. Lin-wen Hu
Title: Principal Research Scientist, Associate Director, The MIT Nuclear Reactor Laboratory

Thesis Reader: Dr. Mujid S. Kazimi
Title: Professor of Nuclear Science and Engineering, Professor of Mechanical Engineering, TEPCO Professor of Nuclear Engineering, Director, Center for Advanced Nuclear Energy Systems (CANES)

Thesis Committee Member: Dr. Michael J. Driscoll
Title: Professor Emeritus of Nuclear Science and Engineering

Acknowledgement

Prof. Jacopo Buongiorno: Without your guidance for every aspect, I could not reach where I am standing now. Your deep and wide insight always inspires me and gave me many causes for getting this thesis work done. I also greatly appreciate the patience that you showed me until this work is finished. It is doubtlessly prestigious to study while I am calling you an advisor.

Dr. Lin-wen Hu: Looking back my 4.5 years graduate study, saying just 'thank you' is not enough to show my hartful gratitude toward you. You always make me to realize where I am and encourage me to move forward. Also your practical research experiences motivate me to explore countless chances of making researches more fruitful.

Prof. Mujid S. Kazimi: I started my graduate study at MIT with you and finally finished this thesis work with your guidance. As my academic advisor and thesis reader, you have showed me something that I really have to take it for valuable as a nuclear engineer.

Profs. Peter Griffith and Michael Driscoll: I appreciate your technical suggestions, which made my thesis work more organized. I deeply appreciate your kind acceptance for being my PhD defense committee.

Dr. Thomas J. McKrell: I have ever imagined that getting things through without your help. If not your help, my thesis work might be delayed sinigificantly. I really appreciate your help not only because you contributed on shortening the duration of my thesis work but also you are the role model for the engineers and experimentalists.

Dr. John Bernard: Any mundane word cannot express my deepest gratitude toward you. You got me out the dark side of my student life and woke my logical senses. I will not forget your priceless help and will remember what you have done for me for nothing.

Prof. Sydney Yip: One incident that I took it very precious was the oral exam in May 2006 for 22.106. Your encouragement when I was struggling by myself has kept my motivation continuing through my graduate study. I am very lucky due to the fact that I could learn many things from you and your enlightening lecture.

Drs. G. P. Celata and Mariani: I appreciate your generous permission in using your numerical routine to predict subcooled flow boiling critical heat flux.

Dr. Pradip Saha: It was one of many fortunate moments that I have worked under your supervision in the beginning of my graduate study. You educated me what should do first as a thermal hydraulic engineer. Your pertaining of a principle even if things seem simple always inspires a young engineer like me.

AREVA: I appreciate AREVA's generous sponsorship for builing flow loop appratus and related supports to conduct most part of this thesis work.

DOE: The latest part of my thesis work was supported by the Department of Energy (DOE) in US and is greatly acknowledged by the author.

MOST/KOSEF: Without 3-year scholarship from the Ministry of Science and Technology (MOST)/the Korea Science and Engineering Foundation (KOSEF) in Republic of Korea, I could not finish this thesis

work. From the candidate nomination for the Korea National Nuclear Scholarship to the end of the supporting, the MOST and KOSEF is greatly acknowdeged for supporting the author.

Prof. Que D. Jeun: You are the very first one who inspired me to step into the thermal hydraulic area. Your lectures given during my undergraduate study at Hanyang University always motivated me to learn more and your encouragement in the lab stimulated my interest. I also would like to show my deepest gratitude to you for giving me many opportunities to broaden my experiences.

Prof. Kune Suh: I greatly appreciate my former advisor at Seoul National University. He has supported me greatly for nothing and finally got me here at MIT.

Dr. Yong-hoon Kim: My senior collegemate during my undergraduate and graduate study is the one who made me to stand here. His endless support has enlightened my life.

Drs. Jeongik Lee and Wesley C. Williams: Without you guys, I wouldn't be able to walk off the MIT with a PhD degree on hands. As a labmate, classmate, and life-long friend, our day-to-day discussion and candid critiques about ourselves made my life fruitful. I have never forgotten the moment that we shared and the places that we walked along and stood for imagining a bright future.

Dr. Christopher Handwerk: You have given me tremendous mental supports from the beginning of my study at MIT. You were like an old brother to me that you never stop motivating and encouraging me.

Dr. In-cheol Bang: I owe you too much about my graduate research. Many of my ideas came from you and you made my work enriched.

Mr. Eric Forrest: I should thank you for conducting dynamic light scattering measurement, which has been an essential piece of the earlier part of my thesis. Your description about DLS measurement helps me make it easy on the nanofluids characterization part, too.

BOSTON3040: With BOSTON3040 member, I have enriched my life by exercising physically and making healthy communication. You guys always have been taking care of me and finally helped me getting through the toughest moment of my student life.

Korean fellows at NSE department: I appreciate your supports and cheering me up to the end. I know how much you guys have concerned about me and for that, I could keep motivating myself to finish thesis work.

Family: My older brother (Daejoong Kim), his wife (Sungnam Kim) and their children (Haneul Kim, Sunho Kim), older sister (Junghoon Kim), her husband (Namkee Lee), and their children (Hyeryung Lee and Kyungmin Lee) have been mental supports behind me. My mother's brothers, sisters and their family have always concerned about my study and my family. I cannot thank them more than anyone can do. I also would like to share this prestigious moment with my late Grandfather Yoonsoo Kim and late grandmother Bongrye Ryoo. Finally, my parents (Yonghee Kim and Ohsoo Kwon) have been lifelong supporting for me. They have given me an avoidable reason to stand strong and kept encouraging me to be a better person that can endure any circumstances. Without their love and support, I would not be able to be here. I love you more than I do myself and thank you for being great parents to me.

Table of Contents

List of Figures

List of Tables

Nomenclature

a	volume of nanofluid [liter]
A_c	hydrodynamic flow area [m^2]
A_h	heated area [m^2]
A_{cx}	heater cross-sectional area [m^2]
A_{TC}	thermocouple sheath cross-sectional area [m^2]
b	volume of nanoparticle which occupies a [liter] or channel height [m]
Bo	Bond number
c	volume of base fluid which occupies a [liter]
C_E	Ergun coefficient
c_h	heater specific heat capacity [J/kg·K]
c_p	average specific heat capacity between T_{in} and T_{out} [J/kg·K]
$c_{p,f}$	specific heat capacity of liquid phase at saturation [J/kg·K]
$c_{p,l}$	specific heat capacity of liquid phase at local bulk temperature [J/kg·K]
$CHFR_{\theta/70^o}$	relative change of CHF value with respect to the CHF at contact angle of 70°
d	volume of water added to dilute concentrated nanofluid [liter], nanoparticle diameter [m] or characteristic diameter of nano-porous layer [m]
D	liquid flow distance [m]
D_b	bubble departure diameter [m]
D_B	vapor blanket diameter [m]
D_c	micro-cavity diameter [m]
D_h	heater characteristic length [m]
D_i	tube inner diameter [m]
D_o	mass self-diffusion coefficient defined by Stokes-Einstein theory [m^2/s] or heater outer diameter [m]

D_{TC}	thermocouple sheath diameter [m]
D^*	minimum bubble diameter [m]
f	friction factor or scattering function
F	force pulled by the Wilhelmy plate [N]
f_b	bubble departure frequency [1/sec]
g	gravity [m/s^2]
G	mass flux [$kg/m^2 \cdot s$]
$g(\beta)$	function of contact angle in Staub's model
h	free elevation difference [m]
h_{air}	natural convective heat transfer coefficient [$W/m^2 \cdot K$]
H_c	micro-cavity height [m]
h_{eff}	effective heat transfer coefficient [$W/m^2 \cdot K$]
h_{fg}	heat of vaporization at saturation [J/kg]
h_{FC}	forced convective heat transfer coefficient [$W/m^2 \cdot K$]
h_{NB}	nucleate boiling heat transfer coefficient [$W/m^2 \cdot K$]
I	electric current [A]
K	ratio of the surface to fluid thermal conductivities or permeability of the wicking structure [m^2]
k_B	Boltzmann constant, 1.3806×10^{-23} J/K
k_{eff}	effective thermal conductivity [$W/m \cdot K$]
k_f	thermal conductivity of liquid phase at saturation [$W/m \cdot K$]
k_h	thermal conductivity of heater material [$W/m \cdot K$]
k_l	thermal conductivity of liquid phase at local bulk temperature [$W/m \cdot K$]
k_m	thermal conductivity of medium [$W/m \cdot K$]
k_p	thermal conductivity of nanoparticle [$W/m \cdot K$]
k_{NF}	thermal conductivity of nanofluid [$W/m \cdot K$]

k_{NL}	effective thermal conductivity of nano-porous layer [W/m·K]
k_{SS316}	effective thermal conductivity of stainless steel heater [W/m·K]
$k_{surface}$	thermal conductivity of heater inner surface [W/m·K]
k_{TC}	thermal conductivity of thermocouple sheath material [W/m·K]
k_w	thermal conductivity of water [W/m·K]
$\bar{k}$	effective thermal conductivity based on thermal resistance theory [W/m·K]
l	wetted perimeter of the Wilhelmy plate [m] or length of the capillary section [m]
L	heater length [m]
L_c	Laplace constant (characteristic length for boiling) [m]
$\dot{m}$	Mass flow rate [kg/s]
m''	number density of micro-cavities [counts/m^2]
n''	number density of nucleation sites [counts/m^2]
N_a	number density of nucleation sites [counts/m^2]
N_{CB}	convective boiling number
Nu_b	Nusselt number for boiling
Nu_{DB}	Nusselt number evaluated by Dittus-Boelter's correlation
Nu_G	Nusselt number evaluated by Gnielinski's correlation
P	pressure [Pa]
P_{cw}	capillary wicking pressure [Pa]
$P_{sat}(T_w)$	saturation pressure corresponding to local wall temperature [Pa]
Pe_m	modified Peclet number
Pr_f	Prandtl number of liquid phase at saturation
Pr_l	Prandtl number of liquid phase at local bulk temperature
Q	volumetric flow rate [m^3/s]
$\dot{Q}$	power [W]

q	scaling factor
q'	linear power [W/m]
q''	heat flux [W/m^2]
q''_{CHF}	critical heat flux [W/m^2]
$q''_{CHF,c}$	critical heat flux limited by capillary wicking [W/m^2]
$q''_{CHF,8mm}$	critical heat flux from 1995 look-up table [kW/m^2]
q_{ev}''	evaporation heat flux [W/m^2]
r	radial distance from the axis of KD2 probe [m] or roughness factor
R	electric resistance [Ω] or radius [m]
R_a	roughness [m]
R_b	interfacial thermal resistance, 2.5×10^{-8} Km^2/W
r_c	cavity mouth radius [m]
$R_{m''}$	ratio of number density of micro-cavities
R^*	specific gas constant for water [J/kg·K]
Re	Reynolds number
Re_m	modified Reynolds number
S	nucleate boiling suppression parameter
t	time [second]
T_b	fluid bulk temperature [°C]
T_i	initial temperature from the probe [m]
T_{in}	inlet bulk temperature [°C]
T_{out}	outlet bulk temperature [°C]
T_{sat}	saturation temperature [°C]
T_w	wall temperature [°C]
$T_{w,o}$	outer wall temperature [°C]
V	voltage [V]

v_{fg}	specific volume change upon evaporation [m^3/kg]
X	flow quality
X_e	exit equilibrium quality

Greek letters

α	thermal diffusivity [m^2/s]
β	contact angle [degree]
γ	Euler's constant, 0.5772
γ_{SV}	surface energy at solid/vapor interface [N/m]
γ_{SL}	surface energy at solid/liquid interface [N/m]
γ_{SV}- γ_{SL}	adhesion tension [N/m]
δ	vapor blanket thickness [m]
δ_{NL}	nanoparticles porous layer thickness [m]
δ_{SS316}	stainless steel 316 heater thickness [m]
ε	surface roughness [μm]
η	dynamic viscosity [kg/m·s]
θ	angle between incident and scattered lights [degree]
θ_a	apparent contact angle [degree]
θ_i	intrinsic contact angle [degree]
λ	wavelength of scattered light [m]
μ_f	dynamic viscosity of liquid phase at saturation [kg/m·s]
μ_l	dynamic viscosity of liquid phase at local bulk temperature [kg/m·s]
μ_{NF}	dynamic viscosity of nanofluid [kg/m·s]
μ_w	dynamic viscosity of liquid phase of water [kg/m·s]
v_{NF}	kinematic viscosity of nanofluid [m^2/s]
v_w	kinematic viscosity of water [m^2/s]

ξ	nanoparticle mass concentration [%wt.]
ρ_{ele}	resistivity of heater material [$\Omega \cdot$m]
ρ_f	density of liquid phase at saturation [kg/m^3]
ρ_g	density of vapor phase at saturation [kg/m^3]
ρ_h	density of the heater material [kg/m^3]
ρ_l	density of vapor phase at local bulk temperature [kg/m^3]
ρ_{NF}	density of nanofluid [kg/m^3]
ρ_p	density of nanoparticle [kg/m^3]
ρ_w	density of water at liquid phase [kg/m^3]
$\overline{\rho}$	mixture density [kg/m^3]
σ	surface tension of fluid [N/m]
τ	time scale during scattering [sec]
φ	nanoparticle volumetric concentration [%vol.]
Φ_s	porosity of nanoparticles porous layer

1 Introduction

1.1 Background and Motivation

Nanofluids are dispersions, or colloidal suspensions, of nano-scale particles (nanoparticles hereafter) in a base liquid. Due to the rapid advancement of nanotechnology, the implementation of nanoparticles has been spawning into many new engineering applications. In particular, use of nanofluids has captured the interest of the thermal fluid engineering community whose primary research objective is to develop new effective energy transfer media. The merits of heat transfer capability of new media can be verified via various measurements such as thermo-physical properties, single-phase convective heat transfer, nucleate boiling heat transfer, and critical heat flux (CHF), to mention a few. The intriguing idea of inventing new media was launched after observing several virtuous characteristics of nanoparticles, including high surface to volume ratio, low mass, and low inertia, which can bring synergies of higher mass/energy transfer rates, high colloid stability, and little erosion.

As a first step to make the use of nanofluids useful/feasible, some researchers have tried to improve their thermo-physical properties by selecting nanoparticle materials and base fluids. The potential candidates for nanoparticle materials are metal (i.e., silver, gold), metal oxides (i.e., alumina, zirconia, zinc oxide, copper oxide), and other chemically stable materials of specific interests (i.e., carbon, diamond). In addition, the base fluids commonly selected are pure water, organic fluids (ethylene glycol and ethanol), and refrigerants, to mention a few. The basic concept is to introduce high conducting nanoparticles into base fluids of relatively low thermal conductivity. Consequently the effective thermal conductivity of the mixture is expected to be higher than that of the base fluid. Chronologically the earliest work in Japan by Masuda et al. (1995) provided the precept for the thermal conductivity

enhancement using addition of nanoparticles such as Al_2O_3, SiO_2, and TiO_2 in water. They showed that the thermal conductivity was enhanced by 32% above the base fluid water value at 5% by volume of Al_2O_3. Choi's work (1995) triggered the nanofluids research. Using Hamilton-Crosser's effective thermal conductivity model, he predicted the increased thermal conductivity by a factor of 3.5 over the base water value using 20 %vol. copper nanoparticles dispersed in water. Later Eastman et al. (1997) experimentally showed that 60% improved thermal conductivity of 5 %vol. copper oxides dispersed in water. Similar result was obtained with copper oxides dispersed in ethylene glycol. Choi and Eastman et al. attributed such consequence to the enlarged surface-to-volume ratio of his smaller particles. However, these results have not been widely reproduced and their validity has been questioned. Following the pioneering work of Choi and his fellows, a number of researchers joined in exploring the anomalous enhancement of the thermal conductivity experimentally and/or theoretically with various combinations of nanoparticles and base liquids (Choi et al., 2001; Das et al., 2003; Eastman and Choi, 2001; Jang and Choi, 2004; Keblinski et al., 2002; Lee et al., 1999; Patel and Das, 2003; Xie et al., 2002a and 2002b). However, continued controversy regarding such abnormal improvements in nanofluids thermo-physical properties instigated further experimental and validation work. MIT's Wesley Williams (Williams, 2006) noted that the nanofluids used in many studies were often poorly characterized and unstable, thus few quantitative conclusions regarding the nanoparticles effects can be drawn with reasonable certainty. In addition, the abnormally high thermal conductivity data were later deemed to be unrepeatable by other groups. In conclusion, the thermal conductivity improvement enabled by nanofluids still needs to be verified thoroughly. A major effort in this sense is underway under the MIT leadership and the auspices of the National Science Foundation. More information on this International Nanofluid Property Benchmark Exercise (INPBE) can be found at http://mit.edu/nse/nanofluids/benchmark/index.html.

As a logical extension of the thermal conductivity enhancement, convective heat transfer might also be enhanced by the use of nanoparticles. The enhanced thermal conductivity will bring an enhanced heat transfer. Another hypothesized benefit from using nanofluids was to promote the turbulence by

particle dispersion without a large change in viscosity. In that perspective, Ahuja's studies (Ahuja, 1975a and 1975b) proposed a convective heat transfer enhancement technique by using dispersions of the 50 to 100 micron diameter polystyrene spheres in aqueous sodium chloride or glycerine flowing in laminar motion. However, the type of the dispersion differs from what is now called 'nanofluid' in that the stability of the suspension was not satisfactory in his work. Also the main heat transfer mechanism was attributed to the particle rotation which creates secondary flow and thus heat transfer. However, Buongiorno (2006) recently reports that such particle rotation effect from nano-scale particle can be discarded. Unlike Ahuja's work, a recent study of Pak and Cho (1998) points out that the nanofluid potential for enhancing the convective heat transfer rate may be hindered by a significant increase in viscosity, which counters the effect of thermal conductivity increase. Indeed, Williams et al.'s recent experimental work (Williams, 2006; Williams et al., 2008) suggests that no significant convective heat transfer enhancement is achieved by enhanced thermal conductivity because of a corresponding increase in viscosity. They also report that using temperature-dependent properties of nanofluids, conventional Dittus-Boelter and Blausis/MacAdams correlations can predict the experimental data well in turbulent flow. An analytical study was conducted by Buongiorno (2006), where the nanoparticle transport mechanisms were interrogated with respect to their potential for enhancing convective heat transfer; it was found that nanoparticle dispersion is a negligible energy transfer mechanism.

Contrary to the mixed outcomes of the conduction and convection heat transfer enhancement, nanofluids are proving to have more promise for boiling heat transfer enhancement. Heat transfer characteristics of nanofluids in pool boiling have been investigated by many research organizations and published in abundance. Nucleate boiling heat transfer and CHF are the main subjects explored (You et al., 2003; Das et al., 2003; Vassallo et al., 2004; Dinh et al., 2004; Moreno et al., 2005; Bang and Change, 2005; Milanova and Kumar, 2005; Wen and Ding, 2005; Kim et al., 2006a; Milanova et al., 2006; Kim et al., 2006b and 2007; Kim, 2007). All the studies report a significant CHF enhancement consistently, but the maximum achievable enhancement varies depending on the adopted nanoparticle concentration,

nanoparticle material, base liquid and heater size and material. On the other hand, the nucleate boiling heat transfer is controversial, with some studies reporting no change of heat transfer in the nucleate boiling regime (You et al., 2003; Vassallo et al., 2004), some reporting heat transfer deterioration (Das et al., 2003; Bang and Change, 2005), and others heat transfer enhancement (Dinh et al., 2004; Wen and Ding, 2005). At MIT, an investigation of CHF and nucleate boiling heat transfer has been under way for 4 years, to identify a plausible mechanism for the significant CHF enhancement observed experimentally (Kim et al., 2006 and 2007; Kim, 2007). In particular, the maximum CHF enhancement of about 52%, 75%, and 80% was observed for boiling of alumina, zirconia, and silica nanofluids, respectively. The nucleate boiling heat transfer coefficients (HTC) of three nanofluids were all lower than the water HTC. The improved surface wettability due to nanoparticle deposition during boiling was determined to be the most likely mechanism of CHF enhancement. Also possible reduction of the nucleation site density was attributed to the deterioration of the nucleate boiling HTC.

Although more study of the basic characteristics of nanofluid boiling is needed, the enhanced CHF is a sure link to some practical applications of nanofluids, e.g., in nuclear reactors. Nanofluids can be beneficial in several aspects of nuclear reactors. One idea is to use the very low-concentration nanofluids as the primary coolant in the pressurized water reactor (PWR). To begin with, since the thermal and transport properties of the diluted nanofluid can be maintained similar to the base liquid, it is expected that the reactor neutronics such as moderation and void coefficients is not likely to change significantly. The improved CHF may afford a higher safety margin because the operation of the PWR is limited by the departure from nucleate boiling ratio (DNBR). Improved CHF could also facilitate the power uprate for the existing PWR systems, as well as the newly developed advanced high power PWR systems such as Advanced Pressurized water Reactor 1400 MWe (APR1400) in Korea and European Pressurized water Reactor 1600 MWe (EPR1600). The nanofluids can also be useful in the standby safety systems such as the Emergency Core Cooling System (ECCS). Likewise, design of residual heat removal systems using nanofluids can be considered. Nanofluids could be used in severe accident mitigation

strategies, such in-vessel retention, which is aimed at ensuring the removal of decay heat from the reactor vessel during severe accidents in high-power density light water reactors (LWRs). The features, potential and shortcomings of using nanofluids in nuclear reactor systems have been investigated at MIT with particular emphasis on evaluating their enhanced economics and safety, and the results are summarized in (Buongiorno et al., 2008).

For all the addressed features, major knowledge gaps remain in the study of nanofluids boiling. In particular, while pool boiling heat transfer has been studied broadly, flow boiling has not. However, flow boiling plays a crucial role in exploring the potential and feasibility of nanofluids for many applications, including the advanced nuclear systems. Before this thesis, no systematic study of the heat transfer characteristics of nanofluids in flow boiling could be found. The only previous relevant study, to the author's best knowledge, is the work of Lee and Mudawar (2006). Their study, in fact, concentrated primarily on convective single-phase heat transfer with alumina nanofluids in a 0.5-mm-diameter channel with few CHF experiments afterwards. According to their short remark, the CHF was triggered by the nanoparticles clogging the micro-channel shortly after the incipience of nucleate boiling. No systematic investigation of flow boiling heat transfer coefficient or CHF was reported, and no assessment of important parameters such as mass flux and nanoparticle concentration was provided. Therefore an extensive study is needed to validate the capability of nanofluids in the flow boiling condition.

1.2 Technical Objectives

The primary goal of this study is to generate and analyze first-of-a-kind data for flow boiling heat transfer coefficient (HTC) and CHF at subcooled conditions. In order to achieve this goal, the following sequential activities have been conducted:

(i) Perform experiments to explore the characteristics of subcooled flow boiling HTC as well as CHF with various experimental conditions for mass flux, equilibrium quality, and type of nanofluids and their concentrations.

(ii) Examine the surface characteristics of the test heaters used in activity (i). Important parameters include surface roughness, area, and wettability, and number of micro-cavities.

(iii) Compare the HTC and CHF data with existing models/correlations. Also, interpret the data in terms of surface parameters acquired by activity (ii).

1.3 Thesis Outline

Chapter 2 provides a review of the subcooled flow boiling heat transfer topic. Studies of subcooled flow HTC and CHF relevant to nanofluids application are presented, and possible surface effects due to the nanoparticle depositions are discussed. The review includes discussion of relevant models or correlations that can be used to interpret the HTC and CHF data.

Chapter 3 reports detailed information related to the experimental activities. In particular, this chapter deals with the nanofluids preparation (0.001, 0.01, and 0.1 %vol. alumina/water, zinc-oxide/water, and diamond/water) and characterization, design and construction of experimental facilities, and finally validation of the experimental apparatus. The nanofluid characterization includes measurement of their thermo-physical properties. In the design and construction of the experimental apparatus, an effort was made to simplify and optimize the current scope of the work given the available experimental resources in

our lab. Calibration of the instruments is also reported and some preliminary experiments are discussed to ensure proper function of the flow loop.

Chapter 4 reports the experimental HTC and CHF data measured with the apparatus described in Chapter 3.

Chapter 5 reports the results of the heater surface characterization effort. To inspect the heater surface characteristics, Scanning Electron Microscopy (SEM) and Energy Dispersive X-ray Spectroscopy (EDS), confocal microscopy, and contact angle measurements are employed. SEM and EDS pictures enable studying the heater surface morphology change before and after nanofluids boiling. Also quantitative information about the surface topography (surface roughness and area changes) is obtained using confocal microscopy. A micro-cavity counting technique was developed based on the confocal microscopy images and ImageJ graphic software. Finally, the wetting behavior of the liquid on the heater coupons of various combinations of liquid/solid is investigated starting from contact angle measurements.

Chapter 6 presents the interpretation of the HTC and CHF experimental data in light of the heater surface characterization. The data are compared to the predictions of traditional HTC and CHF models/correlations. Nanoparticle effects on the HTC and CHF are discussed by interrogating possible important mechanisms. Finally, the possible effects of pressure and radiation on nanofluid boiling (which have not been experimentally explored in this study) are discussed, to guide future research.

2 Review of Subcooled Flow Boiling Heat Transfer Literature

Chapter 2 presents a review of the subcooled flow boiling heat transfer literature, to find HTC and CHF theories/models that could be applicable to this study. Section 2.1 is focused on the subcooled nucleate boiling heat transfer coefficient, while Section 2.2 is focused on the subcooled flow boiling critical heat flux.

2.1 Subcooled flow boiling heat transfer coefficient

Nucleate boiling is the predominant heat transfer mechanism in subcooled flow boiling. It is expected that the nucleate boiling heat transfer coefficient (NBHTC) is likely affected by the presence of nanoparticles. Regarding the nanofluids' NBHTC, some studies were performed in pool boiling condition, but no results have been reported under flow boiling conditions. Therefore, several conventional models/correlations are first reviewed; then some studies related to the effect of surface parameters on the NBHTC are summarized.

2.1.1 Conventional models/correlations for subcooled flow boiling

A typical method of predicting the heat transfer coefficient (HTC) is to solve the wall temperature profile either numerically or to deploy the reliable models developed empirically. This prediction is very challenging especially in the two-phase region, due to the presence of complex phenomena and multiple

distinct regions of subcooled flow boiling. It is accepted that such regions are the single-phase convective heat transfer region, and partial and fully developed subcooled nucleate boiling heat transfer regions (Collier and Thome, 1996). Prediction of single-phase convective heat transfer in simple geometries has been relatively successful through many decades' efforts. The Dittus-Boelter's or Gnielinski's correlations are the best prediction models (Collier and Thome, 1996; Mills, 1999) among existing models for turbulent fully-developed flow in a pipe. In contrast, accurate tools to predict partial and fully developed subcooled nucleate boiling are not available yet, due to the complexity of these regions and their sensitivity to the characteristics of the boiling surface. There are three empirical methods, suggested by Bowring, Bergles and Rosenhow, and Chen, that are quite popular for predicting the NBHTC in subcooled flow boiling. They are described next.

First, Bowring's empirical method hypothesizes that the entire subcooled flow boiling heat transfer regime can be modeled as a linear superposition of the single-phase convective and subcooled nucleate boiling heat transfers. The analytical form is expressed as:

$$q" = q"_{SPL} + q"_{SNB} \tag{2-1}$$

where, q", $q"_{SPL}$, and $q"_{SNB}$ are total surface heat flux, surface heat flux transferred by single-phase forced convection, and surface heat flux transferred by bubble nucleation, respectively. For each flow region, Bowring's empirical method specifies the following assumptions to predict the wall temperature.

(i). $T_w<T_{sat}$ (Single-phase region)

$$q"_{SPL} = h_{lo}\left(T_{w,SPL} - T_b\right);\ q"_{SNB} = 0 \tag{2-2}$$

(ii). $T_{sat}<T_w<T_{w,SNB}$ (Partial subcooled nucleate boiling region)

$$q"_{SPL} = h_{lo}\left(T_{sat} - T_b\right);\ q"_{SNB} = \left[\frac{1}{\psi}\left(T_{w,SNB} - T_{sat}\right)\right]^{1/n} \tag{2-3}$$

(iii). $T_w>T_{w,SNB}$ (Fully-developed subcooled nucleate boiling region)

$$q''_{SPL} = 0;\ q''_{SNB} = \left[\frac{1}{\psi}\left(T_{w,SNB} - T_{sat}\right)\right]^{1/n} \tag{2-4}$$

where T_{sat}, T_w, $T_{w,SPL}$, and $T_{w,SNB}$ are saturation temperature of fluid, wall temperature, and wall temperatures at single phase region and at two-phase region, respectively. ψ is an empirical parameter which usually contains physical property values of the fluid and, in many cases, also includes a function characterizing the particular heating fluid/surface combination. n is an exponent having a value ranging from 0.25 to 0.5. In the calculation of q''_{SPL}, single-phase HTC, h_{lo} can be evaluated using the well-known Dittus-Boelter's or Gnielinski's correlations, respectively as follows (Mills, 1999):

$$h_{lo} = 0.023\left(\frac{k_l}{D_i}\right)\left(\frac{GD_i}{\mu_l}\right)^{0.8}\left(\frac{\mu_l c_{p,l}}{k_l}\right)^{0.4} \quad Dittus-Boelter's\ correlation \text{ for } Re > 10^4 \tag{2-5}$$

$$h_{lo} = \left(\frac{k_l}{D_i}\right)\frac{(f/8)(\mathrm{Re}-1000)\mathrm{Pr}}{1+12.7(f/8)^{1/2}\left(\mathrm{Pr}^{2/3}-1\right)} \quad Gnielinski's\ correlation \text{ for } 3000 < Re < 10^6 \tag{2-6}$$

where, G, D_i, μ_l, $c_{p,l}$, and k_l are the mass flux, heater inner diameter, and viscosity, specific heat capacity, and thermal conductivity of water at local bulk temperature, respectively. Re and Pr are Reynolds and Prandtl numbers, respectively. f is friction factor which can be evaluated using Moody's diagram as:

$$f = [0.790\ln\mathrm{Re} - 1.64]^{-2} \text{ for } 10^4 < Re < 5\times10^6 \tag{2-7}$$

No specific correlation has been recommended for the calculation of q''_{SNB}. This model is recommended for detailed calculations, particularly if other characteristics of the subcooled boiling system are required, such as void fraction and pressure drop (Collier and Thome, 1996).

A second empirical approach is Bergles-Rosenhow's superposition method. This method superposes the single-phase heat transfer and fully developed subcooled nucleate boiling heat transfer, to get the wall temperature in the partial subcooled nucleate boiling region. The explicit form of this method is expressed as:

$$q'' = \left[q''^{\,2}_{SPL} + \left(q''_{SNB} - q''_{SNB,ONB} \right)^2 \right]^{1/n} ; n = 2 \tag{2-8}$$

where, q''_{SPL} is equivalent to Eq. 2-2. q''_{SNB} and $q''_{SNB,ONB}$ are the heat flux at fully developed subcooled nucleate boiling and onset of nucleate boiling, respectively. The ONB point can be evaluated using the model of Davis-Anderson, which is given as:

$$q''_{ONB} = \frac{k_f h_{fg} P}{8 R^* T_{sat}^2 \sigma} \left(T_w - T_{sat} \right)^2_{ONB} \tag{2-9}$$

where k_f, h_{fg}, and σ are the thermal conductivity, heat of vaporization, and surface tension of saturated water at the designated pressure. The specific gas constant for water is R^*=461.9 J/kg·K. In Eq. 2-9, $T_{w,ONB}$ is the unknown that is actually evaluated because from the view point of conducting an experiment, the heat flux is a control variable. Therefore, in order to evaluate $T_{w,ONB}$, Eq. 2-9 is modified as:

$$T_{w,SNB,ONB} = T_{sat} + \sqrt{\frac{8 R^* T_{sat}^2 \sigma}{k_f h_{fg} P_l} q''} \tag{2-10}$$

where, q'' is the control heat flux. Regarding q''_{SNB} in Eq. 2-8, the correlations used in the Bergles-Rohsenhow's methods are the Jens and Lottes' and Thom's correlations. Jens and Lottes correlated their experimental data by a dimensional equation, valid for water only, as follow:

$$\left(T_{w,SNB} - T_{sat} \right) = 25 \left(q''_{SNB} \right)^{0.25} e^{-P/62} \tag{2-11}$$

where, P is the absolute pressure in bar and q''_{SNB} is in MW/m^2 and the temperature are in °C. Thom reported that the wall superheat estimated in Eq. 2-11 is consistently low over the range of their experiments and thus modified it as:

$$\left(T_{w,SNB} - T_{sat} \right) = 22.65 \left(q''_{SNB} \right)^{0.5} e^{-P/87} \text{ or } q''_{SNB} = \left[\frac{1}{22.65} e^{P/87} \left(T_{w,SNB} - T_{sat} \right) \right]^2 \tag{2-12}$$

By replacing $T_{w,SNB}$ with $T_{w,ONB}$ calculated using Eq. 2-10, $q''_{SNB,ONB}$ is then estimated as:

$$q''_{SNB,ONB} = \left[\frac{1}{22.65} e^{P/87} \left(T_{w,SNB,ONB} - T_{sat} \right) \right]^2 \tag{2-13}$$

Then Eq. 2-8 can be solved numerically via an iteration procedure. This model is recommended for rapid

calculations of the complete forced convective subcooled boiling curve when only a limited number of data which fall in the partial subcooled nucleate boiling region are available. A fundamental limitation of using this model in our study is that both the Jens-Lottes' and Thom's correlations were developed for the pressure range of 7 to 172 bar. This pressure range, in fact, is much higher beyond the atmospheric pressure condition of this study.

The third empirical model is Chen's correlation, which is known to have broad applicability and reasonable accuracy. Similarly to the Bowring's method, the Chen's model also superposes the single-phase and nucleate boiling heat transfers linearly. The Chen model is expressed by the following equations:

$$q" = h_{FC}(T_w - T_b) + h_{NB}(T_w - T_{sat}) \tag{2-14}$$

where, h_{FC} is the single-phase forced convection HTC, which is very similar to the Dittus-Boelter correlation:

$$h_{FC} = \left(\frac{k_l}{D_i}\right) 0.023 \left(\frac{G(1-X)D_i}{\mu_l}\right)^{0.8} \left(\frac{\mu_l c_{p,l}}{k_l}\right)^{0.4} \tag{2-15}$$

where the flow quality, X is set equal to zero at subcooled conditions, as recommended by Collier and Thome (1996). k_l, μ_l, and $c_{p,l}$ are the thermo-physical properties corresponding to the local bulk temperature, T_b. h_{NB} is the NBHTC, whose explicit form is given as follows:

$$h_{NB} = 0.00122 \left[\frac{k_f^{0.79} c_{p,f}^{0.45} \rho_f^{0.49}}{\sigma^{0.5} \mu_f^{0.29} h_{fg}^{0.24} \rho_g^{0.24}}\right] (T_w - T_{sat})^{0.24} [P_{sat}(T_w) - P]^{0.75} S \tag{2-16}$$

where k_f, μ_f, ρ_f, ρ_g, and σ are the thermo-physical properties of saturated water. S is the nucleate boiling suppression parameter, which is:

$$S = \frac{1}{1 + 2.53 \times 10^{-6} \left(\frac{G(1-X)D_i}{\mu_l}\right)^{1.17}} \tag{2-17}$$

Eq. 2-16 itself is a rather complex function of T_w and is coupled to Eq. 2-14. Therefore in order to obtain

T_w, Eqs. 2-14 to 17 need to be solved iteratively. Chen's linear superposition method accounts for the forced convection and nucleate boiling suppression effects. However, it does not account for the effect of the boiling surface characteristics on the NBHTC. Nevertheless, it will be used as a starting point for the wall temperature predictions.

2.1.2 Surface effect on flow nucleate boiling heat transfer coefficient

Vandervort et al.'s study (1992) identified several possible mechanisms for subcooled boiling heat transfer as:

(i). Single phase liquid turbulent forced convection.

(ii). Direct wall to vapor transport at the point of bubble attachment

(iii). Micro-layer vaporization of liquid to vapor at the base of the bubble followed by

(iv). Internal micro-convection of vapor across the bubble followed by

(v). Vapor condensation at the bubble tip and convection into the subcooled liquid core

(vi). Bubble-induced turbulent mixing in the liquid phase

(vii). Vapor-liquid exchange

(viii). Thermo-capillary of Marangoni-effect-induced micro-convection

Thom and Collier (1996) suggest that the most dominant heat transfer processes in highly subcooled boiling are mechanisms (iii) and (viii). However, all these mechanisms seem to ignore the effect of the boiling surface characteristics – an effect that can be particularly important when nanoparticles deposition occurs.

A nucleate boiling model that hints to surface effects is Klimenko's model. The model was developed using the experimental data obtained mostly at saturated conditions (Klimenko, 1988; Klimenko, 1990); however here is extrapolated to subcooled boiling conditions as well. His model basically lumps the different two-phase flow and heat transfer regimes into only two, nucleate boiling and forced convection vaporization (annular-flow). Therefore, it consists of two separate correlations, one in the flow regime of the nucleate boiling and one in the forced convective vaporization regime. The transition from one regime to the other is determined by the convective boiling number N_{CB}, which is expressed as following:

$$N_{CB} = \left(\frac{\dot{m}}{A_c}\right)\left(\frac{h_{fg}}{q''}\right)\left[1+x\left(\frac{\rho_f}{\rho_g}-1\right)\right]\left(\frac{\rho_g}{\rho_f}\right)^{1/3} \tag{2-18}$$

The cross-over value of the N_{CB} is 1.6×10^4 with ±25 % uncertainty. By taking the lower bound of the uncertainty, i.e., if $N_{CB} < 1.2\times10^4$, forced convection nucleate boiling prevails. Otherwise, the forced convection vaporization dominates. The correlations are as follows:

$$Nu_{NB} = \frac{h_{NB}L_c}{k_f} = 4.9\times10^{-3}\,Pe_m^{0.6}\,\mathrm{Pr}_f^{-0.33}\left(\frac{P_{sat}L_c}{\sigma}\right)^{0.54}\left(\frac{k_{surface}}{k_f}\right)^{0.12} ; N_{CB} < 1.2\times10^4 \tag{2-19}$$

$$Nu_c = \frac{h_c L_c}{k_f} = 0.087\,\mathrm{Re}_m^{0.6}\,\mathrm{Pr}_f^{1/6}\left(\frac{\rho_g}{\rho_f}\right)^{0.2}\left(\frac{k_{surface}}{k_f}\right)^{0.09} ; N_{CB} > 1.2\times10^4 \tag{2-20}$$

where the modified Peclet number, Pe_m is used to reflect the effect of advection due to boiling. The Prandtl number, Pr_f is implemented to take into account the effect of momentum diffusion with respect to thermal diffusion. L_c is the the Laplace constant or the characteristic length for boiling. Re_m is the Reynolds number of the two-phase mixture.

$$Pe_m = \frac{q'' L_c \rho_f c_{p,f}}{h_{fg}\rho_g k_f} \tag{2-21}$$

$$\mathrm{Pr}_f = \frac{\mu_f c_{p,f}}{k_f} \tag{2-22}$$

$$L_c = \sqrt{\frac{\sigma}{g(\rho_f - \rho_g)}} \tag{2-23}$$

$$\mathrm{Re}_m = \left(\frac{\dot{m}}{A_c}\right)\left[1 + x\left(\frac{\rho_f}{\rho_g} - 1\right)\right]\frac{L_c}{\mu_f} \tag{2-24}$$

Now it is of particular interest to observe that Eq. 2-19 implements the surface effect via surface thermal conductivity change. Since nanoparticle deposition can alter the surface thermal conductivity, implementation of this model in our study seems appropriate.

Tong and Tang (1997) also mention the surface effect on nucleate boiling or effect of fouling on boiling surface explicitly in their book. They report that porous deposits on the surface increase the thermal resistance in forced convection, which results in a penalty in HTC. However, they also report a positive effect from such deposit. That is, in a reactor core such a surface deposit usually called crud exists and is expected to increase the number of active nucleation sites and thus the nucleate boiling HTC. An enhanced capillary wicking force and decreased bubble departure diameter were also observed. Calculation of the wall superheat for a crudded surface is suggested with the assumption that the outer surface temperature of the crud is maintained at saturation.

$$\Delta T_{sat} = (T_w - T_{sat})_{crud} = \frac{q''}{k_{c,B}/s} \tag{2-25}$$

where, $k_{c,B}$ and s are the effective thermal conductivity of crud in nucleate boiling and the thickness of the crud, respectively. Typical crud thickness was reported as ~20 μm at 13.7 MPa. In order to implement this correlation in our case, however, more information would be needed about the effective thermal conductivity and thickness of the nanoparticle porous layer.

Nucleate boiling heat transfer is driven by bubble nucleation at the active nucleation sites, and bubble parameters such as bubble departure diameter and frequency. The pioneering work of Mikic and Rohsenow (1969) proposed the following correlation for nucleate boiling heat transfer.

$$q''_{ev} = 2(\pi k_l \rho_l c_l)^{1/2} f_b^{1/2} D_b^2 N_a (T_w - T_{sat}) \tag{2-26}$$

where, D_b and f_b are bubble departure diameter and its frequency, respectively. (T_w-T_{sat}) is the wall superheat. N_a is the nucleation site density. Eq. 2-26 shows a strong dependency of the heat flux on D_b, f_b, N_a, and (T_w-T_{sat}). However, in order to utilize this model, it is necessary to know the bubble parameters, which are not easily measured or reliably predicted. Moreover, the model was built for pool boiling, while the current study is about flow boiling.

Recently Basu et al. (2005) proposed the following model to predict the subcooled flow boiling heat transfer.

$$q''_w = q''_{tc} + q''_{fc} = q''_l + q''_{ev} \tag{2-27}$$

where, q''_w, q''_{tc}, q''_{fc}, q''_l, and q''_{ev}, are the total heat flux at the wall, and heat fluxes transferred by transient conduction and forced convection, to the liquid, and by evaporation, respectively. Their fundamental idea for the proposed model is that all the energy from the wall is transferred to the superheated liquid layer immediately adjacent to the wall primarily by transient conduction (q''_{tc}) and forced convection (q''_{fc}). The detail models for each heat flux contribution are found as:

(i) $t^* \le t_w$

$$q''_{tc} = \frac{1}{t_w + t_g} \int_0^{t^*} \frac{k_l}{\sqrt{\pi \alpha_l t}} (\Delta T_w + \Delta T_{sub}) dt \tag{2-28}$$

$$q''_{fc} = h_{fc} (\Delta T_w + \Delta T_{sub}) \left[\frac{t_w - t^*}{t_g + t^*} + (1 - A_b N_a) \frac{t_g}{t_g + t_w} \right] \tag{2-29}$$

(ii) $t^* > t_w$

$$q''_{tc} = \frac{1}{t_w + t_g} \left[\int_0^{t_w} \frac{k_l}{\sqrt{\pi \alpha_l t}} (\Delta T_w + \Delta T_{sub}) dt + \int_{t_w}^{t} \frac{k_l}{\sqrt{\pi \alpha_l t}} (\Delta T_w + \Delta T_{sub}) [1 - A_b N_a] dt \right] \tag{2-30}$$

$$\begin{cases} q''_{fc} = h_{fc}\left(\Delta T_w + \Delta T_{sub}\right)\left(1 - A_b N_a\right)\dfrac{t_w + t_g - t^*}{t_w + t_g};\ t_w < t^* < (t_w + t_g) \\ q''_{fc} = 0;\ t^* \geq (t_w + t_g) \end{cases} \tag{2-31}$$

where, t_w, and t_g are the bubble waiting and growth time, respectively. t^* is the time period over which transient conduction is dominant with respect to convection and is expressed as:

$$t^* = \left(\frac{k_l}{h_{fc}}\right)^2 \frac{1}{\pi \alpha_l} \tag{2-32}$$

Then these transferred energies ($q''_{tc} + q''_{fc}$) subsequently go to the liquid (q''_l) and bubble via evaporation (q''_{ev}). The most dominant heat transfer mechanism is from the evaporation of liquid and its expression is given as:

$$q''_{ev} = N_a f_b \frac{\pi}{6} R_f D_l^3 \rho_g h_{fg} \tag{2-33}$$

where, D_l and f_b are bubble lift-off diameter and its frequency, respectively. N_a is nucleation site density. It is clearly seen that Eqs. 2-28 to 31 are closely related to the local subcooling (ΔT_{sub}), wall superheat (ΔT_w), bubble waiting and growth time (t_w and t_g), and nucleation site density (N_a), to mention a few significant variables. In addition, as seen in Eq. 2-33, evaporation carries over the heat transferred by transient conduction and forced convection to the subcooled bulk stream. Also the model shows a strong dependency on nucleation site density (N_a), bubble lift-off diameter and frequency (D_l and f_b). This expression is, in fact, very similar to Eq. 2-26, which is a typical nucleate boiling heat transfer correlation developed for pool boiling conditions. Interestingly, some (t_w, t_g, f_b, D_l, N_a) of the aforementioned parameters are expected to be changed during nanofluids boiling because of the nanoparticle deposition. However, these parameters were not measured in the current study, which makes the application of this model problematic. Therefore, more experimental efforts are needed to make use of Basu et al.'s model for nanofluids.

2.2 Subcooled flow boiling critical heat flux

The previous studies at MIT (Kim et al., 2006b; Kim et al., 2007; Kim, 2007; Truong et al., 2008) have helped identifying the likely parameters affecting the CHF of nanofluids at pool boiling conditions. It was shown that the improved surface wettability was a main factor affecting the CHF enhancement. Regarding the flow CHF, the presence of the convective effect may yield another effect on the CHF. Although has not verified experimentally yet, a possibility exists that the dispersion of the solid particle may agitate the boundary layer and hinder the coalescence of the vapor. In addition, the highly wettable surface may make the liquid film thicker and thus delay the occurrence of the CHF. A detailed analysis of the possible nanoparticle-related effects on CHF is reported in Chapter 6, while in this section four models for flow CHF at low qualities are discussed briefly.

2.2.1 Hydrodynamic Instability Theory (Boundary Layer Separation)

Kutateladze and Leont'ev (1964) suggested that the flow boiling crisis can be analyzed using the concept of boundary-layer separation (blowoff) induced by vapor injection (without condensation). The limiting factor was attributed to the separation of the hydro-dynamic boundary layer when radial bubble injection blows off the liquid layer near the wall. Their physical model led to the following equation:

$$q''_{CHF} = \frac{C_1 h_{fg} \rho_l V_o}{\mathrm{Re}^{0.6}} \tag{2-34}$$

where, h_{fg}, ρ_l, V_o, and μ_l are heat of vaporization, liquid density, free stream velocity, and liquid viscosity, respectively. C_1 is a function of equilibrium quality. An expression for C_1 was proposed by Tong (Tong, 1968) using existing flow boiling crisis data obtained in water at 6.9-13.8 MPa. Furthermore, Celata et al. (1994a) slightly modified Tong's correlation to give a more accurate prediction in the range of pressure

below 5.0 MPa. It is found that their correlation implements only the hydrodynamic and quality effect; that is, no effect of the surface characteristics is envisioned. Note that the diluted nanofluids tend to have similar thermal and transport properties as compared to those of base water (Kim et al., 2006; Kim et al., 2007a, Kim, 2007b), yet they display a much higher CHF. Therefore, this correlation is not very useful for interpreting the nanofluid CHF data, which is most likely due to the alteration of the surface characteristics, as will be shown in Chapter 5 and discussed in some detail in Chapter 6.

2.2.2 Bubble Layer Theory

At highly subcooled flow boiling conditions, the bubbles generated at the wall form a bubble layer. Such observation provided a starting point for many researchers for the modeling of the boiling crisis. Four models adopting the concept of bubble layer are found in the literature (Tong and Tang, 1997).

(i). The analysis of critical enthalpy in a bubble layer was suggested by Tong et al. (1966).

(ii). The analysis of turbulent mixing at the core-bubble layer interface was suggested by Weisman and Pei (1983).

(iii). The analysis of mass and energy balance on the bubble layer was suggested by Chang and Lee (1989).

(iv). The Weisman-Pei model was modified by Lee and Mudawar (1988) based on the Helmholtz instability at the microlayer-vapor interface as a trigger condition for microlayer dryout. Microlayer is a thin liquid layer between bubble and adjacent heated surface. The presence of the microlayer is believed to help delay the triggering of the CHF.

Assumptions (i) ~ (iii) focus exclusively on the bubble layer and thus of limited help in explaining the surface effect on the CHF. On the other hand, a specific variable in the study of Lee and Mudawar (1988) is worthwhile considering for the current study. By choosing the liquid sublayer as a control volume, they set up the following energy conservation for the microlayer:

$$q''_{CHF} = G_m \delta_m \left[\frac{h_{fg} + (h_f - h_m)}{L_m} \right] \tag{2-35}$$

where G_m, δ_m, L_m, and h_m are the liquid mass flux flowing into the microlayer, thickness and length of the microlayer, and liquid enthalpy flowing into the microlayer, respectively. They hypothesized that the microlayer dryout triggers the CHF due to the Helmholtz instability, which determines the scale of the thickness and length of the microlayer. Assuming nanoparticles are deposited on the surface during nanofluids boiling, the wettability change also may alter the occurrence of the Helmholtz instability via the bubble departure dynamics change. Thus, there will be a possibility to interrelate the improved wettability and the microlayer thickness and length without consideration of the Helmholtz instability. This model indeed provides a physical relationship between wettability effect and microlayer formation. However, application of this model may not be viable in the current study as additional experimental setup needs to be devised to visualize the microlayer formation.

2.2.3 Vapor Clot Theory

Katto (1990) developed a model for the CHF at subcooled flow condition, based on the assumption that CHF occurs if a very thin liquid sublayer adjacent to the wall dries out when a vapor clot passes over it. The proposed model has the form of the energy conservation within the control volume of liquid sublayer and adjacent vapor clot. It is found that the Katto model was developed based on the same mechanism as the Lee and Mudawar model, from which it borrows much of the original procedure, e.g.

liquid sublayer dryout mechanism. Celata et al. (1994b), who extended the idea of the dryout of the liquid sublayer, and developed a more mechanistic model based on it. They set up several constitutive models for the liquid sublayer as follows:

$$q''_{CHF} = \frac{\rho_l \delta h_{fg}}{L_B} U_B \tag{2-36}$$

$$\delta = y^* - D_B \tag{2-37}$$

$$D_B = \frac{32}{f} \frac{\sigma g(\beta) \rho_l}{G^2} \tag{2-38}$$

$$\frac{1}{\sqrt{f}} = 1.14 - 2.0 \log\left(\frac{\varepsilon}{D_e} + \frac{9.35}{\mathrm{Re}\sqrt{f}} \right) \tag{2-39}$$

where Eq. (2-36) expresses the power needed to dry out the liquid sublayer, as the vapor clot passes over it. In Eq. (2-36), δ and y^* are the thickness of the liquid sublayer and superheated layer, respectively. It is clearly seen that the decrease in the vapor clot thickness, D_B, will result in an increase in δ and eventually will increase the CHF. In particular, they evaluated D_B by adopting Staub's model (Staub, 1968), which balances the adhesive and dislodging forces of the vapor attached to the heater surface. Note that the model explicitly involves a function of contact angle (β), $g(\beta)$. Furthermore, the friction factor, f, was implemented using Colebrook-White equation combined with Levy's roughness model (Levy, 1967), which also makes use of the surface roughness, ε. Therefore, Celata et al.'s model implicitly suggests a dependence of CHF on the surface characteristics, such as the contact angle and roughness. Since those variables are directly obtainable from measurements, this model will be evaluated in the interpretation of our nanofluids data in Chapter 6.

2.2.4 Wall Overheat Theory (Hot/Dry Spot Theory)

This theory addresses the development of the hot/dry spots within the bases of the bubbles growing at the nucleation sites. The hot/dry spots can be reversible if the rewetting occurs and irreversible if not. The hot/dry spots behavior can be modified by the presence of the nanoparticles on the surface, which was found to be the direct consequence of the nanofluid boiling (Kim et al., 2006, Kim et al., 2007, Kim, 2007). It was also confirmed that the presence of the nanoparticle layer increased the surface wettability significantly. Plausibly the improved wettability can help delay the CHF by promoting the rewetting of hot/dry spots upon bubble departure. In the literature, however, no relevant study about the wettability on subcooled flow boiling CHF is found. Therefore, as an alternative, a pool boiling CHF model that accounts for the wettability effect is introduced (Kandlikar, 2001). Kandlikar (2001) observed significant effect of contact angle on the CHF and modeled its contribution by considering the forces exerted on the bubble due to momentum change from evaporation, surface tension acting on base and top of the bubble, and pressure gradient due to buoyancy. The final form of the model/correlation is expressed as:

$$q''_{CHF,sat} = h_{fg}\rho_g^{1/2}\left(\frac{1+\cos\theta}{16}\right)\left[\frac{2}{\pi}+\frac{\pi}{4}(1+\cos\theta)\cos\phi\right]^{1/2}\left[\sigma g(\rho_f-\rho_g)\right]^{1/4} \tag{2-40}$$

where, θ, ϕ, and σ are receding contact angle of liquid, orientation of heater surface (horizontal up-facing; ϕ=0°), and surface tension, respectively. With a vertical heater surface (ϕ=90°), Eq. 2-41 is reduced as follow:

$$q''_{CHF,sat} = \left(\frac{2}{\pi}\right)^{1/2} h_{fg}\rho_g^{1/2}\left(\frac{1+\cos\theta}{16}\right)\left[\sigma g(\rho_f-\rho_g)\right]^{1/4} \tag{2-41}$$

It is noted that Eq. 2-41 is valid only for saturated pool boiling condition but can be extended to account for the subcooling effect, which is expressed as (Elkassabgi and Lienhard, 1988):

$$q''_{CHF,sub} = q''_{CHF,sat}\left(1+\frac{\Delta T_{sub}}{\Delta T_{sat}}\right)_{sub} \tag{2-42}$$

where, $\Delta T_{sub}=T_{sat}-T_b$ and $\Delta T_{sat}=T_w-T_{sat}$, respectively.

This model provides a basis for the physical consideration of the contact angle, θ. Kandlikar points out that use of the dynamic contact angle (here receding contact angle vs static contact angle) would be the best choice for the model. However, he also recommends use of static contact angle as an alternative if receding contact angle data are unavailable. Since static contact angle is directly measured in this study, the model will be used in our analysis.

Interestingly, in the latest work of Kuan and Kandlikar (2008), an attempt to extend Kandlikar's pool boiling CHF model to flow boiling in micro-channels at saturated conditions was made. The proposed flow CHF model is expressed as:

$$q''_{CHF,sat} = Ch_{fg}\sqrt{\rho_g}\left[\sqrt{\frac{2\sigma\cos\theta}{b}+\frac{G^2}{2\overline{\rho}}}\right] \tag{2-43}$$

where, C is the constant determined by the experimental data and was set as 0.002679 or 0.002492 depending on experimental database that they adopted. h_{fg}, ρ_g, σ, b, G, and θ are heat of vaporization, vapor density, surface tension, channel height, mass flux, and contact angle, respectively. Mixture density, $\overline{\rho}$ is defined as:

$$\frac{1}{\overline{\rho}}=\frac{x}{\rho_g}+\frac{1-x}{\rho_f} \tag{2-44}$$

where, x is thermodynamic quality at the micro-channel exit ($0<x<1$). Their model clearly incorporates the contact angle effect on the flow boiling CHF. As of yet, the validity of this model for subcooled flow boiling in macroscopic channels is not assured because the model was primarily built for micro-channel applications and saturated condition. However, we will employ this model in assessing our CHF experimental data.

In summary, the empirical models of Bowring, Bergles-Rohsenow, and Chen for subcooled flow boiling heat transfer were reviewed and will be used in the analysis of our nanofluid heat transfer coefficient data. Klimenko's model for the forced convective nucleate boiling and Tong and Tang's considerations of the fouling surface effect confirm that surface effects are not negligible. Their works also provide a basis for further modeling work using the measured data. Other studies incorporating the possible surface effects were reviewed, in which the nucleation site density, bubble wait and growth time, bubble departure diameter and frequency were identified as the key parameters. In order to apply such detailed models to the current study, those parameters would need to be measured.

Modeling of the nanofluid CHF was also discussed by reviewing existing theories with particular emphasis on their ability to incorporate surface effects such as roughness and contact angle, which are directly measured in our experiments. Celata et al.'s (Celata et al., 2994b), Kandlikar's (2001), and Kuan and Kandlikar's (2008) models may provide a good starting point for the analysis of the nanofluid CHF data.

3 Experimental Activities

Chapter 3 reports detailed information for the experimental activities related to the subcooled flow boiling study. Section 3.1 describes the procedure for nanofluids preparation from the as-purchased state to dilution. Section 3.2 reports the methods of nanofluid characterization, both the thermo-physical and colloidal properties. Section 3.3 describes the flow boiling loop and associated instrumentation/control. Finally, Section 3.4 describes the efforts undertaken to verify the correct operation of the flow loop.

3.1 Preparation of Nanofluids

Three concentrated nano-dispersions (alumina/water, zinc-oxide/water, and diamond/water) were purchased from vendors. The specifications of the as-received nanofluids were taken from the vendors and some representative data are summarized in Table 3-1.

Table 3-1 Specifications of the tested nanofluids

Nanofluids	Alumina/water	Zinc oxide/water	Diamond/water
Vendor	Nyacol	Nyacol	PlasmaChem GmbH
Particle size (nm)	< 20 nm	< 40 nm	< 10 nm
Particle thermal conductivity (W/m·K)	~40	~100	900~2300
Particle density (g/mL)	3.90	5.75	3.50
Particle weight percent (%wt.)	20	40	5
Appearance	Opaque	Opaque	Opaque

Since the as-received nanofluids were at high concentration (which the vendors typically specify as weight percent, or %wt.), it was necessary to dilute the nanofluids to obtain different (lower) concentrations of nanoparticles. Very dilute nanofluids are desirable for practical applications, including nuclear applications, as the properties of the dilute nanofluids (particularly viscosity) stay similar to those of water, and also dilute nanofluids are typically transparent. Therefore, it is necessary to add a suitable amount of de-ionized (DI) water into the initial high-concentration nanofluids. For example, in order to make φ %vol. nanofluid from a mL of ξ %wt. nanofluid, one needs to determine how much DI water should be added. When the a mL of ξ %wt. nanofluid is said to contain b mL of solid nanoparticles of density ρ_p g/mL and c mL of DI water of density ρ_w g/mL, the required amount of DI water to balance φ %vol. nanofluid can be calculated by means of the following equations:

$$a = b + c \tag{3-1}$$

$$\xi(\%wt.) = \frac{b\rho_p}{b\rho_p + c\rho_w} \times 100 \tag{3-2}$$

$$\varphi(\%vol.) = \frac{b}{b + c + d} \times 100 \tag{3-3}$$

Because the quantity of b and c are not usually known, those variables need to be eliminated. Finally the required amount of water d can be expressed in terms of a, ξ, φ, ρ_p, and ρ_w, and an expression obtained which may be applied to the dilution of any nanofluid.

$$d = a\frac{\frac{1-\varphi}{\varphi} - \frac{1-\xi}{\xi}\cdot\frac{\rho_p}{\rho_w}}{1 + \frac{1-\xi}{\xi}\cdot\frac{\rho_p}{\rho_w}} \tag{3-4}$$

Based on the Eq. (3-4), in order to make 0.1 %vol. alumina from 1 mL of 20 %wt. alumina, 59.2 mL of DI water has to be added, in which the alumina nanoparticles and DI water were assumed to have the density of 3.9 g/mL and 1.0 g/mL, respectively. No surfactants or pH control was used in the dilute nanofluids.

3.2 Characterization of Nanofluids

The thermo-physical and colloidal properties of the prepared nanofluids need to be measured to ensure the changes from those of base water. In this characterization task, density and specific heat capacity changes of the prepared nanofluids over the base water were investigated using a theoretical model. Thermal conductivity, kinematic viscosity, and surface tension of the nanofluids were also measured and resulting values were compared to the existing models. In addition, nanoparticle sizes dispersed in base water were measured using a dynamic light scattering technique.

3.2.1 Nanofluid density

Since this study is mostly focused on the use of very low concentrations of nanoparticles dispersed in base water, the density of the resulting nanofluids is expected to differ negligibly from that of water. The nanofluid density can be calculated as:

$$\rho_{NF} = \varphi\rho_p + (1-\varphi)\rho_w \tag{3-5}$$

where φ is the nanoparticle volume fraction. For example, for φ ~0.1 %vol., ρ_p ~ 4 g/cm^3 and ρ_w ~ 1 g/cm^3 the deviation from DI water is expected to be only 0.3 %. Assuming that the nanoparticles are as volatile as the water molecules, the density of the nanofluid vapor, $\rho_{NF,g}$, can be calculated as

$$\rho_{NF,g} = \rho_g \frac{\rho_p\varphi + \rho_w(1-\varphi)}{\rho_g\varphi + \rho_w(1-\varphi)} \tag{3-6}$$

Eq. 3-6 gives deviations from the pure water vapor density of the order of 0.4 % at the conditions of interest. In reality the deviation will be even smaller because the nanoparticles are less volatile than the water molecules.

3.2.2 Nanofluids specific heat capacity

Specific heat capacity is also one of the important thermo-physical properties which affect the thermal performance of nanofluids. Using the mixing theory for ideal gas mixtures (Smith and Van Ness, 2005), the volume-averaged nanofluids specific heat capacity can be calculated as:

$$c_{p,NF} = \varphi c_{p,p} + (1-\varphi) c_{p,w} \tag{3-7}$$

where, $c_{p,NF}$, $c_{p,p}$, and $c_{p,w}$ are specific heat capacity of nanofluid, nanoparticle suspension, and base water, respectively. Eq. 3-7 actually does not agree with the experimental data, as shown by the recent work of Zhou and Ni (2008). Assuming thermal equilibrium between the particles and the surrounding fluid (actually a good assumption, given the small size of the particles), they recommend the following expression for the specific heat of a liquid/solid mixture:

$$c_{p,NF} = \frac{\varphi \rho_p c_{p,p} + (1-\varphi)\rho_w c_{p,w}}{\varphi \rho_p + (1-\varphi)\rho_w} \tag{3-8}$$

which agrees very well with their data. Using Eq. 3-8, the change of the nanofluids specific heat capacity can be calculated. For example, for the highest alumina nanoparticle volume concentration of φ ~0.1 %vol., $c_{p,p}$ ~ 760 J/kg·K, $c_{p,w}$ ~ 4215.2 J/kg·K (at saturation of 0.1 MPa), ρ_p ~ 4 g/cm^3 and ρ_w ~ 1 g/cm^3 the deviation from DI water is expected to be smaller by only 0.33 %. For zinc oxide and diamond nanofluids, similar results are obtained. Therefore, for the application of low-concentration nanofluids, the specific heat capacity may be treated as identical to that of water.

3.2.3 Thermal conductivity measurement

Models for the prediction of the nanofluid thermal conductivity are much less reliable and controversial, as reported by Williams (2006). Therefore, it was decided to measure the thermal conductivity of our nanofluids. This was done with a KD2 handheld meter and a related apparatus, a schematic diagram of which is given in Fig. 3-1. The measurement range for this instrument is 0.02 to 2.00 W/m·K with an accuracy of 0.01 W/m·K at full range. The operating temperature is from -20 to 40 °C. The KD2 probe uses the single-needle heat pulse technique to measure the thermal conductivity and thermal diffusivity of mixed substance of solid particles and base liquid. With this technique, a 30-second heat pulse is applied to the needle, and the temperature response with time is monitored. The temperature vs time response depends on the thermal properties of the material surrounding the needle. The theory of the thermal conductivity measurement is explained in Appendix A.

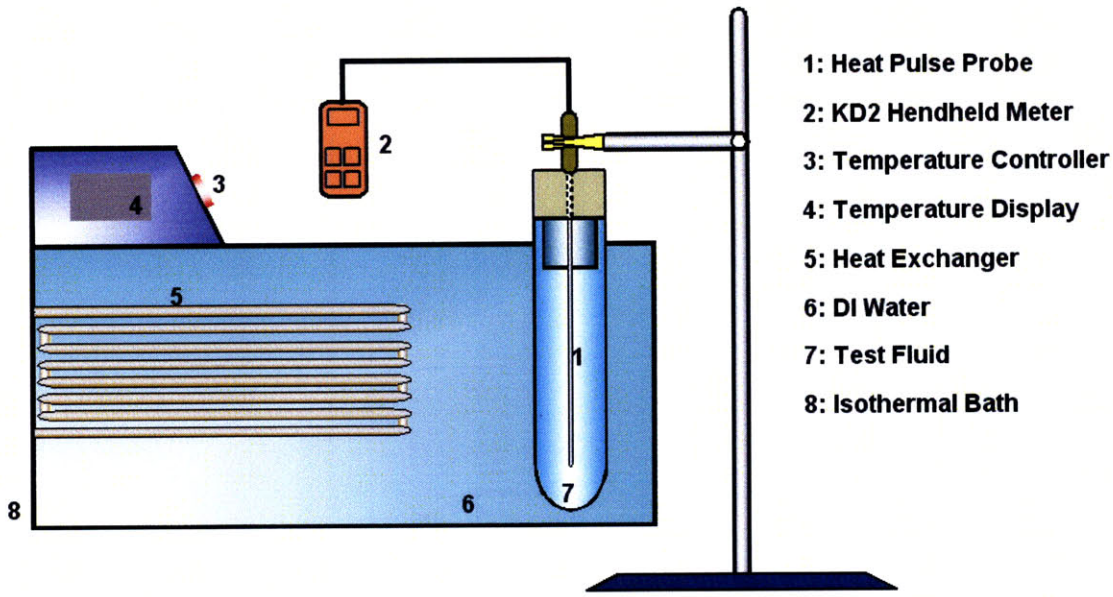

Figure 3-1 A schematic of thermal conductivity measurement

Thermal conductivity was measured at 0.1 MPa and 22.3°C using an isothermal bath. The measurement uncertainty is conservatively less than 5% and the measurement results are given in Table 3-2. The thermal conductivity of dilute nanofluids shows an insignificant change compared to that of water.

The relative error is defined as the ratio of the measured thermal conductivity of nanofluids to water values and estimated to be less than 2 %.

$$relative\ \ error(\%) = \frac{k_{NF,measured} - k_{w,measured}}{k_{w,measured}} \times 100 \tag{3-9}$$

The measured values for water are in good agreement with the ASME steam table value (0.603 W/m·K) for water at 0.1 MPa and 23 °C.

Table 3-2 Thermal conductivity of DI water and nanofluids measured with KD2

	Nanoparticle concentration (%vol.)	Thermal conductivity (W/m·K) Test 1	Thermal conductivity (W/m·K) Test 2	Thermal conductivity (W/m·K) Test 3	Thermal conductivity (W/m·K) Test 4	Thermal conductivity (W/m·K) Test 5	Thermal conductivity (W/m·K) Average	Relative error (%)
DI Water	0	0.58	0.59	0.57	0.59	0.60	0.586	0.0
Alumina /water	0.1	0.58	0.59	0.57	0.60	0.59	0.586	0.0
	0.01	0.57	0.59	0.59	0.60	0.59	0.588	0.3
	0.001	0.57	0.59	0.59	0.59	0.55	0.578	1.4
Zinc oxide /water	0.1	0.56	0.59	0.59	0.60	0.61	0.590	0.7
	0.01	0.59	0.59	0.60	0.60	0.61	0.598	2.0
	0.001	0.58	0.58	0.59	0.59	0.57	0.582	0.7
Diamond /water	0.1	0.60	0.60	0.60	0.59	0.60	0.598	2.0
	0.01	0.59	0.59	0.58	0.59	0.59	0.588	0.3
	0.001	0.60	0.59	0.59	0.58	0.59	0.590	0.7

The measured thermal conductivities of nanofluids are then compared to the well-known prediction, Maxwell-Garnett (MG) relation (1904), whose formula is given as follows:

$$k_{NF} = k_w \left[1 + \frac{1 + 3\varphi(k_p / k_w - 1)}{k_p / k_w + 2 - \varphi(k_p / k_w - 1)} \right] \tag{3-10}$$

where, k_{NF}, k_w, and k_p, are thermal conductivity of the nanoparticles/water, DI water, and nanoparticle, respectively. φ is volumetric fraction of the nanoparticle suspended in base water. The prediction of the MG model is presented in Fig. 3-2. Eq. 3-10 suggests that the thermal conductivity of nanofluids increases with nanoparticle concentration but the increment is not significant as the nanoparticle concentration is very low in this study. Fig. 3-2 suggests that measured thermal conductivities of nanofluids are slightly lower than the predicted values, but within the measurement uncertainty limit of 5%.

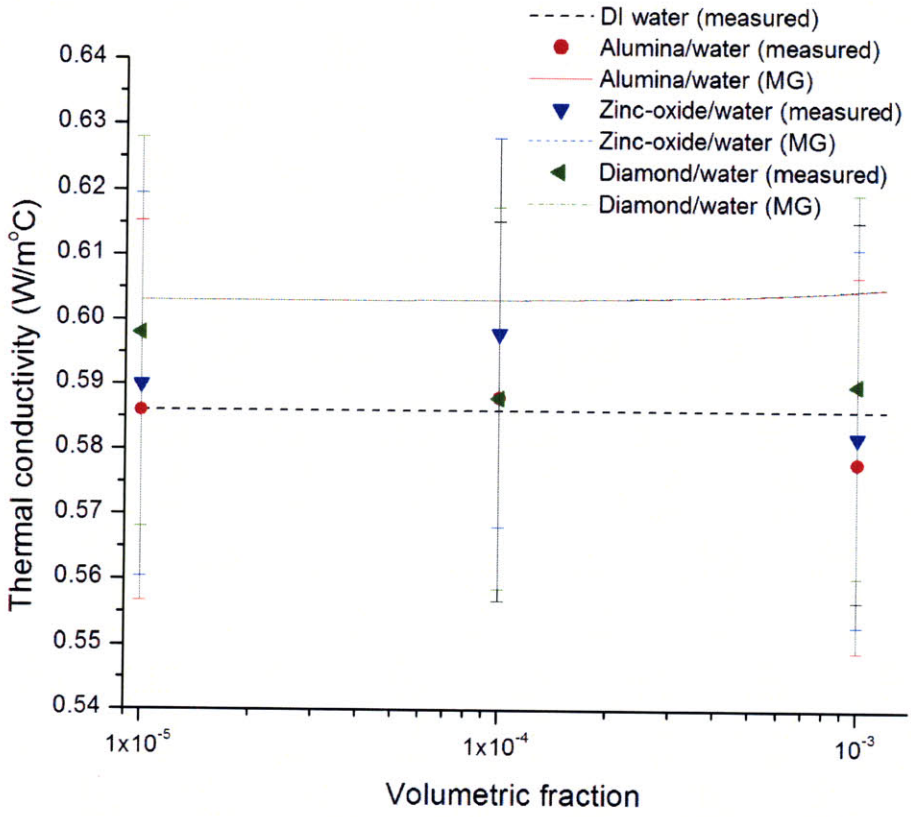

Figure 3-2 Comparison of measured and predicted thermal conductivities within relevant range of nanoparticle volumetric fraction

3.2.4 Kinematic viscosity measurement

Like thermal conductivity, models for the prediction of the nanofluid viscosity are also unreliable and subject of heated debate (Williams, 2006). Therefore, we opted for a direct measurement approach. A reverse-flow type Cannon-Fenske capillary viscometer for both opaque and transparent liquids was used to measure the kinematic viscosity of DI water as well as nanofluids. The measurable range is from 8×10^{-7} to 4×10^{-6} m^2/s. The viscosity of pure water is 9.566×10^{-7} m^2/s at 22 °C, which can be found in the NIST database (http://webbook.nist.gov/chemistry/fluid/). The instrumental uncertainty, 0.16% was provided with 95% confidence of the calibration measurements relative to the primary standard, water at 20 °C and 1 atm. The viscosity measurement of all tested fluids was conducted at 22 °C and atmospheric pressure. Since the viscosity has a high dependence on temperature, the viscometer was housed in a plastic cylinder filled with air, effectively constituting an isothermal vessel without controlling the air temperature. The viscometer is shown in Fig. 3-3. The measurement consists of the following steps. The same procedure was adopted in Williams et al.'s (2008) and Kim et al.'s (2007) studies:

(i). Clean the viscometer using suitable solvents, and dry by forcing clean, dry filtered air through the instrument to remove the final traces of solvents. Periodically, traces of organic deposits should be removed with chromic acid or non-chromium cleaning solution.

(ii). Charge the sample into the viscometer, invert the instrument and apply suction to tube arm F, immersing tube E in the liquid sample, and draw liquid to mark G. Wipe clean arm E, and turn the instrument to its normal vertical position.

(iii). Place the viscometer into the holder, and insert it into the constant temperature bath. Align the viscometer vertically in the bath by means of a small plumb bob in tube F, if a self-aligning holder has not been used.

(iv). Allow sample to flow through capillary tube H and approximately half-fill bulb B, stopping the meniscus in bulb B by placing a rubber stopper in tube E.

(v). Allow approximately 10 minutes for the sample to come to bath temperature at 40 °C and 15 minutes at 100 °C. Make sure the meniscus in bulb B does not reach line K.

(vi). Remove the rubber stopper and allow the meniscus to travel upwards into bulbs C and D, using two clocks to measure the efflux times for the meniscus to pass from mark K to mark J, and from mark J to mark I.

(vii). Calculate the kinematic viscosity of the sample by multiplying the efflux time in seconds for each bulb by the viscometer constant for each bulb. The embedded calculation formula of kinematic viscosity follows the Ostwald flow in the capillary tube as:

$$\nu = \frac{\pi g h r^4}{8 l Q} \tag{3-11}$$

where g, h, r, l, and Q, are the acceleration of the gravity, free elevation difference, capillary radius, length of the capillary section, and volumetric flow rate, respectively. Each capillary viscometer size has a coefficient of calibration in m^2/s^2, which can be converted to the kinematic viscosity by multiplying with counted efflux time.

(viii). Repeat the measurement by evacuating the sample and start over the steps (i) to (vii).

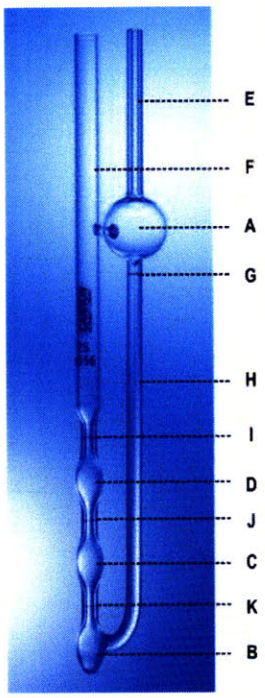

Figure 3-3 Cannon-Fenske capillary viscometer

The measured kinematic viscosity of DI water and nanofluids is tabulated in Table 3-3. In addition, the values are plotted in Fig. 3-4. The measurement uncertainty is less than 5%. The results show that the viscosity of diluted nanofluids is not significantly different from that of DI water. As done in the thermal conductivity characterization, the relative error of viscosity change is also provided for comparison.

$$relative\ \ error(\%) = \frac{\nu_{NF,measured} - \nu_{w,measured}}{\nu_{w,measured}} \times 100 \tag{3-12}$$

The maximum fractional changes were observed for 0.01%vol. alumina, 0.001%vol. zinc oxide, and 0.1%vol. diamond nanofluids, and were up to 2.3%, 2.1%, and 6.6%, respectively. This result reinforces the idea that transport properties do not change significantly in low concentrations of nanofluids.

Table 3-3 Kinematic viscosity of DI water and nanofluids measured at 22 °C and 1 atm

Fluid	Nanoparticle Concentration (%vol.)	Kinematic viscosity (m^2/s) test 1 ($\times 10^7$)	Kinematic viscosity (m^2/s) test 2 ($\times 10^7$)	Average kinematic viscosity (m^2/s) ($\times 10^7$)	Relative error (%)
Pure water	0	9.281	9.443	9.362	0.0
Alumina	0.001	9.370	9.475	9.422	0.6
/water	0.01	9.547	9.605	9.576	2.3
	0.1	9.458	9.410	9.434	0.8
Zinc-oxide	0.001	9.547	9.572	9.560	2.1
/water	0.01	9.370	9.410	9.390	0.3
	0.1	9.458	9.410	9.434	0.8
Diamond	0.001	9.547	9.540	9.543	1.9
/water	0.01	9.635	9.702	9.669	3.3
	0.1	9.900	1.006	9.980	6.6

Viscosities of the nanofluids also can be predicted with existing models. In this study, a prediction developed by Einstein is used (Everett et al., 1988):

$$\mu_{NF} = \mu_w(1+2.5\varphi) \tag{3-13}$$

where, μ_{NF} and μ_w are dynamic viscosity of nanofluids and water, respectively. φ is the volumetric faction of nanoparticle suspended in base water. Eq. 3-13 only considers the liquid-particle interactions (and also assumes that the particles are hard sphere with only short-range interactions) and is hence valid only to volume fractions of about 1 %vol. Since our nanofluids are very dilute (<<1 %vol.), Eq. 3-13 should be valid here. Since the measured viscosity is a kinematic variable, it is necessary to convert Eq. 3-13 into an equivalent form of kinematic viscosity. This can be made simply using the density formula of nanofluids, Eq. 3-5. Then the kinematic viscosity, $v_{NF}=\mu_{NF}/\rho_{NF}$ is obtained simply using Eqs. 3-5 and 3-13. The measured kinematic viscosity values were compared to the prediction (Fig. 3-4).

It is seen that the measured kinematic viscosity values are in good agreement with the prediction as the difference between the measurement and prediction is within 5% uncertainty limit. Therefore, it is concluded that that dilute nanofluids also have negligible changes in kinematic viscosity with respect to water.

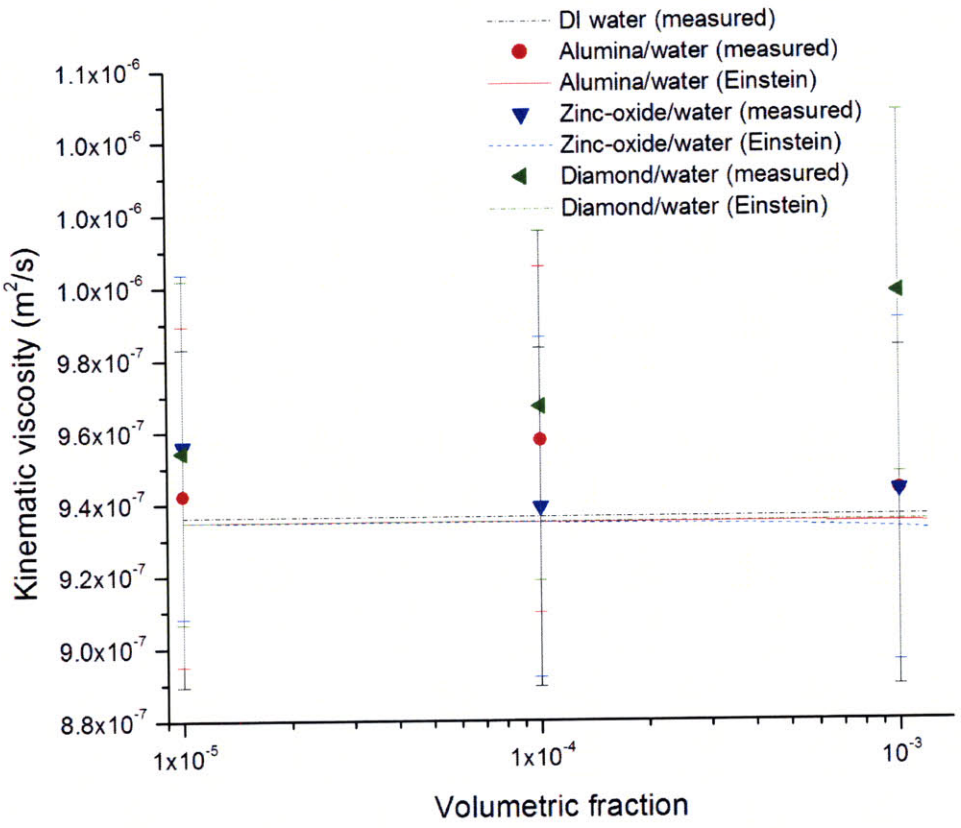

Figure 3-4 Kinematic viscosity of pure water and nanofluids

3.2.5 Surface tension measurement

The surface tension is defined as the force acting over the surface of the liquid per unit length of the surface perpendicular to the force. Surface tension is an effect within the surface sublayer of a liquid that causes that layer to behave as an elastic sheet. This is the property of a liquid in contact with ambient vapor/air or another liquid, respectively. Thus, it changes as the interfacial components change. The surface tension measured in this study is that of the liquid membrane of the nanofluids at the equilibrium state with ambient air. The molecules inside the liquid interact equally with other molecules, from all sides, whereas the molecules at the surface

interact only with the molecules inside the liquid. Therefore the molecules exposed to the air are subject to a net force that tends to keep them within the liquid.

Because surface tension plays an important role in boiling phenomena, and it may also be greatly affected by any surfactants and/or chemicals used by the vendors in the synthesis of the initial high-concentration nanofluids, it was deemed necessary to measure the surface tension of our dilute nanofluids. The measurement device adopted in the current study is a digital tensiometer, Sigma 703 provided by KSV Instruments LTD. A schematic diagram of the apparatus is given in Fig. 3-5. The measurable range is from 0 to 200 mN/m with accuracy of 0.1 mN/m. Additional uncertainty can be generated by the experimental procedure, as described next. The instrument is based on the Wilhelmy Plate method, which measures the force exerted by the liquid on a plate that is drawn through the surface of that liquid. The force is proportional to the surface tension of the liquid. In the Wilhelmy Plate method the plate is first completely immersed into the liquid and then pulled out. Then, the pre-wetted plate is lowered to the surface until its lower edge just touches the surface. At this point the liquid "jumps" onto the edge and sides of the plate. The liquid wets the plate perimeter and exerts a force to some maximum point which is proportional to the surface tension of the liquid (see the point 7 in the bottom right of Fig. 3-5). Corresponding surface tension is calculated by the force exerted on the plate due to wetting.

$$\sigma = \frac{F}{l \cdot \cos\theta} \tag{3-14}$$

where F, l, and θ are force pulled by the Wilhelmy plate, wetted perimeter of the Wilhelmy plate, and contact angle between liquid phase and the Wilhelmy plate, respectively. In practice, complete wetting (θ=0°) is assumed, and to suffice this assumption, a thorough cleansing of the platinum plate is recommended at each measurement. Since the procedure is entirely manual, the results may be affected by it. Following the procedure strictly is important to ensure reliable/repeatable results.

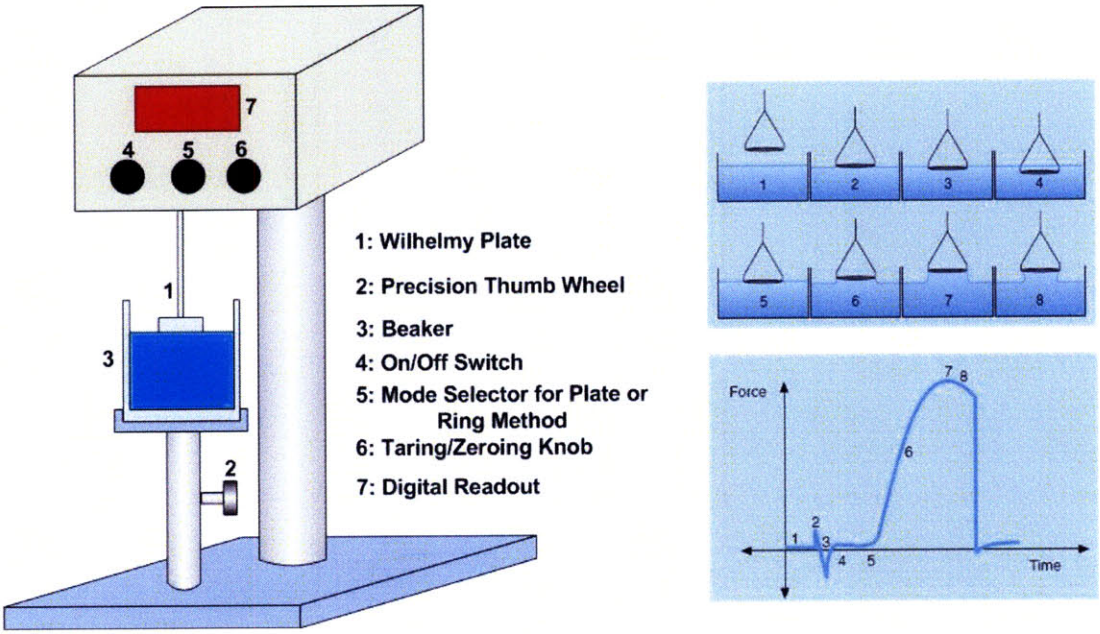

Figure 3-5 A schematic of the surface tension measurement apparatus

The surface tension of various nanofluids was measured and summarized in Table 3-4 and Fig. 3-6. By the same methods used in the thermal conductivity and kinematic viscosity measurements, the relative error of the surface tension change was introduced. It is seen that the maximum relative error is up to about 3.4% for 0.01 %vol. diamond nanofluids. As well, this measurement confirms that the change of surface tension of the low concentration of nanofluid compared to that of water is not significant.

Table 3-4 Surface tension of pure water nanofluids measured in unit of mN/m at 1 atm and 22 °C

Fluid	Nanoparticle Concentration (%vol.)	Surface tension (mN/m) Test 1	Surface tension (mN/m) Test 2	Surface tension (mN/m) Test 3	Surface tension (mN/m) Test 4	Surface tension (mN/m) Test 5	Surface tension (mN/m) Average	Relative error (%)
DI Water	0	72.4	73.0	73.0	73.0	73.0	72.9	0.0
Alumina /water	0.1	75.1	74.8	74.7	74.7	75.1	74.9	2.7
	0.01	73.5	73.3	73.3	73.1	73.5	73.3	0.5
	0.001	73.2	73.1	73.5	72.8	73.2	73.2	0.4
Zinc oxide /water	0.1	73.8	73.7	73.8	73.9	73.8	73.8	1.2
	0.01	73.4	73.3	73.3	73.5	73.4	73.4	0.7
	0.001	73.4	73.4	73.2	73.0	73.4	73.3	0.5
Diamond /water	0.1	71.2	72.0	71.9	72.1	72.2	71.9	1.4
	0.01	69.6	70.2	70.4	70.8	70.9	70.4	3.4
	0.001	71.0	72.0	72.2	72.0	71.8	71.8	1.5

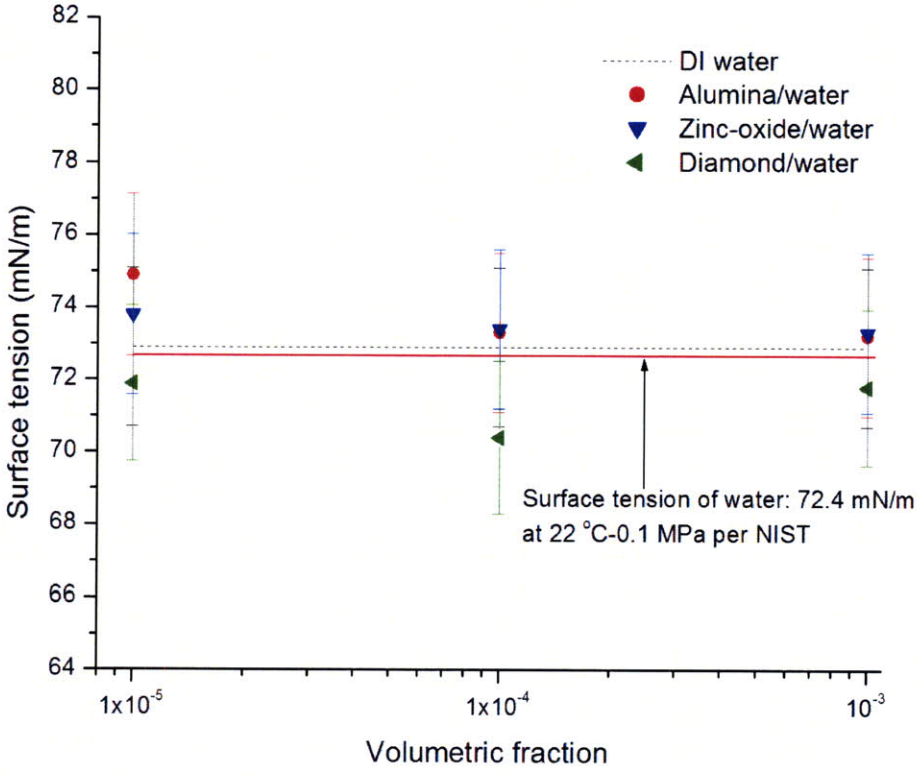

Figure 3-6 Variation of surface tension of tested nanofluids

3.2.6 Nanoparticle size measurement using dynamic light scattering (DLS)

In addition to their thermo-physical properties, it is important to determine also some colloidal properties of the nanofluids. Dynamic light scattering (DLS) theory is a well established technique for measuring particle size over the range from a few nanometers to a few microns. The concept uses the idea that small particles in a suspension move in a random pattern. A microbiologist by the name of Brown first discovered this effect while observing objects thought to be living organisms, by light microscopy. Later it was determined that the "organisms" were actually particles. Thus, the movement of small particles in a resting fluid is termed "Brownian Motion" and can easily be observed for particles of approximately 0.5 to 1.0 μm with a microscope at a magnification of 200 to 400X. Observation of larger particles compared to smaller particles will show that the larger particles move slower than the smaller ones given the same temperature. According to Einstein's developments in his Kinetic Molecular Theory, molecules that are much smaller than the particles can impart a change to the direction of the particle and its velocity. Thus water molecules (0.00033 μm) can move polystyrene particles as large as a couple of microns. The combination of these effects is observed as an overall random motion of the particle. A detailed technical description will help better understand the employed DLS measurements and thus is explained in Appendix B.

The results of the DLS particle size measurements are reported in Table 3-5 and the spectra are shown in Figs. 3-7 to 3-9. The particle sizes of all nanoparticles dispersed in the water seem to be much larger than vendor-specified values. It is believed that particles suspended in the fluid can agglomerate and the process is exacerbated by dilution which resulted in changes in pH. pH controls the surface charge of the particles, and thus can strengthen the electrostatic repulsion force between the particles. Interestingly, at sizes >100 nm, the particles no longer

meet the commonly-accepted definition of the term nanoparticles. Study of these agglomeration effects is beyond the scope of this thesis. We shall note, however, that our nanofluids were observed to be stable (no sedimentation) over long periods of time.

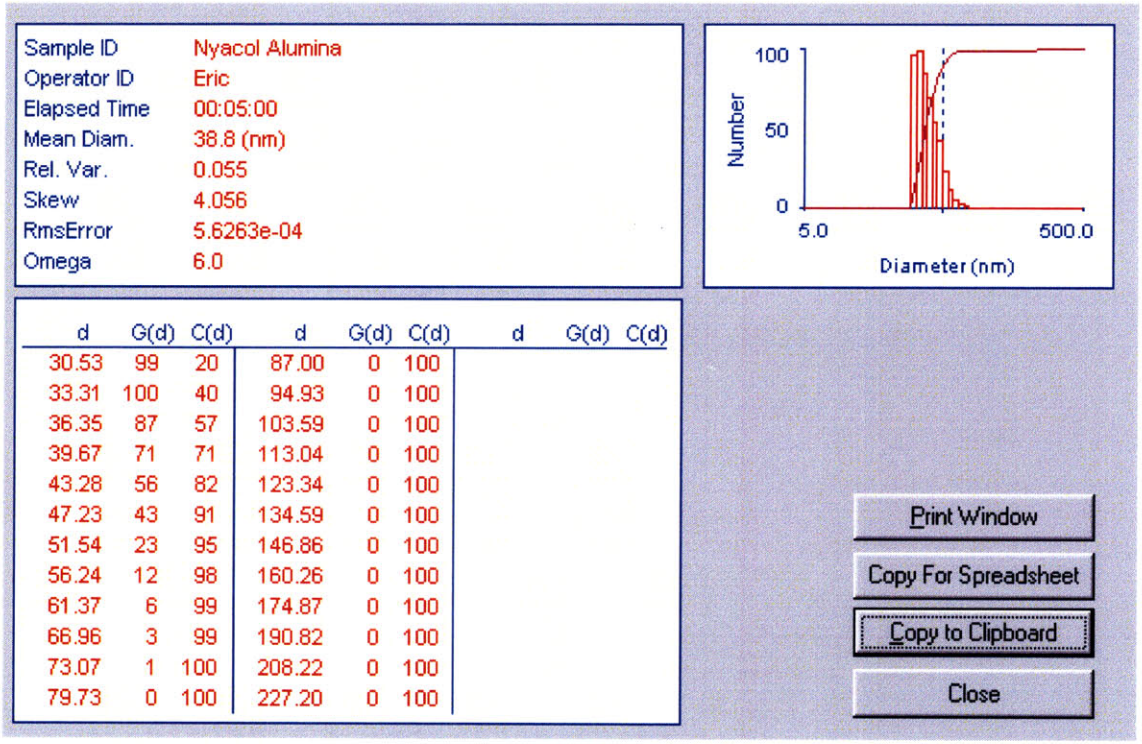

Figure 3-7 Size distribution of alumina nanoparticles in water (at 0.1 %vol.), as measured by the DLS approach

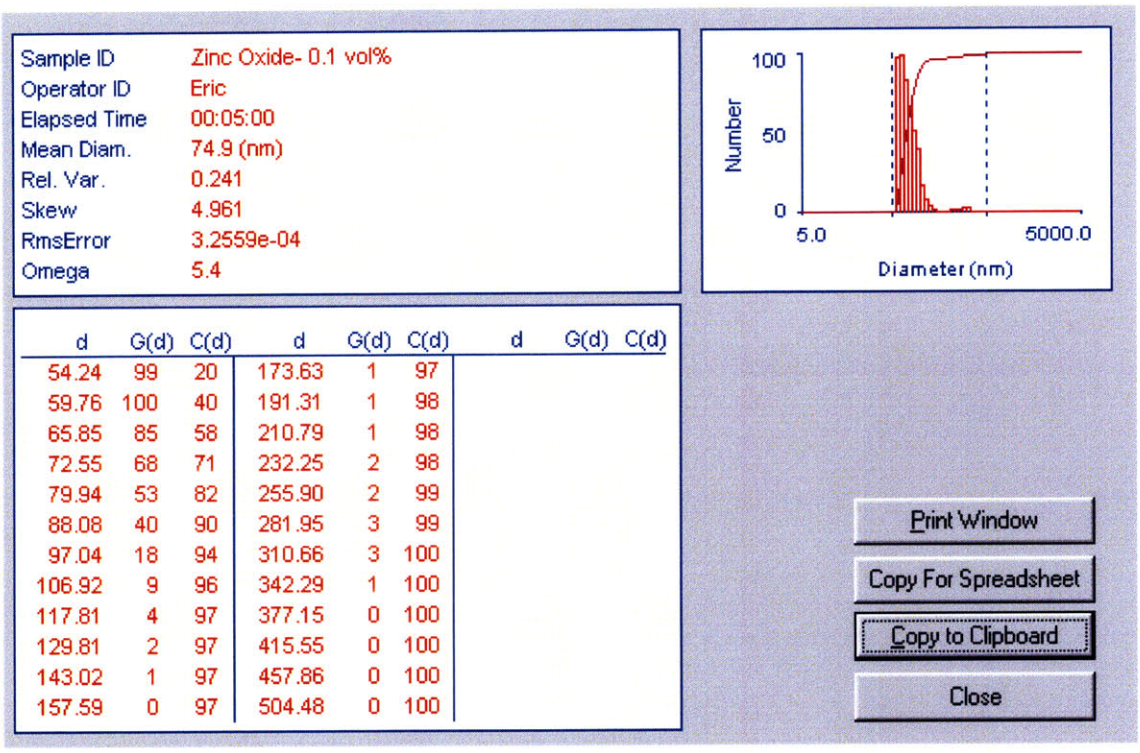

Figure 3-8 Size distribution of zinc oxide nanoparticles in water (at 0.1 %vol.), as measured by the DLS approach

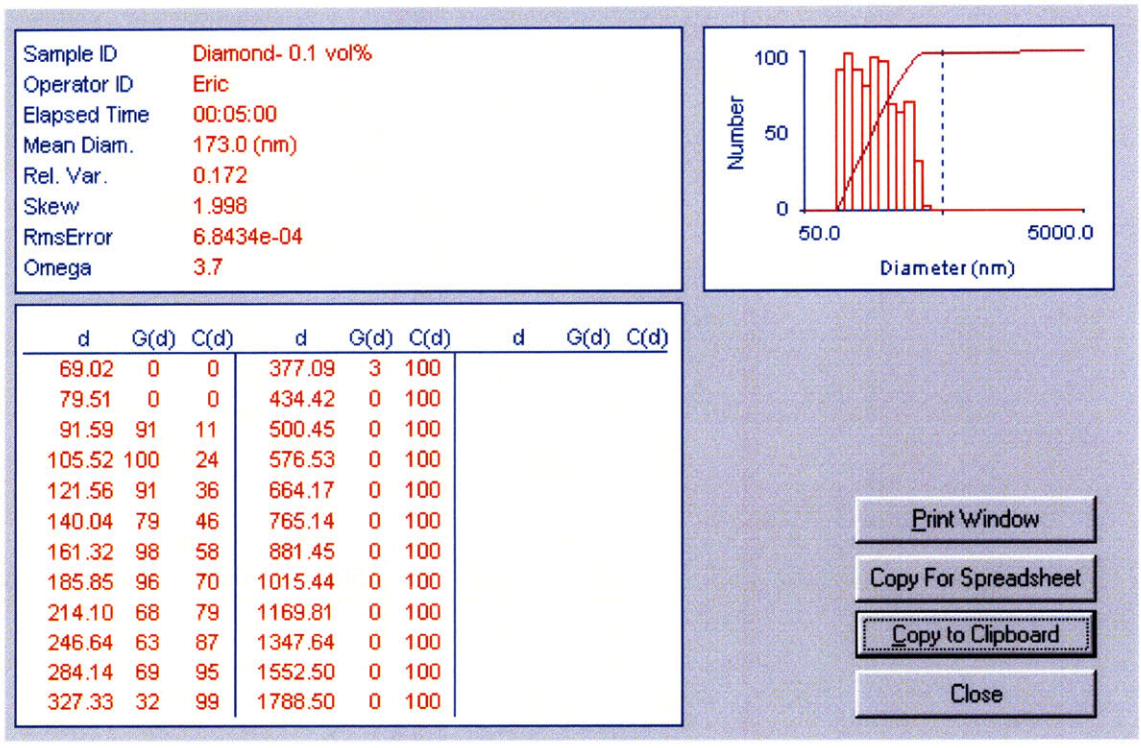

Figure 3-9 Size distribution of diamond nanoparticles in water (at 0.1 %vol.), as measured by the DLS approach

Table 3-5 Particle size measured by DLS technique

Fluid	Nanoparticle Concentration (%vol.)	Mean diameter† (nm)	Effective diameter† (nm)	Vendor specified diameter (nm)
Alumina/water	0.1	38.8	88.3	~20
Zinc oxide /water	0.1	74.9	185.0	~40
Diamond/water	0.1	173.0	266.8	~10

†Effective diameter is the measured diameter (averaged over the experiments) including the hydrodynamic layer. Mean diameter is the average of intensity-weighted diameter and thus it is less than or equal to the effective diameter. If the particle suspension is highly mono-dispersed the difference between those two diameters is small.

3.3 Flow Boiling Experimental Apparatus

3.3.1 Flow loop design

A major effort in this thesis project was the design and construction of a flow loop suitable for measurements of the nanofluids HTC and CHF. A schematic and a picture are shown in Fig. 3-10. The flow loop consists of a heated test section assembly, a pre-heater, a cooler, a pump and an accumulator. The loop is constructed mainly with 25.4 mm OD (1″) stainless steel tubing. Two submerged K-type thermocouples (TCs) measure the fluid bulk temperatures at the entrance and exit of the test section, respectively.

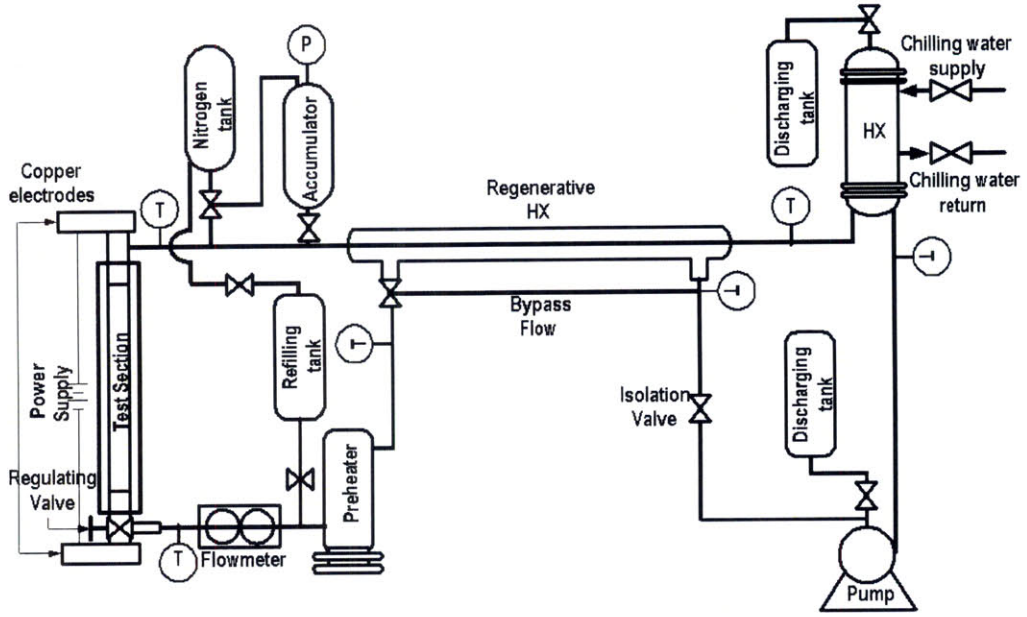

(a)

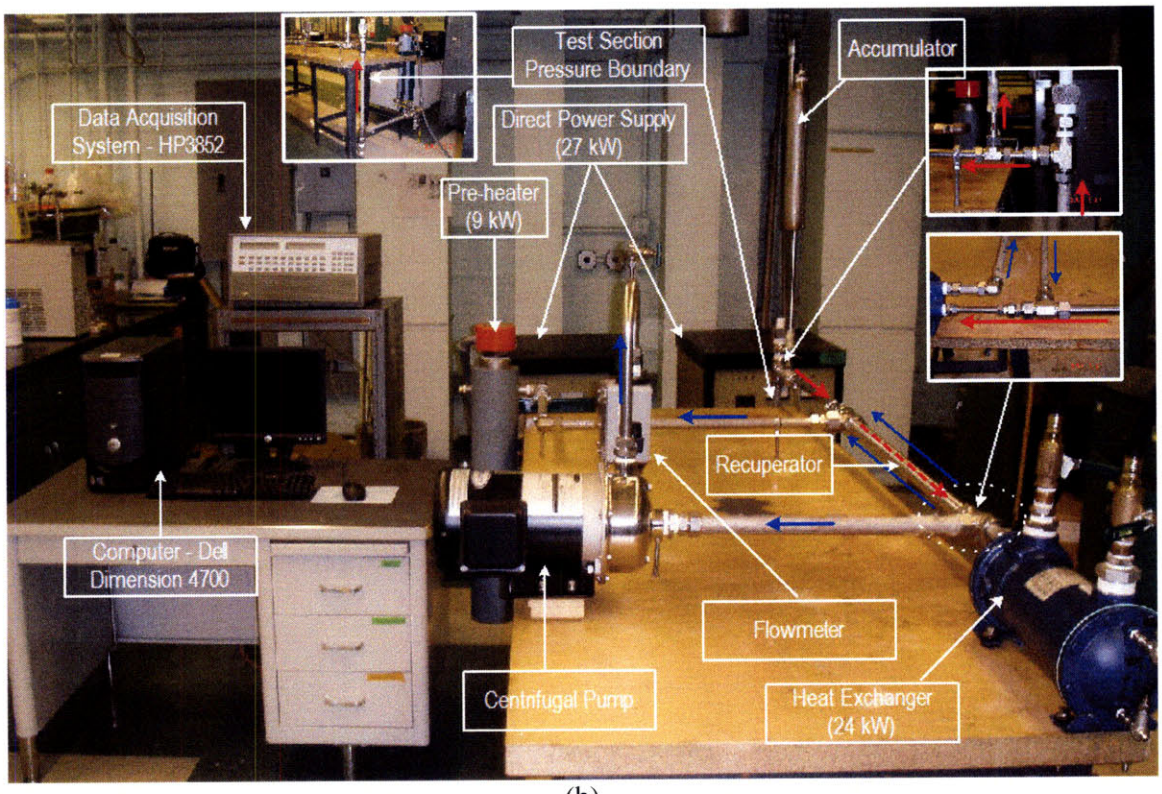

(b)

Figure 3-10 Flow loop apparatus (a) schematic (b) photo

The loop is equipped with a shell-and-tube heat exchanger (maximum 24 kW) to reject the heat and control the test-section inlet subcooling (Fig. 3-11). Pressure can be controlled by an

accumulator and regulated nitrogen overpressure. However, for the experiments presented here the pressure was always atmospheric. Also, the accumulator is used to purge non-condensable gases at the beginning of each run. The flow rate in the loop is controlled with a centrifugal pump of 1.0 HP, which can generate mass flux of about 3300 kg/m^{2}s at current flow loop configuration (Fig. 3-12). Flow rate is measured with a turbine-type flowmeter, whose measurement range is 0.3 to 3.0 GPM (Fig. 3-13).

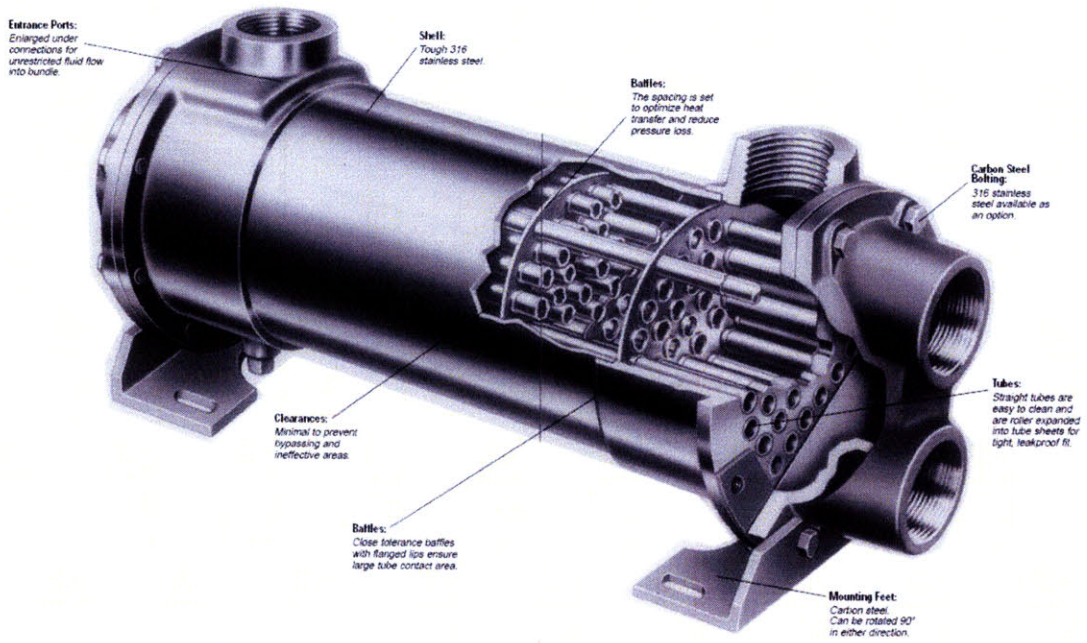

Figure 3-11 Shell-and-tube heat exchanger (Model: SSCF 8" – purchased from ITT Standard)

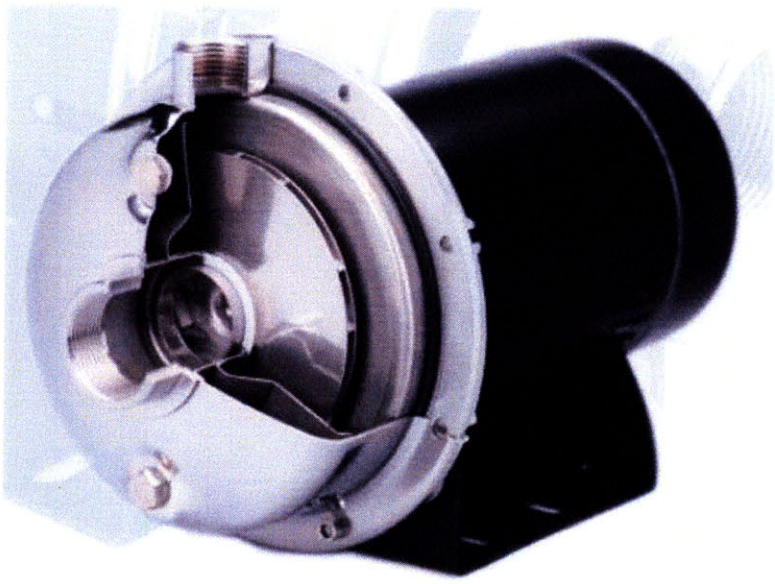

Figure 3-12 Photo of centrifugal pump (Model: SS1XS-3/4" – purchased from Berkeley)

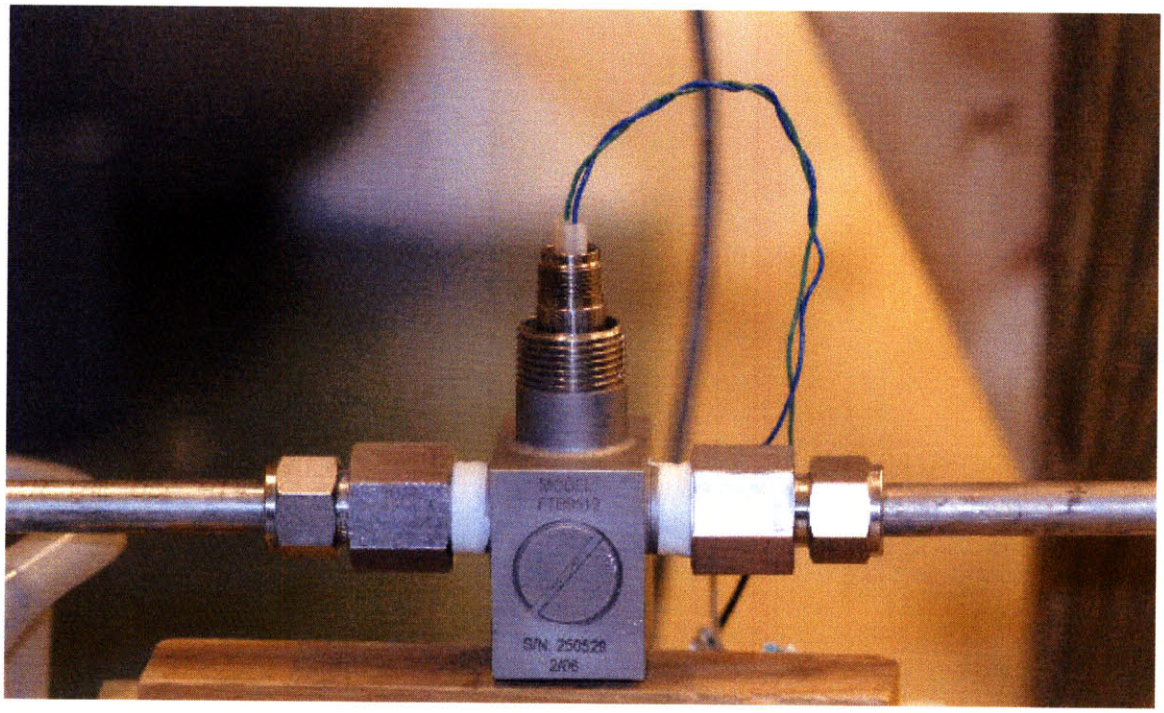

Figure 3-13 Photo of flowmeter (Model: FTB9512 – purchased from OMEGA Engineering)

3.3.2 Heater assembly and power supply design

Two identical DC power supplies operating in parallel were used to provide electric power to the test heater. Each power supply has a capacity of 40V-600A and total maximum power rating is downgraded slightly and expected to be about 35 kW (30V-1150A) from the specification provided by the vendor. The picture of the DC power supply is given in Fig. 3-14.

Figure 3-14 Photo of DC power supplies (Model: EMHP 40-600 – purchased from Lambda Americas)

The tube is electrically heated using the DC power supplies and connected to the tube ends by copper electrodes. The heater test section consists of a tube made of stainless steel seamless grade 316 with 6.35 mm (1/4″) OD, 0.41 mm (0.016″) thickness and 100 mm length

(Fig. 3-15). In this study, test fluids always flow upward. The test tube (ASTM A213-01a/ASME 8A213-01a) was purchased from All-Stainless INC. It mainly consists of elemental composition of 16.48% Cr, 12.14% Ni, 2.53% Mo, and 0.68% Mn according to the vendor-provided specifications. To remove the possible oxides contaminants, the vendor conducted the bright annealed heat treatment at 1070 °C for 20 minutes quenched by liquid nitrogen. The test section assembly is confined by a container in case of flooding by tube heater rupture. The flooding container is constructed using 15 mm thick transparent acryl panels to ensure a clear view of the test section. The photo is given in Fig. 3-16.

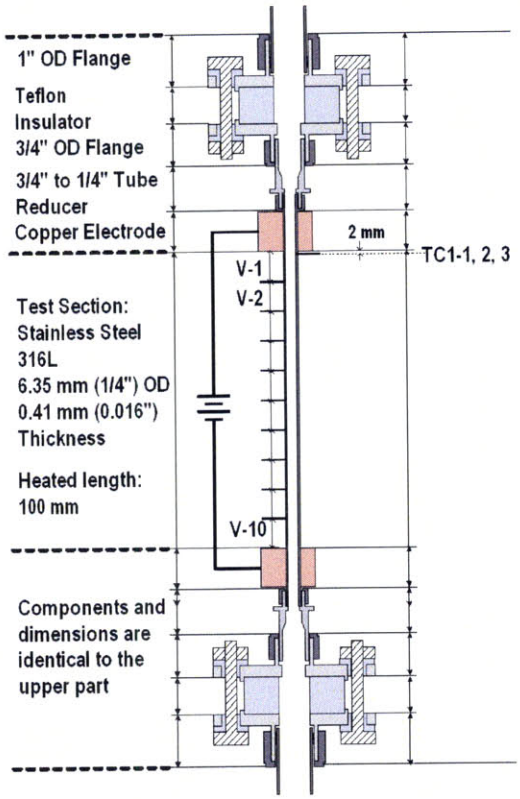

(a)

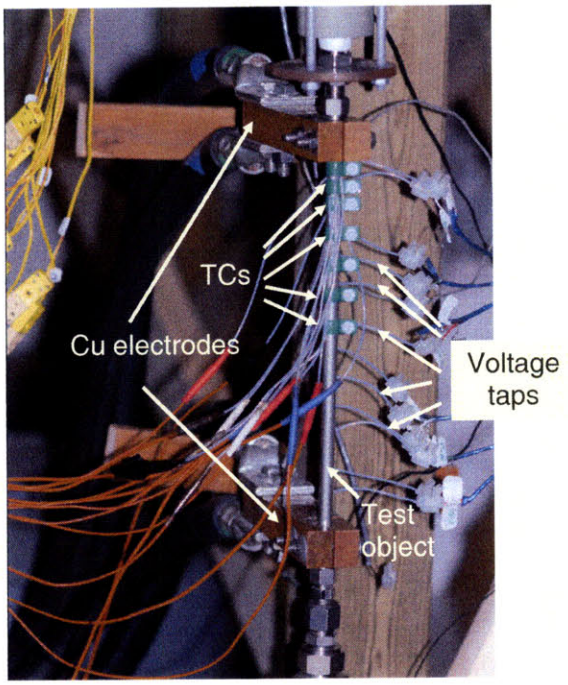

(b)

Figure 3-15 Upflow test section schematic (a) and photo (b)

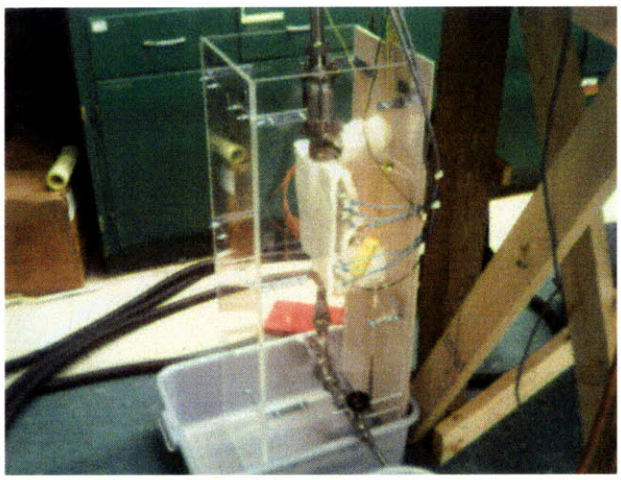

Figure 3-16 Photo of flooding container

The aforementioned heater dimension was determined to secure the mechanical strength and to accommodate the high heat fluxes needed in CHF experiments, particularly as some CHF enhancement is expected when nanofluids are used. The achievable heat flux from the combination of selected heater dimension and DC power supplies was calculated carefully with the Joule-heating method, which suggests the following formula:

$$R = \rho_{ele} \frac{L}{A_{cx}} \tag{3-15}$$

where, R, L, and A_{cx} are electrical resistance, length, and cross-sectional area of the test heater. As a conservative value, the resistivity of the stainless steel grade 316 at room temperature, ρ_{ele}=7.4×10^{-7} ohm·cm, was used for the calculation. Using Eq. 3-15, the electrical resistance of the heater is estimated and its value can be utilized in evaluating the achievable power using Ohm's law as:

$$\dot{Q} = I^2 R \tag{3-16}$$

The maximum electric power upon maximum current input of 1150A is estimated to be around 20 kW. Then, the heat flux delivered to the fluid in the test section, q'', is calculated as:

$$q'' = \frac{VI}{\pi D_i L} \tag{3-17}$$

where V and I are the measured voltage and current, respectively, and D_i and L are the test section inner diameter and length, respectively. The summary of the heat flux calculation with various dimensions of tube heater is given in Table 3-6. The maximum achievable heat flux is calculated to be 11.2 MW/m^2, which is well beyond the typical water CHF value (~5 MW/m^2) at G=2500 kg/m^{2}s with high subcooling under atmospheric pressure. In principle, a possibility of non-uniform axial heat flux exists as the resistivity of the tube material is dependent of the wall temperature. Therefore, in order to confirm the uniformity of the axial heat flux, ten equidistant voltage taps are installed along the tube length. The voltage taps are insulated while installed as any mechanical contact between the conducting cables may realize a closed circuit, which would invalidate the voltage measurement.

Table 3-6 Summary of the heat flux with various tube dimension (CHF value was assumed 5 MW/m^2)

Tube thickness (inch/mm)	ID (mm)	L/D_i	Tube cross-sectional area (m^2)×10^6	Tube heat transfer area (m^2)×10^3	Resistance (ohm)×10^3	Q_{max} (W)	q''_{max} (MW/m^2)	q''_{max}/q''_{CHF}	Voltage (V)
0.035/ 0.8890	4.572	21.9	0.1525	1.4363	7.3433	9,712	6.76	1.35	8.4
0.028/ 0.7112	4.928	20.3	0.1260	1.5481	8.8898	11,757	7.59	1.52	10.2
0.026/ 0.6640	5.029	19.9	0.1180	1.5800	9.4881	12,548	7.94	1.59	10.9
0.024/ 0.6096	5.131	19.5	0.1099	1.6119	10.188	13,473	8.36	1.67	11.7
0.022/ 0.5588	5.232	19.1	0.1017	1.6438	11.016	14,569	8.86	1.77	12.7
0.020/ 0.5080	5.334	18.7	9.3234	1.6757	12.013	15,887	9.48	1.90	13.8
0.018/ 0.4572	5.436	18.4	8.4640	1.7076	13.232	17,500	10.2	2.05	15.2
0.016/ 0.4064	**5.537**	**18.1**	**7.5885**	**1.7396**	**14.759**	**19,519**	**11.2**	**2.24**	**17.0**

Due to the spatial limit around the tube heater circumference, only three K-type thermocouples (TC) were installed to detect the wall temperature. Those were installed azimuthally at 120° from each other at the tube upper end. The configuration of the TC

installation is shown in Fig. 3-17. The thermocouples were also insulated electrically to prevent any improper short circuiting. These thermocouples were secured using Teflon clamps to ensure good thermal contact, and are re-used for later tests if not damaged by temperature excursion during CHF.

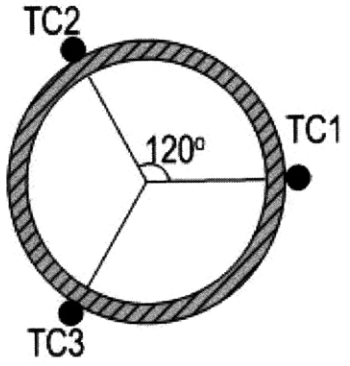

Figure 3-17 TC location azimuthally

3.3.3 Flow loop control systems

To control the flow loop, three systems are used, a Dell Dimension 4700 IBM computer, a HP3852 Data Acquisition System (DAS), and the flow and pressure control panel. They were connected to the instrumentations installed throughout the flow loop facility (Fig. 3-18).

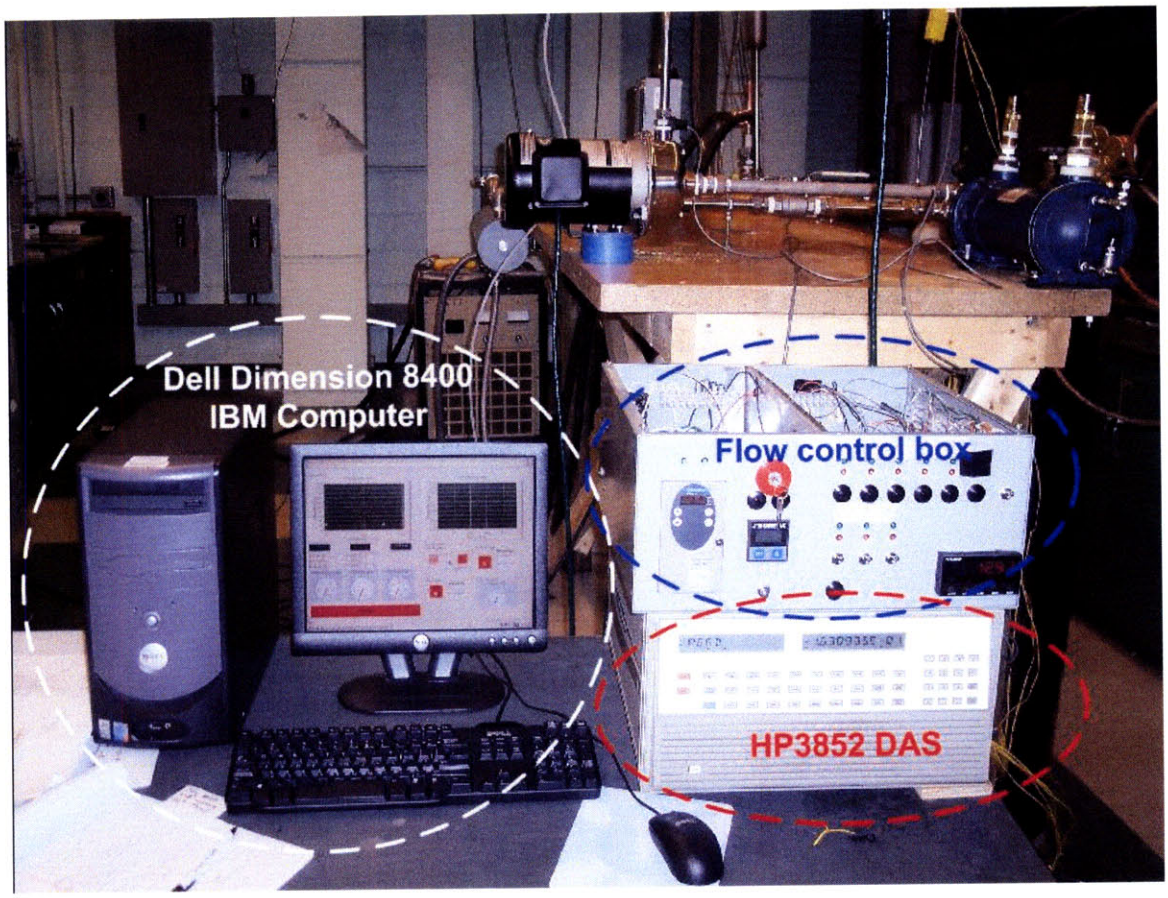

Figure 3-18 A photo of the control systems

The flow and pressure control panel is to regulate the flow rate via pump speed controller (Model: Telemecanique Altivar 31). It was also designed to protect the entire system from over-pressurization by receiving the transmission signal from the pressure transducer installed on the top of the accumulator. The measurement program is built with the Visual Basic (VB) software, which was loaded in the Dell Dimension 8400 IBM computer. Two control panels of the VB measurement program are shown in Fig. 3-19. The control system was designed to allow for rapid shutdown of the DC power supplies via a relay controller installed in the power supplies. If any temperature in the flow loop reaches a preset of high temperature of 350 °C, the relay controller transmits the signal to shut down both DC power supplies.

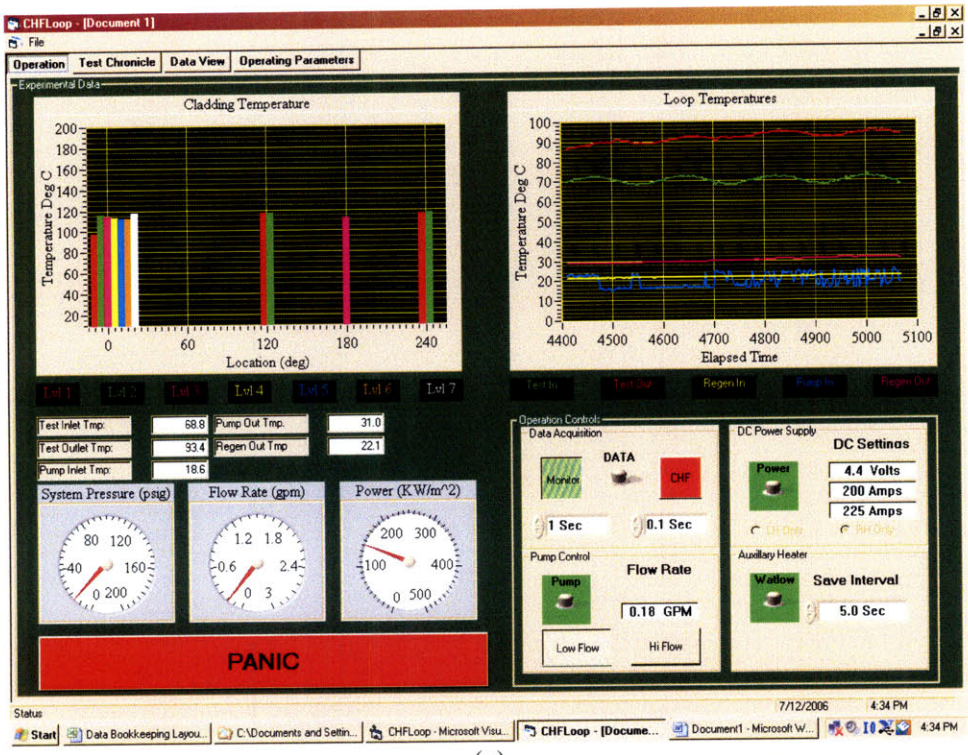

(a)

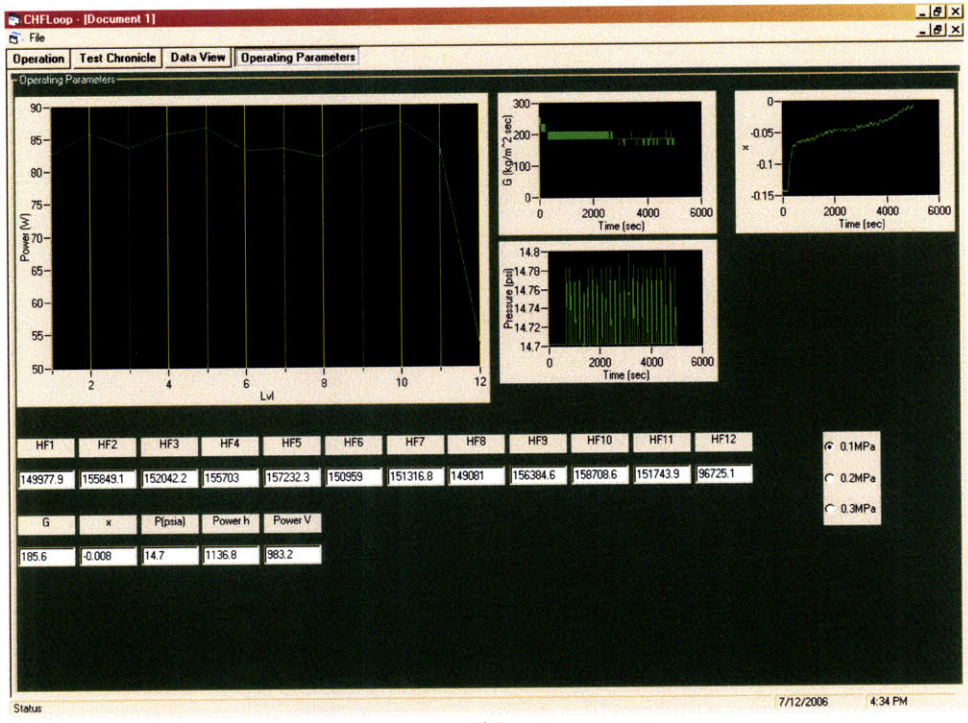

(b)

Figure 3-19 VB Measurement programs (a) main control display (b) auxiliary control display

The HP3852 is the main control unit, which includes many subunits such as HP44713A, HP44728A, HP44715A, HP44726A, and HP44701A. Each subunit has a unique function in collecting an individual experimental signal. Two units of HP44713A (24 Channel High Speed FET Multiflexer) are equipped in the HP3852 main unit and receive all temperature and voltage signals from heater section and flow loop. The HP44728A (8 Channel Relay Actuator) is a relay subunit to communicate with the DC power supplies. The HP44715A (5 Channel Counter/Totalizer: 200 kHz) receives the frequency signal from the flowmeter. The HP44726A (Arbitrary Waveform DAC) is a control unit to regulate the power input of the DC power supplies. Finally, the HP44701A (5.5 Digital Voltmeter) is a subunit to regulate all voltage signals received from other subunits. The integrated control system, the HP3852, then communicates with the VB measurement program via GPIB cable.

3.4 Calibration and Validation of Experimental Apparatus

3.4.1 Current input/output profile and axial heat flux

The electric power is calculated from the measured current and voltage delivered to the test section. Therefore, current calibration was performed first, where multiple points of current were input via in-house visual basic (VB) program. The corresponding current output was read with two current measurement tools, an inductance ammeter (LEM) and a NIST-certified shunt (Lab 800A-100mV shunt) together with a digital voltmeter (DVM890F). The two readings were then compared as displayed in Fig. 3-20. It is observed that the response is linear and the two readings are basically very similar to the input.

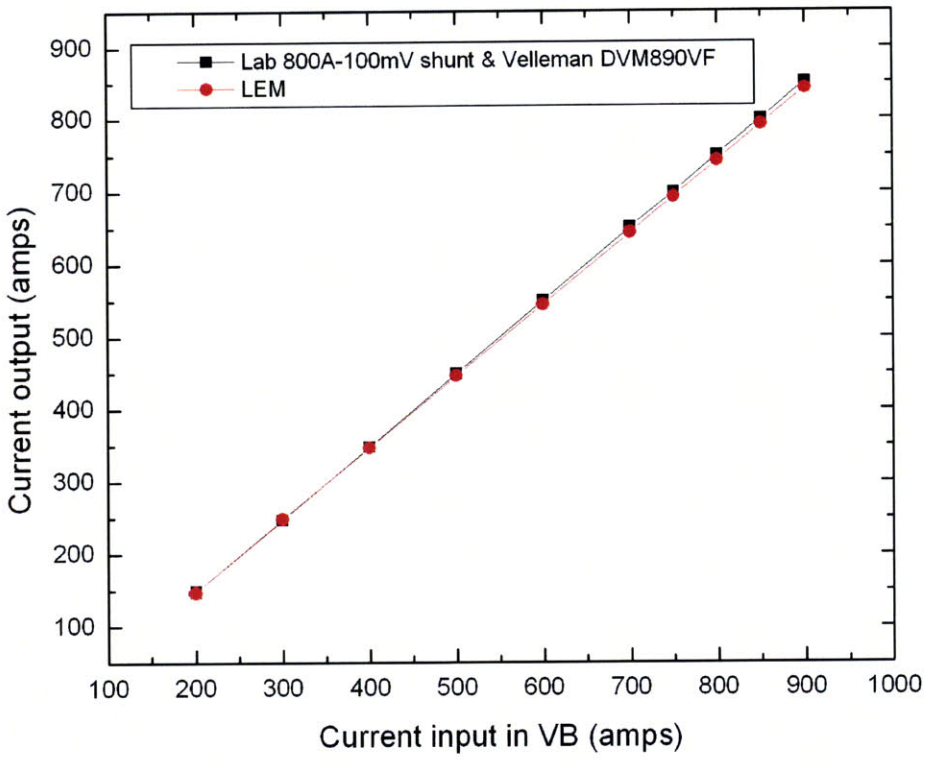

Figure 3-20 Validation of current output using two instrumentations

Secondly, calibration of voltage measurement was performed. In fact, various voltage signals from the various loop instrumentations are regulated by the HP44701A 5.5 digital voltmeter embedded in HP3852. Therefore, the HP44701A was calibrated using a universal voltage source (DVM) generator. The result of the calibration is given in Fig. 3-21. It is also seen that the HP40701A displays voltage almost identical to the applied voltage source. This confirms the proper function of the voltage-related instruments.

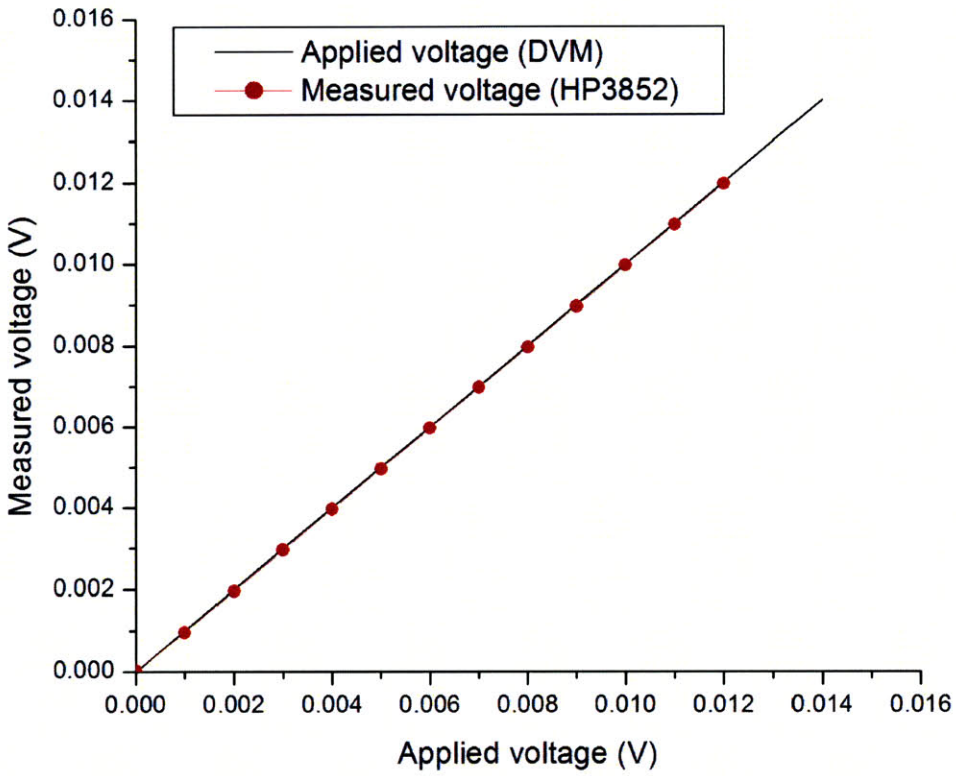

Figure 3-21 Calibration curve of HP40701 5.5 digital voltmeter

After a successful calibration of the current and voltage measurements, the uniformity of the axial heat flux was investigated. As described earlier, ten equidistant voltage taps are installed along the heater length and the segmental values are read and converted to the axial heat flux via VB measurement program. Seven different levels of heat flux were applied in this validation work and its axial heat flux plot was obtained (Fig. 3-22). It is observed that reasonably uniform axial heat flux was achieved as individual fluctuation is within ±5% of the average value. Since the VB measurement software allows monitoring such axial variation visually, it was possible to confirm this uniformity at every test and indeed no abnormal axial variation was ever observed through the entire experimental campaign.

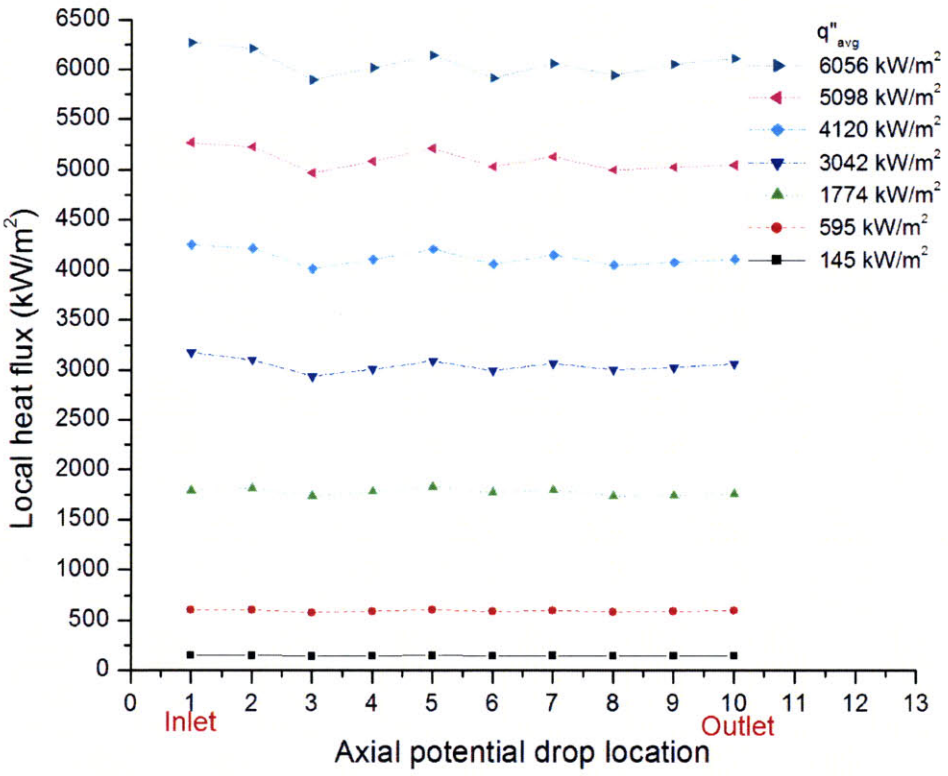

Figure 3-22 Axial distribution of the heat flux at different power level

3.4.2 Flow rate, heat balance and single-phase heat transfer coefficient

The turbine-type flowmeter was purchased from OMEGA Engineering. The vendor provides the calibration curve, but, given the importance of the flow measurement, it was decided to calibrate the instrument independently. Fig. 3-23(a) and (b) show the calibration curves and its linear fit using the data from the vendor and current author, respectively. The in-house calibration was performed by measuring the volume of the water flow given the amount of time, which yields the volumetric flow rate. Corresponding frequency signal was recorded through the

data acquisition system simultaneously. This process was repeated for a broad range of the flow rates by adjusting the water supply valve. A comparison between two calibration curves was made and its result is given in Fig. 3-23(a) and (b). It is seen that both calibration curves generated by the vendor and author are fairly linear. Fig. 3-23(c) also suggests that two individual curves match very well within the calibrated range. Therefore, the vendor-provided curve was safely employed for the flow rate measurement.

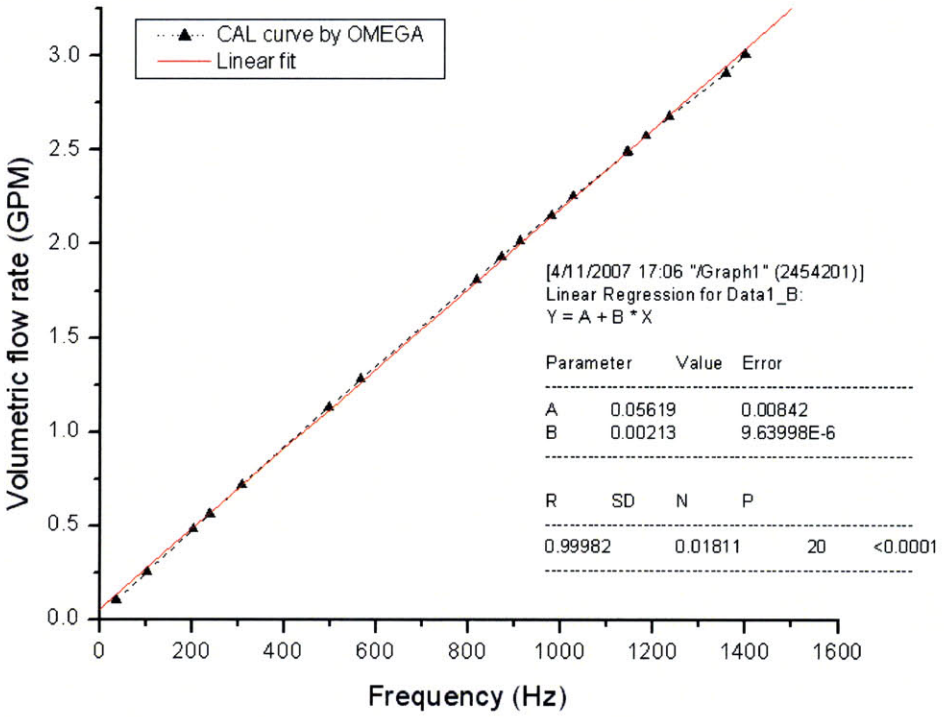

(a)

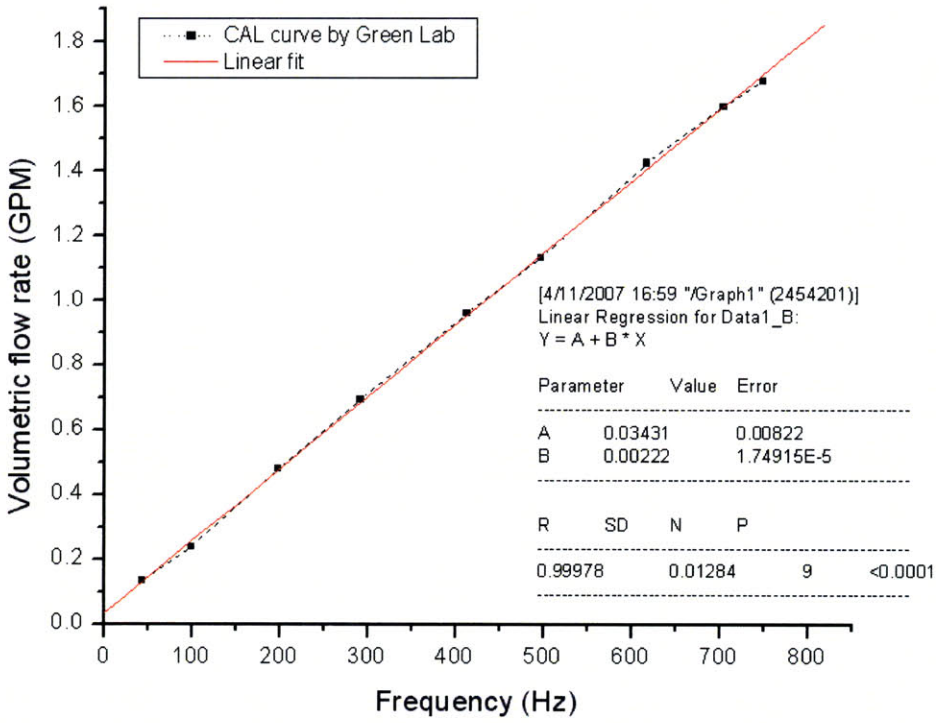

(b)

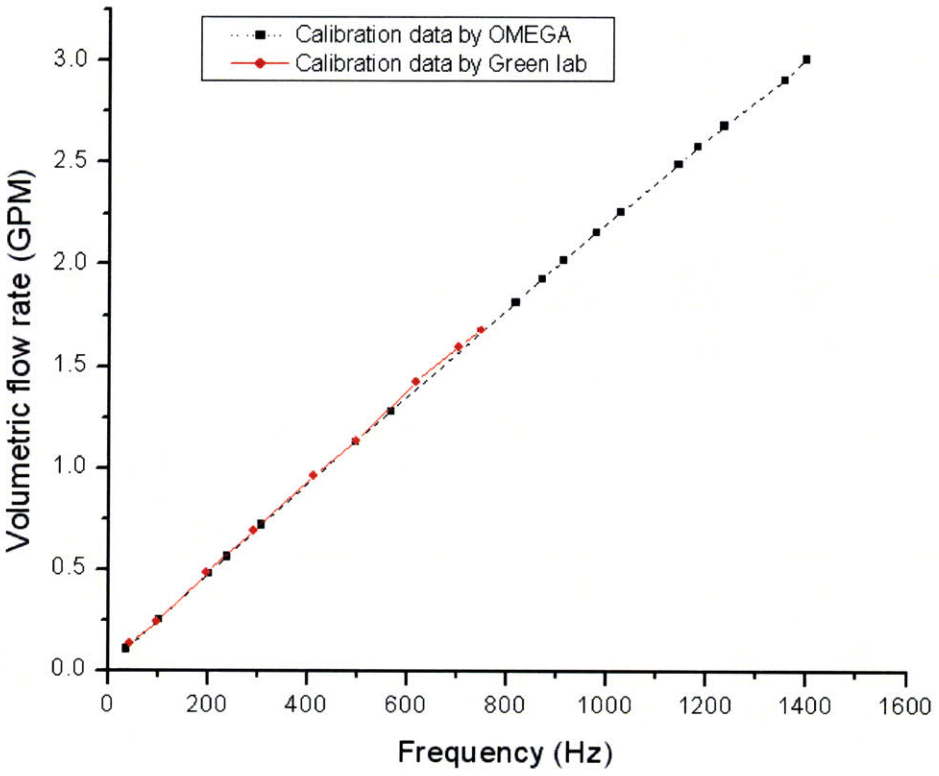

(c)

Figure 3-23 A calibration curve (a) provided by OMEGA (b) generated in Green Lab, and (c) comparison of (a) and (b)

Several preliminary tests with pure water (no nanoparticles present) were then conducted to verify the reliability of the thermal hydraulic measurements in the flow loop. The loop operation was first verified by measuring the single-phase convective heat transfer coefficients at various locations in the test section and comparing them to the well-known Dittus-Boelter and Gnielinski correlations (Mills, 1999). Each expression is given as follows:

$$Nu_{DB} = 0.023\left(\frac{GD_i}{\mu_l}\right)^{0.8}\left(\frac{\mu_l c_{p,l}}{k_l}\right)^{0.4} \tag{3-18}$$

where, Nu_{DB} is the Nusselt number predicted by Dittus-Boelter correlation. G, D_i, μ_l, $c_{p,l}$, and k_l are the mass flux, heater inner diameter, and viscosity, specific heat capacity, and thermal conductivity of water at local bulk temperature, respectively.

$$Nu_G = \frac{(f/8)(\mathrm{Re}-1000)\mathrm{Pr}}{1+12.7(f/8)^{1/2}(\mathrm{Pr}^{2/3}-1)} \quad \text{for } 3000 < Re < 10^6 \tag{3-19}$$

where, Nu_G is the Nusselt number predicted by Gneilinski correlation. Re and Pr are Reynolds and Prandtl numbers, respectively. f is friction factor which can be evaluated using Moody's diagram and was given in Eq. 2-7.

The percentile error of Nusselt number evaluated by Dittus-Boelter and Gnielinski's correlations are defined as:

$$E_{Nu}(\%) = \frac{Nu_{\exp} - Nu_{DB}}{Nu_{DB}} \times 100 \ \ or \ \ \frac{Nu_{\exp} - Nu_G}{Nu_G} \times 100 \tag{3-20}$$

E_{Nu} was evaluated at two different mass fluxes (G=1000 and 1500 kg/m^{2}s). It is observed that for both cases, the values are predominantly within ±20%. Location 1 corresponds to the test section inlet. The large discrepancy after the entrance (Locations 1-2) is due to the thermal entrance effect, which is not accounted for in the Dittus-Boelter and Gnielinski correlations. The overall agreement between the experiments and the correlation is very reasonable (Figs. 3-24 and 25).

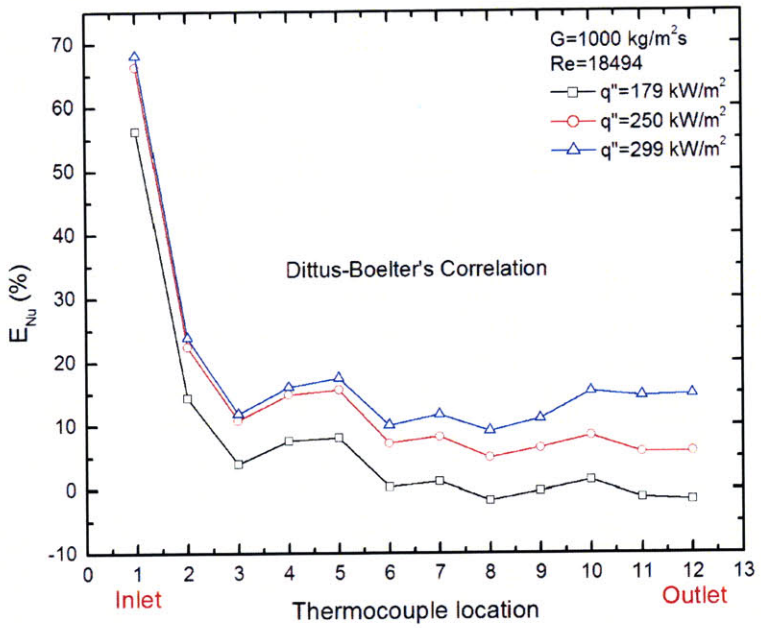

(a)

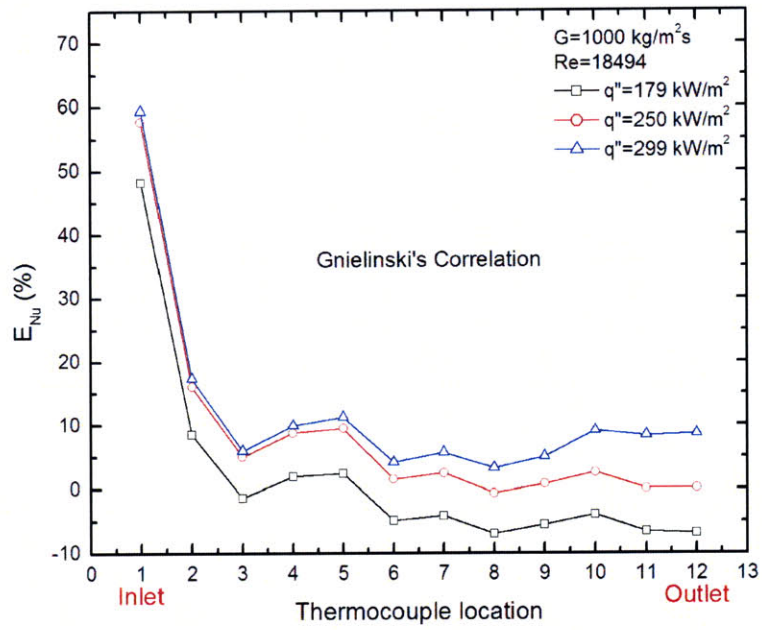

(b)

Figure 3-24 Percentage difference between measured and predicted local Nusselt number by (a) Dittus-Boelter correlation and (b) Gnielinski correlation at G=1000 kg/m^{2}s

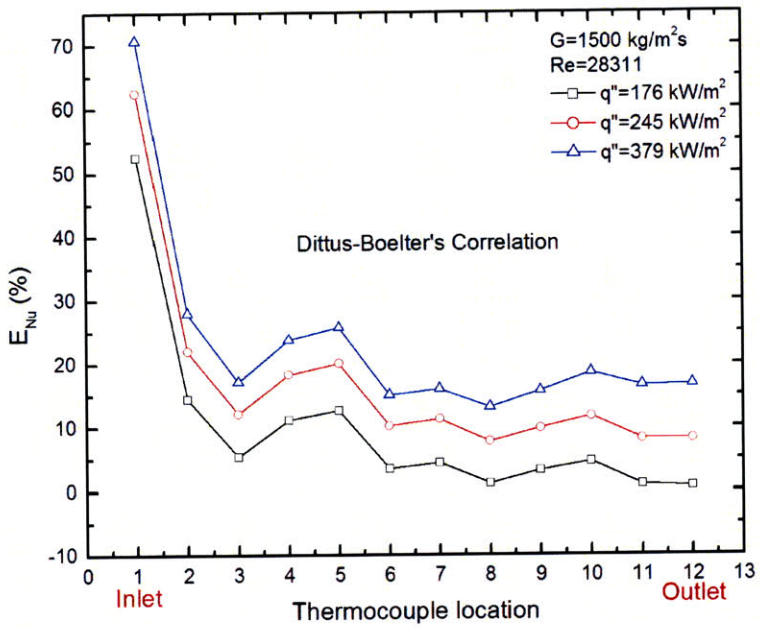

(a)

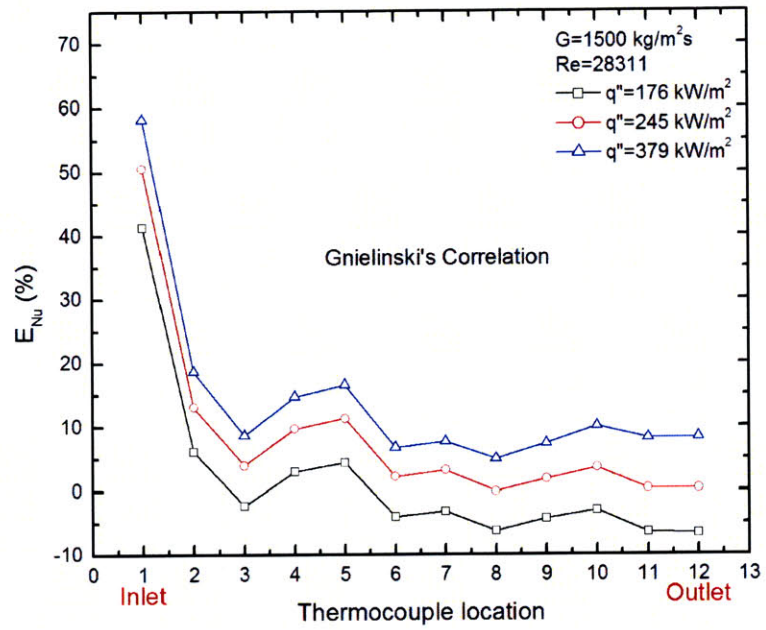

(b)

Figure 3-25 Percentage difference between measured and predicted local Nusselt number by (a) Dittus-Boelter correlation and (b) Gnielinski correlation at G=1500 kg/m^{2}s

Finally, the heat losses in the test section were quantified as follows. The percent heat loss (HL) is defined as the normalized difference between the electric power and the fluid thermal power:

$$HL(\%) = \frac{VI - \dot{m}c_p(T_{out} - T_{in})}{VI} \times 100 \tag{3-21}$$

where $\dot{m}$ is the measured mass flow rate, T_{out} and T_{in} are the measured test-section outlet and inlet temperature, respectively, and c_p is the average specific heat of water between T_{in} and T_{out}. A typical plot of percentage HL at three mass fluxes of 1500, 2000, and 2500 kg/m^{2}s is shown in Fig. 3-26. HL is less than 10% at low heat flux (q''<1.0 MW/m^2) and less than 2% at the high heat fluxes (q''>~4 MW/m^2) of interest to the CHF experiments. This also suggests that the thermal and electric powers are balanced reasonably.

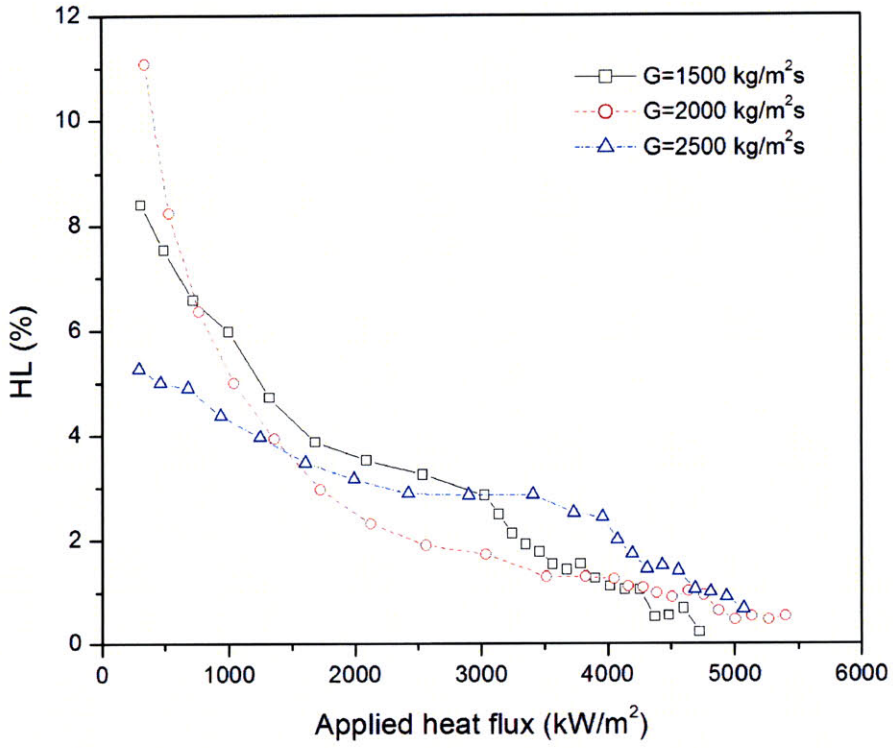

Figure 3-26 Heat loss in the test section as a function of the heat flux

Also the heat loss from the installed thermocouples to the ambient air is calculated using an infinite long fin model (Incropera and DeWitt, 2002):

$$\dot{Q}_{loss} = n\left(h_{air}\pi D_{TC} k_{TC} A_{TC}\right)^{1/2}\left(T_{w,o} - T_{air}\right) \tag{3-22}$$

where, h_{air}, n, D_{TC}, k_{TC}, A_{TC}, $T_{w,o}$, and T_{air}, are the natural convective HTC, number of the installed TCs and stainless steel conducting wires for voltage measurement, TC sheath diameter, thermal conductivity of the TC sheahth, cross-sectional area of the TC sheath, heater tube outer wall temperature, and air temperature, respectively. To evaluate Eq. 3-22, h_{air}=100 W/m^2·K, $T_{w,o}$=220 °C, and T_{air}=25 °C were assumed and n=14 (three TC and eleven voltage wire), D_{TC}=1.016×10^{-3} m, k_{TC}=14.4 W/m·K and A_{TC}=(π/4)(D_{TC})^2 were used. The calculated heat loss is only about 5.3 W (~3 kW/m^2), suggesting that the heat loss is negligible in our experimental setup.

3.4.3 Uncertainty analysis

Uncertainty analysis for the two main experimentally determined parameters, heat flux (q'') and effective heat transfer coefficient (h_{eff}), was performed. To conduct the analysis, a propagation of error method is adopted (Holman, 2001).

3.4.3.1 Uncertainty of heat flux

Heat flux is calculated using Eq. (3-17), where the main source of the heat flux uncertainty is found as voltage (V), current (I), heater diameter (D_i) and length (L). In Section 3.4.1, the uncertainty of the heat flux from the axial variation (i.e., local axial peaking, F_{ax}) was ±5%. The elemental percentage uncertainties of V, I, D_i, L and F_{ax} is less than 1.5%, 1.5%, 0.1%,

3%, and 5% respectively. The propagation of error method suggests the following estimate of heat flux uncertainty:

$$\frac{U_{q''}}{q''} = \sqrt{\left(\frac{U_V}{V}\right)^2 + \left(\frac{U_I}{I}\right)^2 + \left(\frac{U_{D_i}}{D_i}\right)^2 + \left(\frac{U_L}{L}\right)^2 + \left(\frac{U_{F_{ax}}}{F_{ax}}\right)^2}$$
$$= \sqrt{0.015^2 + 0.015^2 + 0.001^2 + 0.03^2 + 0.05^2} \quad (3\text{-}23)$$
$$\approx 0.062$$

Therefore, the measurement uncertainty on the calculated value of the heat flux is <±6.2%.

3.4.3.2 *Uncertainty of heat transfer coefficient*

In this study, effective heat transfer coefficient was defined as follow.

$$h_{eff} = \frac{q''}{\Delta T_b} = \frac{q''}{T_w - T_b} \quad (3\text{-}24)$$

where, T_w and T_b are inner wall temperature and bulk outlet temperature, respectively. The heat flux uncertainty was estimated above and uncertainty of T_w and T_b based on the thermocouple specifications is <±1.1 °C. Corresponding percentage uncertainties of T_w and T_b are estimated to be less than ±1.1% (at T_w=100 °C) and ±2.2% (at T_b=50 °C), respectively. Then the uncertainty of ΔT_b is estimated to be within ±4.4% (maximum 2.2 °C at ΔT_b=50 °C). Therefore, the heat transfer coefficient uncertainty is evaluated as:

$$\frac{U_{he_{ff}}}{h_{eff}} = \sqrt{\left(\frac{U_{q''}}{q''}\right)^2 + \left(\frac{U_{\Delta T_b}}{\Delta T_b}\right)^2}$$
$$= \sqrt{0.062^2 + 0.044^2} \quad (3\text{-}25)$$
$$\approx 0.076$$

Eq. 3-26 suggests that the measurement uncertainty of h_{eff} is <±7.6%.

3.5 Experimental procedure

3.5.1 Flow loop operation procedure

The experimental procedure for the CHF and HTC tests is as follows. After filling the loop with the test fluid, two-step degassing is performed. First, the test fluid is heated up using the preheater and sustained at 80 °C for an hour. Second, for additional 1.5 hour, the test heater is heated using power supplies at heat flux of about 3.0 MW/m^2, while maintaing the entire flow loop at 80 °C. After the successful degassing, the desired flow rate is established and the power is raised in steps lasting a few minutes each until a new steady state is achieved (Fig. 3-27). The flow rate, test-section current and voltage, pressure and wall and bulk temperatures are monitored and recorded at each power step through the measurement software (Fig. 3-19). Since the heat flux is axially uniform, CHF occurs at the test-section exit, and can be detected from the temperature excursion measured by the TCs near the exit. The control system automatically shuts down the power supply when any wall TC detects a runaway temperature excursion. Therefore, the experiment is arrested within 1-2 seconds of CHF occurrence. However, the test-section tube typically experiences burnout at the location of CHF (i.e., the exit), so it has to be replaced after every run. The typical running times are about 2.5, 3.5, and 4.5 hours for the cases of insignificant, moderate, and significant CHF enhancement, respectively. Photos of as-received heater coupon and representative heater coupons undergone CHF are shown in Fig. 3-28. Prior to its use the inner surface of every new tube is cleaned with acetone to remove any dust, grease or other contaminants that could affect CHF.

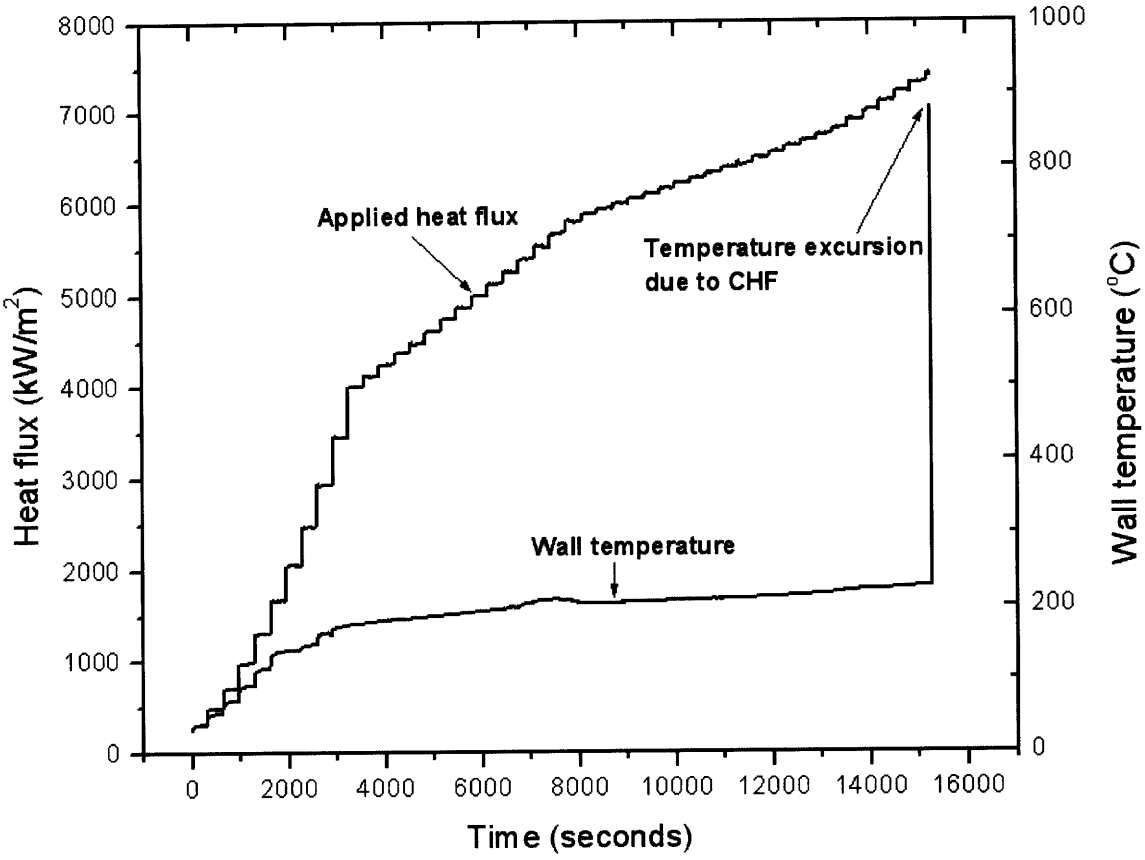

Figure 3-27 Wall temperature and heat flux history in a typical CHF run

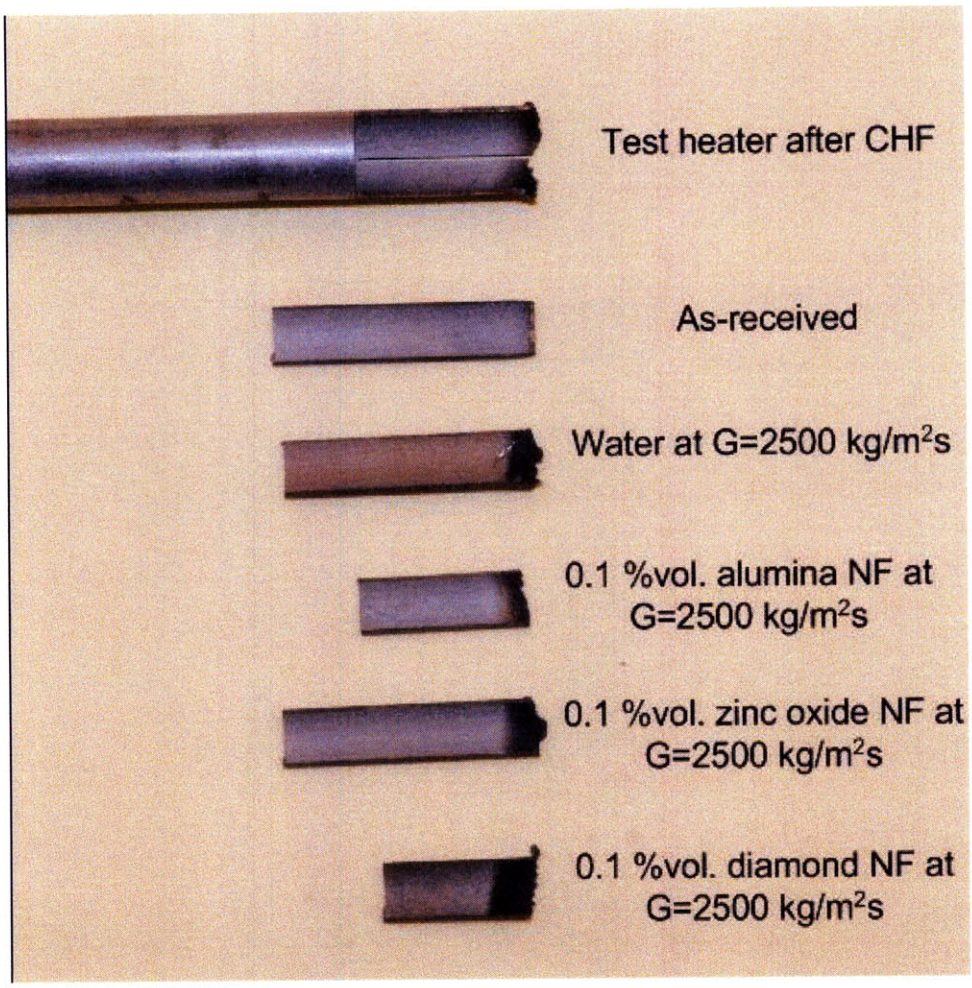

Figure 3-28 Photos of representative heater coupons cut using the electrical discharge machining (EDM) technique

3.5.2 Flow loop cleaning procedure

The nanofluid tests are conducted in order of increasing concentration, to minimize the effect of any holdup in the loop on the next test. However, it is necessary to clean out the flow loop thoroughly when after the tests switch from one type of nanofluid to another. A cleaning process has been set up for this purpose:

(i). Flushing process: The loop was refilled with DI water and the water was circulated in the loop. The water circulation was maintained at room temperature for an hour. This step was repeated 7 times until the discharged water is visibly clean.

(ii). Flushing and heating process: Since nucleate boiling is the main driving force for nanoparticle deposition, a dummy stainless steel grade 316 tube heater was installed in lieu of the test section and heated up to 3.5 MW/m^2 and held at this high heat flux for 4 hours, while the loop was maintained at about 70 °C. This was done to force any residual nanoparticle to deposit on the dummy heater surface. This step was repeated three times.

(iii). Inductively Coupled Plasma (ICP) analysis: After step (i) and (ii), 10 discharged water samples were collected and their weight percent of nanoparticles was measured. An example of ICP analysis after alumina nanoparticle cleaning-out is shown in Table 3-7. It is seen that after flushing 7 times and flushing/heating 3 times, the volume percent of the alumina nanoparticles was reduced significantly as the concentration is very close to the value which water is likely to contain. It is known that about 0.4 ppm of aluminum is contained in water and its concentration can be increased by 5 ppm when water becomes acidic (Emsley, 2003). Therefore, it is concluded that our cleaneup procedure is effective.

Table 3-7 ICP measurement of extracted water samples

Water sample	Measured Al weight fraction (ppm)	Compound (Al_2O_3) volume percent (%vol.)	Dummy heater heating
Flush_01	> 262.6	$> 1.286\times10^{-2}$	No
Flush_02	47.966	2.3×10^{-3}	No
Flush_03	4.997	2.45×10^{-4}	No
Flush_04	1.500	7.340×10^{-5}	No
Flush_05	1.148	5.618×10^{-5}	No
Flush_06	0.720	3.523×10^{-5}	No
Flush_07	0.659	3.225×10^{-5}	No
Flush_08	1.783	8.725×10^{-5}	Yes
Flush_09	0.623	3.049×10^{-5}	Yes
Flush_10	0.598	2.926×10^{-5}	Yes
DI water	0.472	2.309×10^{-5}	

(iv). Heater surface inspection: the dummy heaters that underwent the nucleate boiling process were cut out to examine the inner surface using SEM/EDS. The detailed process of the SEM/EDS will be discussed in Chapter 4. Presence of any porous layer indicates the insufficient cleaning work. However, after repeating flushing and heating process, the SEM pictures taken confirm that the flow loop is cleaned out appropriately as no porous layer was found to exist (Fig. 3-29(c)). EDS also suggests that no alumina nanoparticle is present on the heater surface (Fig. 3-29(d)). The whole procedure was repeated after the zinc-oxide nanofluids tests, prior to loading the diamond nanofluids. The SEM/EDS pictures taken are presented in Fig. 3-30.

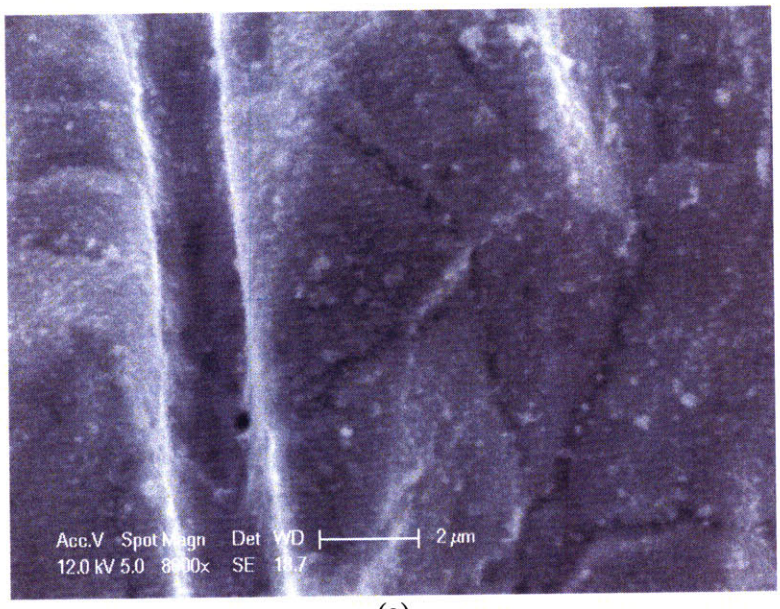
Acc.V Spot Magn Det WD 2 μm
12.0 kV 5.0 8000x SE 11.7

(a)

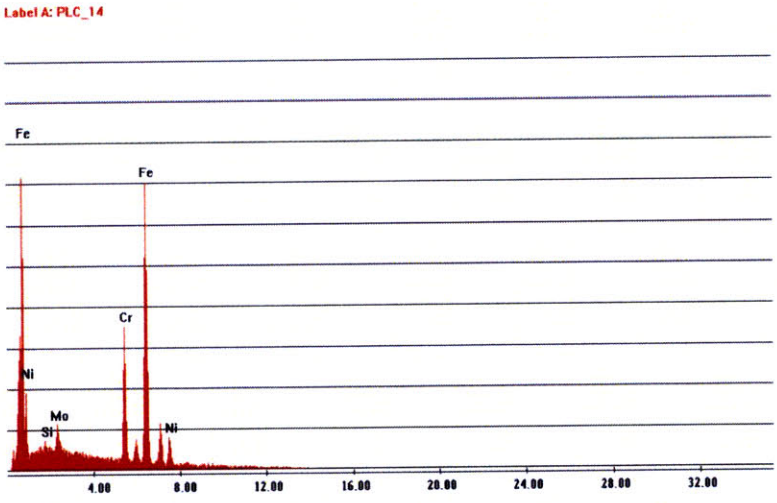
Label A: PLC_14
Fe
Fe
Cr
Ni
Mo
Si
Ni
4.00
8.00
12.00
16.00
20.00
24.00
28.00
32.00

(b)

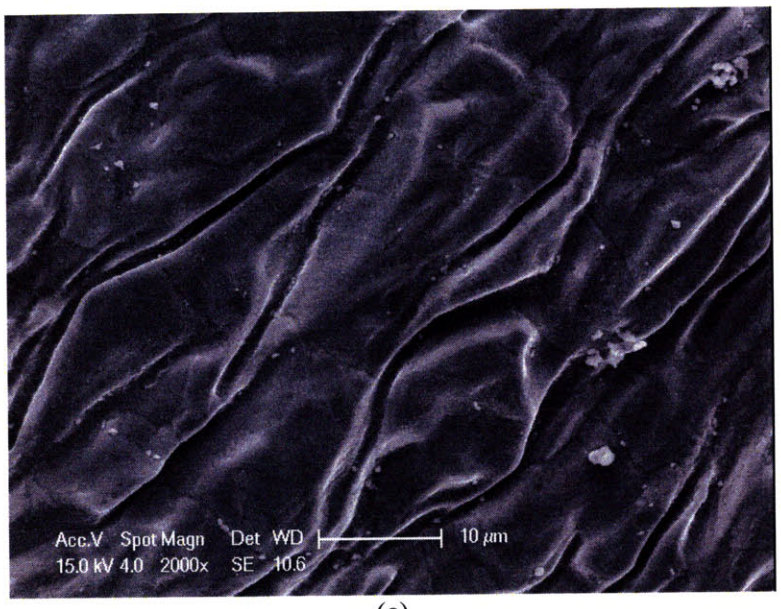

(c)

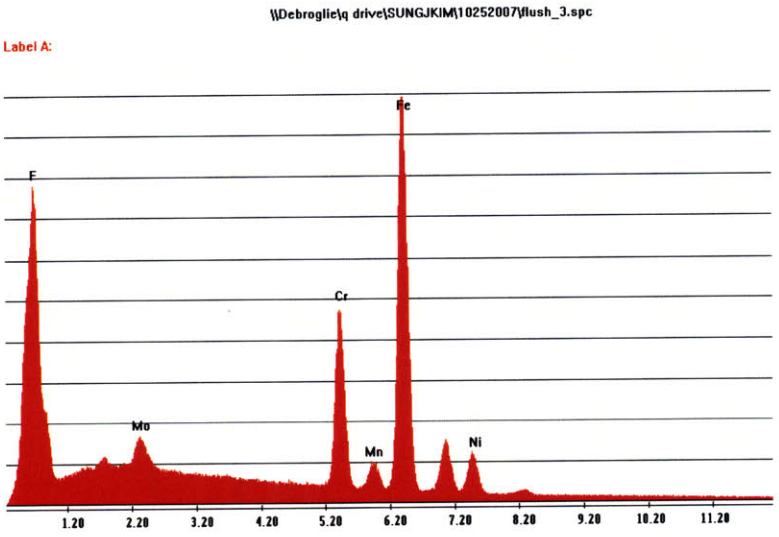

(d)

Figure 3-29 Surface inspection after (a) regular water test (SEM); (b) regular water test (EDS); (c) after the 3rd flushing (SEM); (d) after the 3rd flushing (EDS)

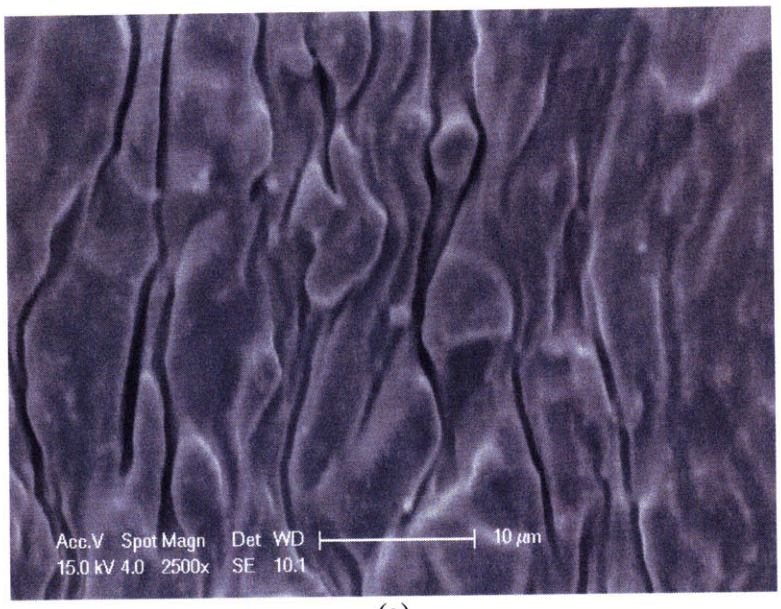

(a)

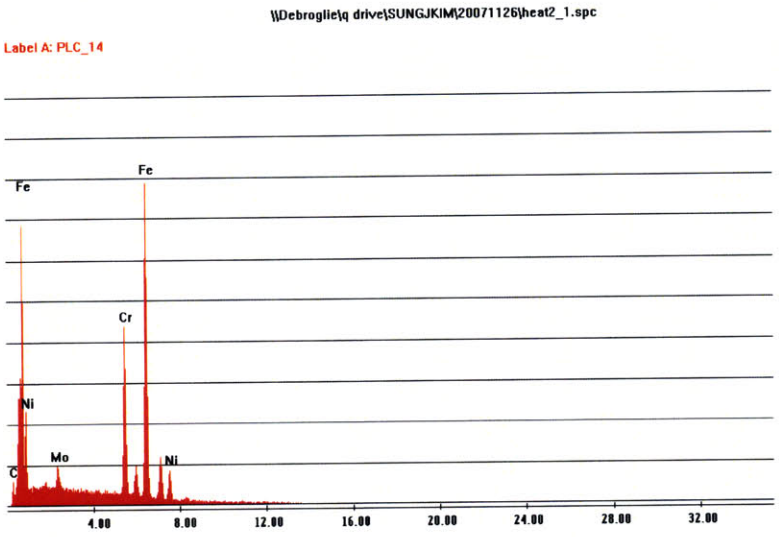

(b)

Figure 3-30 Surface inspection using (a) SEM and (b) EDS at the end of the zinc-oxide tests

4 Results – Heat Transfer Coefficient and Critical Heat Flux

Chapter 4 reports the experimental results for heat transfer coefficient (HTC) and critical heat flux (CHF) measured using the experimental apparatus described in Chapter 3. Section 4.1 reports the wall temperature and HTC experimental data for the water and nanofluid tests. In Section 4.2, the CHF experimental data for deionized water are first presented and compared to the popular 1995 CHF look-up table database. Subsequently, the CHF data of alumina, zinc oxide, and diamonds nanofluids are presented.

4.1 Heat Transfer Coefficient

The heat transfer coefficient was evaluated using three K-type TCs, installed azimuthally at 120° from each other at the end of the test heater, which measured the outer wall temperature, $T_{w,o}$. The inner wall temperatures, T_w, were then derived by solving the radial heat conduction equation in the tube wall with the adiabatic wall condition at the OD (Todreas and Kazimi, 1990):

$$T_w = T_{w,o} - q'' \frac{D_i}{2k_h}\left[\frac{D_o^2}{D_i^2 - D_o^2}\ln\frac{D_i}{D_o} - \frac{1}{2}\right] \tag{4-1}$$

where D_o is the outer tube diameter, k_h is the thermal conductivity of the test heater, whose temperature dependence was accounted for by means of the following equation (ASME, 2004):

$$k_h = 13.79263 + 0.01628T_{w,o} - 5.42692\times10^{-6}T_{w,o}^2 \tag{4-2}$$

The effective heat transfer coefficient, h_{eff}, is calculated from knowledge of the heat flux, the inner wall temperature, and the bulk temperature (measured directly at the test section outlet):

$$h_{eff} = \frac{q''}{T_w - T_b} \tag{4-3}$$

A series of preliminary tests with pure water (no nanoparticles present) were conducted to verify the reliability of the measurements obtained in the loop. As discussed in Chapter 3, the loop operation was first verified by measuring the single-phase convective heat transfer coefficient in the test section and comparing it to the well-known Gnielinski correlation, Eq. 3-25. The agreement between the experiments and the correlation was very reasonable. The instrumental uncertainty for the effective heat transfer coefficient was measured to be less than 7.6%.

Then the flow boiling experiments were run. Water and alumina nanofluids were tested at three different values of the mass flux (G=1500, 2000 and 2500 kg/m^2·s), while zinc oxide and diamond nanofluids were only tested at G=2500 kg/m^{2}s. Flow inlet temperatures increase somewhat with the applied heat flux, and its typical range is 10 to 30 °C from the beginning to the termination of the test, respectively. Figs. 4-1 to 3 show the effective heat transfer coefficient as a function of the applied heat flux for water and alumina nanofluids at the three mass fluxes, respectively. It can be seen that at relatively 'low' heat fluxes (<3000 kW/m^2) the difference between water and the nanofluids is small, while it grows somewhat at higher heat fluxes. Specifically, it appears that at G=1500 and 2000 kg/m^{2}s the water heat transfer coefficient is higher than that of the alumina nanofluids but the differences are not very significant. An interesting feature of the nanofluids data at G=2000 and 2500 kg/m^{2}s is the unexpected reversal of the heat transfer coefficient vs heat flux curve at high heat fluxes. This was also observed in Kim et al.'s (2006a) and Chen et al.'s (2009) studies. Note that all the experiments were terminated at CHF, so this reversal cannot be attributed to transition boiling phenomena. More likely, the slope reversal is due to the accumulation of nanoparticles on the test section surface,

which has been observed systematically in our experiments and can alter the boiling characteristics (e.g., nucleation site density, wettability, capillary wicking) of the surface. However, more work is needed in the interpretation of these data. Similar trends were observed in the tests of zinc oxide nanofluids (Fig. 4-4), but not diamond nanofluids (Fig. 4-5).

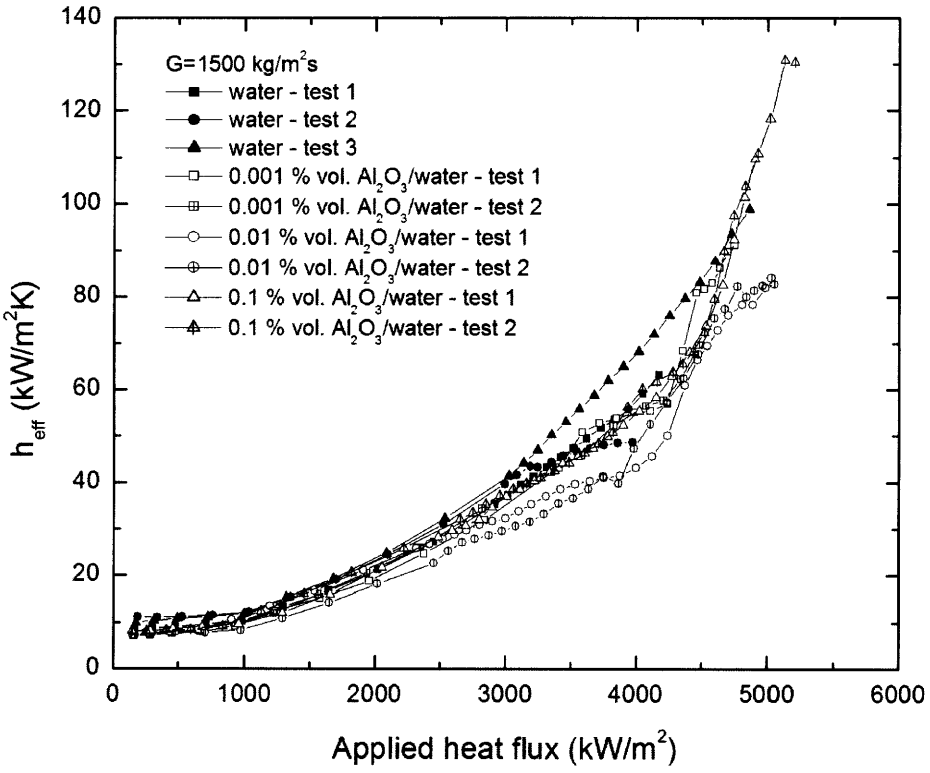

Figure 4-1 Effective heat transfer coefficient of water and alumina nanofluids at G=1500 kg/m^2·s

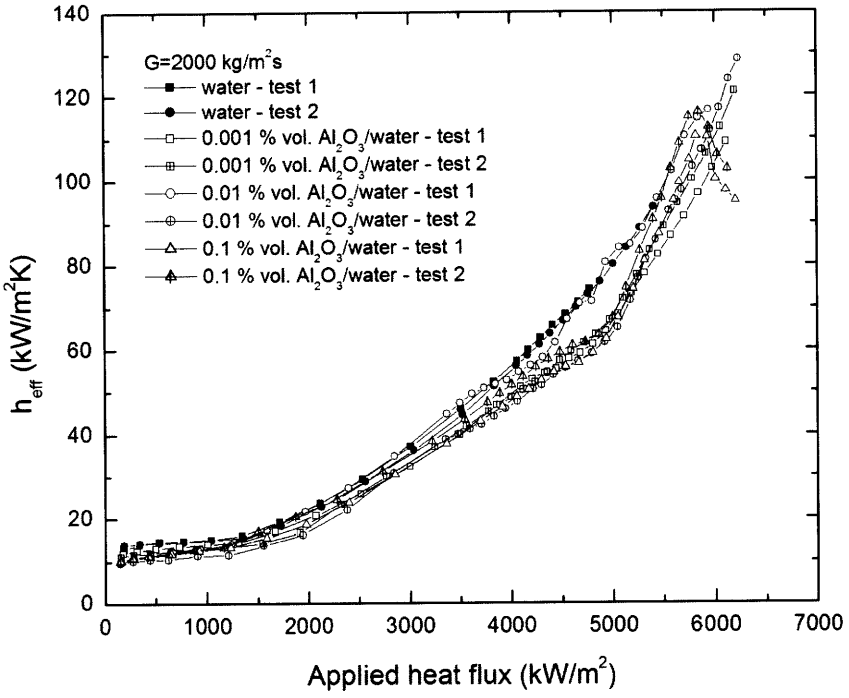

Figure 4-2 Effective heat transfer coefficient of water and alumina nanofluids at G=2000 kg/m^2·s

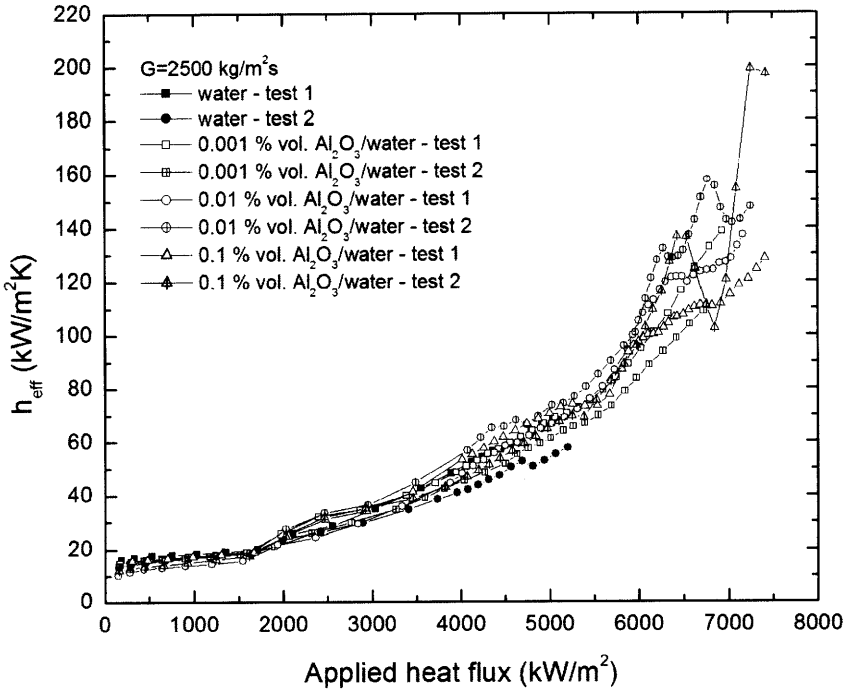

Figure 4-3 Effective heat transfer coefficient of water and alumina nanofluids at G=2500 kg/m^2·s

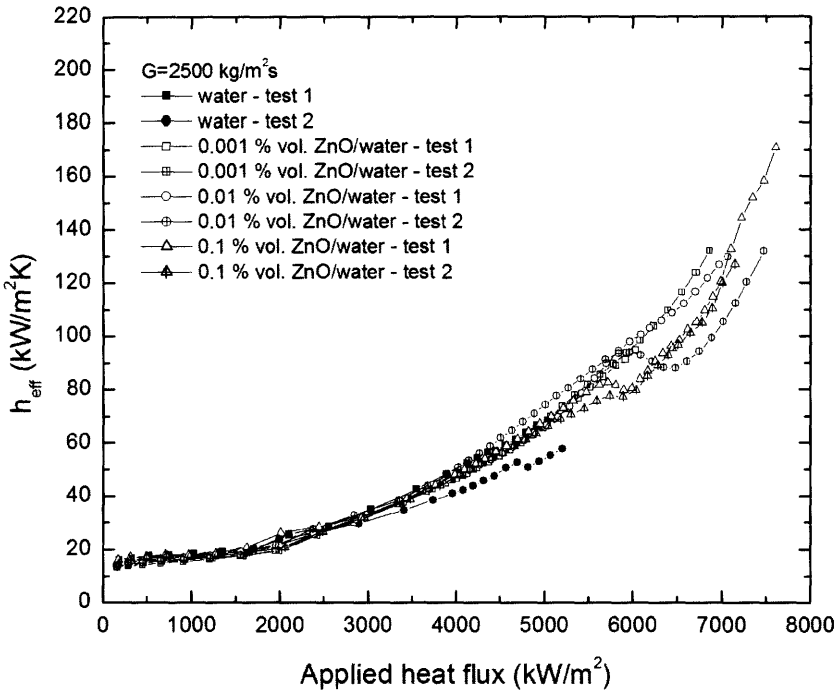

Figure 4-4 Effective heat transfer coefficient of water and zinc oxide nanofluids at G=2500 kg/m^2·s

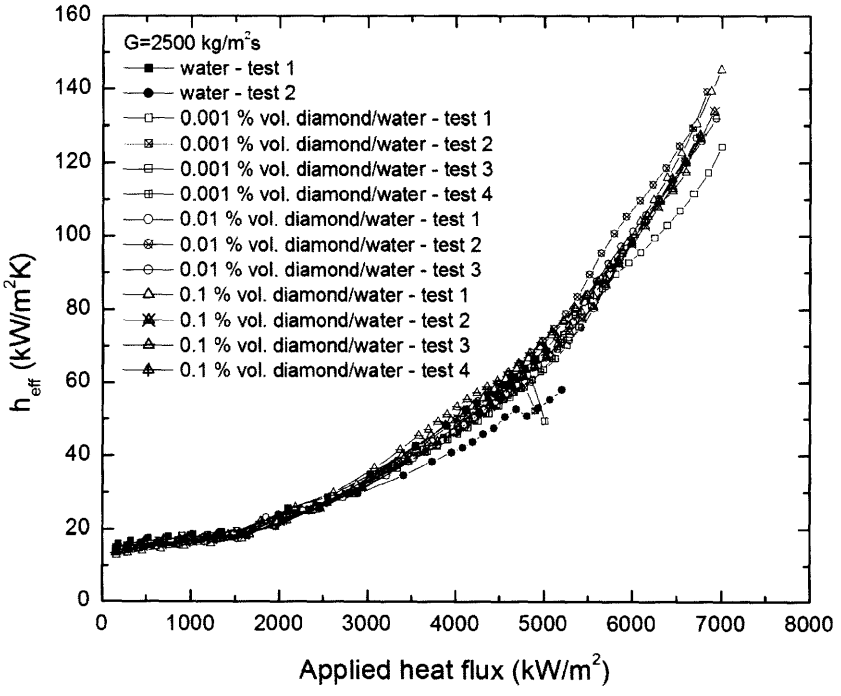

Figure 4-5 Effective heat transfer coefficient of water and diamond nanofluids at G=2500 kg/m^2·s

Figs. 4-6 to 8 summarize the heat transfer coefficient ratios at G=1500, 2000, and 2500 kg/m^{2}s, respectively. The figures show the ratio of the nanofluid to water heat transfer coefficient for the range of heat flux values in which data for both water and nanofluids are available. The measurement uncertainty of this ratio is estimated to be less than 10.7%, which is a propagated uncertainty by two respective HTC uncertainties of 7.6%. It is noted that as nanofluids have higher CHF values, boiling heat transfer coefficient data for nanofluids could be collected over a broader heat flux range than for water. It can be seen that the differences are predominantly within ±20%. Therefore, dilute alumina, zinc oxide and diamond nanofluids do not seem to affect the effective boiling heat transfer coefficients dramatically.

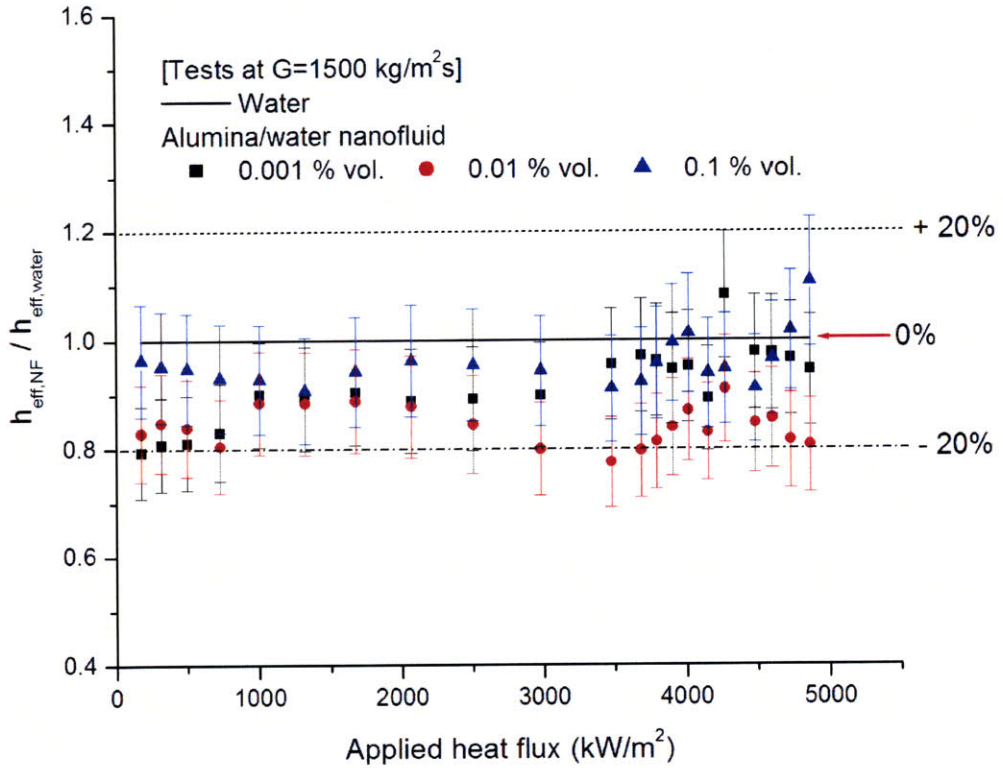

Figure 4-6 Ratio of effective heat transfer coefficient of water and alumina nanofluids at G=1500 kg/m^{2}s

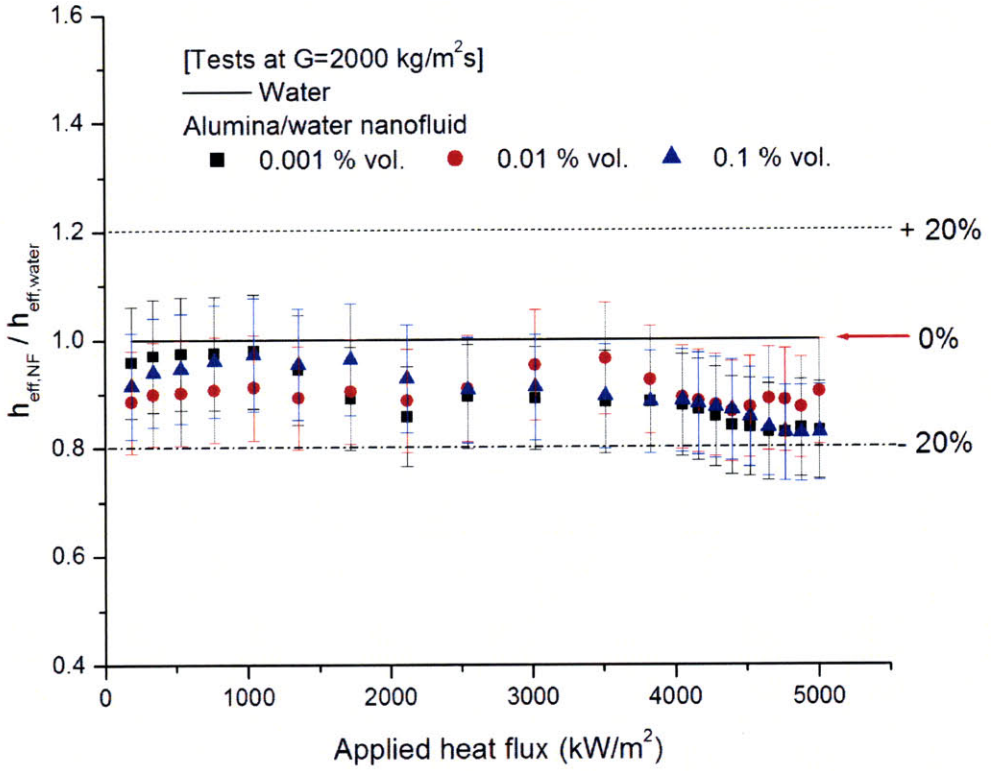

Figure 4-7 Ratio of effective heat transfer coefficient of water and alumina nanofluids at G=2000 kg/m^{2}s

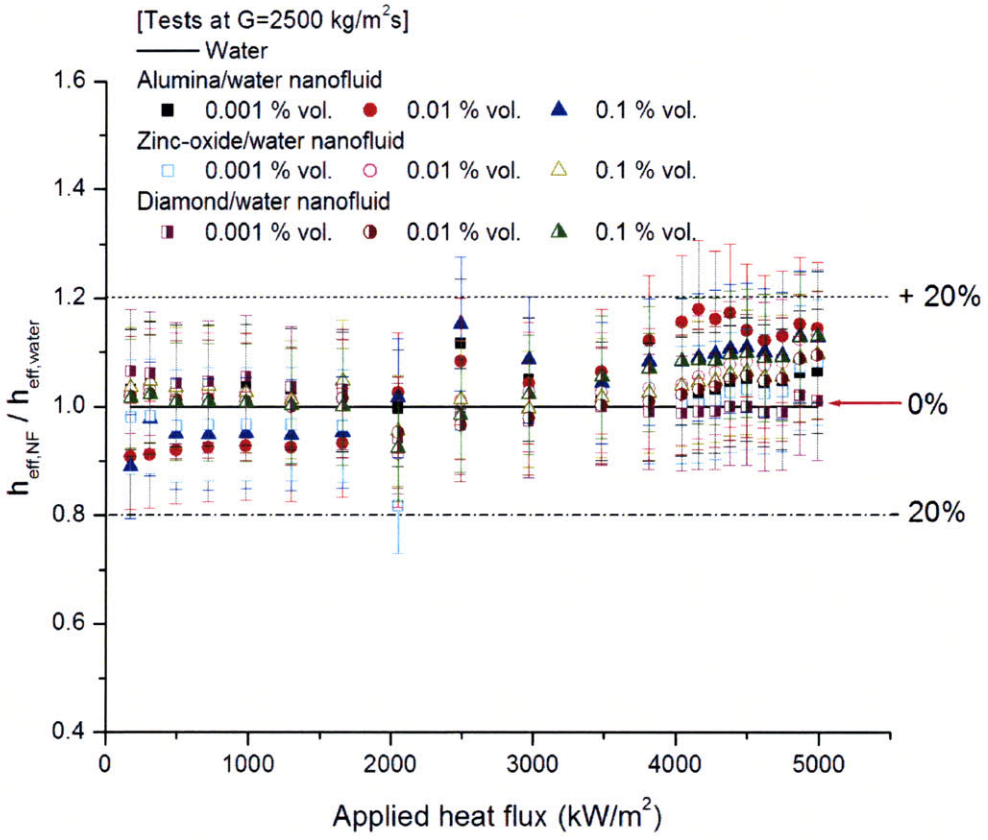

Figure 4-8 Ratio of effective heat transfer coefficient of water and alumina, zinc oxide, and diamond nanofluids at G=2500 kg/m^{2}s

4.2 Critical Heat Flux

Multiple water CHF tests were performed to obtain reliable data and their average values at various experimental conditions. The measured values were then compared to the predictions of the 1995 CHF look-up table (Groeneveld et al., 1996), which is the most accurate tool for predicting the CHF in straight tubes. The root-mean-square (rms) error of the table is about 8%. Since the current study explores the flow CHF at subcooled condition, the exit equilibrium quality, X_e, is always negative and is calculated as:

$$X_e = \frac{c_{p,f}(T_b - T_{sat})}{h_{fg}} < 0 \tag{4-4}$$

where c_p=4.215 kJ/kg·K, T_{sat}=100°C and h_{fg}=2257 kJ/kg are the specific heat, saturation temperature, and heat of vaporization of water at atmospheric pressure, respectively. T_b is the bulk outlet temperature in °C.

Fig. 4-9 shows the CHF experimental data for deionized water at three mass fluxes (G=1500, 2000, and 2500 kg/m^{2}s) and the predictions of the 1995 CHF look-up table. The 1995 look-up table was built based on a vast CHF experimental database normalized to a reference 8-mm inner tube diameter. Therefore, in order to use the table for a heater tube with diameter other than 8 mm, a scaling law is suggested (Groeneveld et al., 1996) as:

$$q''_{CHF} = q''_{CHF,8mm} \times \left(\frac{D_i}{8}\right)^{-0.5} \tag{4-5}$$

where $q''_{CHF,8mm}$ and q''_{CHF} are the 1995 look-up table value and corrected value using the scaling law (Eq. 4-5), respectively. D_i is the inner tube heater diameter in mm. The section of the look-up table that covers the range of the experimental variables of interest to our study is summarized in Table 4-1 and Fig. 4-5, which suggest that the CHF are predominantly dependent of the equilibrium quality, whereas the mass flux effect is negligible when G>1500 kg/m^{2}s. Therefore the ±8% curves in Fig. 4-10 envelop the 1995 CHF look-up table values for all three mass fluxes. In Fig. 4-10, the solid line in the middle represents the 1995 CHF look-up table values, while the dashed lines represent the uncertainty of ±8% rms error band. Note that two different thickness of tube heaters [t=0.012" (D_i=5.7404 mm) and 0.016" (D_i=5.5372 mm)] were tested initially for water CHF tests. It is observed that our water data agree well with the predictions of the look-up table, predominantly within ±8%, which demonstrates that the loop works properly.

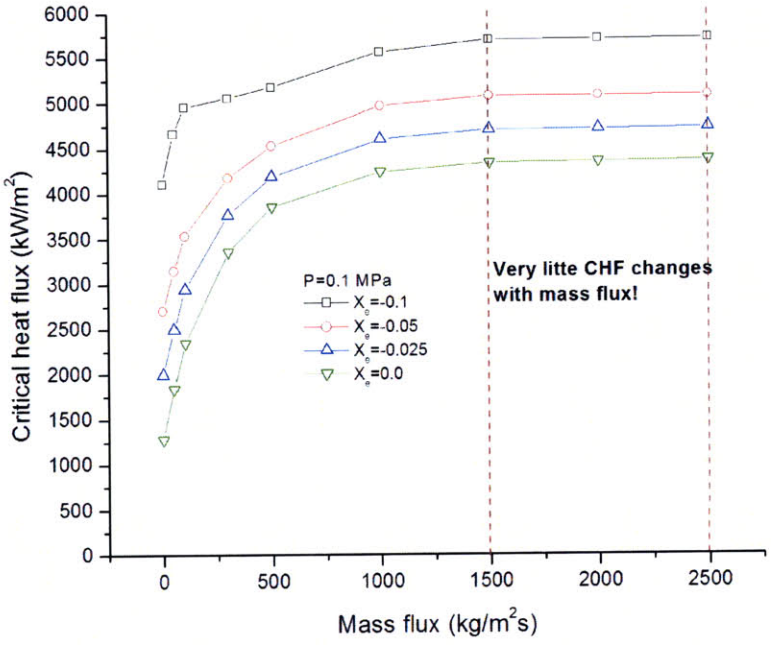

Figure 4-9 Tabular CHF variation according to the mass flux (extracted from 1995 CHF look-up table (Groeneveld et al., 1996))

Table 4-1 Summary of the scaled 1995 Look-up Table at P=0.1 MPa (Groeneveld et al., 1996)

	X_e= -0.1		X_e= -0.05		X_e= -0.025		X_e=0.0	
	LUT D_i=8 mm	Scaled D_i=5.54 mm	LUT D_i=8 mm	Scaled D_i=5.54 mm	LUT D_i=8 mm	Scaled D_i=5.54 mm	LUT D_i=8 mm	Scaled D_i=5.54 mm
G (kg/m^{2}s)	CHF (kW/m^2)	CHF (kW/m^2)	CHF (kW/m^2)	CHF (kW/m^2)	CHF (kW/m^2)	CHF (kW/m^2)	CHF (kW/m^2)	CHF (kW/m^2)
0.0	3419	4,110	2,247	2,701	1,657	1,991	1,066	1,281
50	3881	4,665	2,618	3,147	2,072	2,491	1,526	1,834
100	4124	4,957	2,942	3,536	2,445	2,938	1,947	2,340
300	4206	5,056	3,475	4,177	3,134	3,766	2,792	3,356
500	4305	5,175	3,768	4,529	3,486	4,190	3,204	3,851
1,000	4626	5,560	4,129	4,963	3,828	4,601	3,527	4,239
1,500	4734	5,690	4,216	5,068	3,911	4,701	3,606	4,334
2,000	4739	5,696	4,218	5,070	3,917	4,708	3,616	4,346
2,500	4745	5,703	4,220	5,072	3,926	4,718	3,631	4,364

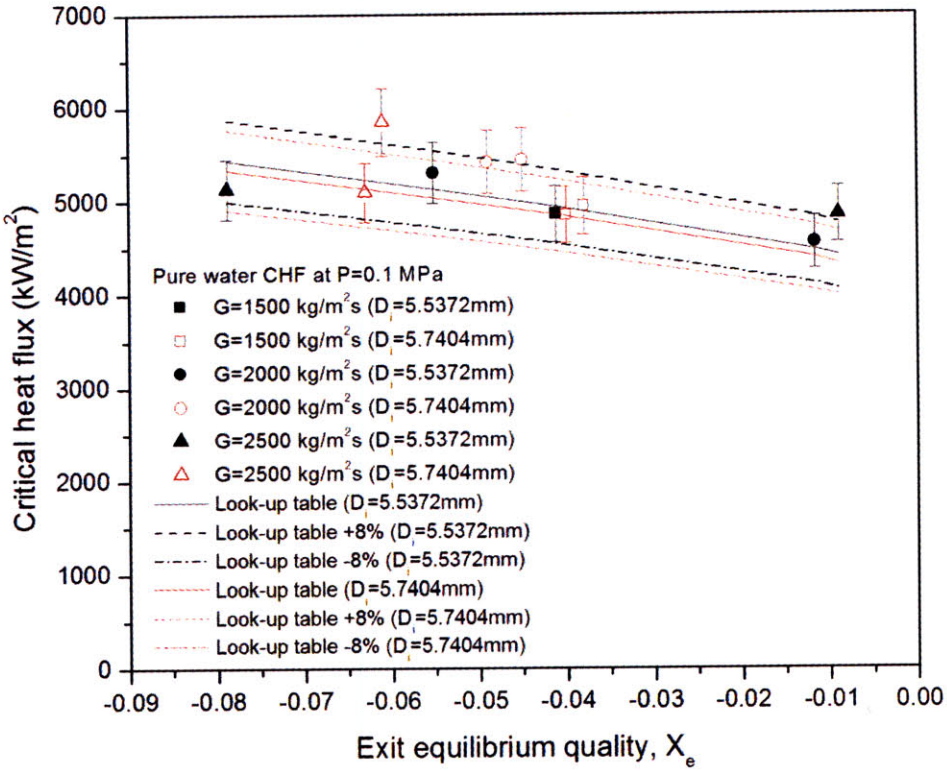

Figure 4-10 Measured CHF values for water at atmospheric pressure

After proper verification of the experizmental apparatus, the alumina nanofluids CHF tests were conducted first. The alumina nanofluid CHF experimental data are shown in Fig. 4-11, where the CHF is displayed as a function of the exit equilibrium quality for three values of the nanoparticle concentration and three values of the mass flux. Note that the marked CHF points are averaged values from multiple runs in the respective conditions of nanoparticle concentration and mass flux. *y*-errors represent the measurement uncertainty of ±6.2% as estimated in Section 3.4.3.1. The data for the low mass flux (G=1500 kg/m^{2}s) fall within the look-up table ±8% 'band', thus indicating that no CHF enhancement is present at these conditions. However, the data for the intermediate and high mass fluxes do show a significant enhancement, well above the estimated experimental uncertainty and the look-up table predictions. The enhancement increases with the mass flux and, to a lesser extent, with the nanoparticle concentration. The maximum

enhancement for the 0.001, 0.01 and 0.1 %vol. alumina nanofluids is 33%, 44% and 53%, respectively, obtained at G=2500 kg/m^{2}s in all three cases.

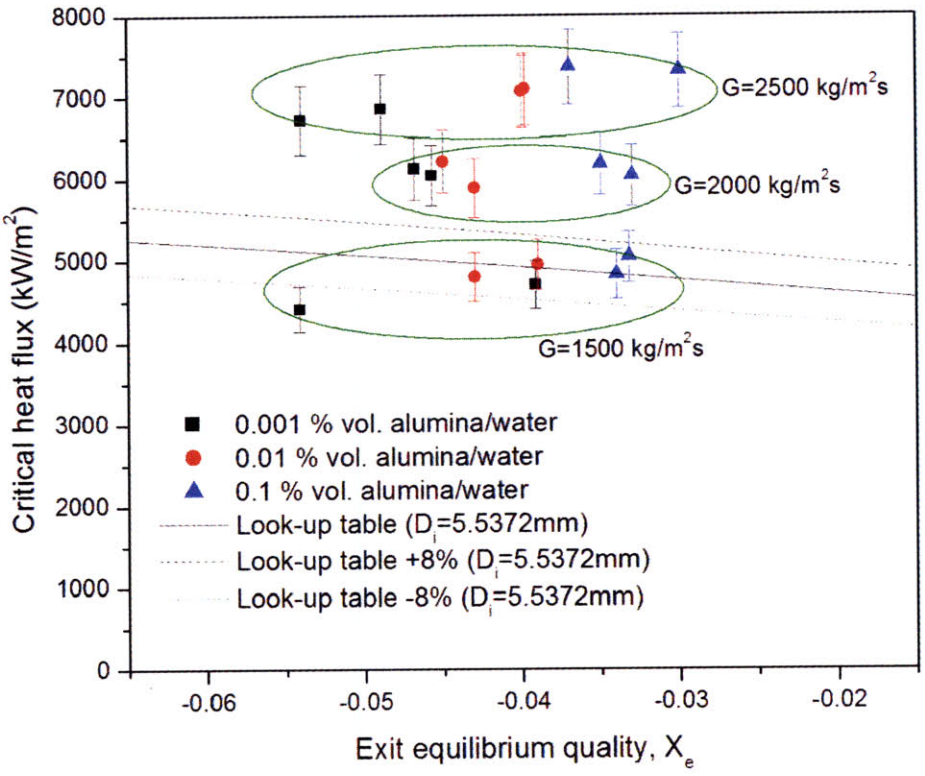

Figure 4-11 Measured CHF values for alumina/water nanofluids at atmospheric pressure

After the alumina nanofluids tests, CHF tests were run for using zinc oxide and diamond nanofluids. The results for the nanofluids with zinc oxide and diamond nanoparticles are shown in Figs. 4-12 and 13, respectively. The maximum measured CHF enhancement for zinc-oxide nanofluids is 53%, while for diamond nanofluids is 38%.

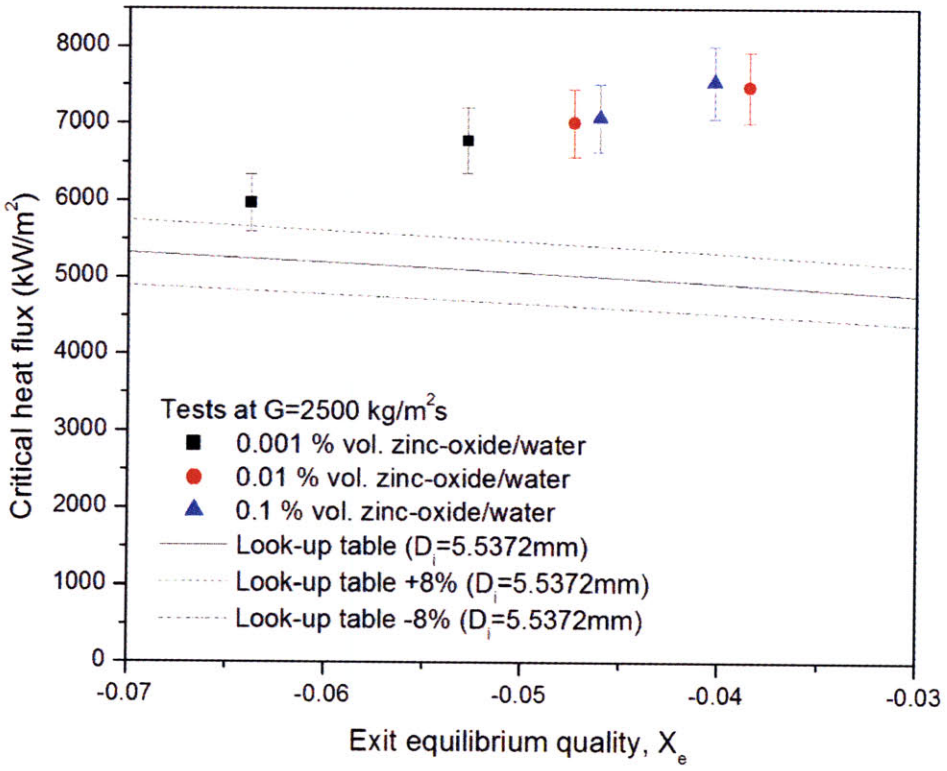

Figure 4-12 Measured CHF values for zinc-oxide/water nanofluids at atmospheric pressure

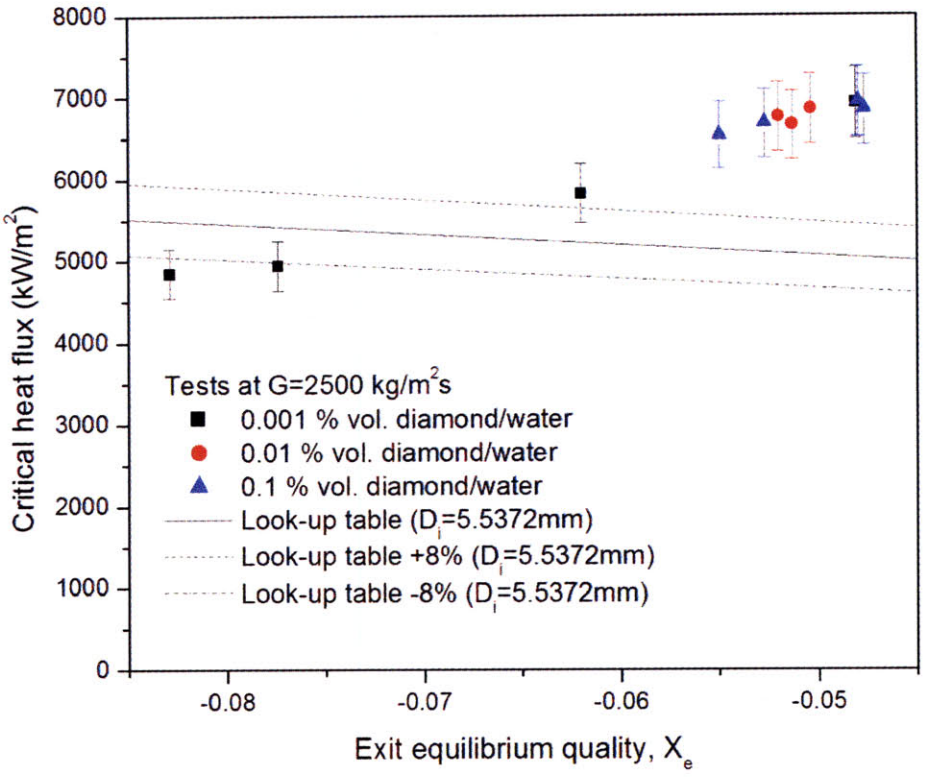

Figure 4-13 Measured CHF values for diamond/water nanofluids at atmospheric pressure

The CHF results from all runs are summarized in Tables 4-2 to 5. In fact, more than 100 CHF runs were performed, where some runs were prematurely terminated accidentally. In the failed tests, some were due to the insufficient de-aeration of the flow loop and thus generation of unstable flow. Others were often caused by oxidization of the copper electrodes, which generates local escalation of the electric resistance. Tables 4-2 to 5 include only the data for the runs that were successfully completed.

Table 4-2 Summary of water CHF values measured at MIT

Test tag	Mass flux (kg/m^2s)	Exit equilibrium quality	T_{in} (°C)	T_{out} (°C)	$q''_{CHF,thermal}$ (kW/m^2)	(a) $q''_{CHF,elec}$ (kW/m^2)	(b) $q''_{CHF,1995LUT}$ (kW/m^2)	Ratio (a)/(b)	Tube thickness (inch)	Remark
W_1	1538.7	-0.0380	24.2	79.0	4,655	4,951	4,810	1.029	0.012	CHF
W_3	1535.2	-0.0400	25.5	78.0	4,462	4,853	4,833	1.004	0.012	CHF
W_12	1500.0	-0.0610	20.0	66.9	n/a	n/a	n/a	n/a	0.016	NBHTC
W_13	1500.0	-0.0650	20.1	64.6	n/a	n/a	n/a	n/a	0.016	NBHTC
W_17	1510.4	-0.0412	22.3	77.6	4,873	4,863	4,943	0.984	0.016	CHF/NBHTC
W_4	2012.5	-0.0490	26.2	73.2	5,246	5,422	4,965	1.092	0.012	CHF
W_5	2011.1	-0.0450	28.5	75.5	5,244	5,448	4,908	1.110	0.012	CHF
W_11	1987.1	-0.0117	52.5	93.4	4,186	4,552	4,476	1.017	0.016	CHF/NBHTC
W_14	2000.0	-0.0690	22.4	62.6	n/a	n/a	n/a	n/a	0.016	NBHTC
W_16	2007.4	-0.0552	24.3	70.0	5,333	5,306	5,135	1.033	0.016	CHF/NBHTC
W_6	2502.3	-0.0610	24.7	67.0	5,862	5,851	5,118	1.143	0.012	CHF
W_7	2505.6	-0.0630	29.0	65.9	5,095	5,099	5,143	0.991	0.012	CHF
W_8	2512.6	-0.0530	27.2	72.2	6,026	6,459	5,110	1.264	0.016	CHF/NBHTC
W_9	2483.4	-0.009	59.2	94.7	4,478	4,852	4,411	1.100	0.016	CHF
W_15	2500.0	-0.0800	22.7	56.4	n/a	n/a	n/a	n/a	0.016	NBHTC
W_18	2545.9	-0.0788	22.8	57.3	5,082	5,132	5,435	0.944	0.016	CHF/NBHTC

Table 4-3 Summary of alumina nanofluids CHF values measured at MIT

Test tag	Nanoparticle concentration (%vol.)	Mass flux (kg/m^2s)	Exit equilibrium quality	T_{in} (°C)	T_{out} (°C)	$q''_{CHF,thermal}$ (kW/m^2)	(a) $q''_{CHF,elec}$ (kW/m^2)	(b) $q''_{CHF,1995LUT}$ (kW/m^2)	Ratio (a)/(b)	Tube thickness (inch)	Remark
AL_01	0.001	1538.7	-0.0391	24.7	78.8	4,781	4,702	4,907	0.958	0.016	CHF/NBHTC
AL_02	0.001	1519.0	-0.0541	20.9	70.5	4,409	4,411	5,110	0.863	0.016	CHF/NBHTC
AL_03	0.001	2496.4	-0.0489	27.1	73.5	6,703	6,858	5,049	1.358	0.016	CHF/NBHTC
AL_04	0.001	2496.1	-0.0540	24.7	70.7	6,647	6,723	5,122	1.313	0.016	CHF/NBHTC
AL_05	0.001	2024.3	-0.0457	24.3	75.0	5,943	6,045	5,008	1.207	0.016	CHF/NBHTC
AL_06	0.001	2010.2	-0.0468	22.5	74.5	6,051	6,126	5,024	1.219	0.016	CHF/NBHTC
AL_01	0.01	1554.5	-0.0430	21.8	76.6	4,936	4,801	4,936	0.973	0.016	CHF/NBHTC
AL_02	0.01	1540.4	-0.0390	22.3	78.7	5,037	4,945	4,907	1.008	0.016	CHF/NBHTC
AL_03	0.01	2002.8	-0.0430	25.7	76.5	5,889	5,888	4,945	1.191	0.016	CHF/NBHTC
AL_05	0.01	2020.0	-0.0450	22.8	75.7	6,183	6,214	4,981	1.248	0.016	CHF/NBHTC
AL_07	0.01	2517.5	-0.0400	29.2	78.1	7,134	7,068	4,930	1.434	0.016	CHF/NBHTC
AL_09	0.01	2502.1	-0.0400	28.4	78.0	7,192	7,095	4,930	1.439	0.016	CHF/NBHTC
AL_01	0.1	2493.8	-0.0370	29.2	80.0	7,346	7,364	4,888	1.507	0.016	CHF/NBHTC
AL_03	0.1	2505.1	-0.0300	33.0	83.6	7,337	7,313	4,789	1.527	0.016	CHF/NBHTC
AL_06	0.1	2001.8	-0.0350	27.8	80.9	6,155	6,184	4,802	1.288	0.016	CHF/NBHTC
AL_07	0.1	1998.5	-0.0330	29.2	81.8	6,076	6,041	4,767	1.267	0.016	CHF/NBHTC
W_AL_05	0.1	2003.6	-0.0370	31.0	79.7	5,647	5,547	4,838	1.147	0.016	CHF/NBHTC
W_AL_04	0.1	2000.0	-0.0460	26.8	74.8	5,553	5,781	4,999	1.156	0.016	CHF/NBHTC
AL_08	0.1	1521.8	-0.0340	25.6	81.2	4,903	4,829	4,833	0.999	0.016	CHF/NBHTC
AL_09	0.1	1521.0	-0.0332	23.2	81.9	5,163	5,041	4,818	1.046	0.016	CHF/NBHTC
AL_pt_11_sub	0.1	1942.8	-0.0048	41.7	97.2	6,243	6,192	4,416	1.402	0.016	CHF/NBHTC

Table 4-4 Summary of zinc oxide nanofluids CHF values measured at MIT

Test tag	Nanoparticle concentration (%vol.)	Mass flux (kg/m^2s)	Exit equilibrium quality	T_{in} (°C)	T_{out} (°C)	$q''_{CHF,thermal}$ (kW/m^2)	(a) $q''_{CHF,elec}$ (kW/m^2)	(b) $q''_{CHF,1995LUT}$ (kW/m^2)	Ratio (a)/(b)	Tube thickness (inch)	Remark
ZN_05	0.001	2510.2	-0.0638	24.9	65.4	5,878	5,975	5,246	1.139	0.016	CHF/NBHTC
ZN_06	0.001	2493.6	-0.0528	25.2	71.3	6,661	6,785	5,107	1.329	0.016	CHF/NBHTC
ZN_03	0.01	2506.6	-0.0474	26.5	74.1	6,906	7,014	5,029	1.395	0.016	CHF/NBHTC
ZN_04	0.01	2468.4	-0.0385	27.8	79.0	7,317	7,472	4,901	1.525	0.016	CHF/NBHTC
ZN_01	0.1	2504.3	-0.0403	26.9	77.9	7,405	7,539	4,935	1.528	0.016	CHF/NBHTC
ZN_02	0.1	2509.2	-0.0461	27.0	74.9	6,960	7,076	5,011	1.412	0.016	CHF/NBHTC

Table 4-5 Summary of diamond nanofluids CHF values measured at MIT

Test tag	Nanoparticle concentration (%vol.)	Mass flux (kg/m^2s)	Exit equilibrium quality	T_{in} (°C)	T_{out} (°C)	$q''_{CHF,thermal}$ (kW/m^2)	(a) $q''_{CHF,elec}$ (kW/m^2)	(b) $q''_{CHF,1995LUT}$ (kW/m^2)	Ratio (a)/(b)	Tube thickness (inch)	Remark
C_01	0.001	2491.9	-0.0481	26.1	73.8	6,876	6,926	5,039	1.374	0.016	CHF/NBHTC
C_02	0.001	2500.0	-0.0829	22.3	55.1	4,771	4,845	5,487	0.883	0.016	CHF/NBHTC
C_03	0.001	2506.9	-0.0620	26.6	66.2	5,757	5,824	5,223	1.115	0.016	CHF/NBHTC
C_04	0.001	2508.1	-0.0774	24.3	57.9	4,883	4,940	5,418	0.912	0.016	CHF/NBHTC
C_05	0.01	2493.4	-0.0513	26.1	72.0	6,622	6,657	5,088	1.308	0.016	CHF/NBHTC
C_06	0.01	2492.3	-0.0520	26.1	71.6	6,565	6,759	5,097	1.326	0.016	CHF/NBHTC
C_07	0.01	2492.7	-0.0504	25.7	72.5	6,754	6,855	5,077	1.350	0.016	CHF/NBHTC
C_08	0.1	2488.7	-0.0480	26.1	73.9	6,875	6,942	5,039	1.378	0.016	CHF/NBHTC
C_09	0.1	2492.2	-0.0477	27.2	74.0	6,760	6,840	5,035	1.358	0.016	CHF/NBHTC
C_10	0.1	2483.3	-0.0550	25.4	70.2	6,446	6,531	5,135	1.272	0.016	CHF/NBHTC
C_11	0.1	2489.2	-0.0527	25.7	71.3	6,570	6,676	5,106	1.307	0.016	CHF/NBHTC

5 Results – Heater Surface Characterization

Chapter 5 reports the results of the heater surface characterization. This task is important because boiling HTC and CHF are affected by the heater surface physico-chemical characteristics, which can be altered by the nanoparticle deposition occurring during nanofluid boiling, as will be shown. The employed characterization measurements are Scanning Electron Microscopy (SEM) and Energy Dispersive X-ray Spectroscopy (EDS), confocal microscopy used to quantify the number of micro-cavities on the surface, and contact angle measurement. Section 5.1 presents the SEM images and EDS spectra of the tested heater coupons, which provide information regarding the surface morphology of the heater surface. Section 5.2 reports more quantitative information about the surface topography, surface roughness and area change. In Section 5.3, the confocal images are utilized to obtain the number density of micro-cavities on the surface. Finally, Section 5.4 reports on effort to characterize the wetting behavior of the liquid on the heater coupons by means of measurements of apparent and intrinsic contact angles.

5.1 Scanning Electron Microscopy and Energy Dispersive X-Ray Spectroscopy

5.1.1 Description of SEM/EDS

In Chapter 4, it was shown that the CHF of water is enhanced when nanoparticles of various materials are added to it. In this section by inspecting the heater surfaces using SEM and

EDS, we present some experimental evidence concerning the possible reasons for such enhancement. A change in CHF can be due to either changes in the thermo-physical properties of the fluid or changes in the surface characteristics of the boiling surface. Since the thermo-physical properties (density, specific heat capacity, thermal conductivity, viscosity, surface tension, etc.) of our nanofluids are almost identical to those of pure water as reported in Chapter 3, the CHF enhancement must come from a surface effect. The morphology of the heater inner surface, which is exposed to the test fluid, is expected to change during a nanofluid run because of nanoparticle precipitation during nucleate boiling. This was confirmed by analyzing representative coupons of the test section heaters, which were prepared by Electron Discharge Machining (EDM) technique (Fig. 5-1). The EDM technique works by eroding material in the path of electrical charges that form an arc between an electrode (the cutting tool) and work piece (heater coupon). Therefore this technique can be used only when the work piece is electrically conductive. Due to its precise machining capability, the EDM can cut very tiny sample in the order of mm and minimize the loss of deposited material on the heater surface by reducing improper contact during cutting process.

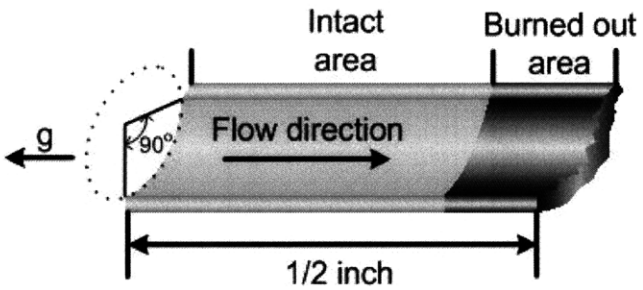

Figure 5-1 Schematic of test coupons cut with EDM technique

The coupons, obtained close to the burnout location of the test heaters, were then examined with a Scanning Electron Microscopy (SEM). The representative SEM pictures of an as-purchased tube heater, as well as tube heaters boiled in pure water and 0.001, 0.01, and

0.1 %vol. alumina, zinc oxide, and diamond nanofluids are shown in Figs. 5-2a to 16a. A significant change in the surface morphology is evident for the coupons boiled in the nanofluids, as the surface seems to cover with a somewhat porous layer. To identify whether the porous layer is indeed made of precipitated nanoparticles, Energy Dispersive X-ray Spectroscopy (EDS) was used concurrently with the imaging capabilities of the SEM. The EDS is an instrument integrated with the SEM allowing for the imaging and subsequent elemental analysis of the features imaged. The EDS technique analyzes the X-rays that are emitted due to the interaction of a high energy electron beam and the surface atoms. Each element emits X-rays at characteristic energy levels. Therefore, measurement of the X-ray spectrum emitted by the surface enables elemental identification and quantification of the surface. The obtained spectra are also shown in Figs. 5-2b to 16b for all test coupons for the surfaces boiled in pure water and nanofluids. The Al, Zn and C peaks in Figs. 5-4 through 5-18 are direct evidence of nanoparticle deposition in their respective tests with alumina, zinc-oxide and diamond nanofluids. In the following section, more detailed observations are discussed to facilitate the interpretation of the experiment results.

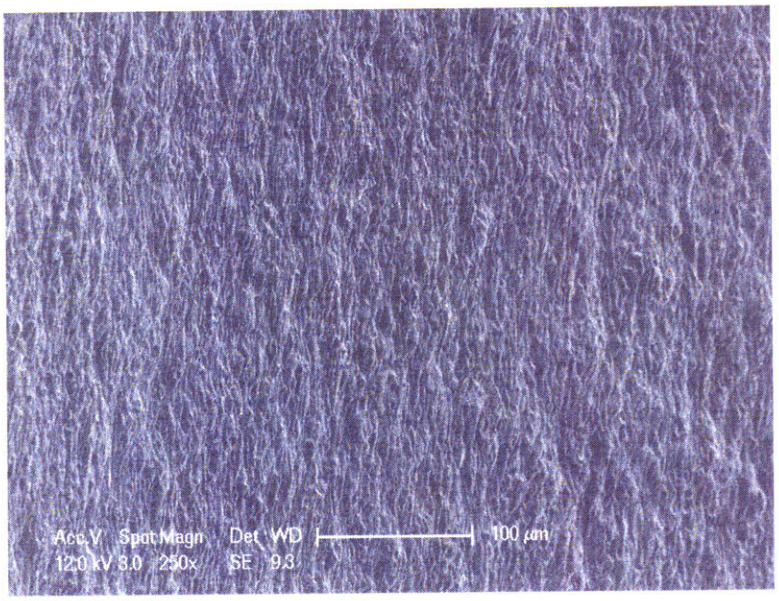

(a)

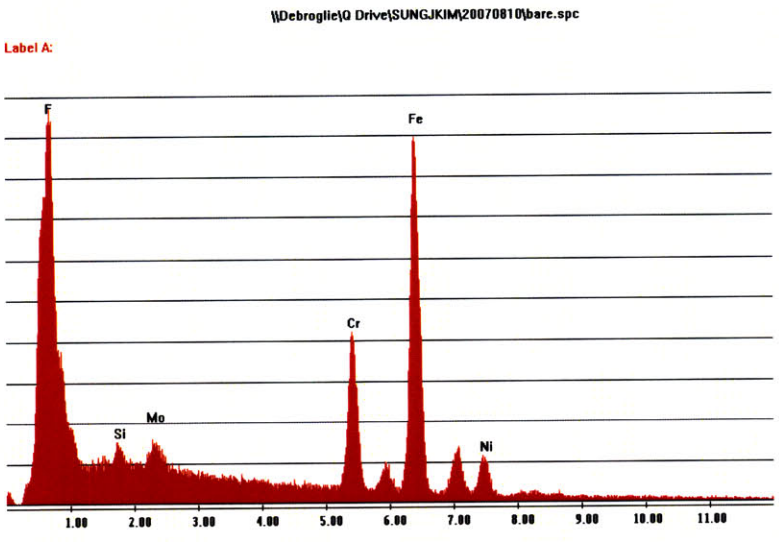

(b)

Figure 5-2 (a) SEM picture and (b) EDS spectrum of as-received stainless steel test heater

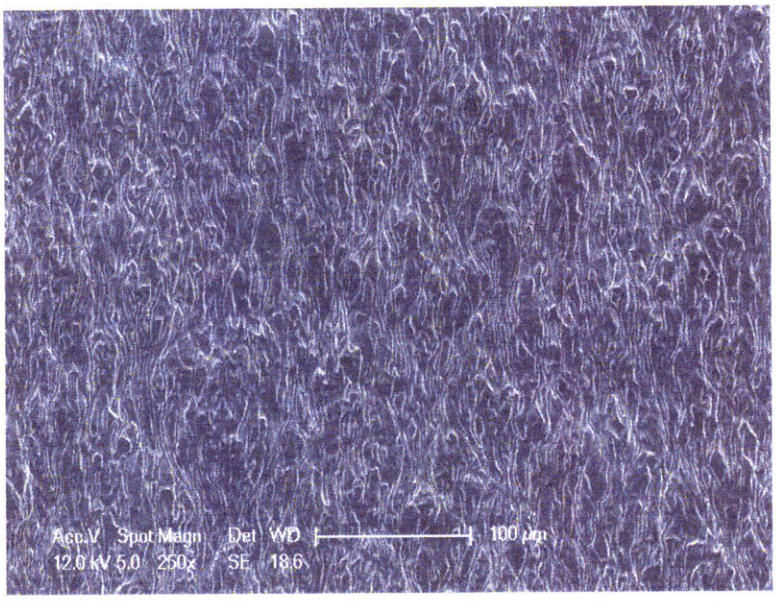

(a)

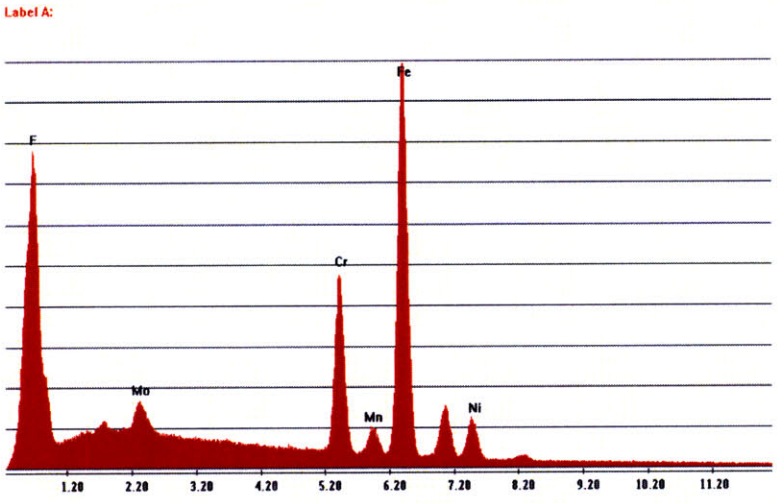

(b)

Figure 5-3 (a) SEM picture and (b) EDS spectrum of stainless steel test heater boiled in pure water

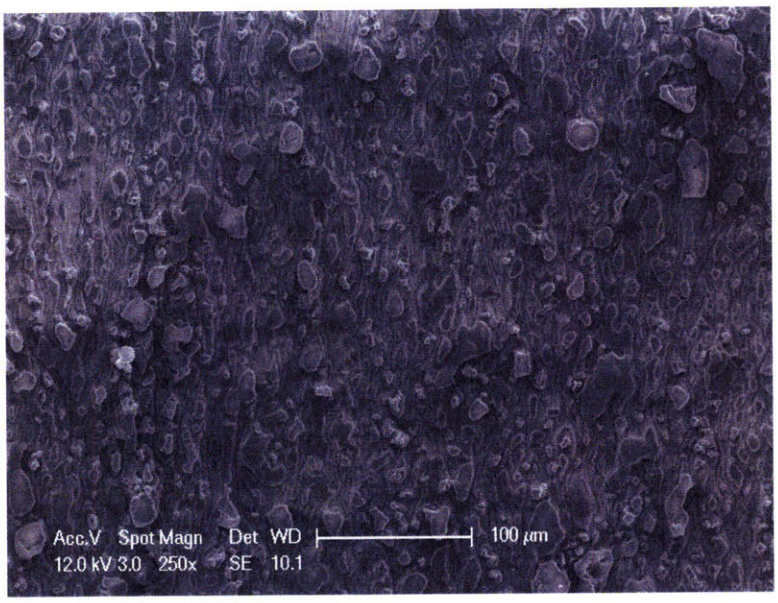

(a)

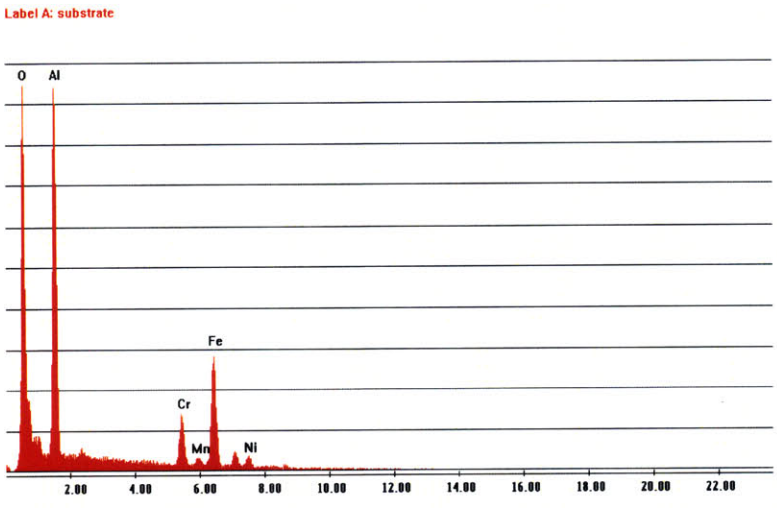

(b)

Figure 5-4 (a) SEM picture and (b) EDS spectrum of stainless steel test heater boiled in 0.001 %vol. alumina nanofluids at G=1500 kg/m^{2}s

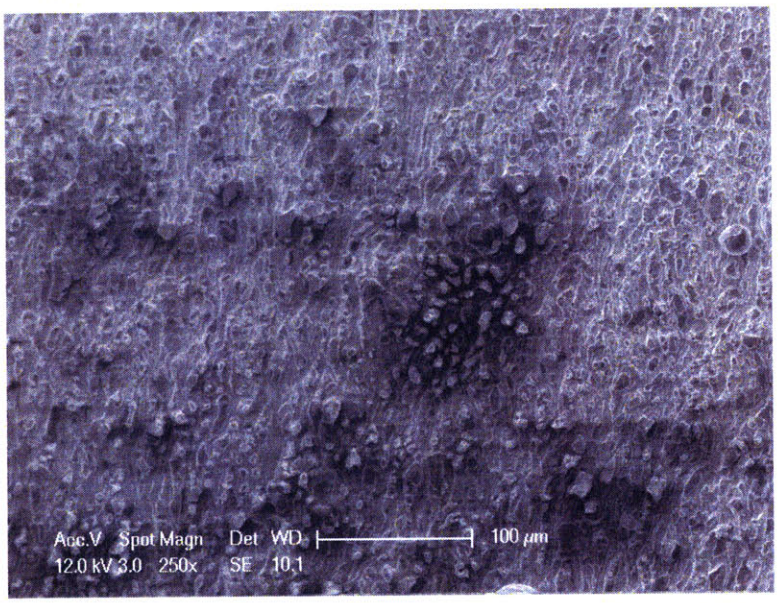

(a)

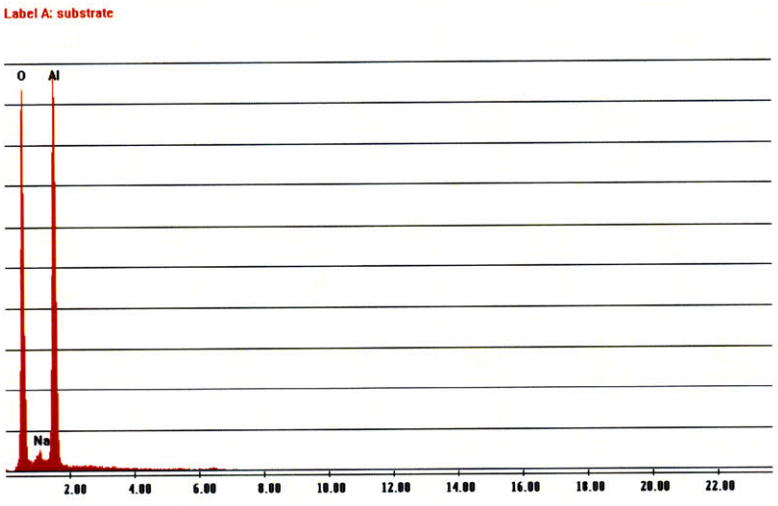

(b)

Figure 5-5 (a) SEM picture and (b) EDS spectrum of stainless steel test heater boiled in 0.001 %vol. alumina nanofluids at G=2000 kg/m^{2}s

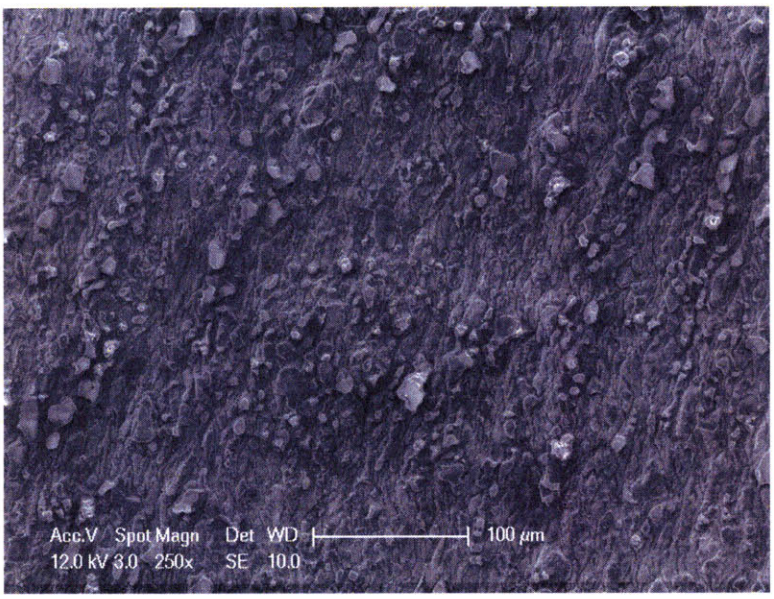

(a)

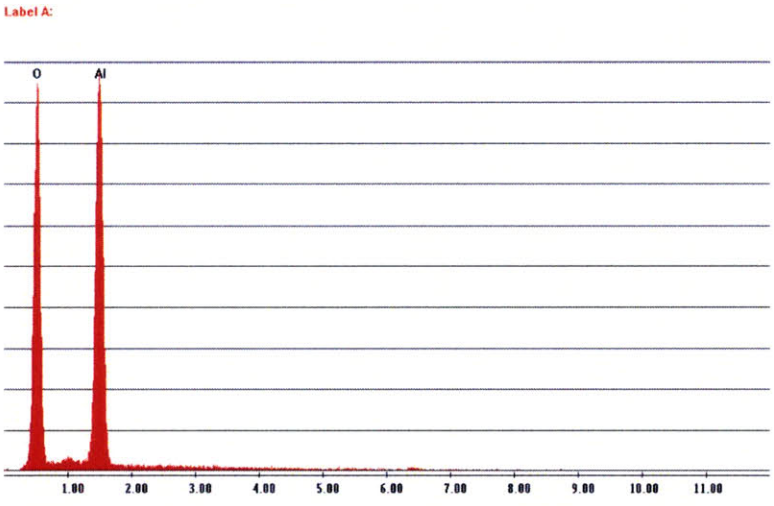

(b)

Figure 5-6 (a) SEM picture and (b) EDS spectrum of stainless steel test heater boiled in 0.001 %vol. alumina nanofluids at G=2500 kg/m^{2}s

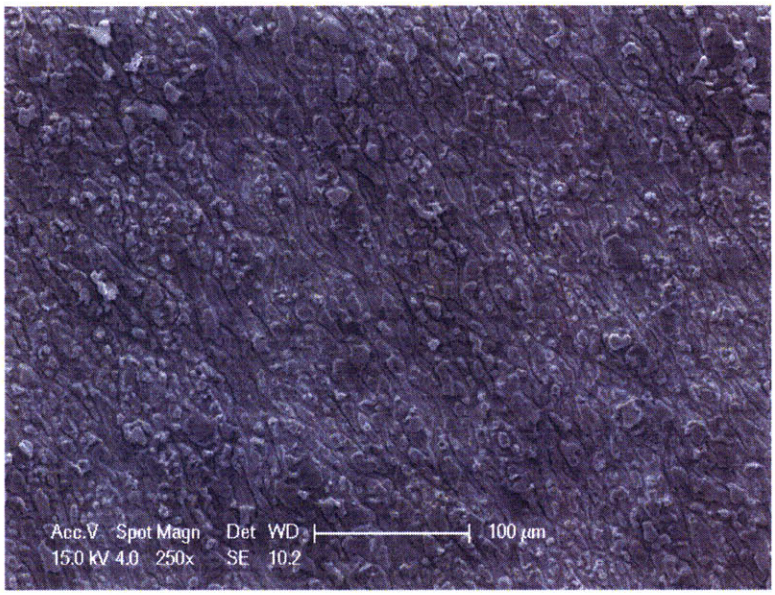

(a)

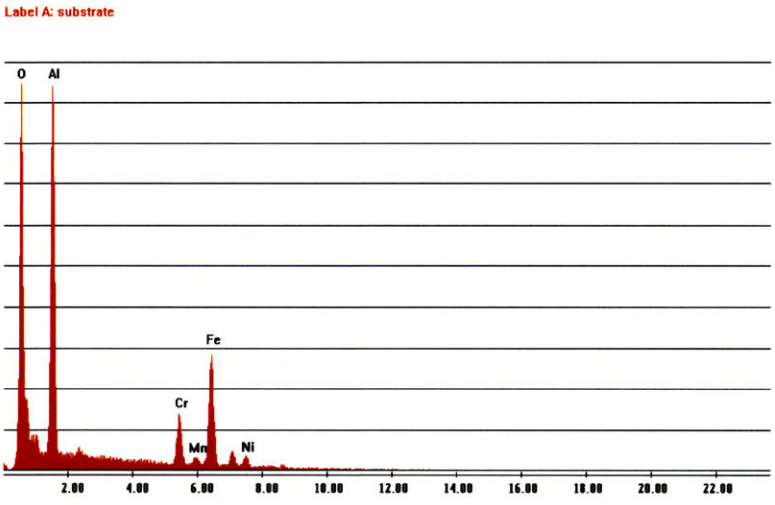

(b)

Figure 5-7 (a) SEM picture and (b) EDS spectrum of stainless steel test heater boiled in 0.01 %vol. alumina nanofluids at G=1500 kg/m^{2}s

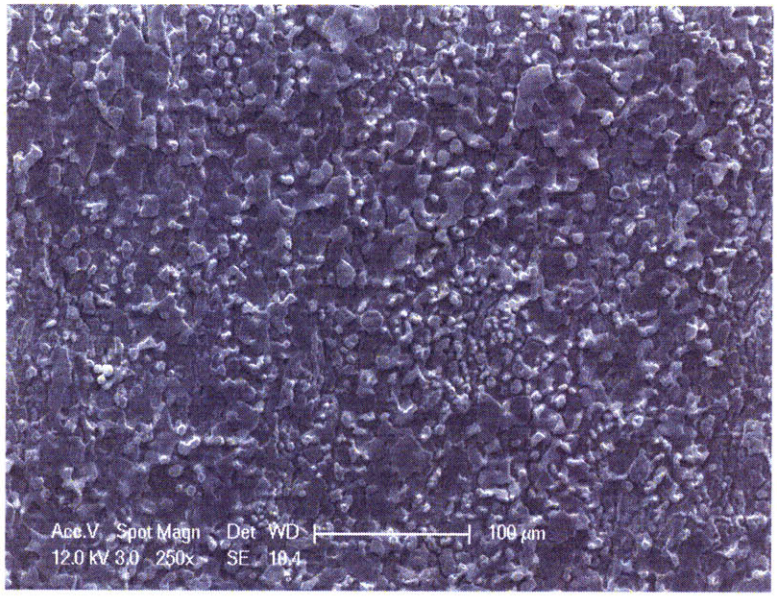

(a)

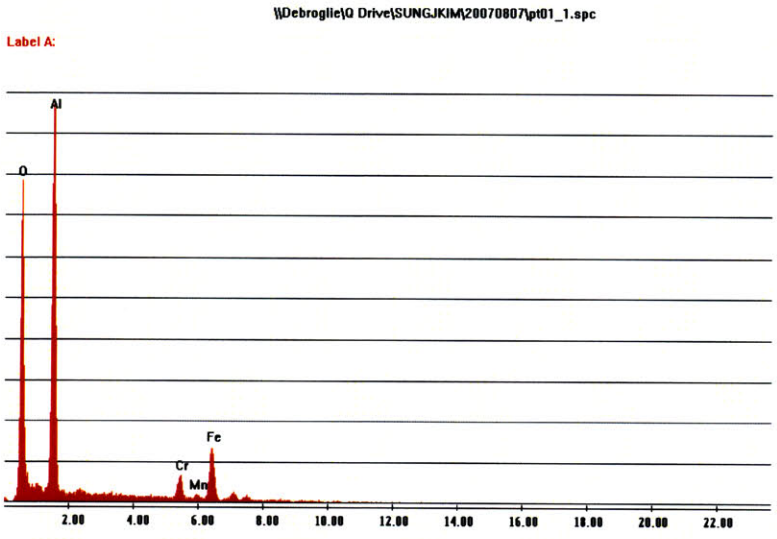

(b)

Figure 5-8 (a) SEM picture and (b) EDS spectrum of stainless steel test heater boiled in 0.01 %vol. alumina nanofluids at G=2000 kg/m^{2}s

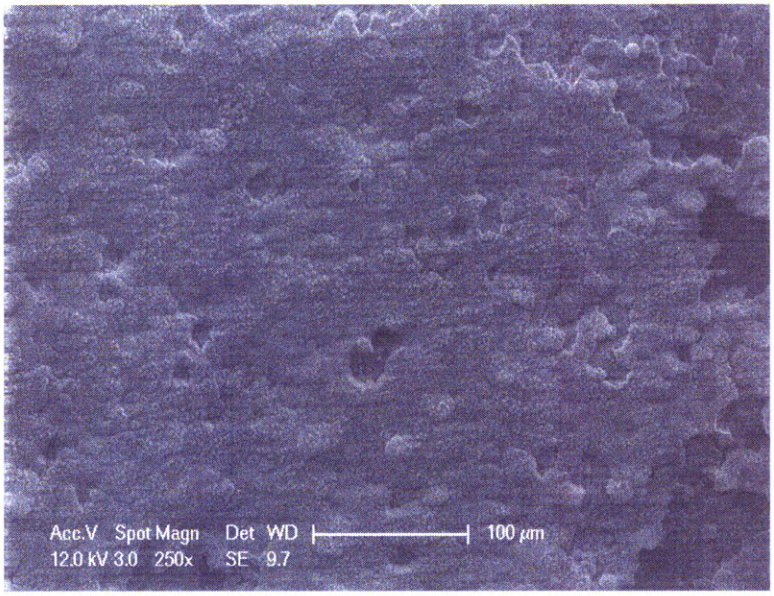

(a)

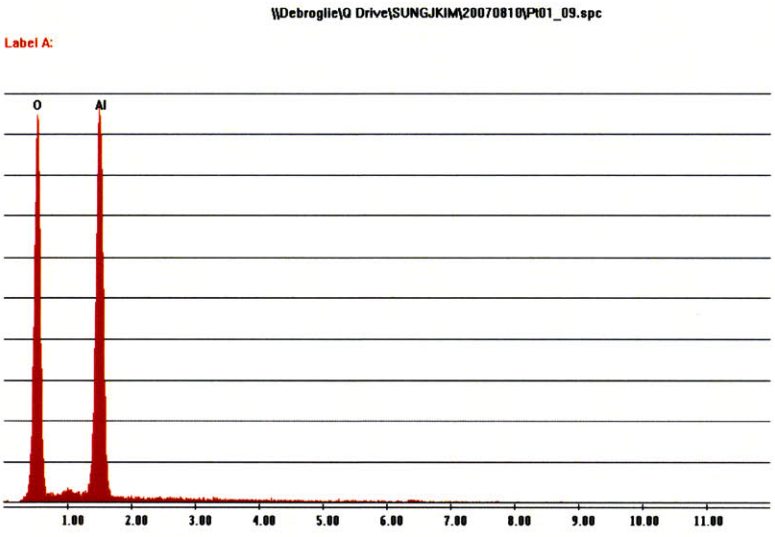

Figure 5-9 (a) SEM picture and (b) EDS spectrum of stainless steel test heater boiled in 0.01 %vol. alumina nanofluids at G=2500 kg/m^{2}s

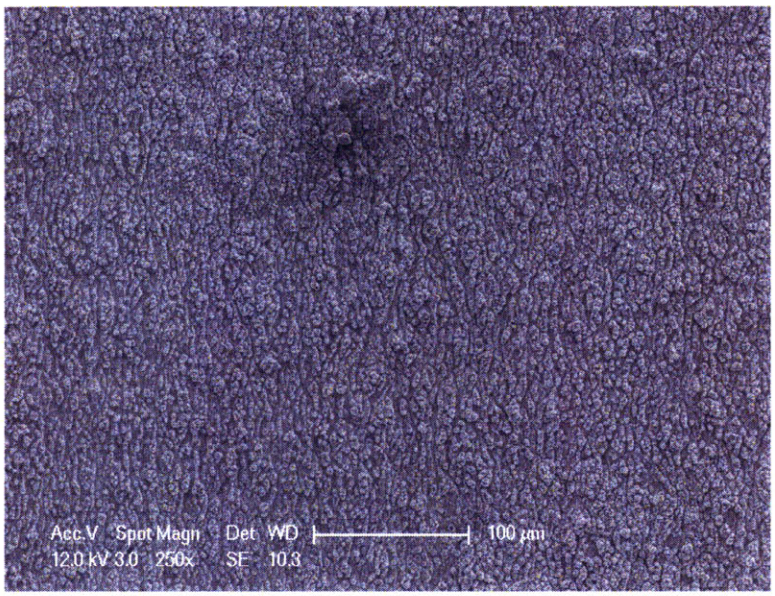

(a)

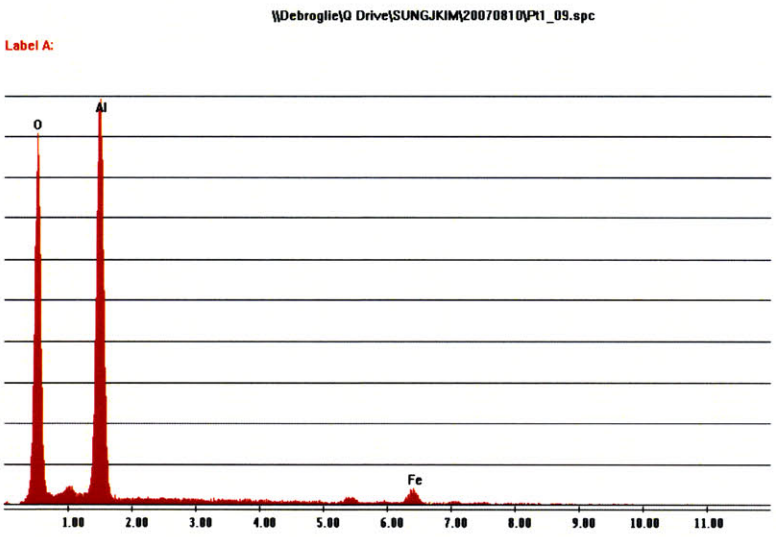

(b)

Figure 5-10 (a) SEM picture and (b) EDS spectrum of stainless steel test heater boiled in 0.1 %vol. alumina nanofluids at G=1500 kg/m^{2}s

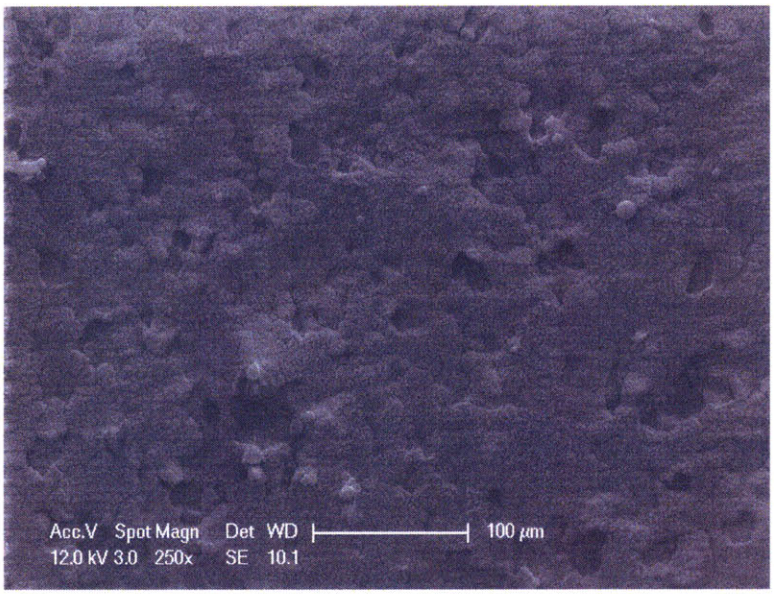

(a)

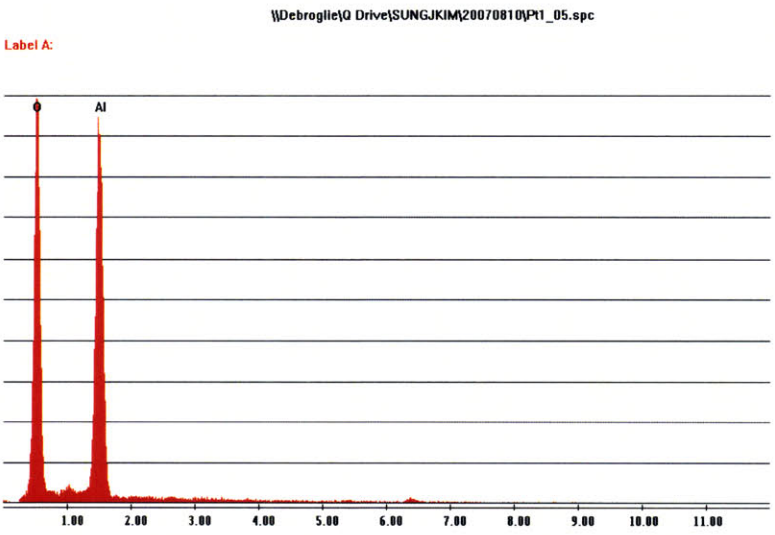

(b)

Figure 5-11 (a) SEM picture and (b) EDS spectrum of stainless steel test heater boiled in 0.1 %vol. alumina nanofluids at G=2000 kg/m^{2}s

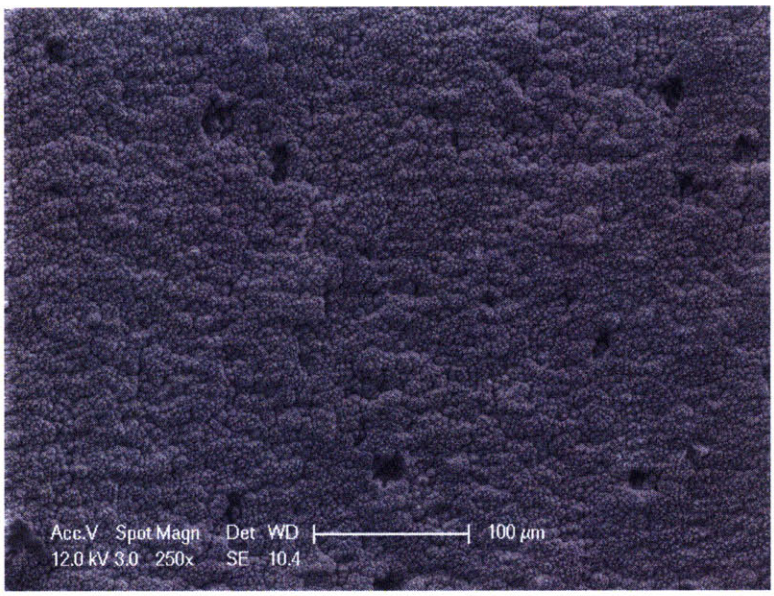

(a)

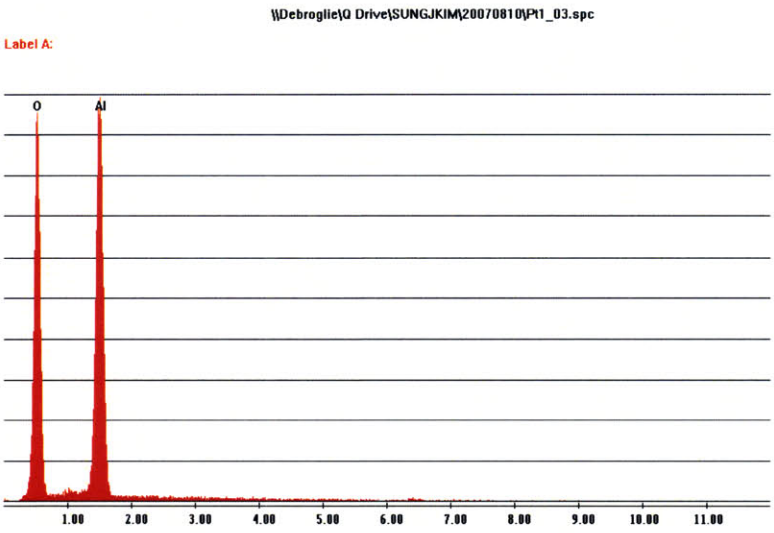

(b)

Figure 5-12 (a) SEM picture and (b) EDS spectrum of stainless steel test heater boiled in 0.1 %vol. alumina nanofluids at G=2500 kg/m^{2}s

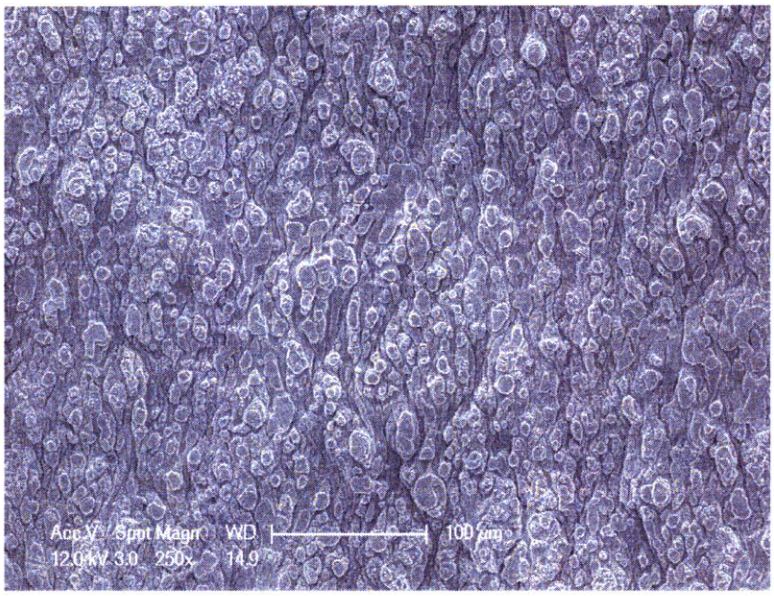

(a)

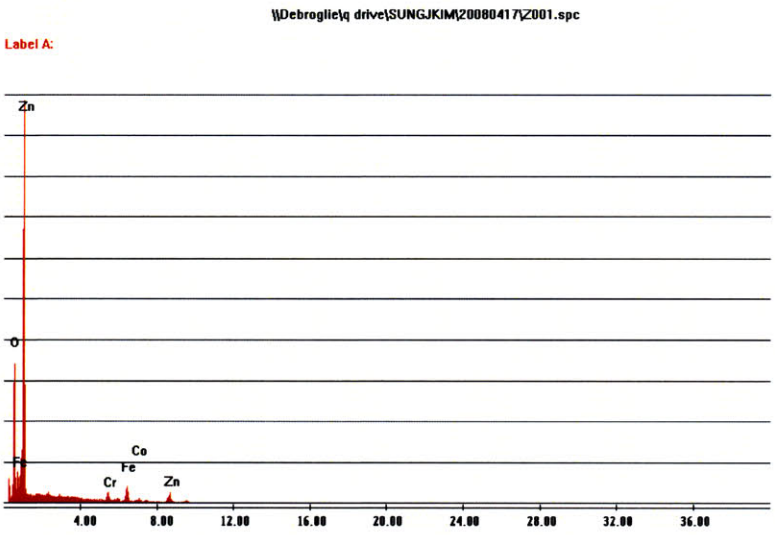

(b)

Figure 5-13 (a) SEM picture and (b) EDS spectrum of stainless steel test heater boiled in 0.001 %vol. zinc oxide nanofluid at G=2500 kg/m^{2}s

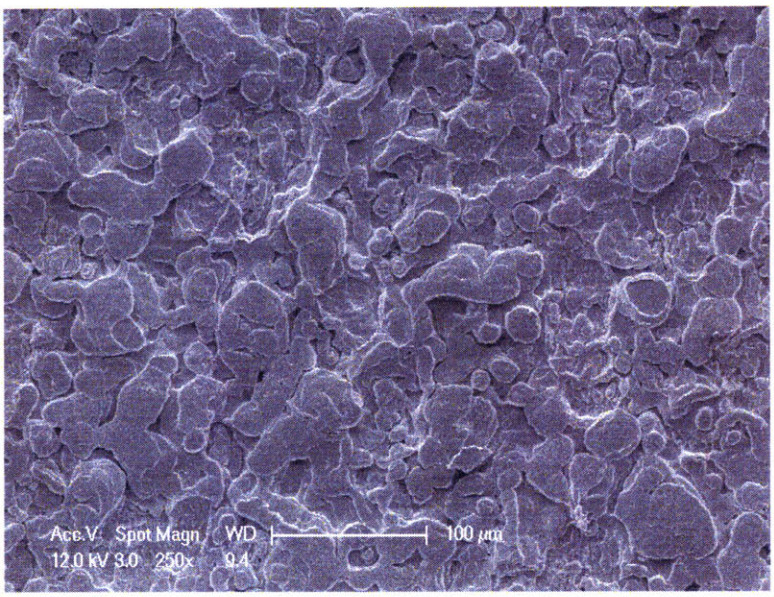

(a)

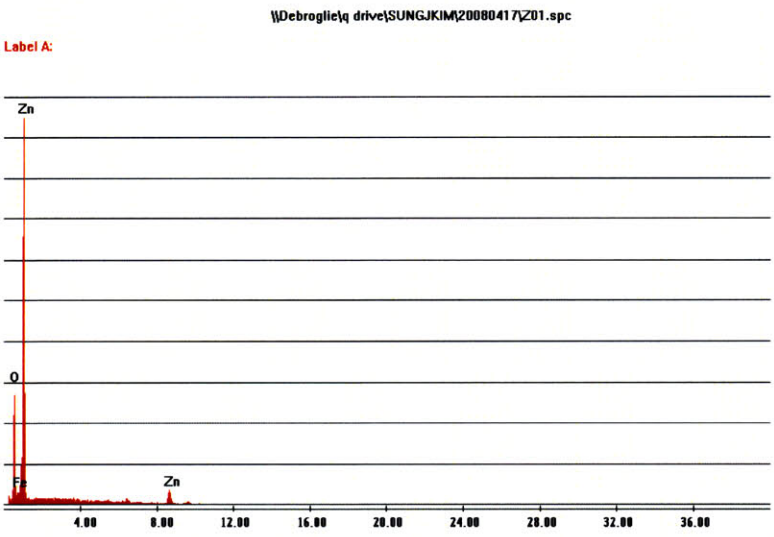

(b)

Figure 5-14 (a) SEM picture and (b) EDS spectrum of stainless steel test heater boiled in 0.01 %vol. zinc oxide nanofluid at G=2500 kg/m^{2}s

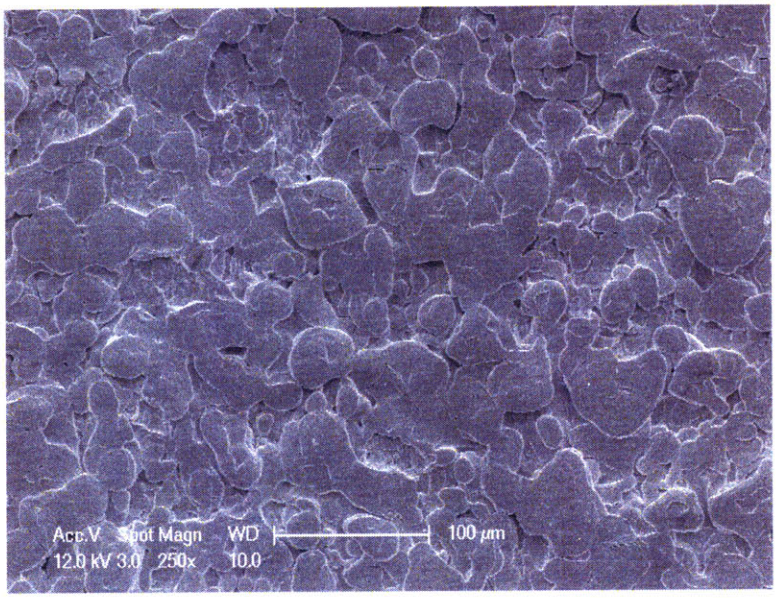

(a)

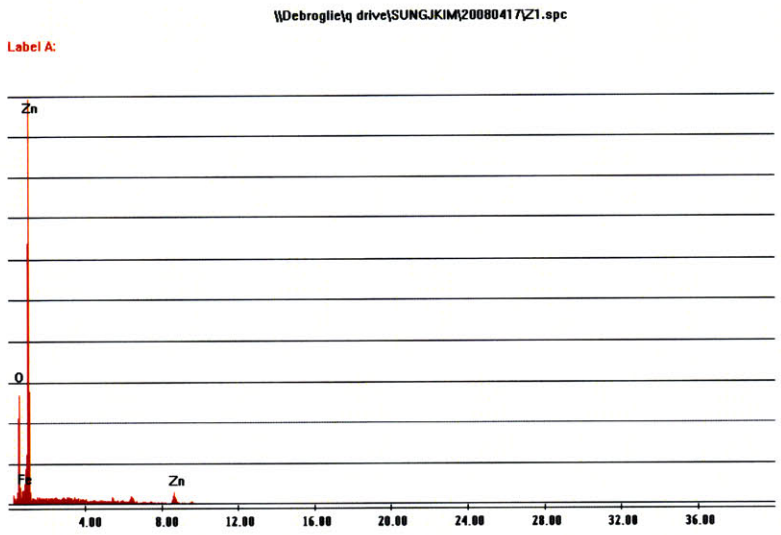

(b)

Figure 5-15 (a) SEM picture and (b) EDS spectrum of stainless steel test heater boiled in 0.1 %vol. zinc oxide nanofluid at G=2500 kg/m^{2}s

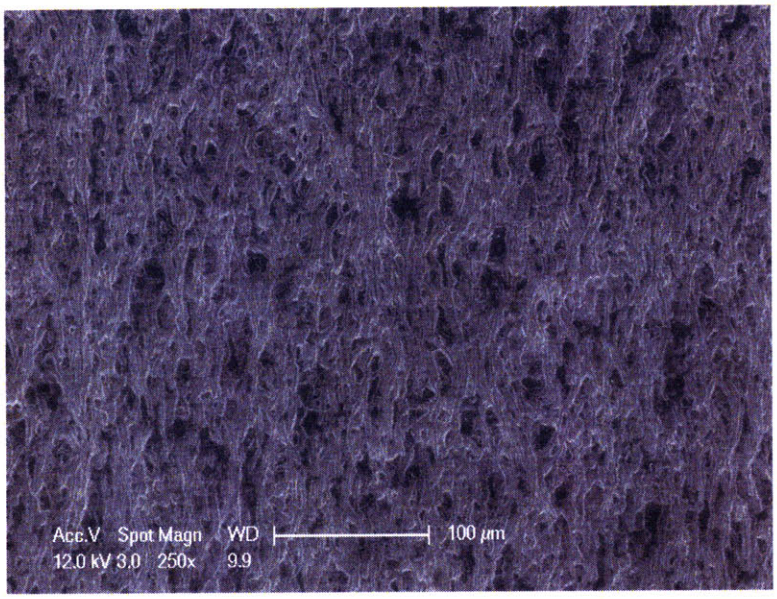

(a)

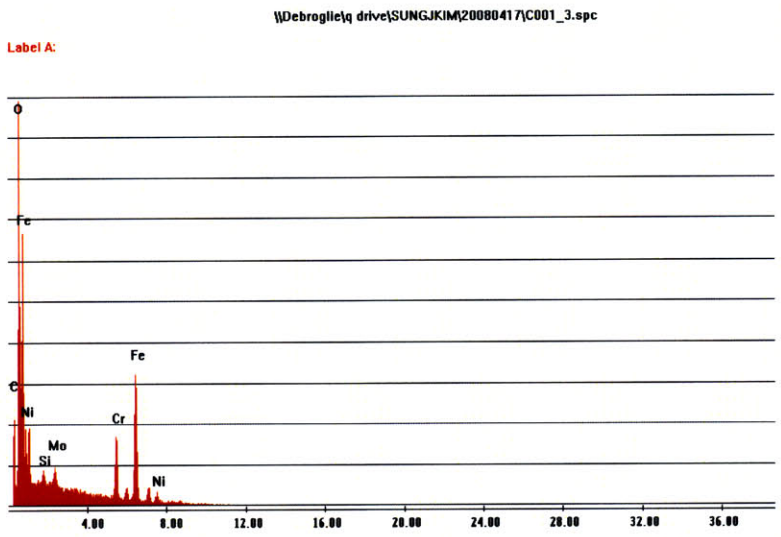

(b)

Figure 5-16 (a) SEM picture and (b) EDS spectrum of stainless steel test heater boiled in 0.001 %vol. diamond nanofluid at G=2500 kg/m^{2}s

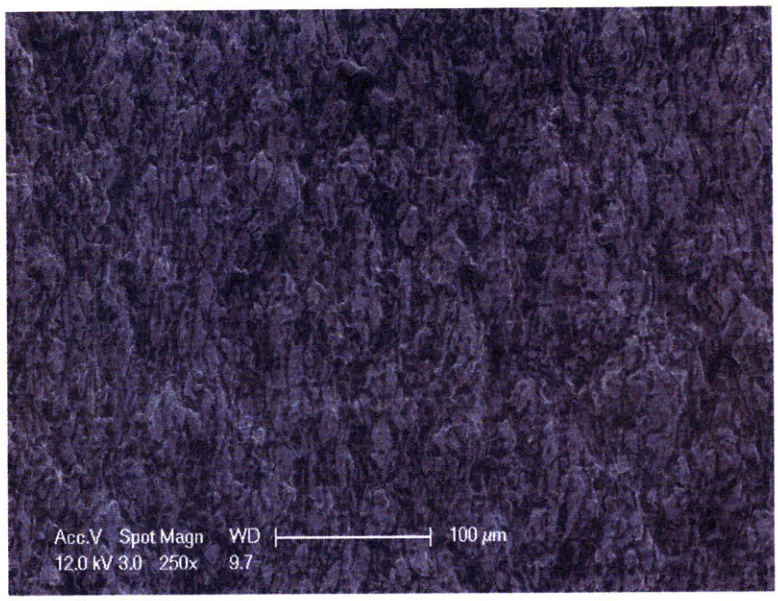

(a)

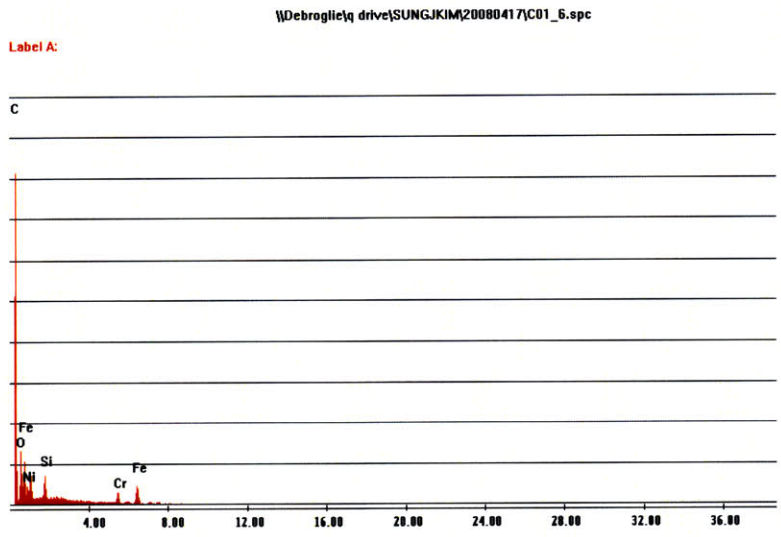

(b)

Figure 5-17 (a) SEM picture and (b) EDS spectrum of stainless steel test heater boiled in 0.01 %vol. diamond nanofluid at G=2500 kg/m^{2}s

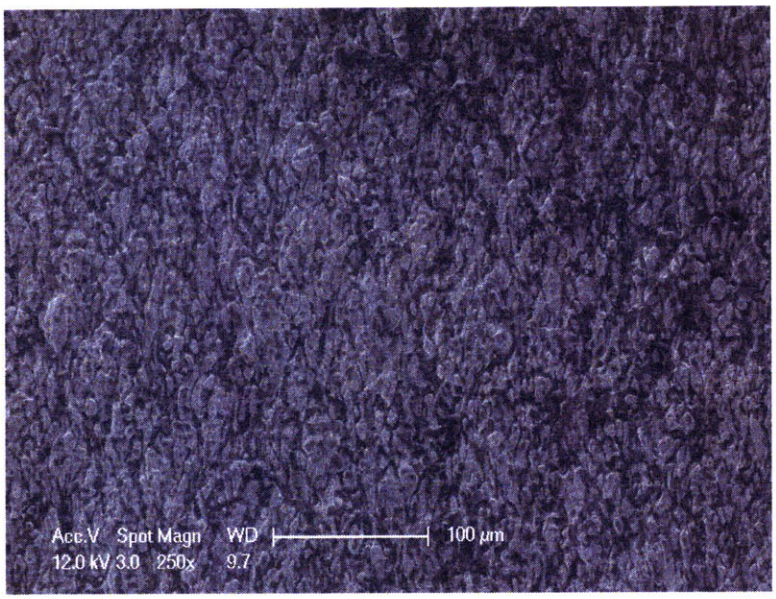

(a)

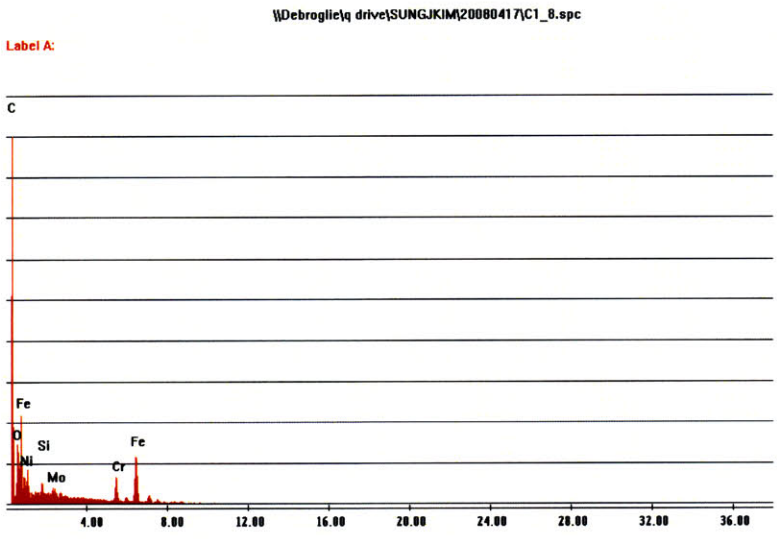

(b)

Figure 5-18 (a) SEM picture and (b) EDS spectrum of stainless steel test heater boiled in 0.1 %vol. diamond nanofluid at G=2500 kg/m^{2}s

5.1.2 Interpretation of SEM Pictures

A more detailed discussion of the morphology changes brought about by nanoparticle deposition is presented here. Figs. 5-2 and 3 clearly show that the surface of the as-purchased heater is clean, and so is the surface boiled in pure water. On the other hand, Figs. 5-4 to 18 indicate the precipitation of a substantial amount of nanoparticles on the heater surface at all nanoparticle concentrations, forming a layer of aggregated particles. It is of interest to observe that some morphological differences are revealed by the SEM pictures with respect to the nanoparticle material and its concentration and, also, the mass flux.

5.1.2.1 Mass flux and concentration effects on porous layer formation of alumina nanoparticles

As shown in Chapter 4, with all three alumina nanoparticle concentrations, no CHF enhancement was achieved at mass flux of G=1500 kg/m^{2}s. Interestingly, a certain trend is found in the SEM images of heater coupons boiled with test fluids at such mass flux. Figs. 5-2a and 3a show the axial peak-and-valley surface morphology of the test coupons as-received and boiled in pure water, respectively. Figs. 5-4a, 7a, and 10a also show the similar morphology developed in one-dimension (along the flow direction), which is now created by the alumina nanoparticle deposition. Figs. 5-2b and 3b confirm that the major components of the stainless steel grade 316 heater are Fe, Cr, Mo, and Ni, as expected. Figs. 5-4b to 12b also show two large peaks correspond to aluminum and oxygen, supporting that the layer is made of aluminum oxide (alumina). Elements of Fe and Cr also appear, suggesting that the thickness of the nanoparticles deposition layer did not completely cover the substrate materials.

It is recalled that significant CHF enhancement was achieved beyond G=1500 kg/m^{2}s. Figs. 5-8a and 9a and 5-11a and 12a show that, as the mass flux increases, the porous layer tends to become more uniform, thicker and less oriented along the flow direction. To a lesser extent, as the concentration increases, a similar trend is observed. Unlike the heater coupons boiled in alumina and zinc oxide nanofluids, the heater coupons boiled in diamond nanofluids have EDS peaks corresponding to the element of stainless steel grade 316, as shown in Figs. 5-16b to 18b, which suggests that less uniform nanoparticles deposition occurs with diamond nanofluids.

5.1.2.2 Nanoparticle materials effect on the porous layer formation

Use of different nanoparticle materials tends to change the deposition patterns significantly. Such changes are found in the representative SEM pictures of Figs. 5-12, 15, and 18 for the test coupons boiled in 0.1 %vol. alumina, zinc oxide, and diamond nanofluids at G=2500 kg/m^{2}s, respectively. In all cases, aggregates of nanoparticles are found to form rather uniformly but the size of such aggregates differs from one nanoparticle material to another. It is observed that alumina and zinc oxide show the finest and largest circular aggregates, while the pattern of the aggregation is somewhat less regular for diamond.

These observations are important because they may suggest that CHF enhancement, which is seen mostly at high mass flux and more prominently with alumina and zinc oxide vs diamond nanofluids, can be obtained provided that a uniform and relatively-thick nanoparticle deposition layer is created on the surface.

5.2 Confocal Microscopy

5.2.1 Surface roughness and area measurements

Two surface parameters that can significantly affect boiling are surface roughness, which is related to the number of micro-cavities available for bubble nucleation, and surface area change, which is related to the wettability of the surface. Both parameters can be changed by the presence of the nanoparticles on the surface, as shown in previous papers (Kim et al. 2006b, Kim et al. 2007, Kim, 2007). Therefore it was decided to measure the surface roughness and area for the test section coupons. This was done by confocal microscopy analysis at multiple locations on each coupon. The confocal microscope scans a laser beam over the sample's surface, creating a high resolution quantitative three dimensional image of the surface. Detailed principle of the confocal microscopy is described in Claxton et al.'s report (http://www.olympusfluoview.com/theory/LSCMIntro.pdf). Coherent light is emitted by the laser system and passes through the light source pinhole aperture. The light is reflected by the dichromatic mirror and reaches the confocal plane (at specified x and y dimension) of the specimen and bounces back to the dichromatic mirror. This secondary light that is only on focus passes through the detector pinhole aperture. This on-focus light density is then transmitted and processed through the computer. This scanning process is repeated at multiple focal planes of z dimension (user can define the number of focal planes) and corresponding light density is processed to construct the three-dimensional image. In our microscopy, Olympus LEXT OLS3100 was used to obtain the confocal microscopy images. The smallest achievable scanning area (xy) resolution is 128×128 μm^2 and respective minimum resolution is 0.12 μm. The maximum height (z) measurement range is 10 mm and minimum movement resolution is 0.01 μm (10 nm).

The numeric values of this surface analysis are shown in Table 5-1 for all tests. Table 5-1 also shows the surface data for the as-purchased test section for comparison. The results are, in effect, best seen in Figs. 5-19 to 22. Figs. 5-19 and 20 show the ratio of the true surface area to the projected surface area with respect to the the nanoparticle concentration and mass flux, respectively. Note that each marked datum is an averaged value from the multiple confocal scans, with which the statistical error of standard deviation was estimated and its respective value was represented as y-axis error in the figures. For the surface area ratio, the maximum standard deviation of 0.467 was estimated for multiple confocal scans of heater coupon boiled in 0.1 % alumina nanofluid at G=2500 kg/m^{2}s. Regarding the surface roughness data, the estimated maximum standard deviation is 1.385 μm for the heater coupon boiled in 0.1 % vol. alumina nanofluid at G=2000 kg/m^{2}s. In Fig. 5-19, the heater coupons boiled in three different concentrations of alumina and zinc oxide nanofluids indicate the tendency of surface area increase compared to water-boiled coupons. Some reduction of surface area is observed in the heater coupons boiled in diamond nanofluids. In particular, no systematic trends of surface area change are observed with respect to the nanoparticle concentration. Fig. 5-20 is more interesting as alumina nanofluids data at all concentrations show the tendency of the surface area increase compared to water case. But, the dependency on the mass flux is not consistent for all cases. For the surface roughness, its variations with nanoparticle concentration and mass flux are shown in Figs. 5-21 and 22, respectively. In Fig. 5-21, the surface roughness of alumina and diamond nanofluids shows the decrease according to the nanoparticle concentration. In case of zinc-oxide nanofluis boiling, the surface roughness increases with respect to the nanoparticle concentration. In Fig. 5-22, heater coupons boiled in alumina nanofluids at all concentrations show the insignificant change of the surface roughness as compared to the water-boiled coupons. The dependency of surface roughness change on the mass flux is not systematic as well. In particular, it can be seen that the surface roughness, R_a, ranges from 1.5 to 3 μm and its average value is about 2 μm for all cases (as-purchased, water-boiled and nanofluid-boiled coupons).

In conclusion, no systematic correlation is found to exist with respect to the CHF enhancement and HTC. Therefore, it must be concluded that the observed boiling characteristics of nanofluids do not come from significant changes in the surface roughness and area.

Table 5-1 Surface roughness and area data for stainless steel coupons from the loop test section after flow boiling tests

Test section surface condition	(a) Projected surface area (μm^2)	(b) Actual surface area (μm^2)	Ratio (b) / (a)	Roughness* *Ra* (μm)
As-received	51,077	71,619	1.40	1.825
DI water (*G*=1500)	53,232	77,688	1.46	2.510
DI water (*G*=2000)	51,060	74,379	1.46	2.193
DI water (*G*=2500)	53,206	73,731	1.39	2.154
0.001 %v alumina NF (*G*=1500)	53,292	88,707	1.66	2.307
0.001 %v alumina NF (*G*=2000)	52,015	85,056	1.63	2.292
0.001 %v alumina NF (*G*=2500)	51,010	81,114	1.59	2.285
0.01 %v alumina NF (*G*=1500)	53,206	82,152	1.54	1.897
0.01 %v alumina NF (*G*=2000)	53,147	99,409	1.87	1.804
0.01 %v alumina NF (*G*=2500)	53,021	99,809	1.88	1.858
0.1 %v alumina NF (*G*=1500)	53,325	97,799	1.83	2.064
0.1 %v alumina NF (*G*=2000)	51,060	79,353	1.55	2.772
0.1 %v alumina NF (*G*=2500)	53,169	133,734	2.52	1.716
0.001 %v zinc oxide NF (*G*=2500)	53,186	80,473	1.51	2.421
0.01 %v zinc oxide NF (*G*=2500)	53,265	89,097	1.67	3.004
0.1 %v zinc oxide NF (*G*=2500)	53,163	84,848	1.60	2.926
0.001 %v diamond NF (*G*=2500)	53,120	74,836	1.41	2.144
0.01 %v diamond NF (*G*=2500)	53,164	69,017	1.30	1.978
0.1 %v diamond NF (*G*=2500)	53,187	68,157	1.28	1.573

* Surface roughness was measured with confocal microscopy (measurement uncertainty ~0.01 μm)

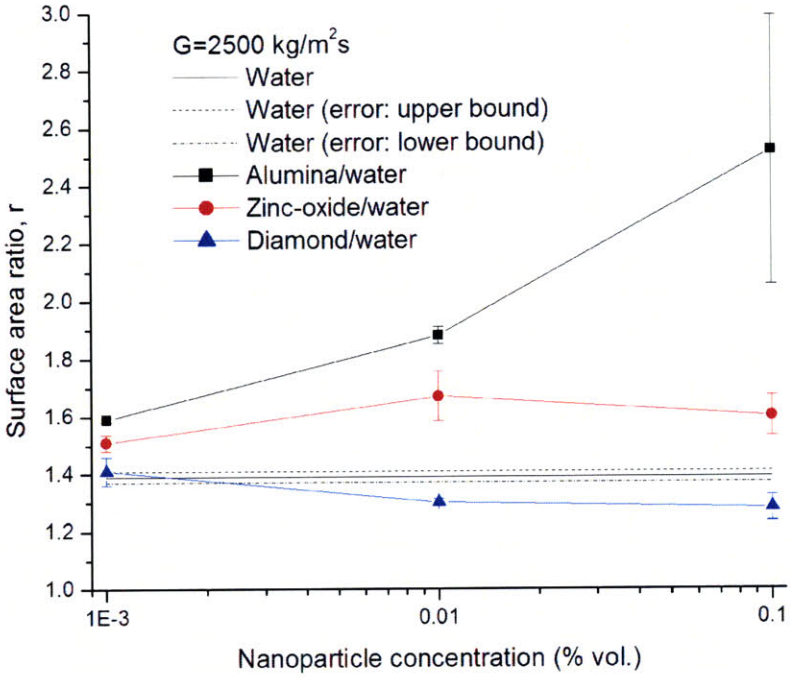

Figure 5-19 Surface area ratio of heater coupons boiled in water and nanofluids at three concentrations at G=2500 kg/m^{2}s

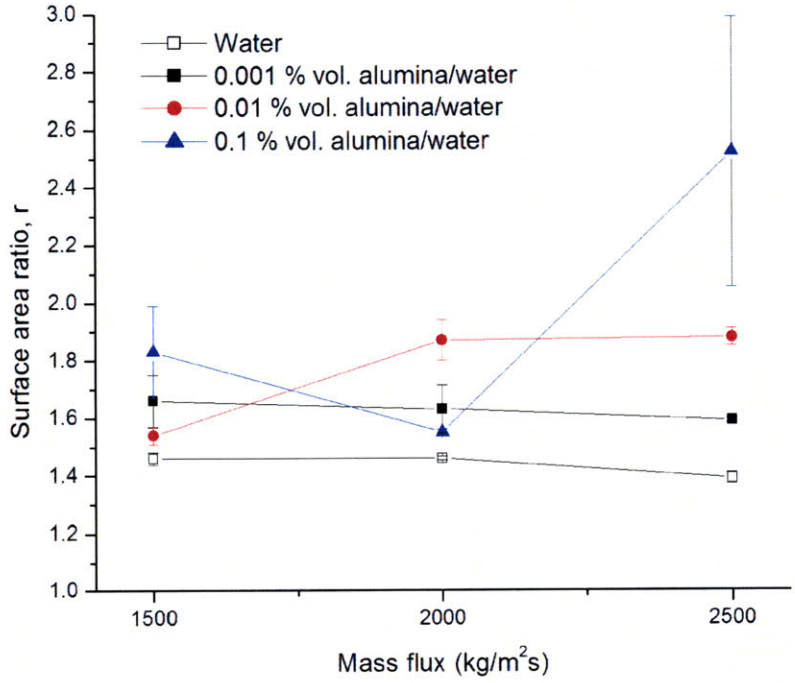

Figure 5-20 Surface area ratio of heater coupons boiled in water and alumina nanofluids at three mass fluxes

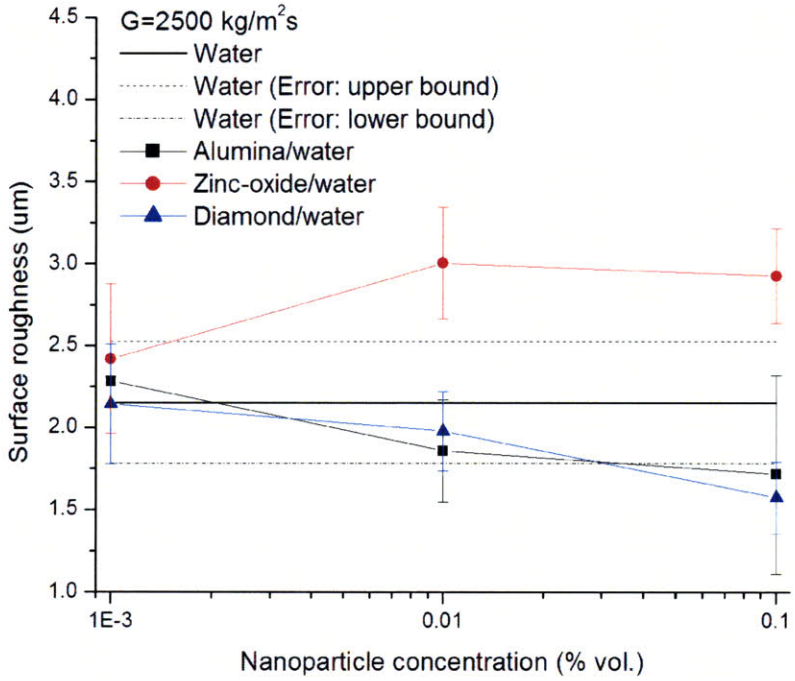

Figure 5-21 Surface roughness of heater coupons boiled in water and nanofluids at three concentrations at G=2500 kg/m^{2}s

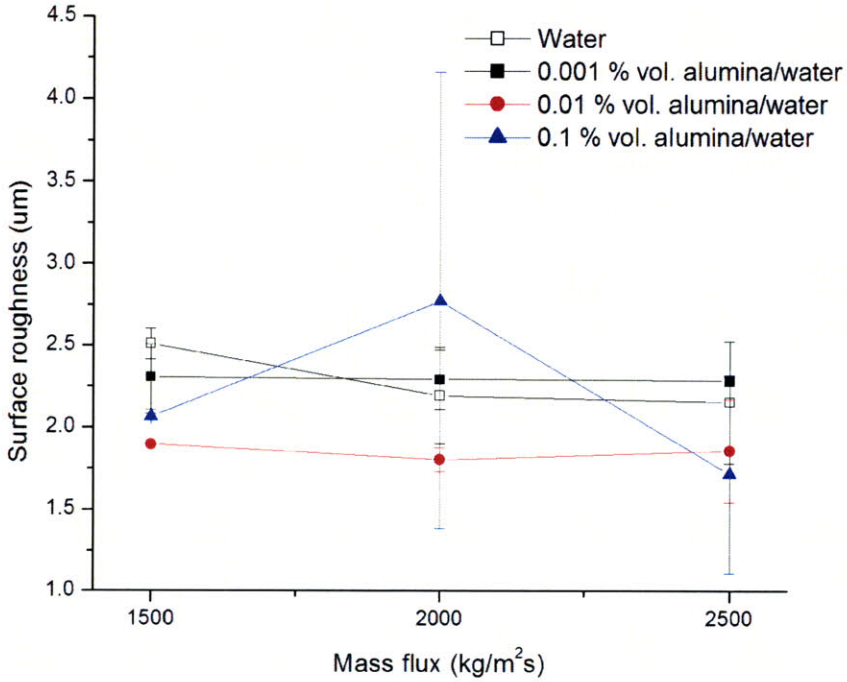

Figure 5-22 Surface roughness of heater coupons boiled in water and alumina nanofluids at three mass fluxes

5.2.2 Three-dimensional images and two-dimensional 8-bit gray images

In this section, representative three-dimensional (3D) and two-dimensional (2D) 8-bit gray confocal images are reported. The 3D confocal images are constructed by the confocal microscopy from a series of 2D images at different elevations. The 3D confocal images supplement the understanding of the surface morphology gained from the SEM images. The 2D 8-bit gray images can be utilized for quantifying of the number of micro-cavities present on the surface, as will be explained in the next section. The representative 3D confocal images are given in Figs. 5-23(a) to 41(a) and the corresponding 2D images are also given in Figs. 5-23b to 41b, respectively.

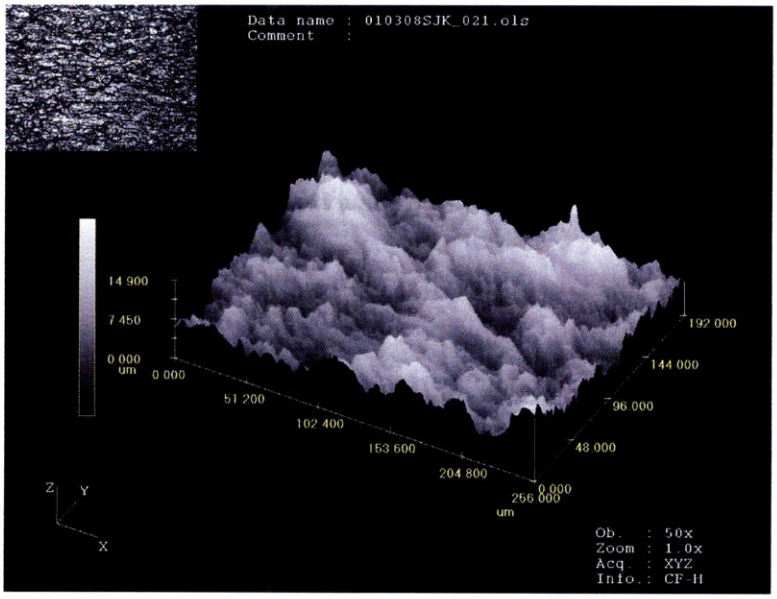

(a)

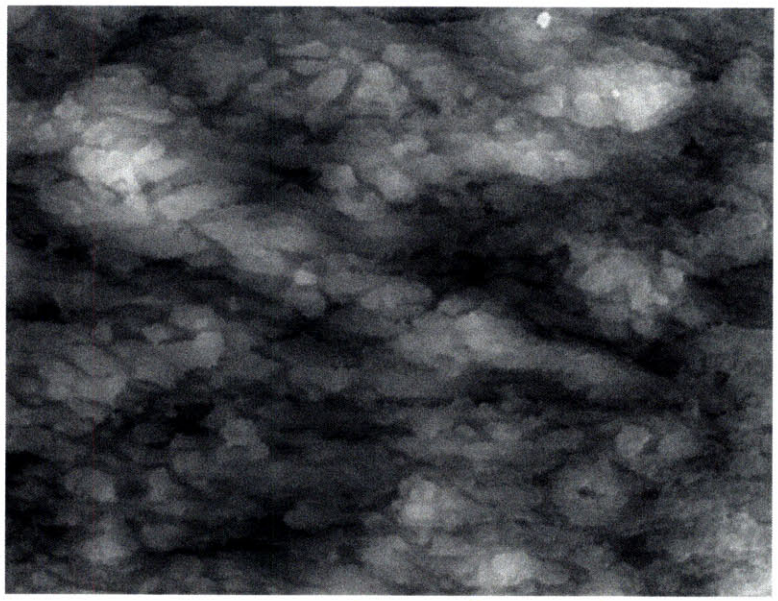

(b)

Figure 5-23 (a) 3D and (b) 2D 8-bit gray confocal images of as-received heater coupon

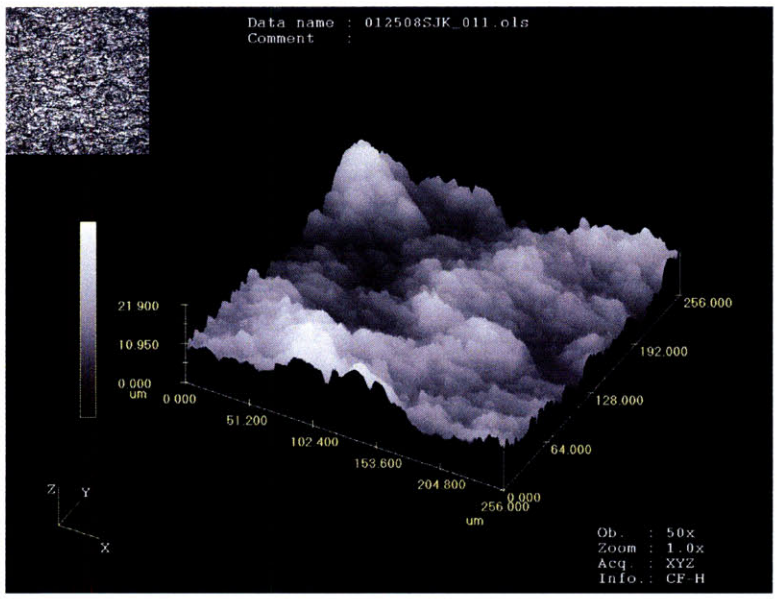

(a)

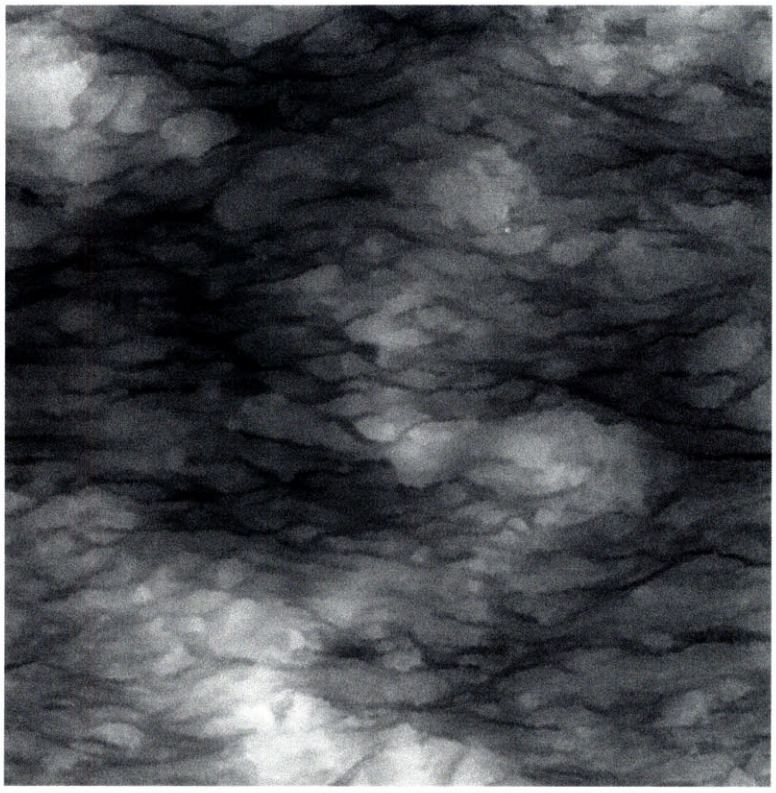

(b)

Figure 5-24 (a) 3D and (b) 2D 8-bit gray confocal images of heater coupon boiled in pure water at G=1500 kg/m^{2}s

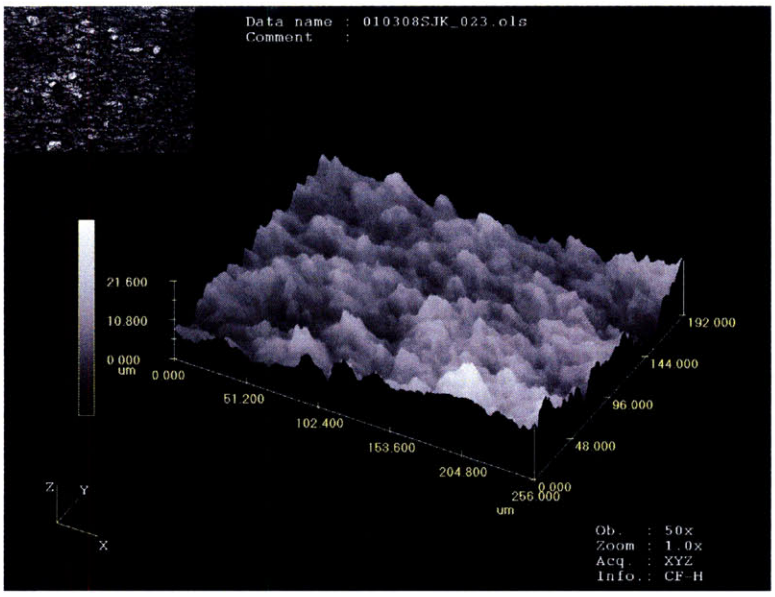

(a)

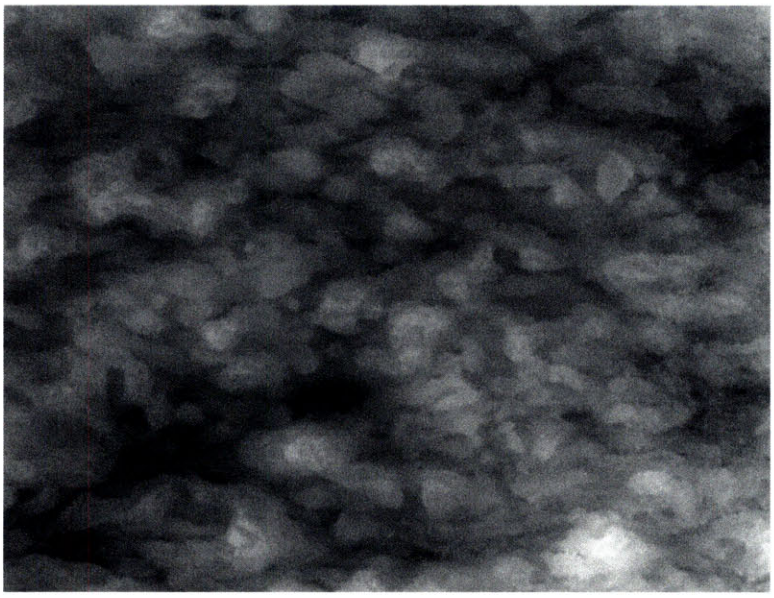

(b)

Figure 5-25 (a) 3D and (b) 2D 8-bit gray confocal images of heater coupon boiled in pure water at G=2000 kg/m^{2}s

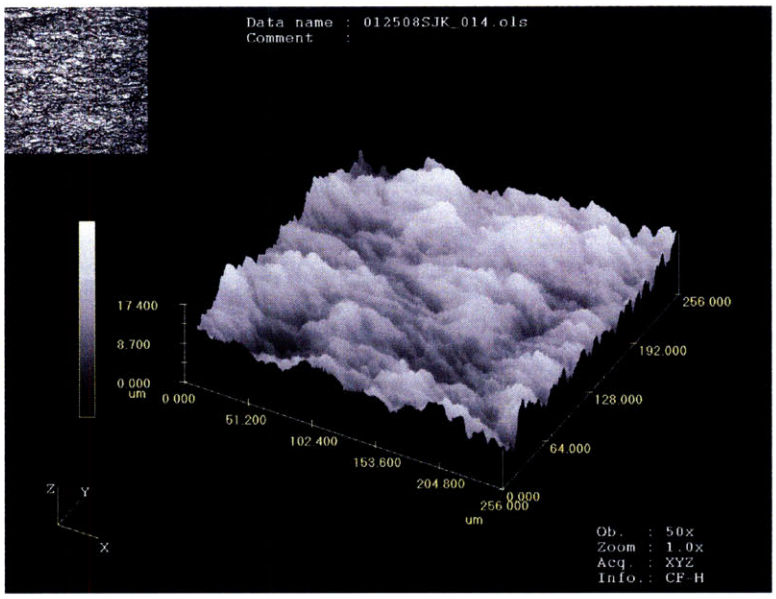

(a)

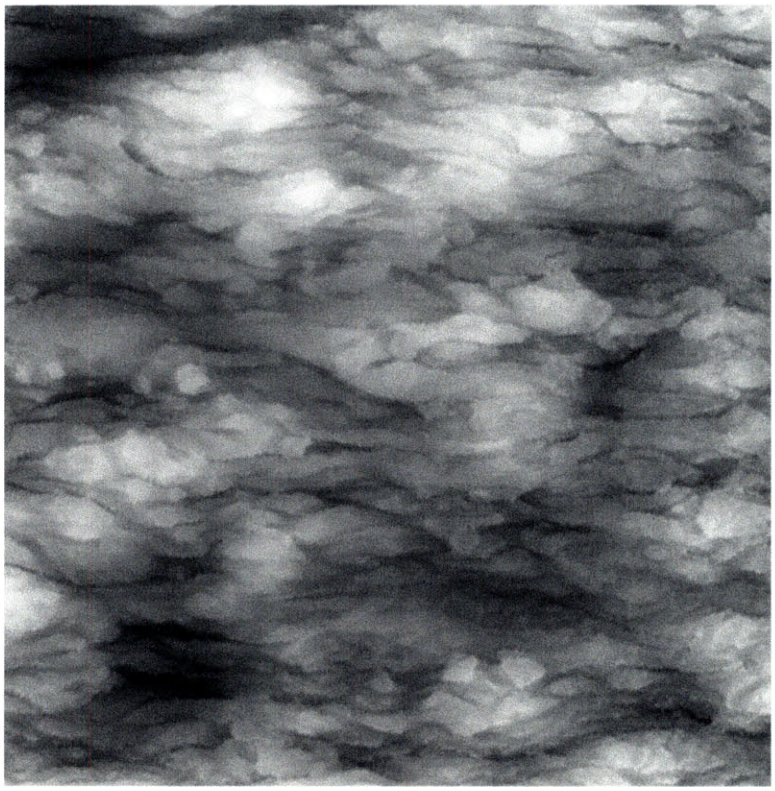

(b)

Figure 5-26 (a) 3D and (b) 2D 8-bit gray confocal images of heater coupon boiled in pure water at G=2500 kg/m^{2}s

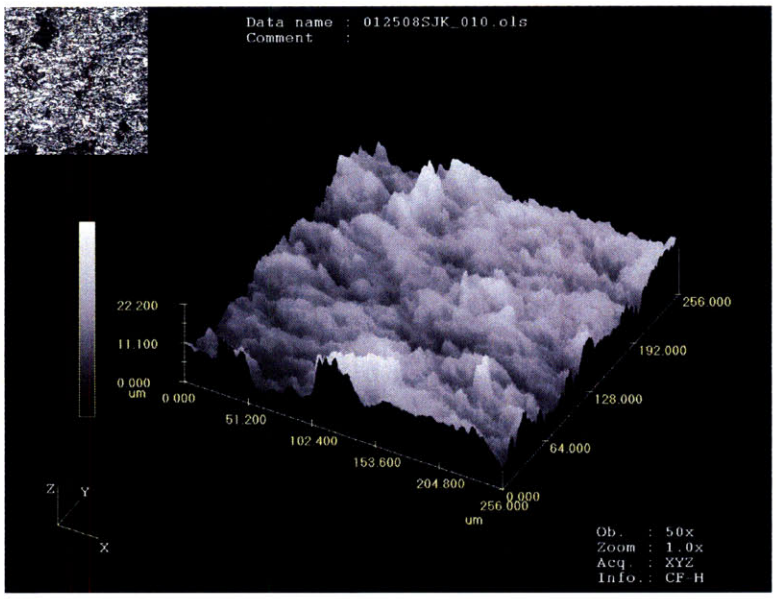

(a)

(b)

Figure 5-27 (a) 3D and (b) 2D 8-bit gray confocal image of heater coupon boiled in 0.001 %vol. alumina nanofluid at G=1500 kg/m^{2}s

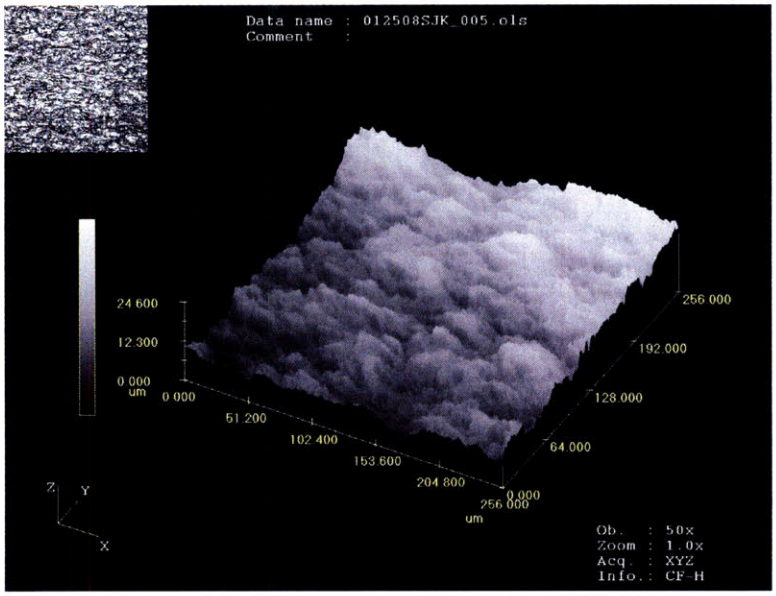

(a)

(b)

Figure 5-28 (a) 3D and (b) 2D 8-bit gray confocal images of heater coupon boiled in 0.001 %vol. alumina nanofluid at G=2000 kg/m^{2}s

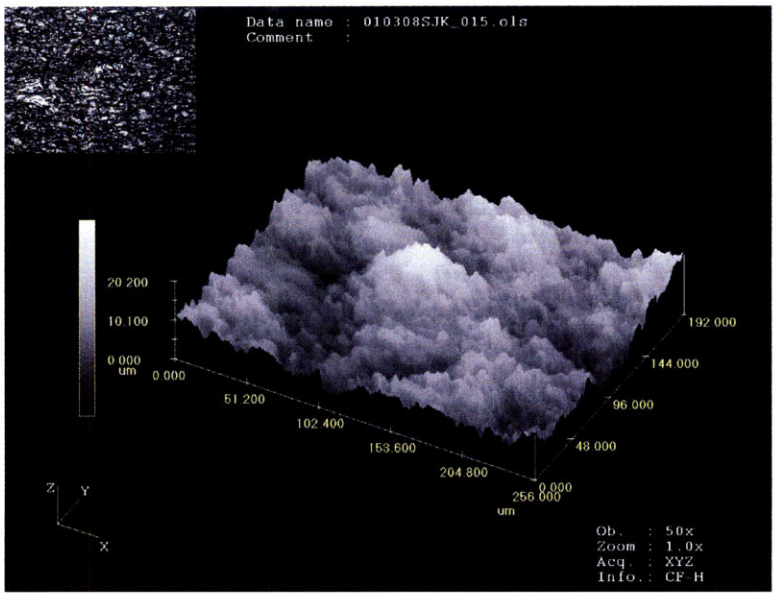

(a)

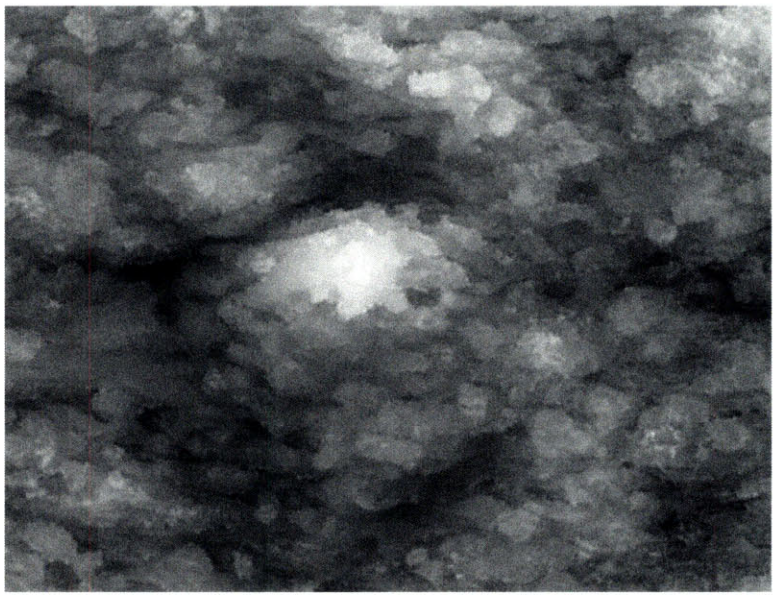

(b)

Figure 5-29 (a) 3D and (b) 2D 8-bit gray confocal images of heater coupon boiled in 0.001 %vol. alumina nanofluid at G=2500 kg/m^{2}s

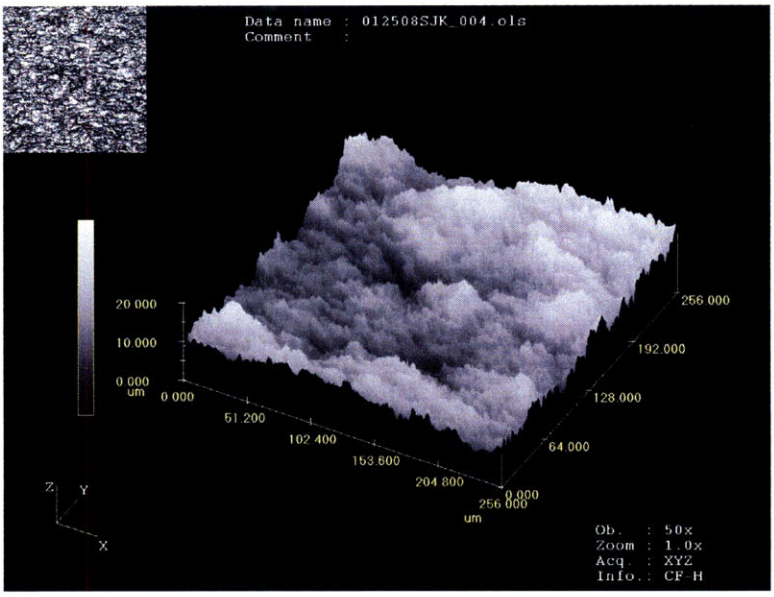

(a)

(b)

Figure 5-30 (a) 3D and (b) 2D 8-bit gray confocal images of heater coupon boiled in 0.01 %vol. alumina nanofluid at G=1500 kg/m^{2}s

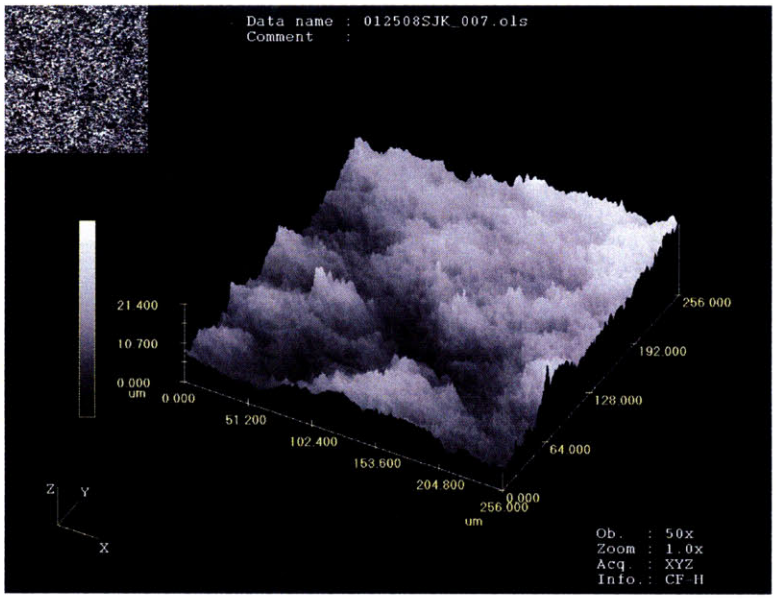

(a)

(b)

Figure 5-31 (a) 3D and (b) 2D 8-bit gray confocal images of heater coupon boiled in 0.01 %vol. alumina nanofluid at G=2000 kg/m^{2}s

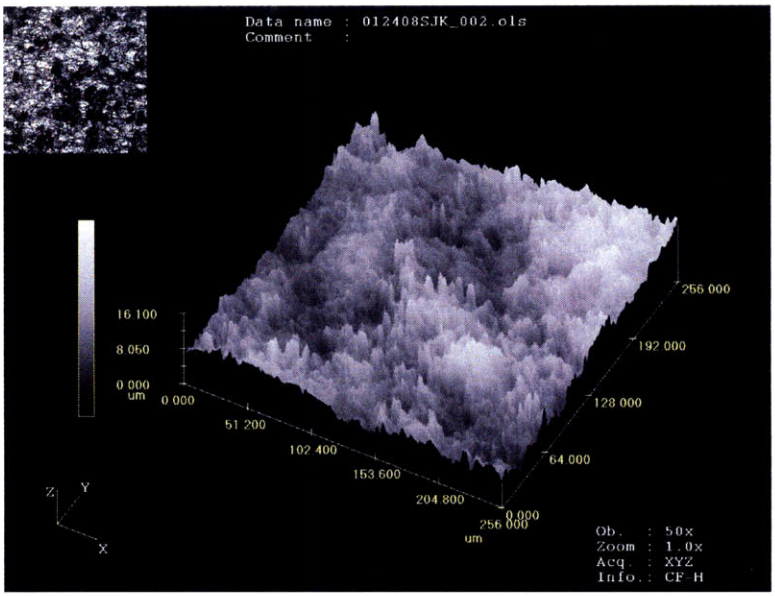

(a)

(b)

Figure 5-32 (a) 3D and (b) 2D 8-bit gray confocal images of heater coupon boiled in 0.01 %vol. alumina nanofluid at G=2500 kg/m^{2}s

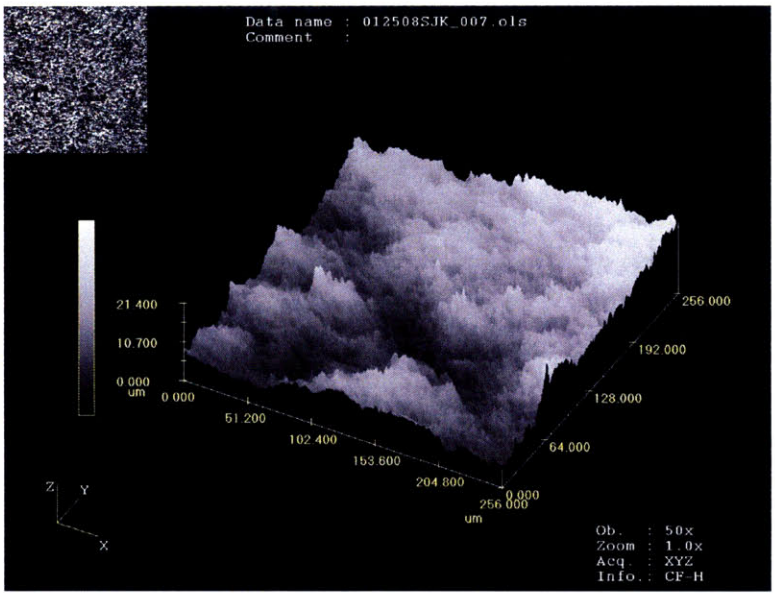

(a)

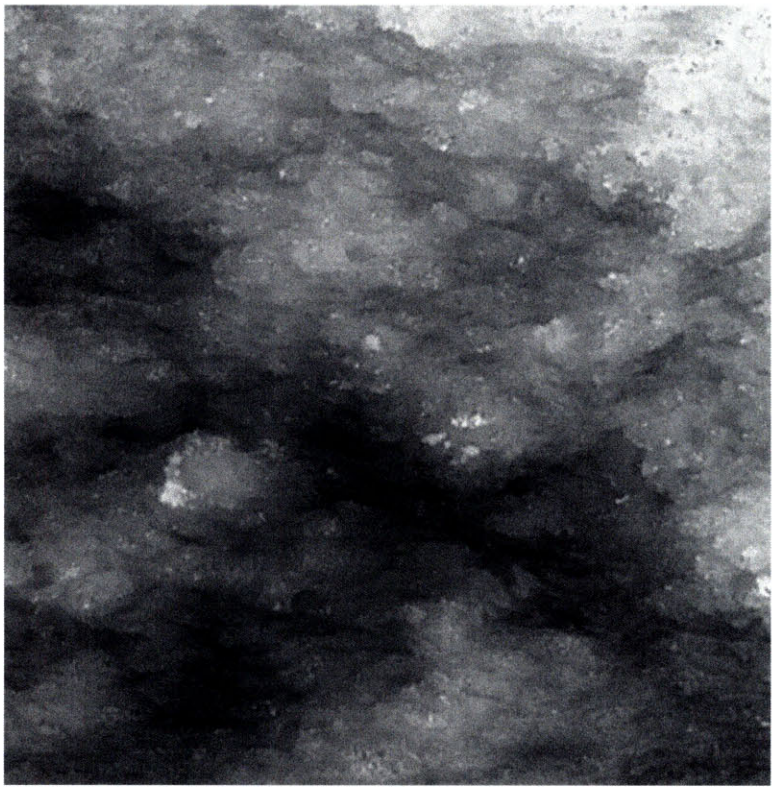

(b)

Figure 5-33 (a) 3D and (b) 2D 8-bit gray confocal images of heater coupon boiled in 0.1 %vol. alumina nanofluid at G=1500 kg/m^{2}s

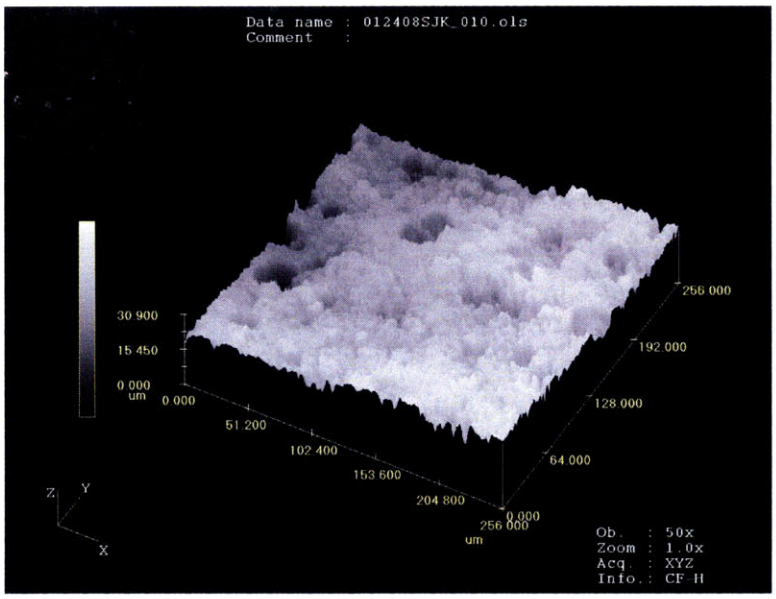

(a)

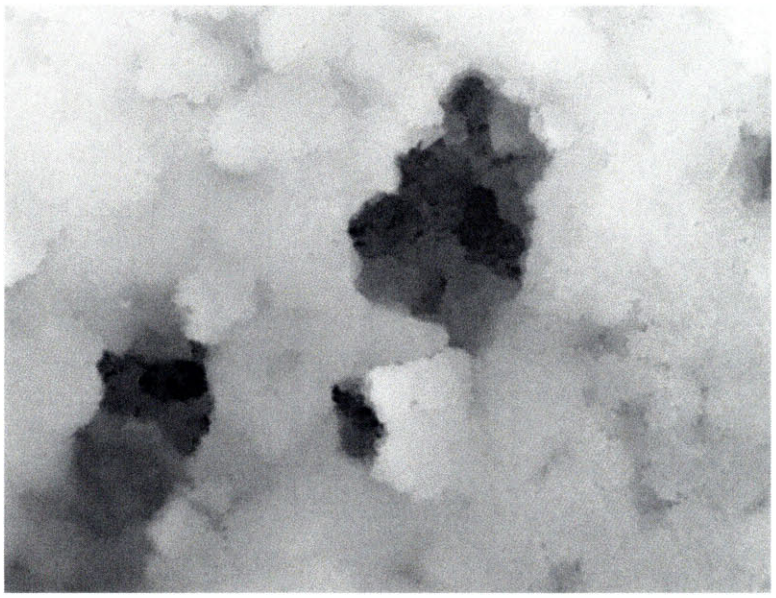

(b)

Figure 5-34 (a) 3D and (b) 2D 8-bit gray confocal image of heater coupon boiled in 0.1 %vol. alumina nanofluid at G=2000 kg/m^{2}s

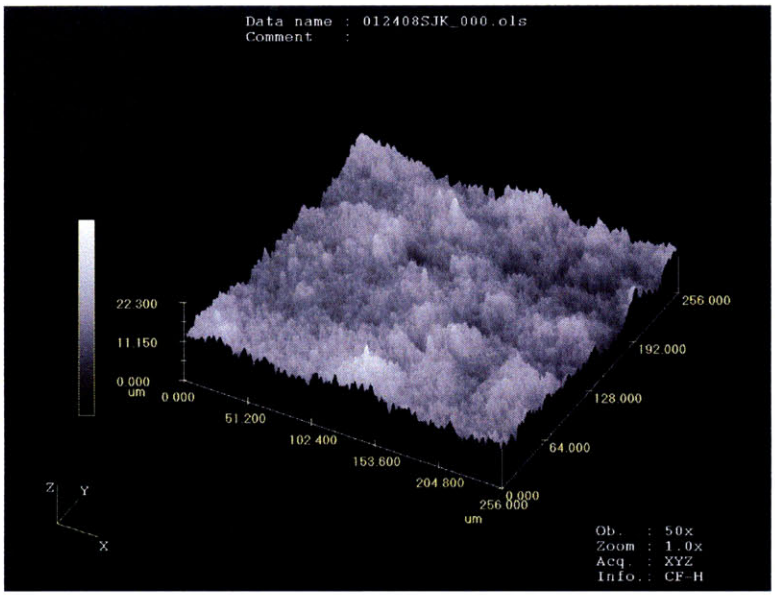

(a)

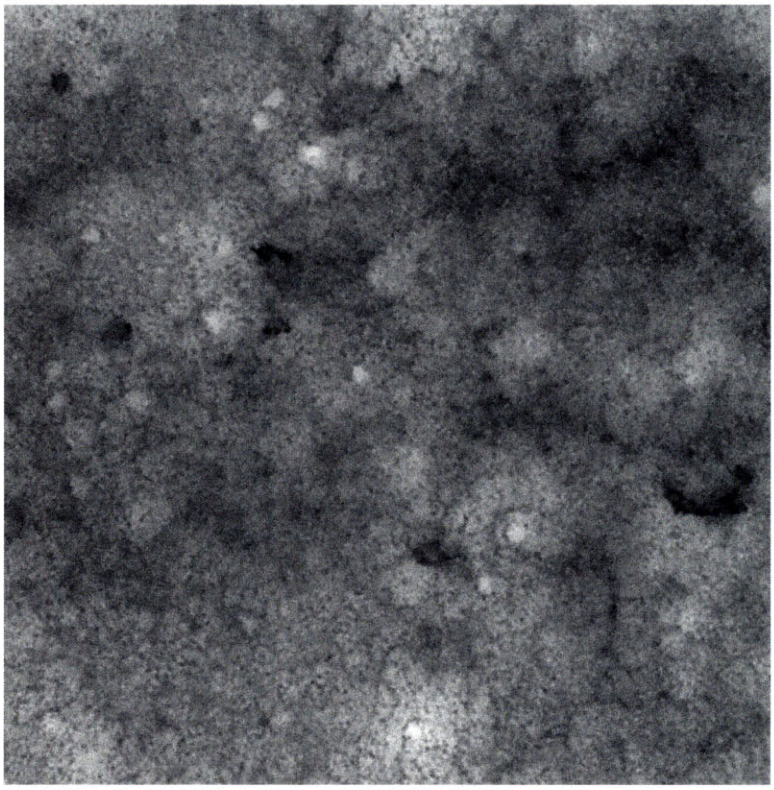

(b)

Figure 5-35 (a) 3D and (b) 2D 8-bit gray confocal images of heater coupon boiled in 0.1 %vol. alumina nanofluid at G=2500 kg/m^{2}s

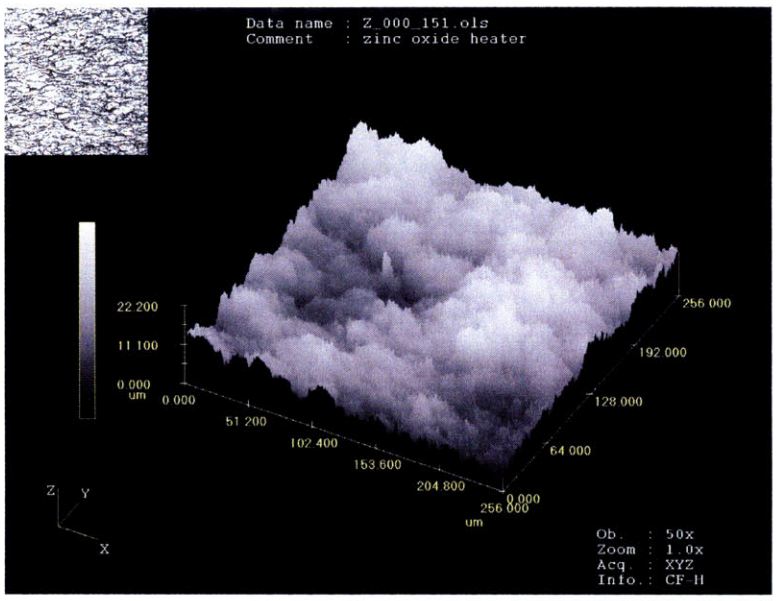

(a)

(b)

Figure 5-36 (a) 3D and (b) 2D 8-bit gray confocal images of heater coupon boiled in 0.001 %vol. zinc oxide nanofluid at G=2500 kg/m^{2}s

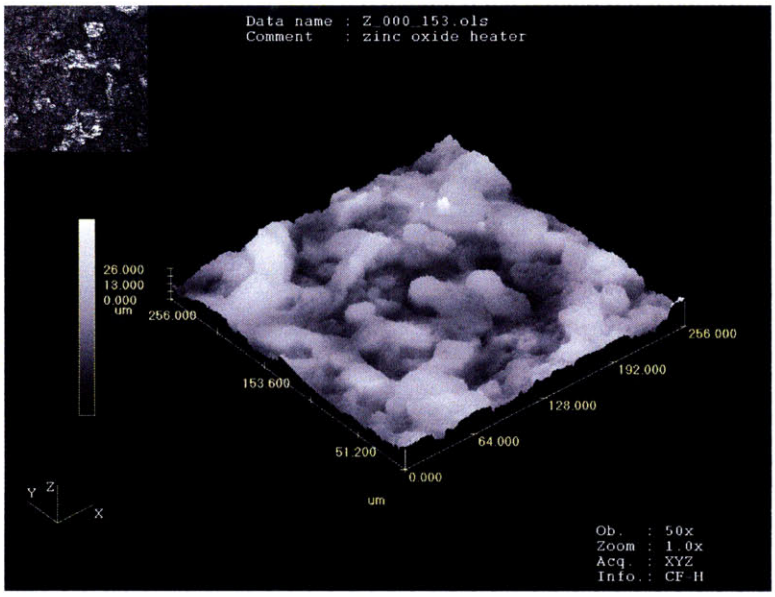

(a)

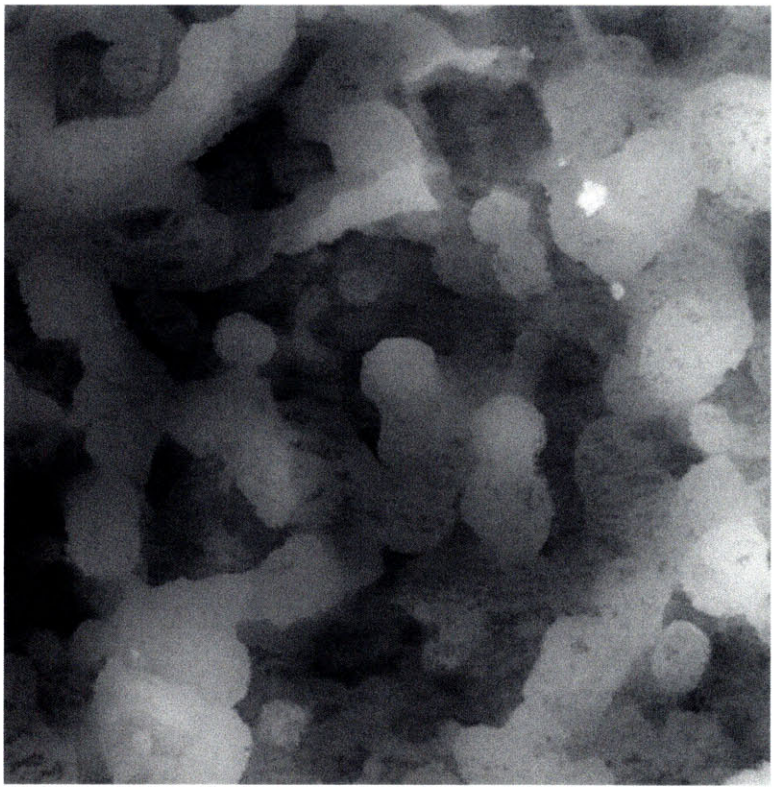

(b)

Figure 5-37 (a) 3D and (b) 2D 8-bit gray confocal images of heater coupon boiled in 0.01 %vol. zinc oxide nanofluid at G=2500 kg/m^{2}s

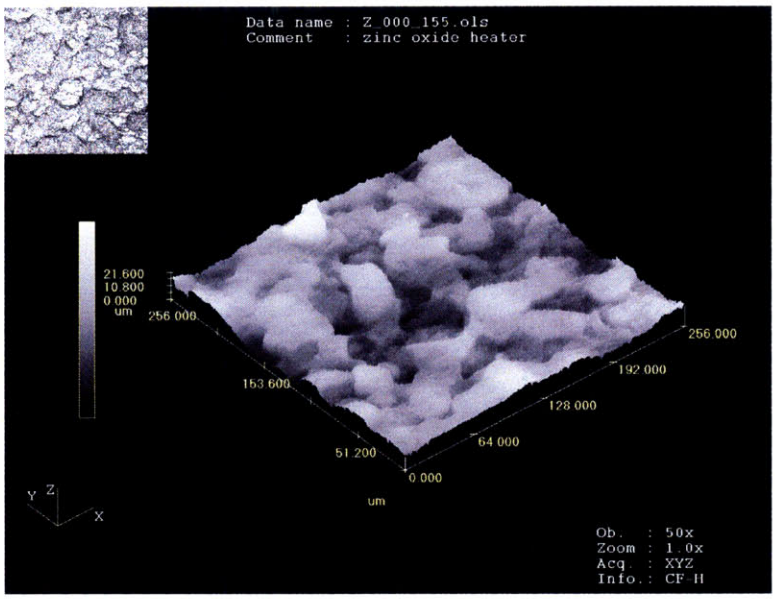

(a)

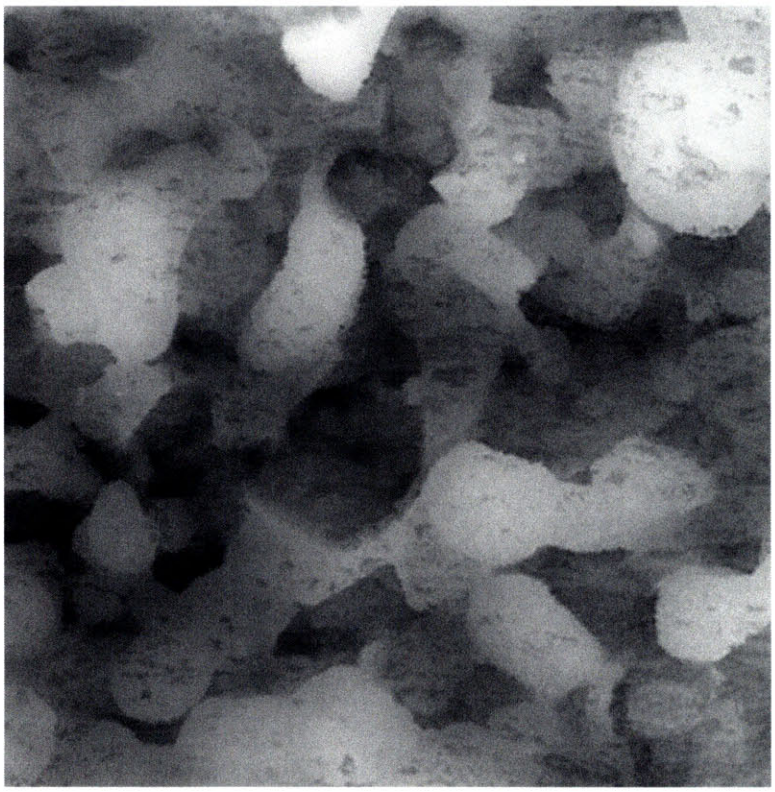

(b)

Figure 5-38 (a) 3D and (b) 2D 8-bit gray confocal images of heater coupon boiled in 0.1 %vol. zinc oxide nanofluid at G=2500 kg/m^{2}s

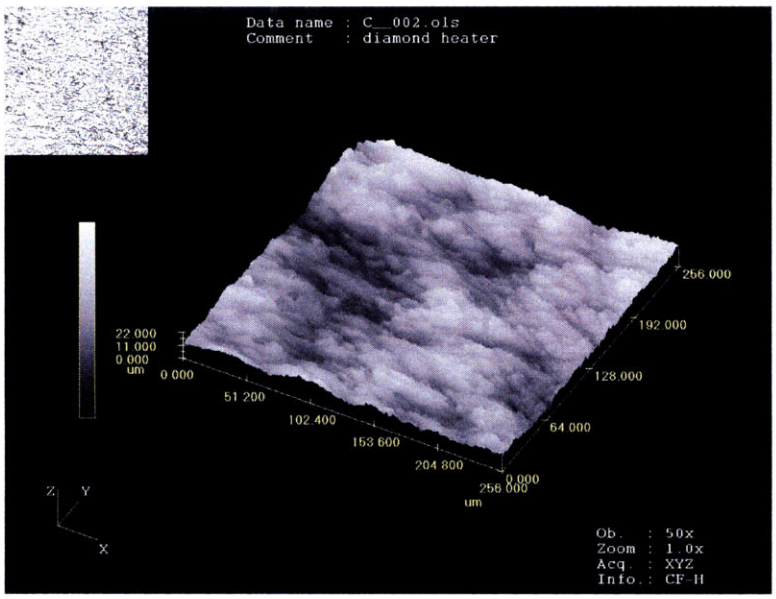

(a)

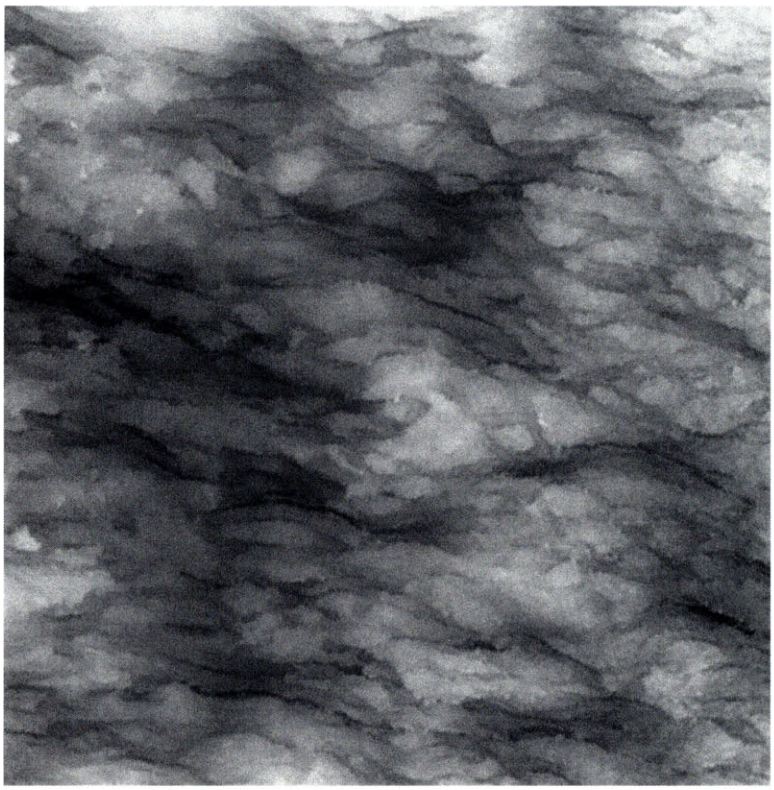

(b)

Figure 5-39 (a) 3D and (b) 2D 8-bit gray confocal images of heater coupon boiled in 0.001 %vol. diamond nanofluid at G=2500 kg/m^{2}s

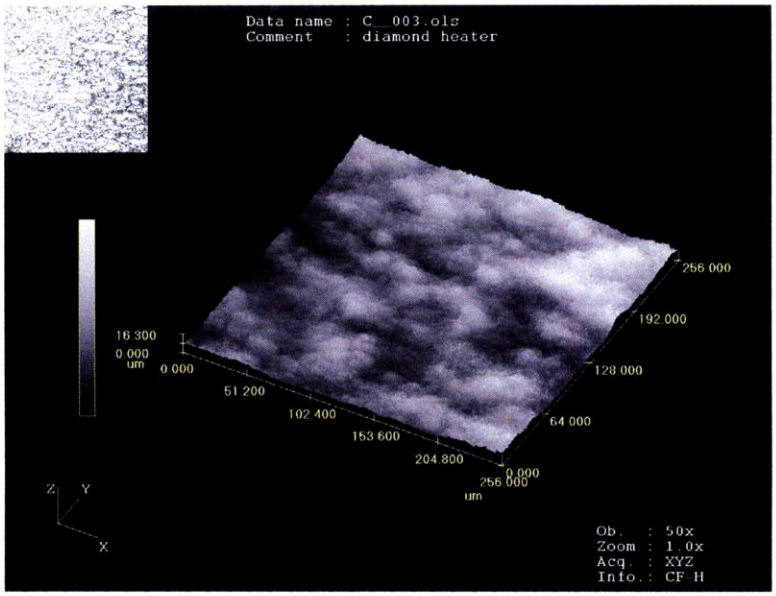

(a)

(b)

Figure 5-40 (a) 3D and (b) 2D 8-bit gray confocal images of heater coupon boiled in 0.01 %vol. diamond nanofluid at G=2500 kg/m^{2}s

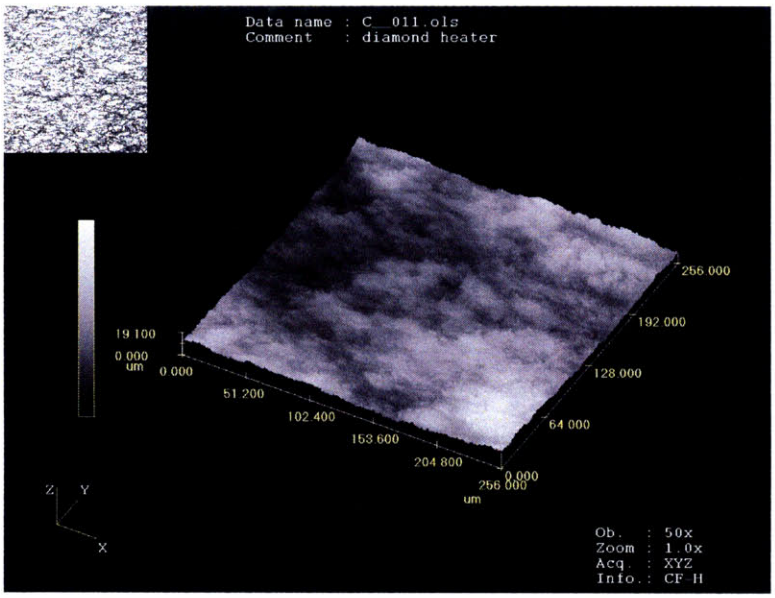

(a)

(b)

Figure 5-41 (a) 3D and (b) 2D 8-bit gray confocal images of heater coupon boiled in 0.1 %vol. diamond nanofluid at G=2500 kg/m^{2}s

5.3 Micro-Cavity Counting Using ImageJ Software

It is commonly accepted that the micro-cavities present on a surface greatly affect the boiling heat transfer behavior of that surface, as they can become active sites for bubble nucleation. In this section, we introduce an effective technique to count the number of micro-cavities using the confocal 2D images presented in the previous section and graphic software package ImageJ.

5.3.1 Micro-cavity counting process using confocal 2D image and ImageJ

As reported in the previous section, 3D tomographic and the corresponding 2D 8-bit gray images of heater coupons were taken by means of confocal microscopy. The number of micro-cavities created on the test section surface by nanoparticle deposition during nanofluid boiling could then be estimated by processing the 2D confocal images with ImageJ, which is a Java-based software package developed at the National Institutes of Health (http://rsb.info.nih.gov/ij/). ImageJ includes a function ('Analyze Particle') to measure and count user-defined objects in multi-dimensional format. The user has to specify the cross-sectional (x and y directions) area range and depth (z direction) of the objects to be found and counted. In this study, we have selected two cross-sectional area ranges, 0.79-79 μm^2, corresponding to cavities of diameter 1-10 μm, and 3.8-79 μm^2, corresponding to cavities of diameter 2.2-10 μm, where 2.2 μm is the calculated minimum bubble diameter, D^*, that can nucleate at the maximum wall superheat, T_w-T_{sat}, measured in our experiments:

$$D^* = \frac{4\sigma T_{sat} v_{fg}}{h_{fg}(T_w - T_{sat})} \tag{5-1}$$

The high end value (10 μm) is recommended by Carey (1992) and Collier and Thome (1996). As for the cavity depth, three different values were selected, ΔH_c=3, 5, and 7 μm. An example of the cavities (0.1 %vol. alumina heater coupon) identified by ImageJ associated with D_c: 1-10 μm and ΔH_c=7 μm is shown in Fig. 5-42, and the corresponding statistics are reported in Table 5-2. Note that not all red regions are counted as micro-cavities, as only the regions which satisfy the prescribed area range of 0.79 to 79 μm^2 are counted and outlined as micro-cavities. A typical example is observed in Fig. 5-42b. This procedure was applied to each test run, to find the values of number density of micro-cavities.

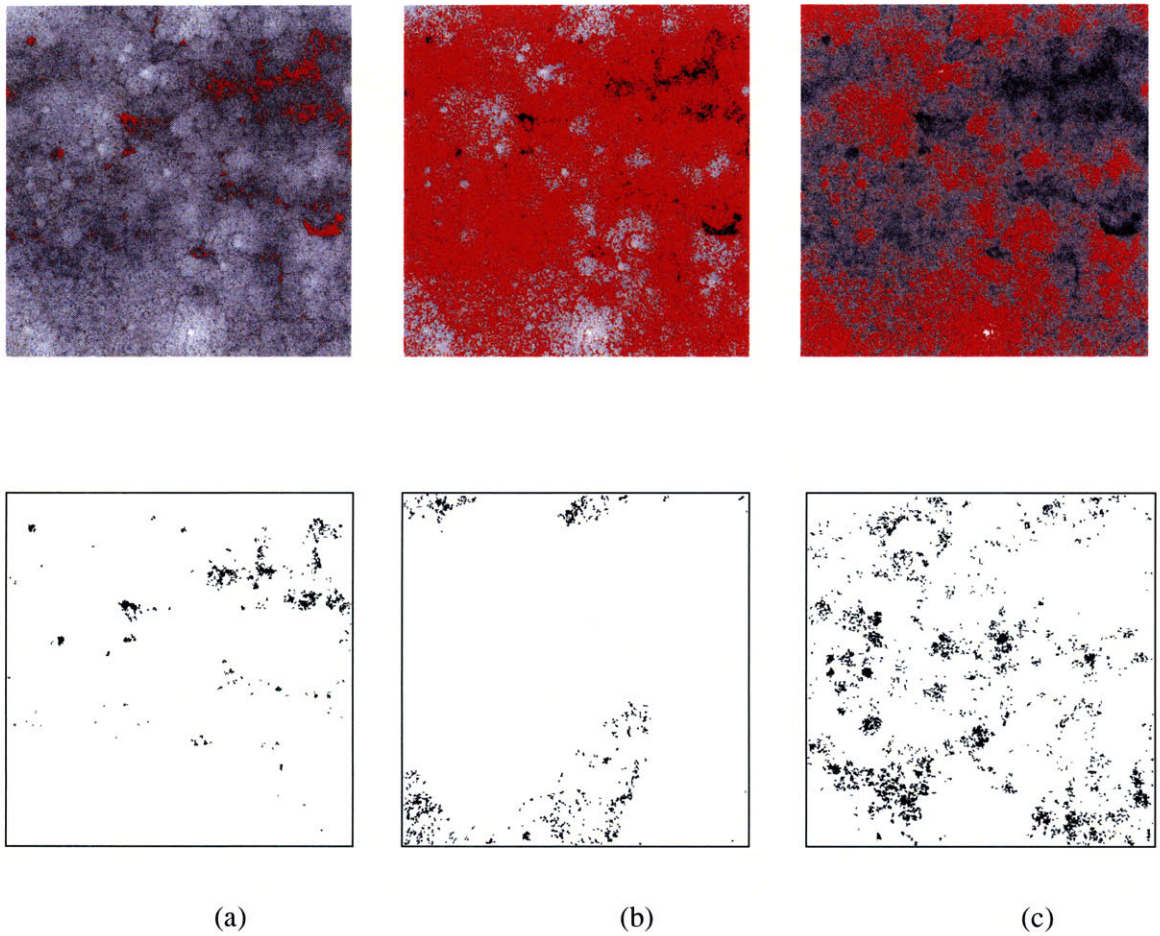

(a) (b) (c)

Figure 5-42 Micro-cavities of various depths identified by ImageJ from a confocal microscopy image of the test section surface; (a) 0<H_c<7 μm, (b) 7 μm <H_c<14 μm, and (c) 14 μm <H_c<21 μm (Image best viewed in color)

Table 5-2 Summary of micro-cavity counting results for a 0.1 %vol. alumina heater coupon (D_c: 1 – 10 μm; ΔH_c= 7 μm; full peak-to-valley height=25.4 μm)

Cavity height range	Count	Average size (μm^2)	Areal fraction (%)
$0<H_c<7$ μm	199	4.266	1.3
$7<H_c<14$ μm	312	2.962	1.4
$14<H_c<21$ μm	1075	3.448	5.7
Sum	1586	3.455	8.4

Using the micro-cavity counting technique described above, about seventy 2D confocal images of all heater-coupons were processed. As a sensitivity analysis, two D_c ranges associated with three H_c were examined. The summary of the results for H_c=3 μm are given in Figs. 5-43 and 44 for $1<D_c<10$ μm and $2.2<D_c<10$ μm, respectively. Also more inclusive results are tabularized in Table 5-3 and 4 for D_c: 1 – 10 μm and 2.2 – 10 μm, respectively. The following sections highlight the results briefly in terms of micro-cavity height and diameter range effects on the counting technique.

5.3.1.1 *Micro-cavity height effect on calculated number of micro-cavities*

In Table 5-3, it is seen that the calculated number of micro-cavities increases as H_c decreases. However, the relative order of the results shown with H_c=3 μm appear similar to those with H_c=5 and 7 μm. The same trend is observed in Table 5-4 for the other D_c range. This suggests that the results obtained from the micro-cavities counting technique are not very sensitive to the selected value of H_c.

5.3.1.2 Micro-cavity diameter effect on calculated number of micro-cavities

The effect of micro-cavity diameter range is more interesting. The results are best analyzed by defining a ratio of micro-cavities density (MC ratio) counted with the heater coupons boiled in water and nanofluids to the as-received heater coupon. Figs. 5-43(a) and 43(b) show the MC ratio counted with $1<D_c<10$ μm (H_c=3 μm) and $2.2<D_c<10$ μm (H_c=3 μm), respectively, and with respect to the nanoparticle concentration. With the aforementioned D_c ranges and H_c, Figs. 5-45(a) and 46(b) also show the respective MC ratio trend according to three tested mass fluxes. In Tables 5-3 and 4, no change of m'', the number of micro-cavity per unit area or micro-cavity density, is observed for water-boiled coupons compared to as-received coupon. This would make sense as no surface morphology was observed with the SEM and confocal images taken. However, in Fig. 5-43(a) (D_c: 1 – 10 μm), a substantial increase of MC ratio is observed for heater coupons boiled in alumina nanofluid. In addition, relatively moderate and insignificant increases of m'' or MC ratio can be seen for heater coupons boiled in zinc oxide and diamond nanofluids. The same trend is not observed in Fig. 5-43(b) (D_c: 2.2 – 10 μm). Although the heater coupons boiled in alumina nanofluids still exhibit the increased m'', invariant and reduced m'' are observed for the heater coupons boiled in zinc oxide and diamond nanofluids, respectively. In addition, no clear trend with regard to the nanoparticle concentration and mass flux is seen from the figures. Therefore it is unlikely that the micro-cavity density can provide the definitive explanation for the CHF and HTC data for nanofluids. However, the micro-cavity information will be used in Chapter 6, where an evaluation of the bubble nucleation sites will be discussed.

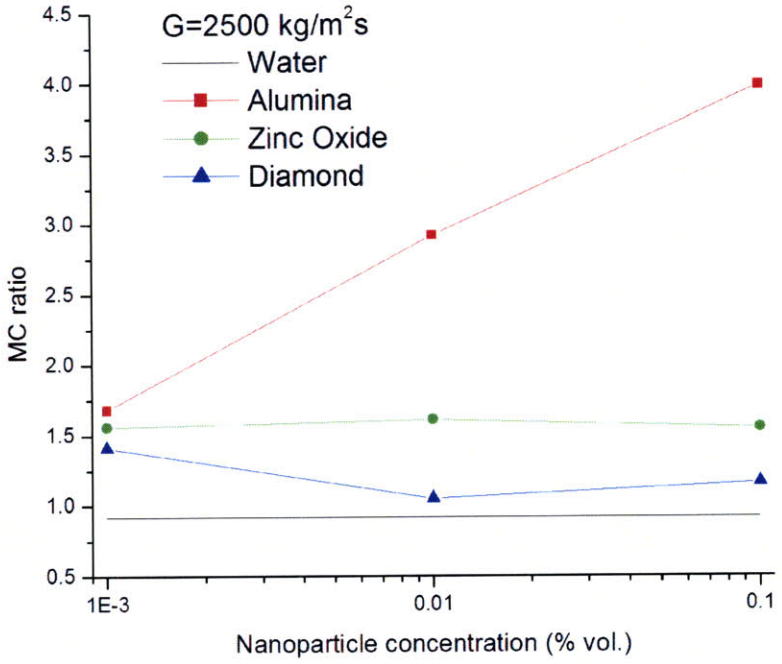

(a)

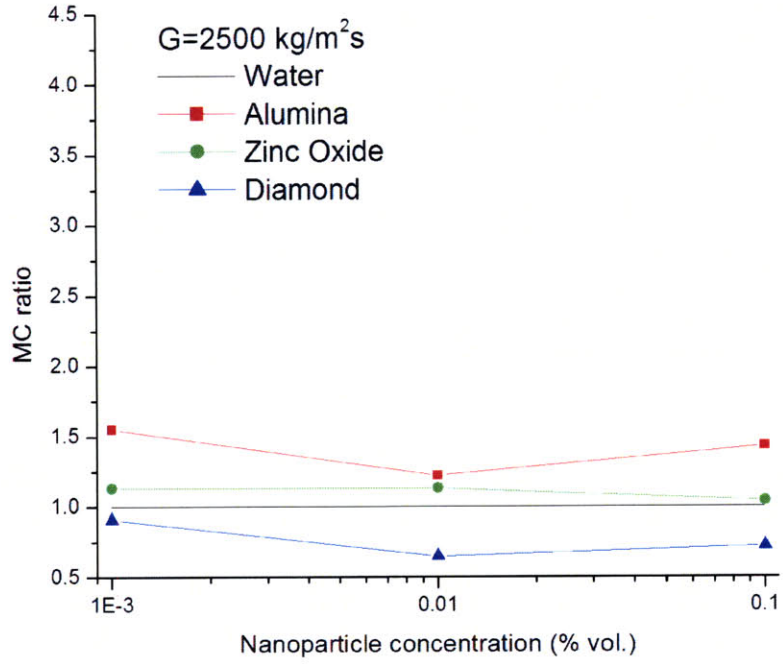

(b)

Figure 5-43 MC ratio with respect to nanoparticle concentration counted in (a) $1<D_c<10$ μm (H_c=3 μm) and (b) $2.2<D_c<10$ μm (H_c=3 μm)

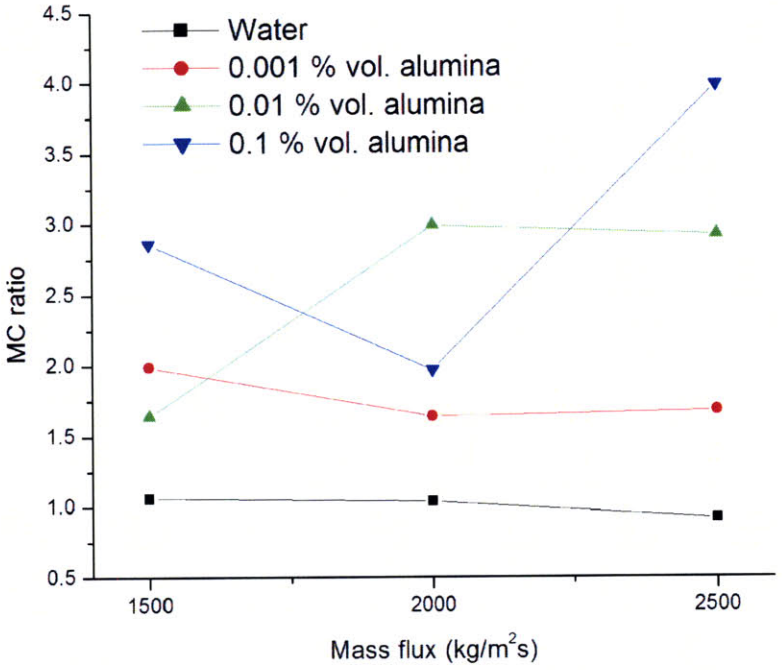

(a)

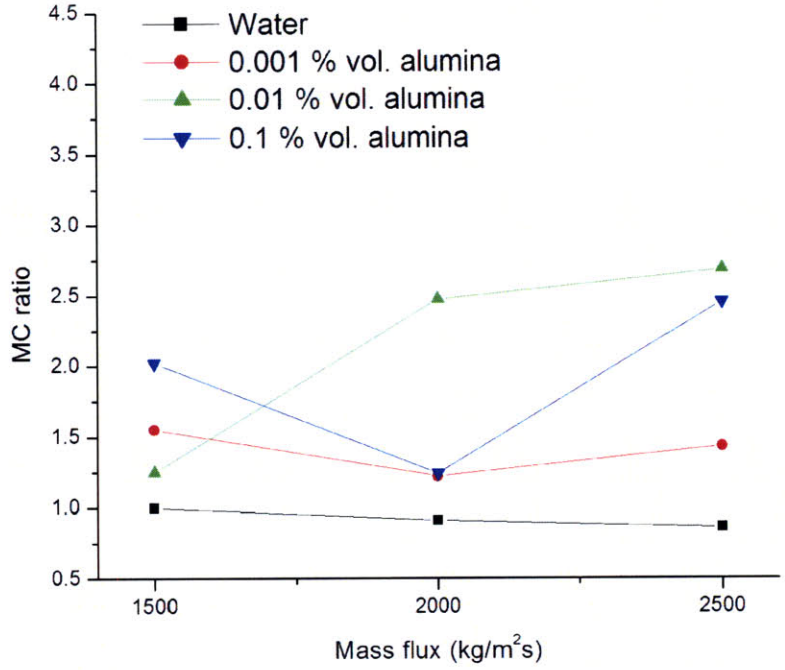

(b)

Figure 5-44 MC ratio with respect to mass flux counted in (a) $1<D_c<10$ μm (H_c=3 μm) and (b) $2.2<D_c<10$ μm (H_c=3 μm)

Table 5-3 Summary of micro-cavity counting results for all heater coupons (D_c: 1 – 10 μm; ΔH_c= 3, 5, and 7 μm)

Surface condition	Nanoparticle Concentration, φ (%vol.)	Mass flux, G (kg/m^{2}s)	Micro-cavity count per 256×256 μm^2, m'' (counts/256×256 μm^2)			Average micro-cavity size (μm^2)			Area fraction occupied by micro-cavities (%)			Ratio of micro-cavity count, $R_{m''}$†		
			ΔH_c 3 μm	ΔH_c 5 μm	ΔH_c 7 μm	ΔH_c 3 μm	ΔH_c 5 μm	ΔH_c 7 μm	ΔH_c 3 μm	ΔH_c 5 μm	ΔH_c 7 μm	ΔH_c 3 μm	ΔH_c 5 μm	ΔH_c 7 μm
As-received	0	0	639	418	318	6.237	6.519	5.736	6.0	4.1	2.8	1.00	1.00	1.00
Water	0	1500	678	384	279	6.467	6.680	6.540	6.7	3.9	2.8	1.06	0.92	0.88
	0	2000	664	371	279	5.944	6.190	7.048	6.1	3.6	3.0	1.04	0.89	0.88
	0	2500	587	328	195	6.044	5.091	6.028	5.4	2.6	1.8	0.92	0.78	0.61
Alumina	0.001	1500	1270	644	425	5.186	5.316	5.294	10.0	5.2	3.4	1.99	1.54	1.34
	0.01	1500	1046	639	416	4.804	4.591	5.313	7.7	4.5	3.4	1.64	1.53	1.31
	0.1	1500	1828	1021	710	3.960	4.243	4.101	11.1	6.7	4.4	2.86	2.44	2.23
	0.001	2000	1047	588	420	4.337	4.590	5.137	6.9	4.1	3.4	1.64	1.41	1.32
	0.01	2000	1914	1159	738	4.392	4.258	4.006	12.8	7.6	4.4	2.99	2.77	2.32
	0.1	2000	1256	551	489	4.100	4.235	3.215	7.9	3.6	2.4	1.97	1.32	1.54
	0.001	2500	1073	568	325	5.158	5.585	5.280	8.5	4.8	2.6	1.68	1.36	1.02
	0.01	2500	1866	1013	681	5.078	5.270	5.134	14.4	8.1	5.3	2.92	2.42	2.14
	0.1	2500	2544	1288	1014	3.819	3.845	3.754	14.6	7.4	5.8	3.98	3.08	3.19
Zinc oxide	0.001	2500	1000	589	380	4.338	4.258	4.006	6.7	3.8	2.4	1.56	1.41	1.19
	0.01	2500	1030	519	388	4.442	4.293	4.620	7.1	3.5	2.7	1.61	1.24	1.22
	0.1	2500	992	481	353	4.226	3.858	4.093	6.4	2.8	2.2	1.55	1.15	1.11
Diamond	0.001	2500	904	510	378	4.239	4.187	5.053	5.8	3.2	3.0	1.41	1.22	1.19
	0.01	2500	672	396	267	4.038	4.034	3.738	4.2	2.4	1.5	1.05	0.95	0.84
	0.1	2500	740	454	286	3.799	3.829	3.825	4.4	2.7	1.7	1.16	1.08	0.90

† Values are obtained by dividing each micro-cavity count by the count for the as-received coupon.

Table 5-4 Summary of micro-cavity counting results for all heater coupons (D_c: 2.2 – 10 μm; ΔH_c= 3, 5, and 7 μm)

Surface condition	Nanoparticle Concentration, φ (%vol.)	Mass flux, G (kg/m^{2}s)	Micro-cavity count per 256×256 μm^2, m'' (counts/256×256 μm^2)			Average micro-cavity size (μm^2)			Area fraction occupied by micro-cavities (%)			Ratio of micro-cavity count, $R_{m''}$†		
			ΔH_c 3 μm	ΔH_c 5 μm	ΔH_c 7 μm	ΔH_c 3 μm	ΔH_c 5 μm	ΔH_c 7 μm	ΔH_c 3 μm	ΔH_c 5 μm	ΔH_c 7 μm	ΔH_c 3 μm	ΔH_c 5 μm	ΔH_c 7 μm
As-received	0	0	213	141	100	15.448	16.110	14.676	5.0	3.4	2.2	1.00	1.00	1.00
Water	0	1500	214	132	100	17.091	16.324	15.392	5.6	3.3	2.3	1.00	0.93	1.00
	0	2000	193	113	94	16.493	16.653	17.787	5.0	2.9	2.6	0.91	0.80	0.94
	0	2500	183	97	63	15.809	13.568	15.308	4.4	2.0	1.5	0.86	0.68	0.63
Alumina	0.001	1500	331	169	112	15.316	15.762	15.700	7.8	4.1	2.5	1.55	1.20	1.12
	0.01	1500	267	161	115	14.030	13.447	15.327	5.7	3.4	2.6	1.25	1.14	1.16
	0.1	1500	431	242	162	11.655	12.925	12.222	7.8	4.7	3.0	2.02	1.71	1.62
	0.001	2000	261	141	109	12.621	13.951	15.156	5.1	3.0	2.5	1.22	1.00	1.09
	0.01	2000	527	324	186	11.543	10.884	10.818	9.3	5.3	3.2	2.47	2.29	1.87
	0.1	2000	263	101	85	13.519	15.535	11.070	5.4	2.3	1.5	1.24	0.72	0.86
	0.001	2500	305	159	93	14.093	15.786	14.466	6.5	3.8	2.0	1.43	1.12	0.94
	0.01	2500	570	303	203	12.826	13.698	13.514	11.1	6.3	4.1	2.68	2.14	2.03
	0.1	2500	522	271	216	12.059	11.868	11.541	9.5	4.9	3.8	2.45	1.92	2.17
Zinc oxide	0.001	2500	240	131	82	14.955	13.386	12.738	4.8	2.7	1.6	1.13	0.93	0.82
	0.01	2500	240	118	91	13.877	13.523	14.393	5.3	2.5	2.0	1.13	0.84	0.91
	0.1	2500	221	101	77	13.315	12.054	12.978	4.5	1.9	1.6	1.04	0.71	0.77
Diamond	0.001	2500	194	114	96	13.917	13.138	15.142	4.1	2.4	2.3	0.91	0.81	0.96
	0.01	2500	138	78	50	13.714	13.866	12.908	2.8	1.7	1.0	0.65	0.55	0.50
	0.1	2500	153	92	60	12.591	12.516	11.909	3.0	1.7	1.1	0.72	0.65	0.60

† Values are obtained by dividing each micro-cavity count by the count for the as-received coupon

5.4 Contact Angle Measurement

Another parameter that may strongly affect CHF and HTC is the contact angle, which is related to the wettability of the surface. The contact angle also can be changed by the presence of the nanoparticles on the surface. Therefore results of the contact angle measurements and their significance are discussed in this section.

5.4.1 Description of contact angle measurements

The sessile drop technique was adopted to measure the static (not advancing or receding) contact angle. Pictures of the contact angle of a still droplet on the surface of interest are taken and the contact angle is estimated from such pictures. A state-of-the-art contact angle goniometer, EasyDrop Contact Angle Instrument by Krüss, was used for this purpose. The apparatus is shown in Fig. 5-45. Because the heater surfaces in our study are curved, fitting the angle was done manually with the help of the software ImageJ. The contact angle photo was imported in ImageJ and its left and right hand sides were read five times and averaged. It is noted that determination of the contact angle value is somewhat subjective with this approach. The estimated uncertainty for these measurements is $\pm 10^{o}$. To obtain reliable contact angle data, it is recommended to use a consistent volume of sessile drop during each test. The volume was kept below 5 μL for all tests. Also, the time duration of the measurement was held short, less than 30 seconds, to minimize the effect of droplet evaporation. The measurements were carried out at 22 ^{o}C in air by depositing each nanofluid droplet on the heater surface coupon from the respective nanofluid test. For example, a sessile droplet of 0.1 %vol. alumina nanofluid was used on the heater surface boiled in the 0.1 %vol. alumina nanofluid.

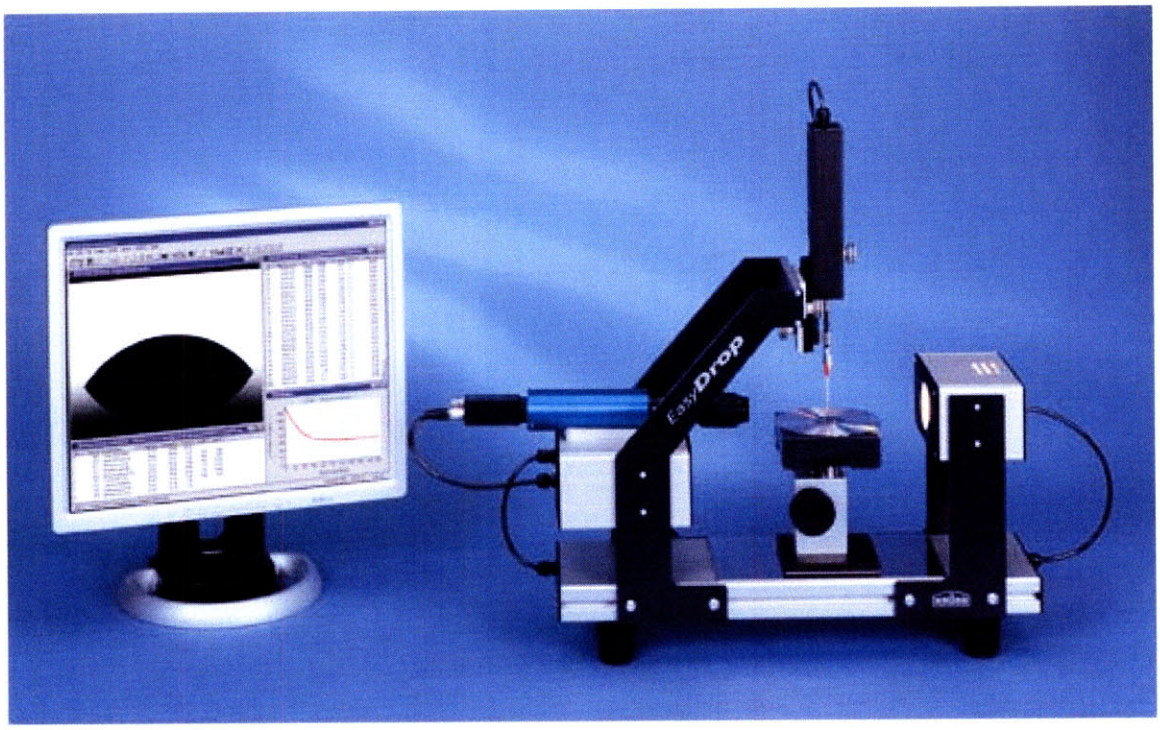

Figure 5-45 Contact angle measurement (EasyDrop Contact Angle Instrumentation by Krüss)

5.4.2 Results

The measured data of apparent contact angle are reported in Table 5-5. The contact angle data are interesting. The as-received coupon and the coupon boiled in water have contact angles around 80°, while the coupons boiled in the alumina nanofluids at G=2500 kg/m^{2}s all have a significantly lower contact angle, ~20-30°. A similar trend is observed in the heater coupons boiled in 0.01 and 0.1 %vol. zinc oxide nanofluids and a smaller but still significant reduction of contact angle is seen in 0.001 %vol. zinc oxide nanofluids. These contact angles are the same whether deionized water or the nanofluids are used in the measurement. In contrast, virtually no reduction of the contact angle is found for the heater coupons boiled in diamond nanofluids at all concentrations. Representative photos of the contact angles are shown in Figs. 5-46 to 64. Recall that the maximum CHF enhancement was observed with alumina nanofluids at G=2500 kg/m^{2}s

and for the zinc-oxide nanofluids, while for diamond nanofluids the CHF enhancement was more modest, so there might be a correlation between contact angle reduction and CHF enhancement. This topic will be discussed in Chapter 6.

Table 5-5 Contact angle data from flow CHF test heaters (NF stands for 'nanofluid')

Surface condition	Nanoparticle concentration φ (%vol.)	Mass flux G (kg/m^{2}s)	Sessile droplet	Apparent contact angle, θ_a (degree)†
As-received	0	0	Water	79
	0	0	0.1 %vol. alumina NF	75
	0	0	0.1 %vol. zinc oxide NF	79
	0	0	1 %vol. diamond NF	123
Water	0	1500	Water	86
	0	1500	0.1 %vol. alumina NF	82
	0	1500	0.1 %vol. zinc oxide NF	92
	0	1500	0.1 %vol. diamond NF	119
	0	2000	Water	86
	0	2000	0.1 %vol. alumina NF	75
	0	2000	0.1 %vol. zinc oxide NF	73
	0	2000	0.1 %vol. diamond NF	127
	0	2500	Water	83
	0	2500	0.1 %vol. alumina NF	96
	0	2500	0.1 %vol. zinc oxide NF	95
	0	2500	0.1 %vol. diamond NF	126
Alumina	0.001	1500	Water	66
	0.001	1500	0.001 %vol. alumina NF	68
	0.01	1500	Water	80
	0.01	1500	0.01 %vol. alumina NF	85
	0.1	1500	Water	87
	0.1	1500	0.1 %vol. alumina NF	82
	0.001	2000	Water	65
	0.001	2000	0.001 %vol. alumina NF	74
	0.01	2000	Water	84
	0.01	2000	0.01 %vol. alumina NF	77
	0.1	2000	Water	40
	0.1	2000	0.1 %vol. alumina NF	27
	0.001	2500	Water	23
	0.001	2500	0.001 %vol. alumina NF	18
	0.01	2500	Water	31
	0.01	2500	0.01 %vol. alumina NF	32
	0.1	2500	Water	20
	0.1	2500	0.1 %vol. alumina NF	19
Zinc oxide	0.001	2500	Water	46
	0.001	2500	0.001 %vol. zinc oxide NF	45
	0.01	2500	Water	41
	0.01	2500	0.01 %vol. zinc oxide NF	29
	0.1	2500	Water	28
	0.1	2500	0.1 %vol. zinc oxide NF	26
Diamond	0.001	2500	Water	122
	0.001	2500	0.001 %vol. diamond NF	125
	0.01	2500	Water	83
	0.01	2500	0.01 %vol. diamond NF	96
	0.1	2500	Water	86
	0.1	2500	0.1 %vol. diamond NF	84

† Contact angle values were measured using the water sessile droplet method (measurement uncertainty ±10°).

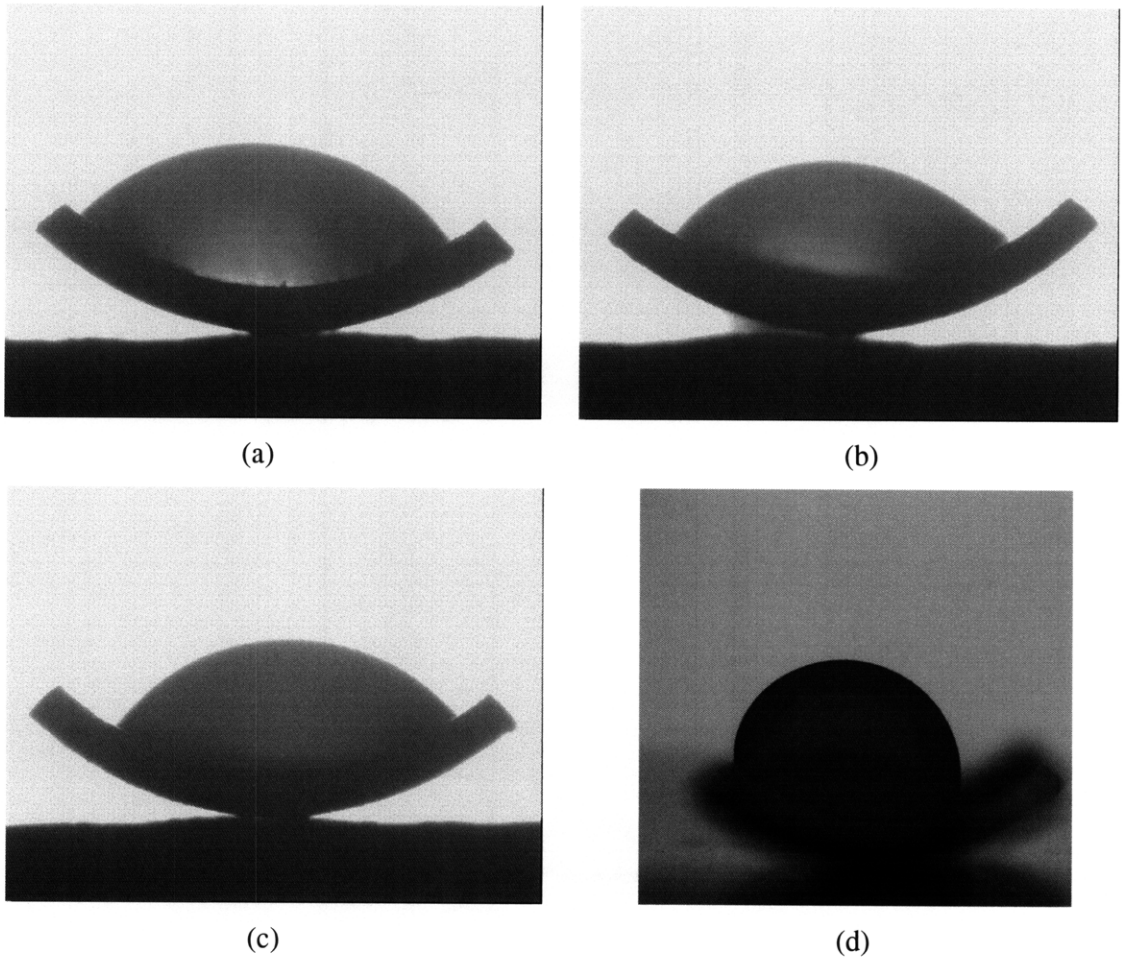

Figure 5-46 Contact angle of (a) DI water and (b) 0.1 %vol. alumina, (c) 0.1 %vol. zinc oxide, and (d) 0.1 %vol. diamond nanofluids on the as-received heater coupon

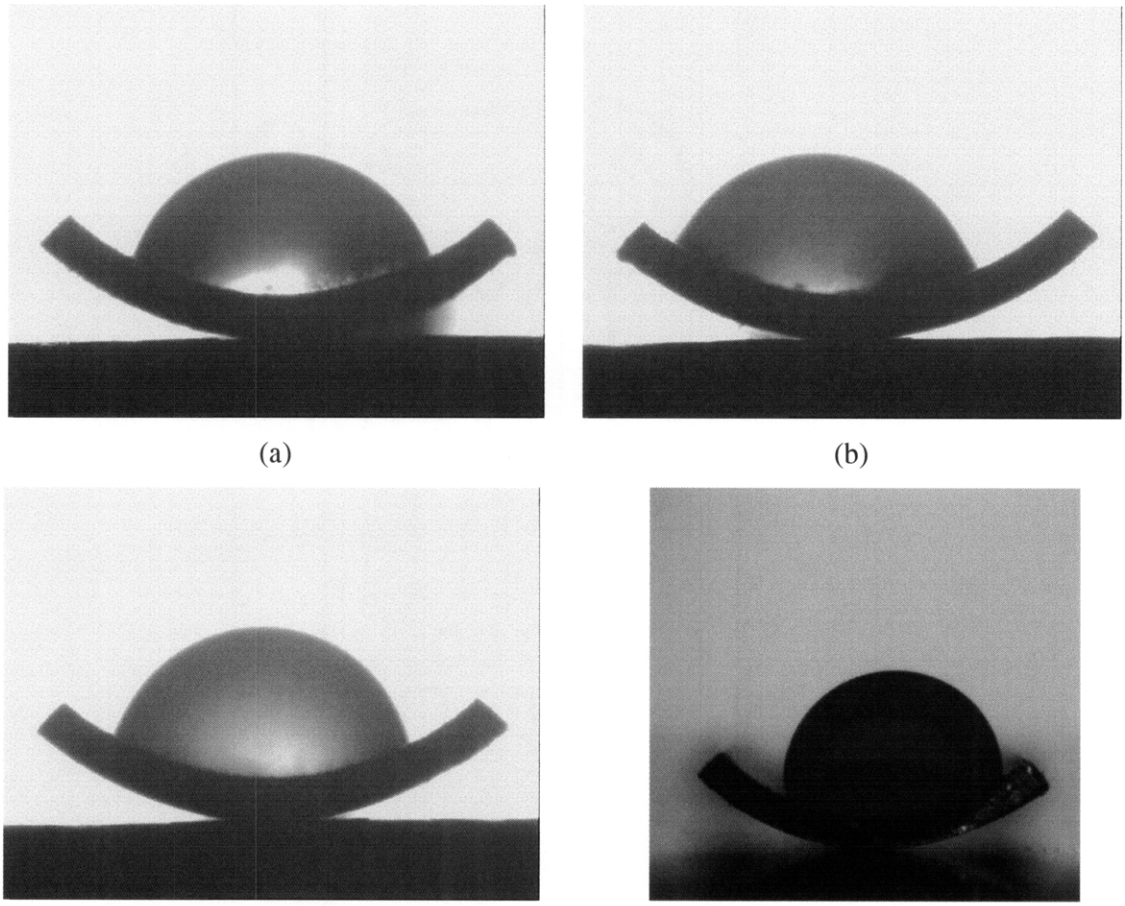

Figure 5-47 Contact angle of (a) DI water and (b) 0.1 %vol. alumina, (c) 0.1 %vol. zinc oxide, (d) 0.1 %vol. diamond nanofluids on the heater coupon boiled in pure water at G=1500 kg/m^{2}s

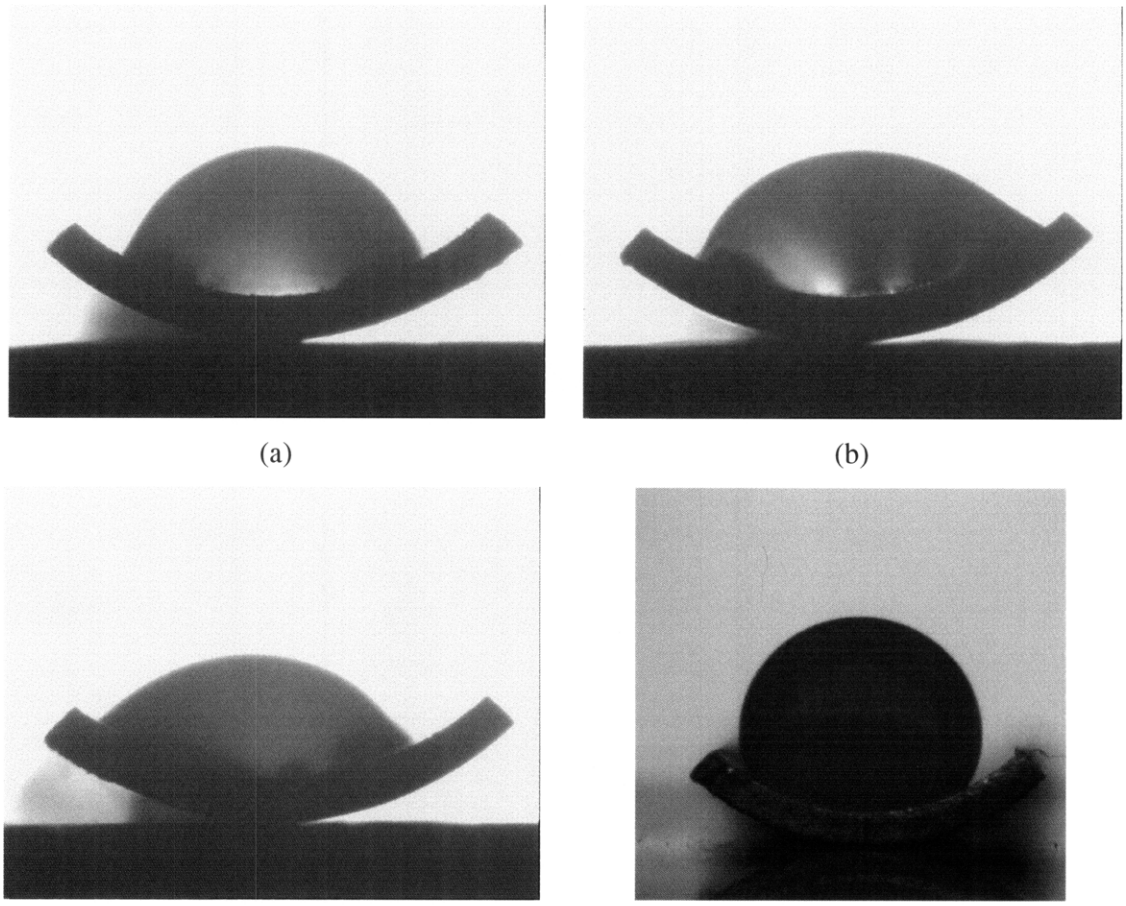

Figure 5-48 Contact angle of (a) DI water and (b) 0.1 %vol. alumina, (c) 0.1 %vol. zinc oxide, and (d) 0.1 %vol. diamond nanofluids on the heater coupon boiled in pure water at G=2000 kg/m^{2}s

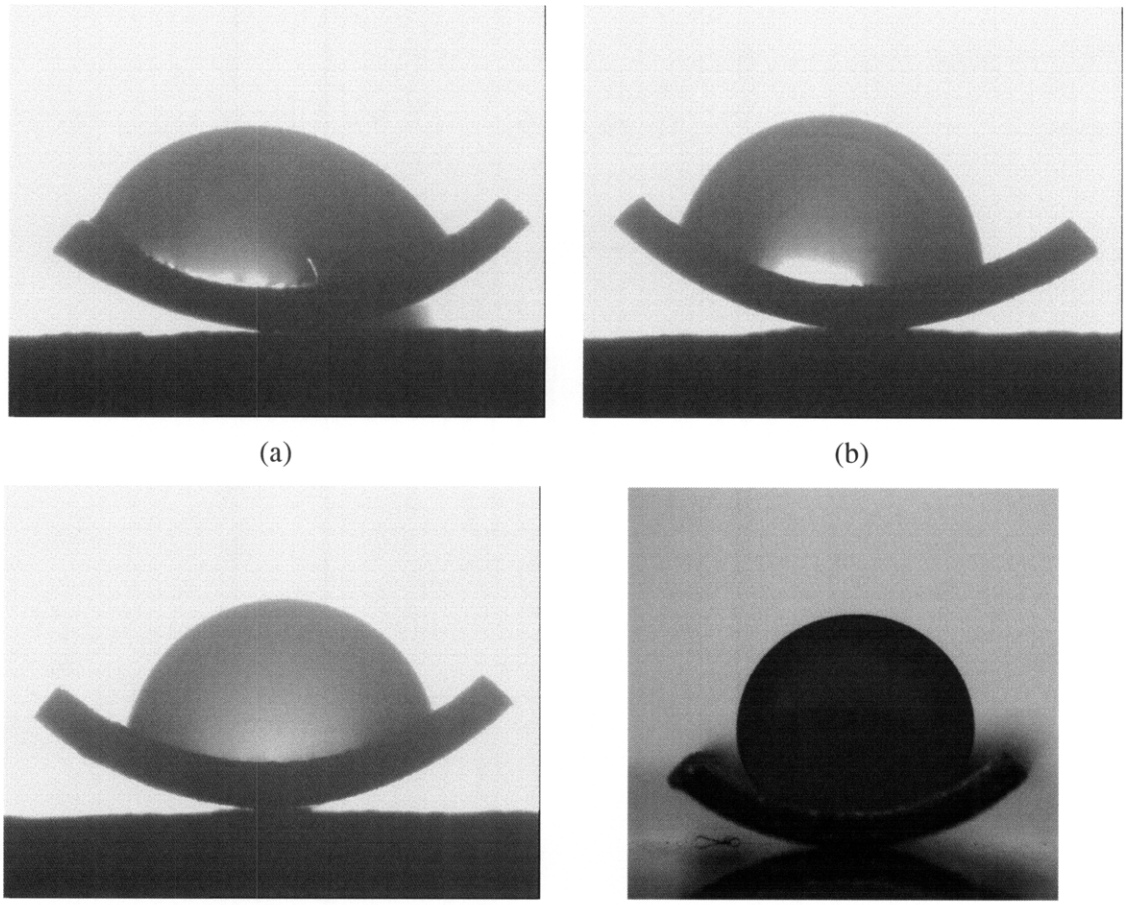

Figure 5-49 Contact angle of (a) DI water and (b) 0.1 %vol. alumina, (c) 0.1 %vol. zinc oxide, (d) 0.1 %vol. diamond nanofluids on the heater coupon boiled in pure water at G=2500 kg/m^{2}s

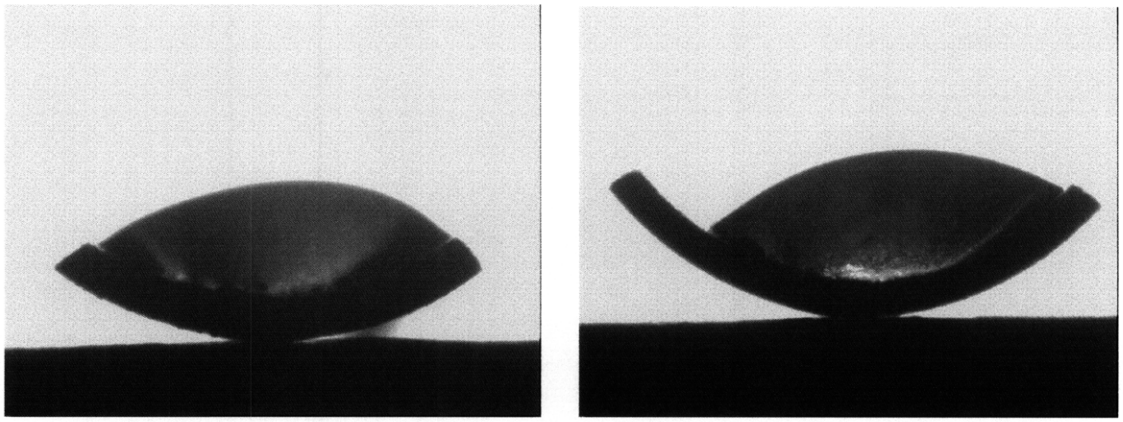

(a) (b)

Figure 5-50 Contact angle of (a) DI water and (b) 0.001 %vol. alumina nanofluid on the heater coupon boiled in 0.001 %vol. alumina nanofluid at G=1500 kg/m^{2}s

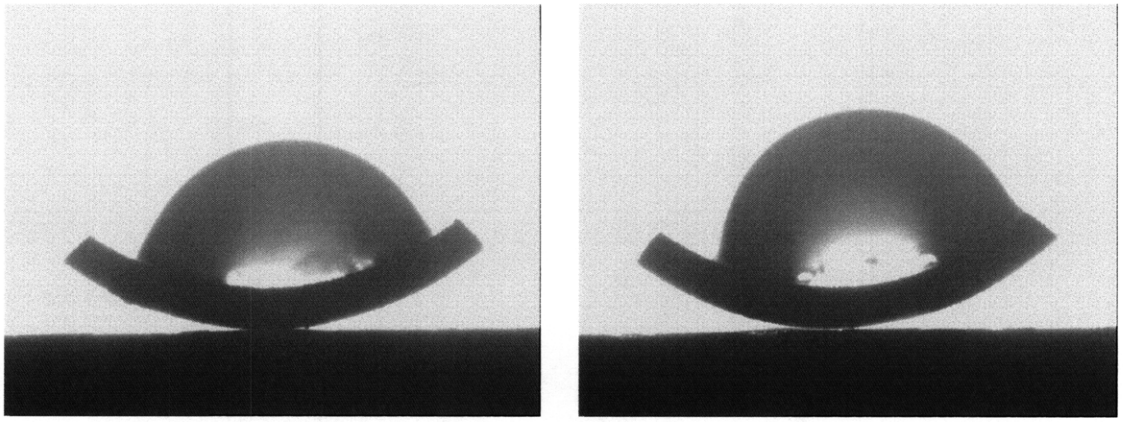

(a) (b)

Figure 5-51 Contact angle of (a) DI water and (b) 0.01 %vol. alumina nanofluid on the heater coupon boiled in 0.01 %vol. alumina nanofluid at G=1500 kg/m^{2}s

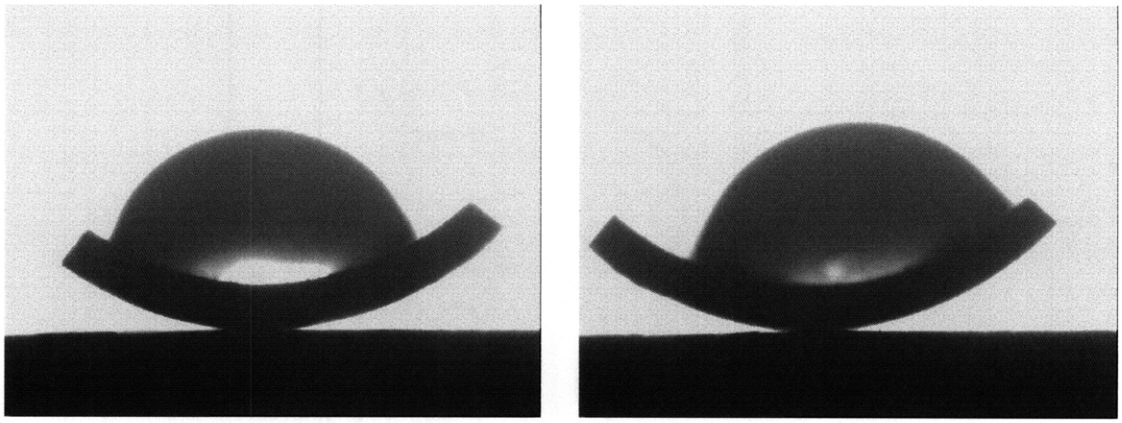

(a) (b)

Figure 5-52 Contact angle of (a) DI water and (b) 0.1 %vol. alumina nanofluid on the heater coupon boiled in 0.01 %vol. alumina nanofluid at G=1500 kg/m^{2}s

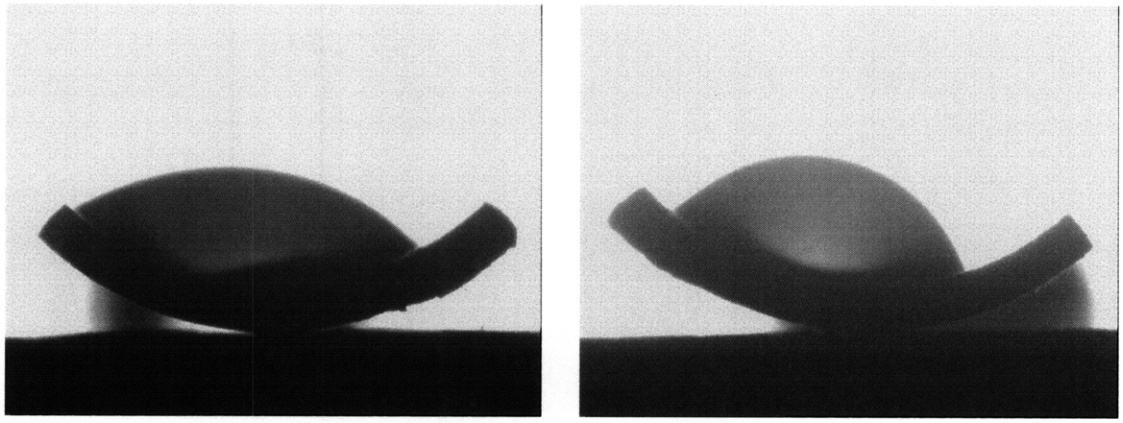

(a) (b)

Figure 5-53 Contact angle of (a) DI water and (b) 0.001 %vol. alumina nanofluid on the heater coupon boiled in 0.001 %vol. alumina nanofluid at G=2000 kg/m^{2}s

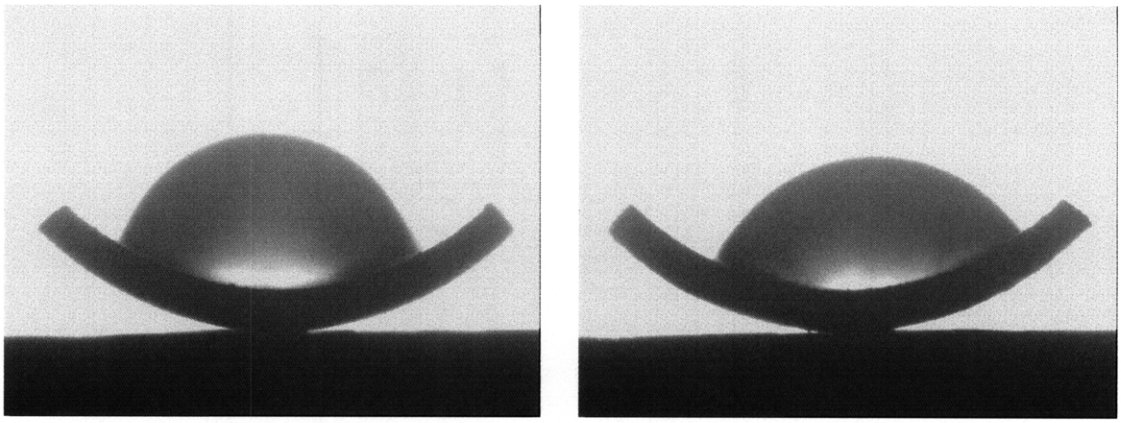

(a) (b)

Figure 5-54 Contact angle of (a) DI water and (b) 0.01 %vol. alumina nanofluid on the heater coupon boiled in 0.01 %vol. alumina nanofluid at G=2000 kg/m^{2}s

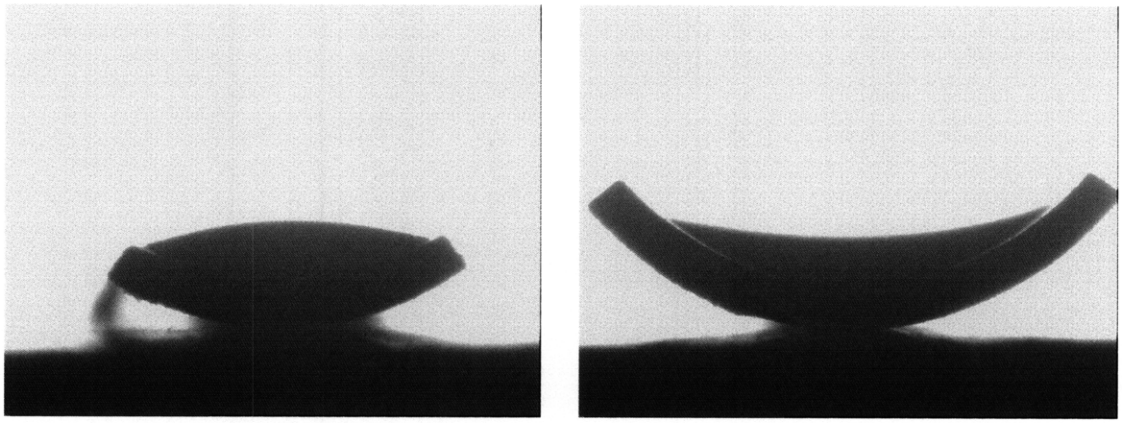

(a) (b)

Figure 5-55 Contact angle of (a) DI water and (b) 0.1 %vol. alumina nanofluid on the heater coupon boiled in 0.1 %vol. alumina nanofluid at G=2000 kg/m^{2}s

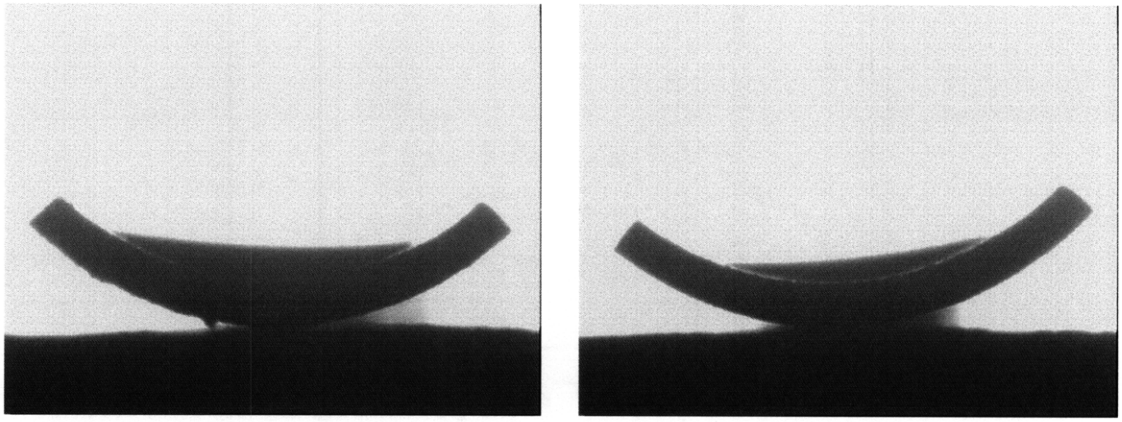

(a) (b)

Figure 5-56 Contact angle of (a) DI water and (b) 0.001 %vol. alumina nanofluid on the heater coupon boiled in 0.001 %vol. alumina nanofluid at G=2500 kg/m^{2}s

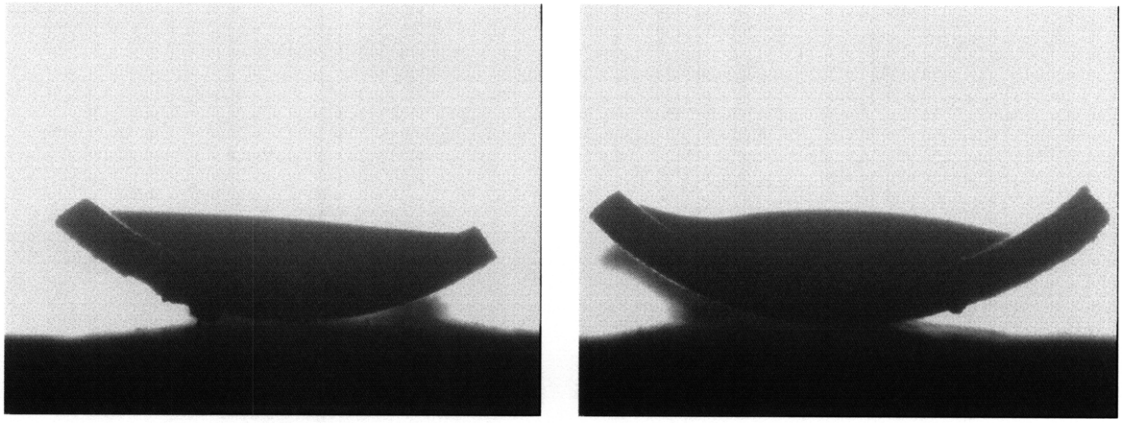

(a) (b)

Figure 5-57 Contact angle of (a) DI water and (b) 0.01 %vol. alumina nanofluid on the heater coupon boiled in 0.01 %vol. alumina nanofluid at G=2500 kg/m^{2}s

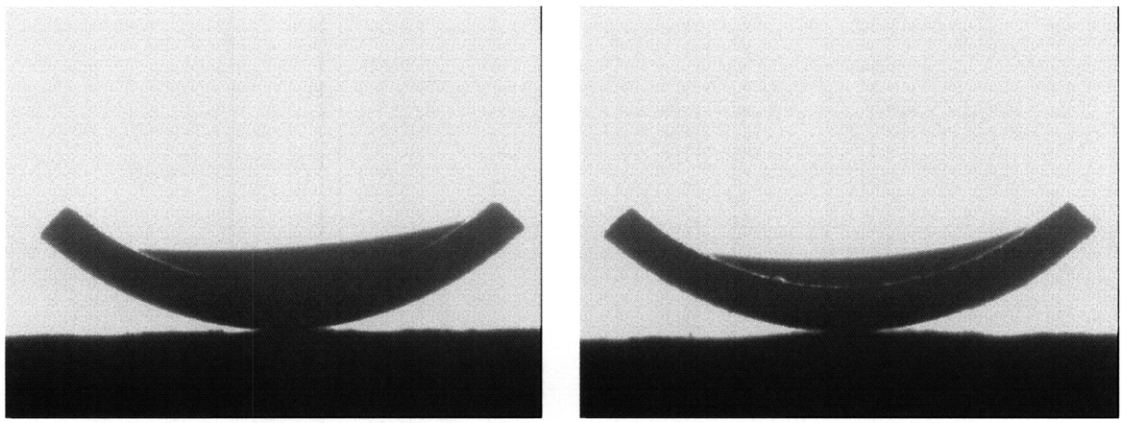

(a) (b)

Figure 5-58 Contact angle of (a) DI water and (b) 0.1 %vol. alumina nanofluid on the heater coupon boiled in 0.1 %vol. alumina nanofluid at G=2500 kg/m^{2}s

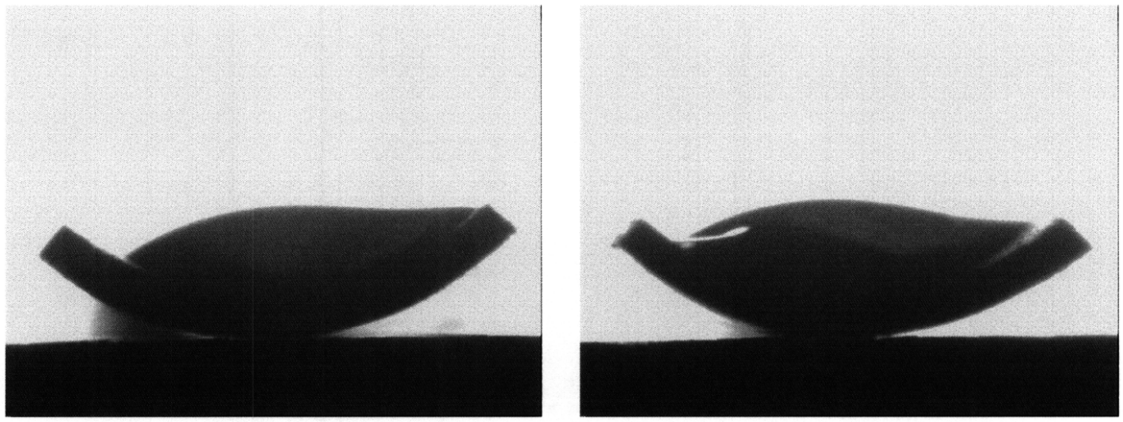

(a) (b)

Figure 5-59 Contact angle of (a) DI water and (b) 0.001 %vol. zinc oxide nanofluid on the heater coupon boiled in 0.001 %vol. zinc oxide nanofluid at G=2500 kg/m^{2}s

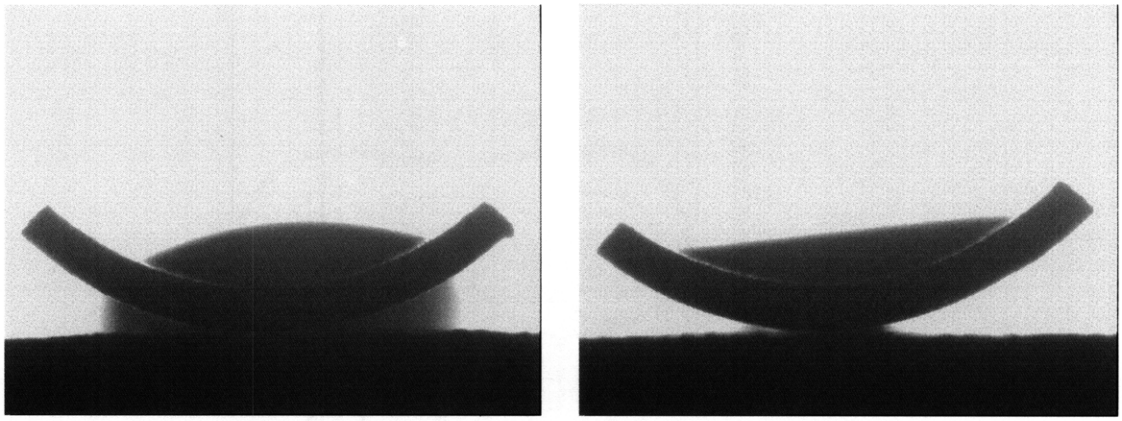

(a) (b)

Figure 5-60 Contact angle of (a) DI water and (b) 0.01 %vol. zinc oxide nanofluid on the heater coupon boiled in 0.01 %vol. zinc oxide nanofluid at G=2500 kg/m^{2}s

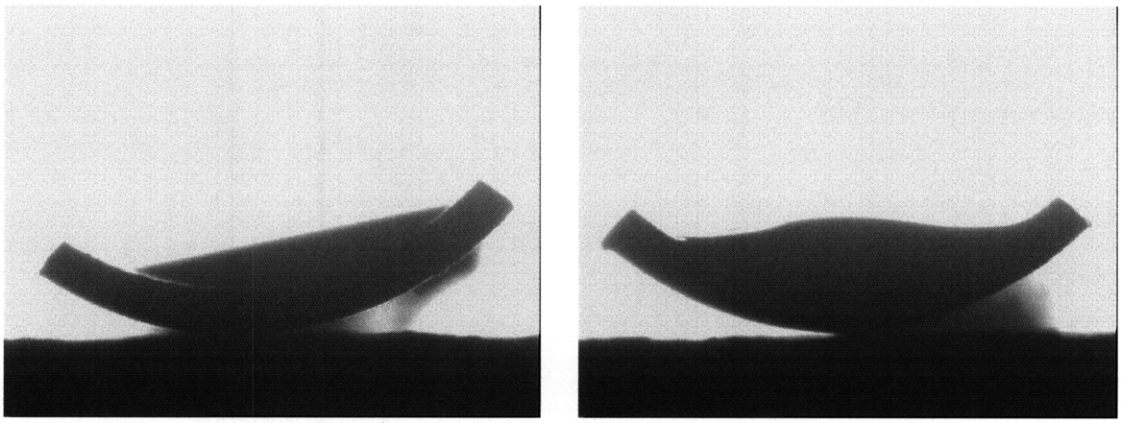

(a) (b)

Figure 5-61 Contact angle of (a) DI water and (b) 0.1 %vol. zinc oxide nanofluid on the heater coupon boiled in 0.1 %vol. zinc oxide nanofluid at G=2500 kg/m^{2}s

(a) (b)

Figure 5-62 Contact angle of (a) DI water and (b) 0.001 %vol. diamond nanofluid on the heater coupon boiled in 0.001 %vol. diamond nanofluid at G=2500 kg/m^{2}s

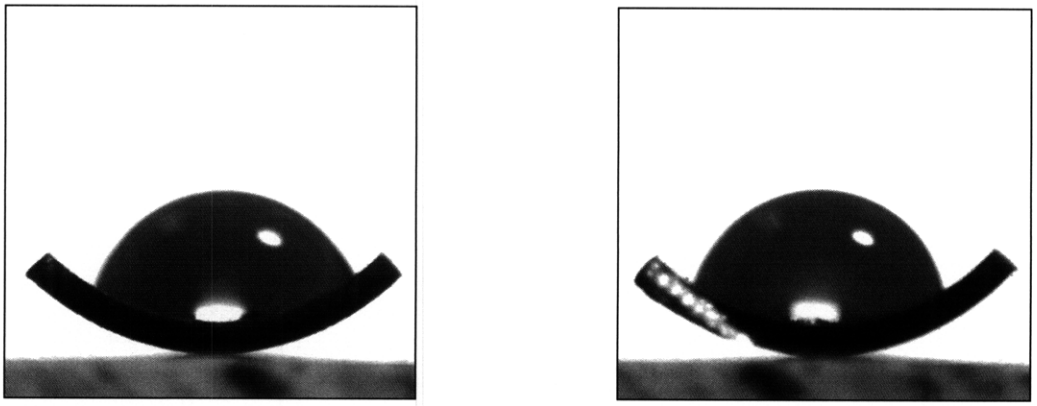

(a) (b)

Figure 5-63 Contact angle of (a) DI water and (b) 0.01 %vol. diamond nanofluid on the heater coupon boiled in 0.01 %vol. diamond nanofluid at G=2500 kg/m^{2}s

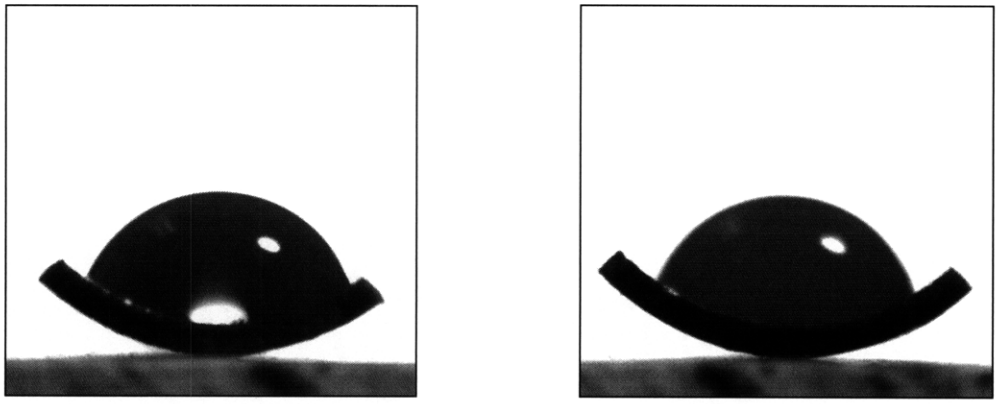

(a) (b)

Figure 5-64 Contact angle of (a) DI water and (b) 0.1 %vol. diamond nanofluid on the heater coupon boiled in 0.1 %vol. diamond nanofluid at G=2500 kg/m^{2}s

5.4.3 Calculation of intrinsic contact angle from the apparent contact angle measurements

The intrinsic contact angle is the contact angle that a droplet would form with a given material if the surface of that material were perfectly flat. On the other hand, the apparent contact angle is the angle formed with the actual surface of interest, which could be highly irregular (rough). The intrinsic contact angle is an important parameter in determining if a micro-cavity present on the surface can become an active site for bubble nucleation (a nucleation site) or not. However, since perfectly flat surfaces are very hard to obtain, the intrinsic contact angle is not easily measured. Fortunately, the intrinsic contact angle can be found from the apparent contact angle with the knowledge of the roughness ratio, as follows. A schematic of the contact angle of liquid is given in Fig. 5-65. The intrinsic contact angle on a perfect smooth surface is found from Young's equation (Carey, 1992):

$$\cos\theta_i = \frac{\gamma_{SV} - \gamma_{SL}}{\sigma_{LV}} \tag{5-2}$$

where θ_i, σ_{LV}, γ_{SV}, and γ_{SL} are the intrinsic contact angle, the surface tension at liquid-vapor

interface, and the surface energies at the solid-vapor and solid-liquid interfaces, respectively. The surface energy difference, γ_{SV}-γ_{SL}, is referred to as the adhesion tension. When the solid surface is rough, the Young's equation has to be modified as follows (Wenzel, 1949):

$$\cos\theta_a = \frac{\gamma_{SV} - \gamma_{SL}}{\sigma_{LV}} \cdot r \tag{5-3}$$

where r is the roughness factor (= ratio of actual surface to projected area), which was obtained by confocal microscopy (see Section 5.2.1), and θ_a is the apparent contact angle, which was measured directly. Then assuming σ_{LV}=72.1 mN/m (for water at 23 °C under P=0.1 MPa), γ_{SV}-γ_{SL} can be estimated from Eq. 5-3, and finally the intrinsic contact angle is found from Eq. 5-2. The intrinsic contact angle results are reported in Table 5-6.

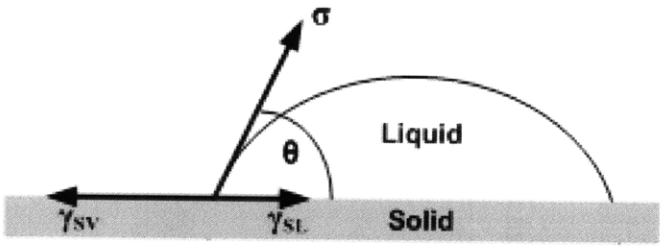

Figure 5-65 A schematic of static contact angle of liquid

Note that some scattering is observed in the calculated values of θ_i. For simplicity, therefore, the average values of θ_i was obtained using the results at G=2500 kg/m^{2}s. The corresponding average values are 86.5, 61.0, 60.8, and 94.5° for water on stainless steel, alumina, zinc oxide, and diamond surfaces, respectively. The relative magnitude of the contact angles appears to be correct, i.e., oxides have the lowest contact angle, and diamond the highest.

Table 5-6 Calculation summary of intrinsic contact angle

Surface condition	Nanoparticle concentration φ (%vol.)	Mass flux G (kg/m^{2}s)	Apparent contact angle, θ_a (degree)	Roughness factor, r	Adhesion tension (γ_{SV}-γ_{SL}), (mN/m)	Intrinsic contact angle, θ_i (degree)
As-received	0	0	79	1.402	9.907	82.2
Water	0	1500	86	1.459	3.480	87.3
	0	2000	86	1.457	3.486	87.3
	0	2500	83	1.386	6.402	85.0
Alumina	0.001	1500	66	1.724	17.174	76.4
	0.01	1500	80	1.544	8.187	83.5
	0.1	1500	87	1.834	2.077	88.4
	0.001	2000	65	1.635	18.815	75.0
	0.01	2000	84	1.870	4.068	86.8
	0.1	2000	40	1.554	35.884	60.5
	0.001	2500	23	1.583	42.338	54.4
	0.01	2500	31	1.882	33.149	62.9
	0.1	2500	20	2.267	30.174	65.5
Zinc oxide	0.001	2500	46	1.513	33.423	62.7
	0.01	2500	41	1.673	32.847	63.2
	0.1	2500	28	1.596	40.275	56.4
Diamond	0.001	2500	122	1.406	-27.706	112.4
	0.01	2500	83	1.298	7.039	84.5
	0.1	2500	86	1.281	4.328	86.6

6 Interpretation of the Experimental Data

In Chapter 6 the CHF and HTC experimental data are interpreted in light of the test section surface characterization presented in Chapter 5. Section 6.1 discusses the HTC predictions using existing models/correlations, which are compared with the measured HTC. In Section 6.2 the CHF models developed by Celata et al. (1994b) and Ku and Kandlikar (2008) are evaluated with respect to their ability to predict the measured CHF in nanofluids. Section 6.3 discusses the potentially relevant nanoparticle effects on HTC and CHF. Finally, Section 6.4 discusses the possible effects of pressure and radiation on nanofluid boiling heat transfer in view of future research efforts in this area.

6.1 Comparison of Heat Transfer Coefficient Data to Models/Correlations

The purpose of this task is to compare the measured HTC to the predictions of traditional models or correlations. As discussed in Chapter 4, Chen's and Klimenko's models were selected for prediction of the HTC, while the Davis and Anderson's model was selected for the onset of nucleate boiling (ONB).

6.1.1 Prediction by Chen's and Klimenko's Models

In our experiments the heat flux is a control variable; therefore, the correlations are used to find the wall temperature and then the HTC.

Chen's model is expressed in Eq. 2-14, in which the applied heat flux, q'' is the control variable in the experiment. T_b is bulk outlet temperature measured during the experiment. Eq. 2-15 is adopted to evaluate the forced convective HTC contribution. In addition, Eq. 2-16 associated with Eq. 2-17 is used to calculate the nucleate boiling contribution. In Eqs. 2-15 and 17, the flow quality X is set equal to zero for subcooled conditions. In Eqs. 2-15 to 17, the thermo-physical properties, k_l, μ_l, and $c_{p,l}$ are evaluated at the local bulk outlet temperature, T_b. Also, k_f, μ_f, ρ_f, ρ_g, and σ are thermo-physical properties of saturated water at 1 bar (1.0×10^5 Pa), which were used in the Chen model also for the nanofluid tests because the thermo-physical properties of dilute nanofluids are very close to those of water, as explained in the Chapter 3. Eq. 2-16 itself is a rather complex function of T_w and is highly coupled with Eq. 2-14. Therefore in order to obtain T_w, Eqs. 2-14 to 17 are solved via an iterative procedure implemented in MATLAB.

In addition to Chen's model, Klimenko's model has been adopted to predict the HTC as well. As reviewed in Chapter 2, the model was developed by correlating the experimental data obtained mostly at saturated conditions (Klimenko, 1988 and 1990). Thus, use of Klimenko's in this analysis is an extrapolation. In utilizing Klimenko's correlation, the selection criterion between nucleate boiling and forced convective vaporization heat transfer regimes is determined by the convective boiling dimensionless number, N_{CB} (Eq. 2-18). N_{CB} could be calculated using our experimental conditions by taking the flow quality X=0, and was found to be always less than the critical value of 1.2×10^4. Therefore, only the forced convection nucleate boiling correlation

(Eq. 2-19) is used for the predictions. To obtain the wall temperature and HTC from Klimenko's correlation, one needs no iterations.

Regarding the ONB prediction, Davis and Anderson's model has been adopted, which provides an expression for the wall temperature at which ONB occurs, Eq. 2-10. T_w at ONB is then evaluated simply by inputting the applied heat flux from the experiments. The predictions by Chen's, Klimenko's, and Davis-Anderson's models are analyzed in Section 6.1.2 below. The numerical routines used to generate these predictions are reported in Appendices C and D.

6.1.2 HTC Predictions and Comparison to Measured Data

Figs. 6-1 to 6-42 show the measured inlet and outlet bulk temperatures along with the measured and predicted inner wall temperatures as a function of the applied heat flux for water, and alumina, zinc-oxide, and diamond nanofluids runs. The inner wall temperature was in fact calculated from the knowledge of measured outer wall temperature using Eqs. 4-1 and 2. The measured and predicted values for the wall temperature, as well as the experimental conditions, are tabulated in Appendix E. The wall temperature curves display the characteristics expected in a flow boiling experiment, with an initial linear behavior in the single-phase region and a significantly lower slope after the onset of nucleate boiling. In general, both Chen's and Klimenko's correlations seem to over-predict the wall temperature for both water and nanofluids.

Chen's model superposes the two modes of forced convective and nucleate boiling heat transfer. Thus, a smooth transition appears between the two regions. Also, Chen's correlation suggests that the HTC depends on the flow parameters (i.e., mass flux, geometry, quality,

pressure) and the thermo-physical properties, but not on the test section surface characteristics. Since all the flow parameters and thermo-physical properties for water and nanofluids are the same, the model shows no effect of the nanoparticles on HTC.

Unlike Chen's model, prediction using Klimenko's model yields a sharp transition at the point of ONB. This is due to the adoption of two different models in each region, where Dittus-Boelter's correlation was used for the single-phase region (T_{wall}<100 °C) and Klimenko's nucleate boiling correlation for T_{wall}>100 °C. In fact for T_{wall}>100 °C Klimenko's model show no dependence on the mass flux, thus convection is assumed to play no role in this region. Instead, the correlation depends on one surface parameter, e.g., the ratio of heater surface thermal conductivity to fluid thermal conductivity. However, the influence of the surface thermal conductivity is uncertain at this moment as the thickness of the porous layer in our experiment is as thin as a few microns. Realistic values of the surface thermal conductivity can be calculated using a model of porous media effective thermal conductivity (Maxwell, 1881) with assumptions of porous layer thickness of about 10 μm and porosity of 50%. The calculated values are 14.042, 14.222, and 14.337 W/m·K for alumina, zinc oxide, and diamond nanoparticles deposited to stainless steel 316 heater surface, respectively. Thermal conductivity of stainless steel 316 heater is 14 W/m·K. As such, no dramatic thermal conductivity change appears after nanofluids boiling. Therefore the thermal conductivity of the original bare surface (i.e., stainless steel grade 316) was utilized for both water and nanofluids runs. The resulting prediction shows no effect of the nanofluid boiling. More detailed calculation and discussion of the surface thermal conductivity effect on the HTC are discussed in Section 6.3.2. Other important surface effects such as micro-structure, number of micro-cavities, and wettability are simply not included in either Chen's or Klimenko's model.

As for ONB, the measured ONB point seems to occur when the applied heat flux exceeds

about 1.0 MW/m^2 at G = 1500 kg/m^2·s, whereas it occurs at higher heat flux for the higher mass fluxes of 2000 and 2500 kg/m^2·s, as expected. The predicted temperatures at ONB are within 105 to 140 °C over the range of the applied heat flux. In many cases, predicted $T_{w,ONB}$ is even higher than the measured T_w at high heat flux region (q''>4 MW/m^2), at which the occurrence of significant nucleate boiling is evident as observed during the experiment. The points of ONB in terms of applied heat flux are not much different between water and nanofluids at G=1500 and 2000 kg/m^{2}s. Often, later ONB seemed to occur in nanofluids boiling compared to water boiling at G=2500 kg/m^{2}s. Note that, like Chen's model, the important surface effects are not included in Davis-Anderson's model.

As far as the behavior of the measured wall temperatures is concerned, an interesting feature is the frequent reversals (more than twice) in temperature vs heat flux curves for the alumina and zinc oxide nanofluids tests at high heat fluxes. This was also observed by Kim et al.'s work (2006a). No such reversals were observed in diamond nanofluids tests at intermediate heat fluxes (q''> 3~4 MW/m^2). Possible reasons for the reversals may include surface morphology changes as the nanoparticles continue to accumulate on the surface as a result of boiling during the experiment, and may also spall off due to the flow-induced shear stress. The particle deposition morphology (and likely the strength of the deposited layer) differs from one material to another, as seen in the SEM pictures shown in Chapter 5, which may explain why certain nanofluids exhibit the reversals and others do not. However, a definitive explanation of these temperature reversals is not available at this time.

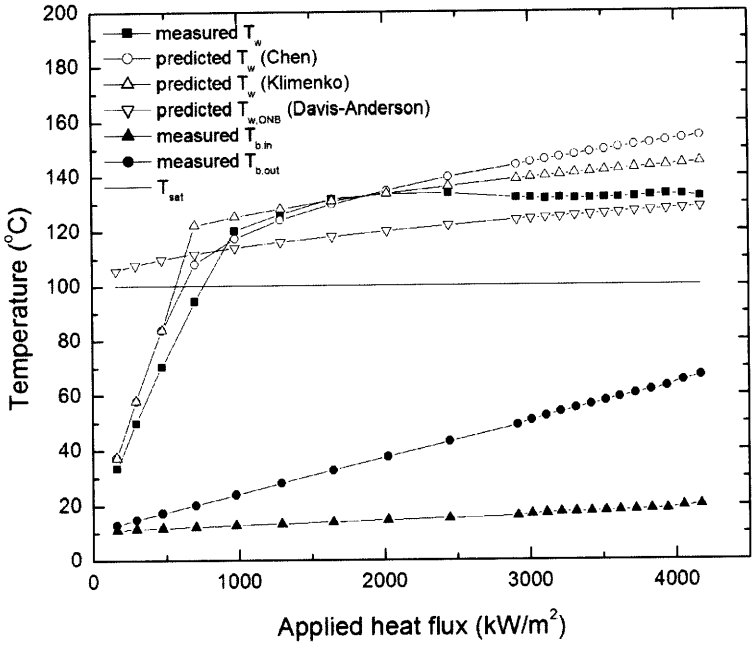

Figure 6-1 Temperature vs heat flux curve for pure water at G=1500 kg/m^2·s (Test 1)

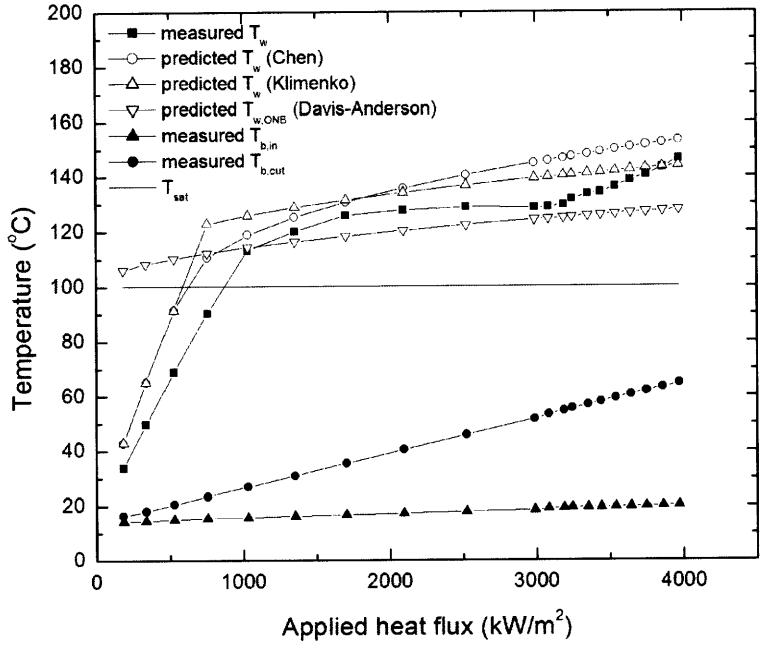

Figure 6-2 Temperature vs heat flux curve for pure water at G=1500 kg/m^2·s (Test 2)

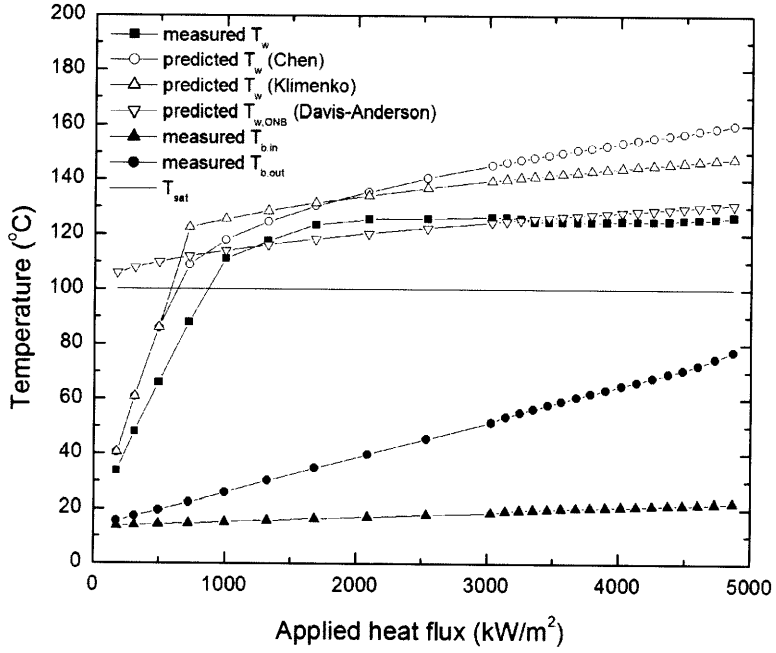

Figure 6-3 Temperature vs heat flux curve for pure water at G=1500 kg/m^2·s (Test 3)

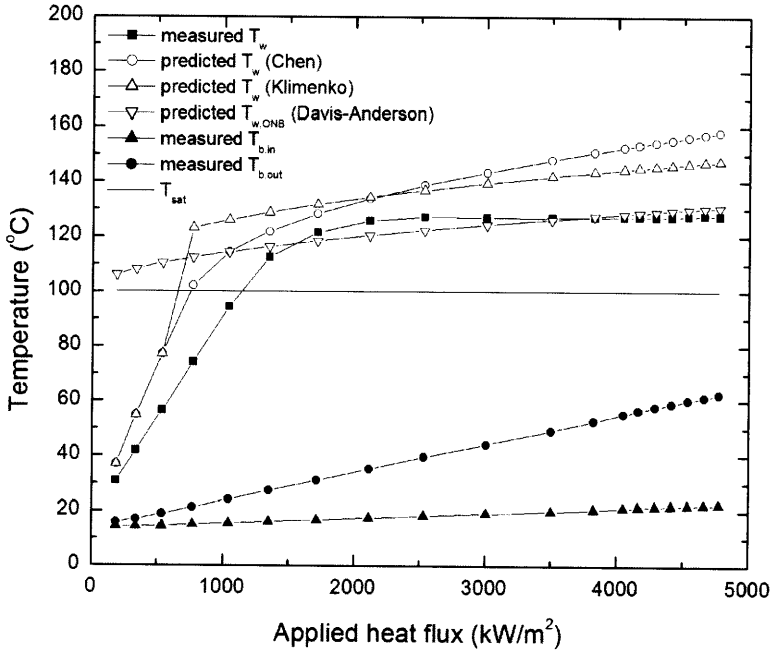

Figure 6-4 Temperature vs heat flux curve for pure water at G=2000 kg/m^2·s (Test 1)

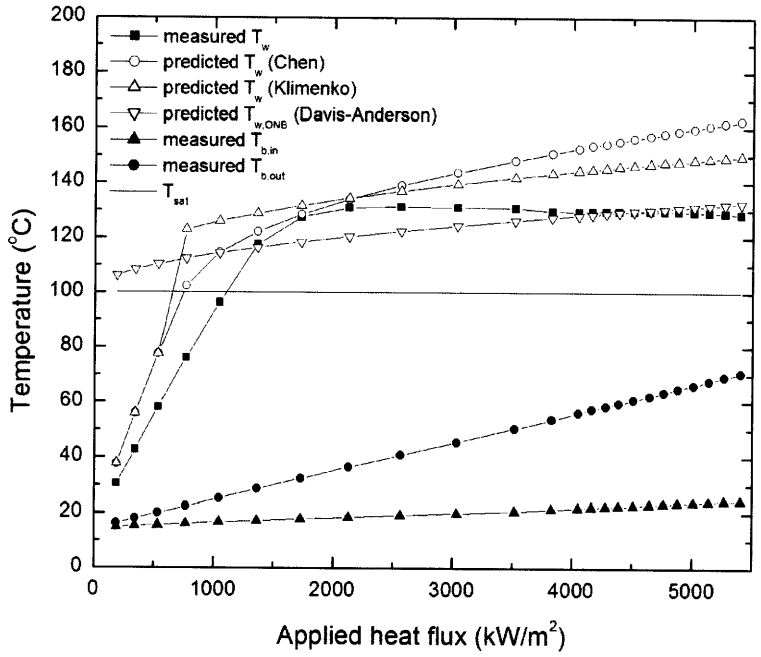

Figure 6-5 Temperature vs heat flux curve for pure water at G=2000 kg/m^2·s (Test 2)

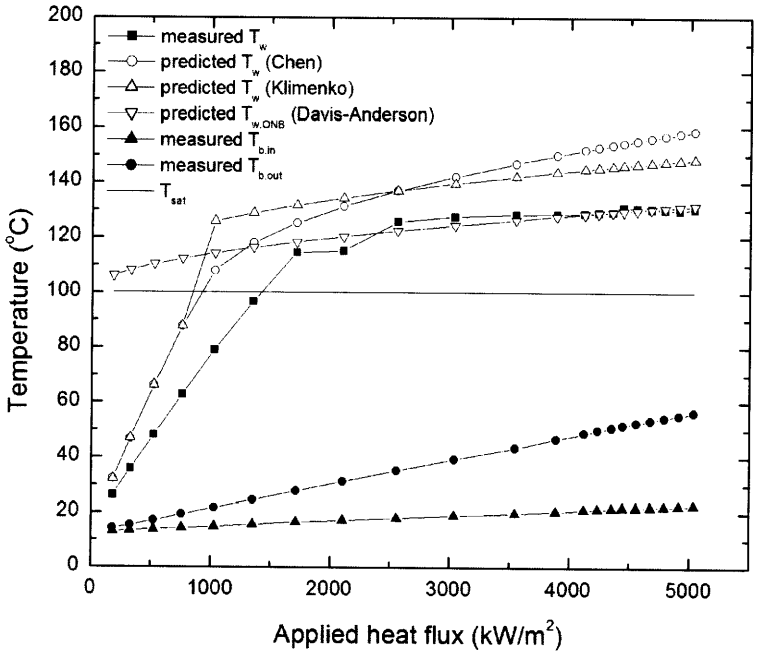

Figure 6-6 Temperature vs heat flux curve for pure water at G=2500 kg/m^2·s (Test 1)

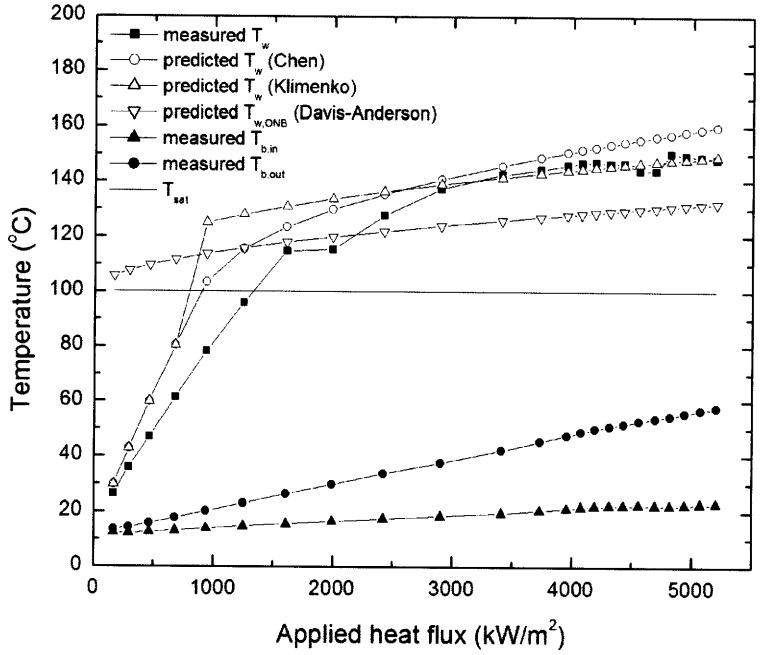

Figure 6-7 Temperature vs heat flux curve for pure water at G=2500 kg/m^2·s (Test 2)

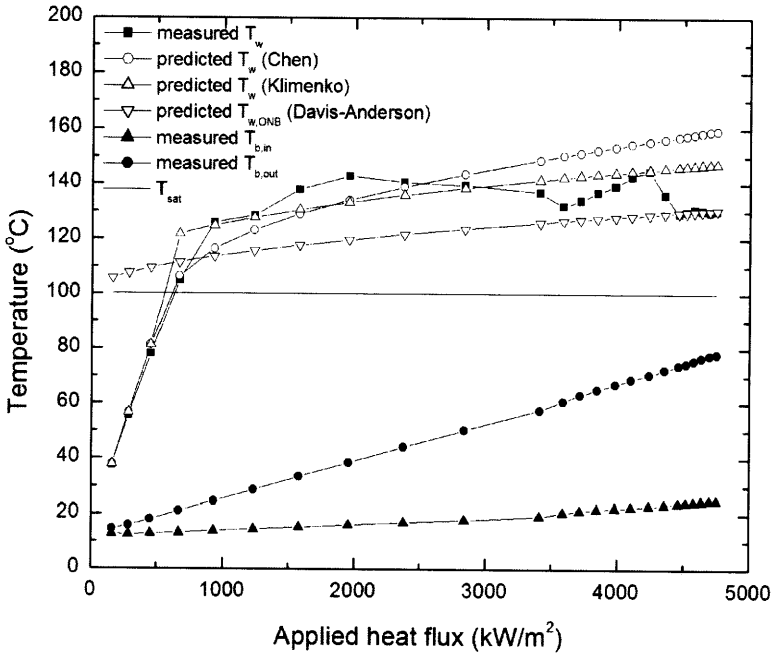

Figure 6-8 Temperature vs heat flux curve for 0.001 %vol. alumina nanofluid at G=1500 kg/m^2·s (Test 1)

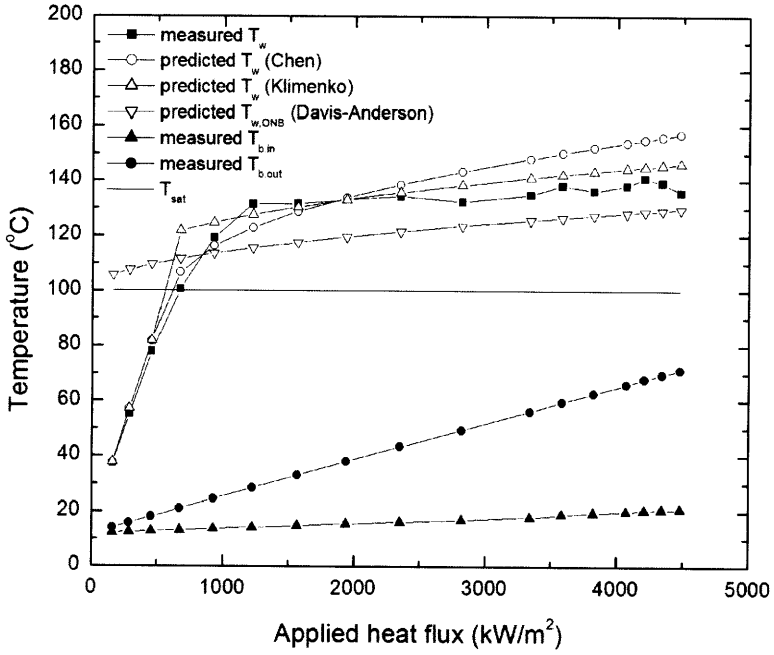

Figure 6-9 Temperature vs heat flux curve for 0.001 %vol. alumina nanofluid at G=1500 kg/m^2·s (Test 2)

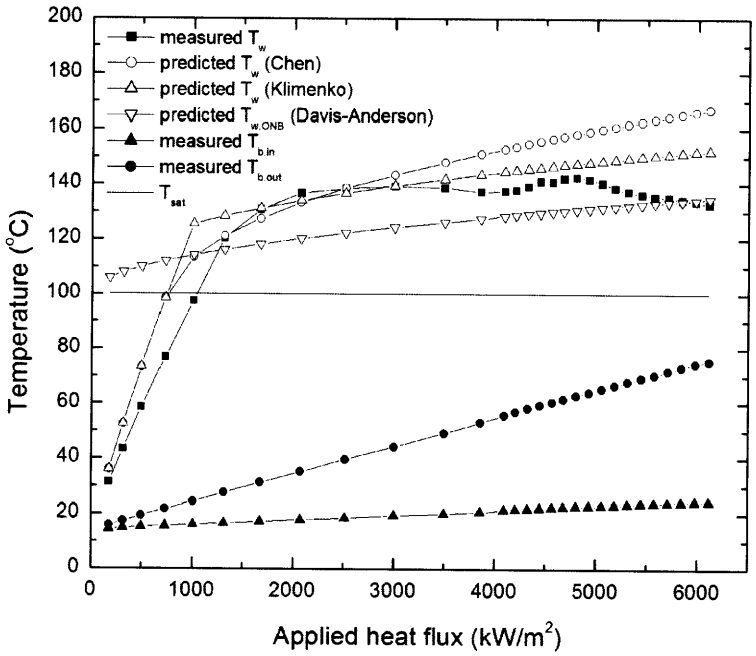

Figure 6-10 Temperature vs heat flux curve for 0.001 %vol. alumina nanofluid at G=2000 kg/m^2·s (Test 1)

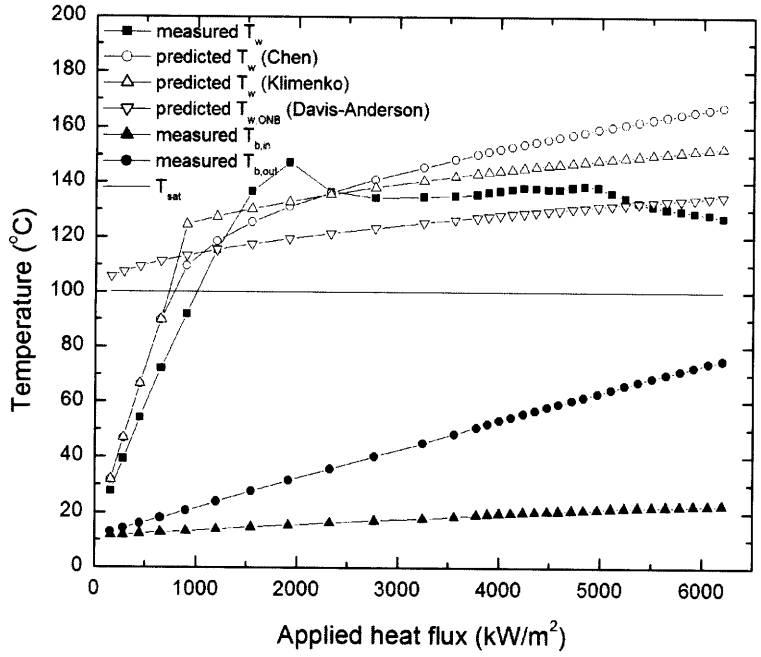

Figure 6-11 Temperature vs heat flux curve for 0.001 %vol. alumina nanofluid at G=2000 kg/m^2·s (Test 2)

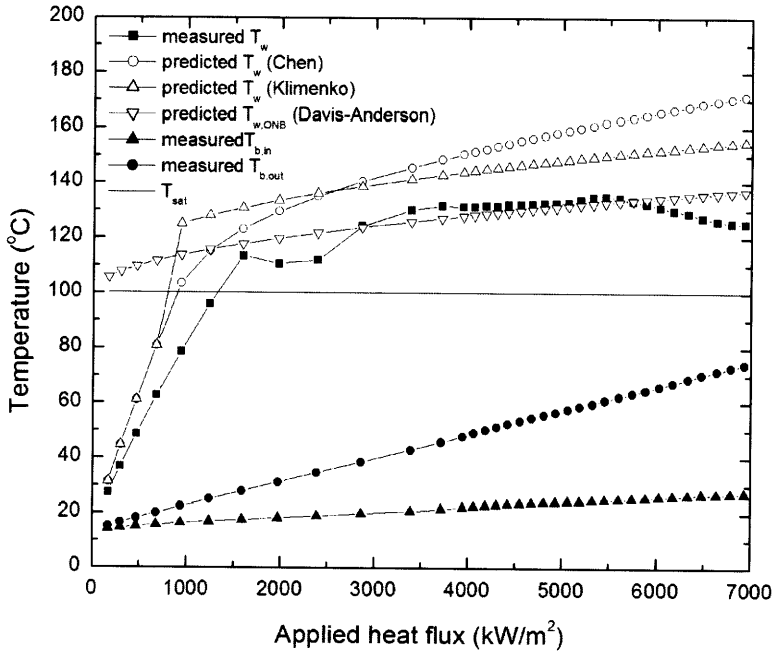

Figure 6-12 Temperature vs heat flux curve for 0.001 %vol. alumina nanofluid at G=2500 kg/m^2·s (Test 1)

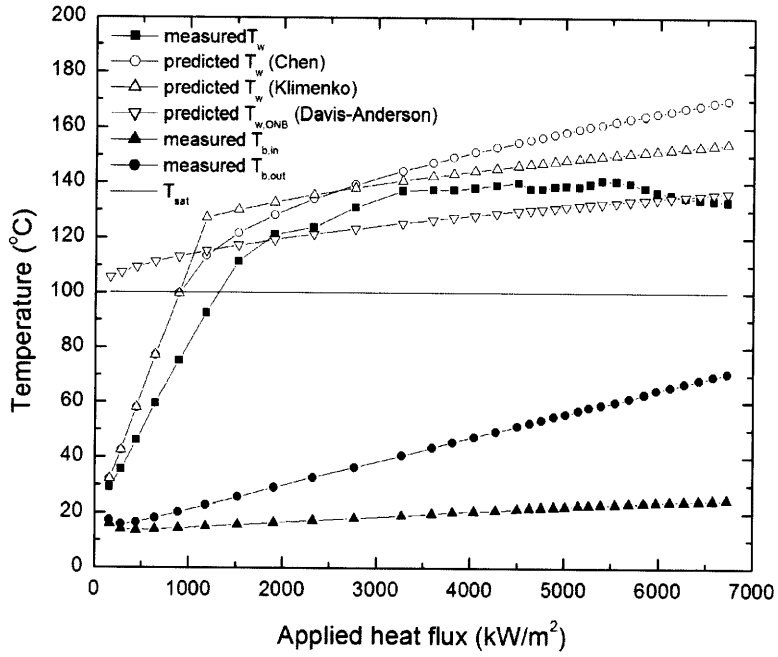

Figure 6-13 Temperature vs heat flux curve for 0.001 %vol. alumina nanofluid at G=2500 kg/m^2·s (Test 2)

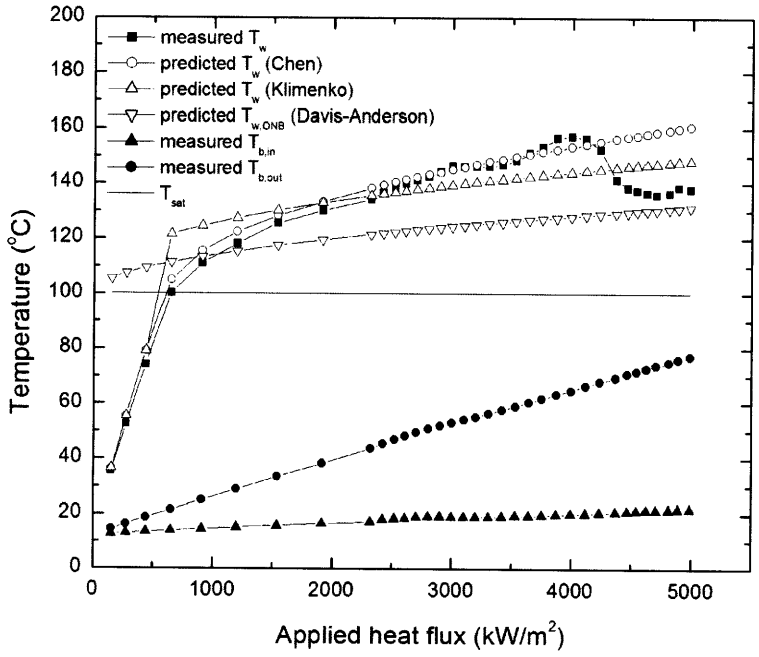

Figure 6-14 Temperature vs heat flux curve for 0.01 %vol. alumina nanofluid at G=1500 kg/m^2·s (Test 1)

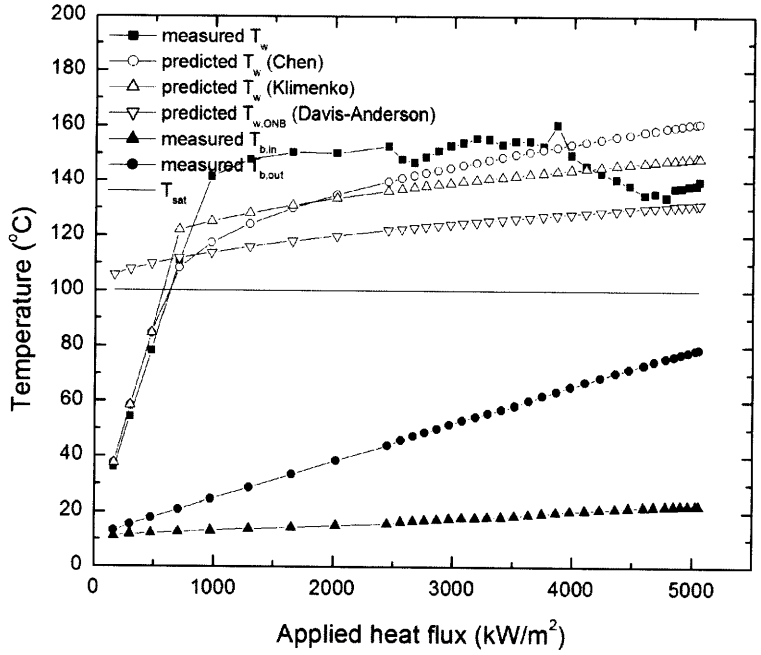

Figure 6-15 Temperature vs heat flux curve for 0.01 %vol. alumina nanofluid at G=1500 kg/m^2·s (Test 2)

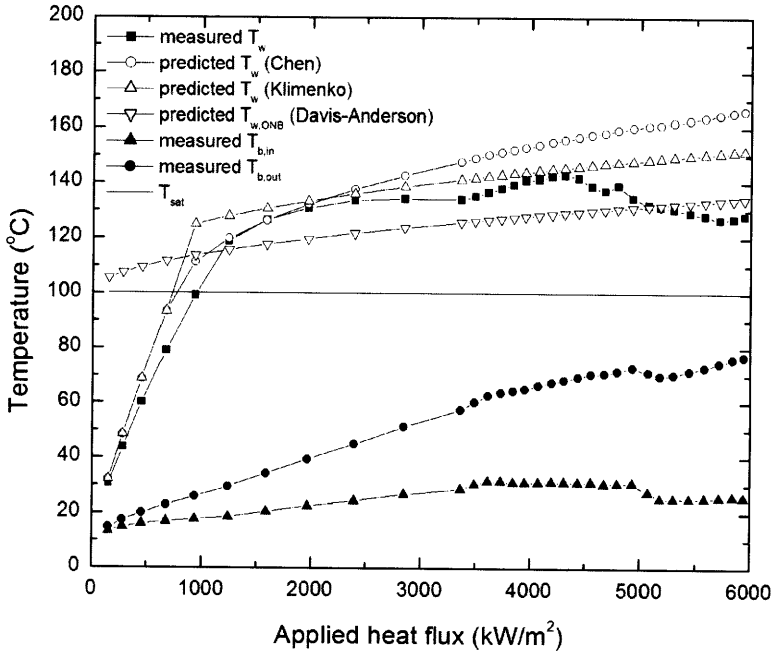

Figure 6-16 Temperature vs heat flux curve for 0.01 %vol. alumina nanofluid at G=2000 kg/m^2·s (Test 1)

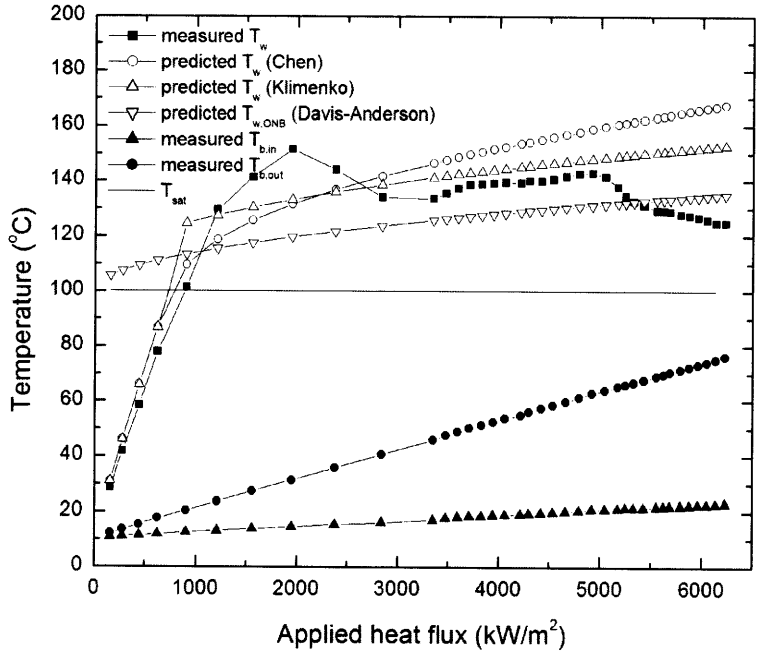

Figure 6-17 Temperature vs heat flux curve for 0.01 %vol. alumina nanofluid at G=2000 kg/m^2·s (Test 2)

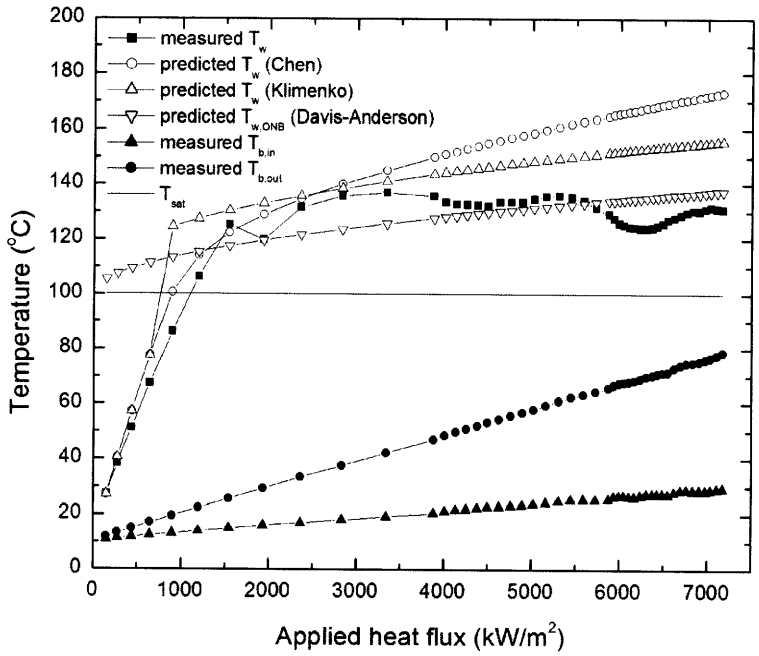

Figure 6-18 Temperature vs heat flux curve for 0.01 %vol. alumina nanofluid at G=2500 kg/m^2·s (Test 1)

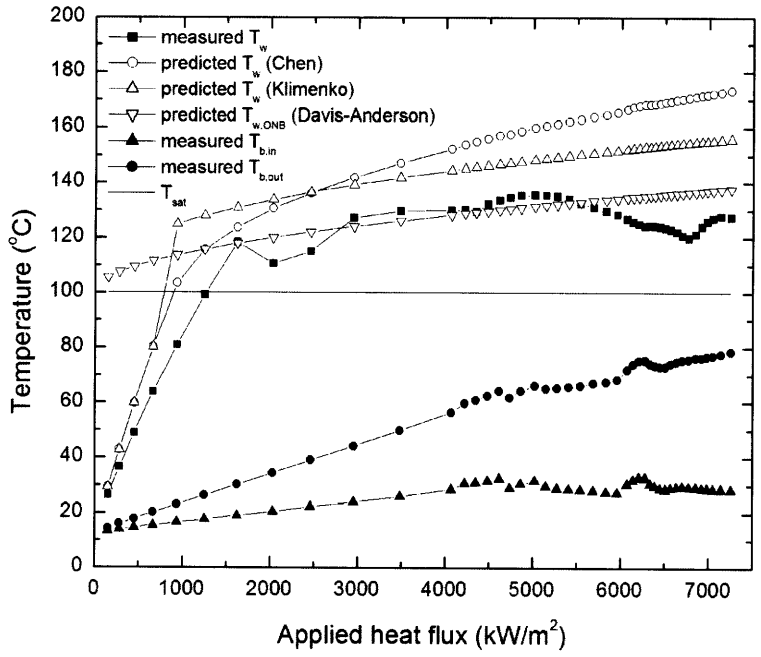

Figure 6-19 Temperature vs heat flux curve for 0.01 %vol. alumina nanofluid at G=2500 kg/m^2·s (Test 2)

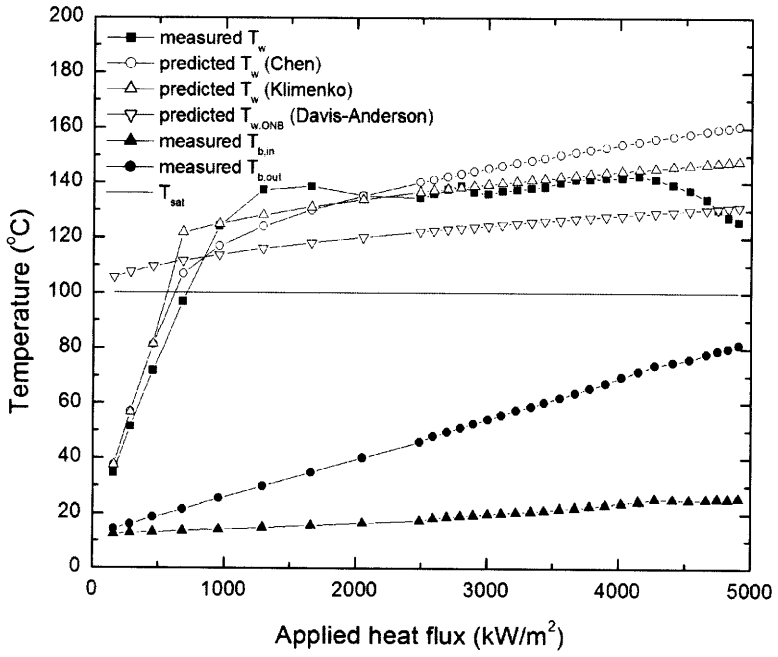

Figure 6-20 Temperature vs heat flux curve for 0.1 %vol. alumina nanofluid at G=1500 kg/m^2·s (Test 1)

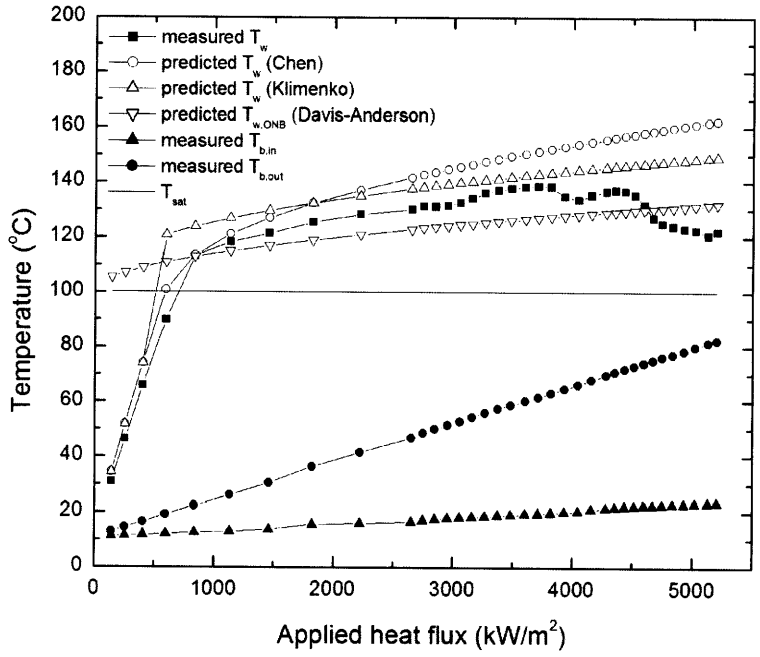

Figure 6-21 Temperature vs heat flux curve for 0.1 %vol. alumina nanofluid at G=1500 kg/m^2·s (Test 2)

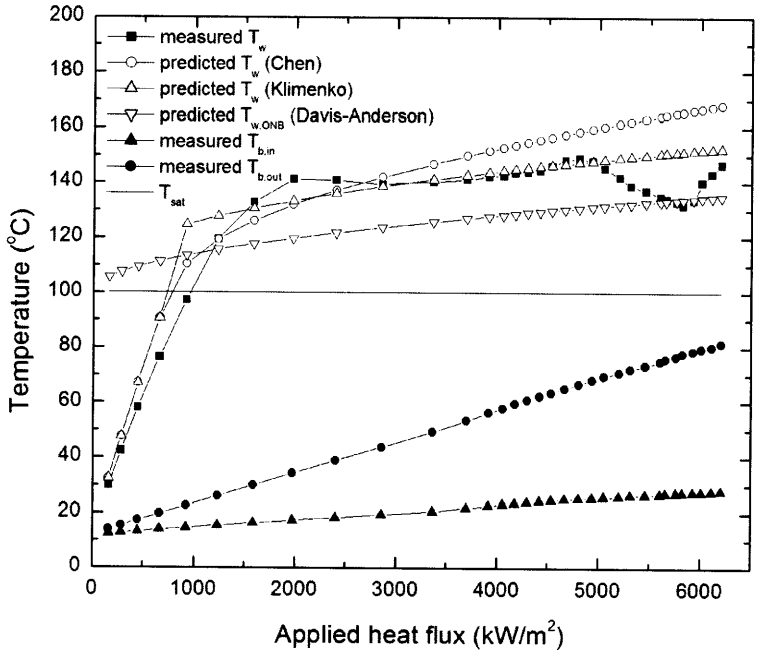

Figure 6-22 Temperature vs heat flux curve for 0.1 %vol. alumina nanofluid at G=2000 kg/m^2·s (Test 1)

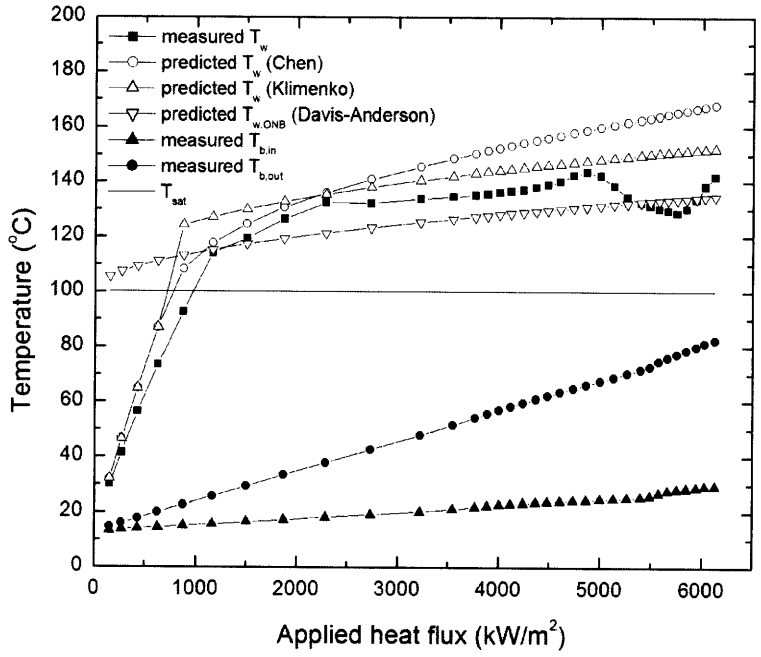

Figure 6-23 Temperature vs heat flux curve for 0.1 %vol. alumina nanofluid at G=2000 kg/m^2·s (Test 2)

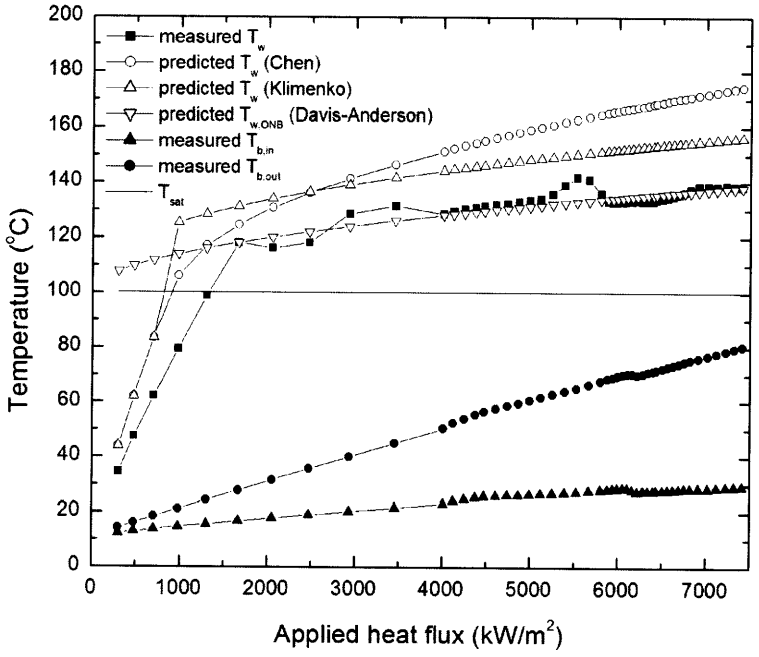

Figure 6-24 Temperature vs heat flux curve for 0.1 %vol. alumina nanofluid at G=2500 kg/m^2·s (Test 1)

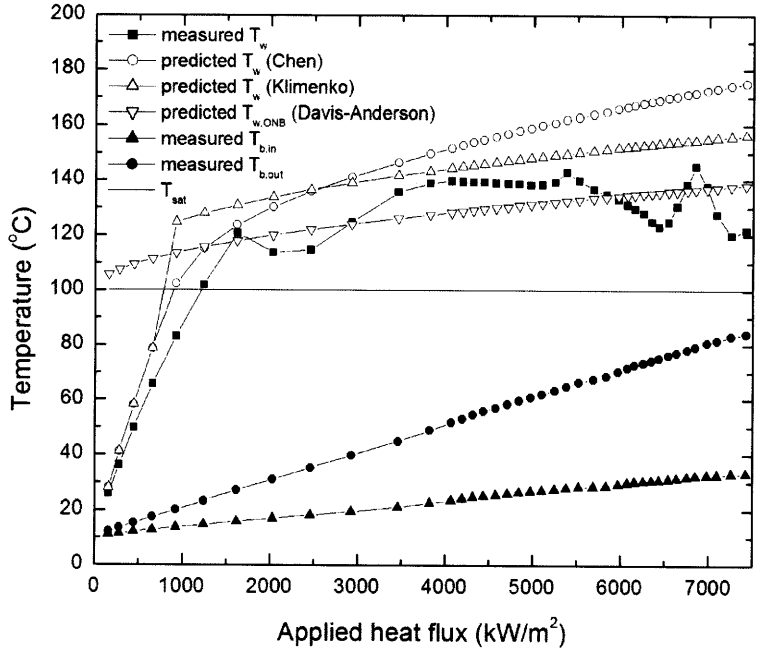

Figure 6-25 Temperature vs heat flux curve for 0.1 %vol. alumina nanofluid at G=2500 kg/m^2·s (Test 2)

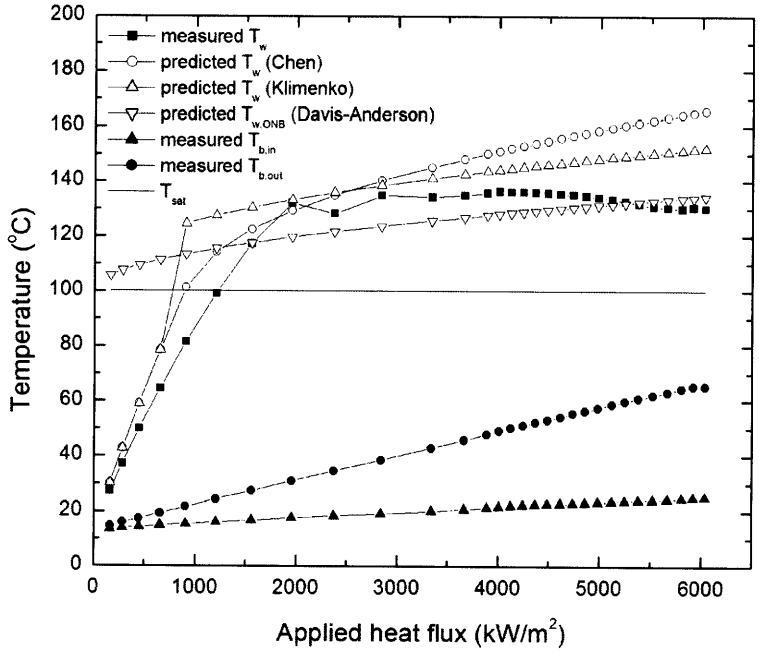

Figure 6-26 Temperature vs heat flux curve for 0.001 %vol. zinc oxide nanofluid at G=2500 kg/m^2·s (Test 1)

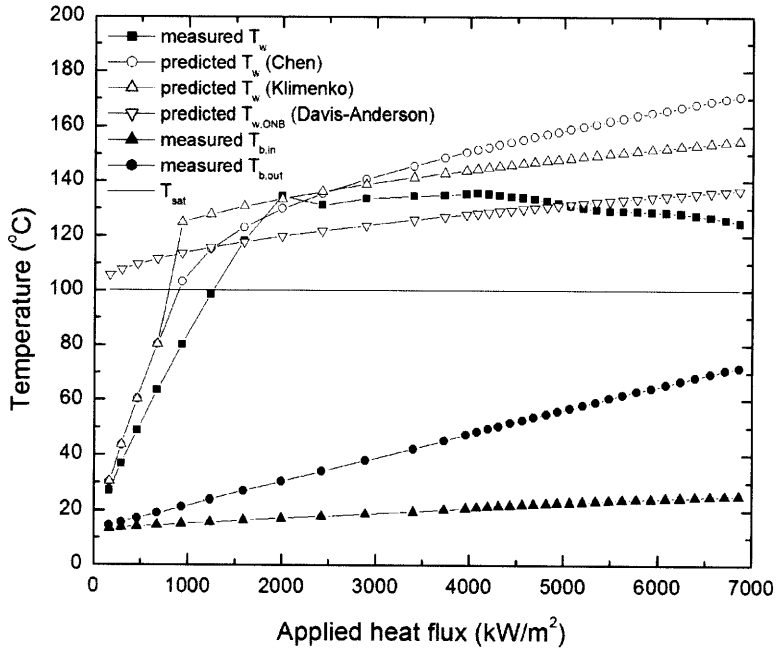

Figure 6-27 Temperature vs heat flux curve for 0.001 %vol. zinc oxide nanofluid at G=2500 kg/m^2·s (Test 2)

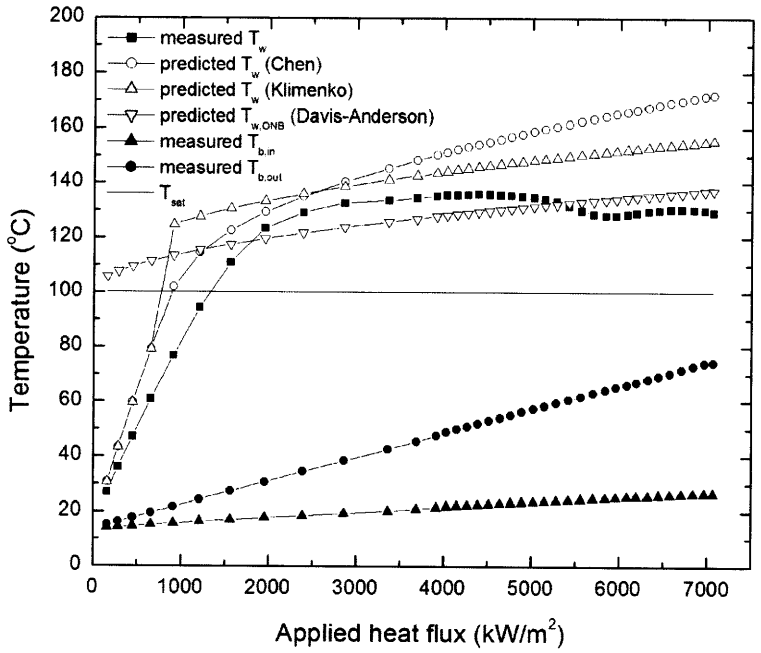

Figure 6-28 Temperature vs heat flux curve for 0.01 %vol. zinc oxide nanofluid at G=2500 kg/m^2·s (Test 1)

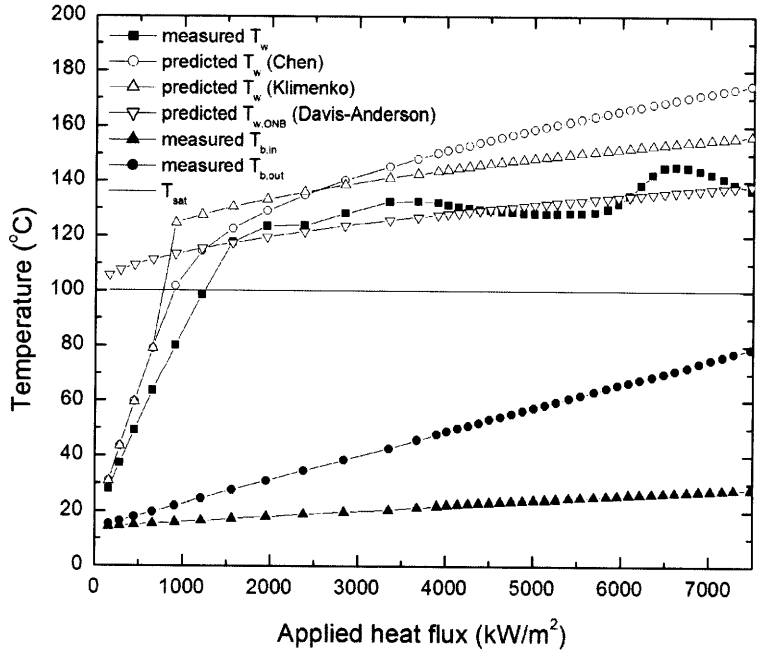

Figure 6-29 Temperature vs heat flux curve for 0.01 %vol. zinc oxide nanofluid at G=2500 kg/m^2·s (Test 2)

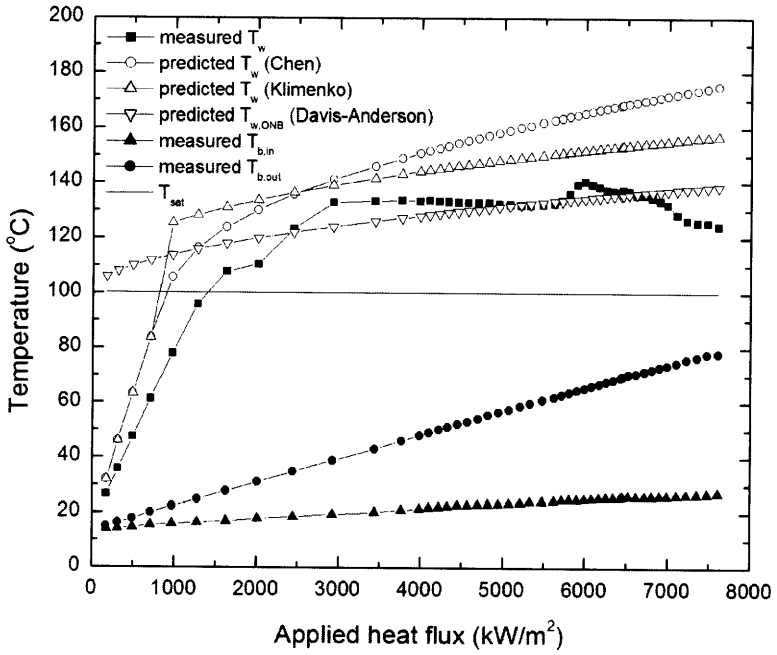

Figure 6-30 Temperature vs heat flux curve for 0.1 %vol. zinc oxide nanofluid at G=2500 kg/m^2·s (Test 1)

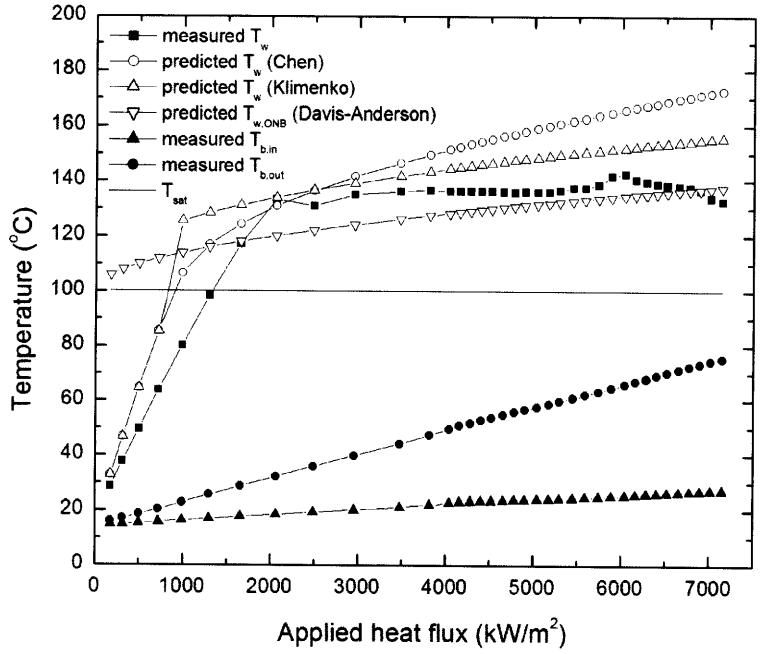

Figure 6-31 Temperature vs heat flux curve for 0.1 %vol. zinc oxide nanofluid at G=2500 kg/m^2·s (Test 2)

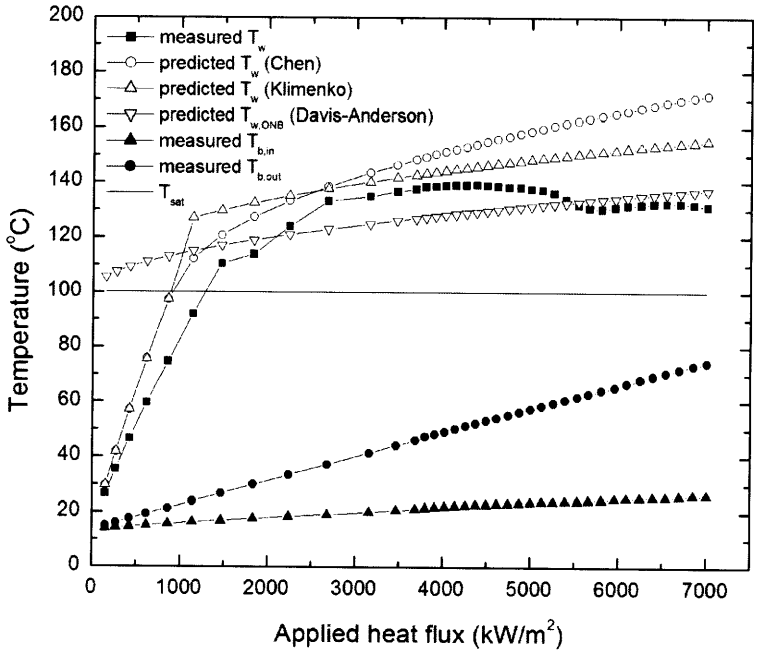

Figure 6-32 Temperature vs heat flux curve for 0.001 %vol. diamond nanofluid at G=2500 kg/m^2·s (Test 1)

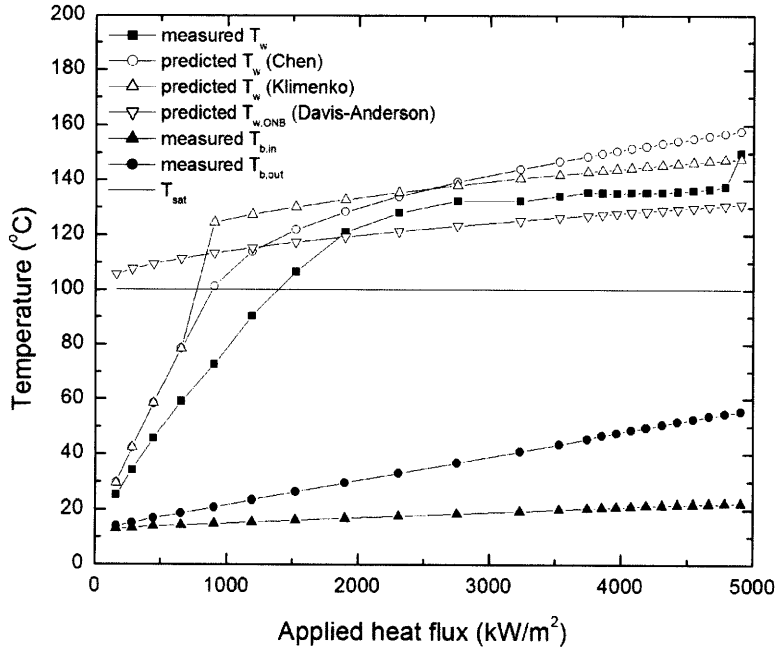

Figure 6-33 Temperature vs heat flux curve for 0.001 %vol. diamond nanofluid at G=2500 kg/m^2·s (Test 2)

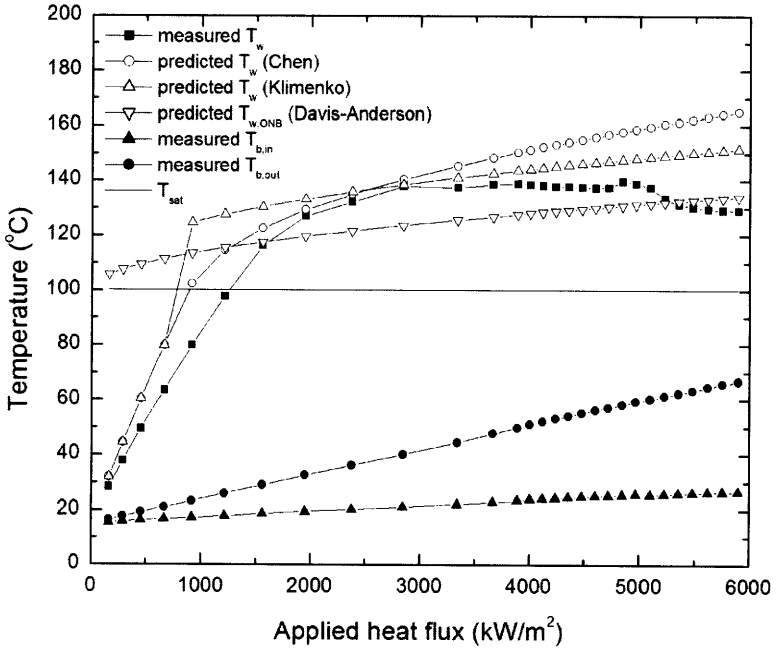

Figure 6-34 Temperature vs heat flux curve for 0.001 %vol. diamond nanofluid at G=2500 kg/m^2·s (Test 3)

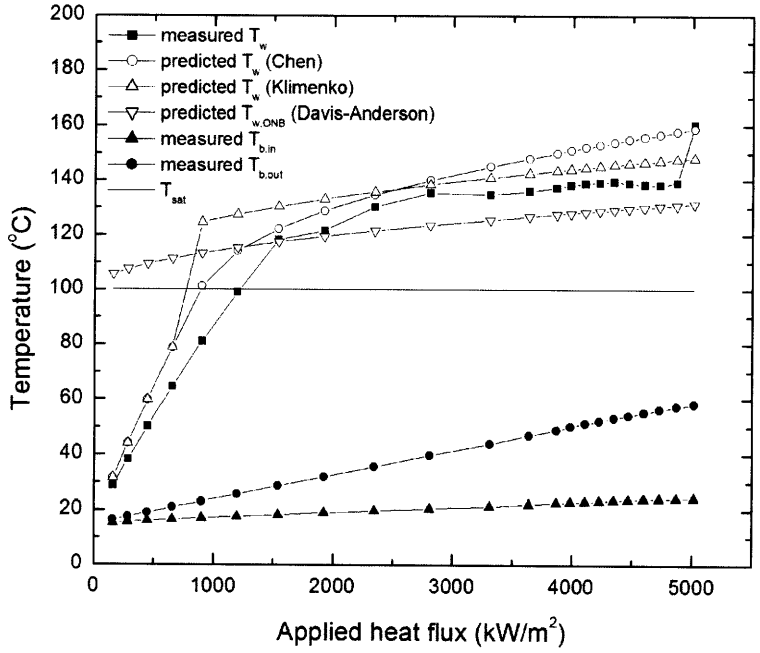

Figure 6-35 Temperature vs heat flux curve for 0.001 %vol. diamond nanofluid at G=2500 kg/m^2·s (Test 4)

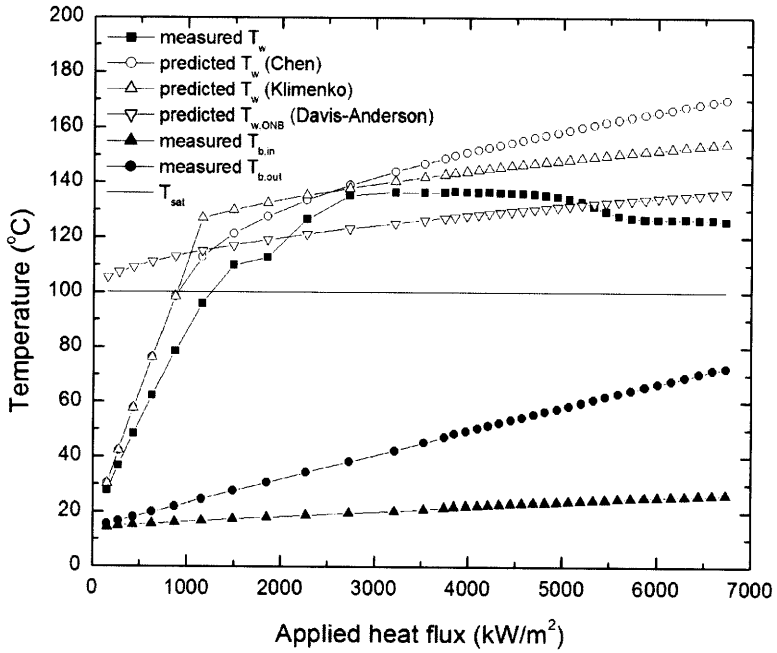

Figure 6-36 Temperature vs heat flux curve for 0.01 %vol. diamond nanofluid at G=2500 kg/m^2·s (Test 1)

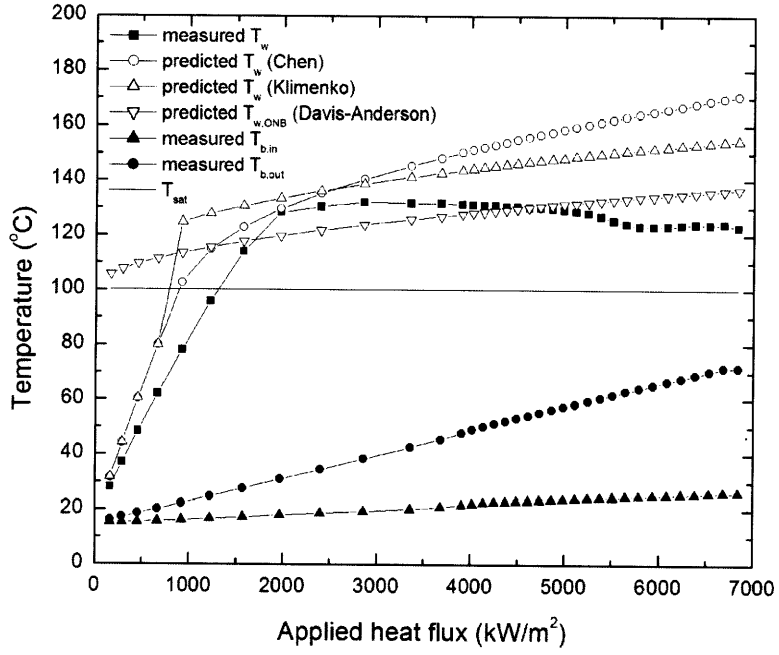

Figure 6-37 Temperature vs heat flux curve for 0.01 %vol. diamond nanofluid at G=2500 kg/m^2·s (Test 2)

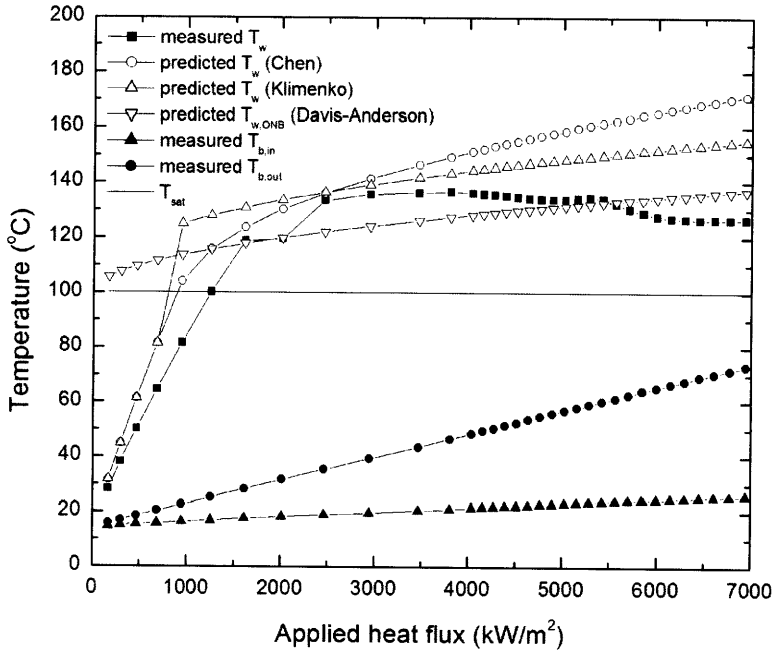

Figure 6-38 Temperature vs heat flux curve for 0.01 %vol. diamond nanofluid at G=2500 kg/m^2·s (Test 3)

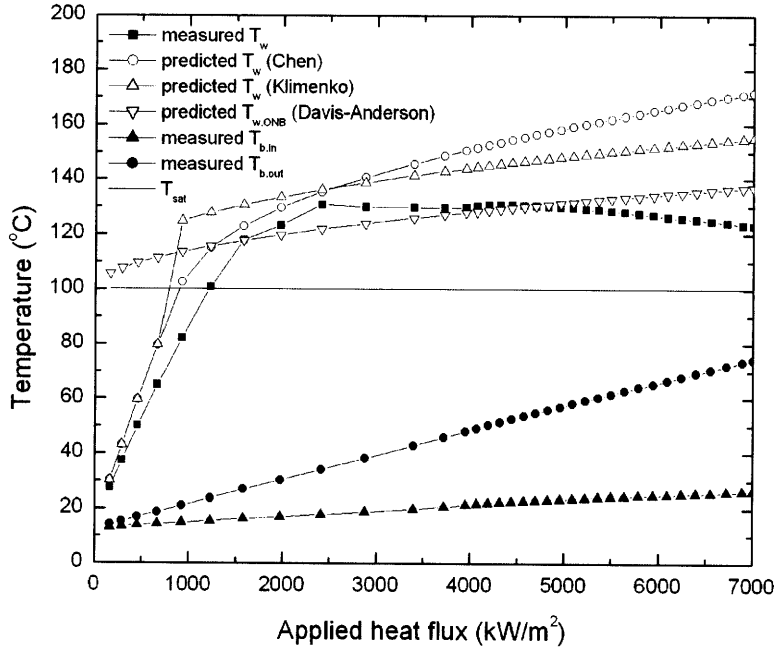

Figure 6-39 Temperature vs heat flux curve for 0.1 %vol. diamond nanofluid at G=2500 kg/m^2·s (Test 1)

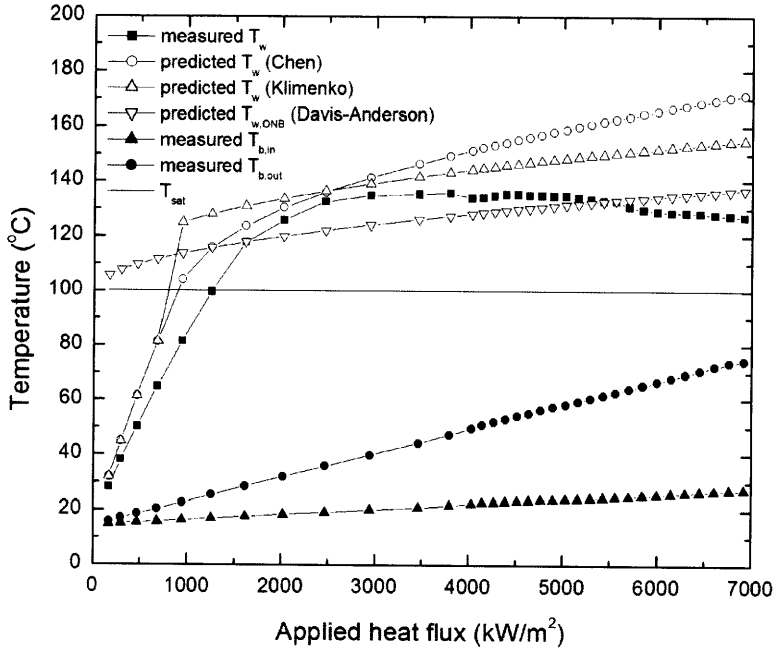

Figure 6-40 Temperature vs heat flux curve for 0.1 %vol. diamond nanofluid at G=2500 kg/m^2·s (Test 2)

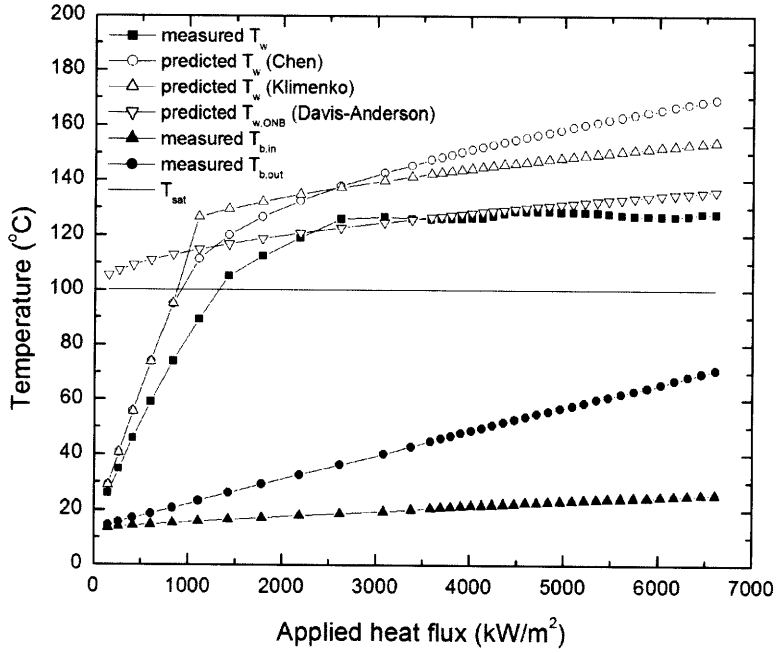

Figure 6-41 Temperature vs heat flux curve for 0.1 %vol. diamond nanofluid at G=2500 kg/m^2·s (Test 3)

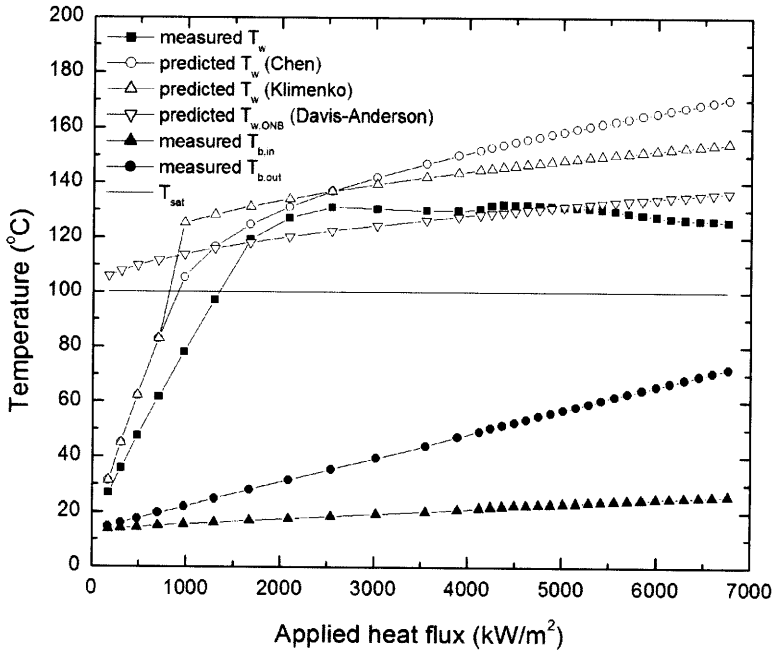

Figure 6-42 Temperature vs heat flux curve for 0.1 %vol. diamond nanofluid at G=2500 kg/m^2·s (Test 4)

The correlation predictions are shown in terms of HTC in Fig 6-43. Obviously, as the correlations over-predict the wall temperature, they underestimate the HTC, which is clearly seen in Fig 6-43 (a) for water and (b) for nanofluids. Chen's and Klimenko's models are in agreement up to intermediate values of the heat flux (~3.0 MW/m^2), beyond which Klimenko's model gives higher HTC values than Chen's, due to its strong dependence on the heat flux. Also, the slope of the HTC vs heat flux curves predicted by Chen's and Klimenko's models is fairly linear, whereas the measured HTC slope increases with increasing heat flux, particularly at high heat flux level (q''>5.0 MW/m^2). To conclude, neither Chen's nor Klimenko's models predict our water and nanofluid data accurately.

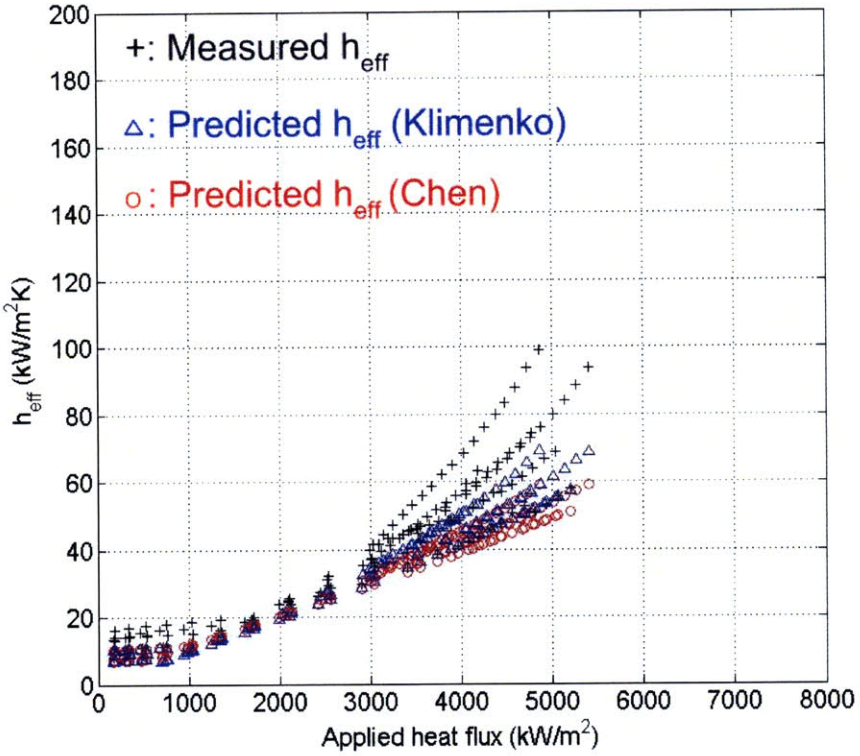

(a)

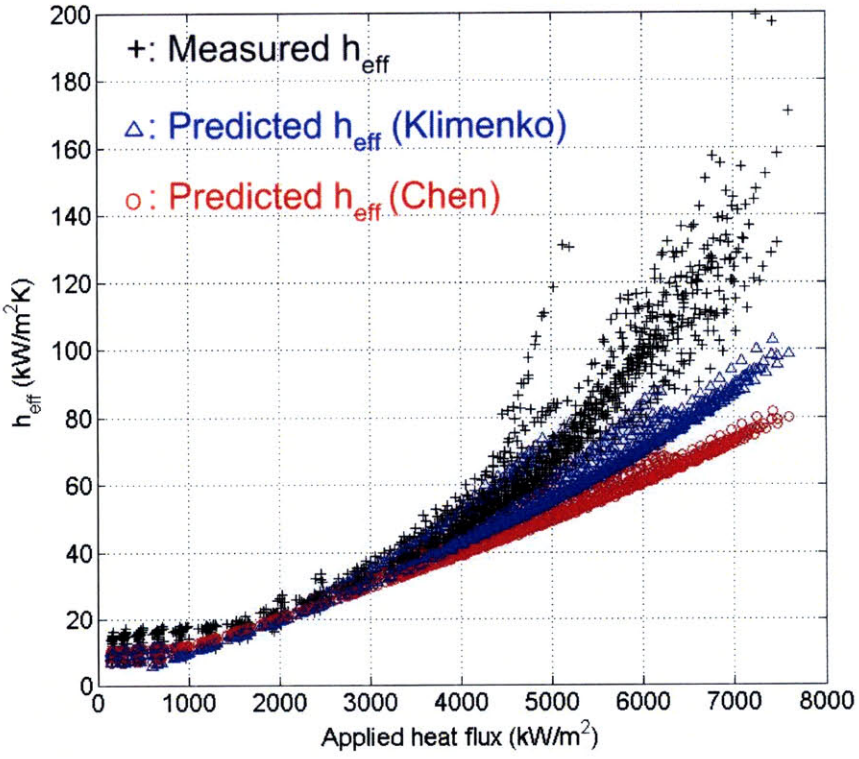

(b)

Figure 6-43 Measured vs predicted heat transfer coefficient for (a) water and (b) nanofluids

6.2 Comparison of CHF Data to Models/correlations

6.2.1 CHF Prediction Using Celata's Model

Celata's model (Celata et al., 1994b) was reviewed in Chapter 2. It was shown that the model implicitly suggests a dependence of the subcooled flow CHF on the contact angle, which was, in fact, adopted from Staub's study (1968). Using Eqs. 2-33 to 36, subcooled flow CHF can be predicted via an iteration procedure with a numerical code. In fact, a FORTRAN 77 routine was obtained from Drs. Celata and Mariani, and used for our calculations.

First, the model was compared to the 1995 CHF look-up table and our measured data for water. As recommended by Celata et al. in their study, $g(\beta)$ =0.03 in Eq. 2-38 was used. Three different mass fluxes (1500, 2000 and 2500 kg/m^{2}s) were considered. The results are given in Fig. 6-44, which shows that Celata et al's predictions exhibit a stronger dependence on the exit equilibrium quality than the data and the look-up table. Regarding the dependency on the mass flux, the CHF trend seems reversed as compared to what is expected (i.e., higher CHF with higher mass flux for DNB). The absolute values of the CHF are also significantly off with respect to the measured water data and look-up table at low (X_e~ -0.08) and high (X_e ~ -0.01) exit equilibrium quality.

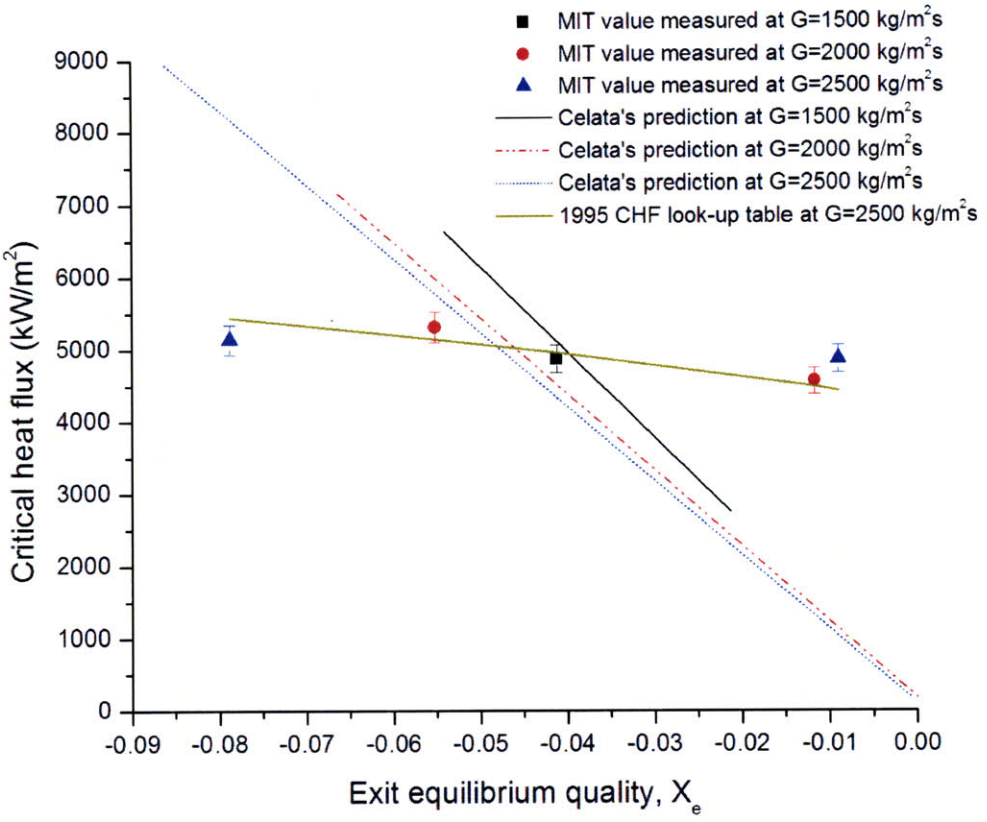

Figure 6-44 Comparison of measured water CHF data with Celata's and 1995 CHF look-up table predictions

Nonetheless, the main objective of interrogating Celata's model is to find the relationship between the contact angle and the CHF. Therefore it was decided to vary the contact angle function $g(\beta)$. Staub's original paper (1968) suggests values from 0.015 to 0.17 for $g(\beta)$ when the contact angle varies from 20 to 70°. Therefore, the contact angle effect was analyzed using $g(\beta)$=0.015, 0.03 and 0.17 for three different mass fluxes of 1500, 2000, and 2500 kg/m^{2}s for an inlet bulk temperature of 30 °C. The results are summarized in Table 6-1. In addition, Fig. 6-45 shows the clear CHF trend according to the contact angle variation.

Table 6-1 Calculation summary for Celata's prediction on contact angle effect

G (kg/m^{2}s)	Contact angle (degree)	$g(\beta)$	T_{in} (°C)	Exit equilibrium quality	D_B (m)	$q''_{CHF,Celata}$ (kW/m^2)
1500	20	0.015	30	-0.0504	1.7239×10^{-4}	3,700
	30	0.03	30	-0.0355	3.4478×10^{-4}	4,400
	70	0.17	30	1.0227	1.9537×10^{-3}	6,100
2000	20	0.015	30	-0.0589	1.1541×10^{-4}	4,400
	30	0.03	30	-0.0477	2.3081×10^{-4}	5,100
	70	0.17	30	1.0223	1.3079×10^{-3}	8,100
2500	20	0.015	30	-0.0653	8.3981×10^{-5}	5,000
	30	0.03	30	-0.0551	1.6825×10^{-4}	5,800
	70	0.17	30	-0.0016	9.5134×10^{-4}	10,000

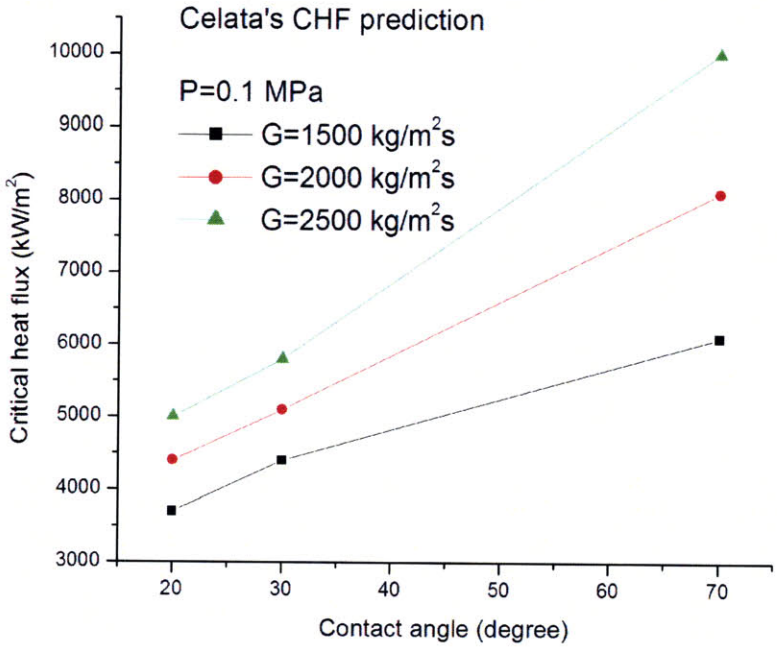

Figure 6-45 Celata et al.'s CHF prediction with three mass fluxes

First, it is seen that the model predicts larger vapor clot sizes (D_B) as the contact angle increases, but, strangely, the values in Table 6-1 increase with increasing contact angle. The trend is seen more clearly in Fig. 6-45. This trend is contrary to what is generally known about the effect of wettability on CHF (Tong and Tang, 1996; Kandlikar, 2001, Dinh et al., 2001, Coursey

and Kim, 2008, Kim et al., 2006b), and more importantly is contrary to our experimental results, which indicate that the CHF enhancement is associated with a reduction in contact angle for the alumina and zinc-oxide nanofluids tests (Table 5-5). We shall note that, while Celata et al.'s model does have the contact angle as one of its parameters through the function $g(\beta)$, the model was never validated with respect to its ability to predict the contact angle effect, and in fact Celata et al. recommend the use of a constant value for $g(\beta)$, i.e., $g(\beta)$=0.03. Therefore, a second flow CHF model including the contact angle, that of Kuan and Kandlikar (2008), is considered next.

6.2.2 CHF Prediction Using Kuan and Kandlikar's Model

Implementation of Kuan and Kandlikar's model for the CHF prediction is rather straightforward. Using Eqs. 2-43 and 44, the relative change of the CHF value with respect to the contact angle can be evaluated. For more simplification, the mixture density was set to equal the liquid phase density by taking the flow quality to zero. The baseline value is the CHF value at contact angle of 70°. Then, the relative changes of the CHF value ($CHFR_{\theta/70^o}$) are obtained by dividing the respective CHF values with the baseline value and corresponding results are tabulated in Table 6-2 with contact angle range from 10 to 70°. Also the visual trend can be seen in Fig. 6-46.

Table 6-2 Calculation summary for Kuan and Kandlikar's prediction on contact angle effect

Contact angle, β (degree)	Mass flux, G (kg/m^{2}s)	Channel height, b (m)	Surface tension, σ (N/m)	Mixture density, $\overline{\rho}$ (kg/m^3)	Relative change, $CHFR_{\theta/70^o}$ (%)
10	1500	0.1	0.05898	958.4	0.032
20	1500	0.1	0.05898	958.4	0.030
30	1500	0.1	0.05898	958.4	0.026
40	1500	0.1	0.05898	958.4	0.021
50	1500	0.1	0.05898	958.4	0.015
60	1500	0.1	0.05898	958.4	0.008
70	1500	0.1	0.05898	958.4	0
10	2000	0.1	0.05898	958.4	0.018
20	2000	0.1	0.05898	958.4	0.017
30	2000	0.1	0.05898	958.4	0.015
40	2000	0.1	0.05898	958.4	0.012
50	2000	0.1	0.05898	958.4	0.008
60	2000	0.1	0.05898	958.4	0.004
70	2000	0.1	0.05898	958.4	0
10	2500	0.1	0.05898	958.4	0.0001
20	2500	0.1	0.05898	958.4	0.0001
30	2500	0.1	0.05898	958.4	0.00009
40	2500	0.1	0.05898	958.4	0.00007
50	2500	0.1	0.05898	958.4	0.00005
60	2500	0.1	0.05898	958.4	0.00003
70	2500	0.1	0.05898	958.4	0

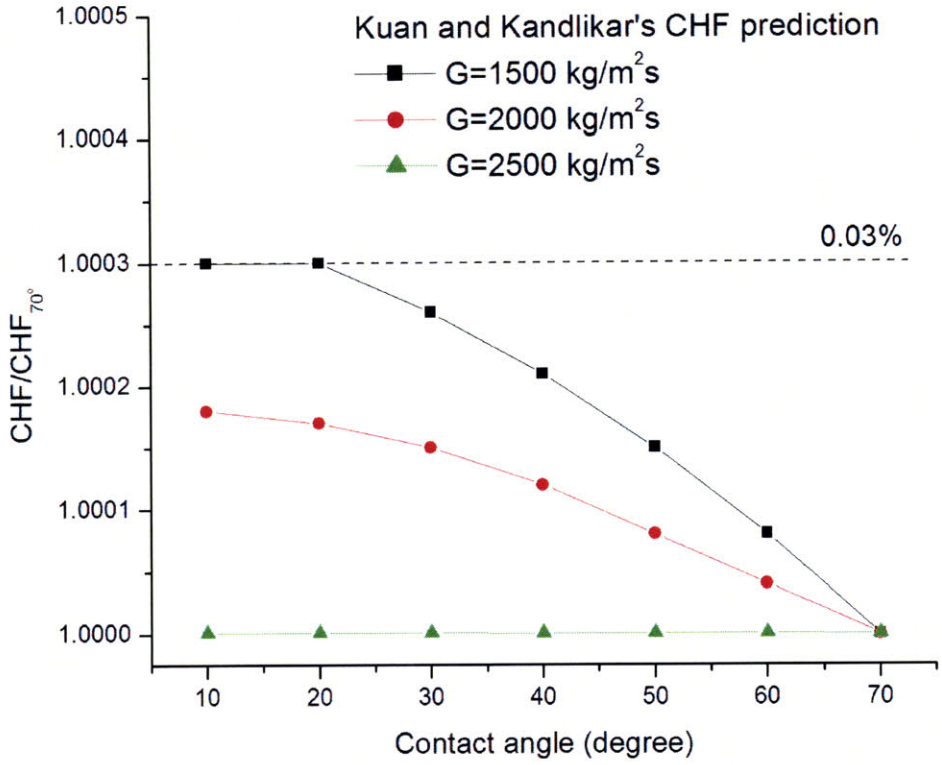

Figure 6-46 Kuan and Kandlikar's CHF prediction with contact angle range from 10° to 70°

In the table and figure, it is seen that the CHF decreases with increasing contact angle; however, the change is negligible (order of 0.03% or less) at any value of the mass flux. The relative increment decreases as the mass flux increases. In Eq. 2-43, the dependency on the contact angle is evident. However, the mass flux effect dominates over the contact angle effect. In fact, Ku and Kandlikar developed the model by correlating their experimental data obtained at relatively low mass flux range of 410.5 – 533.8 kg/m^{2}s, and in micro-channels where the effect of surface effects and wettability are expected to be more pronounced. Therefore, it is not unreasonable to suggest that this model may underpredict the effect of contact angle at high mass fluxes and in relatively large channels.

In summary, the only two available flow CHF models that include the contact angle as a variable, seem to suggest that contact angle changes would not be an important effect in our experiments. However, the contact angle effect in Celata et al.'s model was not validated, and Ku and Kandlikar's was developed for geometry and flow conditions different from ours.

6.3 Discussion of Nanoparticles Effects on HTC and CHF

An apparent consequence of nanofluids boiling is the nanoparticles deposition on the heater surface. Various aspects of this deposition have been discussed in the literature (You et al., 2003; Das et al., 2003, Vassallo et al., 2004; Dinh et al., 2004; Moreno Jr. et al., 2005; Bang and Chang, 2005; Milanova and Kumar, 2005; Wen and Ding, 2005; Milanova et al., 2006; Kim et al., 2006b; Kim et al., 2007; Kim, 2007). In particular, it was shown that the nanoparticle deposition is predominantly fueled by the nucleate boiling process itself, with time and applied heat flux being the governing variables (Kim et al., 2006; Kim et al., 2007; Kim 2007). Accordingly, a deposition layer tends to form on the heater surface. The inspection of the heater surfaces using SEM and confocal microscopes confirmed that such surface morphology changes occurred also in our experiments.

The main experimental results of this study are that the nanoparticles increase the CHF with respect to water, while the HTC is basically unchanged. In principle, the nanoparticles can affect both CHF and HTC either through a change in the thermo-physical properties of the fluid or through a change in the surface characteristics of the heater. Since the nanoparticles have a negligible effect on the thermo-physical properties of the nanofluids at the low concentrations explored in this study (see Chapter 3), we must focus our attention on the effect of nanoparticles

deposition on the surface.

The nanoparticle deposition may affect the surface thermal conductivity, surface roughness and surface area, capillary wicking, wettability, and nucleation site density. Each parameter change may have a unique impact on the boiling characteristics. The relative importance of these parameters in affecting the CHF and HTC has been assessed based on the accepted understanding of boiling phenomena and our engineering judgement, and the outcome of this process is reported in the Table 6-3. The (+) sign beside the parameters denotes an increase of that parameter; the (-) sign denotes a decrease. As this approach is very qualitative, it is accompanied in the following sections by a semi-quantitative analysis of each parameter, an analysis based on the experimental evidence.

Table 6-3 Qualitative assessment of surface parameter effects on CHF and HTC

Parameter	CHF	HTC	Physical mechanism	Support by exp. evidence
Surface thermal conductivity (+)	Affecting (+)	Affecting (+)	Heat dissipation by conduction	Possible
Roughness (+)	Affecting (+)	Affecting (+)	Nucleation site density change	Inconclusive
Surface area change (+)	Affecting (+)	Affecting (-)	Increased wettability	Inconclusive
Capillary wicking (+)	Strong (+)	Strong (+)	Liquid re-entrance	Strong (qualitatively)
Wettability (+)	Strong (+)	Strong (-)	Hot/dry spot reduction	Strong (quantitatively)
Nucleation site density (+)	Strong (+)	Strong (+)	Increased evaporation	Strong (inducible)

6.3.1 Roughness and Surface Area Effects

During subcooled flow boiling, forced convective heat transfer is still at work. First, we quantify its contribution to the overall heat transfer rate. Then, we look at the effect of nanoparticle deposition on it, which can be through a change in surface roughness. We also discuss the effect of roughness on nucleate boiling heat transfer, and the possible effect of surface area change on the CHF.

6.3.1.1 Heat Transfer Coefficient

6.3.1.1.1 Comparison of forced convective and nucleate boiling heat transfer coefficients

For this task, the relative importance of the forced convective and nucleate boiling heat transfer contributions is evaluated using Chen's model. Each heat transfer contribution is expressed, respectively as:

$$q''_{1p} = h_{FC}(T_w - T_b) \tag{6-1}$$

$$q''_{2p} = h_{NB}(T_w - T_{sat}) \tag{6-2}$$

where h_{FC} is given in Eq. 2-15 and h_{NB} was evaluated using Eqs. 2-16 and 17. We define q''_{1p}/q''_{2p} as the ratio of the forced convective heat transfer to the nucleate boiling. Note that this ratio can be evaluated in two different ways. Either using the measured values of T_w, or using the predicted values of T_w (predicted starting from the imposed heat flux). Fig. 6-47 shows the results obtained with the predicted wall temperature along with the test conditions of water and

nanofluids. Raw data of the measured and predicted ratio are given in Appendix F. It can be seen that the relative contribution of forced convective heat transfer decreases with the heat flux, which actually reflects a robust increase in the nucleate boiling contribution; while the forced convective heat transfer tends to increase with the mass flux, as expected, which is due to the $Re^{0.8}$ dependence of h_{FC}, as well the effect of the nucleation suppression factor, S, on h_{NB}.. Fig. 6-48 shows the results obtained using the measured values of T_w, with basically the same trends. The contribution of forced convection is less than 50% of the nucleate boiling heat transfer (or <25% of the overall heat transfer rate) at high heat fluxes, but not entirely negligible. The forced convective heat transfer might be affected by the roughness change due to the nanoparticle deposition, and this effect is analyzed in the next section.

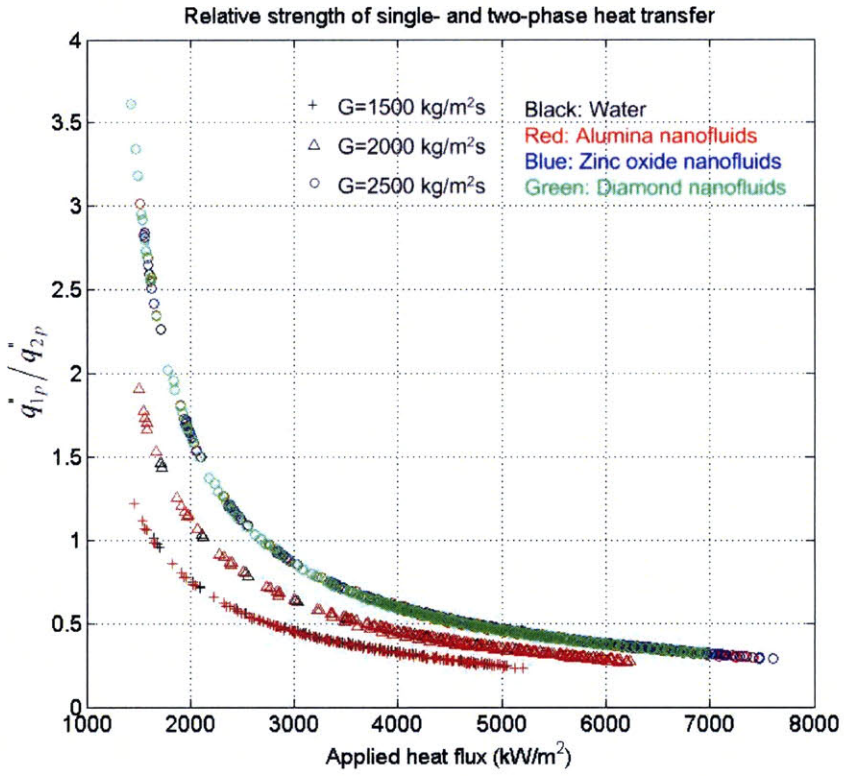

Figure 6-47 Relative strength of forced convective and nucleate boiling heat transfer using the predicted wall temperature values

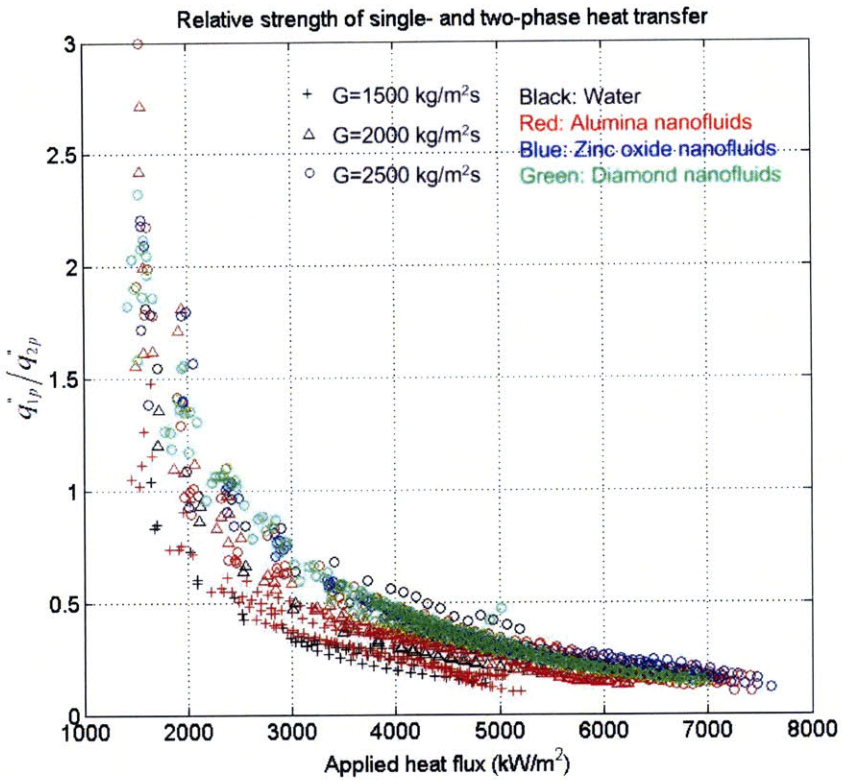

Figure 6-48 Relative strength of forced convective and nucleate boiling heat transfer using the measured wall temperature values

6.3.1.1.2 Roughness effect on forced convective heat transfer coefficient

To get an estimate of the roughness effect on forced convection, the Gnielinski's correlation was selected (Mills, 1999). The correlation is given by Eq. 3-30, where f is the friction factor, which was also given in Eq. 2-7. In the laminar flow, f is obtained using an analytical solution (f=64/Re). Otherwise it should be calculated from the Moody chart or the Colebrook equation. In order to use Eq. 3-30, Re and ε are needed. Thus, instead of using Eq. 2-7, the following formula is introduced to incorporate the roughness effect on the friction factor (http://www.lmnoeng.com/moody.htm).

$$f = \frac{1.325}{\left[\ln\left(\frac{\varepsilon}{3.7D} + \frac{5.74}{\mathrm{Re}^{0.9}}\right)\right]^2} \quad \text{for } 5000 < \mathrm{Re} < 10^8 \text{ and } 10^{-6} < \varepsilon/D < 10^{-2} \tag{6-3}$$

The Reynolds number, *Re*, calculated using the experimental conditions, ranges from 1.7×10^4 to 3.0×10^4 given the local bulk temperature of ~58 °C with varying mass fluxes of 1500 to 2500 kg/m^2·s, respectively. Regarding the surface roughness (ε), its typical value obtained with confocal microscopy is found to range from 1 to 3 μm for all water and nanofluids data (See Table 5-1).

The forced convective HTC estimates vs surface roughness are listed in Table 6-2 for the mass flux range of 1500 to 2500 kg/m^2·s. In detail, Fig. 6-49 shows the HTC trend with roughness change from 1 to 3 μm and its change is less than 4%, which suggests that the roughness effect on the forced convective heat transfer is insignificant in our case. Therefore, it is concluded that nanoparticle deposition does not affect the forced convection component of flow boiling heat transfer.

Table 6-4 Result of HTC calculation with roughness change

Mass flux G (kg/m^2·s)	Re	Roughness ε (μm)	friction factor f	Nu_G	HTC h (W/m^2·K)
1500	~1.7×10^4	1	0.02698	96.1	11255
		2	0.02740	97.2	11391
		3	0.02781	98.3	11522
2000	~2.3×10^4	1	0.02541	119.5	14008
		2	0.02589	121.3	14213
		3	0.02634	122.9	14405
2500	~3.0×10^4	1	0.02406	147.1	17232
		2	0.02460	149.6	17533
		3	0.02510	152.0	17811

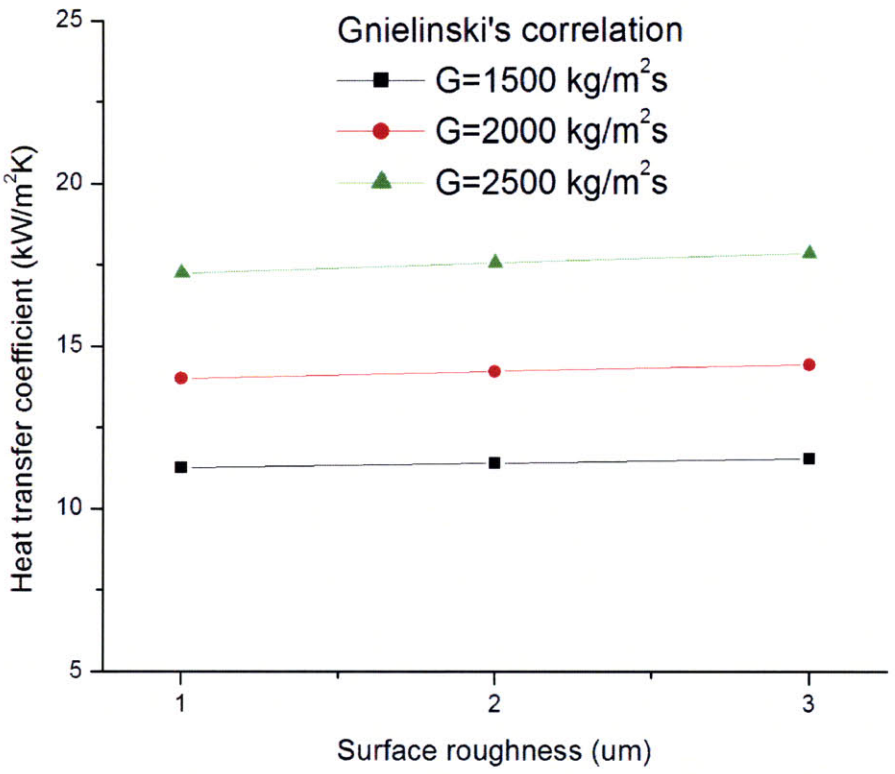

Figure 6-49 Calculated single-phase heat transfer coefficient using Genielinski's correlation at surface roughness range 1 to 3 μm

6.3.1.1.3 Roughness effect on nucleate boiling heat transfer coefficient

A change in surface roughness often reflects a change in surface morphology, which therefore can affect the boiling characteristics significantly. It is generally believed that the main consequence of a higher surface roughness is to increase the number of nucleation sites. In the current study, the surface roughness of the heater coupons was measured using confocal microscope. It was measured that the surface roughness in all tests ranges from 1.3 to 3.0 μm, with no apparent correlation between roughness change and CHF or HTC change.

Chowdhury and Winterton (1985) point out that roughness itself does not affect nucleate boiling directly but rather may be indirectly correlated to the number of nucleation sites on the surface. Furthermore, Pioro et al. (2004) describes roughness as a macro-scale measure of the surface uniformity and does not capture the detail information of the surface micro-structure. Therefore, a realistic interpretation of surface effects on boiling cannot be limited to roughness; instead it has to be based on detailed information of the surface micro-structure, e.g., number of micro-cavities and their size and shape are particularly useful in judging the effect on boiling characteristics. This topic is discussed in Section 6.3.4.1 below.

6.3.1.2 Critical Heat Flux

Another parameter obtainable from the confocal microscopy is the actual surface area of the test section coupons. The surface area change that occurs during nanofluid boiling could, in principle, have an effect on CHF if it is sufficiently high to reduce the effective heat flux delivered to the fluid. However, in our study the surface area changes are small (Table 5-1) and there appears to be no correlation between them and the CHF enhancement. Thus, a direct effect of surface area change on CHF can be excluded. On the other hand, indirect effects cannot be ruled out. For example, surface area change affects the wettability (contact angle) of the surface, as explained in Kim et al.'s study (2006b) and will be discussed in Section 6.3.4.

6.3.2 Surface thermal conductivity and thermal activity

The nanoparticle deposition changes the thermal properties of the surface, i.e., thermal conductivity, specific heat capacity, density. For example, since the thermal conductivities of the tested nanoparticles are usually higher than the thermal conductivity of the heater material (stainless steel grade 316), the effective surface thermal conductivity is expected to increase after nanofluid boiling-driven nanoparticle deposition. In this section, the effects of the surface thermo-physical properties change on the HTC and CHF are analyzed.

6.3.2.1 Heat Transfer Coefficient

It is observed that Klimenko's correlation includes the surface thermal conductivity effect on the nucleate boiling HTC. The correlation is given in Eq. 2-19, with which prediction of the nucleate boiling HTC can be made. We make the assumption that, upon particle deposition, the heater surface consists of the same material of the tested nanoparticles. The effective thermal conductivity of the heater surface, k_{eff}, can be evaluated using thermal conductivity model (Maxwell, 1881).

$$\frac{k_{eff}}{k_h} = \frac{1+2\beta\Phi}{1-\beta\Phi} \tag{6-4}$$

where, k_h is the thermal conductivity of the nanoparticle materials, which are assumed to form a continuous media; Φ is the porosity of the nanoparticle layer, which is assumed to be 50%. $\beta=(k_{air}-k_h)/(k_{air}+2k_h)$. When a finite temperature discontinuity exists at the nanoparticle-fluid interface, Eq. 6-4 is still valid with replacement of k_h with $k_h+\alpha k_{air}$, where $\alpha=2R_b k_h/d$, $R_b=2.5\times10^{-8}$ Km^2/W is the interfacial thermal resistance suggested as a conservative value by Jacob et al. (2008). d is the nanoparticle diameter, whose mean values were reported in Table 3-5.

Using the calculated k_{eff}, the realistic value of the surface thermal conductivity, $\bar{k}$, is calculated using thermal resistance theory with assumption of thin conducting paths of the nanoparticle porous layer and stainless steel heater, where linear temperature drop across the conducting paths is assumed [Todreas and Kazimi (1990)].:

$$\frac{1}{\bar{k}/(\delta_{NL}+\delta_{SS316})} = \frac{1}{k_{SS316}/\delta_{SS316}} + \frac{1}{k_{NL}/\delta_{NL}} \tag{6-5a}$$

Rearranging Eq. (6-5a) gives:

$$\bar{k} = \frac{k_{SS316}k_{NL}}{\delta_{SS316}k_{NL}+\delta_{NL}k_{SS316}}(\delta_{NL}+\delta_{SS316}) \tag{6-5b}$$

where, k_{NL} and k_{SS316} are the effective thermal conductivity of nanoparticles porous layer and stainless steel heater, respectively. δ_{NL}~10 μm, and δ_{SS316}=0.4064 mm are the thicknesses of nanoparticles porous layer and stainless steel heater, respectively. Then, the last term in Eq. 2-19 representing the ratio of the surface to fluid thermal conductivities ($K=k_{surface}/k_f$; $k_{surface}=\bar{k}$) is evaluated according to different nanoparticle materials. The relative HTC change before and after nanofluid boiling is proportional to (K_{NL}/K_{SS316}). The summary of the calculation is given in Table 6-5.

Table 6-5 Summary of surface thermal conductivity change

Surface material	k_h (W/m·K)	k_{eff} (W/m·K)	$\bar{k}$ (W/m·K)	$K=(\bar{k}/k_f)^{0.12}$ *	K_{NL}/K_{SS316}
SS316	14	14	14	1.438	n/a
Al2O3†	40	16	14.042	1.439	1.0007
ZnO†	100	40	14.222	1.441	1.0021
Diamond†	1600	640	14.337	1.442	1.0028

*The thermal conductivity of water at 373 K was used for k_f (0.677 W/m·K).
†The thermal conductivity values are found in Adachi (2004).

These results suggest that surface conductivity changes due to nanoparticle deposition are insignificant and corresponding HTC changes are less than 0.3%. This is consistent with the experimental results, in which the nanofluid HTC is about the same as that of water (see Section 4.1). It is noted that the assumption of a heater made of nanoparticle material is very optimistic. In reality, the thickness of the nanoparticle layer is very small (a few microns) with respect to the steel heater thickness, thus the effective thermal conductivity of the heater is not changed significantly by nanoparticle deposition. From those considerations, it is concluded that the effect of the surface material thermo-physical properties change on the HTC is insignificant.

6.3.2.2 *Critical Heat Flux*

The benefit of having increased surface thermal conductivity for CHF is to dissipate the heat flux radially on the surface more effectively if a hot/dry spot is present. Such hot/dry spot dissipation delays the CHF. Actually, other properties, including specific heat capacity and density, contribute to this effect, and of course the thickness of the deposition layer also affects the dissipation efficacy. Both surface material thermo-physical properties and thickness can be incorporated in a single formula, the so called thermal activity S, proposed by Saylor (1989). The effusivity of the heater material is the measure of the effectiveness of energy exchange with the surroundings and is defined as $(\rho_h c_h k_h)^{1/2}$, and the thermal activity S is the product of the heater effusivity and thickness:

$$S = D_h \sqrt{\rho_h c_h k_h} \tag{6-6}$$

where D_h is the heater thickness. ρ_h, c_h, and k_h are density, specific heat capacity, and thermal conductivity of the heater surface material, respectively. The higher the thermal activity, the higher the ability of the surface to dissipate a hot/dry spot. The summary of our calculation is

given in Table 6-6.

In order to calculate S for the stainless steel substrate, the heater thickness of 0.016" (0.4064 mm) was used, while 10 μm was the assumed thickness for all nanoparticles deposition layers as it typically appears from the confocal microscopy observations. It is reported that the radial conduction dissipation effect saturates when S>8 J/(m·K·s$^{1/2}$) (Arik and Bar-Cohen, 2003). From the calculation, S for the initial heater condition before nanofluid boiling is about 3 J/(m·K·s$^{1/2}$), which is still far less than the saturation value. The results in Table 6-6 show that diamond nanoparticles deposition adds the largest thermal activity to the initial heater condition. However, corresponding CHF enhancement was estimated to be only 2.6% from the CHF vs S curve in Arik and Bar-Cohen's work (2003). This suggests that that hot/dry spot dissipation by the deposition layer is unlikely to be the CHF enhancement mechanism for all nanofluids explored in this study.

Table 6-6 Summary of thermal activity analysis at 373 K

Surface material	k_{eff}† (W/mK)	ρ_h (kg/m^3)	c_h (J/kg·K)	$(\rho_h c_h k_{eff})^{1/2}$ (J/m^2·K·s$^{1/2}$)	D_h (m)	S (J/m·K·s$^{1/2}$)
SS316	14	8,000	500	~7,400	~4.064×10^{-4}	~3.007
Al2O3	16	4,000	760	~6,900	~1×10^{-5}	~0.070
ZnO	40	5,700	500	~10,600	~1×10^{-5}	~0.107
Diamond	640	3,500‡	789	~42,000	~1×10^{-5}	~0.420

† Effective thermal conductivity value calculated using Maxwell effective medium theory (1881). Porosity of 50% and interfacial resistance of 2.5×10^{-8} K·m^2/W were assumed in the calculation. The k_h value for single crystal of diamond is about 1600 W/m·K.

‡ Density value at 300 K was used due to the unavailability of the data at 373 K.

6.3.3 Capillary Wicking

By capillary wicking it is meant the ability of surface pores and cavities to draw liquid into the surface by capillary force. Similar to wettability, capillary wicking is a measure of the liquid affinity to the surface. However, it is worth emphasizing some differences in the context of our study. We measure wettability by the effective contact angle, which is governed mainly by the surface chemistry (surface energy) and surface area, as explained in Section 5.4.3. On the other hand, capillary wicking requires the presence of pores and cavities. These pores can form an interconnected network or can be isolated. In both cases, capillary wicking helps keeping the surface wet and cool; however, in the former case its effectiveness is much greater because liquid is supplied to the nucleation sites without interference from the vapor rising from the nucleation sites. This effect may become particularly important with respect to removing heat from the hot/dry spots on the surface, thus resulting in a delay of CHF.

To begin with, the existence of pores and cavities on the surface of our heaters has to be confirmed. It was shown that nanofluids boiling typically causes formation of a porous layer on the heater surface. In general, capillary wicking can be detected and quantified by immersing a coupon of the test material in the liquid of interest and measuring the change of the free level of the liquid, as it is directly proportional to the amount of liquid adsorbed by the pores. This approach was used by Kim et al. (2006a). In this study, however, this approach would not be feasible because the volume of the coupons themselves is large, which would make it very hard to detect the small volume changes due to liquid adsorption into the pores. Instead, a more qualitative approach has been adopted here. The SEM pictures taken with heater coupons can be utilized to assess if interlinked pores are present or not. As presented in Chapter 5, the SEM pictures of the as-received and water-boiled heaters show no presence of pores and large cavities on the surface. In contrast, the SEM pictures taken for the heater coupons boiled in nanofluids

reveal pores and cavities of various sizes. The SEM pictures at higher magnification in Figs. 6-50, 51, and 52 are particularly beneficial to observe the possible pore formation for alumina, zinc oxide, and diamond nanofluids boiling, respectively. Those are SEM pictures from the runs which yielded the best CHF enhancement for each nanofluid. In Figs. 6-50 and 51, the blue arrows point to the likely pathways underneath particles adjacent to each other and along the crevices formed by the particles. Especially, Fig. 6-50 clearly shows the presence of interlinked pores for the alumina nanofluid case. In fact, the overall alumina porous layer seems to have a layer-by-layer structure, which provides higher possibility of forming interlinked pores. In Fig. 6-51, the 'island' aggregations of zinc oxide nanoparticles are much larger than the alumina nanoparticle aggregations. Accordingly, the possibility of interlinked pore existence seems lower than in the alumina case. Regarding diamond nanofluid boiling, the deposition layer type differs from the previous two cases, appearing flatter and less tortuous, with no indication of interlinked porosity. This SEM pictures analysis suggests that the capillary wicking effect may have a significant effect on boiling of alumina and zinc oxide nanofluids, but not diamond nanofluids. However, the visual approach used here, to assess the importance of porosity is very qualitative, and should be complimented by rigorous porosity measurements (e.g., mercury intrusion porosimetry, nitrogen gas adsorption method). This is left for future research work.

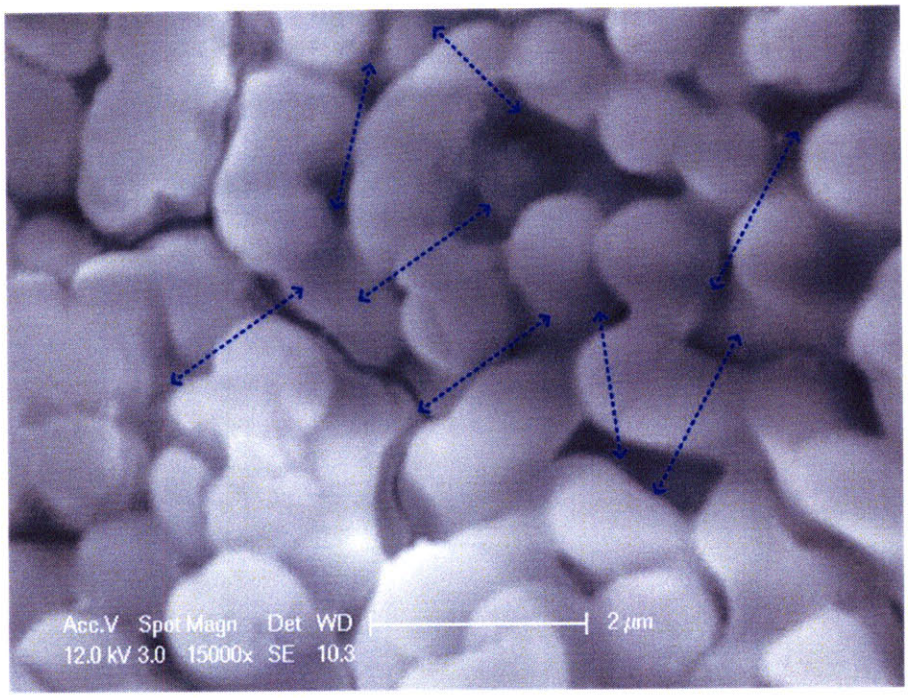

Figure 6-50 SEM picture of test section for 0.1 %vol. alumina nanofluid run at G=2500 kg/m^{2}s

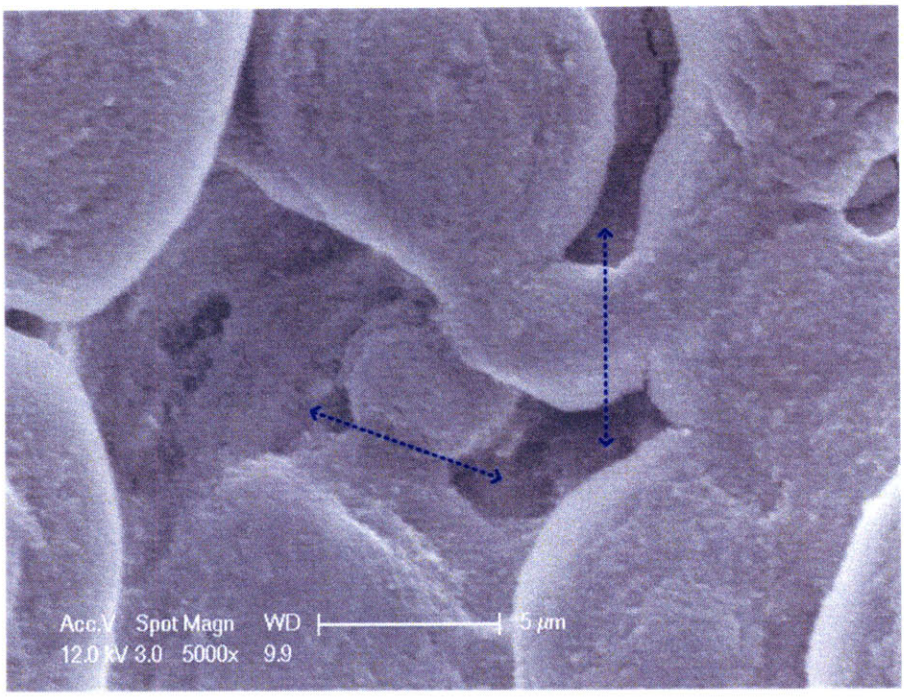

Figure 6-51 SEM picture of test section for 0.1 %vol. zinc oxide nanofluid run at G=2500 kg/m^{2}s

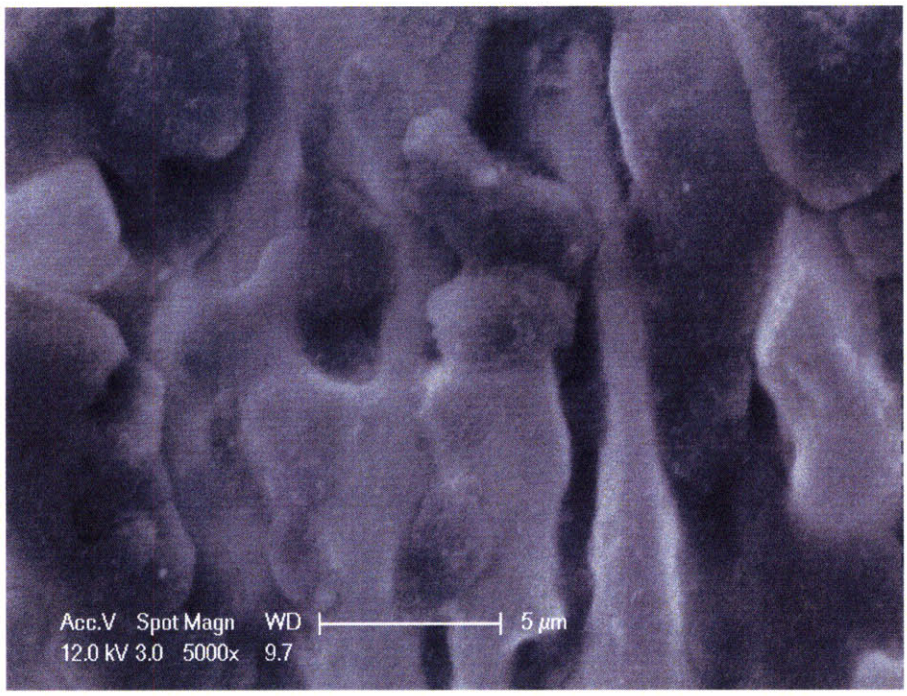

Figure 6-52 SEM picture of test section for 0.1 %vol. diamond nanofluid run at G=2500 kg/m^{2}s

6.3.3.1 Heat Transfer Coefficient

Capillary wicking helps liquid reentrance to the micro-cavities and thus tends to suppress bubble nucleation from the micro-cavities. Although quantitative data are unavailable, careful examination of the SEM pictures suggests that capillary wicking might affect the HTC significantly, moderately, and insignificantly for boiling of the alumina, zinc oxide, and diamond nanofluids, respectively. Accordingly, degradation of the alumina and zinc oxide nanofluids HTC could be expected, while likely the diamond nanofluids HTC would not be affected. However, we have observed that the measured nanofluid HTCs were similar to the water values. Therefore, the connection between capillary wicking and HTC is probably weak.

6.3.3.2 Critical Heat Flux

The major benefit from having increased capillary wicking is to accelerate the supply of liquid to the hot/dry spots that form on the surface at high heat flux. As a result, these dry/hot spots can be dissipated more effectively, which delays the CHF. Therefore capillary wicking would seem to have conflicting effects on HTC and CHF. In a recent study by Kim et al. (2006a), it was proposed that capillary wicking is one of the main mechanisms affecting the CHF.

Recently, Chen et al. (2009) conducted a pool boiling CHF experiment with Cu and Si nanowires in water and reported significant CHF enhancement, by as much as 100%. This was attributed to the presence of capillary wicking. They employed a model to evaluate the CHF limited mainly by capillary wicking ($q''_{CHF,c}$). The model was developed as a balance between the capillary pumping force and the liquid viscous drag along its flow length and is given as (Liter and Kaviany, 2001):

$$\frac{q''_{CHF,c}}{0.53\left(\rho_l \sigma h_{lv} / \mu_l\right)\left((K\Phi_s)^{1/2} / D\right)} = 1 - \frac{C_E}{0.53}\frac{D}{\sqrt{\Phi_s}}\frac{q''^2_{CHF,c}}{\rho_l \sigma h_{lv}^2} \tag{6-7}$$

where μ_l is the viscosity of the liquid, K is the permeability of the wicking structure, C_E is the Ergun coefficient, D is the liquid flow distance, and Φ_s is the porosity of nano-porous layer. $K=\Phi_s d^2/[180(1-\Phi_s)^2]$ and $C_E=(0.018/\Phi_s^3)^{1/2}$ were borrowed from the Carmen-Kozeny model (Kaviany, 1999). With D=50 μm, d=200 nm, and assumption of Φ_s=0.1, they obtained the CHF value of about 2.5 MW/m^2, which was close to their experimental results. However, applying Eq. 6-7 to the current study seems impractical as the parameters of D, d, and Φ_s can be judged only qualitatively because of the random formation of the nanoparticle porous layer. Nonetheless, the model suggests that the effect of capillary wicking on the CHF is potentially optimistic.

In our study, as discussed in the previous section, capillary wicking is likely to be present

in the alumina and zinc oxide nanofluids boiling and in fact these are the two nanofluids with large CHF enhancement. However, the CHF gain using diamond nanofluids is not as significant as alumina and zinc oxide nanofluids (about 35%), which suggests that capillary wicking cannot be the only CHF enhancing effect present in our experiments.

6.3.4 Wettability and Nucleation Site Density

Two other potentially important surface parameters are wettability and nucleation site density. In principle, wettability affects the CHF strongly and, at the same time, influences the nucleation site density and thus the HTC. That is, wettability affects the CHF directly and the HTC via the nucleation site density. The inter-dependence of wettability, nucleation site density, micro-cavities, HTC and CHF is shown schematically in Fig. 6-53.

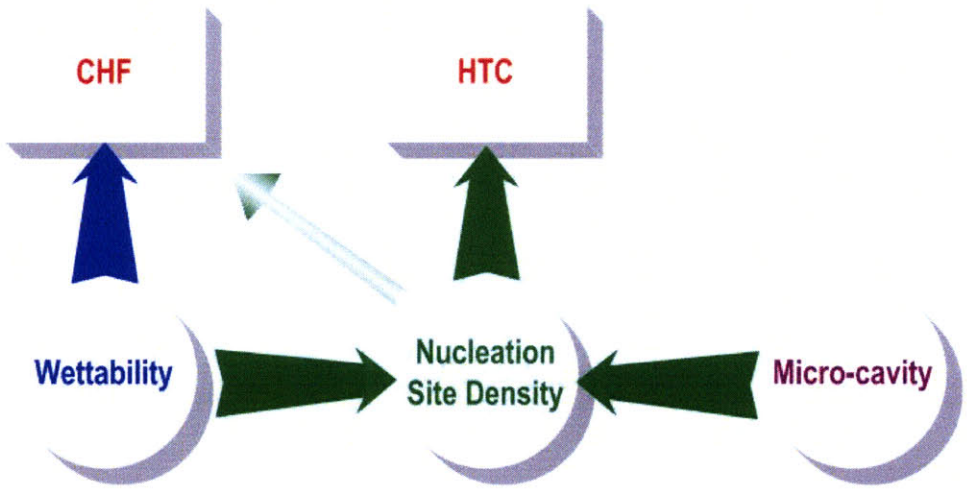

Figure 6-53 Interdependence of CHF, HTC, wettability, nucleation site density and micro-cavity density

Here wettability refers to the affinity of the liquid to the surface of the material, as measured by the intrinsic contact angle of the fluid on the surface. The number of micro-cavities present on the surface is another parameter that affects boiling. The two parameters have opposite effects on the nucleation site density, i.e., the number of micro-cavities per unit area that are actually bubble nucleation sites. Wettability promotes filling of the micro-cavities by the liquid, which makes it more difficult for bubbles to nucleate. On the other hand, the larger the number of micro-cavities, the higher is the possibility of bubble nucleation that can be achieved. These effects have been known since the pioneering work on boiling in the 1950s, and the relation between micro-cavities, contact angle and nucleation site density was quantified by Wang and Dhir (1993). Since in our study we have both wettability and micro-cavity data, the Wang and Dhir's model can be applied to quantify the effect of wettability and micro-cavity changes on the HTC and CHF.

6.3.4.1 Heat Transfer Coefficient

Boiling of nanofluids results in nanoparticle deposition on the boiling surface (Kim et al., 2009). Such deposition can affect the heat transfer coefficient in two ways: (i) change the number of micro-cavities on the surface, and (ii) change the surface wettability. To estimate the relative importance of these two effects, we resort to the conveniently simple Wang and Dhir's model, which provides the number of nucleation site per unit area – the so-called nucleation site density – as a function of the number of micro-cavities on the surface and the contact angle (wettability) of the fluid on the surface:

$$n'' \propto m''(1-\cos\theta_i) \tag{6-8}$$

where n'', m'', and θ_i are densities of nucleation sites and micro-cavities, and the intrinsic contact

angle of water on the surface, respectively. The intrinsic contact angle for alumina, zinc oxide and diamond is not easily obtained from first principles. Therefore, we have estimated it from knowledge of the apparent contact angle, θ_a, and the modified Young's equation (Wenzel, 1949):

$$\cos\theta_a = r \cdot \cos\theta_i \tag{6-9}$$

where r is the roughness factor, defined as the ratio of the actual surface area to the projected surface area. θ_a and r were measured by means of the sessile droplet method and confocal microscopy, respectively. Then θ_i can be calculated from Eq. 6-9. The calculated average values of θ_i are 86.5, 61.0, 60.8, and 94.5° for water on stainless steel, alumina, zinc oxide, and diamond surfaces, respectively. The relative order of the contact angles appears to be correct, i.e., oxides have the lowest contact angle, and diamond the highest. The number of micro-cavities, m'', was estimated from confocal microscopy images of the test section surface, processed with the ImageJ software, as explained in Chapter 5. The ratio of the calculated nucleation site density for the nanofluids to that of water is shown in Figs. 6-54 and 55 for $1<D_c<10$ μm (H_c=3 μm) and $2.2<D_c<10$ μm (H_c=3 μm), respectively. Also the calculated numeric values are tabularized in Table 6-7.

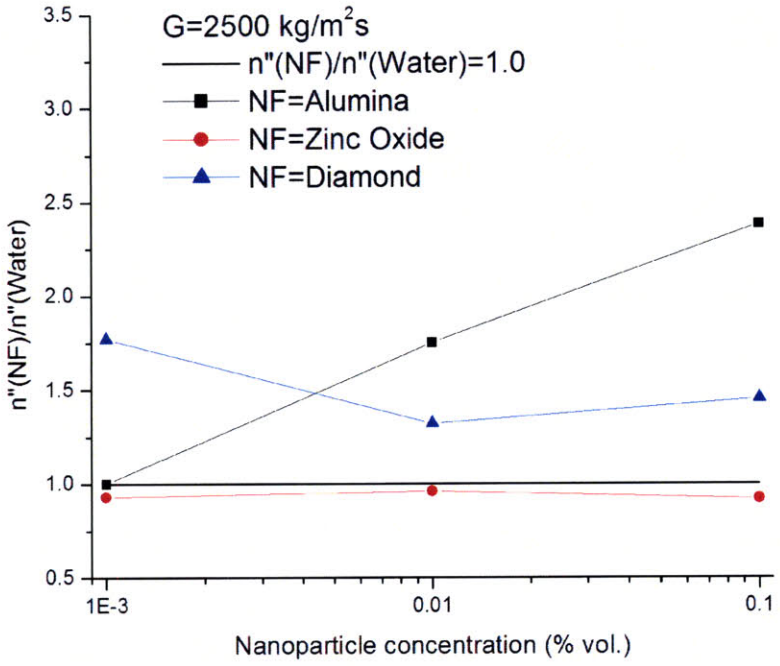

(a)

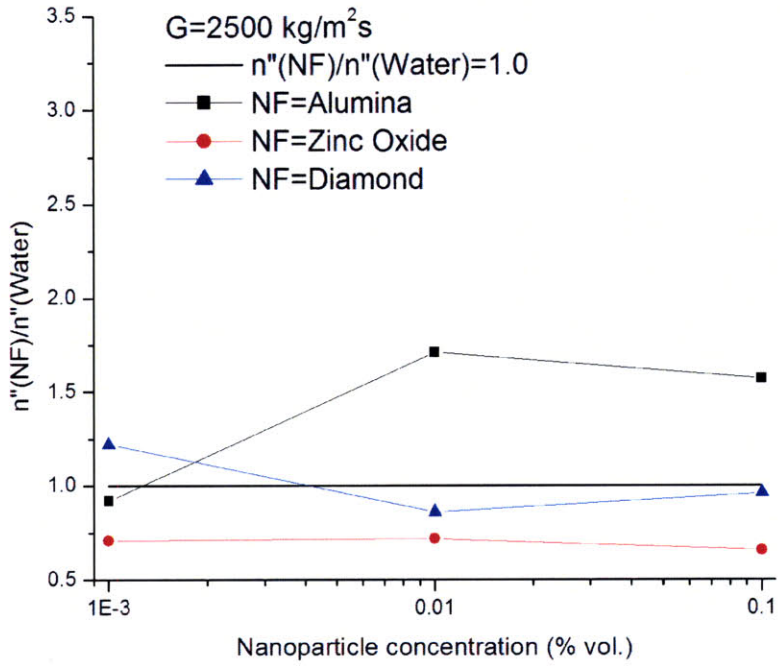

(b)

Figure 6-54 Ratio of nucleation site density according to nanoparticle concentration counted in (a) $1<D_c<10$ μm (H_c=3 μm) and (b) $2.2<D_c<10$ μm (H_c=3 μm)

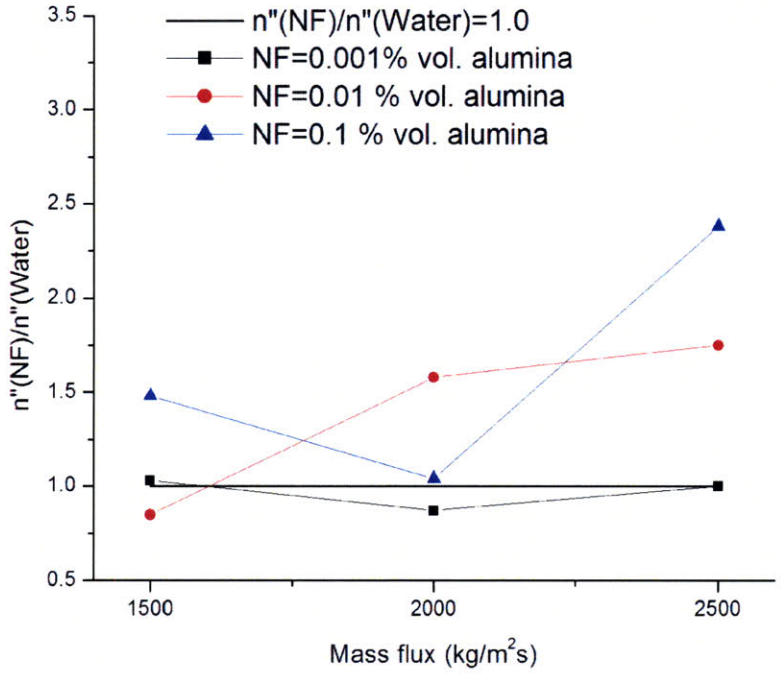

(a)

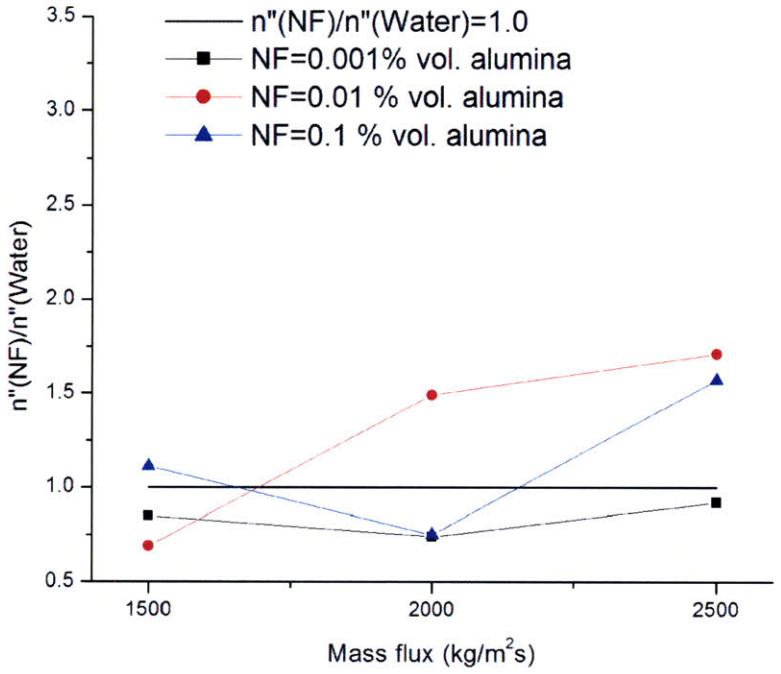

(b)

Figure 6-55 Ratio of nucleation site density according to mass flux counted in (a) $1<D_c<10$ μm (H_c=3 μm) and (b) $2.2<D_c<10$ μm (H_c=3 μm)

Table 6-7 Summary of the nucleation site density calculation using Wang and Dhir's model

Surface condition	Concentration (% vol.)	Mass flux (kg/m^2s)	n''(NF)/ n''(Water) D_c: 1 – 10 μm			n''(NF)/ n''(Water) D_c: 2.2 – 10 μm		
			ΔH_c=3μm	ΔH_c=5μm	ΔH_c=7μm	ΔH_c=3μm	ΔH_c=5μm	ΔH_c=7μm
Alumina	0.001	1500	1.03	0.92	0.84	0.85	0.70	0.62
	0.01	1500	0.85	0.91	0.82	0.69	0.67	0.63
	0.1	1500	1.48	1.46	1.40	1.11	1.01	0.89
		Average	**1.12**	**1.10**	**1.02**	**0.88**	**0.79**	**0.71**
	0.001	2000	0.87	0.87	0.83	0.74	0.69	0.63
	0.01	2000	1.58	1.71	1.45	1.49	1.58	1.09
	0.1	2000	1.04	0.81	0.96	0.75	0.49	0.50
		Average	**1.16**	**1.13**	**1.08**	**0.99**	**0.92**	**0.74**
	0.001	2500	1.00	0.95	0.92	0.92	0.90	0.81
	0.01	2500	1.75	1.70	1.92	1.71	1.72	1.76
	0.1	2500	2.38	2.16	2.85	1.57	1.54	1.88
		Average	**1.71**	**1.60**	**1.90**	**1.40**	**1.39**	**1.49**
Zinc oxide	0.001	2500	0.93	0.98	1.06	0.71	0.74	0.71
	0.01	2500	0.96	0.87	1.09	0.72	0.67	0.78
	0.1	2500	0.92	0.80	0.99	0.66	0.57	0.66
		Average	**0.94**	**0.88**	**1.04**	**0.70**	**0.66**	**0.72**
Diamond	0.001	2500	1.77	1.79	2.23	1.22	1.36	1.75
	0.01	2500	1.32	1.39	1.57	0.86	0.93	0.91
	0.1	2500	1.45	1.59	1.68	0.96	1.09	1.10
		Average	**1.51**	**1.59**	**1.83**	**1.01**	**1.13**	**1.25**

Because the ImageJ-based method for determining the number of micro-cavities is somewhat arbitrary, the sensitivity of the results to the micro-cavity diameter range (D_c) and micro-cavity depth (H_c) is also reported in Table 6-7. With D_c of 1 – 10 μm, heater coupons boiled with alumina nanofluids at G=1500 and 2000 kg/m^{2}s (Fig. 6-55(a)) and zinc oxide nanofluids at G=2500 kg/m^{2}s (Fig. 6-54(a)) show insignificant changes of the nucleation sites compared to water. In contrast, alumina and diamond nanofluids at G=2500 kg/m^{2}s exhibit substantial increases, predominantly more than 50% regardless of the cavity depth (Fig. 6-54(a)). When D_c of 2.2 – 10 μm is implemented (Figs. 6-54(b) and 55(b)), a similar trend is observed for the heater coupons boiled with alumina nanofluids at all mass fluxes as compared to the first cavity diameter range. The nucleation site density of heater coupons boiled in zinc oxide and diamond nanofluids tends to be lower than, and similar to that of water, respectively (Fig. 6-54(b)). For alumina nanofluids it is the increase of the micro-cavity number that drives the increase of nucleation site density in spite of a higher wettability; while for diamond nanofluids is a combination of (moderate) increase in the micro-cavity number and the hydrophobic characteristics of the diamond nanoparticles.

A similar result related to the nucleation site density is reported in Narayan et al's work (2007). They claimed that when the average size of the nanoparticle is much smaller than the heater surface roughness, the number of nucleation sites is greatly increased. The average surface roughness of the bare heater in the current study is about 1.8 μm and the average nanoparticle sizes are 40, 77.4, and 165.4 nm for alumina, zinc oxide, and diamond, respectively. Thus, the calculated increase of the active nucleation sites in this study can be explained as the consequence of the nanofluids boiling.

Assuming that the HTC is proportional only to the nucleation site density, Table 6-7 suggests that the HTC for all nanofluids should be between ~70% and ~230% that of the water

HTC. However, the measured values of the nanofluid HTC exhibit a tighter range of 80% and 120% the measured values of the water HTC. The discrepancy is likely due to differences in other parameters contributing to the HTC, e.g., bubble departure diameter and frequency; however, quantification of their importance would necessitate a different experimental apparatus. This is an area for future contributions.

6.3.4.2 *Critical Heat Flux*

The effect of wettability on the CHF is relatively well understood and was discussed in Section 6.2. Improved wettability should result in CHF enhancement. The alumina and zinc oxide data seem to support this notion. However, the diamonds nanofluids show no wettability improvement but still a 35% CHF enhancement was achieved with respect to the pure water CHF value at G =2500 kg/m^{2}s. This suggests that other mechanisms may be responsible for the enhanced CHF. For example, it was shown in Section 6.3.2.2 that the higher surface thermal activity for the diamond particle deposition layer may help increase the CHF. There could also be other mechanisms affecting the CHF, as discussed in the following section.

6.3.5 Bubble Dynamics Parameters

The interdependency between boiling parameters and HTC/CHF shown in Fig. 6-53 can be refined further by considering additional boiling parameters, which are, however, not measured in the current experimental apparatus. Those are related to the bubble departure dynamics and dynamic nature of wettability. Wettability changes under flow condition (hereafter

dynamic wettability) and bubble departure diameter and frequency may have a substantial impact on the CHF and HTC. It is useful to highlight possible effects of those parameters, recognizing that this is a potential area for future work. The interdependence of the various phenomena and parameters considered here is shown in Fig. 6-56.

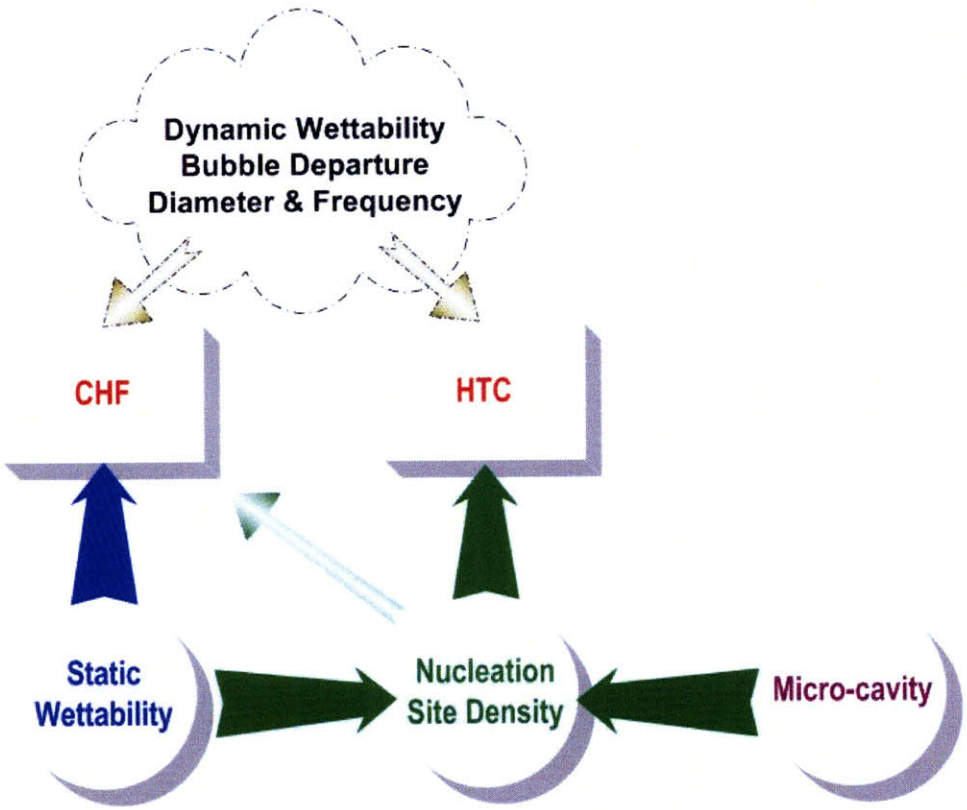

Figure 6-56 Interdependence of important boiling parameters for the CHF and HTC analysis

6.3.5.1 Dynamic wettability

While only the static contact angle was measured in this study, the dynamic contact angle can be significantly different. A study performed by Gajewski (2008) suggests that hydrophobic behavior can be turned into hydrophilic under flow conditions. This phenomenon is called wettability hysteresis, and could be relevant to the diamond particle deposition layers in our study,

which display hydrophobic behavior at static conditions. However, we have no way to test this hypothesis with the current diagnostics in place in our apparatus.

6.3.5.2 *Bubble departure diameter and frequency*

In general, bubble departure size is the resulting force balance between buoyancy, surface tension forces, and the flow drag. The flow drag increases with mass flux and thereby the increasing wall shear force pushes the rising bubble against the heating surface to prevent from departing. This results in a decrease of bubble departure diameter (Levy, 1967; Zeng et al., 1993). Bubble departure diameter is expected to be increasing with wall superheat, which can be driven by high heat flux (Thorncroft et al., 1998). For given bubble departure frequency, having a larger bubble departure diameter is beneficial in increasing the HTC. The bubble departure diameter is also related to surface effects. An ancient, but qualitatively useful prediction implementing such surface effect on the bubble departure diameter was developed by Fritz (1935):

$$D_b = C_d \theta \left[\frac{2\sigma}{g(\rho_l - \rho_g)} \right]^{1/2} \tag{6-10}$$

where the constant C_d=0.0148 for bubbles of hydrogen and water vapor in water and the contact angle θ is in degrees. Eq. 6-10 suggests that with enhanced wettability, the bubble departure diameter decreases. In addition to the bubble departure diameter, the departure frequency also affects the HTC. In many pool boiling studies, the bubble departure frequency is correlated with its departure size as (Ivey, 1967; Situ et al., 2008):

$$f_b \cdot D_b^n = const \tag{6-11}$$

At the hydrodynamic region (f and D_b are assumed to depend on the buoyancy and flow drag), n=1/2, whereas at the thermodynamic region (f and D_b are assumed to be governed solely by

thermodynamic considerations), n=2 fits the water data with, D_b<5 mm (Throncroft et al., 1998). It is reported that such relationship is still valid in convective boiling if the bubble size is much smaller than the channel characteristic length scale (Lee et al., 2005). In our case, calculated D_b using Eq. 6-9 with contact angle of water (θ_i=86.5°) is about 4.8 mm, which is close to but not greater than the flow channel diameter of 5.5 mm. Thus, as the rough estimate, Eq. 6-11 may still be useful in this analysis. Eq. 6-11 suggests that the decreased bubble departure diameter would tend to increase its frequency by square of its decrease rate. As reviewed in Chapter 2, Mikic and Rohsenow's and Basu et al.'s correlations for nucleate boiling heat transfer given in Eqs. 2-26 and 2-33, respectively, can be utilized to evaluate the relative effectiveness of the nanofluids compared to water. Combining Eq. 6-11 with respective Eqs. 2-26 and 2-33 suggests that nucleate boiling heat transfer is simply proportional to D_bN_a. Since we have calculated N_a in Section 5.3, and D_b can be estimated using Eq. 6-11, the nucleate boiling heat transfer of water and nanofluids can be evaluated quantitatively. Finally the ratio of the nucleate boiling heat transfer rate of nanofluids to water ($q''_{ev}(NF)/\ q''_{ev}(Water)$) can be assessed and its result is summarized in Figs. 6-57 and 58. The calculated numeric values are also reported in Table 6-8.

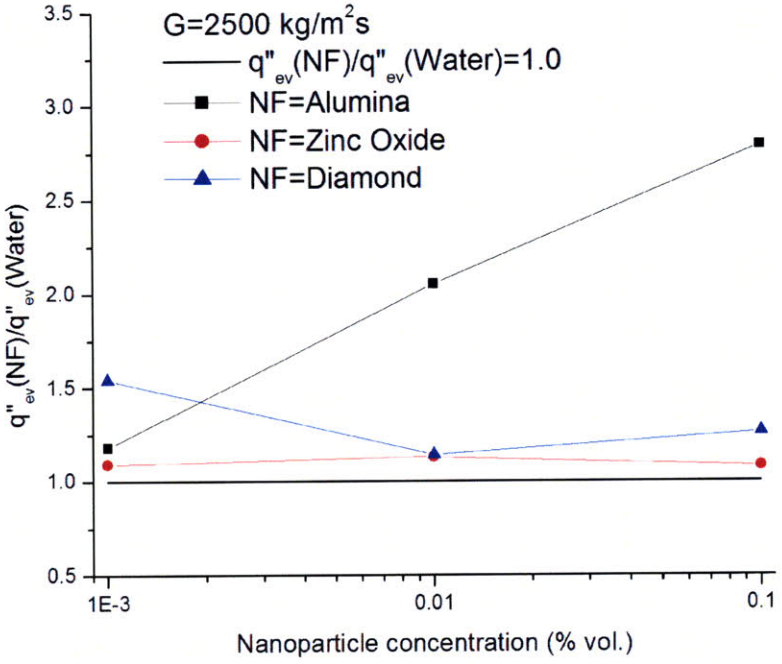

(a)

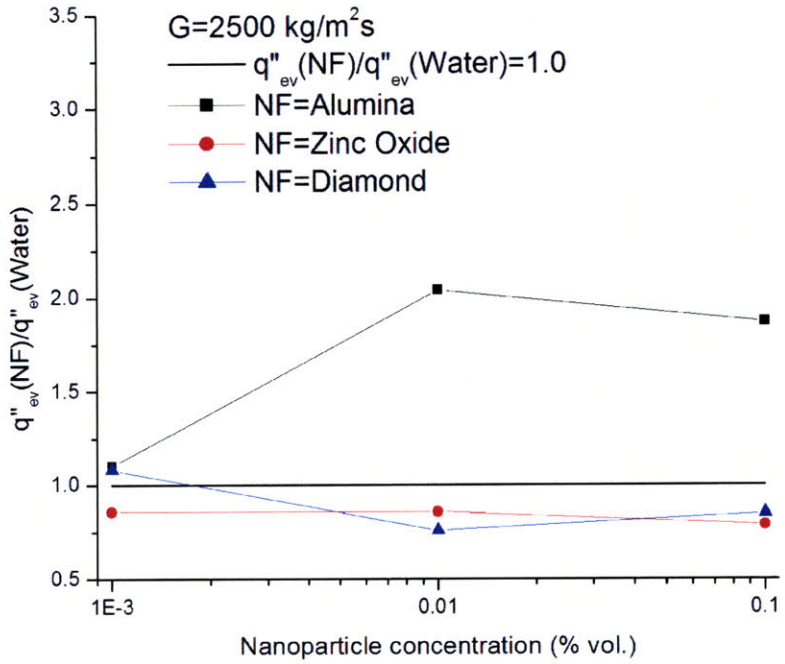

(b)

Figure 6-57 Ratio of evaporative heat flux according to nanoparticle concentration counted in (a) $1<D_c<10$ μm (H_c=3 μm) and (b) $2.2<D_c<10$ μm (H_c=3 μm)

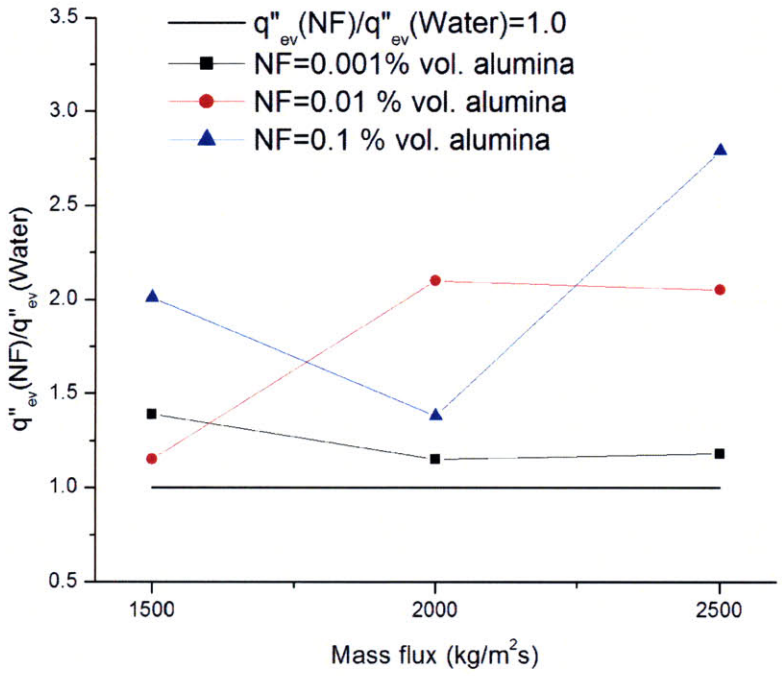

(a)

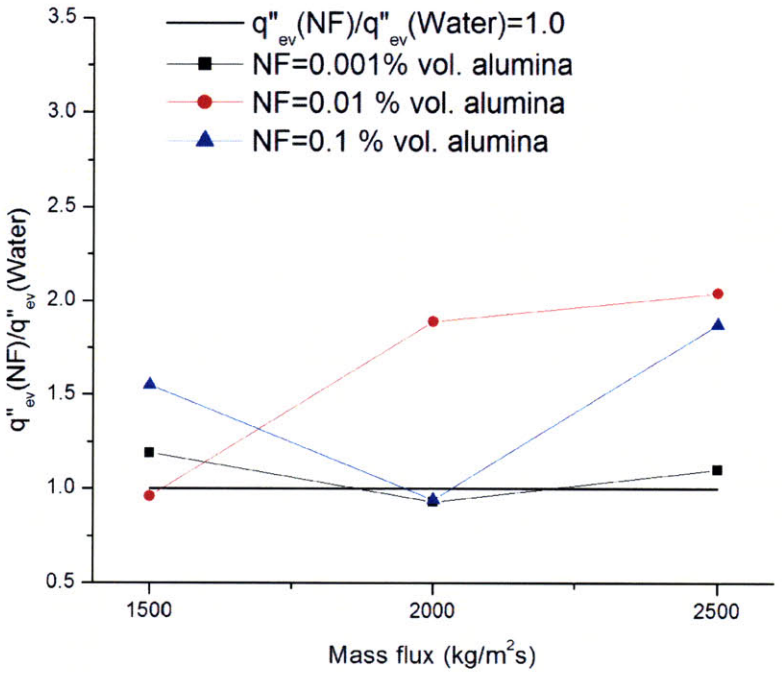

(b)

Figure 6-58 Ratio of evaporative heat flux according to mass flux counted in (a) $1<D_c<10$ μm (H_c=3 μm) and (b) $2.2<D_c<10$ μm (H_c=3 μm)

Table 6-8 Summary of the ratio of nucleate boiling heat transfer calculation

Surface condition	Concentration (% vol.)	Mass flux (kg/m^2s)	$q''_{ev}(NF)/q''_{ev}(Water)$ D_c: 1 – 10 μm			$q''_{ev}(NF)/q''_{ev}(Water)$ D_c: 2.2 – 10 μm		
			ΔH_c=3μm	ΔH_c=5μm	ΔH_c=7μm	ΔH_c=3μm	ΔH_c=5μm	ΔH_c=7μm
Alumina	0.001	1500	1.39	1.26	1.19	1.19	1.05	0.92
	0.01	1500	1.15	1.25	1.17	0.96	1.00	0.95
	0.1	1500	2.01	1.99	1.99	1.55	1.50	1.33
		Average	**1.52**	**1.50**	**1.45**	**1.23**	**1.18**	**1.07**
	0.001	2000	1.15	1.15	1.18	0.93	0.87	0.90
	0.01	2000	2.10	2.26	2.07	1.89	2.01	1.53
	0.1	2000	1.38	1.08	1.37	0.94	0.63	0.70
		Average	**1.54**	**1.50**	**1.54**	**1.26**	**1.17**	**1.04**
	0.001	2500	1.18	1.11	0.91	1.10	0.98	0.77
	0.01	2500	2.05	1.98	1.91	2.04	1.88	1.67
	0.1	2500	2.79	2.52	2.85	1.87	1.68	1.78
		Average	**2.01**	**1.87**	**1.89**	**1.67**	**1.51**	**1.41**
Zinc oxide	0.001	2500	1.09	1.15	1.06	0.86	0.81	0.67
	0.01	2500	1.13	1.01	1.09	0.86	0.73	0.74
	0.1	2500	1.08	0.94	0.99	0.79	0.62	0.63
		Average	**1.10**	**1.03**	**1.05**	**0.84**	**0.72**	**0.68**
Diamond	0.001	2500	1.54	1.55	1.65	1.08	1.10	1.23
	0.01	2500	1.14	1.20	1.16	0.76	0.75	0.64
	0.1	2500	1.26	1.37	1.24	0.85	0.88	0.77
		Average	**1.31**	**1.37**	**1.35**	**0.90**	**0.91**	**0.88**

Similarly to the result of nucleation site density discussed in Section 6.3.4.1, no systematic trend of the nucleate boiling heat transfer of nanofluids compared to water is observed. Primary reason is because the nucleation site density was reutilized in this calculation. Note that the method introduced to calculate the number of micro-cavities and thus the nucleation site density was diagnosed as an arbitrary approach. With D_c of 1 – 10 μm, alumina and diamond nanofluids HTC change compared to water values ranges 0.91 to 2.85 and 1.14 to 1.65, respectively. On the other hand, the zinc oxide nanofluids HTC seems very close to water value as its change ranges 0.94 to 1.15. A similar result is observed with D_c range, 2.2 – 10 μm. Implementation of existing correlations of bubble departure diameter and frequency and nucleate boiling heat transfer does not seem to predict the measured HTC accurately. Therefore modeling of bubble departure diameter and frequency needs to be refined in the future work.

6.4 Pressure and Radiation Effects on Nanofluid Boiling

The current study was conducted at atmospheric pressure. However, higher pressures are employed in power engineering applications as higher energy conversion efficiency can be achieved at elevated pressures and temperatures. If nanofluids are to be used in such applications, high pressure boiling tests ultimately need to be conducted. Also in the perspective of nuclear engineering applications, ionizing radiation effects on nanofluids boiling need to be investigated. High pressure and radiation experiments are beyond the scope of this thesis; however some expected trends are discussed. To facilitate the discussion, it is worthwhile to summarize the variables that are subject to change upon nanofluids boiling:

(i). Heater surface thermo-physical properties

(ii). Capillary wicking

(iii). Wettability (contact angle, static and dynamic)

(iv). Nucleation site density

(v). Bubble departure diameter and frequency

6.4.1 Pressure Effect

It is reasonable to assume that the fluid thermo-physical properties of low-concentration nanofluids will remain similar to those of water at high pressure. Therefore, the discussion is limited to the pressure effect on nanofluids boiling with regards to its impact on the heater surface characteristics.

6.4.1.1 Effect on Heater Surface Thermo-Physical Properties

Nanoparticles deposit on the heater surface and change its thermo-physical properties. The effect of the heater thermo-physical properties on CHF is captured by the 'thermal activity', as explained in Section 6.3.2.2, which depends on the thickness and thermo-physical properties of the deposition layer. Assuming that the thickness of the particle layer is independent of pressure (an assumption that we cannot verify at this time), and since the thermal conductivity, specific heat capacity and density of solids do not change dramatically with pressure and temperature, we predict that the impact of this effect on CHF will be the same at higher pressure. That is, the impact on CHF would be negligible for all nanofluids explored in this study.

6.4.1.2 Effect on Capillary Wicking

Capillary wicking could be a significant effect in alumina and zinc oxide nanofluids boiling due to the formation of interlinked porosity on the surface. The driving force of capillary wicking is the capillary pressure, P_{cw}:

$$P_{cw} = \frac{2\sigma \cos\theta_i}{r_c} \tag{6-12}$$

where σ, θ_i, and r_c are the surface tension of liquid, intrinsic contact angle, and cavity radius, respectively. By increasing capillary wicking pressure, liquid is more prone to be pulled into the cavities. Eq. 6-12 suggests that pressure increase from 0.1 to 15.5 MPa yields reduction of P_{cw} by as much as 93%, which indicates a strong reduction of the benefits of capillary wicking under high pressure. This is mainly due to the significant reduction of the surface tension. Another way to quantify the capillary wicking effect is to calculate the Bond number, which is a measure of importance of surface tension forces compared to body forces and given as:

$$Bo = \frac{\rho g D_c^2}{\sigma} \tag{6-13}$$

where, ρ, g, D_c, and σ are the density of liquid, gravity, cavity diameter, and surface tension, respectively. Given the same D_c, a pressure change from 0.1 to 15.5 MPa results in a substantial increase of the Bo, i.e., 8 times its value at 0.1 MPa. This corroborates the results from Eq. 6-12.

6.4.1.3 Effect on Wettability

Pressure effect on wettability change is of particular interest because the present study shows significant wettability effect on nanofluids boiling under atmospheric pressure. In the literature, a few studies relevant to pressure effect on wettability are found (Zhilina and Markov,

1973; Rajayi and Kantzas, 2008). Zhilina and Markov (1973) reports that the improved wettability at high pressure is due to the formation of an oxide film on the surfaces and desorption of surface-active molecules from the heating surface. Decreasing liquid surface tension with pressure causes the contact angle to decrease as well. This suggests that even without nanofluids boiling, the surface wettability is higher at high pressure. Therefore, the relative benefit of nanofluids on CHF may diminish considerably under higher pressure.

6.4.1.4 *Effect on Nucleation Sites*

At higher pressure, bubble nucleation occurs at low superheats because the surface tension is low. Therefore, most cavities present on the surface will readily activate. A study performed by Barthau and Hahne (2000) suggests in fact that the nucleation site density increases with increasing pressure. As such, the micro-cavities created by the nanoparticle deposition layer should activate readily at high pressure and directly result in higher HTC.

6.4.1.5 *Effect on Bubble Dynamics Parameters*

Pressure effect on bubble dynamics parameters are more complicated. Bubble departure diameter is a function of contact angle (wettability). At high pressure, the wettability effect due to nanoparticle deposition diminishes because of the lowered surface tension (Section 6.4.1.3). This makes the bubble departure diameter independent on the wettability effect due to the nanoparticles deposition. Assuming Eq. 6-11 holds still good, no significant change of bubble departure frequency is expected to occur during nanofluids boiling. Nucleate boiling heat transfer

is then mainly governed by the nucleation site density as seen in Eq. 2-26 or 2-33. However, as pointed out earlier, validation of using Eq. 6-11 needs to be done for accurate prediction.

6.4.2 Radiation Effect

For nuclear engineering applications, radiation effect on nanofluid boiling needs to be studied. First, it is useful to review some experiments conducted in a radiation environment (Sibamoto et al., 2007; Lucas et al., 2007; Lucas, 2008). Sibamoto et al. (2007) identified the so called Radiation Induced Surface Activation (RISA) effect on flow boiling heat transfer. They report that the RISA effect is caused by the photochemical activation of oxidized metal surfaces by heavy irradiation of gamma-ray. Further, the RISA effect enhances the wettability and corrosion resistance of the irradiated surfaces. Since in nanofluids boiling the surface is covered with a particle deposition layer that may be highly wettable to begin with (e.g., for alumina and zinc oxide particles), irradiation may have little relative impact on surface wettability, and thus HTC and CHF.

Lucas et al. (2007) investigated the gamma radiation effect on stability of nanofluids. The acceptance criteria of using nanofluids at nuclear reactor environment were addressed such that no visible agglomeration occurs, pH remains stable and concentration remains unchanged. Those criteria were examined in their study with alumina nanofluids identical to those used in the current study. They showed that at gamma dose of 1×10^7 rad, the use of alumina nanofluids were judged to be acceptable as no agglomeration was found; no significant change of concentration was observed; and pH was maintained as it used to be. However, the other two nanofluids (zinc oxide and diamond nanofluids) have not been examined in our Lab. This is also recommended

for future work and is considered to be valuable. Lucas (2008) also investigated the RISA effect on the pool boiling CHF. After irradiation in a Co-60 gamma source, the CHF enhancement was achieved by as much as 146% and 133% using stainless steel plates pre-coated with titania and alumina nanoparticles, respectively, compared to CHF obtained from plain heaters. However, in-pile boiling tests of nanofluids boiling are needed to confirm and elucidate the effects of the various phenomena.

6.5 Comparison of Pool and Flow Nanofluids Boiling Heat Transfer

Finally, it is of interest to compare the nanofluids boiling characteristics in between pool and flow conditions. To facilitate the comparison, the previous study of pool boiling heat transfer conducted by the current author (Kim et al., 2006 and 2007) is compared to the current study of nanofluids flow boiling heat transfer. The nanofluids tested in the previous study were alumina, zirconia, and silica nanofluids, where the alumina nanofluid differs from the currently employed alumina nanofluid (Nyacol). The former was purchased from Sigma-Aldrich, and thus its colloidal properties must be different with the latter. Since a head-to-head comparison is not viable for any kind of nanofluids, some comparable results of the HTC and CHF from both studies are discussed.

6.5.1 Pool and flow boiling HTC

In the previous study, the HTC was measured using a resistivity-temperature curve for stainless steel wire (Fig. 6-59). It was observed that the HTC of all three nanofluids were deteriorated as compared to the water value. In the current study, with the presence of the forced convective force ($Re>1.7\times10^4$), the measured HTCs of the nanofluids were close to water values and the differences are predominantly within ±20%. In both studies, the surface morphology changes due to the nanoparticle deposition are evident. However, in the previous study, the wettability improvement was dominating over the possible increase of the micro-cavities density, m'' (in fact, m'' was not counted with any method). This countering effect was expected to reduce the nucleation site density and thus the HTC. In flow boiling, we were able to quantify m'' but, no systematic correlation of the mass flux with m'' and wettability is reported. Also, the bubble dynamics parameters, which are expected to have significant impacts on the HTC, are likely to change with the mass flux. This eventually affects the overall HTC trend as well. Therefore, no effective extension of the pool boiling HTC results via mass flux can be applied to the flow boiling HTC results.

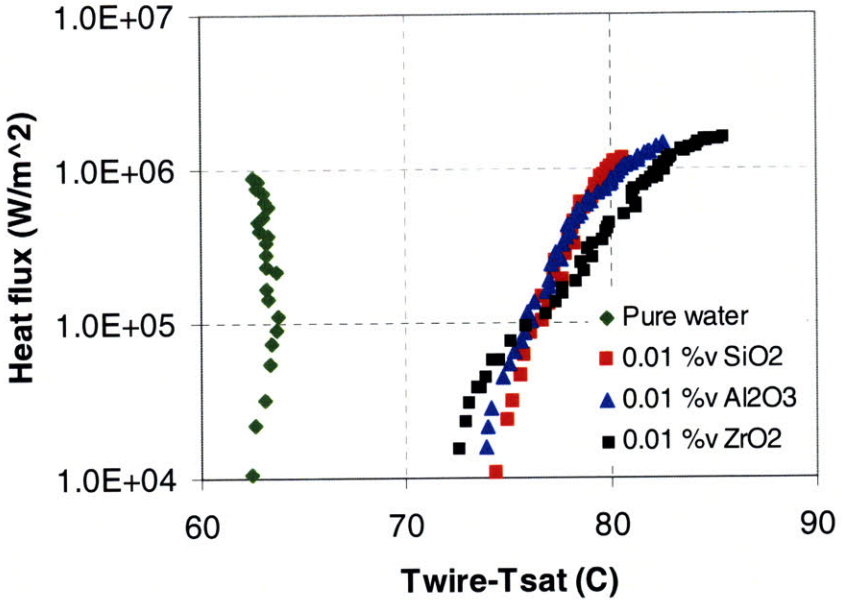

Figure 6-59 Boiling curves for stainless steel wire (cited from (Kim et al. (2007))

6.5.2 Pool and flow boiling CHF

The significant nanofluids pool boiling CHF enhancement was achieved in the previous study (Kim et al., 2007) and corresponding result is shown in Fig. 6-60. The maximum CHF enhancement of about 80% was observed for pool boiling of the silica nanofluid as opposed to 53% maximum flow CHF enhancement with alumina and zinc oxide nanofluids. For both studies, the wettability improvement seems to correlate reasonably well with the observed CHF enhancement.

In the current study, the CHF enhancement increased with the mass flux (no CHF enhancement at G=1500 kg/m^{2}s). In a qualitative viewpoint, if dynamic wettability is assumed at work in our experiments, the observed CHF trend on the mass flux may be explained better. If

this is the case, the mass flux of G=1500 kg/m^{2}s could be a certain threshold value in improving the CHF, because, regardless of the nanoparticle concentrations, enhancing the CHF was not possible at this mass flux. But there is no realistic way to determine whether or not such effect exists during our nanofluids CHF runs. Therefore, no clear correlation between pool and flow boiling CHF can be induced through the surface parameters obtained in this study. In order to explain the observed the CHF dependency on the mass flux, in-situ parameters (e.g., dynamic wettability and bubble dynamics) need to be obtained through an experimental setup. This is also left for the future research work considered to be valuable.

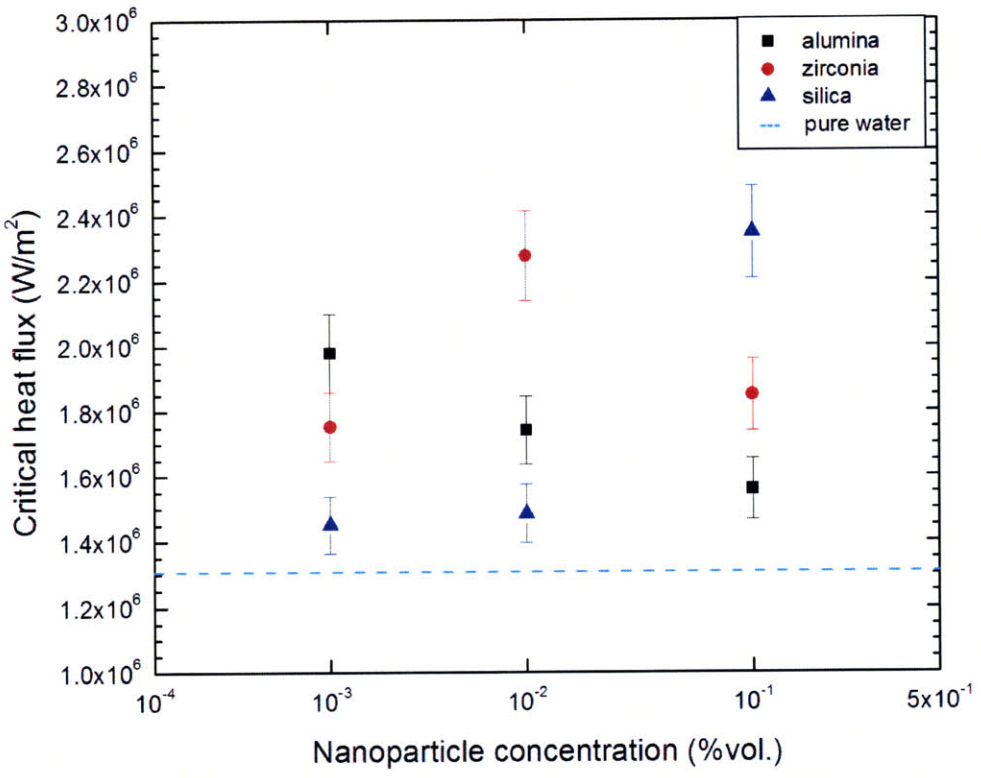

Figure 6-60 CHF data for pure water, alumina, zirconia, and silica nanofluids (cited from Kim et al. (2007))

7 Summary and Conclusions

The current study investigates the flow boiling characteristics of dilute nanofluids under subcooled conditions at atmospheric pressure. In light of previous studies showing significant pool boiling CHF enhancement, using nanofluids seems promising for flow boiling which is the heat transfer mode commonly applied in thermal production and management systems. No systematic study on nanofluids flow boiling heat transfer has been reported in the literature. This thesis presents first-of-its-kinds experimental data demonstrating the effects of alumina, zinc oxide and diamond nanofluids on flow boiling HTC and CHF. In addition, characterization of the heater surfaces is accomplished through various techniques which provide valuable information about the linkage between the surface morphology parameters and the existing boiling HTC and CHF models.

7.1 Experimental Results of Heat Transfer Coefficient, Critical Heat Flux, and Heater Surface Characterization

Alumina/water, zinc-oxide/water, and diamond/water nanofluids at 0.001, 0.01, and 0.1 %vol. were prepared and characterized. The thermo-physical properties of the dilute nanofluids are almost identical to those of de-ionized water. Flow boiling experiments were conducted in the test loop to measure both HTC and CHF. No significant change of the nanofluids' HTC over the water reference values were observed within the available data range. The differences were predominantly within ±20%.

The CHF result seems more promising. The maximum CHF enhancement for the 0.001,

0.01 and 0.1 %vol. alumina nanofluids is 33%, 44% and 53%, respectively, obtained at G=2500 kg/m^{2}s in all three cases. In cases of zinc oxide and diamond nanofluids tests obtained at 0.1 %vol. at G=2500 kg/m^{2}s, the maximum CHF enhancement for zinc-oxide nanofluids is 53%, while for diamond nanofluids is 38%. The enhancement increases with the mass flux and, to a lesser extent, with the nanoparticle concentration.

Closer inspection of surface morphology changes using SEM images suggests that CHF enhancement, which is observed mostly at high mass flux and more prominently with alumina and zinc oxide vs diamond nanofluids, can be obtained provided that a uniform nanoparticle deposition layer is created on the surface.

Using confocal microscopy, the measured surface roughness ranges from 1.5 to 3 μm with an average value about 2 μm for all cases (as-purchased, water-boiled and nanofluid-boiled coupons). Alumina and zinc oxide nanofluids-boiled coupons showed a moderate increase of the surface area as compared to the as-purchased and water-boiled coupons, whereas the diamond nanofluids-boiled coupons showed some reduction of the surface area. As no systematic correlation was observed with respect to the CHF enhancement and HTC, it is concluded that the observed boiling characteristics of nanofluids do not result from significant changes in the surface roughness and area.

The number of micro-cavities was counted with micro-cavity diameters ranging from $1\mu m \le D_c \le 10\mu m$ and $2.2\mu m \le D_c \le 10\mu m$, and cavity heights of 3, 5, and 7 μm. No clear trend with regard to the nanoparticle concentration and mass flux was seen from the analysis. This suggests that the micro-cavity density cannot directly explain the CHF and HTC data for nanofluids. However, the micro-cavity information is expected to be useful for the evaluation of the bubble nucleation sites.

The contact angles of the as-received coupon and the coupon boiled in water was around 80°, while the coupons boiled in the 0.01 and 0.1 %vol. alumina and zinc oxide nanofluids, at G=2500 kg/m^{2}s, all had significantly lower contact angles, ~20-30°. In contrast, virtually no reduction of the contact angle was found for the heater coupons boiled in diamond nanofluids at all concentrations. The measured contact angle data showed a possible correlation with the CHF data as the maximum CHF enhancement was observed with alumina and zinc oxide nanofluids at G=2500 kg/m^{2}s, while for diamond nanofluids the CHF enhancement was more modest.

7.2 Interpretation of the Experimental Data

A detailed review was conducted of relevant subcooled flow boiling heat transfer models or correlations that can be used to interpret the HTC and CHF data. Among many models, the superposition method of heat transfer prediction developed by Chen was deemed as the best boiling heat transfer model for the current study. In addition, Klimenko's correlation can incorporate the possible surface effect of thermal conductivity on the HTC.

Regarding CHF models, four generalized theories were discussed. Those were (i) hydrodynamic instability theory (boundary layer separation); (ii) bubble layer theory; (iii) vapor clot theory; (iv) wall overheat theory (hot/dry spot theory). Celata's model in category (iii) was considered to explain the CHF enhancement with contact angle change. In addition, Kuan and Kandlikar's model in category (iv) also showed the direct implication of the contact angle effect on the CHF enhancement.

Measured HTC and CHF data were compared to the existing models/correlations. Due to

various models and parameters introduced for the analysis, the model limitations and comparison results are summarized in Tables 7-1 and 7.2. Table 7-1 summarizes the comparison results between predictions and the measured HTC and CHF data. Also some functional characteristics of the analyzed models are highlighted in terms of the prediction capability and deficiency of the respective model. Table 7-2 summarizes the parametric effects on the measured HTC and CHF in light of the experimental observations and existing models related to respective parameters.

In summary, due to the complex nature of boiling process, these parameters are often interrelated with one another and hence no single parameter or model analyzed in the current study can explain the observed HTC and CHF phenomena. Nonetheless, rigorous analysis of the models or correlations and interrogation of the key parameters provide more detailed information that can elucidate the needs in new model development.

Table 7-1 Summary of HTC and CHF comparison with existing models/correlations

	Used models or correlations	Predictability	Capability or deficiency of the model	Remark
HTC	Chen (Collier and Thome, 1996)	Underestimates	Mass flux effect on nucleation suppression No consideration for the surface effects	Possible surface effects of nucleation site density, wettability, bubble dynamics appeared as the key
HTC	Klimenko (1988, 1990)	Underestimates	Thermal conductivity effect Strong function of applied heat flux No relation with mass flux	Changes of effective thermal conductivity in our heaters were not significant.
CHF	Celata et al. (1994b)	Predicts oppositely w.r.t. contact angle	Function of contact angle via bubble departure diameter from Staub's model	Trend of bubble departure diameter w.r.t. contact angle seems reasonable. Model was never validated w.r.t. contact angle.
CHF	Kuan and Kandlikar (2008)	Predicts w.r.t. contact angle	Function of contact angle Function of mass flux	Strong dependency on mass flux rather than contact angle. Model was correlated in micro-channel experiments.

Table 7-2 Summary of parametric effects on the HTC and CHF

Parameter	Used data or model Cited study	Interpreted data	Prediction result	Highlight
Surface roughness	Measured roughness Chen (Collier & Thome, 1996) Gnielinski (Mills, 1993)	Forced convective HTC	Negligible effect	Possible surface effects of nucleation site density, wettability, bubble dynamics appeared as the key.
Surface roughness	Measured roughness Chowdhury & Winterton (1985) Pioro et al. (2004)	NBHTC	No direct effect	Indirectly affects nucleation site density.
Surface area	Measured surface area change	CHF	Inconsistent correlation	Indirectly affects the wettability via roughness factor. Used for calculation of intrinsic contact angle.
Surface thermal conductivity	Effective thermal conductivity Klimenko (1988, 1990)	HTC	Negligible effect	No significant change in alumina and zinc oxide NF boiling. Significant change in diamond NF boiling but this does not match with HTC data.
Surface thermal conductivity	Thermal activity Arik-Bar Cohen (2003)	CHF	Strong effect on diamond NF tests	May explain moderate (35%) CHF enhancement in diamond NF boiling.
Capillary wicking	SEM pictures	HTC	Inconsistent correlation	May be at work for alumina and zinc oxide NF but not for diamond NF. This interpretation does not match with HTC data.
Capillary wicking	SEM pictures Kim et al. (2006a) Chen et al. (2009)	CHF	Inconsistent correlation	May explain CHF enhancement in alumina and zinc oxide NF boiling but not in diamond NF boiling.
Nucleation site density	Contact angle Micro-cavity density Wang & Dhir (1993)	HTC	Inconsistent correlation	Potentially showed increased nucleation site density. Estimate does not match with HTC data.
Wettability	Contact angle Celata et al. (1994b) Kuan and Kandlikar (2008) Gajewski (2008)	CHF	Inconsistent correlation	Might explain CHF enhancement for alumina and zinc oxide NF but not for diamond NF. If dynamic wettability was at work during diamond NF boiling, CHF enhancement in our study may be explained.
Bubble dynamics parameters	Departure diameter & frequency, contact angle Nucleation site density Fritz (1935) Mikic-Rohsenow (1969) Basu et al. (2005)	HTC	Inconsistent correlation	Bubble departure diameter & frequency model needs to be validated for nanofluids boiling. Calculation of nucleation site density needs to be refined for accurate prediction.

7.3 Conclusions

An experimental study of flow boiling heat transfer and CHF of water-based nanofluids with alumina, zinc oxide and diamond nanoparticles was presented. The main findings were as follows:

1) The nanofluids exhibited a significant CHF enhancement (up to 40-50%) with respect to pure water at high mass flux (2000-2500 kg/m^{2}s) and for nanoparticle concentration of 0.01-0.1 %vol. The CHF enhancement did not occur at low mass flux (1500 kg/m^{2}s).
2) Some nanoparticles were deposited and formed a porous layer on the boiling surface during the experiments. It was shown that such particle deposition increased the wettability of the boiling surface and that (as opposed to surface area increase) was the main driving force of CHF enhancement for alumina and zinc oxide nanofluids boiling. The CHF enhancement was weakly dependent on nanoparticle concentration for the alumina nanofluids, while it increased more pronouncedly with nanoparticle concentration for the zinc oxide and diamond nanofluids.
3) The measured effective heat transfer coefficients of nanofluids and water were within ±20% of each other at all heat fluxes explored here, and particularly at relatively low heat fluxes (<3000 kW/m^2). The traditional Chen and Klimenko's correlations systematically underestimate the HTC for the nanofluids and water at the operating conditions of our tests. The HTC differences between measurement and prediction were up to by as much as 100%.
4) The calculated nucleation site density data show no clear correlation with the HTC data for nanofluids. Bubble dynamics change along with nucleation site density and wettability data did not establish a direct correlation with the HTC data.

7.4 Future Work

Future research directions are identified upon observing trend of results and some deficiencies of the existing models/correlations and experimental data. Although the current study covered a wide range of surface effect parameter, several additional parameters still need to be identified experimentally. In addition, for applications to power engineering and nuclear power plant, a broader range of thermodynamic conditions, other than low pressure, needs to be investigated. Suggested research topics for future nanofluid study are numerated as follows:

1) Nanofluids boiling at high pressure
2) Dynamic wettability effect on nanofluids boiling
3) Nucleation site density effect on nanofluids boiling
4) Bubble dynamics effect on nanofluids boiling
5) HTC and CHF modeling by incorporating the effects of surface characteristics
6) Radiation effect on nanofluids boiling

Finally prioritizing the addressed topics will promote the idea of utilizing the emegerged outcomes from this study. First, the wettability improvement is believed to explain the significant CHF enhancement in alumina and zinc oxide nanofluids boiling. On the other hand, finding a plausible mechanism to explain the more moderate CHF enhancement in diamond nanofluids boiling was not very successful. Therefore an immediate future research effort should be focused on the dynamic parametric effect on the CHF (e.g., dynamic wettability).

Second, the approach to explain the HTC results is believed to be very inclusive (e.g., coupling of micro-cavity, wettability, nucleation site density, and bubble dynamics). However, the embedded approach of coupling experimental data with existing models was not very effective in predicting the

measured HTC data. Such inherent gap may be due to the validity of using existing models to explain the newly-emerged result. For example, use of Fritz's model for bubble departure diameter and Levy's bubble departure diameter and frequency model were not validated for nanofluids boiling. Therefore, a more research effort is needed to obtain a more accurate bubble dynamics model. Moreover, the inconsistency of the nucleation site density calculation result was inherited from the result of micro-cavity density, whose calculation was also somewhat arbitrary. Therefore direct calculation or measurement of the nucleation site density will improve understanding of the HTC results in this thesis work.

References

Adachi, S., 2004, "Handbook on physical properties of semiconductors", Vol. 1-3, Springer-Verlag, 2004.

Ahuja, A. S., 1975a, "Augmentation of heat transport in laminar flow of polystyrene suspensions. I. Experiments and results", *J. Applied Physics*, Vol. 4, issue 8, pp. 3408-3416.

Ahuja, A. S., 1975b, "Augmentation of heat transport in laminar flow of polystyrene suspensions. II. Analysis of the data", *J. Applied Physics*, Vol. 4, issue 8, pp. 3417-3425.

American Society of Mechanical Engineers (ASME), 2004. ASME Boiler and Preassure Vessel Code. Section II (Properties), Subpart 2, Table TCD.

Arik, M., Bar-Cohen, A., 2003, "Effusivity-based correlation of surface property effects in pool boiling CHF of dielectric liquids", *Int. J. Mass Transfer*, Vol. 46, pp. 3755-3764.

Bang, I. C., Chang, S. H., 2005, "Boiling Heat Transfer Performance and Phenomena of Al_2O_3-Water Nano-fluids from a Plain Surface in a Pool", *Int. J. of Heat and Mass Transfer*, Vol. 48, pp. 2407-2419.

Barthau, G., Hahne, E., 2000, "Nucleation site density and heat transfer in nucleate pool boiling of refrigerant R134a in a wide pressure range", 3rd European Thermal-Sciences Conference, Heidelberg, Germany, Vol. 2, pp. 731-736.

Basu, N., Warrier, G. R., Dhir, V. K., 2005, "Wall Heat Flux Partitioning During Subcooled Flow Boiling: Part 1 – Model Development", J. Heat Transfer, Vol. 127, pp. 131-140.

Buongiorno, J., 2006, "Convective transport in nanofluids", *J. of Heat Transfer*, Vol. 128, pp. 240-250.

Buongiorno, J., Hu, L. W., Kim, S. J., Hannink, R., Truong, B., Forrest, E., 2008, "Nanofluids for enhanced Economics and Safety of Nuclear Reactors: an Evaluation of the Potential Features, Issues and Research Gaps", *Nuclear Technology*, Vol. 162, pp. 80-91.

Carey, V. P., 1992, "Liquid-Vapor Phase-Change Phenomena: An Introduction to the Thermophysics of Vaporization and Condensation Processes in Heat Transfer Equipment", Taylor & Francis, KY.

Celata, G. P., Cumo, M., Mariani, A., 1994a, "Assessment of correlations and models for the prediction of CHF in subcooled flow boiling", Int. J. Heat and Mass Transfer, Vol. 37, pp. 237-255.

Celata, G. P., Cumo, M., Mariani, A., Simoncini, M., Zummo, G., 1994b, "Rationalization of existing mechanistic models for the prediction of water subcooled flow boiling critical heat flux", Int. J. Heat Mass Transfer, Vol. 37, pp. 347-360.

Chang, S. H., Lee, K. W., 1989, "A CHF model based on mass, energy, and momentum balance for upflow boiling at low qualities", Nuclear Engineering and Design, Vol. 113, pp. 35-50.

Chen, R., Lu, M. C., Srinivasan, V., Wang, Z., Cho, H. H., Majumdar, A., 2009, "Nanowires for enhanced boiling heat transfer", Nano Letters, Article ASAP, DOI: 10.1021/nl8026857.

Choi, S. U. S., 1995, "Enhancing thermal conductivity of fluids with nanoparticles". IN: D.A. Siginer, &

H.P. Wang. eds. Developments and Applications of Non-Newtonian Flows, *ASME FED-231/MD-66* pp. 99-105.

Choi, S. U. S., Zhang, Z. G., Yu, W., Lockwood, F. E., Grulke, E. A., 2001, "Anomalous thermal conductivity enhancement in nanotube suspensions", *Applied Physics Letters*, Vol. 79, issue 14, pp. 2252-2254.

Chowdhury, S. K. R., Winterton, R. H. S., 1985, "Surface effects in pool boiling", *Int. J. Heat Mass Transfer*, Vol. 28, pp. 1881-1889.

Claxton, N. S., Fellers, T. J., Davidson, M. W., "Laser scanning confocal microscopy", in http://www.olympusfluoview.com/theory/LSCMIntro.pdf.

Collier, J. G., Thome, J. R., 1996, "Convective boiling and condensation", *Oxford University Press.*

Coursey, J. S., Kim, J., 2008, "Nanofluid boiling: The effect of surface wettability", *Int. J. Heat Fluid Flow*, in press.

Das, S., Putra, N., Roetzel, W., 2003a, "Pool boiling characteristics of nano-fluids", *Int. J. of Heat and Mass Transfer*, Vol. 46, pp. 851-862.

Das, S. K., Putra, N., Thiesen, P., Roetzel, W., 2003b, "Temperature Dependence of Thermal Conductivity Enhancement for Nanofluids", *J. Heat Transfer*, Vol. 125, pp. 567 – 574.

Dinh, T. N., Thu, J. P., Theofanous, T. G., 2004, "Burnout in high heat flux boiling: the hydrodynamic and physico-chemical factors", *42nd AIAA Aerospace Sciences Meeting and Exhibit*, Reno, Nevada, 5-6 January.

Eastman, J. A., Choi, S. U. S., Thompson, L. J., Lee, S., 1997, "Enhanced thermal conductivity through the development of nanofluids", Proceedings of the Symposium on Nanophase and Nanocomposite Materials II. Vol. 457, Materials Research Society, Boston, pp. 3-11.

Eastman, J. A., Choi, S. U. S., 2001, "Anomalously increased effective thermal conductivities of ethylene-glycol-based nanofluids containing copper nanoparticles", *Applied Physics Letters,* Vol. 78, issue, 6, pp. 718-720.

Elkassabgi, Y., Lienhard, J. H., 1988, "Influence of subcooling on burnout of horizontal cylindrical heaters", J. Heat Transfer, Vol. 110, pp. 479-486.

Everett, D. H., 1988, "Basic Principles of Colloid Science", Royal Society of Chemistry London.
Mills, A. F., 1999, "Heat Transfer", Prentice Hall, 2nd Ed.

Fritz, W., 1935, "Maximum volume of vapor bubbles", Phys. Z. Vol. 36, pp. 379-384.

Gajewski, A., 2008, "Contact angle and rivulet width hysteresis on metallic surfaces. Part I: With heated surface", *Int. J. Heat Mass Transfer*, Vol. 51, 5762-5771.

Gnielinski, V., 1976. New Equations for Heat and Mass Transfer in Turbulent Pipe and Channel Flow. Int. Chem. Eng., 16, pp. 359-368.

Groeneveld, D. C., Leung, L. K. H., Kirillov, P. L., Bobkov, V. P., Smogalev, I. P., Vinogradov, V. N.,

Huang, X. C., Royer, E., 1996, "The 1995 Look-up Table for Critical Heat Flux in Tubes", *Nuclear Engineering Design*, 163, pp. 1-23.

Gupta, S. V., 2004, "Capillary action in narrow and wide tubes – a unified approach", Metrologia, Vol. 41, 361-364.

Hatton, A. P., Hall, I. S., 1966, "Photographic study of boiling on prepared surfaces", Paper No. 115, Third International Heat Transfer Conference, Chicago.

Holman, J. P., 2001, "Experimental Methods for Engineers", 7th ed., McGraw-Hill, New York.

Incropera, F. P., DeWitt, D. P., 2002, "Introduction to Heat Transfer", John Willey & Sons, Inc. 4th Ed.

Ivey, H. J., 1967, "Relationships between bubble frequency, departure diameter and rise velocity in nucleate boiling", Int. J. Heat Mass Transfer, Vol. 10, pp. 1023-1040.

Jang, S. P., Choi, S. U. S., 2004, "Role of Brownian motion in the enhanced thermal conductivity of nanofluids", *Applied Physics Letters*, Vol. 84, issue 21, pp. 4316-4318.

Kandlikar, S. G., 2001, "A theoretical model to predict pool boiling CHF incorporating effects of contact angle and orientation", J. Heat Transfer, Vol. 123, pp. 1071-1079.

Katto, Y., 1990, "A physical approach to critical heat flux of subcooled flow boiling in round tubes", Int. J. Heat Mass Transfer, Vol. 33, pp. 611-620.

Kaviany, M., 1999, "Principles of Heat Transfer in Porous Media", Springer: New York.

Keblinski, P., Phillpot, S. R., Choi, S. U. S., Eastman, J. A., 2002, "Mechanisms of heat flow in suspensions of nano-sized particles (nanofluids)", *Int. J. of Heat and Mass Transfer*, Vol. 45, pp. 855-863.

Kim, H., Kim, J., Kim, M., 2006a, "Experimental study on CHF characteristics of water-TiO_2 nano-fluids", *Nuclear Engineering and Technology*, Vol. 38, No. 1.

Kim, S. J., Bang, I. C., Buongiorno, Buongiorno, Hu, L. W., 2006b, "Effects of nanoparticle deposition on surface wettability influencing boiling heat transfer in nanofluids", *Applied Physics Letters*, Vol. 89, 153107.

Kim, S. J., Bang, I. C., Buongiorno, J., Hu, L. W., 2007, "Surface wettability change during pool boiling of nanofuids and its effect on critical heat flux", *Int. J. of Heat and Mass Transfer*, Vol. 50, pp. 4105-4116.

Kim, S. J., 2007, "Pool boiling heat transfer characteristics of nanofluids", *SM thesis*, Nuclear Science and Engineering Department, MIT, Cambridge, MA, USA.

Klimenko, V. V., 1988, "A generalized correlation for two-phase forced flow heat transfer", *Int. J. Heat Mass Transfer*, Vol. 31, pp. 541-552.

Klimenko, V. V., 1990, "A generalized correlation for two-phase forced flow heat transfer – second assessment", *Int. J. Heat Mass Transfer*, Vol. 33, pp. 2073-2088, 1990.

Kuan, W. K., Kandlikar, S. G., 2008, "Experimental study and model on critical heat flux of refrigerant-123 and water in microchannels", J. Heat Transfer, Vol. 130, pp. 034503: 1-5.

Kutateladge, S. S., Leont'ev, A. I., 1964, "Turbulent boundary layers in compressible gases", D. B. Spalding, trans., Academic Press, New York.

Lee, M., Chueng, L. S. L., Lee, Y. K., Zohar, Y., 2005, "Height effect on nucleation-site activity and size-dependent bubble dynamics in microchannel convective boiling", J. Micromech. Microeng., Vol. 15, pp. 2121-2129.

Lee, C. H., Mudawar, I., 1988, "A mechanistic critical heat flux model for subcooled flow boiling based on local bulk flow conditions", *Int. J. Multiphase Flow*, Vol. 14, pp. 711-728.

Lee, J., Mudawar, I., 2006, "Assessment of the effectiveness of nanofluids for single-phase and two-phase heat transfer in micro-channels", *Int. J. Heat and Mass Transfer*, Vol. 50, pp. 452-463.

Lee, S., Choi, S. U. S., Li, S., Eastman, J. A., 1999, "Measuring thermal conductivity of fluids containing oxide nanoparticles", *J. Heat Transfer*, Vol. 121, pp. 280-289.

Levy, S., 1967, "Forced convection subcooled boiling – prediction of the vapor volumetric fraction", Int. J. Heat and Mass Transfer, Vol. 10, pp. 951-965.

Liter, S. G., Kaviany, M., 2001, "Pool-boiling CHF enhancement by modulated porous-layer coating: theory and experiment", International Journal of Heat and Mass Transfer, Vol. 44, pp. 4287-4311.

LMNO Engineering, Research, and Software, Ltd. http://www.lmnoeng.com/moody.htm

Lucas, T., 2008, "Study of chemistry and irradiation effect on nanofluids to be used in Light Water Reactor accident cooling", SM Thesis, Nuclear Science and Engineering Department, MIT.

Lucas, T., Hu, L. W., Buongiorno, J., 2007, "Investigation of gamma radiation effect on nanofluids for nuclear application", Trans. Am. Nuc. Soc., Vol. 96, pp. 487-488.

Masuda, H., Ebata, A., Teramae, K., Hishinuma, N., 1993, "Alteration of thermal conductivity and viscosity of liquid by dispersing ultra-fine particles (dispersion of Al2O3, SiO2, and TiO2 ultra-fine particles)", *Netsu Bussei*, Vol. 4, issue 4, p. 227.

Maxwell, J. C., 1881, "A treatise on electricity and magnetism", 2nd Ed., Clarendon, Oxford.

Maxwell Garnett, J. C., 1904, "Colours in Metal Glasses and in Metallic Films", Royal Society of London Philosophical Transactions Series A, Vol. 203, pp. 385-420.

Mikic, B. B., Rohsenow, W. M., 1969, "A New Correlation of Pool Boiling Data Including the Effect of Heating Surface Characteristics", Trans. ASME, J. Heat Transfer, Vol. 91, 245.

Milanova, D., Kumar, R., 2005, "Role of ions in pool boiling heat transfer of pure and silica nanofluids", *Applied Physics Letters*, Vol. 87, 233107.

Milanova, D., Kumar, R., Kuchibhatla, S., Seal, S., 2006, "Heat transfer behavior of oxide nanoparticles in pool boiling experiment", *Proc. of 4th International Conference on Nanochannels, Microchannels and Minichannels*, Limerick, Ireland, June 19-21.

Mills, A. F., 1999, "Heat Transfer", Prentice Hall, 2nd Ed.

Moreno Jr., G., Oldenburg, S., You, S. M., Kim, J. H., 2005, "Pool Boiling Heat Transfer of Alumina-Water, Zinc Oxide-Water and Alumina-Water Ethylene Glycol Nanofluids", *Proceedings of HT2005*, July 17-22, San Francisco, California, USA.

Narayan, G. P., Anoop, K. B., Das, S. K., 2007, "Mechanism of enhancement/deterioration of boiling heat transfer using stable nanoparticle suspensions over vertical tubes", *Journal of Applied Physics*, Vol. 102, 074317.

Pak, B. C., Cho, Y. I., 1998, "Hydrodynamic and heat transfer study of dispersed fluids with submicron metallic oxide particles", *Experimental Heat Transfer*, Vol. 11, pp. 151-170.

Patel, H. E., Das, S. K., Sundararajan, T., 2003, "Thermal conductivities of naked and monolayer protected metal nanoparticle based nanofluids: Manifestation of anomalous enhancement and chemical effects", *Applied Physics Letters*, Vol. 83, issue 14, pp. 2931-2933.

Pioro, I. L., Wohsenow, W., Doerffer, S. S., 2004, "Nucleate pool-boiling heat transfer. I: review of parametric effects of boiling surface", *Int. J. Heat Mass Transfer*, Vol. 47, pp. 5033-5044.

Rajayi, M., Kantzas, A., 2008, "Effect of temperature and pressure on contact angle of quartz-water-bitumen system", International Symposium of the Society of Core Analysis, Abu Dhabi, UAE, Oct. 29-Nov. 2.

Sibamoto, Y., Yonomot, T., Nakamura, H., Kukita, Y., 2007, "In-pile experiment in JMTR on the radiation induced surface activation (RISA) effect on flow-boiling heat transfer", Journal of Nuclear Science and Technology, Vol. 44, pp. 183-193.

Situ, R., Ishii, M., Hibiki, T., Tu, J. Y., Yeoh, G. H., Mori, M., 2008, "Bubble departure frequency in forced convective subcooled boiling flow", Int. J. Heat Mass Transfer, Vol. 51, pp. 6268-6282.

Staub, F. W., 1968, "The void fraction in subcooled boiling – prediction of the initial point of net vapor generation", J. Heat Transfer, Vol. 90, pp. 151-157.

Theofanous, T. G., Dinh, T. N., 2006, "High heat flux boiling and burnout as microphysical phenomena: mounting evidence and opportunities", Multiphase Sci. Technol. Vol. 18, pp. 1-26.

Thorncroft, G. E., Klausner, J. F., Mei, R., 1998, "An experimental investigation of bubble growth and detachment in vertical upflow and downflow boiling", International Journal of Heat and Mass Transfer, Vol. 41, pp. 3857-3871.

Todreas, N. E., Kazimi, M. S., 1990, "Nuclear Systems I Thermal Hydrualic Fundamentals", Taylor & Francis, 2nd Ed.

Tong, L. S., 1968, "Boundary layer analysis of the flow boiling crisis", Int. J. Heat and Mass Transfer, Vol. 11, pp. 1208-1211.

Tong, L. S., Currin, H. B., Larsen, P. S., Smith, O. G., 1966, Influence of axially non-uniform heat flux on DNB, AIChE Chem. Eng. Prog. Symp. Ser. Vol. 62, pp. 35-40.

Tong, L. S., Tang, Y. S., 1997, "Boiling heat transfer and two-phase flow", *Taylor & Francis*, 2nd Ed.

Truong, B., Hu, L.W., Buongiorno, J., 2008, "Optimizing Critical Heat Flux Enhancement Through Nanoparticle-Based Surface Modifications", International Congress on Advances in Nuclear Power Plants (ICAPP), June 8-12, Anaheim, CA.

You, S. M., Kim, J., Kim, K. H., 2003, "Effect of nanoparticles on critical heat flux of water in pool boiling heat transfer", *Applied Physics Letters*, Vol. 83, *16*, pp. 3374-3376.

Vandervort, C. L., Bergles, A. E., Jensen, M. K.,1992, "Heat transfer mechanisms in very high heat flux subcooled boiling", Presented in Fundamentals of Subcooled Flow Boiling, HTD-Vol. 217, pp. 1-9. Winter Annual Meeting ASME, Anaheim, CA.

Vassallo, P., Kumar, R., D'Amico, S., 2004, "Pool boiling heat transfer experiments in silica-water nano-fluids", *Int. J. of Heat and Mass Transfer*, Vol. 47, pp. 407-411.

Wang, C. H., Dhir, V. K., 1993, "Effect of surface wettability on active nucleation site density during pool boling of water on a vertical surface", *J. Heat Transfer*, Vol. 115, pp. 659-669.

Weisman, J., Pei, B. S., 1983, "Prediction of CHF in flow boiling at low qualities", Int. J. Heat Mass Transfer, Vol. 26, pp. 1463-1477.

Wen, D., Ding, Y., 2005, "Experimental investigation into the pool boiling heat transfer of aqueous based γ-alumina nanofluids", *Journal of Nanoparticle Research*, Vol. 7, pp. 265-274.

Wenzel, R. N., 1949, "Surface roughness and contact angle", J. Phys. Colloid Chem. 53, 1466.

Williams, W. C., 2006, "Experimental and theoretical investigation of transport phenomena in nanoparticle colloids (nanofluids)", *PhD Thesis*, Nuclear Science and Engineering Department, Massachusetts Institute of Technology, Cambridge, MA, USA.

Williams, W. C., Buongiorno, J., Hu, L. W., 2008, "Experimental investigation of turbulent convective heat transfer and pressure loss of alumina/water and zirconia/water nanoparticle colloids (nanofluids) in horizontal tubes", *J. Heat Transfer*, Vol. 130, 042412.

Xie, H., Wang, J., Xi, T., Liu, Y., 2002a, "Thermal Conductivity of Suspensions Containing Nanosized SiC Particles", *International Journal of Thermophysics*, Vol. 23, issue 2, pp. 571-580.

Xie, H., Wang, J., Xi, T., Liu, Y., Ai, F., 2002b, "Thermal conductivity enhancement of suspensions containing nanosized alumina particles", *Journal of Applied Physics*, Vol. 91, issue 7, pp. 4568-4572.

Zeng, L. Z., Klausner, J. F., Mei, R., 1993, "A unified model for the prediction of bubble detachment diameters in boiling systems – I. Flow boiling", International Journal of Heat and Mass Transfer, Vol. 36, pp. 2271-2279.

Zhilina, V. V., Markov, I. I., 1973, "On changes taking place in the separation diameter of a vapor bubble with increasing pressure", Translated from Inzhenerno-Fizicheskii Zhurnal, Vol. 25, pp. 780-784.

Zhou, S. Q., Ni, R., 2008, "Measurement of the specific heat capacity of water-based Al2O3 nanofluid", Applied Physics Letters, Vol. 92, 093123.

Appendix A. Theory of Thermal Conductivity Measurement

First the transient heat conduction equation for cylindrical coordinate in a homogeneous and isotropic medium is considered as the governing equation:

$$\frac{\partial T}{\partial t} = \alpha\left(\frac{\partial^2 T}{\partial r^2} + \frac{1}{r}\frac{\partial T}{\partial r}\right) \tag{A-1}$$

where T is temperature (°C), t is time (second), α is thermal diffusivity of the medium (m^2/s), and r is the radial distance (m) from the axis of the probe. Eq. A-1 assumes negligible axial conduction and no convection effects. When a long, electrically heated probe is inserted into a medium, the temperature rise from an initial temperature, T_i, at some radial distance from the probe is

$$T - T_i = \left(\frac{q'}{4\pi k_m}\right) Ei\left(-\frac{r^2}{4\alpha t}\right) \tag{A-2}$$

where q' is the heat rate supplied per unit length (W/m) and Ei is the exponential integral function given by

$$-Ei(-a) = \int_a^\infty \left(\frac{1}{u}\right)\exp(-u)du = -\gamma - \ln\left(\frac{r^2}{4\alpha t}\right) + \frac{r^2}{4\alpha t} - \left(\frac{r^2}{8\alpha t}\right) + \ldots \tag{A-3}$$

where $a=r^2/4\alpha t$ and γ is Euler's constant (0.5772). When t is large, the higher order terms can be ignored, thus combining Eqs. A-2 and A-3 yields

$$\Delta T = T - T_i \cong \frac{q'}{4\pi k_m}\left[\ln t - \gamma - \ln\left(\frac{r^2}{4\alpha t}\right)\right] \tag{A-4}$$

where k_m is the thermal conductivity of the medium (W/m·K). It is apparent from the relationship between thermal conductivity and $\Delta T=T-T_i$, shown in Eq. A-4, that ΔT and $\ln(t)$ are linearly related with a slope $n=q'/4\pi k_m$. Linearly regressing ΔT on $\ln(t)$ yields a slope that, after arranging, gives the thermal conductivity as

$$k_m = \frac{q'}{4\pi m} \tag{A-5}$$

Where q' is known from power supplied to the probe. The diffusivity can also be obtained from Eq. A-6. The intersection of regression line with the t axis ($\Delta T=0$) gives

$$\ln(t_o) = \left[\gamma + \ln\left(\frac{r^2}{4\alpha} \right) \right] \tag{A-6}$$

From the calculated t_o (from the intercept of ΔT vs. $\ln(t)$) and finite r, Eq. A-6 gives diffusivity, α. Because the higher order terms of Eq. A-3 have been neglected, Eq. A-4 is not exact. However, if the slope of intercept are computed only for ΔT and $\ln(t)$ values, where t is large enough to ignore the higher order terms, Eqs. A-5 and A-6 give correct values for k_m and α. This procedure is automatically performed by the KD2 probe; the user simply has to read the probe output.

From a physical view point, thermal conductivity of a material is a measure of how well the material transfers heat from one point to another in response to a temperature difference between those two points. Conduction is defined as the transfer of energy from the more energetic to the less energetic particles of a substance due to interactions between particles at atomic and molecular levels at rest. Therefore it is important to eliminate any free convective heat transfer condition during the entire measurement. This is done by eliminating large thermal gradients within the system. That is, the test fluid sample is maintained at constant temperature by an isothermal bath, and the duration of the heat pulse in the probe is kept relatively short (a few seconds), to prevent the onset of free convective flow.

Appendix B. Theory of Dynamic Light Scattering Measurement

When a coherent source of light such as a laser having a known frequency is directed at the moving particles, the light is scattered, but at a different frequency. The change in the frequency is quite similar to the change in frequency or pitch one hears when an ambulance with its wailing siren approaches and finally passes. The shift is termed a Doppler shift or broadening, and the concept is the same for light when it interacts with small moving particles. For the purposes of particle measurement, the shift in light frequency is related to the size of the particles causing the shift. Due to their average higher Brownian velocity, smaller particles cause a greater shift in the light frequency than larger particles. Thus, the difference in the frequency of the scattered light among particles of different sizes is used to determine the sizes of the particles present.

The DLS equipment used for this study consists of mainly three components. A laser provided by Spectra-Physics emits a 514 nm wavelength of argon. A goniometer from Brookhaven receives any scattering between the incident laser and present nano-size particle, which is placed onto a bath. Finally, a detector from Brookhaven detects the light scattered at 90 degrees from the incident laser beam since the angle between the goniometer and detector is fixed at 90 degrees. This configuration is shown in Fig. B-1. Since the expected particle size of nanoparticles is smaller than the wavelength of the incident laser light, the type of scattering of interest in our case is called Rayleigh scattering, which is defined as the scattering of light, or other electromagnetic radiation, by particles much smaller than the wavelength of the light.

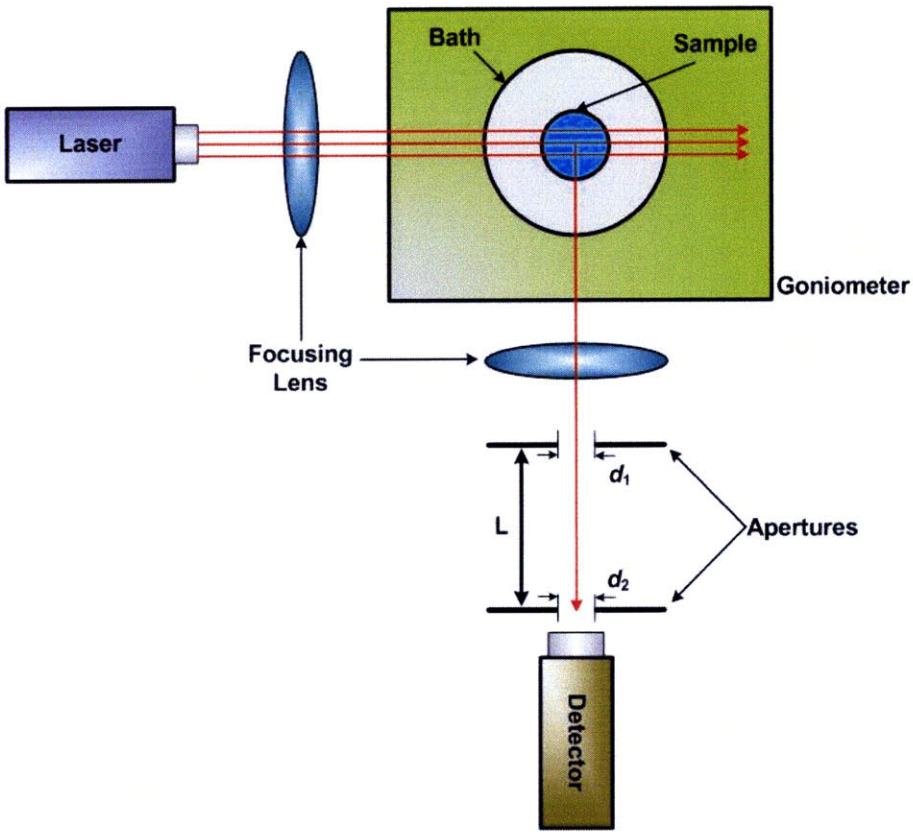

Figure B-1 A schematic of the light scattering measurement apparatus operating in the dynamic mode

There exists an alternative mode of operation for the DLS measurements, the static light scattering, which is also viable if the configuration allows the goniometer to rotate automatically. In such a case, scattered laser light will be detected as a function of the angle, which gives the angular distribution of particle size. In the dynamic and static modes, the so-called hydrodynamic and gyration particle diameters can be obtained, respectively. The equations governing the dynamic mode of operation are discussed next.

When measuring a particle size, it is necessary to start with several assumptions. First the particles can be assumed to be in Brownian motion. Second, it assumed that the particle do not interact with each other. In a practical measurement, the second assumption can be valid when the fluid contains

a small number of particles. With those assumptions, the average motion of a particle can be described by using an intermediate scattering function, $f(q,\tau)$ expressed as:

$$f(q,\tau) = \langle \exp\{-iq \cdot [r(0) - r(\tau)]\} \rangle = \langle \exp[iq \cdot \Delta r(\tau)] \rangle \quad \text{(B-1)}$$

where $q=(4\pi/\lambda)\sin(\theta/2)$ is a scattering factor, λ is a wavelength of scattered light, θ is an angle between incident and scattered lights, τ is the time scale during the scattering, and $\Delta r(\tau) \equiv r(\tau) - r(0)$ is displacement of particle in time τ (Berne and Pecora, 1976).

For particle in Brownian motion, $\Delta r(\tau)$ is a real 3-D Gaussian variable and therefore $f(q, \tau)$ and the mean square displacement $\langle \Delta r^2(\tau) \rangle$ become:

$$f(q,\tau) = \exp\left[-\frac{q^2}{6} \langle \Delta r^2(\tau) \rangle \right] \quad \text{(B-2)}$$

$$\langle \Delta r^2(\tau) \rangle = 6 D_o \tau \quad \text{(B-3)}$$

Combining Eqs. B-2 and B-3 yields:

$$f(q,\tau) = \exp[-q^2 D_o \tau] \quad \text{(B-4)}$$

where D_o is a mass self-diffusion coefficient defined by Stokes-Einstein theory as:

$$D_o = \frac{k_B T}{6\pi\eta R} \quad \text{(B-5)}$$

where k_B is the Boltzmann constant, T is the temperature, η is viscosity, and R is a radius of the particle that is measured.

In the measurement, the measured quantity indeed is the diffusion constant D_o based on the known scaling factor q and time τ in the Eq. B-4. Using the obtained $f(q,\tau)$, the diffusion constant is found from Eq. B-4. Finally, the radius of particle size R is determined from Eq. B-5.

Appendix C. Numerical Routine of Chen's Model in MATLAB

This section describes a numerical routine, which has implemented Chen's correlation for inner wall temperature prediction. The prediction was made using several parameters obtained during the experimental activities. The utilized parameters are applied heat flux, bulk inlet temperature, mass flux, and outer wall temperature, all of which are read as the input for running this routine. The input file, 'test1.xls', shown below involves those four variables. This routine also contains a subroutine of evaluating the relative importance of single-phase HTC over the two-phase HTC. The evaluation was conducted using both measured and predicted wall temperatures. Prediction of T_w at ONB can be made using Davis-Anderson's model (Eq. 2-9) and is also viable through this routine.

Prediction of inner wall temperature starts by calculating the inner wall temperature using imported outer wall temperature. If the calculated inner wall temperature is below T_{sat}, then the forced convective HTC in Chen's correlation predicts $T_{w,i}$. Otherwise, Chen's nucleate boiling HTC correlation is used for $T_{w,i}$ prediction via an iteration method. A simple iteration method has been introduced in this routine. First, a reasonable wall temperature (Tw_o in the routine) is guessed (e.g., Tw_o=T_{sat} + 3). Tw_o is then used for calculating the pressure differential term, $[P_{sat}(T_w)-P]$ in Eq. 2-16 by replacing T_w with Tw_o. The guessed Tw_o and resulting local pressure differential along with Eq. 2-17 estimate Eq. 2-16. Finally, in Eq. 2-14, T_w becomes the only unknown variable as h_{FC} and h_{NB} are estimated using Eq. 2-15 and Eqs. 2-16 and 17, respectively. The estimated T_w (Tw_2p in the numerical routine) is then compared with the initial guess of Tw_o and this interation process continues until the difference between two values converges below 10^{-3} °C.

Following routine shows the corresponding source script built in MATLAB.

```
clear all; close all; clc;

TOL = 1e-3;

%THERMODYNAMIC PROPERTIES OF WATER AT 1 BAR
P=1.01e5; Tsat=100;

%SPEICIFIC GAS CONSTANT FOR WATER VAPOR AT STD
R=461.9;

%TUBE HEATER OUTER DIAMETER IN m
Do=1/4*25.4*0.001;

%TUBE HEATER THICKNESS IN m
th=0.016*25.4*0.001;

%TUBE HEATER INNER DIAMETER IN m
Di=Do-2*th; L=0.1;

%FLOW CHANNEL HYDRAULIC AREA IN m
A=pi/4*Di^2;
pi=3.141592;

%READ EXPERIMENTAL DATA AS INPUT FOR RUNNING SCRIPT
input=xlsread('test1.xls');
[m,n]=size(input);

%AXIAL NDOE FOR HEATER
Z=0.01:0.01:0.1;

%SIZE OF THE AXIAL NODE
t=length(Z);

Tw = zeros(m, t);
Xe = zeros(m, t);
Tbtemp = zeros(m, t);
hFC = zeros(m, t);
Tb = zeros(m, t);
iXtt = zeros(m, t);
F = zeros(m, t);
S = zeros(m, t);
hNB = zeros(m, t);
flag = zeros(m, t);
eps = ones(m, t);


%CONSTANT OF CHEN CORRELATION OF NUCLEATE BOILING HTC
hNB_coeff=0.00122*(kf(Tsat)^0.79*(cpf(Tsat)*1e3)^0.45*(1/vf(Tsat))^0.49)/(sigma(Tsat)^0.5*muf(Tsat)^0.29*(hf
g(Tsat)*1e3)^0.24*(1/vg(Tsat))^0.24);

%SATURATION TEMPERATURE IN CELSIUS
Tsat_table=[0:10:370,374.15];
Psat_table=[0.006112,0.012271,0.023368,0.042418,0.073750,0.12335,0.19919,0.31161,0.47358,0.70109,1.01325,1.
4327,1.9854,2.7011,3.6136,4.7597,6.1804,7.9202,10.027,12.553,15.550,19.080,23.202,27.979,33.480,39.776,46.94
1,55.052,64.191,74.449,85.917,98.694,112.89,128.64,146.08,165.37,186.74,210.53,221.2];
```

```
for i=1:m
   disp(['m = ', num2str(i)]);

   %INPUT: HEAT FLUX IN kW/m^2
   q=input(:,1);

   %INPUT: BULK INLET TEMP IN °C
   Tin=input(:,2);

   %INPUT: MASS FLUX IN kg/m^2s
   G=input(:,3);

   %INLET ENTHALPY IN J/kg
   h_in=cpf(Tin(i))*1e3*Tin(i);

   %MEASURED OUTER WALL TEMPERATURE
   Twall_out=input(:,4);
   for ii=1:t

     %LOCAL BULK TEMPERATURE
    Tbtemp(i,ii)=Tin(i)+pi*Di/G(i)/A/(cpf(Tin(i))*1e3)*q(i)*1e3*Z(ii);
    %CALCULATION OF WALL TEMPERATURE AT ONB
    Tw_ONB(i,ii)=Tsat+sqrt(8*R*(Tsat+273.1)^2*sigma(Tsat)*q(i)*1e3/(Kf(Tsat)*hfg(Tsat)*1e3*P*1e6));

     %DITTUS-BOELTER CORRELATION
hFC(i,ii)=kf(Tbtemp(i,ii))/Di*0.023*(G(i)*Di/muf(Tbtemp(i,ii)))^0.8*(muf(Tbtemp(i,ii))*cpf(Tbtemp(i,ii))*1e3/kf(
Tbtemp(i,ii)))^0.4;

     %ESTIMATE OF WALL TEMPERATURE TO JUDGE WHETHER BOILING MIGHT OCCUR
     Tw(i,ii)=Tbtemp(i,ii)+q(i)*1e3/hFC(i,ii);

     %LOCAL EQUILIBRIUM QUALITY
     Xe(i,ii)=1/(hfg(Tsat)*1e3)*(pi*Di*q(i)*1e3/G(i)/A)*Z(ii)-(hf(Tsat)*1e3-h_in)/(hfg(Tsat)*1e3);

     if Tw(i,ii)<=Tsat

       %LOCAL BULK TEMPERATURE WHEN T_wall IS BELOW T_sat
       Tb(i,ii)=Tin(i)+pi*Di/G(i)/A/(cpf(Tin(i))*1e3)*q(i)*1e3*Z(ii);

       %LOCAL WALL TEMPERATURE WHEN T_wall IS BELOW T_sat
       Tw(i,ii)=Tb(i,ii)+q(i)*1e3/hFC(i,ii);

     else
       flag(i, ii) = 1;
       if Xe(i,ii)<0

         %LOCAL BULK TEMPERATURE WHEN T_wall IS BEYOND T_sat BUT STILL AT SUBCOOLED
         CONTITION
         Tb(i,ii)=Tin(i)+pi*Di/G(i)/A/(cpf(Tin(i))*1e3)*(q(i)*1e3)*Z(ii);
         X=0;
       else

         %LOCAL BULK TEMPERATURE AT SATURATED CONDITION
         Tb(i,ii)=Tsat;
         X=Xe(i,ii);
       end
```

```
        %INVERSE MARTINELLI PARAMETER
        iXtt(i,ii)=((1/vf(Tsat))/(1/vg(Tsat)))^0.5*(mug(Tsat)/muf(Tsat))^0.1*(X/(1-X))^0.9;
        if iXtt(i,ii)<0.1;

          %FORCED CONVECTION ENHANCEMENT PARAMETER AT SUBCOOLED CONDITION
          F(i,ii)=1;
        else

          %FORCED CONVECTION ENHANCEMENT PARAMETER
          F(i,ii)=2.35*(0.213+iXtt(i,ii))^0.736;
        end

        %DITTUS-BOELTER-LIKE CORRELATION: A PART OF CHEN CORRELATION
         hFC(i,ii)=kf(Tbtemp(i,ii))/Di*0.023*(G(i)*(1-
         X)*Di/muf(Tbtemp(i,ii)))^0.8*(muf(Tbtemp(i,ii))*(cpf(Tbtemp(i,ii))*1e3)/kf(Tbtemp(i,ii)))^0.4*F(i,ii);

        %NUCLEATE BOILING SUPPRESSION FACTOR: A PART OF CHEN CORRELATION
        S(i,ii)=1/(1+2.53e-6*(G(i)*(1-X)*Di/muf(Tbtemp(i,ii))*F(i,ii)^1.25)^1.17);
        Tw_0=Tsat+3;
        numIter = 1;
        while 1
          Psat0=interp1(Tsat_table, Psat_table, Tw_0)*10^5;

          %h_NB CORRESPONDING TO INITIAL GUESS
          hNB(i,ii)=hNB_coeff*(Tw_0-Tsat)^0.24*(Psat0-P)^0.75*S(i,ii);

          %WALL TEMPERATURE OBTAINED ITERATIVELY
          Tw_2p=(hNB(i,ii)*Tsat+hFC(i,ii)*Tb(i,ii)+q(i)*1e3)/(hNB(i,ii)+hFC(i,ii));
          eps(i, ii) = abs(Tw_2p-Tw_0);
          if Tw_2p <= Tsat || Psat0 < P
            Tw_2p = Tsat;
            break;
          elseif eps(i,ii) > TOL
            Tw_0 = (Tw_2p+Tw_0)/2;
          else
            break;
          end
          numIter = numIter+1;
        end
        Tw(i,ii) = Tw_2p;
        hNB_pred(i,ii)=0.001*(q(i)*1e3-hFC(i,ii)*(Tw(i,ii)-Tb(i,ii)))/(Tw(i,ii)-Tsat); % in kW/m2K
        q_1p(i,ii)=0.001*hFC(i,ii)*(Tw(i,ii)-Tb(i,ii));
        q_2p(i,ii)=hNB_pred(i,ii)*(Tw(i,ii)-Tsat);
        ratio_pred(i,ii)=q_1p(i,ii)/q_2p(i,ii);
        q_check(i,ii)=q_1p(i,ii)+q_2p(i,ii);
      end
      heff_pred(i,ii)=q(i)*1e3/(Tw(i,ii)-Tb(i,ii));
      disp(['Z = ', num2str(Z(ii),'%.2f'), ': Tw = ',num2str(Tw(i,ii))]);
    end
end


%CALCULATION OF FORCED CONVECTIVE HEAT TRANSFER AND NUCLEATE BOILING USING
MEASURED INNER WALL TEMPERATURE
for i=1:m
```

```
    %INPUT: HEAT FLUX IN kW/m^2
    q=input(:,1);

    %INPUT: BULK INLET TEMPERATURE IN °C
    Tin=input(:,2);

    %INPUT: MASS FLUX IN kg/m^2s
    G=input(:,3);

    %MEASURED OUTER WALL TEMPERATURE IN °C
    Twall_out=input(:,4);

    %ASME Code Cases : Nuclear Components. Case N-47-30, Section III, Division
    %1. 1992 ASME Boiler and Pressure Vessel Code.
    k_sus=13.00857+0.01687*Twall_out(i)-2.08333e-6*Twall_out(i)^2;

    %MEASURED INNER WALL TEMPERATURE BY SOLVING CONDUCTION EQUATION
    Twall_in=Twall_out-Di*q*1e3/(2*k_sus)*(Do^2/(Di^2-Do^2)*log(Di/Do)-1/2);

    %LOCAL BULK TEMPERATURE AT HEATER EXIT
    Tb2(i)=Tin(i)+pi*Di/G(i)/A/(cpf(Tin(i))*1e3)*q(i)*1e3*0.1;
    Ref(i)=G(i)*Di/muf(Tb2(i));
    Prf(i)=muf(Tb2(i))*cpf(Tb2(i))*1e3/kf(Tb2(i));
    Nuf(i)=muf(Tb2(i))*vf(Tb2(i));

    %DITTUS-BOELTER CORRELATION
    hFC2(i)=kf(Tb2(i))/Di*0.023*Ref(i)^0.8*Prf(i)^0.4;
    k_G(i)=kf(Tb2(i));

    %TO DEFINE AN EFFECTIVE h_NB FOR EXPERIMENTAL RESULTS
    heff(i)=q(i)*1e3/(Twall_in(i)-Tb2(i));

    %CALCULATION OF MINIMUM RADIUS FOR NUCLEATION
    r_min(i)=2*sigma(Tsat)*(Tsat+273.15)*(vg(Tsat)-vf(Tsat))/(hfg(Tsat)*1.e3*(Twall_in(i)-Tsat));
    if Twall_in(i) <= Tsat
       hNB_in(i)=0;
       ratio(i)=0;
    else
       hNB_in(i)=(q(i)*1e3-hFC2(i)*(Twall_in(i)-Tb2(i)))/(Twall_in(i)-Tsat);
       q_1pex(i)=0.001*hFC2(i)*(Twall_in(i)-Tb2(i));
       q_2pex(i)=0.001*hNB_in(i)*(Twall_in(i)-Tsat);
       ratio(i)=q_1pex(i)/q_2pex(i);
       q_check2(i)=q_1pex(i)+q_2pex(i);
    end

    %h_NB USING MEASURED INNER WALL TEMPERATURE in kW/m^2K
    hNB_meas=transpose(hNB_in)/1e3;
    ratio_ex(i)=ratio(i);
end
heff_exp=transpose(heff);
ratio_meas=transpose(ratio_ex);
q_checkmeas=transpose(q_check2);
q_1pmeas=transpose(q_1pex);
q_2pmeas=transpose(q_2pex);
Re=transpose(Ref);
```

```
Pr=transpose(Prf);
Nu=transpose(Nuf);
k=transpose(k_G);
rmin=transpose(r_min);

figure;
plot(q,Tw(:,10),q,Twall_in,q,Twall_out); hold on; grid on;
xlabel('Heat Flux, kW/m^2');
ylabel('Wall Temperature, ^oC');
figure;
plot(q,heff_pred(:,10),q,heff_exp); hold on; grid on;
xlabel('Heat Flux, kW/m^2');
ylabel('Nucleate boiling heat transfer coefficient, kW/m^2K');
figure;
plot(q,ratio_pred(:,10)); hold on; grid on;
xlabel('Heat Flux, kW/m^2');
ylabel('ratio_pred');
figure;
plot(q,ratio_meas); hold on; grid on;
xlabel('Heat Flux, kW/m^2');
ylabel('ratio_ex');
plot(q,rmin); hold on; grid on;
xlabel('Heat Flux, kW/m^2');
ylabel('r_m_i_n');

%PREDICTED INNER WALL TEMPERATURE USING CHEN CORRELATION
Twall=Tw(:,10);

%PRESSURE CORRESPONDING TO PREDICTED INNER WALL TEMPERATURE
Ps_wall=interp1(Tsat_table, Psat_table, real(Twall))*10^5;
disp('Wall Temperature:');
disp(num2str(Twall, '%3.3f'));
```

Appendix D. Numerical Routine of Klimenko's model in MATLAB

T_w prediction using Klimenko's correlation is rather simpler than Chen's prediction. As far as T_w prediction below T_{sat}, Dittus-Boelter's correlation is introduced. Beyond T_{sat}, the convective boiling number, N_{CB} in Eq. 2-18, should be estimated first to select a proper correlation among Eqs. 2-19 and 2-20. Beyond T_{sat} and $N_{CB}<1.2\times10^4$, Klimenko's forced convective nucleate boiling correlation, Eq. 2-19, is utilized. Eq. 2-19 contains only one variable of heat flux, which is the control variable in the experiment. Therefore h_{NB} can be calculated straightforwardly and thus T_w. Following routine shows the detailed process of the numerical script built in MATLAB.

```
clear all; close all; clc;

%THERMODYNAMIC OPERATING CONDITION
Psat=1.01e5; Tsat=100;

%TUBE HEATER OUTER DIAMETER IN m
Do=1/4*25.4*0.001;

%TUBE HEATER THICKNESS IN m
th=0.016*25.4*0.001;

%TUBE HEATER INNER DIAMETER IN m
Di=Do-2*th; L=0.1;

%FLOW CHANNEL HYDRAULIC AREA IN m
A=pi/4*Di^2;
pi=3.141592;

%GRAVITY
g=9.8;

%READ EXPERIMENTAL ATA AS INPUT FOR RUNNING SCRIPT
input=xlsread('test1.xls');
[m,n]=size(input);

%AXIAL NODE FOR HEATER
Z=0.01:0.01:0.1;

%SIZE OF THE AXIAL NODE
t=length(Z);
Tw = zeros(m, t);
```

```
Tb = zeros(m, t);
hFC = zeros(m, t);
Tb = zeros(m, t);
flag = zeros(m, t);

%SATURATION TEMPERATURE IN °C
Tsat_table=[0:10:370,374.15];
Psat_table=[0.006112,0.012271,0.023368,0.042418,0.073750,0.12335,0.19919,0.31161,0.47358,0.70109,1.01325,1.
4327,1.9854,2.7011,3.6136,4.7597,6.1804,7.9202,10.027,12.553,15.550,19.080,23.202,27.979,33.480,39.776,46.94
1,55.052,64.191,74.449,85.917,98.694,112.89,128.64,146.08,165.37,186.74,210.53,221.2];

for i=1:m
   disp(['m = ', num2str(i)]);

   %INPUT: HEAT FLUX IN kW/m^2
   q=input(:,1);

   %INPUT: BULK INLET TEMPERATURE IN °C
   Tin=input(:,2);

   %INPUT: MASS FLUX IN kg/m^2s
   G=input(:,3);

   %INLET ENTHALPY IN J/kg
   h_in=cpf(Tin(i))*1e3*Tin(i);

   %MEASURED OUTER WALL TEMPERATURE
   Twall_out=input(:,4);

   %ASME Code Cases : Nuclear Components. Case N-47-30, Section III, Division
   %1. 1992 ASME Boiler and Pressure Vessel Code.
   k_sus=13.00857+0.01687*Twall_out(i)-2.08333e-6*Twall_out(i)^2;
   for ii=1:t

      %LOCAL BULK TEMPERATURE
      Tb(i,ii)=Tin(i)+pi*Di/G(i)/A/(cpf(Tin(i))*1e3)*q(i)*1e3*Z(ii);

      %DITTUS-BOELTER CORRELATION
hFC(i,ii)=kf(Tb(i,ii))/Di*0.023*(G(i)*Di/muf(Tb(i,ii)))^0.8*(muf(Tb(i,ii))*cpf(Tb(i,ii))*1e3/kf(Tb(i,ii)))^0.4;
      %ESTIMATE OF WALL TEMPERATURE TO JUDGE WHETHER BOILING MIGHT OCCUR
      Twtemp(i,ii)=Tb(i,ii)+q(i)*1e3/hFC(i,ii);
      NCB(i,ii)=G(i)*hfg(Tsat)*1e3/(q(i)*1e3)*((1/vg(Tsat))/(1/vf(Tsat)))^(1/3);

      %LAPALCE CHARACTERISTIC LENGTH
      Lc=sqrt(sigma(Tsat)/g/(1/vf(Tsat)-1/vg(Tsat)));

      %LIQUID PRANDTL NUMBER AT SATURATION
      Prf=muf(Tsat)*cpf(Tsat)*1e3/kf(Tsat);
      if Twtemp(i,ii)<=Tsat

         %LOCAL WALL TEMPERATURE WHEN T_wall IS BELOW T_sat
         Tw(i,ii)=Twtemp(i,ii);
      else
         flag(i, ii) = 1;
         if NCB(i,ii)<1.2e4
```

```
        %MODIFIED PECLET NUMBER
        Pem(i,ii)=q(i)*1e3*Lc*(1/vf(Tsat))*(cpf(Tsat)*1e3)/(hfg(Tsat)*1e3/vg(Tsat)*kf(Tsat));

        %NUSSELT NUMBER AT FLORCED CONVECTIVE NUCLEATE BOILING
        Nu(i,ii)=4.9e-3*Pem(i,ii)^0.6*Prf^(-0.33)*(Psat*Lc/sigma(Tsat))^0.54*(k_sus/kf(Tsat))^0.12;
        h(i,ii)=Nu(i,ii)/Lc*kf(Tsat);
      else

        %MODIFIED REYNOLDS NUMBER IN BOILING CONDITION
        Rem(i,ii)=G(i)*Lc/muf(Tsat);

        %NUSSELT NUMBER AT FLORCED CONVECTIVE VAPORIZATION
        Nu(i,ii)=0.087*Rem(i,ii)^0.6*Prf^(1/6)*(1/vg(Tsat)*1/vf(Tsat))^0.2*(k_sus/kf(Tsat))^0.09;
        h(i,ii)=Nu(i,ii)/Lc*kf(Tsat);
      end
      Tw(i,ii)=Tsat+q(i)*1e3/h(i,ii);
    end
    Tw_pred(i,ii)=Tw(i,ii);
    heff_pred(i,ii)=q(i)*1e3/(Tw_pred(i,ii)-Tb(i,ii));
    disp(['Z = ', num2str(Z(ii),'%.2f'), ': Tw = ',num2str(Tw_pred(i,ii))]);
  end

  % INNER WALL TEMPERATURE
  for i=1:m

    %ASME Code Cases : Nuclear Components. Case N-47-30, Section III, Division
    %1. 1992 ASME Boiler and Pressure Vessel Code.
    k_sus=13.00857+0.01687*Twall_out(i)-2.08333e-6*Twall_out(i)^2;

    %MEASURED INNER WALL TEMPERATURE BY SOLVING CONDUCTION EQUATION
    Twall_in=Twall_out-Di*q*1e3/(2*k_sus)*(Do^2/(Di^2-Do^2)*log(Di/Do)-1/2);

    %PRESURE CORRESPONDING TO INNER WALL TEMPERATURE
    Ps_in=interp1(Tsat_table, Psat_table, Twall_in)*10^5;

    %TO DEFINE AN EFFECTIVE h_NB FOR EXPERIMENTAL RESULTS
    heff(i)=q(i)*1e3/(Twall_in(i)-Tb(i,10));
  end
  heff_exp=transpose(heff);
end
 figure;
plot(q,Tw_pred(:,10),q,Twall_in,q,Twall_out); hold on; grid on;
xlabel('Heat Flux, kW per m^2');
ylabel('Wall Temperature, ^oC');
figure;
plot(q,heff_pred(:,10)/1e3,q,heff_exp/1e3); hold on; grid on;
xlabel('Heat Flux, kW per m^2');
ylabel('heff, kW per m^2 K');

%PREDICTED INNER WALL TEMPERATURE USING CHEN CORRELATION
Twall=Tw(:,10);

%PRESSURE CORRESPONDING TO PREDICTED INNER WALL TEMPERATURE
Ps_wall=interp1(Tsat_table, Psat_table, real(Twall))*10^5;
disp('Wall Temperature:');
disp(num2str(Twall, '%3.3f'));
```

Appendix E. Measured and Predicted Wall Temperature

Table E-1 Test_W_12_G_1500_11_02_2007_NBHT

Experiment Heat flux, q" (kW/m^2)	Experiment $T_{w,o}$ (°C)	Experiment $T_{w,i}$ (°C)	Chen's prediction $T_{w,i}$ (°C)	Klimenko's prediction $T_{w,i}$ (°C)	Davis-Anderson's prediction $T_{w,ONB}$ (°C)	Experiment Mass flux, G (kg/m^2s)	Experiment $T_{b,in}$ (°C)	Experiment $T_{b,out}$ (°C)
1.662E+02	35.5	33.4	37.4	37.4	105.7	1504.6	11.1	13.0
3.000E+02	53.6	49.9	58.0	58.0	107.7	1504.6	11.5	14.9
4.772E+02	76.3	70.4	83.8	83.8	109.7	1503.1	11.9	17.3
7.036E+02	103.0	94.3	107.9	122.2	111.8	1505.3	12.3	20.2
9.799E+02	132.3	120.2	117.4	125.3	113.9	1509.8	12.8	23.8
1.294E+03	142.2	126.2	124.0	128.2	116.0	1517.4	13.4	28.0
1.647E+03	152.1	131.7	129.8	131.1	118.0	1521.6	14.0	32.6
2.024E+03	158.5	133.5	134.7	133.7	120.0	1523.1	14.7	37.5
2.450E+03	164.0	133.7	139.6	136.3	122.0	1524.8	15.3	43.0
2.916E+03	168.1	132.0	144.0	138.9	124.0	1530.1	16.1	48.9
3.015E+03	169.3	132.0	145.0	139.5	124.4	1536.2	16.8	50.8
3.115E+03	170.1	131.6	145.9	140.0	124.8	1534.2	17.1	52.3
3.215E+03	171.7	132.0	146.8	140.5	125.1	1532.7	17.4	53.7
3.318E+03	172.8	131.8	147.7	141.0	125.5	1539.0	17.5	55.0
3.422E+03	174.0	131.8	148.6	141.5	125.9	1541.8	17.7	56.4
3.520E+03	175.5	132.0	149.4	142.0	126.3	1543.2	17.9	57.7
3.619E+03	176.7	132.0	150.3	142.4	126.7	1543.6	18.1	59.1
3.727E+03	178.3	132.3	151.1	142.9	127.1	1546.9	18.3	60.4
3.832E+03	180.2	132.8	151.9	143.4	127.5	1551.6	18.5	61.7
3.939E+03	181.9	133.2	152.7	143.8	127.8	1553.6	18.6	63.0
4.050E+03	183.2	133.1	153.6	144.3	128.2	1553.8	19.6	65.2
4.171E+03	183.8	132.2	154.5	144.9	128.6	1557.8	20.0	66.9

Table E-2 Test _W_13_G_1500_11_07_2007_NBHT

Experiment	Experiment	Experiment	Chen's prediction	Klimenko's prediction	Davis-Anderson's prediction	Experiment	Experiment	Experiment
Heat flux, q" (kW/m^2)	$T_{w,o}$ (°C)	$T_{w,i}$ (°C)	$T_{w,i}$ (°C)	$T_{w,i}$ (°C)	$T_{w,ONB}$ (°C)	Mass flux, G (kg/m^2s)	$T_{b,in}$ (°C)	$T_{b,out}$ (°C)
1.868E+02	36.1	33.8	42.9	42.9	106.1	1500.9	14.5	16.4
3.391E+02	53.9	49.8	65.1	65.1	108.2	1501.1	14.6	18.1
5.277E+02	75.5	69.0	91.3	91.3	110.2	1504.1	15.0	20.6
7.566E+02	99.6	90.3	110.5	122.9	112.2	1508.0	15.4	23.5
1.034E+03	125.8	113.1	118.8	125.9	114.3	1512.1	15.7	26.9
1.355E+03	136.6	120.0	125.2	128.8	116.3	1518.1	16.2	30.9
1.703E+03	146.7	125.9	130.7	131.5	118.3	1521.7	16.7	35.4
2.096E+03	153.3	127.7	135.7	134.2	120.3	1520.8	17.2	40.4
2.526E+03	159.8	128.9	140.5	136.8	122.3	1522.3	17.8	45.8
2.992E+03	165.3	128.7	144.9	139.4	124.3	1528.2	18.4	51.6
3.085E+03	166.6	128.9	145.8	139.8	124.6	1529.9	19.0	53.3
3.189E+03	168.6	129.6	146.7	140.4	125.0	1531.3	19.2	54.7
3.246E+03	171.5	131.8	147.2	140.6	125.3	1531.7	19.3	55.5
3.353E+03	174.6	133.6	148.2	141.2	125.7	1532.9	19.4	56.8
3.442E+03	176.4	134.3	149.0	141.6	126.0	1530.9	19.5	58.0
3.542E+03	179.6	136.3	149.9	142.0	126.4	1528.7	19.6	59.3
3.645E+03	183.1	138.6	150.7	142.5	126.8	1531.7	19.7	60.6
3.749E+03	186.3	140.5	151.5	143.0	127.2	1533.0	19.8	61.9
3.860E+03	190.4	143.2	152.3	143.4	127.6	1533.5	20.0	63.2
3.970E+03	194.9	146.3	153.1	143.9	127.9	1535.8	20.1	64.6

Table E-3 Test _W_17_G_1500_11_13_2007_CHF

Experiment	Experiment	Experiment	Chen's prediction	Klimenko's prediction	Davis-Anderson's prediction	Experiment	Experiment	Experiment
Heat flux, q" (kW/m^2)	$T_{w,o}$ (°C)	$T_{w,i}$ (°C)	$T_{w,i}$ (°C)	$T_{w,i}$ (°C)	$T_{w,ONB}$ (°C)	Mass flux, G (kg/m^2s)	$T_{b,in}$ (°C)	$T_{b,out}$ (°C)
1.750E+02	35.9	33.7	40.5	40.5	105.9	1505.4	13.7	15.5
3.114E+02	52.0	48.1	60.8	60.8	107.8	1506.0	14.0	17.3
4.920E+02	72.0	66.0	86.0	86.0	109.8	1507.8	14.3	19.5

7.194E+02	96.8	87.9	108.8	122.5	111.9	1511.0	14.7	22.3
9.974E+02	123.3	111.0	117.9	125.5	114.0	1513.7	15.1	25.8
1.320E+03	133.7	117.4	124.5	128.5	116.1	1519.9	15.8	30.1
1.683E+03	144.2	123.5	130.4	131.4	118.2	1526.6	16.4	34.7
2.088E+03	151.2	125.5	135.5	134.1	120.3	1529.1	17.1	39.8
2.536E+03	157.1	125.8	140.6	136.9	122.3	1532.2	17.8	45.4
3.027E+03	163.6	126.3	145.2	139.6	124.4	1536.9	18.5	51.5
3.139E+03	165.0	126.3	146.3	140.1	124.9	1537.8	19.2	53.6
3.246E+03	165.9	125.9	147.2	140.7	125.3	1540.9	19.5	55.1
3.351E+03	166.0	124.7	148.2	141.2	125.7	1542.6	19.7	56.5
3.460E+03	167.3	124.7	149.1	141.7	126.1	1545.0	19.9	57.9
3.564E+03	168.4	124.5	150.0	142.2	126.5	1547.2	20.1	59.3
3.677E+03	170.0	124.7	150.9	142.7	126.9	1549.9	20.3	60.7
3.786E+03	171.2	124.6	151.7	143.2	127.3	1547.6	20.4	62.0
3.902E+03	172.8	124.7	152.6	143.7	127.7	1552.0	20.6	63.4
4.019E+03	174.5	124.9	153.5	144.2	128.1	1555.0	20.8	64.9
4.135E+03	175.8	124.8	154.4	144.7	128.5	1555.9	20.9	66.3
4.253E+03	177.2	124.8	155.3	145.2	128.9	1555.9	21.1	67.8
4.373E+03	178.8	124.9	156.2	145.7	129.3	1563.6	21.3	69.3
4.483E+03	180.5	125.2	157.0	146.2	129.7	1561.9	21.4	70.7
4.600E+03	182.2	125.4	157.9	146.7	130.1	1553.2	21.6	72.4
4.726E+03	183.8	125.6	158.8	147.2	130.5	1539.9	21.9	74.8
4.863E+03	186.4	126.4	159.9	147.7	130.9	1526.2	22.2	77.4

Table E-4 Test _W_14_G_2000_11_08_2007_NBHT

Experiment	Experiment	Experiment	Chen's prediction	Klimenko's prediction	Davis-Anderson's prediction	Experiment	Experiment	Experiment
Heat flux, q" (kW/m^2)	$T_{w,o}$ (°C)	$T_{w,i}$ (°C)	$T_{w,i}$ (°C)	$T_{w,i}$ (°C)	$T_{w,ONB}$ (°C)	Mass flux, G (kg/m^2s)	$T_{b,in}$ (°C)	$T_{b,out}$ (°C)
1.855E+02	33.0	30.7	36.9	36.9	106.0	1987.4	14.3	15.8
3.371E+02	46.1	41.9	54.8	54.8	108.1	1989.4	14.3	16.9
5.343E+02	63.1	56.5	77.2	77.2	110.3	1992.4	14.5	18.8
7.669E+02	83.6	74.2	102.1	123.1	112.3	1997.0	15.0	21.2
1.040E+03	107.2	94.4	114.3	126.0	114.3	2000.4	15.5	24.1

1.347E+03	129.0	112.4	121.8	128.7	116.3	2001.4	16.1	27.3
1.714E+03	142.6	121.5	128.2	131.6	118.4	2002.6	16.8	31.1
2.111E+03	151.9	125.8	133.7	134.3	120.4	2008.2	17.5	35.2
2.530E+03	158.4	127.2	138.7	136.8	122.3	2010.6	18.3	39.5
3.005E+03	164.0	126.9	143.4	139.4	124.3	2012.4	19.1	44.3
3.502E+03	170.0	126.8	148.0	141.9	126.2	2012.9	19.9	49.3
3.826E+03	174.2	127.0	150.7	143.4	127.4	2021.2	20.6	52.8
4.051E+03	177.0	127.1	152.5	144.4	128.2	2022.1	21.1	55.3
4.164E+03	178.5	127.2	153.4	144.9	128.6	2021.9	21.5	56.6
4.288E+03	179.9	127.1	154.3	145.4	129.0	2023.8	21.7	57.9
4.410E+03	181.4	127.1	155.2	145.9	129.5	2023.7	21.9	59.1
4.536E+03	183.3	127.4	156.2	146.4	129.9	2025.6	22.1	60.3
4.659E+03	185.0	127.6	157.1	146.9	130.3	2025.3	22.3	61.5
4.773E+03	186.3	127.5	157.9	147.3	130.6	2025.4	22.4	62.6

Table E-5 Test _W_16_G_2500_11_09_2007_CHF

Experiment	Experiment	Experiment	Chen's prediction	Klimenko's prediction	Davis-Anderson's prediction	Experiment	Experiment	Experiment
Heat flux, q" (kW/m^2)	$T_{w,o}$ (°C)	$T_{w,i}$ (°C)	$T_{w,i}$ (°C)	$T_{w,i}$ (°C)	$T_{w,ONB}$ (°C)	Mass flux, G (kg/m^2s)	$T_{b,in}$ (°C)	$T_{b,out}$ (°C)
1.882E+02	32.7	30.4	37.7	37.7	106.1	1980.7	14.8	16.2
3.420E+02	47.0	42.8	56.0	56.0	108.2	1982.1	15.3	17.9
5.329E+02	64.7	58.2	77.5	77.5	110.2	1986.5	15.6	19.9
7.637E+02	85.5	76.1	102.2	123.0	112.3	1991.8	16.1	22.3
1.043E+03	109.0	96.2	114.5	126.0	114.3	1992.8	16.7	25.2
1.360E+03	134.1	117.4	122.1	128.8	116.4	1994.0	17.2	28.6
1.726E+03	148.6	127.5	128.5	131.7	118.4	1997.1	17.9	32.4
2.126E+03	156.9	130.9	134.0	134.4	120.4	1998.5	18.5	36.5
2.561E+03	162.6	131.3	139.1	137.0	122.4	2001.6	19.2	40.8
3.035E+03	168.2	131.1	143.8	139.6	124.4	2004.1	19.9	45.6
3.519E+03	173.8	130.8	148.2	142.0	126.3	2008.7	20.6	50.5
3.828E+03	176.6	129.8	150.8	143.4	127.4	2012.8	21.3	53.7
4.050E+03	179.1	129.5	152.6	144.4	128.2	2013.7	21.8	56.1
4.161E+03	180.5	129.7	153.5	144.8	128.6	2015.3	22.1	57.4

4.278E+03	182.1	129.7	154.3	145.3	129.0	2015.0	22.3	58.6
4.386E+03	183.3	129.7	155.2	145.8	129.4	2016.5	22.5	59.7
4.511E+03	184.7	129.5	156.1	146.3	129.8	2016.8	22.7	60.9
4.640E+03	186.2	129.5	157.1	146.8	130.2	2017.2	23.0	62.3
4.759E+03	187.8	129.7	158.0	147.3	130.6	2018.7	23.3	63.6
4.877E+03	189.4	129.7	158.8	147.7	131.0	2021.2	23.5	64.9
5.006E+03	190.7	129.4	159.8	148.2	131.4	2022.8	23.8	66.3
5.135E+03	192.1	129.3	160.7	148.7	131.8	2020.5	24.0	67.7
5.265E+03	193.4	129.0	161.6	149.2	132.2	2008.7	24.3	69.3
5.401E+03	194.6	128.6	162.5	149.7	132.6	2006.2	24.4	70.7

Table E-6 Test _W_15_G_2500_11_08_2007_NBHT

Experiment	Experiment	Experiment	Chen's prediction	Klimenko's prediction	Davis-Anderson's prediction	Experiment	Experiment	Experiment
Heat flux, q" (kW/m^2)	$T_{w,o}$ (°C)	$T_{w,i}$ (°C)	$T_{w,i}$ (°C)	$T_{w,i}$ (°C)	$T_{w,ONB}$ (°C)	Mass flux, G (kg/m^2s)	$T_{b,in}$ (°C)	$T_{b,out}$ (°C)
1.838E+02	28.4	26.2	32.1	32.1	106.0	2487.2	13.1	14.2
3.287E+02	39.8	35.8	46.9	46.9	108.0	2488.0	13.4	15.4
5.254E+02	54.6	48.1	66.2	66.2	110.2	2493.9	13.8	17.1
7.564E+02	72.1	62.8	87.7	87.7	112.2	2500.1	14.3	19.2
1.026E+03	91.6	79.0	107.8	125.9	114.2	2510.3	14.9	21.6
1.349E+03	113.2	96.6	118.0	128.8	116.3	2516.0	15.7	24.5
1.711E+03	135.5	114.5	125.2	131.6	118.3	2519.0	16.5	27.8
2.104E+03	140.9	115.1	131.3	134.3	120.3	2519.3	17.3	31.3
2.555E+03	157.0	125.7	136.9	137.0	122.4	2523.2	18.1	35.1
3.036E+03	164.8	127.5	142.1	139.6	124.4	2512.9	18.9	39.3
3.548E+03	171.8	128.3	146.9	142.1	126.4	2520.8	19.8	43.6
3.889E+03	176.2	128.5	149.9	143.7	127.7	2526.9	20.5	46.7
4.122E+03	179.2	128.7	151.8	144.7	128.5	2526.1	21.1	48.9
4.237E+03	181.0	129.0	152.7	145.2	128.9	2521.8	21.4	50.0
4.356E+03	182.4	129.1	153.6	145.6	129.3	2524.1	21.6	51.0
4.444E+03	185.3	130.8	154.3	146.0	129.6	2518.9	21.9	51.9
4.558E+03	186.5	130.7	155.2	146.5	129.9	2518.3	21.9	52.7
4.673E+03	187.7	130.4	156.0	146.9	130.3	2522.1	22.1	53.6

4.787E+03	188.8	130.1	156.8	147.4	130.7	2533.0	22.3	54.4
4.910E+03	190.1	129.9	157.8	147.8	131.1	2534.7	22.5	55.4
5.035E+03	192.1	130.4	158.7	148.3	131.5	2536.4	22.7	56.4

Table E-7 Test _W_18_G_2500_11_15_2007

Experiment	Experiment	Experiment	Chen's prediction	Klimenko's prediction	Davis-Anderson's prediction	Experiment	Experiment	Experiment
Heat flux, q" (kW/m^2)	$T_{w,o}$ (°C)	$T_{w,i}$ (°C)	$T_{w,i}$ (°C)	$T_{w,i}$ (°C)	$T_{w,ONB}$ (°C)	Mass flux, G (kg/m^2s)	$T_{b,in}$ (°C)	$T_{b,out}$ (°C)
1.652E+02	28.3	26.3	29.7	29.7	105.7	2480.0	12.4	13.5
2.940E+02	39.3	35.8	42.8	42.8	107.6	2480.2	12.2	14.2
4.640E+02	52.6	47.0	59.9	59.9	109.6	2484.2	12.6	15.7
6.764E+02	69.6	61.4	80.4	80.4	111.5	2489.5	13.2	17.7
9.358E+02	89.5	78.2	103.3	125.0	113.6	2495.6	14.0	20.1
1.247E+03	110.8	95.8	115.5	127.9	115.7	2497.2	14.7	23.0
1.607E+03	134.0	114.7	123.4	130.8	117.8	2509.2	15.6	26.3
1.992E+03	139.3	115.3	129.8	133.6	119.8	2506.9	16.5	29.8
2.421E+03	156.7	127.6	135.3	136.2	121.8	2514.6	17.5	33.6
2.899E+03	172.2	137.3	140.7	138.8	123.9	2521.2	18.4	37.7
3.411E+03	183.5	142.4	145.6	141.4	125.9	2523.4	19.5	42.2
3.733E+03	189.2	144.3	148.6	142.9	127.1	2524.7	20.5	45.4
3.957E+03	193.5	145.9	150.5	143.9	127.9	2525.7	21.2	47.6
4.076E+03	195.8	146.7	151.5	144.4	128.3	2534.3	21.7	48.9
4.192E+03	197.6	147.1	152.4	144.9	128.7	2538.6	22.0	50.0
4.312E+03	198.3	146.4	153.3	145.4	129.1	2543.3	22.2	51.0
4.432E+03	199.8	146.5	154.2	145.9	129.5	2538.3	22.2	51.9
4.558E+03	199.0	144.1	155.2	146.4	129.9	2538.8	22.4	52.9
4.689E+03	200.3	143.8	156.1	146.9	130.4	2540.2	22.3	53.8
4.813E+03	208.0	150.1	157.0	147.4	130.8	2537.1	22.2	54.7
4.937E+03	208.9	149.5	157.9	147.8	131.2	2538.4	22.5	55.8
5.067E+03	209.8	148.8	158.9	148.3	131.6	2543.2	22.8	56.9
5.198E+03	210.6	148.0	159.8	148.8	132.0	2548.6	22.9	57.7

Table E-8 Test _AL_pt_001v_01_G_1500_05_24_2007

Experiment Heat flux, q" (kW/m^2)	Experiment $T_{w,o}$ (°C)	Experiment $T_{w,i}$ (°C)	Chen's prediction $T_{w,i}$ (°C)	Klimenko's prediction $T_{w,i}$ (°C)	Davis-Anderson's prediction $T_{w,ONB}$ (°C)	Experiment Mass flux, G (kg/m^2s)	Experiment $T_{b,in}$ (°C)	Experiment $T_{b,out}$ (°C)
1.600E+02	39.4	37.5	37.8	37.8	105.6	1483.0	12.7	14.5
2.843E+02	59.0	55.5	56.6	56.6	107.5	1482.7	12.5	15.8
4.526E+02	83.5	78.0	81.2	81.2	109.4	1484.2	12.8	18.0
6.660E+02	113.0	104.8	106.3	121.7	111.4	1487.8	13.2	21.0
9.302E+02	137.4	125.9	116.3	124.8	113.5	1489.9	13.8	24.6
1.234E+03	143.7	128.5	123.1	127.7	115.6	1494.3	14.5	28.7
1.578E+03	157.2	137.8	128.9	130.5	117.6	1501.9	15.2	33.4
1.956E+03	166.9	142.9	134.0	133.2	119.6	1506.1	16.1	38.5
2.376E+03	169.9	140.6	138.9	135.9	121.6	1510.7	17.0	44.1
2.838E+03	174.5	139.6	143.5	138.5	123.6	1513.4	17.9	50.3
3.409E+03	178.8	136.9	148.7	141.4	125.9	1527.6	19.1	57.6
3.587E+03	176.1	132.0	150.3	142.3	126.6	1530.8	20.4	60.8
3.717E+03	179.7	134.0	151.3	142.9	127.0	1527.7	21.2	63.2
3.847E+03	184.2	136.9	152.4	143.4	127.5	1531.4	21.7	65.1
3.983E+03	188.3	139.3	153.4	144.0	128.0	1530.3	22.1	67.1
4.106E+03	193.3	142.8	154.4	144.5	128.4	1529.0	22.5	68.9
4.236E+03	196.8	144.7	155.4	145.1	128.9	1532.2	22.9	70.6
4.354E+03	189.6	136.0	156.3	145.6	129.3	1534.9	23.3	72.3
4.459E+03	184.0	129.2	157.1	146.1	129.6	1536.6	23.7	73.8
4.518E+03	185.6	130.0	157.6	146.3	129.8	1541.2	24.0	74.6
4.578E+03	187.2	130.9	158.0	146.5	130.0	1536.1	24.2	75.7
4.636E+03	187.5	130.4	158.5	146.8	130.2	1536.0	24.5	76.6
4.695E+03	187.6	129.9	159.0	147.0	130.4	1536.8	24.7	77.5
4.748E+03	188.6	130.2	159.3	147.2	130.6	1536.0	24.7	78.1

Table E-9 Test _AL_pt_001v_02_G_1500_05_25_2007

Experiment	Experiment	Experiment	Chen's prediction	Klimenko's prediction	Davis-Anderson's prediction	Experiment	Experiment	Experiment
Heat flux, q" (kW/m^2)	$T_{w,o}$ (°C)	$T_{w,i}$ (°C)	$T_{w,i}$ (°C)	$T_{w,i}$ (°C)	$T_{w,ONB}$ (°C)	Mass flux, G (kg/m^2s)	$T_{b,in}$ (°C)	$T_{b,out}$ (°C)
1.598E+02	39.1	37.2	37.7	37.7	105.6	1473.4	12.3	14.1
2.867E+02	58.6	55.1	57.1	57.1	107.5	1475.0	12.5	15.8
4.553E+02	83.5	77.9	81.8	81.8	109.5	1476.5	12.8	18.1
6.689E+02	108.7	100.5	106.6	121.8	111.5	1479.0	13.2	21.0
9.254E+02	130.6	119.2	116.2	124.7	113.5	1481.2	13.7	24.5
1.222E+03	146.4	131.4	122.9	127.6	115.5	1486.2	14.2	28.4
1.564E+03	150.8	131.6	128.7	130.4	117.5	1492.9	14.9	33.0
1.938E+03	156.9	133.1	133.8	133.1	119.5	1494.2	15.6	38.0
2.350E+03	163.2	134.3	138.6	135.7	121.5	1494.5	16.2	43.4
2.820E+03	166.9	132.3	143.3	138.4	123.6	1500.2	17.0	49.5
3.341E+03	175.8	134.8	148.0	141.1	125.6	1510.3	17.9	56.2
3.582E+03	182.2	138.2	150.1	142.2	126.5	1517.7	18.9	59.6
3.823E+03	183.2	136.3	152.0	143.3	127.4	1525.0	19.5	62.8
4.074E+03	188.2	138.2	153.9	144.4	128.3	1529.9	20.0	66.0
4.208E+03	192.5	140.9	154.9	145.0	128.8	1531.3	20.5	67.9
4.338E+03	192.5	139.3	155.9	145.5	129.2	1532.4	20.8	69.6
4.480E+03	190.7	135.7	157.0	146.1	129.7	1536.7	20.9	71.3

Table E-10 Test _AL_pt_001v_05_G_2000_11_20_2007

Experiment	Experiment	Experiment	Chen's prediction	Klimenko's prediction	Davis-Anderson's prediction	Experiment	Experiment	Experiment
Heat flux, q" (kW/m^2)	$T_{w,o}$ (°C)	$T_{w,i}$ (°C)	$T_{w,i}$ (°C)	$T_{w,i}$ (°C)	$T_{w,ONB}$ (°C)	Mass flux, G (kg/m^2s)	$T_{b,in}$ (°C)	$T_{b,out}$ (°C)
1.778E+02	33.4	31.3	36.0	36.0	105.9	1992.8	14.4	15.8
3.160E+02	47.2	43.3	52.6	52.6	107.9	1994.9	14.8	17.3
4.983E+02	64.6	58.6	73.3	73.3	109.9	1996.9	15.2	19.2
7.281E+02	85.6	76.8	98.5	98.5	112.0	1999.2	15.6	21.6
1.008E+03	109.6	97.4	113.3	125.6	114.1	2000.9	16.1	24.4

1.313E+03	136.0	120.2	121.1	128.4	116.1	2002.8	16.6	27.5
1.672E+03	151.0	130.8	127.5	131.2	118.1	2005.9	17.2	31.2
2.072E+03	161.7	136.7	133.2	134.0	120.2	2008.3	17.9	35.2
2.514E+03	168.7	138.4	138.5	136.7	122.2	2013.2	18.6	39.6
3.000E+03	175.4	139.2	143.4	139.4	124.3	2016.2	19.3	44.3
3.495E+03	180.9	138.7	147.9	141.8	126.2	2019.8	20.0	49.3
3.857E+03	183.8	137.2	151.0	143.5	127.5	2021.2	20.7	53.1
4.092E+03	186.8	137.4	152.8	144.5	128.4	2020.5	21.3	55.7
4.205E+03	188.7	137.9	153.7	145.0	128.8	2021.1	21.6	57.1
4.326E+03	191.5	139.2	154.6	145.5	129.2	2022.9	21.8	58.3
4.445E+03	194.7	141.0	155.5	145.9	129.6	2023.3	22.0	59.4
4.566E+03	196.0	140.8	156.4	146.4	130.0	2024.4	22.2	60.6
4.680E+03	198.7	142.1	157.3	146.9	130.3	2025.6	22.4	61.7
4.803E+03	200.5	142.5	158.2	147.4	130.7	2026.5	22.6	62.9
4.928E+03	201.4	141.8	159.1	147.8	131.1	2028.5	22.8	64.1
5.056E+03	201.5	140.4	160.0	148.3	131.5	2029.8	22.9	65.4
5.184E+03	201.1	138.5	160.8	148.8	131.9	2030.6	23.1	66.6
5.314E+03	201.4	137.2	161.7	149.3	132.3	2030.6	23.3	67.9
5.446E+03	202.1	136.3	162.6	149.8	132.7	2032.0	23.5	69.2
5.571E+03	202.9	135.5	163.4	150.2	133.1	2029.9	23.7	70.4
5.707E+03	204.1	135.2	164.3	150.7	133.5	2027.1	23.9	71.9
5.840E+03	204.9	134.3	165.1	151.2	133.9	2027.6	24.1	73.2
5.977E+03	205.7	133.5	166.0	151.7	134.3	2026.0	24.3	74.6
6.113E+03	206.6	132.7	166.9	152.1	134.7	2022.6	24.4	75.5

Table E-11 Test _AL_pt_001v_06_G_2000_11_21_2007

Experiment	Experiment	Experiment	Chen's prediction	Klimenko's prediction	Davis-Anderson's prediction	Experiment	Experiment	Experiment
Heat flux, q" (kW/m^2)	$T_{w,o}$ (°C)	$T_{w,i}$ (°C)	$T_{w,i}$ (°C)	$T_{w,i}$ (°C)	$T_{w,ONB}$ (°C)	Mass flux, G (kg/m^2s)	$T_{b,in}$ (°C)	$T_{b,out}$ (°C)
1.585E+02	29.5	27.6	31.7	31.7	105.6	1986.0	11.7	13.0
2.818E+02	42.7	39.3	46.9	46.9	107.4	1987.4	11.9	14.2
4.449E+02	59.6	54.2	66.5	66.5	109.4	1988.6	12.3	15.9
6.502E+02	80.0	72.1	89.8	89.8	111.3	1991.1	12.8	18.1

9.000E+02	102.8	91.9	109.5	124.5	113.3	1993.8	13.3	20.7
1.198E+03	129.9	115.4	118.5	127.4	115.4	1997.4	13.9	23.8
1.544E+03	155.4	136.7	125.4	130.2	117.4	1999.8	14.7	27.5
1.915E+03	170.5	147.2	131.1	132.9	119.4	2001.7	15.5	31.5
2.324E+03	164.7	136.5	136.2	135.6	121.4	2006.1	16.3	35.7
2.767E+03	168.0	134.4	141.0	138.1	123.3	2011.0	17.1	40.2
3.245E+03	174.1	134.7	145.5	140.6	125.3	2013.7	17.9	45.0
3.556E+03	178.2	135.1	148.3	142.1	126.4	2016.3	18.6	48.4
3.772E+03	181.4	135.6	150.2	143.1	127.2	2020.8	19.1	50.8
3.886E+03	183.6	136.4	151.1	143.6	127.6	2024.9	19.5	52.1
4.001E+03	185.5	136.9	152.0	144.1	128.1	2023.9	19.7	53.3
4.119E+03	187.5	137.5	152.9	144.6	128.5	2025.6	19.9	54.5
4.236E+03	189.5	138.1	153.8	145.1	128.9	2024.9	20.1	55.7
4.354E+03	190.6	137.8	154.6	145.6	129.3	2025.5	20.3	56.8
4.478E+03	191.7	137.4	155.6	146.1	129.7	2025.8	20.5	58.1
4.587E+03	193.0	137.4	156.4	146.5	130.0	2025.1	20.6	59.2
4.716E+03	195.4	138.2	157.3	147.0	130.5	2025.7	20.8	60.5
4.834E+03	197.3	138.7	158.2	147.5	130.8	2025.8	21.0	61.7
4.969E+03	198.5	138.2	159.2	148.0	131.3	2027.1	21.2	63.0
5.102E+03	198.0	136.1	160.1	148.5	131.7	2028.6	21.5	64.4
5.236E+03	197.8	134.3	161.0	149.0	132.1	2018.0	21.7	65.9
5.368E+03	197.7	132.6	161.9	149.5	132.5	2014.1	21.9	67.3
5.504E+03	198.1	131.3	162.8	150.0	132.9	2015.5	22.0	68.7
5.640E+03	198.8	130.4	163.6	150.5	133.3	2015.0	22.1	69.9
5.781E+03	199.8	129.7	164.5	151.0	133.7	2014.9	22.2	71.3
5.915E+03	200.7	128.9	165.4	151.5	134.1	2012.7	22.4	72.6
6.057E+03	201.8	128.3	166.3	152.0	134.5	2013.1	22.5	74.0
6.195E+03	202.4	127.2	167.2	152.4	134.9	2007.2	22.6	75.1

Table E-12 Test _AL_pt_001v_03_G_2500_11_16_2007

Experiment	Experiment	Experiment	Chen's prediction	Klimenko's prediction	Davis-Anderson's prediction	Experiment	Experiment	Experiment
Heat flux, q" (kW/m^2)	$T_{w,o}$ (°C)	$T_{w,i}$ (°C)	$T_{w,i}$ (°C)	$T_{w,i}$ (°C)	$T_{w,ONB}$ (°C)	Mass flux, G (kg/m^2s)	$T_{b,in}$ (°C)	$T_{b,out}$ (°C)
1.679E+02	29.2	27.2	31.3	31.3	105.7	2492.3	14.1	15.1
2.975E+02	40.3	36.7	44.6	44.6	107.7	2494.3	14.6	16.5
4.676E+02	54.2	48.6	61.1	61.1	109.6	2500.1	15.1	18.1
6.789E+02	70.8	62.7	80.9	80.9	111.6	2504.5	15.7	20.0
9.345E+02	89.8	78.6	103.3	125.0	113.6	2507.9	16.3	22.3
1.239E+03	110.7	95.8	115.2	127.9	115.6	2508.0	16.9	24.9
1.590E+03	132.5	113.3	123.1	130.7	117.7	2513.7	17.5	27.8
1.973E+03	134.3	110.5	129.5	133.5	119.7	2517.4	18.2	31.1
2.389E+03	140.7	111.9	135.0	136.1	121.7	2520.0	19.0	34.6
2.860E+03	158.7	124.2	140.5	138.7	123.7	2523.1	19.8	38.5
3.385E+03	171.0	130.1	145.5	141.3	125.8	2528.9	20.7	42.9
3.712E+03	176.4	131.6	148.5	142.8	127.0	2536.0	21.5	45.8
3.941E+03	178.9	131.3	150.5	143.9	127.8	2543.4	22.1	47.9
4.060E+03	180.3	131.3	151.4	144.4	128.3	2548.2	22.5	49.1
4.182E+03	182.0	131.6	152.4	144.9	128.7	2539.3	22.8	50.3
4.302E+03	183.3	131.4	153.4	145.4	129.1	2528.3	23.0	51.4
4.422E+03	185.4	132.1	154.3	145.9	129.5	2528.1	23.3	52.5
4.550E+03	187.0	132.1	155.3	146.4	129.9	2530.3	23.5	53.6
4.676E+03	188.8	132.4	156.2	146.9	130.3	2532.7	23.7	54.6
4.804E+03	190.5	132.5	157.2	147.4	130.7	2533.6	24.0	55.7
4.929E+03	192.0	132.6	158.1	147.9	131.1	2535.8	24.1	56.7
5.061E+03	194.0	132.9	159.1	148.4	131.6	2537.4	24.3	57.7
5.189E+03	196.5	133.9	160.0	148.9	132.0	2537.6	24.4	58.8
5.322E+03	198.8	134.7	160.9	149.4	132.4	2538.5	24.6	59.8
5.454E+03	200.8	135.0	161.8	149.8	132.8	2524.5	24.8	61.1
5.601E+03	202.0	134.5	162.8	150.4	133.2	2518.0	25.0	62.4
5.744E+03	202.7	133.4	163.7	150.9	133.6	2519.8	25.3	63.6
5.884E+03	203.3	132.3	164.6	151.4	134.0	2524.4	25.6	64.8
6.027E+03	203.7	131.1	165.6	151.8	134.4	2526.4	25.9	66.1
6.172E+03	204.4	129.9	166.5	152.3	134.8	2527.5	26.2	67.3

6.329E+03	205.2	128.9	167.6	152.9	135.3	2515.0	26.4	68.8
6.477E+03	205.4	127.3	168.6	153.3	135.7	2498.2	26.7	70.3
6.633E+03	206.1	126.1	169.5	153.9	136.1	2496.4	26.8	71.6
6.785E+03	207.1	125.3	170.5	154.3	136.5	2497.0	27.0	72.9
6.931E+03	208.8	125.2	171.3	154.8	136.9	2495.7	27.1	74.0

Table E-13 Test _AL_pt_001v_04_G_2500_11_17_2007

Experiment	Experiment	Experiment	Chen's prediction	Klimenko's prediction	Davis-Anderson's prediction	Experiment	Experiment	Experiment
Heat flux, q" (kW/m^2)	$T_{w,o}$ (°C)	$T_{w,i}$ (°C)	$T_{w,i}$ (°C)	$T_{w,i}$ (°C)	$T_{w,ONB}$ (°C)	Mass flux, G (kg/m^2s)	$T_{b,in}$ (°C)	$T_{b,out}$ (°C)
1.576E+02	30.9	29.0	32.0	32.0	105.6	2458.6	16.0	17.2
2.800E+02	38.9	35.6	42.5	42.5	107.4	2478.1	13.9	15.8
4.412E+02	51.4	46.1	58.0	58.0	109.3	2497.0	13.6	16.5
6.434E+02	67.3	59.6	77.2	77.2	111.3	2501.1	13.9	18.1
8.888E+02	85.9	75.2	99.6	99.6	113.2	2504.5	14.4	20.2
1.179E+03	106.8	92.6	113.4	127.3	115.2	2508.2	15.0	22.7
1.519E+03	129.6	111.4	121.7	130.1	117.3	2513.0	15.7	25.6
1.903E+03	144.0	121.1	128.3	132.9	119.3	2517.0	16.4	29.0
2.320E+03	151.7	123.9	134.1	135.6	121.4	2520.6	17.3	32.6
2.766E+03	164.3	131.1	139.3	138.1	123.3	2524.2	18.1	36.4
3.270E+03	176.3	137.1	144.3	140.7	125.4	2530.1	18.9	40.6
3.593E+03	180.6	137.5	147.2	142.3	126.6	2534.2	19.7	43.5
3.813E+03	183.2	137.5	149.2	143.3	127.4	2536.9	20.3	45.6
4.039E+03	186.7	138.2	151.1	144.3	128.2	2538.3	20.6	47.5
4.270E+03	190.4	139.2	152.9	145.2	129.0	2539.7	21.0	49.4
4.501E+03	194.1	140.1	154.6	146.2	129.8	2540.6	21.3	51.3
4.631E+03	193.5	137.9	155.6	146.7	130.2	2542.8	21.7	52.6
4.755E+03	194.8	137.8	156.5	147.2	130.6	2543.0	21.9	53.6
4.889E+03	197.2	138.6	157.5	147.7	131.0	2546.5	22.1	54.8
5.009E+03	199.0	138.9	158.4	148.2	131.4	2548.9	22.3	55.8
5.150E+03	200.5	138.7	159.5	148.7	131.8	2548.7	22.6	57.0
5.262E+03	202.7	139.5	160.3	149.1	132.2	2536.8	22.7	58.1
5.392E+03	205.5	140.8	161.1	149.6	132.6	2538.4	22.9	59.1

5.544E+03	207.1	140.6	162.1	150.1	133.0	2540.5	23.0	60.2
5.691E+03	208.1	139.8	163.1	150.6	133.5	2543.4	23.3	61.4
5.846E+03	208.2	138.1	164.1	151.2	133.9	2522.0	23.5	63.0
5.971E+03	208.4	136.7	164.9	151.6	134.3	2500.0	23.7	64.4
6.119E+03	209.0	135.6	165.9	152.1	134.7	2496.3	23.9	65.6
6.271E+03	210.0	134.7	166.9	152.6	135.1	2497.8	24.1	66.9
6.426E+03	211.2	134.1	167.9	153.1	135.6	2495.4	24.3	68.2
6.573E+03	212.4	133.5	168.8	153.6	136.0	2494.4	24.5	69.5
6.723E+03	213.8	133.2	169.8	154.1	136.4	2496.1	24.7	70.7

Table E-14 Test _AL_pt_01v_01_G_1500_06_01_2007

Experiment	Experiment	Experiment	Chen's prediction	Klimenko's prediction	Davis-Anderson's prediction	Experiment	Experiment	Experiment
Heat flux, q" (kW/m^2)	$T_{w,o}$ (°C)	$T_{w,i}$ (°C)	$T_{w,i}$ (°C)	$T_{w,i}$ (°C)	$T_{w,ONB}$ (°C)	Mass flux, G (kg/m^2s)	$T_{b,in}$ (°C)	$T_{b,out}$ (°C)
1.507E+02	37.5	35.6	36.4	36.4	105.4	1487.9	12.7	14.4
2.751E+02	55.9	52.5	55.4	55.4	107.4	1490.0	13.1	16.3
4.386E+02	79.5	74.1	79.1	79.1	109.3	1492.4	13.5	18.6
6.458E+02	108.1	100.2	104.9	121.5	111.3	1495.0	14.0	21.4
9.031E+02	121.9	110.9	115.4	124.5	113.3	1497.5	14.5	24.9
1.197E+03	132.6	118.1	122.4	127.4	115.3	1501.4	15.1	28.9
1.535E+03	144.1	125.5	128.2	130.2	117.4	1508.0	15.8	33.4
1.913E+03	153.4	130.1	133.4	133.0	119.4	1515.3	16.5	38.3
2.319E+03	162.4	134.2	138.3	135.6	121.4	1515.4	17.2	43.7
2.420E+03	166.3	136.8	139.4	136.2	121.8	1518.5	18.0	45.5
2.518E+03	168.9	138.3	140.5	136.7	122.3	1520.3	18.4	47.0
2.609E+03	171.6	139.8	141.4	137.2	122.7	1519.6	18.6	48.3
2.703E+03	174.2	141.3	142.3	137.8	123.1	1519.3	18.9	49.6
2.802E+03	176.6	142.4	143.2	138.3	123.5	1521.2	19.1	50.9
2.899E+03	179.6	144.3	144.1	138.8	123.9	1520.5	19.1	52.0
2.998E+03	182.8	146.3	145.0	139.3	124.3	1521.7	19.0	53.1
3.099E+03	184.0	146.2	145.9	139.8	124.7	1521.3	19.0	54.2
3.199E+03	185.1	146.1	146.8	140.3	125.1	1521.3	18.9	55.2
3.307E+03	186.4	146.1	147.8	140.9	125.5	1524.5	19.0	56.5

3.419E+03	188.5	146.9	148.7	141.4	125.9	1527.4	19.1	57.8
3.532E+03	191.4	148.4	149.7	141.9	126.4	1531.0	19.3	59.1
3.644E+03	195.5	151.1	150.6	142.4	126.8	1533.5	19.4	60.5
3.754E+03	199.0	153.3	151.5	142.9	127.2	1534.0	19.6	61.9
3.873E+03	203.8	156.6	152.4	143.4	127.6	1537.2	19.8	63.3
3.996E+03	205.8	157.2	153.3	144.0	128.0	1539.9	20.0	64.8
4.117E+03	206.4	156.3	154.2	144.5	128.5	1541.9	20.2	66.4
4.236E+03	203.9	152.4	155.1	145.0	128.9	1543.4	20.5	67.9
4.369E+03	194.7	141.5	156.1	145.6	129.3	1547.2	20.7	69.4
4.467E+03	192.8	138.4	156.8	146.1	129.6	1546.1	20.9	70.8
4.542E+03	192.9	137.5	157.4	146.4	129.9	1547.5	21.1	71.8
4.622E+03	192.9	136.6	158.0	146.7	130.2	1548.6	21.3	72.8
4.702E+03	193.2	135.9	158.6	147.0	130.4	1550.9	21.4	73.8
4.808E+03	195.1	136.6	159.3	147.4	130.8	1555.2	21.5	74.9
4.886E+03	198.0	138.5	159.9	147.7	131.0	1553.3	21.7	76.0
4.985E+03	198.8	138.0	160.6	148.1	131.3	1555.7	21.8	77.2

Table E-15 Test _AL_pt_01v_02_G_1500_06_05_2007

Experiment Heat flux, q" (kW/m^2)	Experiment $T_{w,o}$ (°C)	Experiment $T_{w,i}$ (°C)	Chen's prediction $T_{w,i}$ (°C)	Klimenko's prediction $T_{w,i}$ (°C)	Davis-Anderson's prediction $T_{w,ONB}$ (°C)	Experiment Mass flux, G (kg/m^2s)	Experiment $T_{b,in}$ (°C)	Experiment $T_{b,out}$ (°C)
1.642E+02	37.9	35.9	37.5	37.5	105.7	1476.1	11.1	13.1
2.987E+02	58.1	54.4	58.5	58.5	107.7	1477.7	11.8	15.3
4.762E+02	83.9	78.2	84.6	84.6	109.7	1480.3	12.2	17.8
6.995E+02	119.4	110.9	108.1	122.1	111.7	1483.5	12.7	20.8
9.711E+02	153.3	141.5	117.4	125.1	113.8	1485.1	13.2	24.5
1.292E+03	163.4	147.7	124.2	128.1	115.9	1489.8	13.8	28.7
1.649E+03	170.3	150.3	130.0	131.0	118.0	1493.8	14.4	33.5
2.019E+03	174.6	150.1	134.8	133.6	119.9	1494.9	15.1	38.4
2.451E+03	182.3	152.6	139.7	136.3	122.0	1496.5	15.7	44.0
2.564E+03	179.1	147.9	140.9	136.9	122.5	1499.9	16.4	45.9
2.667E+03	179.1	146.7	141.9	137.5	122.9	1501.8	16.7	47.4
2.764E+03	182.2	148.7	142.8	138.1	123.3	1501.9	17.0	48.8

2.869E+03	185.9	151.0	143.8	138.6	123.8	1504.3	17.2	50.1
2.972E+03	188.9	152.8	144.7	139.1	124.2	1505.5	17.5	51.6
3.077E+03	191.3	153.9	145.7	139.7	124.6	1506.3	17.9	53.2
3.188E+03	194.3	155.6	146.7	140.2	125.0	1509.1	17.9	54.4
3.293E+03	195.2	155.2	147.6	140.8	125.5	1511.2	18.0	55.7
3.405E+03	194.5	153.2	148.6	141.3	125.9	1515.6	18.2	57.0
3.516E+03	197.3	154.6	149.6	141.8	126.3	1517.6	18.5	58.5
3.635E+03	198.8	154.6	150.5	142.4	126.7	1522.5	19.0	60.3
3.748E+03	198.3	152.7	151.4	142.9	127.2	1524.1	19.5	62.0
3.865E+03	207.5	160.5	152.4	143.4	127.6	1525.9	19.9	63.7
3.981E+03	197.9	149.6	153.3	144.0	128.0	1527.8	20.3	65.3
4.106E+03	195.4	145.5	154.2	144.5	128.4	1531.3	20.6	67.0
4.230E+03	194.2	142.9	155.2	145.0	128.8	1532.3	21.0	68.6
4.359E+03	193.5	140.6	156.1	145.6	129.3	1534.8	21.2	70.3
4.470E+03	192.6	138.3	157.0	146.1	129.7	1535.5	21.5	71.8
4.594E+03	190.6	134.8	157.9	146.6	130.1	1535.9	21.7	73.3
4.677E+03	192.3	135.5	158.5	146.9	130.3	1536.3	21.9	74.5
4.772E+03	192.1	134.1	159.2	147.3	130.6	1537.2	22.0	75.6
4.842E+03	196.1	137.3	159.7	147.5	130.9	1540.7	22.1	76.4
4.901E+03	197.1	137.6	160.1	147.8	131.1	1541.4	22.2	77.1
4.962E+03	198.5	138.2	160.5	148.0	131.2	1541.2	22.2	77.8
5.026E+03	199.5	138.4	160.9	148.2	131.4	1541.1	22.2	78.6
5.049E+03	201.3	140.0	161.1	148.3	131.5	1539.7	22.3	78.9

Table E-16 Test _AL_pt_01v_03_G_2000_06_11_2007

Experiment	Experiment	Experiment	Chen's prediction	Klimenko's prediction	Davis-Anderson's prediction	Experiment	Experiment	Experiment
Heat flux, q" (kW/m^2)	$T_{w,o}$ (°C)	$T_{w,i}$ (°C)	$T_{w,i}$ (°C)	$T_{w,i}$ (°C)	$T_{w,ONB}$ (°C)	Mass flux, G (kg/m^2s)	$T_{b,in}$ (°C)	$T_{b,out}$ (°C)
1.506E+02	32.3	30.5	32.0	32.0	105.4	1986.4	13.3	14.6
2.803E+02	47.1	43.7	48.4	48.4	107.4	1993.2	14.8	17.3
4.525E+02	65.6	60.1	68.7	68.7	109.4	1983.8	16.0	19.9
6.712E+02	87.1	79.0	93.3	93.3	111.5	1978.8	16.9	22.8
9.342E+02	110.5	99.1	111.2	124.9	113.6	1982.7	17.7	25.8

1.240E+03	133.9	118.8	119.7	127.8	115.6	1987.0	18.6	29.4
1.587E+03	145.8	126.5	126.4	130.6	117.7	1996.4	20.4	34.2
1.967E+03	154.8	130.8	132.2	133.3	119.7	2002.6	22.5	39.4
2.390E+03	162.7	133.6	137.6	136.0	121.7	2003.2	24.4	45.0
2.847E+03	168.9	134.3	142.7	138.6	123.7	1998.8	26.7	51.3
3.364E+03	174.9	134.0	147.7	141.2	125.7	1999.6	28.6	57.6
3.491E+03	177.6	135.2	149.1	141.8	126.2	2001.0	30.3	60.4
3.611E+03	180.6	136.7	150.3	142.4	126.7	1991.5	31.4	62.7
3.730E+03	183.5	138.1	151.2	142.9	127.1	1992.3	31.4	63.8
3.843E+03	186.2	139.4	152.1	143.4	127.5	1988.4	31.0	64.4
3.952E+03	189.0	140.9	152.9	143.9	127.9	1988.4	30.9	65.2
4.074E+03	191.1	141.5	153.9	144.4	128.3	1990.7	31.0	66.4
4.192E+03	193.6	142.6	154.8	144.9	128.7	1990.7	31.2	67.5
4.309E+03	195.5	143.0	155.7	145.4	129.1	1990.1	31.1	68.5
4.435E+03	195.8	141.9	156.7	145.9	129.5	1989.3	31.0	69.5
4.553E+03	194.3	138.9	157.5	146.4	129.9	1987.9	31.1	70.6
4.674E+03	194.0	137.2	158.3	146.9	130.3	2001.1	30.4	70.8
4.795E+03	197.5	139.2	159.2	147.3	130.7	2013.3	30.6	71.7
4.929E+03	194.5	134.6	160.2	147.9	131.1	2011.7	30.7	73.0
5.067E+03	193.7	132.1	160.7	148.4	131.6	1998.6	27.5	71.3
5.177E+03	194.3	131.3	161.1	148.8	131.9	1998.1	25.1	69.9
5.300E+03	195.1	130.6	161.9	149.3	132.3	2013.9	25.0	70.4
5.443E+03	195.3	129.1	162.8	149.8	132.7	2013.8	25.1	71.8
5.582E+03	195.9	128.1	163.7	150.3	133.1	2012.8	25.2	73.1
5.716E+03	196.2	126.7	164.6	150.8	133.5	2011.3	25.5	74.6
5.840E+03	198.1	127.1	165.4	151.2	133.9	2006.3	25.7	76.0
5.938E+03	200.2	128.0	166.0	151.6	134.2	1999.3	25.6	76.9

Table E-17 Test _AL_pt_01v_05_G_2000_06_13_2007

Experiment	Experiment	Experiment	Chen's prediction	Klimenko's prediction	Davis-Anderson's prediction	Experiment	Experiment	Experiment
Heat flux, q" (kW/m^2)	$T_{w,o}$ (°C)	$T_{w,i}$ (°C)	$T_{w,i}$ (°C)	$T_{w,i}$ (°C)	$T_{w,ONB}$ (°C)	Mass flux, G (kg/m^2s)	$T_{b,in}$ (°C)	$T_{b,out}$ (°C)
1.570E+02	30.5	28.6	30.9	30.9	105.6	1983.5	10.9	12.2

2.782E+02	45.2	41.8	46.1	46.1	107.4	1984.8	11.2	13.6
4.420E+02	63.8	58.5	65.9	65.9	109.3	1986.8	11.5	15.4
6.240E+02	85.5	77.9	86.8	86.8	111.1	1988.9	12.0	17.7
9.023E+02	112.3	101.3	109.5	124.5	113.3	1992.5	12.6	20.4
1.207E+03	144.1	129.4	118.7	127.4	115.4	1995.5	13.2	23.7
1.558E+03	160.3	141.3	125.6	130.3	117.5	1997.2	13.9	27.4
1.946E+03	175.0	151.4	131.5	133.1	119.6	1999.4	14.6	31.4
2.377E+03	173.0	144.1	136.8	135.9	121.6	2002.3	15.4	35.9
2.838E+03	168.6	134.1	141.7	138.5	123.6	2006.0	16.2	40.7
3.348E+03	174.2	133.5	146.4	141.1	125.7	2009.5	17.1	45.9
3.473E+03	177.7	135.5	147.5	141.7	126.1	2012.6	17.8	47.6
3.592E+03	180.9	137.2	148.6	142.3	126.6	2014.5	18.2	49.0
3.708E+03	183.7	138.7	149.6	142.8	127.0	2015.4	18.5	50.3
3.827E+03	185.4	138.9	150.6	143.3	127.4	2016.7	18.6	51.4
3.942E+03	187.1	139.2	151.5	143.8	127.8	2015.8	18.8	52.6
4.060E+03	188.8	139.5	152.3	144.3	128.3	2017.3	19.0	53.7
4.214E+03	190.5	139.3	153.5	145.0	128.8	2016.3	19.1	54.9
4.297E+03	192.4	140.1	154.1	145.3	129.1	2019.2	19.4	56.1
4.416E+03	193.6	139.9	155.0	145.8	129.5	2018.6	19.6	57.4
4.535E+03	195.7	140.6	155.9	146.3	129.9	2019.4	19.8	58.6
4.659E+03	198.4	141.7	156.9	146.8	130.3	2019.1	20.1	59.9
4.791E+03	200.9	142.7	157.8	147.3	130.7	2021.5	20.4	61.4
4.920E+03	202.7	142.9	158.8	147.8	131.1	2023.4	21.0	63.0
5.049E+03	203.0	141.6	159.7	148.3	131.5	2023.3	21.0	64.1
5.174E+03	200.7	137.8	160.6	148.8	131.9	2023.2	21.2	65.4
5.250E+03	198.4	134.6	161.0	149.1	132.1	2024.7	21.3	66.1
5.327E+03	197.4	132.6	161.5	149.4	132.4	2023.3	21.3	66.8
5.426E+03	197.1	131.2	162.2	149.8	132.7	2023.9	21.4	67.7
5.553E+03	196.8	129.3	163.0	150.2	133.1	2024.6	21.7	69.0
5.622E+03	197.5	129.1	163.5	150.5	133.3	2025.0	21.8	69.8
5.681E+03	198.0	128.9	163.9	150.7	133.4	2024.4	22.0	70.6
5.788E+03	198.2	127.8	164.5	151.0	133.7	2024.1	22.1	71.5
5.875E+03	198.8	127.4	165.1	151.3	134.0	2023.5	22.3	72.4
5.960E+03	199.1	126.7	165.6	151.6	134.2	2024.1	22.4	73.3
6.045E+03	199.4	126.0	166.2	151.9	134.5	2023.9	22.5	74.1
6.136E+03	199.4	124.8	166.8	152.2	134.7	2021.6	22.7	75.1

6.229E+03	200.5	124.8	167.4	152.6	135.0	2018.4	23.0	76.3

Table E-18 Test _AL_pt_01v_07_G_2500_06_15_2007

Experiment Heat flux, q" (kW/m^2)	Experiment $T_{w,o}$ (°C)	Experiment $T_{w,i}$ (°C)	Chen's prediction $T_{w,i}$ (°C)	Klimenko's prediction $T_{w,i}$ (°C)	Davis-Anderson's prediction $T_{w,ONB}$ (°C)	Experiment Mass flux, G (kg/m^2s)	Experiment $T_{b,in}$ (°C)	Experiment $T_{b,out}$ (°C)
1.513E+02	29.1	27.3	27.1	27.1	105.5	2467.0	10.9	11.9
2.762E+02	41.8	38.4	40.5	40.5	107.4	2470.6	11.4	13.3
4.386E+02	56.5	51.2	57.2	57.2	109.3	2473.7	11.9	14.9
6.447E+02	75.1	67.4	77.5	77.5	111.3	2478.5	12.5	17.0
8.943E+02	96.9	86.2	100.6	124.5	113.3	2482.7	13.2	19.4
1.195E+03	120.5	106.2	114.0	127.4	115.3	2488.0	14.0	22.3
1.544E+03	143.7	125.2	122.3	130.3	117.4	2493.4	15.0	25.7
1.934E+03	143.0	119.8	128.9	133.1	119.5	2496.1	16.0	29.4
2.364E+03	160.0	131.7	134.7	135.8	121.6	2503.9	17.0	33.4
2.836E+03	169.7	135.8	140.1	138.5	123.6	2509.8	18.1	37.6
3.340E+03	177.0	137.0	145.0	141.1	125.6	2515.1	19.2	42.2
3.881E+03	182.2	135.7	149.9	143.6	127.6	2519.2	20.4	47.0
4.012E+03	181.7	133.6	151.0	144.2	128.1	2525.1	21.2	48.6
4.135E+03	182.3	132.8	151.9	144.7	128.5	2528.5	21.6	49.9
4.256E+03	183.6	132.7	152.9	145.2	128.9	2531.6	21.9	51.0
4.380E+03	184.9	132.5	153.9	145.7	129.4	2535.7	22.3	52.1
4.499E+03	186.0	132.1	154.8	146.2	129.8	2526.8	22.6	53.3
4.631E+03	189.1	133.6	155.8	146.7	130.2	2522.7	22.8	54.5
4.765E+03	190.7	133.7	156.8	147.3	130.6	2524.7	23.1	55.7
4.894E+03	192.3	133.7	157.8	147.8	131.0	2525.3	23.3	56.8
5.022E+03	194.8	134.7	158.7	148.2	131.4	2527.2	23.7	58.0
5.164E+03	197.5	135.7	159.8	148.8	131.9	2531.3	24.3	59.5
5.310E+03	199.4	135.9	160.9	149.3	132.3	2533.8	24.9	61.1
5.450E+03	200.5	135.3	161.8	149.8	132.7	2534.5	25.3	62.5
5.592E+03	201.0	134.0	162.7	150.3	133.2	2533.9	25.4	63.5
5.730E+03	200.1	131.5	163.6	150.8	133.6	2531.0	25.3	64.4
5.877E+03	199.6	129.3	164.6	151.4	134.0	2531.9	25.6	65.7

5.936E+03	198.6	127.6	165.1	151.6	134.2	2533.1	26.3	66.8
5.995E+03	197.7	126.0	165.5	151.8	134.3	2533.5	26.6	67.5
6.050E+03	197.6	125.2	165.8	152.0	134.5	2533.2	26.6	67.8
6.110E+03	197.6	124.5	166.2	152.2	134.7	2532.7	26.4	68.0
6.169E+03	198.2	124.3	166.5	152.4	134.8	2533.5	26.2	68.3
6.238E+03	198.6	124.0	167.0	152.6	135.0	2536.8	26.7	69.1
6.301E+03	199.4	124.0	167.5	152.8	135.2	2538.3	27.1	69.9
6.368E+03	200.4	124.2	167.9	153.0	135.4	2539.4	27.1	70.4
6.422E+03	201.8	124.9	168.2	153.2	135.5	2538.9	27.2	70.9
6.487E+03	203.4	125.7	168.6	153.4	135.7	2539.2	27.1	71.2
6.545E+03	205.5	127.2	169.0	153.6	135.9	2538.4	27.0	71.5
6.617E+03	207.1	127.9	169.6	153.8	136.1	2541.5	27.9	72.9
6.690E+03	208.9	128.8	170.1	154.0	136.3	2543.0	28.6	74.0
6.759E+03	210.7	129.8	170.5	154.2	136.5	2540.9	28.8	74.7
6.833E+03	212.2	130.5	170.9	154.5	136.7	2538.2	28.5	75.0
6.901E+03	213.0	130.4	171.3	154.7	136.8	2534.9	28.4	75.4
6.970E+03	214.5	131.1	171.7	154.9	137.0	2532.7	28.5	76.0
7.030E+03	215.7	131.6	172.1	155.1	137.2	2526.0	28.7	76.8
7.100E+03	216.2	131.2	172.5	155.3	137.4	2522.6	29.1	77.7
7.167E+03	216.7	131.0	173.0	155.5	137.5	2512.4	29.3	78.6

Table E-19 Test _Al_pt_01v_09_G_2500_06_20_2007

Experiment	Experiment	Experiment	Chen's prediction	Klimenko's prediction	Davis-Anderson's prediction	Experiment	Experiment	Experiment
Heat flux, q" (kW/m^2)	$T_{w,o}$ (°C)	$T_{w,i}$ (°C)	$T_{w,i}$ (°C)	$T_{w,i}$ (°C)	$T_{w,ONB}$ (°C)	Mass flux, G (kg/m^2s)	$T_{b,in}$ (°C)	$T_{b,out}$ (°C)
1.541E+02	28.1	26.3	29.2	29.2	105.5	2484.0	13.3	14.3
2.836E+02	39.9	36.5	42.8	42.8	107.5	2485.0	13.9	15.9
4.539E+02	54.5	49.0	59.8	59.8	109.4	2490.2	14.6	17.8
6.704E+02	71.9	63.9	80.2	80.2	111.5	2496.4	15.5	20.1
9.345E+02	92.0	80.8	103.4	124.9	113.6	2500.6	16.5	23.0
1.251E+03	114.1	99.1	115.6	128.0	115.7	2509.4	17.7	26.3
1.622E+03	137.7	118.3	123.7	130.9	117.9	2511.7	19.0	30.1
2.032E+03	135.0	110.6	130.6	133.8	120.0	2512.1	20.5	34.4

2.462E+03	144.5	115.0	136.2	136.5	122.0	2510.7	22.2	39.1
2.954E+03	162.7	127.3	141.8	139.2	124.1	2510.1	23.9	44.2
3.484E+03	171.5	129.7	147.0	141.8	126.2	2511.1	26.0	49.9
4.067E+03	178.7	129.9	152.3	144.4	128.3	2508.4	28.4	56.4
4.223E+03	180.8	130.1	153.8	145.1	128.8	2504.2	30.7	59.8
4.348E+03	181.6	129.4	154.8	145.6	129.2	2496.5	30.9	60.9
4.484E+03	186.1	132.3	156.0	146.2	129.7	2499.5	31.6	62.6
4.620E+03	189.0	133.6	157.1	146.7	130.1	2503.1	32.4	64.3
4.739E+03	191.4	134.6	157.5	147.2	130.5	2488.3	29.0	61.9
4.864E+03	193.8	135.5	158.7	147.6	130.9	2495.4	30.6	64.3
5.021E+03	195.8	135.6	160.0	148.2	131.4	2502.7	31.6	66.2
5.148E+03	197.2	135.5	160.5	148.7	131.8	2502.1	29.7	65.2
5.276E+03	198.4	135.1	161.3	149.2	132.2	2499.6	28.9	65.4
5.409E+03	198.8	134.0	162.1	149.7	132.6	2517.5	28.6	65.7
5.543E+03	199.0	132.5	162.9	150.2	133.0	2517.2	28.3	66.3
5.688E+03	199.3	131.1	163.8	150.7	133.5	2514.9	28.0	67.1
5.834E+03	199.6	129.7	164.6	151.2	133.9	2511.6	27.5	67.6
5.962E+03	200.1	128.5	165.4	151.6	134.2	2509.0	27.3	68.3
6.074E+03	199.6	126.8	166.6	152.0	134.6	2521.2	30.4	72.0
6.141E+03	199.5	125.8	167.3	152.3	134.8	2524.3	31.9	73.9
6.208E+03	199.4	125.0	167.8	152.5	134.9	2527.2	32.8	75.2
6.277E+03	199.5	124.2	168.3	152.7	135.1	2524.8	32.6	75.5
6.333E+03	200.3	124.4	168.3	152.9	135.3	2518.0	30.6	74.1
6.381E+03	200.7	124.2	168.4	153.1	135.4	2512.7	29.6	73.4
6.445E+03	201.3	124.0	168.7	153.3	135.6	2519.5	28.8	73.0
6.502E+03	201.6	123.6	169.0	153.5	135.8	2518.1	28.4	73.0
6.564E+03	201.6	122.9	169.4	153.7	135.9	2519.1	29.0	74.0
6.633E+03	201.8	122.2	169.9	153.9	136.1	2519.0	29.2	74.7
6.696E+03	201.2	120.9	170.3	154.1	136.3	2517.5	29.4	75.4
6.770E+03	201.0	119.8	170.7	154.3	136.5	2514.0	29.2	75.7
6.850E+03	203.4	121.3	171.1	154.6	136.7	2511.8	29.1	76.2
6.918E+03	207.0	124.0	171.5	154.8	136.9	2515.7	28.8	76.3
6.980E+03	209.7	126.0	171.8	154.9	137.1	2513.6	28.7	76.6
7.046E+03	211.6	127.1	172.1	155.1	137.2	2506.9	28.4	77.0
7.135E+03	213.3	127.8	172.6	155.4	137.5	2500.3	28.4	77.7
7.250E+03	214.4	127.5	173.3	155.8	137.8	2503.9	28.3	78.4

Table E-20 Test _AL_pt_1v_08_G_1500_07_31_2007

Experiment	Experiment	Experiment	Chen's prediction	Klimenko's prediction	Davis-Anderson's prediction	Experiment	Experiment	Experiment
Heat flux, q" (kW/m^2)	$T_{w,o}$ (°C)	$T_{w,i}$ (°C)	$T_{w,i}$ (°C)	$T_{w,i}$ (°C)	$T_{w,ONB}$ (°C)	Mass flux, G (kg/m^2s)	$T_{b,in}$ (°C)	$T_{b,out}$ (°C)
1.592E+02	36.5	34.5	37.4	37.4	105.6	1495.0	12.4	14.3
2.865E+02	54.9	51.4	56.8	56.8	107.5	1496.4	12.8	16.1
4.571E+02	77.5	71.8	81.4	81.4	109.5	1498.0	13.2	18.5
6.788E+02	105.0	96.7	106.8	121.9	111.6	1501.1	13.6	21.4
9.562E+02	136.0	124.2	116.9	125.0	113.8	1499.3	14.2	25.3
1.290E+03	153.2	137.3	124.1	128.2	116.0	1500.0	14.9	29.8
1.657E+03	159.0	138.6	130.1	131.1	118.1	1502.2	15.7	34.7
2.052E+03	160.5	135.2	135.2	133.9	120.2	1503.5	16.5	40.1
2.487E+03	165.1	134.4	140.2	136.6	122.2	1504.6	17.4	45.9
2.591E+03	167.9	135.9	141.2	137.2	122.7	1506.6	18.3	48.0
2.695E+03	170.8	137.6	142.2	137.7	123.1	1508.9	18.8	49.6
2.797E+03	173.5	139.0	143.2	138.3	123.5	1509.0	19.2	51.2
2.896E+03	172.2	136.5	144.2	138.8	123.9	1508.1	19.5	52.7
3.005E+03	172.9	135.9	145.2	139.4	124.4	1509.5	19.9	54.2
3.111E+03	175.3	137.0	146.2	139.9	124.8	1507.1	20.2	55.8
3.221E+03	177.2	137.5	147.2	140.5	125.3	1509.1	20.5	57.4
3.333E+03	179.2	138.1	148.2	141.0	125.7	1512.2	20.8	58.9
3.435E+03	180.8	138.4	149.1	141.5	126.1	1513.8	21.2	60.4
3.553E+03	184.0	140.2	150.2	142.1	126.5	1518.0	21.7	62.1
3.669E+03	186.5	141.2	151.1	142.6	127.0	1518.7	22.1	63.8
3.779E+03	188.0	141.4	152.0	143.1	127.4	1518.4	22.6	65.6
3.900E+03	189.8	141.8	152.9	143.6	127.8	1521.5	23.1	67.4
4.022E+03	191.5	141.9	154.0	144.2	128.2	1517.4	23.8	69.6
4.150E+03	193.7	142.5	155.0	144.7	128.7	1519.4	24.5	71.7
4.271E+03	194.1	141.4	156.0	145.2	129.1	1521.2	25.3	73.8
4.405E+03	193.7	139.3	156.9	145.8	129.5	1523.0	25.1	75.0
4.531E+03	193.1	137.2	157.8	146.3	130.0	1524.8	24.8	76.1
4.660E+03	191.6	134.1	158.8	146.8	130.4	1521.2	25.1	78.0

4.744E+03	188.9	130.4	159.4	147.2	130.6	1521.5	25.4	79.2
4.825E+03	186.9	127.5	160.0	147.5	130.9	1522.5	25.2	79.9
4.903E+03	186.4	125.9	160.5	147.8	131.2	1521.8	25.6	81.2

Table E-21 Test _AL_pt_1v_09_G_1500_08_01_2007

Experiment Heat flux, q" (kW/m^2)	Experiment $T_{w,o}$ (°C)	Experiment $T_{w,i}$ (°C)	Chen's prediction $T_{w,i}$ (°C)	Klimenko's prediction $T_{w,i}$ (°C)	Davis-Anderson's prediction $T_{w,ONB}$ (°C)	Experiment Mass flux, G (kg/m^2s)	Experiment $T_{b,in}$ (°C)	Experiment $T_{b,out}$ (°C)
1.436E+02	32.6	30.8	34.3	34.3	105.3	1486.8	11.3	13.0
2.558E+02	49.6	46.4	51.7	51.7	107.1	1487.3	11.5	14.5
4.050E+02	70.8	65.8	74.0	74.0	108.9	1488.4	11.8	16.5
5.956E+02	97.2	89.8	100.7	120.8	110.8	1491.1	12.2	19.1
8.353E+02	123.4	113.1	113.4	123.8	112.8	1492.5	12.6	22.2
1.130E+03	132.2	118.2	121.0	126.8	114.9	1497.1	13.1	26.1
1.457E+03	139.4	121.4	126.9	129.6	116.9	1504.1	13.7	30.4
1.822E+03	147.9	125.4	132.3	132.3	118.9	1512.1	15.6	36.4
2.222E+03	155.7	128.3	137.1	135.0	120.9	1510.7	16.0	41.5
2.651E+03	162.8	130.1	141.7	137.5	122.8	1512.3	16.4	46.7
2.749E+03	165.2	131.3	142.6	138.1	123.3	1513.2	17.1	48.5
2.849E+03	166.3	131.2	143.6	138.6	123.7	1513.1	17.5	50.0
2.955E+03	168.0	131.5	144.6	139.2	124.1	1515.2	17.8	51.5
3.057E+03	170.3	132.6	145.5	139.7	124.5	1517.6	18.0	52.8
3.158E+03	173.2	134.2	146.4	140.2	124.9	1510.8	18.3	54.4
3.266E+03	176.4	136.1	147.4	140.7	125.3	1504.2	18.6	56.0
3.375E+03	178.7	137.1	148.4	141.2	125.8	1508.1	18.8	57.5
3.485E+03	180.9	137.9	149.4	141.8	126.2	1510.8	19.0	58.9
3.603E+03	182.7	138.3	150.3	142.3	126.6	1515.3	19.3	60.3
3.711E+03	184.3	138.6	151.2	142.8	127.0	1516.2	19.5	61.7
3.819E+03	185.5	138.4	152.0	143.3	127.4	1519.4	19.7	63.2
3.931E+03	183.2	134.8	152.9	143.8	127.8	1518.8	20.0	64.7
4.047E+03	183.6	133.7	153.8	144.3	128.2	1521.8	20.3	66.2
4.156E+03	186.6	135.3	154.6	144.8	128.6	1522.4	20.9	68.0
4.280E+03	189.4	136.7	155.6	145.3	129.0	1526.1	21.3	69.7

4.355E+03	190.8	137.1	156.2	145.6	129.3	1526.8	21.6	70.9
4.436E+03	191.5	136.8	156.8	145.9	129.5	1528.2	21.9	72.0
4.517E+03	191.0	135.3	157.4	146.3	129.8	1526.7	22.0	73.1
4.595E+03	188.4	131.8	158.0	146.6	130.1	1527.0	22.2	74.1
4.667E+03	184.7	127.1	158.5	146.9	130.3	1523.9	22.2	75.1
4.743E+03	183.5	125.0	159.1	147.2	130.5	1523.3	22.4	76.2
4.832E+03	183.5	124.0	159.7	147.6	130.8	1526.5	22.6	77.2
4.927E+03	183.9	123.1	160.4	147.9	131.1	1526.6	22.8	78.5
5.018E+03	184.5	122.6	161.0	148.3	131.4	1518.7	23.0	80.0
5.125E+03	184.0	120.8	161.7	148.7	131.8	1519.6	23.2	81.5
5.202E+03	186.3	122.2	162.2	149.0	132.0	1522.4	23.3	82.3

Table E-22 Test _AL_pt_1v_06_G_2000_07_26_2007

Experiment	Experiment	Experiment	Chen's prediction	Klimenko's prediction	Davis-Anderson's prediction	Experiment	Experiment	Experiment
Heat flux, q" (kW/m^2)	$T_{w,o}$ (°C)	$T_{w,i}$ (°C)	$T_{w,i}$ (°C)	$T_{w,i}$ (°C)	$T_{w,ONB}$ (°C)	Mass flux, G (kg/m^2s)	$T_{b,in}$ (°C)	$T_{b,out}$ (°C)
1.595E+02	31.8	29.9	32.4	32.4	105.6	1984.4	12.5	13.9
2.823E+02	45.6	42.3	47.6	47.6	107.5	1986.8	12.8	15.3
4.463E+02	63.3	58.0	67.0	67.0	109.4	1989.1	13.3	17.2
6.580E+02	84.3	76.4	90.6	90.6	111.4	1992.8	13.9	19.6
9.198E+02	108.2	97.2	110.3	124.7	113.5	1997.4	14.6	22.5
1.230E+03	134.1	119.4	119.3	127.7	115.6	2002.2	15.4	26.0
1.585E+03	151.7	132.8	126.0	130.6	117.7	2005.5	16.3	30.0
1.975E+03	164.9	141.3	132.0	133.3	119.7	2008.9	17.3	34.3
2.397E+03	169.5	140.9	137.2	136.0	121.7	2009.4	18.3	38.9
2.855E+03	173.4	139.4	142.0	138.6	123.7	2012.3	19.3	43.8
3.361E+03	180.4	140.3	146.8	141.2	125.7	2011.4	20.6	49.4
3.695E+03	185.1	141.1	149.9	142.7	127.0	2010.0	21.8	53.5
3.912E+03	189.0	142.3	151.7	143.7	127.7	1999.4	22.6	56.4
4.054E+03	190.9	142.6	152.8	144.3	128.2	2013.4	23.2	58.0
4.172E+03	193.2	143.5	153.7	144.8	128.6	2006.2	23.6	59.6
4.294E+03	195.1	143.9	154.7	145.3	129.1	2004.7	24.0	61.0
4.418E+03	197.2	144.5	155.6	145.8	129.5	2006.3	24.4	62.4

4.535E+03	200.2	146.1	156.5	146.3	129.9	2004.8	24.7	63.7
4.664E+03	203.9	148.3	157.5	146.8	130.3	2005.7	25.0	65.1
4.804E+03	206.1	148.9	158.6	147.3	130.7	2003.7	25.3	66.7
4.935E+03	206.8	148.0	159.6	147.8	131.2	2000.9	25.6	68.2
5.052E+03	205.6	145.3	160.4	148.3	131.5	1993.4	25.8	69.6
5.202E+03	204.0	142.0	161.4	148.9	132.0	2001.7	26.0	70.9
5.314E+03	202.4	139.0	162.2	149.3	132.3	1997.6	26.3	72.2
5.458E+03	202.2	137.1	163.1	149.8	132.8	2009.1	26.5	73.4
5.600E+03	201.8	135.0	164.0	150.4	133.2	2007.2	26.7	74.9
5.656E+03	201.6	134.1	164.4	150.6	133.4	1995.8	27.0	75.9
5.759E+03	201.7	133.1	165.1	150.9	133.7	2001.2	27.1	76.8
5.822E+03	201.2	131.8	165.5	151.1	133.8	1989.5	27.2	77.8
5.926E+03	204.3	133.7	166.2	151.5	134.1	1988.8	27.4	78.8
6.008E+03	211.8	140.2	166.7	151.7	134.4	1992.2	27.5	79.6
6.108E+03	216.1	143.3	167.4	152.0	134.7	2005.8	27.7	80.3
6.202E+03	220.7	146.7	168.0	152.3	134.9	1997.9	27.9	81.5

Table E-23 Test _AL_pt_1v_07_G_2000_07_27_2007

Experiment	Experiment	Experiment	Chen's prediction	Klimenko's prediction	Davis-Anderson's prediction	Experiment	Experiment	Experiment
Heat flux, q" (kW/m^2)	$T_{w,o}$ (°C)	$T_{w,i}$ (°C)	$T_{w,i}$ (°C)	$T_{w,i}$ (°C)	$T_{w,ONB}$ (°C)	Mass flux, G (kg/m^2s)	$T_{b,in}$ (°C)	$T_{b,out}$ (°C)
1.513E+02	31.8	30.0	32.0	32.0	105.5	1995.2	13.4	14.7
2.697E+02	44.7	41.5	46.5	46.5	107.3	1997.2	13.8	16.1
4.270E+02	61.5	56.4	64.9	64.9	109.2	1999.0	14.1	17.8
6.264E+02	81.0	73.5	87.0	87.0	111.1	2000.9	14.5	20.0
8.707E+02	103.0	92.6	108.1	124.2	113.1	2003.6	15.1	22.6
1.162E+03	127.9	114.0	117.6	127.1	115.1	2006.0	15.7	25.7
1.501E+03	137.3	119.3	124.6	130.0	117.2	2008.5	16.5	29.4
1.870E+03	148.8	126.4	130.6	132.7	119.2	2003.6	17.3	33.4
2.282E+03	159.8	132.5	135.9	135.3	121.2	1994.7	18.2	37.9
2.731E+03	164.8	132.1	140.9	138.0	123.2	2001.2	19.2	42.7
3.219E+03	172.3	133.8	145.5	140.5	125.2	2005.1	20.2	47.9
3.541E+03	177.1	134.6	148.5	142.0	126.4	2007.6	21.1	51.6

3.764E+03	180.2	135.1	150.4	143.1	127.2	2005.0	21.8	54.2
3.883E+03	182.2	135.6	151.4	143.6	127.6	2007.8	22.3	55.7
4.003E+03	184.1	136.1	152.3	144.1	128.1	2011.3	22.6	57.0
4.115E+03	186.0	136.7	153.2	144.6	128.5	2010.2	22.9	58.3
4.239E+03	187.9	137.1	154.2	145.1	128.9	2003.4	23.2	59.7
4.363E+03	190.3	138.1	155.1	145.6	129.3	2004.6	23.5	61.1
4.480E+03	192.8	139.1	156.0	146.1	129.7	2004.6	23.7	62.3
4.603E+03	195.4	140.3	156.9	146.6	130.1	2005.6	23.9	63.6
4.732E+03	199.2	142.5	157.9	147.1	130.5	2008.1	24.2	64.9
4.863E+03	202.0	143.7	158.9	147.6	130.9	2010.1	24.4	66.2
4.999E+03	202.2	142.3	159.9	148.1	131.4	2010.9	24.6	67.5
5.132E+03	200.1	138.6	160.8	148.6	131.8	2010.8	24.8	68.9
5.265E+03	197.7	134.6	161.7	149.2	132.2	2011.0	25.1	70.3
5.399E+03	197.1	132.4	162.5	149.7	132.6	2010.4	25.3	71.7
5.483E+03	196.9	131.3	163.1	150.0	132.8	2011.7	25.7	72.8
5.573E+03	196.9	130.2	163.9	150.3	133.1	2015.3	26.9	74.7
5.661E+03	197.3	129.5	164.5	150.6	133.4	2015.7	27.6	76.1
5.751E+03	197.6	128.7	165.1	150.9	133.6	2014.9	28.1	77.4
5.844E+03	200.2	130.2	165.8	151.2	133.9	2011.1	28.5	78.7
5.940E+03	204.7	133.6	166.5	151.5	134.2	2006.2	28.8	80.0
6.026E+03	210.6	138.4	167.1	151.8	134.4	1999.9	29.2	81.2
6.125E+03	215.4	142.0	167.7	152.1	134.7	1997.2	29.3	82.3

Table E-24 Test _Al_pt_1v_01_G_2500_07_06

Experiment Heat flux, q" (kW/m^2)	Experiment $T_{w,o}$ (°C)	Experiment $T_{w,i}$ (°C)	Chen's prediction $T_{w,i}$ (°C)	Klimenko's prediction $T_{w,i}$ (°C)	Davis-Anderson's prediction $T_{w,ONB}$ (°C)	Experiment Mass flux, G (kg/m^2s)	Experiment $T_{b,in}$ (°C)	Experiment $T_{b,out}$ (°C)
3.045E+02	38.1	34.5	44.0	44.0	107.7	2469.8	12.3	14.2
4.817E+02	53.1	47.4	62.0	62.0	109.7	2473.5	13.0	16.1
7.052E+02	70.7	62.3	83.5	83.5	111.8	2476.2	13.7	18.3
9.800E+02	91.1	79.4	106.0	125.4	113.9	2486.7	14.6	21.0
1.303E+03	114.2	98.7	117.0	128.4	116.0	2487.3	15.6	24.2
1.666E+03	137.9	118.1	124.6	131.3	118.1	2491.1	16.7	27.7

2.055E+03	140.5	116.1	130.8	134.0	120.1	2494.7	17.8	31.6
2.476E+03	147.6	118.2	136.2	136.6	122.1	2497.2	19.0	35.7
2.936E+03	163.4	128.6	141.3	139.1	124.0	2502.7	20.2	40.0
3.459E+03	172.4	131.4	146.3	141.7	126.1	2500.1	21.5	45.0
4.011E+03	176.2	128.6	151.2	144.2	128.1	2489.2	23.0	50.4
4.124E+03	178.5	129.6	152.3	144.7	128.5	2476.6	24.1	52.5
4.251E+03	180.9	130.4	153.3	145.2	128.9	2480.6	24.7	54.0
4.375E+03	182.7	130.9	154.3	145.7	129.3	2482.3	25.4	55.5
4.476E+03	184.5	131.4	155.1	146.1	129.7	2488.5	25.8	56.6
4.610E+03	186.7	132.0	156.1	146.7	130.1	2486.6	25.9	57.7
4.741E+03	188.4	132.2	157.1	147.2	130.5	2485.5	26.2	58.8
4.869E+03	190.9	133.1	158.1	147.7	130.9	2489.4	26.2	59.7
4.995E+03	193.0	133.7	159.0	148.2	131.3	2485.7	26.3	60.7
5.121E+03	194.9	134.1	160.0	148.6	131.7	2494.1	26.6	61.8
5.254E+03	198.1	135.8	160.8	149.1	132.2	2503.8	26.9	62.9
5.395E+03	203.2	139.2	161.8	149.6	132.6	2500.2	27.0	64.0
5.531E+03	207.5	141.9	162.7	150.1	133.0	2505.4	27.3	65.2
5.672E+03	208.2	141.0	163.6	150.6	133.4	2507.2	27.6	66.5
5.807E+03	205.0	136.2	164.5	151.1	133.8	2509.0	28.0	67.8
5.886E+03	203.0	133.2	165.1	151.4	134.0	2508.7	28.2	68.6
5.942E+03	203.2	132.8	165.5	151.6	134.2	2509.3	28.3	69.1
5.997E+03	204.0	132.9	165.8	151.7	134.3	2511.3	28.4	69.6
6.054E+03	204.8	133.0	166.2	151.9	134.5	2510.0	28.6	70.1
6.107E+03	205.6	133.2	166.6	152.1	134.7	2508.6	28.6	70.5
6.165E+03	206.3	133.2	166.8	152.3	134.8	2508.2	27.9	70.3
6.223E+03	207.1	133.3	167.1	152.5	135.0	2506.2	27.3	70.0
6.280E+03	207.7	133.2	167.4	152.7	135.1	2505.7	27.4	70.5
6.335E+03	208.3	133.2	167.8	152.9	135.3	2504.7	27.5	71.0
6.394E+03	208.9	133.1	168.2	153.1	135.5	2503.9	27.5	71.5
6.431E+03	209.8	133.5	168.4	153.2	135.6	2504.9	27.6	71.8
6.502E+03	211.2	134.1	168.9	153.4	135.8	2504.0	27.7	72.3
6.562E+03	212.2	134.4	169.3	153.6	135.9	2503.3	27.8	73.0
6.625E+03	213.3	134.8	169.7	153.8	136.1	2501.1	27.9	73.5
6.689E+03	214.8	135.5	170.1	154.0	136.3	2502.5	28.1	74.1
6.751E+03	216.5	136.5	170.5	154.2	136.4	2500.4	28.3	74.8
6.819E+03	218.6	137.7	170.9	154.4	136.6	2499.2	28.3	75.3

6.914E+03	220.8	138.8	171.4	154.7	136.9	2494.2	28.4	76.1
7.019E+03	221.8	138.6	172.0	155.0	137.2	2493.9	28.5	77.0
7.119E+03	222.8	138.4	172.6	155.3	137.4	2501.7	28.8	77.8
7.225E+03	224.5	138.9	173.2	155.6	137.7	2504.4	29.0	78.7
7.318E+03	225.5	138.7	173.8	155.9	137.9	2500.8	29.1	79.6
7.409E+03	226.3	138.4	174.3	156.2	138.2	2486.7	29.2	80.5

Table E-25 Test _AL_pt_1v_02_G_2500_07_09_2007

Experiment	Experiment	Experiment	Chen's prediction	Klimenko's prediction	Davis-Anderson's prediction	Experiment	Experiment	Experiment
Heat flux, q" (kW/m^2)	$T_{w,o}$ (°C)	$T_{w,i}$ (°C)	$T_{w,i}$ (°C)	$T_{w,i}$ (°C)	$T_{w,ONB}$ (°C)	Mass flux, G (kg/m^2s)	$T_{b,in}$ (°C)	$T_{b,out}$ (°C)
1.594E+02	27.8	25.9	28.0	28.0	105.6	2472.6	11.1	12.2
2.817E+02	39.6	36.2	41.2	41.2	107.4	2471.4	11.6	13.6
4.485E+02	55.2	49.8	58.2	58.2	109.4	2485.6	12.2	15.4
6.611E+02	73.6	65.7	78.8	78.8	111.4	2493.3	12.9	17.5
9.220E+02	94.3	83.2	102.3	124.8	113.5	2498.7	13.8	20.1
1.241E+03	116.7	101.8	115.2	127.9	115.6	2504.3	14.8	23.3
1.618E+03	140.1	120.7	123.6	130.9	117.8	2508.3	15.9	27.1
2.029E+03	138.0	113.6	130.3	133.8	120.0	2507.8	17.1	31.1
2.461E+03	144.2	114.6	135.9	136.5	122.0	2506.0	18.3	35.3
2.927E+03	160.0	124.8	141.2	139.0	124.0	2496.8	19.6	39.8
3.460E+03	177.3	135.7	146.3	141.7	126.1	2504.9	21.1	44.9
3.823E+03	185.0	139.0	149.7	143.3	127.4	2507.3	22.6	48.9
4.069E+03	188.6	139.7	151.7	144.4	128.3	2500.6	23.6	51.7
4.196E+03	190.0	139.5	152.8	144.9	128.7	2498.0	24.2	53.2
4.317E+03	191.4	139.4	153.8	145.4	129.1	2495.4	24.7	54.6
4.440E+03	192.8	139.4	154.7	145.9	129.6	2494.7	25.1	55.9
4.578E+03	194.1	139.1	155.8	146.5	130.0	2501.0	25.4	57.1
4.713E+03	195.6	138.9	156.9	147.0	130.4	2503.4	26.0	58.5
4.840E+03	197.0	138.8	157.9	147.5	130.9	2501.4	26.4	59.8
4.974E+03	198.2	138.3	158.9	148.0	131.3	2503.5	26.7	61.0
5.104E+03	199.8	138.4	159.9	148.5	131.7	2505.8	27.0	62.1
5.249E+03	202.6	139.4	160.9	149.1	132.1	2509.1	27.4	63.5

5.383E+03	207.8	143.0	161.8	149.5	132.5	2506.2	27.9	65.0
5.525E+03	206.4	139.9	162.8	150.1	133.0	2506.3	28.3	66.4
5.688E+03	205.3	136.8	163.9	150.7	133.5	2513.9	28.5	67.6
5.835E+03	204.9	134.7	164.8	151.2	133.9	2511.7	28.6	68.7
5.973E+03	205.0	133.1	165.8	151.7	134.3	2511.3	29.2	70.3
6.074E+03	204.3	131.2	166.5	152.0	134.6	2505.4	29.8	71.7
6.159E+03	203.8	129.7	167.2	152.3	134.8	2499.2	30.2	72.8
6.257E+03	203.3	128.0	167.8	152.6	135.1	2501.5	30.3	73.5
6.346E+03	201.4	125.0	168.4	152.9	135.3	2502.1	30.6	74.4
6.431E+03	200.5	123.1	168.9	153.2	135.6	2497.2	30.7	75.2
6.538E+03	203.5	124.9	169.7	153.6	135.9	2499.6	31.1	76.3
6.633E+03	210.4	130.6	170.3	153.8	136.1	2499.9	31.4	77.2
6.748E+03	219.6	138.4	171.0	154.1	136.4	2511.7	31.8	78.2
6.846E+03	227.5	145.1	171.6	154.4	136.7	2501.6	32.2	79.4
6.975E+03	221.8	137.9	172.4	154.8	137.0	2498.4	32.5	80.8
7.088E+03	212.8	127.6	173.1	155.3	137.3	2493.2	32.6	81.7
7.253E+03	207.2	120.0	174.1	155.8	137.8	2496.3	33.0	83.2
7.420E+03	211.0	121.7	175.0	156.3	138.2	2514.0	33.1	84.1

Table E-26 Test _ZN_pt_001v_05_G_2500_12_13_2007

Experiment	Experiment	Experiment	Chen's prediction	Klimenko's prediction	Davis-Anderson's prediction	Experiment	Experiment	Experiment
Heat flux, q" (kW/m^2)	$T_{w,o}$ (°C)	$T_{w,i}$ (°C)	$T_{w,i}$ (°C)	$T_{w,i}$ (°C)	$T_{w,ONB}$ (°C)	Mass flux, G (kg/m^2s)	$T_{b,in}$ (°C)	$T_{b,out}$ (°C)
1.601E+02	29.2	27.2	30.1	30.1	105.6	2496.4	13.6	14.7
2.841E+02	40.6	37.1	42.8	42.8	107.5	2495.5	14.0	15.9
4.480E+02	55.3	49.9	59.0	59.0	109.4	2498.2	14.4	17.4
6.544E+02	72.5	64.5	78.5	78.5	111.3	2501.3	14.9	19.3
9.050E+02	92.5	81.5	101.2	124.6	113.3	2504.9	15.5	21.6
1.204E+03	113.6	99.0	114.2	127.5	115.4	2508.0	16.1	24.3
1.554E+03	136.0	117.2	122.4	130.4	117.5	2513.0	16.8	27.3
1.952E+03	155.7	132.1	129.3	133.2	119.6	2499.1	17.6	30.9
2.372E+03	156.9	128.2	134.9	135.9	121.6	2491.8	18.4	34.6
2.838E+03	169.2	134.8	140.3	138.5	123.6	2496.6	19.2	38.6

3.337E+03	174.8	134.3	145.1	141.1	125.6	2500.6	20.1	42.9
3.661E+03	179.4	135.0	148.1	142.6	126.8	2504.3	20.8	45.8
3.887E+03	182.9	135.8	150.1	143.6	127.7	2506.4	21.3	47.9
4.006E+03	185.0	136.4	151.0	144.1	128.1	2508.7	21.7	49.1
4.125E+03	186.2	136.2	152.0	144.6	128.5	2510.5	22.0	50.2
4.243E+03	187.6	136.2	152.9	145.1	128.9	2510.4	22.2	51.2
4.365E+03	188.9	136.0	153.8	145.6	129.3	2511.4	22.4	52.2
4.486E+03	190.2	135.8	154.7	146.1	129.7	2512.8	22.6	53.2
4.610E+03	191.4	135.5	155.7	146.6	130.1	2514.1	22.8	54.3
4.736E+03	192.6	135.2	156.6	147.1	130.5	2501.1	22.9	55.5
4.858E+03	193.6	134.7	157.5	147.6	130.9	2496.7	23.1	56.5
4.985E+03	194.6	134.2	158.5	148.1	131.3	2498.5	23.3	57.6
5.120E+03	195.5	133.5	159.5	148.6	131.7	2499.4	23.5	58.8
5.249E+03	196.4	132.7	160.4	149.1	132.1	2499.6	23.8	59.9
5.385E+03	197.0	131.8	161.3	149.6	132.5	2501.1	23.9	61.0
5.521E+03	197.7	130.8	162.2	150.1	133.0	2509.0	24.1	62.0
5.664E+03	199.2	130.5	163.1	150.6	133.4	2510.7	24.4	63.2
5.806E+03	200.5	130.1	164.0	151.1	133.8	2510.8	24.6	64.5
5.916E+03	202.3	130.6	164.8	151.5	134.1	2511.6	24.9	65.4
6.033E+03	203.3	130.2	165.5	151.9	134.5	2508.9	25.0	65.3

Table E-27 Test _ZN_pt_001v_06_G_2500_12_14_2007

Experiment	Experiment	Experiment	Chen's prediction	Klimenko's prediction	Davis-Anderson's prediction	Experiment	Experiment	Experiment
Heat flux, q" (kW/m^2)	$T_{w,o}$ (°C)	$T_{w,i}$ (°C)	$T_{w,i}$ (°C)	$T_{w,i}$ (°C)	$T_{w,ONB}$ (°C)	Mass flux, G (kg/m^2s)	$T_{b,in}$ (°C)	$T_{b,out}$ (°C)
1.641E+02	28.9	27.0	30.3	30.3	105.7	2479.0	13.3	14.4
2.922E+02	40.3	36.8	43.6	43.6	107.6	2482.7	13.7	15.6
4.607E+02	54.5	49.0	60.3	60.3	109.5	2485.4	14.1	17.1
6.720E+02	71.7	63.6	80.3	80.3	111.5	2488.2	14.6	19.0
9.286E+02	91.4	80.2	103.1	124.9	113.5	2491.6	15.1	21.2
1.234E+03	113.4	98.5	115.1	127.8	115.6	2495.5	15.7	23.9
1.589E+03	137.4	118.2	123.1	130.7	117.7	2499.3	16.4	27.0
1.994E+03	158.5	134.5	129.9	133.5	119.8	2503.8	17.1	30.4

2.422E+03	160.6	131.3	135.4	136.2	121.8	2506.6	17.9	34.1
2.891E+03	168.6	133.7	140.7	138.8	123.8	2509.6	18.7	38.0
3.400E+03	175.6	134.6	145.6	141.4	125.9	2513.5	19.5	42.2
3.727E+03	179.8	134.8	148.6	142.9	127.1	2503.5	20.3	45.3
3.958E+03	183.2	135.4	150.6	143.9	127.9	2498.6	20.8	47.4
4.075E+03	184.9	135.7	151.5	144.4	128.3	2500.9	21.1	48.6
4.195E+03	185.9	135.3	152.4	144.9	128.7	2502.0	21.4	49.7
4.311E+03	186.8	134.8	153.3	145.4	129.1	2502.4	21.6	50.6
4.435E+03	187.9	134.4	154.3	145.9	129.5	2503.7	21.8	51.7
4.561E+03	189.0	134.0	155.2	146.5	130.0	2504.8	22.0	52.7
4.685E+03	190.1	133.5	156.2	147.0	130.4	2506.3	22.2	53.8
4.819E+03	190.9	132.7	157.2	147.5	130.8	2507.3	22.4	54.9
4.936E+03	191.6	132.0	158.0	147.9	131.2	2508.6	22.6	55.9
5.068E+03	192.3	131.2	159.0	148.4	131.6	2509.8	22.8	57.0
5.203E+03	193.1	130.3	160.0	148.9	132.0	2511.5	23.0	58.1
5.344E+03	194.2	129.6	160.9	149.5	132.4	2512.9	23.3	59.3
5.485E+03	195.4	129.2	161.9	150.0	132.8	2499.0	23.5	60.7
5.627E+03	197.1	129.1	162.8	150.5	133.3	2494.5	23.7	61.9
5.776E+03	198.7	129.0	163.8	151.0	133.7	2493.4	23.9	63.2
5.928E+03	200.4	128.8	164.7	151.5	134.2	2494.5	24.0	64.3
6.080E+03	202.0	128.6	165.7	152.0	134.6	2495.5	24.3	65.6
6.237E+03	203.4	128.1	166.7	152.6	135.0	2494.4	24.5	66.9
6.396E+03	204.8	127.5	167.7	153.1	135.5	2494.8	24.7	68.2
6.552E+03	205.8	126.7	168.8	153.6	135.9	2495.1	24.9	69.5
6.711E+03	206.9	125.9	169.7	154.1	136.3	2494.9	25.1	70.8
6.859E+03	207.5	124.7	170.6	154.6	136.7	2492.3	25.2	71.8

Table E-28 Test _ZN_pt_01v_03_G_2500_12_05_2007

Experiment	Experiment	Experiment	Chen's prediction	Klimenko's prediction	Davis-Anderson's prediction	Experiment	Experiment	Experiment
Heat flux, q" (kW/m^2)	$T_{w,o}$ (°C)	$T_{w,i}$ (°C)	$T_{w,i}$ (°C)	$T_{w,i}$ (°C)	$T_{w,ONB}$ (°C)	Mass flux, G (kg/m^2s)	$T_{b,in}$ (°C)	$T_{b,out}$ (°C)
1.610E+02	28.8	26.9	30.6	30.6	105.6	2487.6	14.1	15.1
2.862E+02	39.4	36.0	43.3	43.3	107.5	2489.7	14.4	16.3

4.514E+02	52.5	47.1	59.6	59.6	109.4	2491.8	14.7	17.7
6.591E+02	68.8	60.9	79.1	79.1	111.4	2495.0	15.2	19.5
9.108E+02	87.6	76.7	124.7	101.8	113.4	2498.3	15.7	21.7
1.210E+03	108.8	94.3	127.6	114.4	115.4	2505.5	16.4	24.3
1.559E+03	129.5	110.8	130.5	122.6	117.5	2505.8	17.0	27.3
1.954E+03	146.9	123.5	133.3	129.3	119.6	2507.9	17.8	30.7
2.387E+03	157.8	129.2	136.0	135.0	121.7	2514.2	18.6	34.5
2.860E+03	166.9	132.6	138.6	140.4	123.7	2514.8	19.4	38.4
3.365E+03	174.0	133.6	141.2	145.3	125.7	2519.2	20.2	42.6
3.689E+03	178.8	134.5	142.7	148.3	126.9	2521.8	21.0	45.5
3.916E+03	182.2	135.2	143.7	150.3	127.8	2523.2	21.5	47.6
4.032E+03	184.0	135.6	144.2	151.3	128.2	2498.6	21.9	49.0
4.149E+03	185.4	135.6	144.8	152.2	128.6	2495.4	22.1	50.0
4.269E+03	187.0	135.7	145.3	153.1	129.0	2497.9	22.3	51.0
4.391E+03	188.6	135.9	145.8	154.0	129.4	2499.4	22.5	52.0
4.515E+03	189.9	135.8	146.3	155.0	129.8	2504.7	22.7	53.1
4.640E+03	191.2	135.6	146.8	155.9	130.2	2508.9	22.9	54.1
4.765E+03	192.6	135.5	147.3	156.9	130.6	2508.9	23.2	55.2
4.891E+03	193.8	135.1	147.7	157.8	131.0	2509.1	23.4	56.3
5.024E+03	195.0	134.7	148.3	158.8	131.4	2509.6	23.6	57.4
5.150E+03	196.0	134.2	148.7	159.7	131.8	2509.1	23.8	58.5
5.284E+03	196.7	133.3	149.2	160.6	132.2	2510.3	24.0	59.6
5.422E+03	196.7	131.7	149.7	161.5	132.7	2511.3	24.2	60.7
5.562E+03	196.6	129.9	150.2	162.5	133.1	2511.7	24.5	61.9
5.702E+03	197.0	128.6	150.7	163.4	133.5	2512.7	24.7	63.1
5.843E+03	198.1	128.0	151.2	164.3	133.9	2513.6	24.9	64.3
5.961E+03	199.5	128.0	151.6	165.1	134.2	2514.1	25.1	65.3
6.090E+03	201.6	128.6	152.1	165.9	134.6	2514.9	25.3	66.3
6.194E+03	203.3	129.0	152.4	166.6	134.9	2514.9	25.5	67.2
6.322E+03	205.4	129.5	152.8	167.4	135.3	2514.7	25.6	68.2
6.445E+03	207.3	130.0	153.2	168.2	135.6	2514.8	25.8	69.2
6.572E+03	209.1	130.3	153.6	169.0	136.0	2514.4	26.0	70.3
6.701E+03	210.7	130.3	154.0	169.8	136.3	2500.6	26.2	71.6
6.835E+03	212.2	130.2	154.5	170.7	136.7	2485.1	26.3	72.9
6.963E+03	213.5	130.0	154.9	171.4	137.0	2482.6	26.5	74.0
7.064E+03	214.0	129.3	155.2	171.9	137.3	2530.5	26.5	74.2

Table E-29 Test _ZN_pt_01v_04_G_2500_12_10_2007

Experiment Heat flux, q" (kW/m^2)	Experiment $T_{w,o}$ (°C)	Experiment $T_{w,i}$ (°C)	Chen's prediction $T_{w,i}$ (°C)	Klimenko's prediction $T_{w,i}$ (°C)	Davis-Anderson's prediction $T_{w,ONB}$ (°C)	Experiment Mass flux, G (kg/m^2s)	Experiment $T_{b,in}$ (°C)	Experiment $T_{b,out}$ (°C)
1.611E+02	29.7	27.8	30.8	30.8	105.6	2495.0	14.3	15.3
2.861E+02	40.7	37.3	43.4	43.4	107.5	2496.6	14.7	16.5
4.513E+02	54.7	49.3	59.6	59.6	109.4	2499.4	15.0	17.9
6.588E+02	71.6	63.7	79.0	79.0	111.4	2501.8	15.5	19.8
9.107E+02	91.0	80.1	101.7	124.7	113.4	2504.6	16.0	22.0
1.211E+03	112.6	98.3	114.4	127.6	115.4	2508.2	16.6	24.6
1.561E+03	136.2	117.7	122.6	130.5	117.5	2512.7	17.3	27.6
1.954E+03	146.8	123.6	129.2	133.3	119.6	2517.6	18.1	30.9
2.379E+03	152.1	123.8	134.9	136.0	121.6	2517.0	18.9	34.6
2.845E+03	162.0	128.2	140.3	138.6	123.7	2524.0	19.7	38.5
3.353E+03	172.3	132.5	145.2	141.2	125.7	2522.9	20.5	42.7
3.679E+03	176.2	132.6	148.2	142.7	126.9	2512.8	21.3	45.8
3.904E+03	178.5	132.2	150.2	143.7	127.7	2516.1	21.9	47.8
4.019E+03	179.0	131.3	151.1	144.2	128.1	2518.7	22.2	49.0
4.140E+03	179.7	130.6	152.1	144.7	128.5	2521.2	22.5	50.0
4.262E+03	180.8	130.2	153.0	145.3	129.0	2522.7	22.7	51.0
4.383E+03	181.8	129.8	154.0	145.8	129.4	2524.1	22.9	52.1
4.503E+03	182.8	129.4	154.9	146.3	129.8	2509.4	23.1	53.3
4.630E+03	183.9	129.0	155.9	146.8	130.2	2504.0	23.3	54.3
4.754E+03	185.1	128.7	156.8	147.3	130.6	2504.6	23.5	55.4
4.884E+03	186.4	128.4	157.8	147.8	131.0	2506.0	23.7	56.5
5.011E+03	187.6	128.1	158.8	148.2	131.4	2506.1	23.9	57.5
5.138E+03	188.9	128.0	159.7	148.7	131.8	2506.7	24.1	58.6
5.263E+03	190.5	128.1	160.6	149.2	132.2	2508.0	24.3	59.7
5.409E+03	192.5	128.3	161.5	149.7	132.6	2508.3	24.6	60.9
5.544E+03	194.2	128.4	162.4	150.2	133.0	2510.1	24.8	62.1
5.695E+03	196.3	128.7	163.4	150.7	133.5	2509.5	25.1	63.3
5.839E+03	199.1	129.9	164.3	151.2	133.9	2509.2	25.3	64.6
5.962E+03	202.6	131.9	165.2	151.6	134.2	2509.9	25.6	65.7
6.092E+03	207.0	134.7	166.0	152.0	134.6	2511.6	25.8	66.7

6.220E+03	212.4	138.6	166.8	152.5	135.0	2511.8	26.0	67.8
6.348E+03	217.8	142.4	167.7	152.8	135.3	2512.5	26.2	68.9
6.481E+03	221.8	144.9	168.5	153.3	135.7	2512.8	26.4	70.0
6.611E+03	223.9	145.4	169.4	153.7	136.1	2513.0	26.6	71.1
6.747E+03	225.0	145.0	170.2	154.1	136.4	2513.8	26.9	72.2
6.883E+03	225.6	143.9	171.0	154.5	136.8	2503.9	27.1	73.6
7.018E+03	225.8	142.6	171.8	155.0	137.2	2493.1	27.3	74.9
7.152E+03	225.7	140.9	172.6	155.4	137.5	2488.3	27.4	76.1
7.281E+03	225.3	138.9	173.3	155.8	137.8	2479.4	27.6	77.3
7.472E+03	225.5	136.9	174.5	156.4	138.3	2468.4	27.8	79.0

Table E-30 Test _ZN_pt_1v_01_G_2500_11_28_2007

Experiment	Experiment	Experiment	Chen's prediction	Klimenko's prediction	Davis-Anderson's prediction	Experiment	Experiment	Experiment
Heat flux, q" (kW/m^2)	$T_{w,o}$ (°C)	$T_{w,i}$ (°C)	$T_{w,i}$ (°C)	$T_{w,i}$ (°C)	$T_{w,ONB}$ (°C)	Mass flux, G (kg/m^2s)	$T_{b,in}$ (°C)	$T_{b,out}$ (°C)
1.749E+02	28.6	26.5	31.9	31.9	105.9	2489.1	13.9	15.0
3.154E+02	39.5	35.7	46.1	46.1	107.9	2491.6	14.2	16.2
4.942E+02	53.3	47.4	63.4	63.4	109.9	2503.4	14.6	17.7
7.111E+02	69.8	61.3	83.6	83.6	111.8	2512.5	15.4	20.0
9.695E+02	89.5	77.9	105.5	125.3	113.8	2488.6	15.9	22.2
1.275E+03	110.9	95.7	116.3	128.2	115.8	2492.1	16.3	24.7
1.625E+03	127.2	107.7	123.8	131.0	117.9	2498.3	16.9	27.7
2.009E+03	134.4	110.3	130.1	133.7	119.9	2502.4	17.8	31.1
2.444E+03	152.5	123.2	135.7	136.4	121.9	2500.9	18.5	34.8
2.923E+03	167.9	132.8	141.1	139.0	124.0	2505.7	19.3	38.8
3.434E+03	174.4	133.3	145.9	141.5	126.0	2506.7	20.1	43.1
3.761E+03	178.7	133.6	148.9	143.1	127.2	2512.8	20.9	46.1
3.983E+03	181.1	133.3	150.8	144.1	128.0	2516.8	21.4	48.1
4.099E+03	182.6	133.5	151.7	144.5	128.4	2520.4	21.8	49.3
4.216E+03	183.8	133.3	152.6	145.0	128.8	2525.1	22.0	50.3
4.325E+03	185.0	133.2	153.4	145.5	129.2	2532.5	22.3	51.2
4.447E+03	186.2	133.0	154.4	146.0	129.6	2536.0	22.6	52.2
4.569E+03	187.6	132.8	155.3	146.5	130.0	2529.9	22.6	53.2

4.693E+03	189.0	132.8	156.2	147.0	130.4	2531.9	22.9	54.3
4.821E+03	190.5	132.7	157.2	147.5	130.8	2508.9	23.0	55.6
4.945E+03	191.6	132.4	158.2	148.0	131.2	2508.8	23.1	56.6
5.076E+03	193.0	132.1	159.1	148.5	131.6	2511.2	23.3	57.6
5.212E+03	194.4	131.9	160.1	149.0	132.0	2526.3	23.6	58.7
5.326E+03	195.7	131.9	160.9	149.4	132.4	2518.5	23.9	59.9
5.478E+03	197.7	132.1	161.9	149.9	132.8	2518.8	24.1	61.1
5.621E+03	199.9	132.5	162.8	150.4	133.3	2523.7	24.3	62.2
5.715E+03	202.2	133.7	163.4	150.8	133.5	2531.1	24.6	63.0
5.805E+03	205.6	136.0	164.0	151.1	133.8	2521.1	24.7	63.9
5.900E+03	210.1	139.4	164.6	151.4	134.1	2516.9	24.7	64.7
5.990E+03	212.3	140.5	165.2	151.7	134.3	2515.5	24.8	65.4
6.079E+03	212.2	139.4	165.8	152.0	134.6	2519.0	25.0	66.2
6.166E+03	212.3	138.5	166.4	152.3	134.8	2527.2	25.3	66.9
6.254E+03	212.5	137.5	166.9	152.6	135.1	2518.7	25.4	67.8
6.341E+03	213.0	137.0	167.5	152.9	135.3	2514.4	25.4	68.5
6.431E+03	213.7	136.7	168.1	153.1	135.6	2514.7	25.6	69.2
6.451E+03	214.8	137.5	168.2	153.2	135.6	2527.7	25.7	69.6
6.524E+03	215.0	136.9	168.7	153.4	135.8	2520.3	25.9	70.3
6.619E+03	214.9	135.6	169.2	153.8	136.1	2521.6	25.7	70.7
6.718E+03	216.0	135.5	169.8	154.1	136.4	2519.1	25.7	71.5
6.799E+03	216.0	134.5	170.3	154.3	136.6	2513.9	25.8	72.2
6.897E+03	216.0	133.4	170.9	154.6	136.8	2513.7	25.9	72.9
6.985E+03	215.7	132.0	171.4	154.9	137.1	2511.6	26.0	73.7
7.103E+03	213.6	128.5	172.0	155.3	137.4	2520.5	26.1	74.5
7.221E+03	212.8	126.3	172.8	155.7	137.7	2507.7	26.3	75.8
7.348E+03	213.6	125.5	173.5	156.1	138.0	2510.6	26.5	76.7
7.474E+03	214.9	125.4	174.2	156.4	138.3	2512.6	26.7	77.8
7.605E+03	215.3	124.2	175.0	156.8	138.7	2496.0	27.0	78.0

Table E-31 Test _ZN_pt_1v_02_G_2500_12_03_2007

Experiment Heat flux, q" (kW/m^2)	Experiment $T_{w,o}$ (°C)	Experiment $T_{w,i}$ (°C)	Chen's prediction $T_{w,i}$ (°C)	Klimenko's prediction $T_{w,i}$ (°C)	Davis-Anderson's prediction $T_{w,ONB}$ (°C)	Experiment Mass flux, G (kg/m^2s)	Experiment $T_{b,in}$ (°C)	Experiment $T_{b,out}$ (°C)
176.8	30.7	28.6	32.8	32.8	105.9	2478.7	14.8	16.0
315.9	41.5	37.7	46.7	46.7	107.9	2478.4	14.9	17.0
500.5	55.5	49.5	64.6	64.6	109.9	2481.6	15.3	18.5
723.7	72.5	63.9	85.4	85.4	111.9	2486.7	15.8	20.4
987.6	92.0	80.2	106.5	125.5	113.9	2490.8	16.3	22.8
1296.8	113.7	98.2	116.9	128.4	116.0	2494.0	17.0	25.5
1652.4	136.9	117.2	124.3	131.2	118.0	2496.9	17.8	28.6
2058.2	157.8	133.2	130.9	133.9	120.1	2500.5	18.6	32.2
2487.9	160.7	130.9	136.3	136.6	122.1	2510.4	19.4	35.9
2955.5	170.4	135.0	141.5	139.1	124.1	2512.2	20.2	39.9
3478.2	177.8	136.2	146.4	141.7	126.2	2520.7	21.2	44.3
3816.6	182.1	136.5	149.5	143.3	127.4	2522.9	22.0	47.4
4042.0	184.5	136.2	151.4	144.3	128.2	2517.7	22.6	49.7
4158.4	186.0	136.3	152.3	144.8	128.6	2509.0	23.0	50.9
4280.8	187.5	136.3	153.3	145.3	129.0	2512.9	23.2	51.9
4403.6	188.9	136.3	154.2	145.8	129.4	2513.0	23.3	52.9
4521.4	190.3	136.3	155.1	146.3	129.8	2515.8	23.4	53.9
4656.9	191.7	136.0	156.1	146.8	130.3	2514.7	23.5	54.8
4782.8	192.9	135.8	157.0	147.3	130.7	2517.7	23.7	55.9
4903.3	194.6	136.0	157.9	147.8	131.1	2517.7	23.8	56.8
5044.3	196.2	135.9	159.0	148.3	131.5	2518.3	23.9	57.8
5178.1	197.8	135.9	159.9	148.8	131.9	2519.2	24.0	58.9
5298.3	199.9	136.6	160.7	149.3	132.3	2520.6	24.2	59.9
5449.4	202.6	137.4	161.7	149.8	132.7	2521.4	24.4	61.1
5589.3	204.3	137.5	162.6	150.3	133.2	2520.8	24.6	62.3
5741.2	207.3	138.7	163.6	150.8	133.6	2522.6	24.7	63.5
5890.1	212.2	141.8	164.6	151.3	134.0	2520.0	25.0	64.7
6040.8	214.8	142.6	165.6	151.8	134.5	2521.3	25.2	65.9
6162.7	214.1	140.5	166.4	152.2	134.8	2522.1	25.5	67.0
6282.5	214.6	139.6	167.2	152.6	135.2	2521.9	25.7	68.1

6400.2	215.5	139.0	167.9	153.0	135.5	2522.5	26.0	69.2
6513.1	216.3	138.4	168.7	153.4	135.8	2515.8	26.2	70.3
6649.5	217.4	138.0	169.6	153.8	136.2	2513.1	26.4	71.5
6774.1	218.6	137.6	170.3	154.2	136.5	2511.0	26.6	72.5
6888.9	218.8	136.5	171.0	154.6	136.8	2511.6	26.8	73.5
7008.0	217.5	133.8	171.7	155.0	137.1	2508.9	27.0	74.6
7144.0	218.0	132.6	172.5	155.4	137.5	2509.5	27.1	75.3

Table E-32 Test _C_pt_001v_01_G_2500_2_4_2008

Experiment	Experiment	Experiment	Chen's prediction	Klimenko's prediction	Davis-Anderson's prediction	Experiment	Experiment	Experiment
Heat flux, q" (kW/m^2)	$T_{w,o}$ (°C)	$T_{w,i}$ (°C)	$T_{w,i}$ (°C)	$T_{w,i}$ (°C)	$T_{w,ONB}$ (°C)	Mass flux, G (kg/m^2s)	$T_{b,in}$ (°C)	$T_{b,out}$ (°C)
152.7	28.2	26.4	29.6	29.6	105.5	2494.1	14.0	14.9
271.2	38.6	35.4	41.8	41.8	107.3	2496.0	14.3	16.1
427.3	51.7	46.6	57.1	57.1	109.2	2498.7	14.7	17.5
622.8	67.1	59.7	75.6	75.6	111.1	2501.5	15.1	19.2
859.3	84.9	74.6	97.3	97.3	113.0	2504.0	15.7	21.3
1139.4	105.7	92.0	112.2	127.0	115.0	2507.9	16.3	23.8
1466.3	127.9	110.3	120.7	129.7	117.0	2511.6	16.9	26.7
1832.4	135.8	113.8	127.3	132.5	119.0	2515.3	17.6	29.9
2240.2	150.9	124.0	133.2	135.1	121.0	2518.1	18.4	33.4
2683.5	165.4	133.2	138.5	137.7	123.0	2509.4	19.2	37.3
3161.2	172.7	134.8	143.5	140.2	124.9	2496.4	20.0	41.4
3472.1	178.3	136.7	146.4	141.7	126.1	2500.0	20.7	44.3
3687.2	181.8	137.6	148.3	142.7	126.9	2501.8	21.2	46.2
3798.9	183.9	138.4	149.3	143.2	127.3	2504.3	21.5	47.4
3911.8	185.4	138.5	150.3	143.7	127.7	2505.9	21.8	48.3
4025.9	187.1	138.9	151.2	144.2	128.1	2507.9	22.0	49.3
4140.6	188.7	139.1	152.1	144.7	128.5	2509.7	22.2	50.3
4258.8	190.2	139.1	153.0	145.2	128.9	2511.2	22.4	51.3
4378.4	191.7	139.2	153.9	145.7	129.3	2511.5	22.6	52.3
4497.5	192.9	139.0	154.8	146.2	129.7	2513.0	22.8	53.3
4619.8	193.9	138.6	155.8	146.7	130.1	2514.2	23.0	54.3

4748.1	195.2	138.3	156.7	147.2	130.6	2515.5	23.1	55.4
4875.5	196.6	138.2	157.7	147.7	131.0	2516.0	23.3	56.4
5003.3	197.7	137.7	158.6	148.2	131.4	2517.1	23.5	57.5
5132.2	198.7	137.2	159.6	148.6	131.8	2513.2	23.7	58.6
5260.7	199.1	136.1	160.5	149.1	132.2	2511.0	23.8	59.7
5397.4	198.6	133.9	161.4	149.6	132.6	2511.0	23.9	60.8
5539.9	198.2	131.8	162.3	150.2	133.0	2511.3	24.1	61.9
5666.4	198.6	130.7	163.1	150.6	133.4	2509.2	24.3	63.0
5812.0	200.1	130.4	164.0	151.1	133.8	2510.8	24.5	64.2
5959.6	202.4	131.0	165.0	151.6	134.2	2512.2	24.8	65.4
6097.3	204.8	131.7	165.9	152.1	134.6	2502.8	25.0	66.8
6249.6	206.8	131.9	166.9	152.6	135.1	2494.5	25.2	68.2
6391.9	208.9	132.3	167.8	153.0	135.5	2494.9	25.4	69.4
6537.3	210.8	132.4	168.8	153.5	135.9	2492.9	25.6	70.6
6692.3	212.6	132.4	169.7	154.0	136.3	2494.8	25.8	71.9
6849.9	214.1	132.0	170.7	154.5	136.7	2493.8	26.1	73.3
7002.8	215.1	131.2	171.6	155.0	137.1	2490.0	26.2	74.3

Table E-33 Test _C_pt_001v_02_G_2500_2_6_2008

Experiment	Experiment	Experiment	Chen's prediction	Klimenko's prediction	Davis-Anderson's prediction	Experiment	Experiment	Experiment
Heat flux, q" (kW/m^2)	$T_{w,o}$ (°C)	$T_{w,i}$ (°C)	$T_{w,i}$ (°C)	$T_{w,i}$ (°C)	$T_{w,ONB}$ (°C)	Mass flux, G (kg/m^2s)	$T_{b,in}$ (°C)	$T_{b,out}$ (°C)
158.7	26.9	25.0	29.5	29.5	105.6	2484.0	13.0	13.9
282.4	37.5	34.1	42.3	42.3	107.5	2486.4	13.4	15.2
444.4	51.0	45.7	58.5	58.5	109.4	2491.9	13.9	16.8
651.9	67.0	59.1	78.4	78.4	111.3	2489.2	14.4	18.6
903.2	83.6	72.7	101.3	124.6	113.3	2489.0	14.9	20.8
1190.1	104.7	90.3	113.9	127.4	115.3	2493.2	15.5	23.4
1523.3	124.9	106.5	121.9	130.2	117.3	2498.3	16.2	26.2
1900.6	143.9	121.0	128.4	132.9	119.3	2503.5	16.9	29.5
2308.7	155.9	128.0	134.0	135.5	121.3	2503.9	17.7	33.0
2754.0	165.6	132.4	139.3	138.1	123.3	2505.3	18.5	36.8
3232.8	171.4	132.4	144.0	140.6	125.2	2509.1	19.3	40.8

3531.7	176.8	134.2	146.8	142.0	126.4	2512.2	20.0	43.6
3746.3	180.7	135.5	148.7	143.0	127.1	2509.6	20.4	45.6
3856.6	181.8	135.3	149.7	143.5	127.5	2509.6	20.7	46.7
3966.8	183.0	135.2	150.6	144.0	127.9	2511.5	21.0	47.7
4076.6	184.6	135.5	151.5	144.4	128.3	2507.8	21.1	48.7
4189.9	186.0	135.5	152.4	144.9	128.7	2505.3	21.3	49.7
4308.2	187.4	135.5	153.3	145.4	129.1	2504.1	21.5	50.7
4425.4	189.2	135.8	154.2	145.9	129.5	2510.2	21.7	51.7
4543.8	191.0	136.2	155.1	146.4	129.9	2509.8	21.9	52.7
4663.8	192.9	136.7	156.0	146.9	130.3	2506.0	22.1	53.7
4784.3	195.3	137.6	156.9	147.3	130.7	2510.0	22.2	54.6
4905.5	208.9	149.8	157.8	147.7	131.1	2510.9	22.3	55.6

Table E-34 Test _C_pt_001v_03_G_2500_2_8_2008

Experiment Heat flux, q" (kW/m^2)	Experiment $T_{w,o}$ (°C)	Experiment $T_{w,i}$ (°C)	Chen's prediction $T_{w,i}$ (°C)	Klimenko's prediction $T_{w,i}$ (°C)	Davis-Anderson's prediction $T_{w,ONB}$ (°C)	Experiment Mass flux, G (kg/m^2s)	Experiment $T_{b,in}$ (°C)	Experiment $T_{b,out}$ (°C)
161.8	30.3	28.3	31.8	31.8	105.6	2491.6	15.5	16.4
287.6	41.3	37.8	44.5	44.5	107.5	2491.7	15.9	17.7
453.8	55.1	49.5	60.4	60.4	109.4	2495.9	16.3	19.2
662.0	71.6	63.5	79.8	79.8	111.4	2501.3	16.7	21.0
914.2	90.9	79.8	102.2	124.7	113.4	2505.6	17.3	23.3
1213.4	112.4	97.7	114.5	127.6	115.5	2508.1	17.9	25.9
1559.6	135.1	116.2	122.6	130.4	117.5	2500.8	18.7	29.0
1950.2	150.7	127.0	129.3	133.2	119.6	2508.4	19.5	32.5
2375.9	161.2	132.3	135.0	135.9	121.6	2505.5	20.3	36.2
2842.6	172.4	137.9	140.4	138.5	123.6	2514.1	21.1	40.1
3340.8	178.0	137.4	145.3	141.1	125.6	2508.8	22.1	44.5
3663.1	183.1	138.6	148.4	142.6	126.8	2487.4	22.9	47.8
3889.5	186.2	138.9	150.3	143.6	127.7	2495.9	23.5	49.9
4003.8	187.1	138.5	151.3	144.1	128.1	2498.1	23.9	51.1
4118.8	188.2	138.2	152.2	144.6	128.5	2500.6	24.2	52.2
4235.0	189.4	137.9	153.1	145.1	128.9	2501.3	24.4	53.3

4353.9	190.8	137.8	154.0	145.6	129.3	2501.8	24.6	54.3
4476.7	192.2	137.7	155.0	146.1	129.7	2502.5	24.8	55.3
4598.9	193.2	137.3	155.9	146.6	130.1	2504.8	25.0	56.3
4719.2	194.8	137.4	156.8	147.1	130.5	2505.2	25.2	57.3
4845.0	198.6	139.7	157.8	147.5	130.9	2506.4	25.4	58.4
4968.7	199.4	139.0	158.7	148.0	131.3	2507.4	25.7	59.5
5093.0	199.3	137.4	159.6	148.5	131.7	2507.3	25.6	60.3
5223.2	197.0	133.5	160.5	149.0	132.1	2507.5	25.7	61.3
5352.8	196.4	131.3	161.3	149.5	132.5	2506.7	25.9	62.4
5482.0	197.0	130.4	162.2	150.0	132.8	2506.7	26.1	63.4
5618.8	197.8	129.5	163.1	150.4	133.2	2506.8	26.3	64.6
5753.2	199.2	129.3	164.0	150.9	133.6	2506.9	26.5	65.7
5895.6	200.8	129.1	164.9	151.4	134.1	2506.8	26.6	66.8

Table E-35 Test _C_pt_001v_04_G_2500_2_11_2008

Experiment	Experiment	Experiment	Chen's prediction	Klimenko's prediction	Davis-Anderson's prediction	Experiment	Experiment	Experiment
Heat flux, q" (kW/m^2)	$T_{w,o}$ (°C)	$T_{w,i}$ (°C)	$T_{w,i}$ (°C)	$T_{w,i}$ (°C)	$T_{w,ONB}$ (°C)	Mass flux, G (kg/m^2s)	$T_{b,in}$ (°C)	$T_{b,out}$ (°C)
160.4	30.6	28.7	31.5	31.5	105.6	2492.9	15.3	16.4
284.7	41.7	38.3	44.1	44.1	107.5	2495.1	15.8	17.6
447.5	55.6	50.2	59.8	59.8	109.4	2496.1	16.1	19.1
651.4	72.3	64.5	78.8	78.8	111.3	2499.4	16.6	20.9
898.7	91.7	81.0	101.1	124.6	113.3	2503.4	17.1	23.1
1193.9	113.3	99.0	114.0	127.4	115.3	2507.5	17.7	25.7
1538.3	136.5	118.1	122.2	130.3	117.4	2507.5	18.3	28.7
1921.6	144.5	121.5	128.8	133.1	119.4	2509.4	19.1	32.0
2344.7	158.2	130.2	134.6	135.7	121.5	2504.7	19.8	35.7
2808.2	168.8	135.3	140.0	138.4	123.5	2512.0	20.6	39.7
3311.0	174.2	134.7	145.0	140.9	125.5	2508.0	21.4	43.9
3637.8	179.4	136.0	148.0	142.5	126.8	2502.8	22.1	47.0
3866.7	183.3	137.2	150.0	143.5	127.6	2507.9	22.6	49.0
3984.8	185.7	138.2	151.0	144.0	128.0	2504.3	22.9	50.2
4107.2	187.9	138.9	152.0	144.6	128.4	2503.4	23.1	51.3

4227.0	189.6	139.2	152.9	145.1	128.8	2502.2	23.3	52.3
4346.9	191.4	139.5	153.8	145.6	129.2	2502.7	23.5	53.3
4471.3	192.3	139.0	154.8	146.1	129.7	2504.8	23.7	54.3
4598.3	193.3	138.4	155.7	146.6	130.1	2505.9	23.9	55.4
4725.4	194.7	138.3	156.7	147.1	130.5	2507.6	24.1	56.4
4866.9	197.2	139.2	157.7	147.6	130.9	2508.1	24.2	57.5
5013.2	220.1	160.3	158.8	148.1	131.4	2508.2	24.3	58.3

Table E-36 Test _C_pt_01v_05_G_2500_2_12_2008

Experiment	Experiment	Experiment	Chen's prediction	Klimenko's prediction	Davis-Anderson's prediction	Experiment	Experiment	Experiment
Heat flux, q" (kW/m^2)	$T_{w,o}$ (°C)	T_{w_i} (°C)	T_{w_i} (°C)	T_{w_i} (°C)	$T_{w,ONB}$ (°C)	Mass flux, G (kg/m^2s)	$T_{b,in}$ (°C)	$T_{b,out}$ (°C)
154.1	29.5	27.6	30.2	30.2	105.5	2492.3	14.5	15.5
273.7	40.1	36.8	42.3	42.3	107.3	2503.9	14.9	16.7
431.0	53.6	48.4	57.7	57.7	109.2	2506.2	15.3	18.1
629.0	69.9	62.3	76.2	76.2	111.1	2508.4	15.7	19.9
869.3	89.0	78.5	98.3	98.3	113.1	2503.4	16.2	22.0
1155.3	109.8	95.8	112.8	127.1	115.1	2501.5	16.8	24.6
1488.4	127.8	109.8	121.2	129.9	117.1	2505.2	17.4	27.5
1850.7	135.1	112.7	127.6	132.6	119.1	2508.6	18.1	30.6
2269.0	154.0	126.6	133.6	135.3	121.1	2499.6	18.8	34.3
2725.8	168.2	135.2	139.1	137.9	123.2	2498.6	19.6	38.2
3214.1	175.2	136.4	144.0	140.5	125.1	2503.4	20.3	42.3
3525.6	179.0	136.4	146.9	142.0	126.3	2507.3	21.0	45.2
3739.5	181.5	136.4	148.8	142.9	127.1	2506.8	21.5	47.2
3846.2	183.3	136.8	149.8	143.4	127.5	2486.7	21.9	48.5
3974.2	184.6	136.6	150.9	144.0	128.0	2488.9	22.1	49.5
4098.0	185.9	136.4	151.8	144.5	128.4	2490.8	22.3	50.5
4211.9	187.3	136.5	152.7	145.0	128.8	2492.9	22.5	51.5
4329.6	188.6	136.3	153.6	145.5	129.2	2494.5	22.7	52.5
4448.1	190.0	136.2	154.5	146.0	129.6	2496.0	22.9	53.5
4569.9	191.2	136.0	155.4	146.5	130.0	2497.4	23.1	54.5
4694.5	192.5	135.8	156.4	147.0	130.4	2498.2	23.3	55.6

4815.3	193.5	135.4	157.3	147.5	130.8	2499.0	23.4	56.6
4940.6	194.5	134.8	158.2	147.9	131.2	2499.0	23.6	57.6
5067.9	195.4	134.2	159.1	148.4	131.6	2502.3	23.7	58.6
5197.4	195.9	133.1	160.1	148.9	132.0	2498.6	24.0	59.8
5327.8	195.7	131.3	161.0	149.4	132.4	2495.8	24.2	60.9
5456.6	195.3	129.4	161.8	149.9	132.8	2499.9	24.4	62.0
5592.2	195.4	127.9	162.7	150.4	133.2	2500.3	24.6	63.2
5729.4	196.3	127.1	163.6	150.9	133.6	2499.8	24.8	64.3
5868.2	197.5	126.6	164.5	151.3	134.0	2501.2	25.0	65.5
6005.9	199.1	126.5	165.4	151.8	134.4	2502.1	25.2	66.6
6152.6	200.8	126.5	166.3	152.3	134.8	2501.9	25.4	67.8
6295.5	202.6	126.6	167.3	152.8	135.2	2502.4	25.6	69.0
6442.1	204.2	126.4	168.2	153.2	135.6	2496.5	25.8	70.3
6586.1	206.0	126.4	169.1	153.7	136.0	2494.1	26.0	71.6
6727.3	207.2	125.9	170.0	154.2	136.4	2492.8	26.2	72.4

Table E-37 Test _C_pt_01v_06_G_2500_2_14_2008

Experiment	Experiment	Experiment	Chen's prediction	Klimenko's prediction	Davis-Anderson's prediction	Experiment	Experiment	Experiment
Heat flux, q" (kW/m^2)	$T_{w,o}$ (°C)	$T_{w,i}$ (°C)	$T_{w,i}$ (°C)	$T_{w,i}$ (°C)	$T_{w,ONB}$ (°C)	Mass flux, G (kg/m^2s)	$T_{b,in}$ (°C)	$T_{b,out}$ (°C)
162.0	29.9	28.0	31.6	31.6	105.6	2480.0	15.2	16.3
289.2	40.6	37.1	44.3	44.3	107.5	2480.7	15.3	17.2
455.6	54.0	48.5	60.4	60.4	109.5	2483.1	15.5	18.5
664.5	70.3	62.2	80.0	80.0	111.4	2485.3	15.8	20.1
918.0	89.2	78.1	102.6	124.8	113.4	2488.1	16.2	22.2
1219.4	110.5	95.7	114.8	127.7	115.5	2491.9	16.7	24.7
1570.4	132.9	113.9	122.8	130.5	117.6	2496.7	17.3	27.6
1967.3	152.0	128.2	129.5	133.3	119.7	2499.2	18.0	31.0
2395.4	159.4	130.4	135.2	136.0	121.7	2503.2	18.7	34.5
2856.9	166.6	132.0	140.4	138.6	123.7	2508.1	19.4	38.4
3354.6	172.2	131.6	145.3	141.2	125.7	2502.4	20.2	42.6
3676.9	176.1	131.6	148.2	142.7	126.9	2507.2	21.0	45.5
3904.6	178.5	131.3	150.3	143.7	127.7	2487.9	21.6	47.9

4016.9	179.7	131.1	151.2	144.2	128.1	2488.8	22.0	49.2
4135.1	180.9	130.9	152.1	144.7	128.5	2491.5	22.4	50.3
4251.2	182.2	130.8	153.0	145.2	128.9	2493.6	22.6	51.3
4371.5	183.4	130.5	153.9	145.7	129.3	2495.0	22.8	52.3
4489.7	184.7	130.4	154.8	146.2	129.7	2496.8	23.0	53.3
4614.1	186.0	130.1	155.8	146.7	130.1	2498.0	23.2	54.3
4734.3	187.2	130.0	156.7	147.2	130.5	2500.8	23.4	55.4
4862.2	188.4	129.5	157.6	147.7	130.9	2501.0	23.6	56.4
4985.5	189.4	129.1	158.6	148.1	131.3	2501.7	23.8	57.5
5113.9	190.5	128.7	159.5	148.6	131.7	2503.1	24.0	58.5
5246.6	191.5	128.0	160.4	149.1	132.1	2503.8	24.2	59.6
5377.1	191.8	126.8	161.3	149.6	132.5	2504.6	24.4	60.7
5513.5	192.0	125.3	162.2	150.1	132.9	2493.6	24.5	61.9
5648.7	192.4	124.1	163.1	150.6	133.3	2491.7	24.7	63.1
5790.7	193.5	123.4	164.0	151.1	133.8	2492.5	24.9	64.2
5933.4	195.0	123.2	164.9	151.6	134.2	2493.9	25.0	65.4
6081.7	197.0	123.4	165.9	152.1	134.6	2494.6	25.2	66.6
6229.3	199.1	123.7	166.8	152.6	135.0	2495.2	25.4	67.8
6378.0	201.1	124.0	167.8	153.0	135.4	2494.9	25.6	69.0
6529.7	202.8	123.8	168.8	153.5	135.8	2494.6	25.9	70.3
6681.4	204.9	124.1	169.7	154.0	136.3	2493.6	26.1	71.6
6837.0	205.5	122.8	170.6	154.5	136.7	2490.9	26.2	71.7

Table E-38 Test _C_pt_01v_07_G_2500_2_21_2008

Experiment	Experiment	Experiment	Chen's prediction	Klimenko's prediction	Davis-Anderson's prediction	Experiment	Experiment	Experiment
Heat flux, q" (kW/m^2)	$T_{w,o}$ (°C)	$T_{w,i}$ (°C)	$T_{w,i}$ (°C)	$T_{w,i}$ (°C)	$T_{w,ONB}$ (°C)	Mass flux, G (kg/m^2s)	$T_{b,in}$ (°C)	$T_{b,out}$ (°C)
167.0	30.2	28.2	31.6	31.6	105.7	2490.3	14.6	15.7
296.4	41.5	38.0	44.8	44.8	107.6	2486.4	15.0	16.9
467.8	55.8	50.1	61.4	61.4	109.6	2489.1	15.4	18.4
682.4	72.9	64.6	81.5	81.5	111.6	2491.8	15.8	20.3
943.2	93.0	81.6	104.1	125.0	113.6	2494.2	16.3	22.5
1253.5	115.3	100.2	115.7	128.0	115.7	2497.7	16.9	25.2

1612.7	138.2	118.8	123.6	130.8	117.8	2501.7	17.6	28.3
2010.7	143.7	119.5	130.2	133.7	119.9	2504.6	18.3	31.7
2462.0	163.1	133.5	136.0	136.4	122.0	2506.6	18.9	35.4
2945.6	171.2	135.7	141.4	139.1	124.1	2499.2	19.6	39.4
3466.0	178.0	136.3	146.3	141.7	126.1	2502.2	20.4	43.6
3803.5	182.5	136.7	149.3	143.2	127.4	2505.1	21.0	46.6
4034.8	184.8	136.2	151.2	144.3	128.2	2507.3	21.5	48.6
4151.7	185.8	135.8	152.1	144.8	128.6	2501.6	21.7	49.7
4271.2	187.1	135.6	153.1	145.3	129.0	2502.4	21.8	50.6
4392.5	188.1	135.2	154.0	145.8	129.4	2504.8	22.0	51.6
4513.1	189.1	134.7	154.9	146.3	129.8	2506.5	22.1	52.5
4637.8	190.1	134.3	155.9	146.8	130.2	2491.8	22.3	53.8
4764.8	191.5	134.1	156.8	147.3	130.6	2492.7	22.6	54.9
4892.3	192.9	133.9	157.8	147.8	131.0	2499.0	22.8	56.0
5024.8	194.4	133.9	158.7	148.3	131.4	2502.1	23.1	57.1
5154.5	196.4	134.3	159.7	148.7	131.8	2504.4	23.3	58.1
5285.6	198.2	134.5	160.6	149.2	132.2	2504.8	23.5	59.2
5426.2	199.5	134.2	161.5	149.7	132.7	2505.6	23.7	60.4
5562.8	199.3	132.3	162.4	150.2	133.1	2507.6	23.9	61.5
5701.5	199.0	130.4	163.3	150.7	133.5	2508.6	24.2	62.7
5848.1	199.4	129.0	164.3	151.3	133.9	2490.9	24.4	64.2
5993.7	199.9	127.7	165.2	151.8	134.3	2492.7	24.5	65.4
6143.5	201.1	127.1	166.2	152.3	134.8	2492.1	24.7	66.6
6294.3	202.5	126.7	167.2	152.8	135.2	2493.7	24.9	67.8
6447.1	204.2	126.5	168.2	153.3	135.6	2493.5	25.2	69.2
6606.3	206.2	126.6	169.2	153.8	136.1	2492.3	25.4	70.5
6771.4	208.1	126.5	170.2	154.3	136.5	2493.4	25.6	71.8
6939.3	210.2	126.6	171.1	154.8	136.9	2492.0	25.8	73.2

Table E-39 Test _C_pt_1v_08_G_2500_2_23_2008

Experiment Heat flux, q" (kW/m^2)	Experiment $T_{w,o}$ (°C)	Experiment $T_{w,i}$ (°C)	Chen's prediction $T_{w,i}$ (°C)	Klimenko's prediction $T_{w,i}$ (°C)	Davis-Anderson's prediction $T_{w,ONB}$ (°C)	Experiment Mass flux, G (kg/m^2s)	Experiment $T_{b,in}$ (°C)	Experiment $T_{b,out}$ (°C)
163.0	29.4	27.4	30.1	30.1	105.7	2486.9	13.2	14.2
289.4	40.9	37.4	43.1	43.1	107.5	2489.2	13.5	15.4
456.1	55.5	50.0	59.6	59.6	109.5	2489.3	13.9	16.9
665.8	73.2	65.1	79.6	79.6	111.4	2491.1	14.3	18.7
920.7	93.2	82.1	102.4	124.8	113.5	2494.5	14.9	21.0
1224.8	115.4	100.7	114.9	127.7	115.5	2498.5	15.5	23.7
1577.6	136.9	117.8	122.9	130.6	117.6	2498.5	16.3	26.8
1971.9	146.9	123.1	129.6	133.4	119.7	2493.7	17.0	30.3
2408.9	159.8	130.7	135.3	136.1	121.8	2498.1	17.9	34.1
2876.3	164.6	129.9	140.6	138.7	123.8	2502.1	18.8	38.2
3392.1	170.7	129.7	145.6	141.4	125.8	2486.3	19.8	42.8
3719.6	174.4	129.5	148.6	142.9	127.1	2489.5	20.7	45.9
3949.0	177.4	129.7	150.6	143.9	127.9	2492.9	21.3	48.1
4067.5	179.2	130.1	151.5	144.4	128.3	2496.9	21.7	49.3
4190.4	181.2	130.6	152.5	145.0	128.7	2501.9	22.0	50.4
4314.7	182.6	130.6	153.4	145.5	129.1	2505.7	22.2	51.5
4439.7	184.2	130.6	154.4	146.0	129.6	2497.4	22.5	52.7
4567.6	185.6	130.5	155.4	146.5	130.0	2491.5	22.7	53.8
4693.9	187.0	130.3	156.4	147.0	130.4	2484.9	22.9	54.9
4824.2	188.4	130.1	157.3	147.5	130.8	2494.3	23.1	56.0
4954.9	189.7	129.9	158.3	148.0	131.2	2494.4	23.3	57.1
5088.6	191.0	129.5	159.3	148.5	131.6	2495.4	23.6	58.3
5222.0	192.3	129.2	160.2	149.0	132.1	2497.0	23.8	59.4
5359.1	193.6	128.9	161.1	149.5	132.5	2499.3	24.1	60.6
5496.4	194.8	128.5	162.0	150.0	132.9	2504.7	24.3	61.7
5639.4	196.1	128.0	163.0	150.5	133.3	2498.3	24.4	63.0
5787.4	197.4	127.5	163.9	151.1	133.7	2492.0	24.6	64.2
5937.8	198.6	126.9	164.9	151.6	134.2	2493.6	24.7	65.4
6089.1	199.7	126.2	165.9	152.1	134.6	2492.9	24.9	66.7
6240.0	201.1	125.7	166.9	152.6	135.0	2489.4	25.2	68.0

6393.0	202.5	125.3	167.9	153.1	135.5	2491.2	25.4	69.4
6550.4	203.9	124.8	168.9	153.6	135.9	2490.6	25.6	70.7
6718.9	205.2	124.1	169.9	154.1	136.4	2489.2	25.9	72.1
6886.8	206.6	123.4	170.9	154.7	136.8	2488.6	26.1	73.5
6996.7	207.5	123.0	171.5	155.0	137.1	2488.8	26.2	74.2

Table E-40 Test _C_pt_1v_09_G_2500_3_6_2008

Experiment	Experiment	Experiment	Chen's prediction	Klimenko's prediction	Davis-Anderson's prediction	Experiment	Experiment	Experiment
Heat flux, q" (kW/m^2)	$T_{w,o}$ (°C)	$T_{w,i}$ (°C)	$T_{w,i}$ (°C)	$T_{w,i}$ (°C)	$T_{w,ONB}$ (°C)	Mass flux, G (kg/m^2s)	$T_{b,in}$ (°C)	$T_{b,out}$ (°C)
166.9	30.3	28.2	31.8	31.8	105.7	2485.2	14.8	15.8
296.1	41.6	38.0	44.8	44.8	107.6	2483.4	15.1	17.0
466.5	55.8	50.2	61.4	61.4	109.6	2485.9	15.4	18.5
680.8	73.0	64.8	81.4	81.4	111.6	2488.7	15.8	20.3
941.4	92.8	81.5	104.0	125.0	113.6	2491.6	16.3	22.6
1252.7	114.6	99.6	115.7	128.0	115.7	2493.1	17.0	25.3
1614.4	137.3	117.8	123.6	130.9	117.8	2498.2	17.7	28.5
2020.6	150.1	125.8	130.4	133.7	119.9	2497.8	18.4	32.0
2464.2	162.3	132.6	136.0	136.4	122.0	2502.0	19.2	35.8
2944.9	170.3	134.8	141.4	139.1	124.1	2495.3	20.1	39.9
3462.7	177.1	135.4	146.3	141.7	126.1	2499.3	20.9	44.3
3793.3	181.3	135.7	149.3	143.2	127.3	2507.2	21.7	47.3
4025.0	182.5	134.1	151.3	144.2	128.1	2496.4	22.3	49.6
4143.5	184.1	134.2	152.2	144.7	128.6	2486.3	22.6	51.0
4265.9	186.1	134.7	153.2	145.2	129.0	2483.2	22.8	52.0
4389.1	188.3	135.4	154.1	145.8	129.4	2478.1	23.0	53.1
4515.6	189.7	135.4	155.1	146.3	129.8	2481.3	23.3	54.2
4637.1	190.9	135.0	156.0	146.8	130.2	2481.8	23.4	55.2
4765.7	192.3	134.9	157.0	147.3	130.6	2483.1	23.7	56.3
4895.5	193.7	134.7	158.0	147.8	131.0	2483.9	23.8	57.4
5028.0	195.2	134.7	158.9	148.3	131.5	2488.9	24.0	58.4
5159.4	196.1	134.0	159.9	148.8	131.9	2490.8	24.1	59.5
5293.0	197.3	133.6	160.8	149.3	132.3	2486.0	24.3	60.6

5427.3	198.3	133.0	161.7	149.7	132.7	2487.1	24.5	61.7
5558.9	199.8	132.8	162.5	150.2	133.1	2487.7	24.7	62.8
5699.7	199.4	130.8	163.4	150.7	133.5	2489.9	24.9	64.0
5845.5	200.1	129.7	164.4	151.2	133.9	2490.6	25.2	65.3
5993.8	201.1	129.0	165.4	151.7	134.3	2500.2	25.5	66.6
6143.2	202.7	128.7	166.4	152.3	134.8	2494.7	25.8	68.0
6295.8	204.4	128.6	167.4	152.8	135.2	2492.7	26.2	69.4
6447.3	205.9	128.3	168.4	153.2	135.6	2492.4	26.5	70.8
6603.5	207.3	127.8	169.4	153.8	136.0	2492.4	26.8	72.3
6763.2	209.0	127.5	170.4	154.3	136.5	2491.8	27.1	73.6
6917.2	210.2	126.9	171.2	154.7	136.9	2492.6	27.2	74.4

Table E-41 Test _C_pt_1v_10_G_2500_3_18_2008

Experiment	Experiment	Experiment	Chen's prediction	Klimenko's prediction	Davis-Anderson's prediction	Experiment	Experiment	Experiment
Heat flux, q" (kW/m^2)	$T_{w,o}$ (°C)	$T_{w,i}$ (°C)	$T_{w,i}$ (°C)	$T_{w,i}$ (°C)	$T_{w,ONB}$ (°C)	Mass flux, G (kg/m^2s)	$T_{b,in}$ (°C)	$T_{b,out}$ (°C)
148.2	27.6	25.8	28.8	28.8	105.4	2493.8	13.6	14.5
262.7	37.9	34.7	40.7	40.7	107.2	2486.4	13.9	15.6
413.5	50.9	45.9	55.7	55.7	109.0	2488.2	14.3	17.0
602.9	66.4	59.1	73.8	73.8	110.9	2492.7	14.7	18.7
832.4	84.1	74.0	94.9	94.9	112.8	2496.3	15.2	20.7
1106.1	102.5	89.1	111.2	126.7	114.8	2500.5	15.9	23.2
1424.6	122.3	105.1	119.9	129.4	116.7	2503.6	16.5	26.0
1784.6	133.9	112.3	126.6	132.1	118.7	2488.3	17.2	29.2
2182.8	145.3	118.9	132.5	134.8	120.7	2490.6	18.0	32.6
2617.3	157.6	126.0	137.8	137.3	122.7	2492.7	18.7	36.3
3082.0	163.9	126.7	142.6	139.8	124.6	2501.3	19.5	40.2
3375.8	166.9	126.1	145.4	141.3	125.8	2503.3	20.2	42.9
3581.9	169.2	126.0	147.4	142.3	126.5	2494.8	20.7	44.9
3690.0	170.8	126.2	148.3	142.8	126.9	2502.5	21.0	46.0
3797.8	172.1	126.2	149.3	143.3	127.3	2497.9	21.2	46.9
3906.4	173.4	126.2	150.2	143.7	127.7	2494.2	21.4	47.8
4016.3	174.8	126.3	151.1	144.2	128.1	2494.3	21.6	48.8

4129.4	176.3	126.4	152.0	144.7	128.5	2499.7	21.7	49.7
4240.8	178.2	127.0	152.9	145.2	128.9	2498.1	21.9	50.7
4355.9	180.5	127.9	153.8	145.7	129.3	2488.3	22.1	51.8
4475.0	182.7	128.7	154.7	146.1	129.7	2484.3	22.3	52.8
4594.8	184.3	128.8	155.6	146.6	130.1	2489.8	22.6	53.8
4713.9	185.7	128.7	156.5	147.1	130.5	2498.6	22.7	54.8
4837.2	187.1	128.7	157.4	147.6	130.8	2495.9	22.9	55.8
4963.9	188.5	128.6	158.3	148.1	131.2	2494.3	23.1	56.8
5090.7	190.0	128.5	159.2	148.5	131.6	2501.8	23.3	57.8
5219.7	191.3	128.3	160.2	149.0	132.0	2507.9	23.5	58.9
5349.0	192.7	128.1	161.0	149.5	132.4	2502.5	23.7	60.0
5473.2	193.9	127.9	161.8	149.9	132.8	2505.6	23.9	61.0
5607.9	195.2	127.4	162.7	150.4	133.2	2510.7	24.1	62.1
5743.9	196.4	127.1	163.6	150.9	133.6	2506.9	24.3	63.2
5885.1	197.9	126.9	164.5	151.4	134.0	2507.8	24.4	64.3
6026.2	199.6	126.8	165.4	151.9	134.4	2505.9	24.6	65.6
6168.4	201.2	126.7	166.4	152.3	134.8	2480.7	24.8	67.1
6312.4	203.3	127.1	167.3	152.8	135.2	2479.4	25.0	68.3
6457.5	205.8	127.9	168.2	153.3	135.6	2484.7	25.3	69.6
6604.7	207.4	127.7	169.2	153.8	136.0	2481.9	25.4	70.8

Table E-42 Test _C_pt_1v_11_G_2500_3_23_2008

Experiment	Experiment	Experiment	Chen's prediction	Klimenko's prediction	Davis-Anderson's prediction	Experiment	Experiment	Experiment
Heat flux, q" (kW/m^2)	$T_{w,o}$ (°C)	$T_{w,i}$ (°C)	$T_{w,i}$ (°C)	$T_{w,i}$ (°C)	$T_{w,ONB}$ (°C)	Mass flux, G (kg/m^2s)	$T_{b,in}$ (°C)	$T_{b,out}$ (°C)
171.5	28.8	26.7	31.3	31.3	105.8	2488.8	13.7	14.8
304.8	39.5	35.8	45.0	45.0	107.7	2491.2	14.1	16.1
480.1	53.3	47.5	62.2	62.2	109.7	2494.8	14.5	17.6
701.4	70.1	61.6	82.9	82.9	111.7	2497.5	15.0	19.6
970.5	89.7	78.0	105.4	125.3	113.8	2501.1	15.6	21.9
1293.1	112.7	97.0	116.7	128.3	115.9	2504.8	16.2	24.7
1672.0	139.4	119.2	124.7	131.3	118.1	2496.7	17.0	28.0
2088.6	152.4	127.2	131.2	134.1	120.3	2498.9	17.7	31.6

2540.3	161.8	131.1	136.9	136.9	122.4	2502.7	18.5	35.4
3022.7	167.0	130.5	142.0	139.5	124.4	2508.1	19.3	39.5
3549.3	172.8	130.0	147.0	142.1	126.4	2504.1	20.2	43.9
3888.6	176.8	129.9	150.1	143.7	127.7	2487.6	20.9	47.2
4121.6	180.2	130.4	151.9	144.7	128.5	2489.6	21.5	49.3
4242.1	183.0	131.8	152.9	145.2	128.9	2490.5	21.9	50.5
4366.9	184.8	132.1	153.8	145.7	129.3	2498.3	22.1	51.5
4494.0	186.3	132.0	154.8	146.2	129.7	2502.6	22.4	52.6
4621.5	187.7	131.9	155.7	146.7	130.2	2507.6	22.5	53.6
4752.2	189.0	131.7	156.7	147.2	130.6	2496.7	22.7	54.8
4882.2	190.4	131.4	157.7	147.7	131.0	2485.3	22.8	56.0
5013.3	191.8	131.3	158.7	148.2	131.4	2484.4	23.0	57.0
5149.6	193.2	131.0	159.7	148.7	131.8	2490.3	23.2	58.1
5286.6	194.6	130.7	160.6	149.3	132.2	2493.6	23.5	59.2
5417.3	195.7	130.3	161.5	149.7	132.6	2484.5	23.7	60.6
5559.1	196.9	129.8	162.4	150.2	133.1	2475.4	24.0	61.9
5698.3	197.7	128.9	163.3	150.7	133.5	2480.7	24.2	63.0
5844.6	198.9	128.3	164.3	151.2	133.9	2487.2	24.4	64.2
5992.9	200.1	127.7	165.2	151.8	134.3	2492.7	24.7	65.5
6141.7	201.1	126.9	166.2	152.3	134.8	2487.7	24.9	66.8
6296.1	202.6	126.6	167.2	152.8	135.2	2484.5	25.1	68.1
6452.3	204.2	126.3	168.2	153.3	135.6	2483.2	25.3	69.4
6594.9	206.0	126.3	169.1	153.7	136.0	2488.1	25.6	70.6
6757.4	207.3	125.7	170.1	154.3	136.5	2490.3	25.8	72.0

Appendix F. Effective Heat Transfer Coefficient Data

In Section 4.1, the results of the effective heat transfer coefficient, h_{eff} (calculated from the knowledge of applied heat flux and measured T_w and $T_{b,o}$ were presented for all runs of water and nanofluids boiling. In Section 6.1.2, T_w was also predicted using Chen's and Klimenko's correlations. The numeric values of the measured and predicted T_w were reported in Appendix E. Both measured and predicted T_w were used for the calculation of the effective HTC and its result was given in Fig. (6-43). Considering the importance of the h_{eff} result, the raw data are also tabularized in this section for more detailed information.

In Section 6.3.1.1.1, the relative importance of the forced convective and nucleate boiling heat transfer contribution was analyzed. Eqs. 6-1 and 6-2 were used to quantify each contribution and its ratio (q''_{1p}/q''_{2p}) was compared through Figs. 6-47 and 48 using the predicted and measured T_w, respectively. In this section, corresponding raw data are also reported for more detail information.

Table F-1 Test _W_12_G_1500_11_02_2007_NBHT

Experiment	Experiment	Chen's prediction	Klimenko's prediction	Exp/Pred	Exp/Pred	Chen's prediction			Experiment		
q" (kW/m^2)	h_{eff} ($W/m^2 \cdot K$) (a)	h_{eff} ($W/m^2 \cdot K$) (b)	h_{eff} ($W/m^2 \cdot K$) (c)	Ratio (a)/(b)	Ratio (a)/(c)	$q"_{1p}$ (kW/m^2) (d)	$q"_{2p}$ (kW/m^2) (e)	Ratio (d)/(e)	$q"_{1p}$ (kW/m^2) (f)	$q"_{2p}$ (kW/m^2) (g)	Ratio (f)/(g)
1.662E+02	8301	6820	6820	1.217	1.217	0	0	0	0	0	0
3.000E+02	8718	6973	6973	1.250	1.250	0	0	0	0	0	0
4.772E+02	9115	7179	7179	1.270	1.270	0	0	0	0	0	0
7.036E+02	9617	8036	6907	1.197	1.392	654.151	49.4867	13.2187	0	0	0
9.799E+02	10258	10495	9676	0.977	1.060	725.1733	254.7372	2.8468	741.4187	238.4918	3.1088
1.294E+03	13292	13495	12926	0.985	1.028	781.3214	512.8153	1.5236	792.7838	501.3529	1.5813
1.647E+03	16754	16965	16751	0.988	1.000	829.3654	817.944	1.014	839.3638	807.9456	1.0389
2.024E+03	21262	20857	21068	1.019	1.009	868.0001	1156.423	0.7506	851.0532	1173.37	0.7253
2.450E+03	27205	25386	26260	1.072	1.036	905.6352	1543.921	0.5866	844.693	1604.864	0.5263
2.916E+03	35349	30674	32406	1.152	1.091	939.877	1976.045	0.4756	815.2244	2100.697	0.3881
3.015E+03	37339	31982	33962	1.168	1.099	948.1239	2067.325	0.4586	811.7415	2203.707	0.3684
3.115E+03	39469	33241	35479	1.187	1.112	951.2832	2163.752	0.4396	800.8452	2314.19	0.3461
3.215E+03	41269	34482	36988	1.197	1.116	954.9904	2259.751	0.4226	797.5962	2417.146	0.33
3.318E+03	43311	35698	38472	1.213	1.126	963.3407	2354.191	0.4092	793.6685	2523.863	0.3145
3.422E+03	45446	36970	40045	1.229	1.135	969.9475	2451.855	0.3956	788.7244	2633.078	0.2995
3.520E+03	47374	38195	41577	1.240	1.139	975.5809	2544.66	0.3834	786.2404	2734.001	0.2876
3.619E+03	49499	39464	43164	1.254	1.147	980.4682	2638.695	0.3716	781.3999	2837.763	0.2754
3.727E+03	51679	40860	44897	1.265	1.151	986.9489	2740.088	0.3602	780.0321	2947.004	0.2647
3.832E+03	53570	42213	46587	1.269	1.150	992.4372	2839.855	0.3495	781.7443	3050.547	0.2563
3.939E+03	55703	43623	48369	1.277	1.152	996.2862	2942.74	0.3386	779.9423	3159.084	0.2469
4.050E+03	59163	45520	50830	1.300	1.164	996.2277	3054.059	0.3262	766.2084	3284.078	0.2333
4.171E+03	63230	47253	53084	1.338	1.191	1001.062	3169.681	0.3158	747.8342	3422.908	0.2185

Table F-2 Test _W_13_G_1500_11_07_2007_NBHT

Experiment	Experiment	Chen's prediction	Klimenko's prediction	Exp/Pred	Exp/Pred	Chen's prediction			Experiment		
q" (kW/m^2)	h_{eff} (W/m^2·K) (a)	h_{eff} (W/m^2·K) (b)	h_{eff} (W/m^2·K) (c)	Ratio (a)/(b)	Ratio (a)/(c)	$q"_{1p}$ (kW/m^2) (d)	$q"_{2p}$ (kW/m^2) (e)	Ratio (d)/(e)	$q"_{1p}$ (kW/m^2) (f)	$q"_{2p}$ (kW/m^2) (g)	Ratio (f)/(g)
1.868E+02	11183	7108	7108	1.573	1.573	0	0	0	0	0	0
3.391E+02	11080	7275	7275	1.523	1.523	0	0	0	0	0	0
5.277E+02	11203	7512	7512	1.491	1.491	0	0	0	0	0	0
7.566E+02	11580	8753	7652	1.323	1.513	670.738	85.8388	7.8139	0	0	0
1.034E+03	12219	11330	10517	1.078	1.162	736.8857	297.3084	2.4785	682.856	351.338	1.9436
1.355E+03	15501	14475	13940	1.071	1.112	790.1818	565.0684	1.3984	737.4727	617.7775	1.1938
1.703E+03	19169	17982	17835	1.066	1.075	833.5307	869.6828	0.9584	781.5154	921.698	0.8479
2.096E+03	24499	22142	22496	1.106	1.089	872.5174	1223.776	0.713	788.1858	1308.107	0.6025
2.526E+03	31056	26853	27953	1.157	1.111	906.3837	1619.243	0.5598	783.3881	1742.238	0.4496
2.992E+03	39720	32285	34341	1.230	1.157	938.2421	2054.234	0.4567	762.2899	2230.186	0.3418
3.085E+03	41663	33535	35852	1.242	1.162	942.5519	2142.604	0.4399	758.3322	2326.823	0.3259
3.189E+03	43438	34829	37432	1.247	1.160	948.1591	2240.607	0.4232	759.9173	2428.849	0.3129
3.246E+03	43310	35551	38325	1.218	1.130	951.1659	2295.018	0.4144	780.4241	2465.759	0.3165
3.353E+03	44359	36858	39948	1.204	1.110	957.3525	2395.833	0.3996	795.1111	2558.074	0.3108
3.442E+03	45806	37987	41366	1.206	1.107	960.8805	2481.173	0.3873	796.5271	2645.527	0.3011
3.542E+03	46620	39259	42982	1.188	1.085	965.0797	2577.132	0.3745	812.3495	2729.862	0.2976
3.645E+03	47205	40578	44629	1.163	1.058	970.1378	2675.062	0.3627	833.6074	2811.593	0.2965
3.749E+03	48042	41941	46340	1.145	1.037	973.6422	2775.393	0.3508	849.6691	2899.366	0.2931
3.860E+03	48515	43434	48238	1.117	1.006	976.7356	2882.821	0.3388	874.0981	2985.459	0.2928
3.970E+03	48695	44944	50180	1.083	0.970	980.8691	2989.467	0.3281	904.9597	3065.377	0.2952

Table F-3 Test _W_17_G_1500_11_13_2007_CHF

Experiment	Experiment	Chen's prediction	Klimenko's prediction	Exp/Pred	Exp/Pred	Chen's prediction			Experiment		
q" (kW/m^2)	h_{eff} (W/m^2·K) (a)	h_{eff} (W/m^2·K) (b)	h_{eff} (W/m^2·K) (c)	Ratio (a)/(b)	Ratio (a)/(c)	$q"_{1p}$ (kW/m^2) (d)	$q"_{2p}$ (kW/m^2) (e)	Ratio (d)/(e)	$q"_{1p}$ (kW/m^2) (f)	$q"_{2p}$ (kW/m^2) (g)	Ratio (f)/(g)
1.750E+02	9893	7037	7037	1.406	1.406	0	0	0	0	0	0
3.114E+02	10389	7208	7208	1.441	1.441	0	0	0	0	0	0

4.920E+02	10874	7442	7442	1.461	1.461	0	0	0	0	0	0
7.194E+02	11216	8377	7224	1.339	1.553	659.667	59.7666	11.0374	0	0	0
9.974E+02	11914	10916	10073	1.091	1.183	729.8695	267.5073	2.7284	668.2929	329.084	2.0308
1.320E+03	15403	14081	13510	1.094	1.140	786.5944	533.2593	1.4751	718.6626	601.1911	1.1954
1.683E+03	19333	17730	17555	1.090	1.101	833.5903	849.9077	0.9808	764.1	919.398	0.8311
2.088E+03	24884	21999	22324	1.131	1.115	875.8665	1211.818	0.7228	773.9483	1313.736	0.5891
2.536E+03	32300	26917	28014	1.200	1.153	911.9627	1624.525	0.5614	759.6595	1776.829	0.4275
3.027E+03	41504	32656	34775	1.271	1.194	944.5026	2082.768	0.4535	742.8357	2284.434	0.3252
3.139E+03	44239	34200	36652	1.294	1.207	949.009	2190.485	0.4332	733.3459	2406.148	0.3048
3.246E+03	46974	35552	38308	1.321	1.226	955.6606	2290.717	0.4172	722.9927	2523.385	0.2865
3.351E+03	50303	36863	39929	1.365	1.260	961.7991	2389.208	0.4026	704.5245	2646.483	0.2662
3.460E+03	53041	38235	41647	1.387	1.274	968.6978	2491.455	0.3888	697.9918	2762.161	0.2527
3.564E+03	55857	39542	43300	1.413	1.290	975.3927	2588.819	0.3768	690.2345	2873.977	0.2402
3.677E+03	58705	41022	45139	1.431	1.301	979.9374	2697.151	0.3633	684.5009	2992.588	0.2287
3.786E+03	61930	42517	47022	1.457	1.317	981.2765	2804.654	0.3499	673.4286	3112.502	0.2164
3.902E+03	64995	44035	48944	1.476	1.328	987.0266	2914.884	0.3386	668.4621	3233.449	0.2067
4.019E+03	68219	45616	50974	1.495	1.338	991.9176	3026.705	0.3277	663.0146	3355.608	0.1976
4.135E+03	71951	47231	53075	1.523	1.356	995.6447	3139.124	0.3172	653.3282	3481.441	0.1877
4.253E+03	75956	48910	55288	1.553	1.374	999.0375	3254.354	0.307	643.0551	3610.337	0.1781
4.373E+03	79719	50520	57430	1.578	1.388	1007.302	3365.73	0.2993	638.1085	3734.924	0.1708
4.483E+03	83240	52151	59635	1.596	1.396	1008.096	3474.519	0.2901	631.3412	3851.274	0.1639
4.600E+03	87719	54055	62252	1.623	1.409	1003.617	3596.072	0.2791	618.2169	3981.471	0.1553
4.726E+03	93665	56336	65456	1.663	1.431	995.4944	3730.952	0.2668	598.5223	4127.924	0.145
4.863E+03	98932	58869	69091	1.681	1.432	987.217	3876.14	0.2547	587.206	4276.151	0.1373

Table F-4 Test _W_14_G_2000_11_08_2007_NBHT

Experiment	Experiment	Chen's prediction	Klimenko's prediction	Exp/Pred	Exp/Pred	Chen's prediction			Experiment		
q" (kW/m^2)	h_{eff} ($W/m^2 \cdot K$) (a)	h_{eff} ($W/m^2 \cdot K$) (b)	h_{eff} ($W/m^2 \cdot K$) (c)	Ratio (a)/(b)	Ratio (a)/(c)	$q"_{1p}$ (kW/m^2) (d)	$q"_{2p}$ (kW/m^2) (e)	Ratio (d)/(e)	$q"_{1p}$ (kW/m^2) (f)	$q"_{2p}$ (kW/m^2) (g)	Ratio (f)/(g)
1.855E+02	12927	8816	8816	1.466	1.466	0	0	0	0	0	0
3.371E+02	14008	8963	8963	1.563	1.563	0	0	0	0	0	0
5.343E+02	14697	9207	9207	1.596	1.596	0	0	0	0	0	0
7.669E+02	14899	9524	7559	1.564	1.971	763.2516	3.6336	210.0565	0	0	0

1.040E+03	15139	11586	10253	1.307	1.476	878.0261	162.4141	5.4061	0	0	0
1.347E+03	16116	14329	13342	1.125	1.208	952.2292	395.1677	2.4097	846.1434	501.2536	1.6881
1.714E+03	19267	17734	17136	1.086	1.124	1018.032	695.5918	1.4635	936.5329	777.0905	1.2052
2.111E+03	23665	21537	21408	1.099	1.105	1073.808	1037.258	1.0352	976.8089	1134.258	0.8612
2.530E+03	29329	25647	26128	1.144	1.123	1127.95	1402.141	0.8044	985.8721	1544.219	0.6384
3.005E+03	36985	30478	31769	1.214	1.164	1172.132	1832.847	0.6395	965.5241	2039.455	0.4734
3.502E+03	45975	35715	38082	1.287	1.207	1217.542	2284.266	0.533	945.4614	2556.347	0.3698
3.826E+03	52297	39268	42475	1.332	1.231	1242.922	2582.865	0.4812	932.9377	2892.849	0.3225
4.051E+03	57167	41871	45710	1.365	1.251	1256.733	2794.26	0.4498	920.153	3130.841	0.2939
4.164E+03	59714	43234	47434	1.381	1.259	1263.305	2900.273	0.4356	914.3212	3249.257	0.2814
4.288E+03	62699	44678	49275	1.403	1.272	1272.186	3015.851	0.4218	906.2148	3381.823	0.268
4.410E+03	65601	46090	51096	1.423	1.284	1280.206	3129.428	0.4091	899.1364	3510.498	0.2561
4.536E+03	68281	47545	52987	1.436	1.289	1288.127	3248.041	0.3966	896.6381	3639.53	0.2464
4.659E+03	71128	48992	54889	1.452	1.296	1293.664	3365.042	0.3844	890.7436	3767.962	0.2364
4.773E+03	74206	50350	56694	1.474	1.309	1299.141	3473.883	0.374	881.189	3891.835	0.2264

Table F-5 Test _W_16_G_2500_11_09_2007_CHF

Experiment	Experiment	Chen's prediction	Klimenko's prediction	Exp/Pred	Exp/Pred	Chen's prediction			Experiment		
q" (kW/m^2)	h_{eff} ($W/m^2 \cdot K$) (a)	h_{eff} ($W/m^2 \cdot K$) (b)	h_{eff} ($W/m^2 \cdot K$) (c)	Ratio (a)/(b)	Ratio (a)/(c)	$q"_{1p}$ (kW/m^2) (d)	$q"_{2p}$ (kW/m^2) (e)	Ratio (d)/(e)	$q"_{1p}$ (kW/m^2) (f)	$q"_{2p}$ (kW/m^2) (g)	Ratio (f)/(g)
1.882E+02	13918	8851	8851	1.572	1.572	0	0	0	0	0	0
3.420E+02	14318	9058	9058	1.581	1.581	0	0	0	0	0	0
5.329E+02	14411	9311	9311	1.548	1.548	0	0	0	0	0	0
7.637E+02	14620	9611	7614	1.521	1.920	759.9426	3.7605	202.085	0	0	0
1.043E+03	15052	11745	10400	1.282	1.447	876.6466	166.7491	5.2573	0	0	0
1.360E+03	15567	14607	13623	1.066	1.143	953.2501	406.5205	2.3449	893.9842	465.7865	1.9193
1.726E+03	18428	18035	17462	1.022	1.055	1016.908	709.1454	1.434	994.7033	731.3496	1.3601
2.126E+03	22849	21889	21803	1.044	1.048	1071.689	1053.85	1.0169	1026.149	1099.39	0.9334
2.561E+03	28759	26171	26748	1.099	1.075	1125.587	1435.083	0.7843	1023.832	1536.838	0.6662
3.035E+03	36090	31036	32445	1.163	1.112	1170.034	1864.536	0.6275	1005.786	2028.784	0.4958
3.519E+03	44540	36157	38646	1.232	1.153	1214.796	2304.572	0.5271	985.7628	2533.605	0.3891
3.828E+03	51210	39597	42912	1.293	1.193	1236.802	2590.843	0.4774	955.9907	2871.654	0.3329
4.050E+03	56071	42167	46117	1.330	1.216	1250.694	2799.026	0.4468	940.2309	3109.489	0.3024

4.161E+03	58501	43512	47823	1.344	1.223	1258.244	2902.929	0.4334	935.5306	3225.642	0.29
4.278E+03	61059	44875	49568	1.361	1.232	1265.697	3012.502	0.4201	929.9042	3348.294	0.2777
4.386E+03	63619	46143	51207	1.379	1.242	1273.364	3112.482	0.4091	923.2639	3462.582	0.2666
4.511E+03	66693	47593	53090	1.401	1.256	1279.54	3231.596	0.3959	912.7772	3598.359	0.2537
4.640E+03	69965	49171	55175	1.423	1.268	1285.305	3354.323	0.3832	903.0012	3736.627	0.2417
4.759E+03	72927	50652	57156	1.440	1.276	1291.347	3467.389	0.3724	896.6053	3862.131	0.2322
4.877E+03	75923	52087	59096	1.458	1.285	1298.401	3578.566	0.3628	890.4611	3986.506	0.2234
5.006E+03	79910	53702	61309	1.488	1.303	1305.407	3700.85	0.3527	876.9646	4129.293	0.2124
5.135E+03	83931	55382	63591	1.515	1.320	1309.514	3825.952	0.3423	863.8169	4271.649	0.2022
5.265E+03	88627	57226	66126	1.549	1.340	1307.838	3957.469	0.3305	844.1985	4421.109	0.1909
5.401E+03	93645	59013	68587	1.587	1.365	1310.597	4090.401	0.3204	825.6582	4575.34	0.1805

Table F-6 Test _W_15_G_2500_11_08_2007_NBHT

Experiment	Experiment	Chen's prediction	Klimenko's prediction	Exp/Pred	Exp/Pred	Chen's prediction			Experiment		
q" (kW/m^2)	h_{eff} (W/m^2·K) (a)	h_{eff} (W/m^2·K) (b)	h_{eff} (W/m^2·K) (c)	Ratio (a)/(b)	Ratio (a)/(c)	$q"_{1p}$ (kW/m^2) (d)	$q"_{2p}$ (kW/m^2) (e)	Ratio (d)/(e)	$q"_{1p}$ (kW/m^2) (f)	$q"_{2p}$ (kW/m^2) (g)	Ratio (f)/(g)
1.838E+02	16162	10354	10354	1.561	1.561	0	0	0	0	0	0
3.287E+02	16970	10521	10521	1.613	1.613	0	0	0	0	0	0
5.254E+02	17703	10773	10773	1.643	1.643	0	0	0	0	0	0
7.564E+02	18014	11096	11096	1.624	1.624	0	0	0	0	0	0
1.026E+03	18448	11946	9870	1.544	1.869	980.965	44.7011	21.945	0	0	0
1.349E+03	19196	14502	12987	1.324	1.478	1097.477	251.3907	4.3656	0	0	0
1.711E+03	20133	17648	16555	1.141	1.216	1186.542	524.7848	2.261	1039.523	671.8042	1.5474
2.104E+03	25644	21125	20508	1.214	1.250	1262.023	841.9388	1.4989	1039.133	1064.829	0.9759
2.555E+03	28715	25206	25192	1.139	1.140	1331.45	1223.304	1.0884	1168.231	1386.522	0.8426
3.036E+03	35004	29662	30413	1.180	1.151	1395.415	1640.51	0.8506	1182.033	1853.892	0.6376
3.548E+03	42564	34503	36188	1.234	1.176	1454.482	2093.418	0.6948	1178.597	2369.303	0.4974
3.889E+03	48244	37825	40283	1.275	1.198	1494.437	2394.528	0.6241	1171.259	2717.706	0.431
4.122E+03	52356	40205	43206	1.302	1.212	1517.649	2604.407	0.5827	1165.029	2957.026	0.394
4.237E+03	54271	41412	44713	1.311	1.214	1526.355	2710.367	0.5632	1164.332	3072.39	0.379
4.356E+03	56464	42612	46214	1.325	1.222	1536.739	2819.031	0.5451	1159.366	3196.404	0.3627
4.444E+03	56936	43603	47480	1.306	1.199	1540.605	2903.872	0.5305	1179.451	3265.027	0.3612
4.558E+03	59084	44701	48874	1.322	1.209	1549.638	3008.111	0.5152	1172.035	3385.714	0.3462

4.673E+03	61417	45853	50348	1.339	1.220	1560.892	3112.11	0.5016	1164.974	3508.028	0.3321
4.787E+03	63838	46971	51787	1.359	1.233	1575.748	3211.496	0.4907	1159.053	3628.191	0.3195
4.910E+03	66483	48226	53428	1.379	1.244	1586.781	3323.696	0.4774	1150.674	3759.802	0.306
5.035E+03	68571	49496	55107	1.385	1.244	1598.152	3436.699	0.465	1153.216	3881.635	0.2971

Table F-7 Test _W_18_G_2500_11_15_2007

Experiment	Experiment	Chen's prediction	Klimenko's prediction	Exp/Pred	Exp/Pred	Chen's prediction			Experiment		
q" (kW/m^2)	h_{eff} ($W/m^2 \cdot K$) (a)	h_{eff} ($W/m^2 \cdot K$) (b)	h_{eff} ($W/m^2 \cdot K$) (c)	Ratio (a)/(b)	Ratio (a)/(c)	$q"_{1p}$ (kW/m^2) (d)	$q"_{2p}$ (kW/m^2) (e)	Ratio (d)/(e)	$q"_{1p}$ (kW/m^2) (f)	$q"_{2p}$ (kW/m^2) (g)	Ratio (f)/(g)
1.652E+02	13322	10227	10227	1.303	1.303	0	0	0	0	0	0
2.940E+02	14134	10319	10319	1.370	1.370	0	0	0	0	0	0
4.640E+02	15365	10526	10526	1.460	1.460	0	0	0	0	0	0
6.764E+02	16035	10824	10824	1.481	1.481	0	0	0	0	0	0
9.358E+02	16634	11294	8951	1.473	1.858	927.7548	8.0554	115.1724	0	0	0
1.247E+03	17602	13532	11919	1.301	1.477	1062.552	184.6178	5.7554	0	0	0
1.607E+03	18590	16612	15427	1.119	1.205	1159.724	447.7288	2.5902	1035.761	571.691	1.8118
1.992E+03	23939	20022	19287	1.196	1.241	1240.499	751.9463	1.6497	1037.009	955.4362	1.0854
2.421E+03	26361	23912	23710	1.102	1.112	1308.506	1112.698	1.176	1186.425	1234.778	0.9608
2.899E+03	29674	28295	28829	1.049	1.029	1379.949	1518.59	0.9087	1315.296	1583.242	0.8308
3.411E+03	34651	33192	34623	1.044	1.001	1440.88	1969.963	0.7314	1379.688	2031.154	0.6793
3.733E+03	38364	36397	38542	1.054	0.995	1476.079	2256.767	0.6541	1399.88	2332.966	0.6
3.957E+03	40850	38683	41381	1.056	0.987	1500.66	2456.466	0.6109	1420.584	2536.543	0.56
4.076E+03	42213	39955	42948	1.057	0.983	1516.82	2559.15	0.5927	1435.206	2640.764	0.5435
4.192E+03	43703	41146	44428	1.062	0.984	1529.449	2663.029	0.5743	1439.516	2752.961	0.5229
4.312E+03	45727	42338	45917	1.080	0.996	1541.194	2770.466	0.5563	1426.539	2885.122	0.4944
4.432E+03	47401	43526	47419	1.089	1.000	1548.54	2883.149	0.5371	1421.502	3010.187	0.4722
4.558E+03	50604	44782	49010	1.130	1.033	1559.186	2999.208	0.5199	1379.341	3179.053	0.4339
4.689E+03	52634	46003	50571	1.144	1.041	1570.995	3117.624	0.5039	1372.619	3316	0.4139
4.813E+03	50694	47178	52109	1.075	0.973	1580.223	3233.244	0.4887	1470.166	3343.3	0.4397
4.937E+03	52941	48483	53824	1.092	0.984	1590.952	3346.157	0.4755	1456.514	3480.595	0.4185
5.067E+03	55315	49805	55576	1.111	0.995	1604.318	3462.202	0.4634	1444.062	3622.457	0.3986
5.198E+03	57819	51105	57313	1.131	1.009	1618.487	3579.198	0.4522	1430.119	3767.566	0.3796

Table F-8 Test _AL_pt_001v_01_G_1500_05_24_2007

Experiment	Experiment	Chen's prediction	Klimenko's prediction	Exp/Pred	Exp/Pred	Chen's prediction			Experiment		
q" (kW/m^2)	h_{eff} (W/m^2·K) (a)	h_{eff} (W/m^2·K) (b)	h_{eff} (W/m^2·K) (c)	Ratio (a)/(b)	Ratio (a)/(c)	$q"_{1p}$ (kW/m^2) (d)	$q"_{2p}$ (kW/m^2) (e)	Ratio (d)/(e)	$q"_{1p}$ (kW/m^2) (f)	$q"_{2p}$ (kW/m^2) (g)	Ratio (f)/(g)
1.600E+02	7085	6859	6859	1.033	1.033	0	0	0.000	0.0	0.0	0.000
2.843E+02	7250	6965	6965	1.041	1.041	0	0	0.000	0.0	0.0	0.000
4.526E+02	7638	7167	7167	1.066	1.066	0	0	0.000	0.0	0.0	0.000
6.660E+02	8008	7808	6610	1.026	1.212	635	31	20.439	618.8	47.3	13.091
9.302E+02	9235	10147	9287	0.910	0.994	709	221	3.200	778.2	152.0	5.120
1.234E+03	12454	13073	12464	0.953	0.999	765	469	1.630	802.2	431.4	1.859
1.578E+03	15208	16515	16246	0.921	0.936	812	766	1.061	881.8	696.3	1.266
1.956E+03	18830	20480	20650	0.919	0.912	854	1102	0.775	928.0	1027.7	0.903
2.376E+03	24754	25060	25890	0.988	0.956	891	1485	0.600	901.2	1474.4	0.611
2.838E+03	31964	30453	32186	1.050	0.993	924	1914	0.483	879.7	1958.4	0.449
3.409E+03	43251	37451	40696	1.155	1.063	958	2451	0.391	829.4	2579.6	0.322
3.587E+03	50808	40119	44065	1.266	1.153	965	2622	0.368	762.0	2825.4	0.270
3.717E+03	52786	42157	46650	1.252	1.132	964	2752	0.351	770.0	2946.5	0.261
3.847E+03	53762	44075	49109	1.220	1.095	969	2879	0.337	794.0	3053.5	0.260
3.983E+03	55118	46110	51763	1.195	1.065	971	3012	0.322	811.9	3170.7	0.256
4.106E+03	55351	48004	54278	1.153	1.020	973	3133	0.311	843.4	3262.8	0.259
4.236E+03	56924	49982	56935	1.139	1.000	977	3259	0.300	857.3	3378.5	0.254
4.354E+03	68360	51859	59447	1.318	1.150	979	3376	0.290	742.1	3612.2	0.205
4.459E+03	80938	53530	61716	1.512	1.311	980	3479	0.282	648.0	3811.2	0.170
4.518E+03	81763	54472	63031	1.501	1.297	983	3535	0.278	654.6	3863.8	0.169
4.578E+03	83074	55601	64636	1.494	1.285	979	3598	0.272	655.3	3922.3	0.167
4.636E+03	86264	56635	66107	1.523	1.305	979	3657	0.268	642.7	3993.3	0.161
4.695E+03	89766	57659	67576	1.557	1.328	980	3715	0.264	629.1	4065.7	0.155
4.748E+03	91194	58478	68749	1.559	1.326	980	3768	0.260	628.4	4119.7	0.153

Table F-9 Test _AL_pt_001v_02_G_1500_05_25_2007

Experiment	Experiment	Chen's prediction	Klimenko's prediction	Exp/Pred	Exp/Pred	Chen's prediction			Experiment		
q" (kW/m^2)	h_{eff} (W/m^2·K) (a)	h_{eff} (W/m^2·K) (b)	h_{eff} (W/m^2·K) (c)	Ratio (a)/(b)	Ratio (a)/(c)	$q"_{1p}$ (kW/m^2) (d)	$q"_{2p}$ (kW/m^2) (e)	Ratio (d)/(e)	$q"_{1p}$ (kW/m^2) (f)	$q"_{2p}$ (kW/m^2) (g)	Ratio (f)/(g)
1.598E+02	7048	6792	6792	1.038	1.038	0	0	0	0	0	0
2.867E+02	7408	6938	6938	1.068	1.068	0	0	0	0	0	0
4.553E+02	7704	7146	7146	1.078	1.078	0	0	0	0	0	0
6.689E+02	8493	7816	6639	1.087	1.279	634.392	34.4662	18.4062	0	0	0
9.254E+02	9844	10089	9233	0.976	1.066	705.0588	220.3559	3.1996	722.1118	203.3029	3.5519
1.222E+03	11944	12931	12324	0.924	0.969	759.8121	462.1837	1.644	822.1726	399.8232	2.0563
1.564E+03	15984	16325	16045	0.979	0.996	807.5803	756.5941	1.0674	824.3659	739.8085	1.1143
1.938E+03	20538	20212	20356	1.016	1.009	846.9126	1090.715	0.7765	833.0787	1104.549	0.7542
2.350E+03	26065	24664	25439	1.057	1.025	882.2145	1467.915	0.601	834.4058	1515.723	0.5505
2.820E+03	34385	30039	31690	1.145	1.085	917.4509	1902.39	0.4823	801.1511	2018.69	0.3969
3.341E+03	42817	36359	39330	1.178	1.089	947.8858	2393.257	0.3961	804.5758	2536.567	0.3172
3.582E+03	45820	39578	43380	1.158	1.056	962.5103	2619.321	0.3675	831.0606	2750.771	0.3021
3.823E+03	52294	42856	47479	1.220	1.101	972.1605	2850.851	0.341	796.4059	3026.606	0.2631
4.074E+03	56502	46333	51948	1.219	1.088	980.9315	3092.604	0.3172	804.0826	3269.453	0.2459
4.208E+03	57593	48354	54618	1.191	1.054	984.4598	3223.546	0.3054	826.2152	3381.79	0.2443
4.338E+03	62243	50283	57189	1.238	1.088	988.4287	3349.861	0.2951	798.1928	3540.097	0.2255
4.480E+03	69634	52304	59897	1.331	1.163	993.3231	3487.081	0.2849	745.8274	3734.577	0.1997

Table F-10 Test _AL_pt_001v_05_G_2000_11_20_2007

Experiment	Experiment	Chen's prediction	Klimenko's prediction	Exp/Pred	Exp/Pred	Chen's prediction			Experiment		
q" (kW/m^2)	h_{eff} (W/m^2·K) (a)	h_{eff} (W/m^2·K) (b)	h_{eff} (W/m^2·K) (c)	Ratio (a)/(b)	Ratio (a)/(c)	$q"_{1p}$ (kW/m^2) (d)	$q"_{2p}$ (kW/m^2) (e)	Ratio (d)/(e)	$q"_{1p}$ (kW/m^2) (f)	$q"_{2p}$ (kW/m^2) (g)	Ratio (f)/(g)
1.778E+02	11924	8834	8834	1.350	1.350	0	0	0	0	0	0
3.160E+02	12593	9022	9022	1.396	1.396	0	0	0	0	0	0
4.983E+02	13076	9261	9261	1.412	1.412	0	0	0	0	0	0
7.281E+02	13564	9508	9508	1.427	1.427	0	0	0	0	0	0
1.008E+03	14126	11377	9988	1.242	1.414	868.3153	139.1856	6.2385	0	0	0

1.313E+03	14419	14093	13067	1.023	1.104	945.8947	366.8094	2.5787	923.9595	388.7446	2.3768
1.672E+03	17053	17427	16780	0.979	1.016	1012.205	659.3146	1.5352	1033.868	637.6512	1.6214
2.072E+03	20752	21244	21079	0.977	0.984	1068.68	1003.29	1.0652	1093.485	978.485	1.1175
2.514E+03	25906	25561	26036	1.013	0.995	1126.854	1387.354	0.8122	1111.379	1402.83	0.7922
3.000E+03	32245	30487	31796	1.058	1.014	1173.146	1827.153	0.6421	1108.761	1891.538	0.5862
3.495E+03	39874	35665	38039	1.118	1.048	1220.126	2274.984	0.5363	1090.905	2404.205	0.4537
3.857E+03	46792	39646	42965	1.180	1.089	1244.63	2612.532	0.4764	1054.182	2802.98	0.3761
4.092E+03	51069	42372	46369	1.205	1.101	1258.284	2833.503	0.4441	1043.647	3048.139	0.3424
4.205E+03	52945	43741	48109	1.210	1.101	1265.44	2940.039	0.4304	1045.09	3160.389	0.3307
4.326E+03	54332	45138	49902	1.204	1.089	1274.135	3051.833	0.4175	1058.157	3267.811	0.3238
4.445E+03	55314	46526	51707	1.189	1.070	1282.265	3162.524	0.4055	1078.16	3366.63	0.3202
4.566E+03	57748	47942	53555	1.205	1.078	1288.497	3277.437	0.3931	1069.351	3496.583	0.3058
4.680E+03	58957	49290	55337	1.196	1.065	1294.446	3385.67	0.3823	1081.815	3598.301	0.3006
4.803E+03	61089	50748	57284	1.204	1.066	1300.854	3502.518	0.3714	1080.279	3723.093	0.2902
4.928E+03	64192	52232	59285	1.229	1.083	1308.023	3619.824	0.3613	1063.965	3863.881	0.2754
5.056E+03	68182	53763	61372	1.268	1.111	1315.11	3740.41	0.3516	1036.665	4018.855	0.258
5.184E+03	73128	55381	63538	1.320	1.151	1320.771	3862.734	0.3419	999.9259	4183.579	0.239
5.314E+03	77802	57053	65807	1.364	1.182	1326.332	3987.962	0.3326	972.314	4341.981	0.2239
5.446E+03	82268	58731	68115	1.401	1.208	1332.966	4113.012	0.3241	951.3028	4494.675	0.2117
5.571E+03	86801	60384	70408	1.437	1.233	1335.127	4235.809	0.3152	928.5023	4642.434	0.2
5.707E+03	91359	62221	72994	1.468	1.252	1336.768	4370.045	0.3059	910.1422	4796.671	0.1897
5.840E+03	96778	63992	75516	1.512	1.282	1340.605	4499.255	0.298	886.1734	4953.687	0.1789
5.977E+03	102746	65873	78238	1.560	1.313	1343.285	4633.444	0.2899	860.9566	5115.773	0.1683
6.113E+03	108956	67737	80967	1.609	1.346	1345.305	4767.891	0.2822	836.1053	5277.091	0.1584

Table F-11 Test _AL_pt_001v_06_G_2000_11_21_2007

Experiment	Experiment	Chen's prediction	Klimenko's prediction	Exp/Pred	Exp/Pred	Chen's prediction			Experiment		
q" (kW/m^2)	h_{eff} (W/m^2·K) (a)	h_{eff} (W/m^2·K) (b)	h_{eff} (W/m^2·K) (c)	Ratio (a)/(b)	Ratio (a)/(c)	$q"_{1p}$ (kW/m^2) (d)	$q"_{2p}$ (kW/m^2) (e)	Ratio (d)/(e)	$q"_{1p}$ (kW/m^2) (f)	$q"_{2p}$ (kW/m^2) (g)	Ratio (f)/(g)
1.585E+02	11220	8520	8520	1.317	1.317	0	0	0	0	0	0
2.818E+02	11606	8656	8656	1.341	1.341	0	0	0	0	0	0
4.449E+02	11992	8849	8849	1.355	1.355	0	0	0	0	0	0
6.502E+02	12357	9112	9112	1.356	1.356	0	0	0	0	0	0

9.000E+02	12932	10186	8701	1.270	1.486	832.447	67.5668	12.3203	0	0	0
1.198E+03	13320	12713	11618	1.048	1.147	918.0997	279.9976	3.279	875.7594	322.3379	2.7169
1.544E+03	14330	15863	15103	0.903	0.949	987.8823	556.4658	1.7753	1092.992	451.3558	2.4216
1.915E+03	16740	19334	18988	0.866	0.882	1047.402	868.0145	1.2067	1209.155	706.2612	1.7121
2.324E+03	23455	23268	23412	1.008	1.002	1099.799	1224.32	0.8983	1090.551	1233.567	0.8841
2.767E+03	29939	27611	28433	1.084	1.053	1153.095	1613.464	0.7147	1062.998	1703.561	0.624
3.245E+03	36919	32502	34182	1.136	1.080	1195.725	2049.107	0.5835	1052.256	2192.576	0.4799
3.556E+03	41847	35821	38210	1.168	1.095	1224.68	2330.847	0.5254	1047.917	2507.61	0.4179
3.772E+03	45324	38179	41130	1.187	1.102	1243.226	2529.09	0.4916	1046.883	2725.433	0.3841
3.886E+03	46876	39475	42718	1.187	1.097	1251.577	2634.23	0.4751	1053.611	2832.196	0.372
4.001E+03	48631	40778	44330	1.193	1.097	1257.851	2742.962	0.4586	1054.376	2946.437	0.3578
4.119E+03	50408	42112	45995	1.197	1.096	1265.784	2853.009	0.4437	1057.115	3061.678	0.3453
4.236E+03	52204	43446	47677	1.202	1.095	1272.718	2963.535	0.4295	1058.819	3177.434	0.3332
4.354E+03	54596	44783	49378	1.219	1.106	1280.5	3073.896	0.4166	1049.986	3304.409	0.3178
4.478E+03	57294	46204	51206	1.240	1.119	1288.654	3189.305	0.4041	1038.863	3439.096	0.3021
4.587E+03	59507	47478	52865	1.253	1.126	1295.528	3291.946	0.3935	1033.304	3554.17	0.2907
4.716E+03	61416	48970	54823	1.254	1.120	1302.302	3413.891	0.3815	1038.036	3678.158	0.2822
4.834E+03	63454	50368	56680	1.260	1.120	1307.653	3525.873	0.3709	1037.628	3795.898	0.2734
4.969E+03	66804	51979	58840	1.285	1.135	1314.732	3654.414	0.3598	1022.628	3946.518	0.2591
5.102E+03	71929	53593	61019	1.342	1.179	1321.66	3780.835	0.3496	984.4396	4118.055	0.2391
5.236E+03	77568	55388	63425	1.400	1.223	1320.518	3915.228	0.3373	942.6453	4293.101	0.2196
5.368E+03	83393	57111	65756	1.460	1.268	1323.563	4044.183	0.3273	906.1447	4461.601	0.2031
5.504E+03	89015	58832	68110	1.513	1.307	1330.323	4173.979	0.3187	878.9768	4625.325	0.19
5.640E+03	94489	60542	70470	1.561	1.341	1335.299	4304.707	0.3102	855.2971	4784.709	0.1788
5.781E+03	100171	62350	72993	1.607	1.372	1339.101	4441.898	0.3015	833.2554	4947.744	0.1684
5.915E+03	106199	64122	75499	1.656	1.407	1341.456	4573.885	0.2933	809.7104	5105.631	0.1586
6.057E+03	112514	65970	78150	1.706	1.440	1345.78	4710.832	0.2857	788.8307	5267.781	0.1497
6.195E+03	120919	67917	80992	1.780	1.493	1345.901	4849.52	0.2775	755.7298	5439.691	0.1389

Table F-12 Test _AL_pt_001v_03_G_2500_11_16_2007

Experiment	Experiment	Chen's prediction	Klimenko's prediction	Exp/Pred	Exp/Pred	Chen's prediction			Experiment		
q" (kW/m^2)	h_{eff} (W/m^2·K) (a)	h_{eff} (W/m^2·K) (b)	h_{eff} (W/m^2·K) (c)	Ratio (a)/(b)	Ratio (a)/(c)	$q"_{1p}$ (kW/m^2) (d)	$q"_{2p}$ (kW/m^2) (e)	Ratio (d)/(e)	$q"_{1p}$ (kW/m^2) (f)	$q"_{2p}$ (kW/m^2) (g)	Ratio (f)/(g)
1.679E+02	14691	10488	10488	1.401	1.401	0	0	0	0	0	0
2.975E+02	15405	10673	10673	1.443	1.443	0	0	0	0	0	0
4.676E+02	15996	10920	10920	1.465	1.465	0	0	0	0	0	0
6.789E+02	16554	11218	11218	1.476	1.476	0	0	0	0	0	0
9.345E+02	17192	11595	9138	1.483	1.881	926.4953	8.0148	115.5975	0	0	0
1.239E+03	18001	13790	12088	1.305	1.489	1061.982	176.6951	6.0103	0	0	0
1.590E+03	19082	16801	15553	1.136	1.227	1159.132	431.149	2.6885	1020.013	570.2674	1.7887
1.973E+03	25651	20174	19398	1.271	1.322	1238.87	733.7373	1.6884	973.8529	998.7548	0.9751
2.389E+03	32083	23971	23723	1.338	1.352	1305.473	1083.237	1.2052	974.9722	1413.738	0.6896
2.860E+03	34459	28303	28805	1.218	1.196	1377.142	1483.218	0.9285	1130.682	1729.678	0.6537
3.385E+03	39942	33292	34718	1.200	1.150	1439.105	1945.915	0.7396	1199.059	2185.961	0.5485
3.712E+03	44515	36487	38626	1.220	1.152	1478.321	2233.432	0.6619	1211.258	2500.495	0.4844
3.941E+03	48637	38789	41482	1.254	1.172	1506.995	2433.885	0.6192	1201.448	2739.432	0.4386
4.060E+03	50863	40054	43044	1.270	1.182	1521.536	2538.643	0.5993	1197.81	2862.369	0.4185
4.182E+03	52970	41349	44664	1.281	1.186	1526.554	2655.299	0.5749	1191.242	2990.611	0.3983
4.302E+03	55400	42613	46260	1.300	1.198	1530.668	2770.902	0.5524	1176.987	3124.583	0.3767
4.422E+03	57193	43869	47856	1.304	1.195	1540.167	2882.174	0.5344	1180.988	3241.353	0.3644
4.550E+03	59571	45175	49527	1.319	1.203	1551.616	2997.953	0.5176	1176.275	3373.294	0.3487
4.676E+03	61840	46484	51223	1.330	1.207	1563.229	3112.868	0.5022	1174.686	3501.411	0.3355
4.804E+03	64260	47816	52968	1.344	1.213	1574.376	3229.167	0.4875	1171.122	3632.42	0.3224
4.929E+03	66712	49096	54659	1.359	1.221	1586.343	3342.847	0.4745	1167.069	3762.12	0.3102
5.061E+03	69079	50439	56455	1.370	1.224	1598.806	3462.688	0.4617	1167.024	3894.47	0.2997
5.189E+03	70732	51759	58243	1.367	1.214	1610.244	3578.936	0.4499	1177.971	4011.209	0.2937
5.322E+03	72709	53183	60124	1.367	1.209	1618.971	3703.312	0.4372	1183.865	4138.418	0.2861
5.454E+03	75311	54709	62173	1.377	1.211	1618.595	3835.167	0.422	1175.483	4278.279	0.2748
5.601E+03	79383	56391	64450	1.408	1.232	1623.32	3977.306	0.4081	1152.835	4447.791	0.2592
5.744E+03	84048	57983	66623	1.450	1.262	1632.774	4111.468	0.3971	1126.096	4618.146	0.2438
5.884E+03	89021	59560	68808	1.495	1.294	1643.609	4240.518	0.3876	1099.354	4784.772	0.2298
6.027E+03	94763	61205	71123	1.548	1.332	1653.233	4373.326	0.378	1067.492	4959.066	0.2153
6.172E+03	100815	62883	73516	1.603	1.371	1663.031	4509.18	0.3688	1037.024	5135.187	0.2019

6.329E+03	107735	64798	76301	1.663	1.412	1665.934	4662.803	0.3573	1001.714	5327.023	0.188
6.477E+03	116424	66702	79088	1.745	1.472	1662.163	4814.494	0.3452	952.0176	5524.639	0.1723
6.633E+03	124840	68509	81754	1.822	1.527	1668.677	4964.802	0.3361	915.4766	5718.002	0.1601
6.785E+03	132545	70340	84459	1.884	1.569	1675.305	5109.664	0.3279	888.8297	5896.139	0.1507
6.931E+03	138457	72082	87015	1.921	1.591	1680.653	5250.526	0.3201	874.7371	6056.441	0.1444

Table F-13 Test _AL_pt_001v_04_G_2500_11_17_2007

Experiment	Experiment	Chen's prediction	Klimenko's prediction	Exp/Pred	Exp/Pred	Chen's prediction			Experiment		
q" (kW/m^2)	h_{eff} ($W/m^2 \cdot K$) (a)	h_{eff} ($W/m^2 \cdot K$) (b)	h_{eff} ($W/m^2 \cdot K$) (c)	Ratio (a)/(b)	Ratio (a)/(c)	$q"_{1p}$ (kW/m^2) (d)	$q"_{2p}$ (kW/m^2) (e)	Ratio (d)/(e)	$q"_{1p}$ (kW/m^2) (f)	$q"_{2p}$ (kW/m^2) (g)	Ratio (f)/(g)
1.576E+02	13664	10606	10606	1.288	1.288	0	0	0	0	0	0
2.800E+02	14732	10510	10510	1.402	1.402	0	0	0	0	0	0
4.412E+02	15526	10681	10681	1.454	1.454	0	0	0	0	0	0
6.434E+02	16099	10924	10924	1.474	1.474	0	0	0	0	0	0
8.888E+02	16710	11233	11233	1.488	1.488	0	0	0	0	0	0
1.179E+03	17371	13058	11315	1.330	1.535	1042.894	136.5702	7.6363	0	0	0
1.519E+03	18164	15888	14599	1.143	1.244	1140.729	378.4053	3.0146	997.3152	521.8187	1.9112
1.903E+03	21144	19248	18393	1.099	1.150	1226.14	676.4454	1.8126	1115.634	786.9516	1.4177
2.320E+03	26082	22989	22642	1.135	1.152	1295.621	1023.913	1.2654	1141.495	1178.039	0.969
2.766E+03	29914	27032	27344	1.107	1.094	1362.645	1403.347	0.971	1230.835	1535.156	0.8018
3.270E+03	34670	31744	32874	1.092	1.055	1429.175	1840.903	0.7763	1308.084	1961.995	0.6667
3.593E+03	39134	34868	36639	1.122	1.068	1465.351	2127.276	0.6888	1305.163	2287.464	0.5706
3.813E+03	42444	37017	39284	1.147	1.080	1490.519	2321.997	0.6419	1299.457	2513.059	0.5171
4.039E+03	45488	39229	42009	1.160	1.083	1514.713	2523.91	0.6001	1305.894	2732.729	0.4779
4.270E+03	48545	41530	44858	1.169	1.082	1539.119	2731.351	0.5635	1316.265	2954.205	0.4456
4.501E+03	51671	43830	47753	1.179	1.082	1557.661	2943.065	0.5293	1320.863	3179.863	0.4154
4.631E+03	55347	45185	49478	1.225	1.119	1568.822	3061.822	0.5124	1280.361	3350.284	0.3822
4.755E+03	57641	46459	51121	1.241	1.128	1578.9	3176.064	0.4971	1272.187	3482.778	0.3653
4.889E+03	59404	47819	52894	1.242	1.123	1591.699	3297.566	0.4827	1280.889	3608.377	0.355
5.009E+03	61298	49047	54513	1.250	1.124	1602.887	3406.167	0.4706	1282.146	3726.909	0.344
5.150E+03	64051	50499	56449	1.268	1.135	1614.766	3535.13	0.4568	1272.736	3877.16	0.3283
5.262E+03	65572	51746	58124	1.267	1.128	1617.739	3644.394	0.4439	1276.272	3985.861	0.3202
5.392E+03	66852	53104	59917	1.259	1.116	1628.776	3763.666	0.4328	1293.467	4098.975	0.3156

5.544E+03	69809	54696	62029	1.276	1.125	1639.83	3904.168	0.42	1284.478	4259.519	0.3016
5.691E+03	73391	56275	64145	1.304	1.144	1649.878	4041.249	0.4083	1264.752	4426.375	0.2857
5.846E+03	78830	58144	66701	1.356	1.182	1646.44	4199.967	0.392	1214.039	4632.368	0.2621
5.971E+03	83695	59735	68914	1.401	1.214	1640.811	4330.633	0.3789	1170.751	4800.693	0.2439
6.119E+03	88724	61411	71257	1.445	1.245	1647.465	4471.395	0.3684	1139.994	4978.865	0.229
6.271E+03	93648	63094	73637	1.484	1.272	1657.766	4613.013	0.3594	1116.586	5154.193	0.2166
6.426E+03	98731	64877	76205	1.522	1.296	1666.122	4759.544	0.3501	1094.514	5331.152	0.2053
6.573E+03	103823	66557	78658	1.560	1.320	1675.025	4897.997	0.342	1073.493	5499.53	0.1952
6.723E+03	108599	68262	81163	1.591	1.338	1682.87	5039.762	0.3339	1057.501	5665.131	0.1867

Table F-14 Test _AL_pt_01v_01_G_1500_06_01_2007

Experiment	Experiment	Chen's prediction	Klimenko's prediction	Exp/Pred	Exp/Pred	Chen's prediction			Experiment		
q" (kW/m^2)	h_{eff} ($W/m^2 \cdot K$) (a)	h_{eff} ($W/m^2 \cdot K$) (b)	h_{eff} ($W/m^2 \cdot K$) (c)	Ratio (a)/(b)	Ratio (a)/(c)	$q"_{1p}$ (kW/m^2) (d)	$q"_{2p}$ (kW/m^2) (e)	Ratio (d)/(e)	$q"_{1p}$ (kW/m^2) (f)	$q"_{2p}$ (kW/m^2) (g)	Ratio (f)/(g)
1.507E+02	7225	6869	6869	1.052	1.052	0	0	0	0	0	0
2.751E+02	7713	7035	7035	1.096	1.096	0	0	0	0	0	0
4.386E+02	8001	7253	7253	1.103	1.103	0	0	0	0	0	0
6.458E+02	8278	7737	6456	1.070	1.282	626.6384	19.1951	32.6458	0	0	0
9.031E+02	10611	9974	9066	1.064	1.170	705.0504	198.0142	3.5606	662.3201	240.7445	2.7511
1.197E+03	13578	12805	12149	1.060	1.118	761.6556	435.3965	1.7493	717.8986	479.1534	1.4983
1.535E+03	16863	16177	15847	1.042	1.064	809.2869	725.9122	1.1149	775.9327	759.2664	1.022
1.913E+03	21096	20103	20204	1.049	1.044	853.0537	1059.968	0.8048	812.5117	1100.51	0.7383
2.319E+03	25928	24512	25238	1.058	1.027	888.0176	1431.456	0.6204	839.1275	1480.346	0.5668
2.420E+03	26786	25759	26692	1.040	1.004	896.383	1523.393	0.5884	861.583	1558.193	0.5529
2.518E+03	27861	26929	28057	1.035	0.993	904.0973	1613.574	0.5603	873.4712	1644.2	0.5312
2.609E+03	28790	28028	29335	1.027	0.981	909.9846	1699.102	0.5356	885.4966	1723.59	0.5138
2.703E+03	29742	29161	30663	1.020	0.970	916.3859	1786.586	0.5129	898.0918	1804.88	0.4976
2.802E+03	30880	30358	32079	1.017	0.963	922.6247	1879.56	0.4909	906.6228	1895.562	0.4783
2.899E+03	31641	31464	33399	1.006	0.947	927.5255	1971.68	0.4704	921.9244	1977.281	0.4663
2.998E+03	32347	32594	34758	0.992	0.931	933.37	2064.373	0.4521	940.0731	2057.67	0.4569
3.099E+03	33881	33780	36195	1.003	0.936	938.4329	2160.133	0.4344	935.2526	2163.314	0.4323
3.199E+03	35410	34923	37589	1.014	0.942	943.9962	2254.711	0.4187	930.6116	2268.095	0.4103
3.307E+03	37074	36211	39174	1.024	0.946	951.3395	2355.602	0.4039	928.779	2378.163	0.3905

3.419E+03	38527	37574	40874	1.025	0.943	958.6224	2459.918	0.3897	934.5294	2484.011	0.3762
3.532E+03	39695	38977	42644	1.018	0.931	966.5095	2565.536	0.3767	948.615	2583.431	0.3672
3.644E+03	40288	40432	44470	0.996	0.906	972.2594	2672.064	0.3639	975.3588	2668.965	0.3654
3.754E+03	41064	41916	46337	0.980	0.886	975.1195	2779.21	0.3509	994.9743	2759.356	0.3606
3.873E+03	41416	43503	48356	0.952	0.856	979.9449	2893.492	0.3387	1028.935	2844.502	0.3617
3.996E+03	43123	45165	50488	0.955	0.854	984.6181	3010.888	0.327	1030.825	2964.681	0.3477
4.117E+03	45590	46858	52686	0.973	0.865	988.8165	3127.875	0.3161	1015.929	3100.762	0.3276
4.236E+03	49979	48545	54894	1.030	0.910	992.8544	3242.896	0.3062	964.0008	3271.749	0.2946
4.369E+03	60812	50419	57350	1.206	1.060	998.931	3370.106	0.2964	827.8877	3541.15	0.2338
4.467E+03	66437	51928	59381	1.279	1.119	999.5748	3467.319	0.2883	780.9723	3685.921	0.2119
4.542E+03	69453	53071	60937	1.309	1.140	1000.989	3541.079	0.2827	764.579	3777.489	0.2024
4.622E+03	72846	54258	62564	1.343	1.164	1002.569	3619.215	0.277	746.4582	3875.326	0.1926
4.702E+03	76038	55455	64222	1.371	1.184	1004.834	3696.897	0.2718	732.5525	3969.178	0.1846
4.808E+03	78311	56982	66360	1.374	1.180	1009.237	3799.04	0.2657	734.074	4074.203	0.1802
4.886E+03	78284	58245	68169	1.344	1.148	1008.827	3877.009	0.2602	750.3066	4135.529	0.1814
4.985E+03	81909	59784	70313	1.370	1.165	1011.136	3974.258	0.2544	737.754	4247.64	0.1737

Table F-15 Test _AL_pt_01v_02_G_1500_06_05_2007

Experiment	Experiment	Chen's prediction	Klimenko's prediction	Exp/Pred	Exp/Pred	Chen's prediction			Experiment		
q" (kW/m^2)	h_{eff} (W/m^2·K) (a)	h_{eff} (W/m^2·K) (b)	h_{eff} (W/m^2·K) (c)	Ratio (a)/(b)	Ratio (a)/(c)	$q"_{1p}$ (kW/m^2) (d)	$q"_{2p}$ (kW/m^2) (e)	Ratio (d)/(e)	$q"_{1p}$ (kW/m^2) (f)	$q"_{2p}$ (kW/m^2) (g)	Ratio (f)/(g)
1.642E+02	7297	6718	6718	1.086	1.086	0	0	0	0	0	0
2.987E+02	7744	6901	6901	1.122	1.122	0	0	0	0	0	0
4.762E+02	7987	7129	7129	1.120	1.120	0	0	0	0	0	0
6.995E+02	7830	8012	6904	0.977	1.134	647.5203	51.9999	12.4523	662.1518	37.3684	17.7196
9.711E+02	8338	10450	9648	0.798	0.864	715.6783	255.4402	2.8017	896.4051	74.7135	11.9979
1.292E+03	10911	13532	12990	0.806	0.840	771.4591	520.0856	1.4833	956.2117	335.333	2.8515
1.649E+03	14189	17071	16899	0.831	0.840	818.0327	830.6663	0.9848	983.6791	665.0198	1.4792
2.019E+03	18182	20950	21205	0.868	0.857	855.488	1163.877	0.735	985.2084	1034.156	0.9527
2.451E+03	22692	25604	26560	0.886	0.854	891.7531	1559.329	0.5719	1005.694	1445.388	0.6958
2.564E+03	25291	26989	28152	0.937	0.898	900.2797	1663.491	0.5412	960.2733	1603.497	0.5989
2.667E+03	27034	28216	29572	0.958	0.914	907.8635	1758.779	0.5162	947.1625	1719.48	0.5508
2.764E+03	27843	29386	30945	0.948	0.900	914.4367	1849.822	0.4943	964.6855	1799.573	0.5361

2.869E+03	28583	30625	32411	0.933	0.882	922.6763	1946.547	0.474	988.1862	1881.037	0.5253
2.972E+03	29499	31918	33958	0.924	0.869	927.4994	2044.829	0.4536	1003.123	1969.205	0.5094
3.077E+03	30668	33258	35578	0.922	0.862	932.1827	2144.72	0.4346	1010.497	2066.406	0.489
3.188E+03	31577	34537	37135	0.914	0.850	939.3737	2248.226	0.4178	1026.996	2160.603	0.4753
3.293E+03	33157	35809	38696	0.926	0.857	945.7104	2347.449	0.4029	1020.943	2272.217	0.4493
3.405E+03	35521	37189	40402	0.955	0.879	953.4956	2451.673	0.3889	997.8377	2407.331	0.4145
3.516E+03	36638	38611	42195	0.949	0.868	959.8857	2555.908	0.3756	1011.149	2504.645	0.4037
3.635E+03	38568	40257	44262	0.958	0.871	966.9734	2667.735	0.3625	1008.916	2625.793	0.3842
3.748E+03	41356	41895	46317	0.987	0.893	969.3728	2778.28	0.3489	981.6143	2766.039	0.3549
3.865E+03	39800	43588	48495	0.913	0.821	972.3572	2892.66	0.3361	1064.471	2800.546	0.3801
3.981E+03	47353	45272	50631	1.046	0.935	975.6839	3005.43	0.3246	932.4613	3048.652	0.3059
4.106E+03	52479	47067	52956	1.115	0.991	980.563	3125.743	0.3137	879.1152	3227.191	0.2724
4.230E+03	57268	48887	55354	1.171	1.035	984.1342	3245.621	0.3032	839.7803	3389.974	0.2477
4.359E+03	62415	50789	57895	1.229	1.078	988.5499	3370.395	0.2933	804.1025	3554.842	0.2262
4.470E+03	67641	52471	60167	1.289	1.124	989.9158	3480.411	0.2844	767.6115	3702.715	0.2073
4.594E+03	75454	54354	62737	1.388	1.203	991.4382	3602.627	0.2752	713.9132	3880.152	0.184
4.677E+03	77340	55681	64593	1.389	1.197	992.1809	3685.134	0.2692	714.0499	3963.265	0.1802
4.772E+03	82326	57120	66608	1.441	1.236	994.0348	3777.646	0.2631	689.4161	4082.264	0.1689
4.842E+03	79947	58153	68091	1.375	1.174	997.2336	3844.397	0.2594	725.1002	4116.531	0.1761
4.901E+03	81421	59088	69420	1.378	1.173	998.3347	3903.062	0.2558	724.243	4177.154	0.1734
4.962E+03	82454	60030	70737	1.374	1.166	998.887	3962.754	0.2521	726.9722	4234.669	0.1717
5.026E+03	84123	61047	72167	1.378	1.166	999.509	4026.637	0.2482	725.0646	4301.081	0.1686
5.049E+03	82692	61460	72767	1.345	1.136	998.6847	4050.1	0.2466	741.9956	4306.789	0.1723

Table F-16 Test _AL_pt_01v_03_G_2000_06_11_2007

Experiment	Experiment	Chen's prediction	Klimenko's prediction	Exp/Pred	Exp/Pred	Chen's prediction			Experiment		
q'' (kW/m^2)	h_{eff} (W/m^2·K) (a)	h_{eff} (W/m^2·K) (b)	h_{eff} (W/m^2·K) (c)	Ratio (a)/(b)	Ratio (a)/(c)	q''_{1p} (kW/m^2) (d)	q''_{2p} (kW/m^2) (e)	Ratio (d)/(e)	q''_{1p} (kW/m^2) (f)	q''_{2p} (kW/m^2) (g)	Ratio (f)/(g)
1.506E+02	9707	8674	8674	1.119	1.119	0	0	0	0	0	0
2.803E+02	10841	8984	8984	1.207	1.207	0	0	0	0	0	0
4.525E+02	11511	9265	9265	1.242	1.242	0	0	0	0	0	0
6.712E+02	12171	9516	9516	1.279	1.279	0	0	0	0	0	0
9.342E+02	12948	10950	9432	1.183	1.373	839.8211	94.4272	8.8938	0	0	0

1.240E+03	14045	13734	12611	1.023	1.114	926.707	313.7281	2.9539	905.6276	334.8075	2.7049
1.587E+03	17396	17204	16451	1.011	1.057	991.7016	594.8164	1.6672	980.2543	606.2637	1.6169
1.967E+03	21789	21207	20952	1.027	1.040	1051.278	915.9452	1.1478	1022.693	944.5304	1.0828
2.390E+03	27301	25806	26263	1.058	1.040	1098.348	1291.856	0.8502	1037.72	1352.484	0.7673
2.847E+03	34743	31145	32609	1.116	1.065	1139.253	1707.418	0.6672	1020.842	1825.829	0.5591
3.364E+03	44702	37352	40274	1.197	1.110	1176.431	2187.941	0.5377	982.5779	2381.795	0.4125
3.491E+03	47302	39374	42895	1.201	1.103	1182.79	2308.144	0.5124	984.1196	2506.815	0.3926
3.611E+03	49380	41234	45337	1.198	1.089	1180.93	2430.38	0.4859	985.7387	2625.571	0.3754
3.730E+03	50714	42662	47166	1.189	1.075	1187.79	2542.431	0.4672	998.83	2731.391	0.3657
3.843E+03	51666	43828	48655	1.179	1.062	1193.936	2648.653	0.4508	1012.407	2830.183	0.3577
3.952E+03	52602	45060	50252	1.167	1.047	1200.765	2751.4	0.4364	1028.208	2923.958	0.3516
4.074E+03	54568	46567	52238	1.172	1.045	1208.286	2865.565	0.4217	1030.742	3043.109	0.3387
4.192E+03	56101	48053	54224	1.167	1.035	1214.593	2977.83	0.4079	1039.953	3152.469	0.3299
4.309E+03	58030	49438	56084	1.174	1.035	1221.327	3088.167	0.3955	1040.093	3269.4	0.3181
4.435E+03	61546	50928	58103	1.208	1.059	1228.49	3206.56	0.3831	1016.182	3418.868	0.2972
4.553E+03	67001	52408	60127	1.278	1.114	1233.295	3319.894	0.3715	964.3167	3588.872	0.2687
4.674E+03	70791	53412	61447	1.325	1.152	1249.897	3424.206	0.365	942.6964	3731.407	0.2526
4.795E+03	71293	54833	63437	1.300	1.124	1261.886	3532.761	0.3572	970.181	3824.466	0.2537
4.929E+03	80535	56575	65870	1.424	1.223	1265.97	3663.236	0.3456	889.0242	4040.181	0.22
5.067E+03	83933	56667	65692	1.481	1.278	1279.229	3787.353	0.3378	863.3876	4203.194	0.2054
5.177E+03	84799	56744	65577	1.494	1.293	1294.436	3882.421	0.3334	865.9076	4310.949	0.2009
5.300E+03	88522	57970	67207	1.527	1.317	1309.544	3989.974	0.3282	857.3013	4442.217	0.193
5.443E+03	95604	59831	69773	1.598	1.370	1313.355	4129.588	0.318	821.6698	4621.273	0.1778
5.582E+03	102193	61663	72338	1.657	1.413	1316.643	4265.285	0.3087	794.2164	4787.711	0.1659
5.716E+03	110371	63555	75041	1.737	1.471	1318.713	4396.809	0.2999	759.1187	4956.403	0.1532
5.840E+03	114625	65347	77646	1.754	1.476	1318.807	4521.574	0.2917	751.6061	5088.775	0.1477
5.938E+03	116411	66689	79606	1.746	1.462	1317.849	4620.121	0.2852	754.7193	5183.251	0.1456

Table F-17 Test _AL_pt_01v_05_G_2000_06_13_2007

Experiment	Experiment	Chen's prediction	Klimenko's prediction	Exp/Pred	Exp/Pred	Chen's prediction			Experiment		
q" (kW/m^2)	h_{eff} ($W/m^2 \cdot K$) (a)	h_{eff} ($W/m^2 \cdot K$) (b)	h_{eff} ($W/m^2 \cdot K$) (c)	Ratio (a)/(b)	Ratio (a)/(c)	$q"_{1p}$ (kW/m^2) (d)	$q"_{2p}$ (kW/m^2) (e)	Ratio (d)/(e)	$q"_{1p}$ (kW/m^2) (f)	$q"_{2p}$ (kW/m^2) (g)	Ratio (f)/(g)
1.570E+02	9838	8430	8430	1.167	1.167	0	0	0	0	0	0

2.782E+02	10094	8566	8566	1.178	1.178	0	0	0	0	0	0
4.420E+02	10466	8756	8756	1.195	1.195	0	0	0	0	0	0
6.240E+02	10488	8989	8989	1.167	1.167	0	0	0	0	0	0
9.023E+02	11294	10123	8664	1.116	1.304	833.572	68.6921	12.1349	746.6737	155.5904	4.799
1.207E+03	11502	12691	11627	0.906	0.989	919.6072	287.4204	3.1995	1014.064	192.9638	5.2552
1.558E+03	13763	15861	15128	0.868	0.910	988.6304	569.3181	1.7365	1138.682	419.2663	2.7159
1.946E+03	16297	19443	19130	0.838	0.852	1051.099	894.5214	1.175	1253.436	692.1846	1.8108
2.377E+03	22139	23563	23776	0.940	0.931	1104.665	1272.595	0.868	1175.216	1202.043	0.9777
2.838E+03	30751	28097	29001	1.094	1.060	1158.629	1679.82	0.6897	1058.196	1780.253	0.5944
3.348E+03	38704	33312	35152	1.162	1.101	1203.695	2144.663	0.5613	1035.623	2312.736	0.4478
3.473E+03	39975	34765	36915	1.150	1.083	1215.815	2257.615	0.5385	1056.942	2416.488	0.4374
3.592E+03	41095	36054	38498	1.140	1.067	1227.354	2364.589	0.5191	1076.369	2515.574	0.4279
3.708E+03	42309	37320	40069	1.134	1.056	1237.886	2470.355	0.5011	1091.474	2616.767	0.4171
3.827E+03	44089	38588	41625	1.143	1.059	1245.961	2581.18	0.4827	1090.102	2737.038	0.3983
3.942E+03	45839	39863	43190	1.150	1.061	1252.211	2690.168	0.4655	1088.593	2853.786	0.3815
4.060E+03	47640	41157	44789	1.158	1.064	1259.93	2799.585	0.45	1088.085	2971.43	0.3662
4.214E+03	50467	42881	46945	1.177	1.075	1268.878	2945.45	0.4308	1077.782	3136.546	0.3436
4.297E+03	51404	43844	48165	1.172	1.067	1275.209	3021.65	0.422	1087.286	3209.573	0.3388
4.416E+03	53801	45242	49951	1.189	1.077	1282.237	3134.239	0.4091	1077.881	3338.594	0.3229
4.535E+03	55523	46612	51722	1.191	1.073	1290.198	3244.867	0.3976	1082.764	3452.302	0.3136
4.659E+03	57033	48067	53627	1.187	1.064	1298.125	3360.709	0.3863	1093.674	3565.16	0.3068
4.791E+03	58946	49680	55761	1.187	1.057	1304.995	3486.388	0.3743	1099.491	3691.891	0.2978
4.920E+03	61454	51357	58017	1.197	1.059	1310.742	3609.148	0.3632	1095.017	3824.873	0.2863
5.049E+03	65007	52818	59978	1.231	1.084	1317.34	3731.388	0.353	1069.976	3978.751	0.2689
5.174E+03	71421	54363	62032	1.314	1.151	1322.478	3851.697	0.3433	1006.318	4167.857	0.2414
5.250E+03	76770	55288	63253	1.389	1.214	1326.497	3923.605	0.3381	955.0205	4295.081	0.2224
5.327E+03	81144	56223	64498	1.443	1.258	1329.113	3998.254	0.3324	920.6372	4406.729	0.2089
5.426E+03	85844	57463	66175	1.494	1.297	1333.617	4092.566	0.3259	892.4451	4533.738	0.1968
5.553E+03	92609	59105	68426	1.567	1.353	1339.296	4214.078	0.3178	854.514	4698.86	0.1819
5.622E+03	95100	60022	69704	1.584	1.364	1342.405	4279.714	0.3137	846.9993	4775.119	0.1774
5.681E+03	97529	60827	70829	1.603	1.377	1343.597	4337.867	0.3097	837.7226	4843.742	0.1729
5.788E+03	103125	62231	72790	1.657	1.417	1346.068	4442.231	0.303	812.042	4976.257	0.1632
5.875E+03	107116	63388	74426	1.690	1.439	1347.851	4526.875	0.2977	797.3781	5077.348	0.157
5.960E+03	111813	64530	76054	1.733	1.470	1350.36	4609.961	0.2929	779.0897	5181.232	0.1504
6.045E+03	116839	65676	77703	1.779	1.504	1352.418	4692.761	0.2882	759.9775	5285.201	0.1438
6.136E+03	123696	66947	79548	1.848	1.555	1353.33	4782.788	0.283	732.2273	5403.89	0.1355

6.229E+03	128460	68386	81692	1.878	1.572	1352.987	4876.508	0.2775	720.047	5509.448	0.1307

Table F-18 Test _AL_pt_01v_07_G_2500_06_15_2007

Experiment	Experiment	Chen's prediction	Klimenko's prediction	Exp/Pred	Exp/Pred	Chen's prediction			Experiment		
q" (kW/m^2)	h_{eff} (W/m^2·K) (a)	h_{eff} (W/m^2·K) (b)	h_{eff} (W/m^2·K) (c)	Ratio (a)/(b)	Ratio (a)/(c)	$q"_{1p}$ (kW/m^2) (d)	$q"_{2p}$ (kW/m^2) (e)	Ratio (d)/(e)	$q"_{1p}$ (kW/m^2) (f)	$q"_{2p}$ (kW/m^2) (g)	Ratio (f)/(g)
1.513E+02	10094	10003	10003	1.009	1.009	0	0	0	0	0	0
2.762E+02	11293	10172	10172	1.110	1.110	0	0	0	0	0	0
4.386E+02	12429	10379	10379	1.197	1.197	0	0	0	0	0	0
6.447E+02	13113	10659	10659	1.230	1.230	0	0	0	0	0	0
8.943E+02	13691	11020	8511	1.242	1.609	894.0099	0.2718	3288.678	0	0	0
1.195E+03	14490	13026	11366	1.112	1.275	1043.908	150.9017	6.9178	937.9264	256.883	3.6512
1.544E+03	15739	15987	14764	0.985	1.066	1140.394	403.4013	2.8269	1157.722	386.0735	2.9987
1.934E+03	21816	19431	18638	1.123	1.171	1224.949	708.8937	1.728	1090.463	843.3792	1.293
2.364E+03	24438	23332	23064	1.047	1.060	1296.204	1067.904	1.2138	1237.051	1127.057	1.0976
2.836E+03	29377	27661	28105	1.062	1.045	1366.938	1468.741	0.9307	1286.596	1549.083	0.8306
3.340E+03	35815	32488	33773	1.102	1.060	1429.925	1910.413	0.7485	1296.609	2043.729	0.6344
3.881E+03	44535	37720	40170	1.181	1.109	1490.066	2390.956	0.6232	1261.579	2619.443	0.4816
4.012E+03	48159	39213	42001	1.228	1.147	1505.947	2506.011	0.6009	1225.805	2786.153	0.44
4.135E+03	50933	40513	43607	1.257	1.168	1520.227	2614.319	0.5815	1208.826	2925.72	0.4132
4.256E+03	53191	41770	45172	1.273	1.178	1531.306	2725.018	0.5619	1202.124	3054.2	0.3936
4.380E+03	55674	43056	46789	1.293	1.190	1542.824	2837.252	0.5438	1192.775	3187.301	0.3742
4.499E+03	58310	44344	48435	1.315	1.204	1547.693	2951.712	0.5243	1176.634	3322.772	0.3541
4.631E+03	59663	45714	50201	1.305	1.188	1556.193	3074.67	0.5061	1191.985	3438.879	0.3466
4.765E+03	62272	47131	52043	1.321	1.197	1568.111	3197.385	0.4904	1186.454	3579.042	0.3315
4.894E+03	64880	48482	53821	1.338	1.205	1579.052	3315.044	0.4763	1179.572	3714.524	0.3176
5.022E+03	66615	49846	55642	1.336	1.197	1590.785	3431.21	0.4636	1189.954	3832.041	0.3105
5.164E+03	68886	51484	57875	1.338	1.190	1604.842	3558.691	0.451	1199.031	3964.502	0.3024
5.310E+03	72113	53241	60232	1.354	1.197	1614.247	3695.281	0.4368	1191.451	4118.077	0.2893
5.450E+03	75957	54856	62400	1.385	1.217	1622.047	3827.772	0.4238	1171.112	4278.707	0.2737
5.592E+03	80483	56358	64416	1.428	1.249	1630.591	3961.173	0.4116	1141.494	4450.27	0.2565
5.730E+03	86859	57777	66324	1.503	1.310	1638.165	4092.276	0.4003	1089.372	4641.069	0.2347
5.877E+03	94190	59452	68639	1.584	1.372	1647.333	4230.145	0.3894	1039.494	4837.984	0.2149

5.936E+03	99703	60410	70028	1.650	1.424	1649.796	4286.016	0.3849	999.3271	4936.485	0.2024
5.995E+03	105010	61207	71170	1.716	1.475	1653.047	4341.731	0.3807	963.2315	5031.547	0.1914
6.050E+03	107943	61745	71913	1.748	1.501	1656.932	4393.565	0.3771	947.5232	5102.973	0.1857
6.110E+03	110914	62277	72640	1.781	1.527	1661.322	4449.103	0.3734	932.5584	5177.866	0.1801
6.169E+03	112801	62814	73383	1.796	1.537	1666.226	4502.883	0.37	927.5971	5241.512	0.177
6.238E+03	116605	63756	74775	1.829	1.559	1671.762	4566.173	0.3661	913.8088	5324.125	0.1716
6.301E+03	119530	64611	76050	1.850	1.572	1676.154	4624.647	0.3624	905.7726	5395.028	0.1679
6.368E+03	121093	65327	77084	1.854	1.571	1680.485	4687.376	0.3585	906.3248	5461.537	0.1659
6.422E+03	121464	65994	78072	1.841	1.556	1682.319	4739.233	0.355	913.7799	5507.772	0.1659
6.487E+03	121359	66623	78977	1.822	1.537	1686.64	4800.165	0.3514	925.669	5561.136	0.1665
6.545E+03	119509	67187	79795	1.779	1.498	1689.887	4854.9	0.3481	949.7762	5595.011	0.1698
6.617E+03	121877	68465	81799	1.780	1.490	1691.558	4925.877	0.3434	949.9745	5667.461	0.1676
6.690E+03	123415	69635	83632	1.772	1.476	1693.258	4996.282	0.3389	955.1551	5734.385	0.1666
6.759E+03	123809	70582	85055	1.754	1.456	1694.112	5064.733	0.3345	965.5507	5793.295	0.1667
6.833E+03	124028	71269	86019	1.740	1.442	1697.268	5135.275	0.3305	975.0384	5857.504	0.1665
6.901E+03	126389	72042	87146	1.754	1.450	1698.786	5202.258	0.3265	968.0608	5932.983	0.1632
6.970E+03	126901	72877	88396	1.741	1.436	1700.51	5269.335	0.3227	976.3266	5993.518	0.1629
7.030E+03	128421	73803	89833	1.740	1.430	1697.981	5331.53	0.3185	975.5704	6053.941	0.1611
7.100E+03	132934	74904	91559	1.775	1.452	1697.616	5402.858	0.3142	956.3102	6144.164	0.1556
7.167E+03	136897	75973	93245	1.802	1.468	1693.271	5473.375	0.3094	939.4633	6227.183	0.1509

Table F-19 Test _Al_pt_01v_09_G_2500_06_20_2007

Experiment	Experiment	Chen's prediction	Klimenko's prediction	Exp/Pred	Exp/Pred	Chen's prediction			Experiment		
q'' (kW/m^2)	h_{eff} (W/m^2·K) (a)	h_{eff} (W/m^2·K) (b)	h_{eff} (W/m^2·K) (c)	Ratio (a)/(b)	Ratio (a)/(c)	q''_{1p} (kW/m^2) (d)	q''_{2p} (kW/m^2) (e)	Ratio (d)/(e)	q''_{1p} (kW/m^2) (f)	q''_{2p} (kW/m^2) (g)	Ratio (f)/(g)
1.541E+02	13333	10339	10339	1.290	1.290	0	0	0	0	0	0
2.836E+02	14212	10534	10534	1.349	1.349	0	0	0	0	0	0
4.539E+02	15016	10809	10809	1.389	1.389	0	0	0	0	0	0
6.704E+02	15792	11165	11165	1.414	1.414	0	0	0	0	0	0
9.345E+02	16609	11610	9163	1.431	1.813	925.64	8.8157	104.9986	0	0	0
1.251E+03	17565	14010	12302	1.254	1.428	1066.134	184.596	5.7755	0	0	0
1.622E+03	18724	17322	16088	1.081	1.164	1167.406	454.4169	2.569	1079.425	542.3976	1.9901
2.032E+03	27411	21132	20438	1.297	1.341	1245.436	786.3422	1.5838	959.7046	1072.074	0.8952

2.462E+03	33403	25365	25288	1.317	1.321	1314.303	1148.177	1.1447	997.6193	1464.861	0.681
2.954E+03	36404	30275	31113	1.202	1.170	1377.202	1576.377	0.8737	1144.883	1808.697	0.633
3.484E+03	44713	35887	37933	1.246	1.179	1439.131	2045.208	0.7037	1154.632	2329.707	0.4956
4.067E+03	56719	42430	46218	1.337	1.227	1486.93	2580.269	0.5763	1111.952	2955.247	0.3763
4.223E+03	61560	44932	49533	1.370	1.243	1494.297	2728.447	0.5477	1090.294	3132.45	0.3481
4.348E+03	65130	46324	51364	1.406	1.268	1499.749	2848.721	0.5265	1066.35	3282.12	0.3249
4.484E+03	65717	48022	53654	1.368	1.225	1508.731	2975.115	0.5071	1102.11	3381.737	0.3259
4.620E+03	68056	49798	56092	1.367	1.213	1517.915	3102.113	0.4893	1110.31	3509.719	0.3164
4.739E+03	66465	49582	55620	1.340	1.195	1532.672	3206.473	0.478	1142.978	3596.167	0.3178
4.864E+03	69505	51540	58364	1.349	1.191	1539.989	3324.309	0.4633	1141.566	3722.731	0.3066
5.021E+03	73558	53580	61244	1.373	1.201	1552.742	3468.41	0.4477	1130.626	3890.526	0.2906
5.148E+03	74411	54032	61694	1.377	1.206	1567.864	3579.641	0.438	1138.13	4009.375	0.2839
5.276E+03	76849	55045	62991	1.396	1.220	1577.846	3698.461	0.4266	1129.833	4146.474	0.2725
5.409E+03	80446	56155	64444	1.433	1.248	1597.911	3810.618	0.4193	1115.098	4293.431	0.2597
5.543E+03	85115	57432	66153	1.482	1.287	1607.785	3935.229	0.4086	1084.559	4458.456	0.2433
5.688E+03	90228	58823	68035	1.534	1.326	1617.286	4070.398	0.3973	1054.072	4633.613	0.2275
5.834E+03	95575	60130	69793	1.589	1.369	1627.017	4207.269	0.3867	1023.332	4810.954	0.2127
5.962E+03	100780	61434	71604	1.640	1.407	1634.718	4327.772	0.3777	996.2223	4966.268	0.2006
6.074E+03	113210	64252	75972	1.762	1.490	1636.036	4437.69	0.3687	928.2516	5145.475	0.1804
6.141E+03	120940	65821	78443	1.837	1.542	1634.37	4507.056	0.3626	889.2354	5252.191	0.1693
6.208E+03	127729	67060	80395	1.905	1.589	1635.753	4572.568	0.3577	858.5456	5349.775	0.1605
6.277E+03	132062	67724	81356	1.950	1.623	1639.312	4637.554	0.3535	840.4311	5436.435	0.1546
6.333E+03	128699	67250	80377	1.914	1.601	1647.587	4685.059	0.3517	860.6741	5471.972	0.1573
6.381E+03	128457	67216	80187	1.911	1.602	1652.066	4729.212	0.3493	864.209	5517.069	0.1566
6.445E+03	129032	67375	80306	1.915	1.607	1663.736	4781.541	0.3479	868.4823	5576.794	0.1557
6.502E+03	131136	67788	80866	1.934	1.622	1667.715	4834.039	0.345	861.848	5639.906	0.1528
6.564E+03	136928	68776	82399	1.991	1.662	1669.353	4895.114	0.341	838.2391	5726.228	0.1464
6.633E+03	142602	69689	83801	2.046	1.702	1671.928	4960.897	0.337	816.8296	5815.995	0.1404
6.696E+03	150847	70561	85109	2.138	1.772	1673.037	5023.246	0.3331	782.3882	5913.894	0.1323
6.770E+03	157564	71302	86151	2.210	1.829	1675.357	5094.594	0.3288	757.9452	6012.005	0.1261
6.850E+03	155222	72197	87470	2.150	1.775	1678.128	5171.777	0.3245	780.3321	6069.573	0.1286
6.918E+03	147080	72751	88253	2.022	1.667	1685.245	5232.999	0.322	833.3643	6084.879	0.137
6.980E+03	142489	73368	89155	1.942	1.598	1687.739	5292.406	0.3189	868.8021	6111.343	0.1422
7.046E+03	141474	74078	90195	1.910	1.569	1687.458	5358.043	0.3149	883.3477	6162.153	0.1434
7.135E+03	142829	75164	91832	1.900	1.555	1687.772	5447.305	0.3098	887.9639	6247.113	0.1421
7.250E+03	147616	76411	93708	1.932	1.575	1695.913	5553.723	0.3054	877.6426	6371.994	0.1377

Table F-20 Test _AL_pt_1v_08_G_1500_07_31_2007

Experiment	Experiment	Chen's prediction	Klimenko's prediction	Exp/Pred	Exp/Pred	Chen's prediction			Experiment		
q" (kW/m^2)	h_{eff} (W/m^2·K) (a)	h_{eff} (W/m^2·K) (b)	h_{eff} (W/m^2·K) (c)	Ratio (a)/(b)	Ratio (a)/(c)	$q"_{1p}$ (kW/m^2) (d)	$q"_{2p}$ (kW/m^2) (e)	Ratio (d)/(e)	$q"_{1p}$ (kW/m^2) (f)	$q"_{2p}$ (kW/m^2) (g)	Ratio (f)/(g)
1.592E+02	8011	6883	6883	1.164	1.164	0	0	0	0	0	0
2.865E+02	8239	7039	7039	1.170	1.170	0	0	0	0	0	0
4.571E+02	8673	7259	7259	1.195	1.195	0	0	0	0	0	0
6.788E+02	9113	7955	6755	1.146	1.349	642.6813	36.0934	17.8061	0	0	0
9.562E+02	9721	10431	9581	0.932	1.015	716.9459	239.2089	2.9972	768.854	187.3007	4.1049
1.290E+03	12058	13677	13112	0.882	0.920	775.8306	514.5177	1.5079	879.5071	410.8411	2.1407
1.657E+03	16038	17362	17188	0.924	0.933	821.3229	835.1826	0.9834	888.6417	767.8638	1.1573
2.052E+03	21733	21573	21875	1.007	0.994	862.3076	1189.423	0.725	855.5337	1196.197	0.7152
2.487E+03	28318	26385	27436	1.073	1.032	895.7968	1590.888	0.5631	834.2855	1652.4	0.5049
2.591E+03	29669	27793	29067	1.068	1.021	902.8979	1688.459	0.5347	845.4247	1745.932	0.4842
2.695E+03	30808	29089	30583	1.059	1.007	910.916	1784.037	0.5106	859.7231	1835.23	0.4685
2.797E+03	32009	30371	32101	1.054	0.997	915.8851	1880.702	0.487	868.6411	1927.946	0.4506
2.896E+03	34746	31638	33610	1.098	1.034	919.6465	1976.417	0.4653	837.0119	2059.052	0.4065
3.005E+03	37045	33033	35291	1.121	1.050	925.1073	2080.035	0.4448	824.5606	2180.582	0.3781
3.111E+03	38552	34431	37000	1.120	1.042	928.5232	2182.703	0.4254	828.909	2282.317	0.3632
3.221E+03	40383	35855	38757	1.126	1.042	934.7277	2286.315	0.4088	829.5579	2391.485	0.3469
3.333E+03	42235	37318	40583	1.132	1.041	941.7163	2390.909	0.3939	831.7274	2500.897	0.3326
3.435E+03	44166	38718	42355	1.141	1.043	946.6966	2487.907	0.3805	829.5452	2605.059	0.3184
3.553E+03	45566	40358	44446	1.129	1.025	951.7731	2601.186	0.3659	842.6503	2710.309	0.3109
3.669E+03	47412	42057	46595	1.127	1.018	954.0534	2714.59	0.3515	845.9509	2822.693	0.2997
3.779E+03	49846	43756	48776	1.139	1.022	955.4658	2823.904	0.3383	838.4059	2940.964	0.2851
3.900E+03	52339	45591	51161	1.148	1.023	959.305	2940.594	0.3262	835.3075	3064.592	0.2726
4.022E+03	55414	47672	53928	1.162	1.028	958.4762	3063.524	0.3129	824.2318	3197.768	0.2578
4.150E+03	58316	49841	56852	1.170	1.026	959.0833	3190.831	0.3006	819.3678	3330.546	0.246
4.271E+03	62858	52017	59840	1.208	1.050	958.5957	3312.786	0.2894	792.9542	3478.428	0.228
4.405E+03	68098	53810	62274	1.266	1.094	963.3792	3441.318	0.2799	760.9474	3643.75	0.2088
4.531E+03	73705	55487	64575	1.328	1.141	968.227	3562.364	0.2718	728.6174	3801.973	0.1916
4.660E+03	82586	57683	67691	1.432	1.220	967.122	3693.046	0.2619	675.217	3984.951	0.1694
4.744E+03	92378	59156	69813	1.562	1.323	967.6758	3776.584	0.2562	619.4188	4124.841	0.1502
4.825E+03	101478	60267	71390	1.684	1.421	970.6991	3854.016	0.2519	576.2741	4248.441	0.1356

4.903E+03	109709	61825	73631	1.775	1.490	967.6946	3934.916	0.2459	545.1296	4357.481	0.1251

Table F-21 Test _AL_pt_1v_09_G_1500_08_01_2007

Experiment	Experiment	Chen's prediction	Klimenko's prediction	Exp/Pred	Exp/Pred	Chen's prediction			Experiment		
q" (kW/m^2)	h_{eff} (W/m^2·K) (a)	h_{eff} (W/m^2·K) (b)	h_{eff} (W/m^2·K) (c)	Ratio (a)/(b)	Ratio (a)/(c)	$q"_{1p}$ (kW/m^2) (d)	$q"_{2p}$ (kW/m^2) (e)	Ratio (d)/(e)	$q"_{1p}$ (kW/m^2) (f)	$q"_{2p}$ (kW/m^2) (g)	Ratio (f)/(g)
1.436E+02	8220	6753	6753	1.217	1.217	0	0	0	0	0	0
2.558E+02	8142	6874	6874	1.184	1.184	0	0	0	0	0	0
4.050E+02	8335	7049	7049	1.182	1.182	0	0	0	0	0	0
5.956E+02	8503	7298	5854	1.165	1.453	595.2226	0.4118	1445.428	0	0	0
8.353E+02	9264	9164	8226	1.011	1.126	688.691	146.5963	4.6979	680.7751	154.5122	4.406
1.130E+03	12378	11907	11227	1.040	1.102	748.4927	381.9859	1.9595	719.6012	410.8774	1.7514
1.457E+03	16166	15099	14685	1.071	1.101	800.2862	656.5206	1.219	747.0737	709.7332	1.0526
1.822E+03	20674	19000	18983	1.088	1.089	842.5841	979.4637	0.8603	773.9998	1048.048	0.7385
2.222E+03	25844	23224	23754	1.113	1.088	880.1044	1342.368	0.6556	790.5004	1431.972	0.552
2.651E+03	32093	27916	29189	1.150	1.099	912.1689	1738.763	0.5246	793.091	1857.841	0.4269
2.749E+03	33516	29211	30704	1.147	1.092	918.682	1830.761	0.5018	800.3348	1949.108	0.4106
2.849E+03	35403	30450	32165	1.163	1.101	925.354	1923.77	0.481	795.5454	2053.579	0.3874
2.955E+03	37239	31744	33706	1.173	1.105	931.0598	2024.22	0.46	793.3361	2161.944	0.367
3.057E+03	38623	32980	35191	1.171	1.098	936.9311	2119.979	0.442	799.6974	2257.212	0.3543
3.158E+03	39809	34301	36806	1.161	1.082	937.7689	2219.774	0.4225	807.6609	2349.882	0.3437
3.266E+03	40999	35728	38570	1.148	1.063	939.1469	2326.483	0.4037	818.0448	2447.585	0.3342
3.375E+03	42550	37106	40281	1.147	1.056	946.4474	2428.672	0.3897	825.003	2550.116	0.3235
3.485E+03	44236	38514	42051	1.149	1.052	953.3041	2532.159	0.3765	829.6342	2655.829	0.3124
3.603E+03	46323	40022	43945	1.157	1.054	960.8258	2641.875	0.3637	829.7929	2772.907	0.2993
3.711E+03	48363	41493	45783	1.166	1.056	963.7193	2747.523	0.3508	826.5038	2884.738	0.2865
3.819E+03	50809	42980	47659	1.182	1.066	967.814	2851.635	0.3394	818.3744	3001.075	0.2727
3.931E+03	56198	44560	49668	1.261	1.131	969.8902	2960.887	0.3276	768.7479	3162.03	0.2431
4.047E+03	60095	46225	51818	1.300	1.160	974.1239	3072.542	0.317	749.0017	3297.665	0.2271
4.156E+03	61717	47985	54149	1.286	1.140	975.9241	3180.107	0.3069	758.4917	3397.539	0.2232
4.280E+03	63763	49847	56639	1.279	1.126	980.8048	3298.87	0.2973	766.453	3513.222	0.2182
4.355E+03	65575	51071	58297	1.284	1.125	981.3188	3373.409	0.2909	763.9794	3590.748	0.2128
4.436E+03	68167	52332	60011	1.303	1.136	982.5259	3453.295	0.2845	753.9953	3681.826	0.2048

4.517E+03	72412	53616	61768	1.351	1.172	982.2808	3535.06	0.2779	727.0283	3790.313	0.1918
4.595E+03	79558	54824	63423	1.451	1.254	983.1823	3611.98	0.2722	677.2538	3917.908	0.1729
4.667E+03	89883	55969	65000	1.606	1.383	982.1016	3684.519	0.2665	611.2993	4055.321	0.1507
4.743E+03	97629	57258	66817	1.705	1.461	981.995	3760.817	0.2611	575.6977	4167.114	0.1382
4.832E+03	103835	58595	68712	1.772	1.511	985.3897	3846.829	0.2562	555.8388	4276.38	0.13
4.927E+03	110823	60189	70975	1.841	1.561	985.818	3940.718	0.2502	535.2173	4391.319	0.1219
5.018E+03	118261	61974	73534	1.908	1.608	980.3765	4037.228	0.2428	513.5752	4504.029	0.114
5.125E+03	130852	63868	76240	2.049	1.716	979.3533	4146.063	0.2362	477.8393	4647.577	0.1028
5.202E+03	130392	65080	77993	2.004	1.672	980.9516	4220.571	0.2324	489.4253	4712.097	0.1039

Table F-22 Test _AL_pt_1v_06_G_2000_07_26_2007

Experiment	Experiment	Chen's prediction	Klimenko's prediction	Exp/Pred	Exp/Pred	Chen's prediction			Experiment		
q" (kW/m^2)	h_{eff} (W/m^2·K) (a)	h_{eff} (W/m^2·K) (b)	h_{eff} (W/m^2·K) (c)	Ratio (a)/(b)	Ratio (a)/(c)	$q"_{1p}$ (kW/m^2) (d)	$q"_{2p}$ (kW/m^2) (e)	Ratio (d)/(e)	$q"_{1p}$ (kW/m^2) (f)	$q"_{2p}$ (kW/m^2) (g)	Ratio (f)/(g)
1.595E+02	10254	8594	8594	1.193	1.193	0	0	0	0	0	0
2.823E+02	10737	8748	8748	1.227	1.227	0	0	0	0	0	0
4.463E+02	11199	8962	8962	1.250	1.250	0	0	0	0	0	0
6.580E+02	11825	9260	9260	1.277	1.277	0	0	0	0	0	0
9.198E+02	12542	10479	8998	1.197	1.394	839.7815	79.9688	10.5014	0	0	0
1.230E+03	13355	13179	12090	1.013	1.105	927.114	302.5724	3.0641	914.3451	315.3413	2.8995
1.585E+03	15606	16491	15748	0.946	0.991	999.2122	585.4025	1.7069	1055.343	529.2714	1.994
1.975E+03	18680	20213	19930	0.924	0.937	1056.633	918.3432	1.1506	1142.818	832.1579	1.3733
2.397E+03	23832	24388	24677	0.977	0.966	1110.614	1286.288	0.8634	1136.015	1260.886	0.901
2.855E+03	30390	29061	30123	1.046	1.009	1157.987	1696.538	0.6826	1106.908	1747.618	0.6334
3.361E+03	37633	34509	36637	1.091	1.027	1203.274	2157.924	0.5576	1102.933	2258.265	0.4884
3.695E+03	42979	38356	41424	1.121	1.038	1225.495	2469.922	0.4962	1093.244	2602.174	0.4201
3.912E+03	46341	41085	44838	1.128	1.034	1232.092	2680.034	0.4597	1091.956	2820.17	0.3872
4.054E+03	48772	42795	46993	1.140	1.038	1247.58	2806.593	0.4445	1094.29	2959.883	0.3697
4.172E+03	50508	44309	48946	1.140	1.032	1251.06	2920.484	0.4284	1097.106	3074.439	0.3568
4.294E+03	52622	45826	50913	1.148	1.034	1256.179	3037.751	0.4135	1093.565	3200.365	0.3417
4.418E+03	54612	47395	52971	1.152	1.031	1262.042	3155.99	0.3999	1094.879	3323.153	0.3295
4.535E+03	55821	48880	54947	1.142	1.016	1266.252	3269.012	0.3874	1108.405	3426.859	0.3234
4.664E+03	56683	50488	57115	1.123	0.992	1272.63	3391.226	0.3753	1133.14	3530.716	0.3209

4.804E+03	59055	52287	59571	1.129	0.991	1278.072	3526.3	0.3624	1131.196	3673.176	0.308
4.935E+03	62454	54005	61950	1.156	1.008	1282.676	3652.329	0.3512	1108.75	3826.255	0.2898
5.052E+03	67504	55631	64196	1.213	1.052	1283.429	3768.697	0.3405	1057.364	3994.762	0.2647
5.202E+03	74255	57513	66749	1.291	1.112	1293.118	3909.124	0.3308	1001.242	4201	0.2383
5.314E+03	80943	59116	68970	1.369	1.174	1292.775	4021.588	0.3215	943.8708	4370.492	0.216
5.458E+03	87332	60897	71448	1.434	1.222	1303.844	4153.83	0.3139	908.8963	4548.778	0.1998
5.600E+03	95199	62876	74260	1.514	1.282	1306.298	4293.849	0.3042	862.4943	4737.652	0.1821
5.656E+03	99356	63934	75817	1.554	1.310	1299.555	4356.841	0.2983	835.9818	4820.414	0.1734
5.759E+03	104796	65260	77734	1.606	1.348	1306.018	4452.739	0.2933	813.049	4945.708	0.1644
5.822E+03	110487	66363	79371	1.665	1.392	1299.936	4521.907	0.2875	780.5437	5041.299	0.1548
5.926E+03	110280	67833	81574	1.626	1.352	1302.596	4623.075	0.2818	800.9697	5124.702	0.1563
6.008E+03	100218	68966	83327	1.453	1.203	1307.131	4700.87	0.2781	899.2237	5108.777	0.176
6.108E+03	97530	70169	85161	1.390	1.145	1318.589	4789.686	0.2753	948.3648	5159.91	0.1838
6.202E+03	95087	71720	87577	1.326	1.086	1313.864	4888.599	0.2688	990.6738	5211.789	0.1901

Table F-23 Test _AL_pt_1v_07_G_2000_07_27_2007

Experiment	Experiment	Chen's prediction	Klimenko's prediction	Exp/Pred	Exp/Pred	Chen's prediction			Experiment		
q" (kW/m^2)	h_{eff} (W/m^2·K) (a)	h_{eff} (W/m^2·K) (b)	h_{eff} (W/m^2·K) (c)	Ratio (a)/(b)	Ratio (a)/(c)	$q"_{1p}$ (kW/m^2) (d)	$q"_{2p}$ (kW/m^2) (e)	Ratio (d)/(e)	$q"_{1p}$ (kW/m^2) (f)	$q"_{2p}$ (kW/m^2) (g)	Ratio (f)/(g)
1.513E+02	10153	8711	8711	1.165	1.165	0	0	0	0	0	0
2.697E+02	10891	8871	8871	1.228	1.228	0	0	0	0	0	0
4.270E+02	11343	9070	9070	1.251	1.251	0	0	0	0	0	0
6.264E+02	11946	9335	9335	1.280	1.280	0	0	0	0	0	0
8.707E+02	12677	10179	8567	1.245	1.480	820.9992	49.7306	16.5089	0	0	0
1.162E+03	13354	12643	11460	1.056	1.165	911.7886	249.8747	3.649	862.735	298.9284	2.8861
1.501E+03	16973	15767	14923	1.076	1.137	984.796	516.2699	1.9075	914.3686	586.6974	1.5585
1.870E+03	20452	19244	18838	1.063	1.086	1040.696	828.8211	1.2556	978.7871	890.7296	1.0989
2.282E+03	24533	23296	23422	1.053	1.047	1090.137	1191.779	0.9147	1034.715	1247.202	0.8296
2.731E+03	31163	27828	28685	1.120	1.086	1142.013	1589.259	0.7186	1019.408	1711.864	0.5955
3.219E+03	38239	32972	34764	1.160	1.100	1187.278	2031.816	0.5843	1023.348	2195.747	0.4661
3.541E+03	43502	36554	39151	1.190	1.111	1214.472	2326.901	0.5219	1020.109	2521.264	0.4046
3.764E+03	47469	39137	42379	1.213	1.120	1227.269	2536.327	0.4839	1011.475	2752.12	0.3675
3.883E+03	49545	40586	44180	1.221	1.121	1235.381	2647.506	0.4666	1011.632	2871.254	0.3523

4.003E+03	51602	41997	45950	1.229	1.123	1244.504	2758.995	0.4511	1012.514	2990.985	0.3385
4.115E+03	53463	43357	47679	1.233	1.121	1250.747	2864.095	0.4367	1013.95	3100.892	0.327
4.239E+03	55780	44887	49653	1.243	1.123	1255.153	2983.404	0.4207	1009.687	3228.87	0.3127
4.363E+03	57643	46389	51602	1.243	1.117	1261.652	3101.1	0.4068	1014.988	3347.763	0.3032
4.480E+03	59257	47817	53477	1.239	1.108	1266.75	3212.824	0.3943	1021.85	3457.724	0.2955
4.603E+03	60885	49309	55457	1.235	1.098	1272.977	3329.573	0.3823	1030.593	3571.957	0.2885
4.732E+03	61672	50869	57555	1.212	1.072	1280.586	3451.411	0.371	1055.896	3676.101	0.2872
4.863E+03	63319	52470	59734	1.207	1.060	1288.093	3575.074	0.3603	1067.007	3796.16	0.2811
4.999E+03	67519	54138	62027	1.247	1.089	1295.43	3703.999	0.3497	1038.341	3961.088	0.2621
5.132E+03	74557	55859	64354	1.335	1.159	1301.029	3831.356	0.3396	974.4478	4157.937	0.2344
5.265E+03	83251	57630	66771	1.445	1.247	1306.084	3958.85	0.3299	903.8426	4361.092	0.2073
5.399E+03	90663	59440	69269	1.525	1.309	1308.738	4090.208	0.32	857.7641	4541.181	0.1889
5.483E+03	95729	60696	71044	1.577	1.347	1310.405	4172.383	0.3141	830.5815	4652.207	0.1785
5.573E+03	102804	62542	73772	1.644	1.394	1309.619	4263.61	0.3072	796.4696	4776.76	0.1667
5.661E+03	108715	64095	76071	1.696	1.429	1309.548	4351.578	0.3009	771.8158	4889.31	0.1579
5.751E+03	114901	65561	78254	1.753	1.468	1310.014	4440.51	0.295	747.2388	5003.285	0.1493
5.844E+03	115921	67086	80562	1.728	1.439	1309.249	4534.533	0.2887	757.4474	5086.335	0.1489
5.940E+03	112490	68698	83054	1.637	1.354	1307.929	4632.257	0.2824	798.498	5141.688	0.1553
6.026E+03	105982	70209	85418	1.510	1.241	1303.252	4722.912	0.2759	863.0742	5163.09	0.1672
6.125E+03	102663	71729	87790	1.431	1.169	1302.497	4822.496	0.2701	909.749	5215.244	0.1744

Table F-24 Test _Al_pt_1v_01_G_2500_07_06

Experiment	Experiment	Chen's prediction	Klimenko's prediction	Exp/Pred	Exp/Pred	Chen's prediction			Experiment		
q" (kW/m^2)	h_{eff} ($W/m^2 \cdot K$) (a)	h_{eff} ($W/m^2 \cdot K$) (b)	h_{eff} ($W/m^2 \cdot K$) (c)	Ratio (a)/(b)	Ratio (a)/(c)	$q"_{1p}$ (kW/m^2) (d)	$q"_{2p}$ (kW/m^2) (e)	Ratio (d)/(e)	$q"_{1p}$ (kW/m^2) (f)	$q"_{2p}$ (kW/m^2) (g)	Ratio (f)/(g)
3.045E+02	1.578E+04	1.030E+04	10303	1.532	1.532	0	0	0	0	0	0
4.817E+02	1.609E+04	1.056E+04	10556	1.524	1.524	0	0	0	0	0	0
7.052E+02	1.670E+04	1.087E+04	10874	1.535	1.535	0	0	0	0	0	0
9.800E+02	1.740E+04	1.158E+04	9418	1.503	1.848	953.6597	26.3547	36.1856	0	0	0
1.303E+03	1.804E+04	1.410E+04	12552	1.280	1.437	1076.816	225.914	4.7665	0	0	0
1.666E+03	1.892E+04	1.729E+04	16172	1.094	1.170	1168.588	497.8303	2.3474	1067.338	599.0802	1.7816
2.055E+03	2.509E+04	2.081E+04	20160	1.206	1.245	1245.285	810.097	1.5372	1032.352	1023.03	1.0091
2.476E+03	3.106E+04	2.474E+04	24639	1.255	1.260	1310.119	1165.393	1.1242	1043.049	1432.464	0.7282

2.936E+03	3.419E+04	2.912E+04	29772	1.174	1.148	1378.382	1557.765	0.8848	1173.334	1762.813	0.6656
3.459E+03	4.133E+04	3.428E+04	35945	1.206	1.150	1433.895	2024.958	0.7081	1189.015	2269.838	0.5238
4.011E+03	5.326E+04	3.996E+04	42979	1.333	1.239	1486.953	2524.015	0.5891	1115.361	2895.607	0.3852
4.124E+03	5.541E+04	4.149E+04	44920	1.336	1.234	1487.279	2637.219	0.564	1113.224	3011.274	0.3697
4.251E+03	5.759E+04	4.296E+04	46781	1.341	1.231	1498.307	2752.525	0.5443	1117.188	3133.644	0.3565
4.375E+03	6.013E+04	4.443E+04	48681	1.353	1.235	1508.203	2866.439	0.5262	1113.996	3260.646	0.3416
4.476E+03	6.187E+04	4.556E+04	50142	1.358	1.234	1519.411	2956.928	0.5138	1118.426	3357.914	0.3331
4.610E+03	6.414E+04	4.696E+04	51981	1.366	1.234	1529.916	3080.19	0.4967	1119.909	3490.197	0.3209
4.741E+03	6.678E+04	4.836E+04	53834	1.381	1.241	1540.643	3200.298	0.4814	1115.29	3625.651	0.3076
4.869E+03	6.843E+04	4.962E+04	55507	1.379	1.233	1554.229	3314.884	0.4689	1126.602	3742.511	0.301
4.995E+03	7.060E+04	5.097E+04	57330	1.385	1.232	1560.924	3434.471	0.4545	1126.551	3868.844	0.2912
5.121E+03	7.294E+04	5.232E+04	59159	1.394	1.233	1573.74	3547.751	0.4436	1128.36	3993.131	0.2826
5.254E+03	7.411E+04	5.378E+04	61118	1.378	1.213	1586.401	3667.787	0.4325	1150.813	4103.376	0.2805
5.395E+03	7.342E+04	5.536E+04	63258	1.326	1.161	1592.915	3802.256	0.4189	1200.609	4194.562	0.2862
5.531E+03	7.346E+04	5.688E+04	65348	1.292	1.124	1603.801	3927.557	0.4083	1241.39	4289.967	0.2894
5.672E+03	7.762E+04	5.852E+04	67631	1.326	1.148	1613.072	4058.938	0.3974	1215.779	4456.23	0.2728
5.807E+03	8.699E+04	6.013E+04	69879	1.447	1.245	1622.12	4185.154	0.3876	1120.958	4686.316	0.2392
5.886E+03	9.361E+04	6.112E+04	71279	1.532	1.313	1626.616	4259.706	0.3819	1061.717	4824.605	0.2201
5.942E+03	9.599E+04	6.176E+04	72206	1.554	1.329	1630.49	4311.08	0.3782	1048.838	4892.732	0.2144
5.997E+03	9.734E+04	6.238E+04	73097	1.560	1.332	1635.329	4361.711	0.3749	1047.762	4949.279	0.2117
6.054E+03	9.879E+04	6.309E+04	74119	1.566	1.333	1637.602	4416.487	0.3708	1045.443	5008.645	0.2087
6.107E+03	1.001E+05	6.369E+04	74994	1.571	1.335	1639.39	4467.737	0.3669	1042.985	5064.142	0.206
6.165E+03	1.003E+05	6.393E+04	75244	1.569	1.333	1645.817	4518.888	0.3642	1048.394	5116.311	0.2049
6.223E+03	1.008E+05	6.424E+04	75621	1.569	1.333	1650.754	4572.317	0.361	1051.618	5171.453	0.2034
6.280E+03	1.026E+05	6.491E+04	76604	1.581	1.340	1652.848	4626.725	0.3572	1045.146	5234.427	0.1997
6.335E+03	1.044E+05	6.557E+04	77565	1.592	1.346	1654.744	4680.247	0.3536	1039.2	5295.792	0.1962
6.394E+03	1.064E+05	6.626E+04	78573	1.605	1.354	1657.037	4736.604	0.3498	1032.013	5361.629	0.1925
6.431E+03	1.066E+05	6.668E+04	79194	1.598	1.346	1659.44	4771.415	0.3478	1037.88	5392.975	0.1925
6.502E+03	1.075E+05	6.749E+04	80401	1.593	1.337	1662.383	4839.207	0.3435	1043.145	5458.445	0.1911
6.562E+03	1.090E+05	6.828E+04	81588	1.596	1.336	1664.336	4897.856	0.3398	1042.558	5519.634	0.1889
6.625E+03	1.102E+05	6.902E+04	82707	1.597	1.333	1666.18	4959.246	0.336	1042.954	5582.472	0.1868
6.689E+03	1.109E+05	6.983E+04	83936	1.588	1.321	1669.513	5019.976	0.3326	1051.217	5638.272	0.1864
6.751E+03	1.111E+05	7.068E+04	85216	1.572	1.304	1670.073	5081.113	0.3287	1062.304	5688.882	0.1867
6.819E+03	1.106E+05	7.149E+04	86415	1.547	1.280	1672.307	5146.54	0.3249	1080.914	5737.934	0.1884
6.914E+03	1.115E+05	7.271E+04	88253	1.533	1.263	1673.053	5241.167	0.3192	1090.809	5823.411	0.1873
7.019E+03	1.150E+05	7.401E+04	90207	1.554	1.275	1677.314	5341.782	0.314	1079.294	5939.801	0.1817

7.119E+03	1.185E+05	7.525E+04	92125	1.574	1.286	1685.964	5433.21	0.3103	1070.582	6048.593	0.177
7.225E+03	1.207E+05	7.655E+04	94132	1.577	1.282	1692.38	5532.944	0.3059	1073.015	6152.309	0.1744
7.318E+03	1.242E+05	7.778E+04	96062	1.596	1.293	1694.074	5623.547	0.3012	1060.969	6256.651	0.1696
7.409E+03	1.284E+05	7.912E+04	98172	1.623	1.308	1687.537	5721.902	0.2949	1039.695	6369.744	0.1632

Table F-25 Test _AL_pt_1v_02_G_2500_07_09_2007

Experiment	Experiment	Chen's prediction	Klimenko's prediction	Exp/Pred	Exp/Pred	Chen's prediction			Experiment		
q" (kW/m^2)	h_{eff} (W/m^2·K) (a)	h_{eff} (W/m^2·K) (b)	h_{eff} (W/m^2·K) (c)	Ratio (a)/(b)	Ratio (a)/(c)	$q"_{1p}$ (kW/m^2) (d)	$q"_{2p}$ (kW/m^2) (e)	Ratio (d)/(e)	$q"_{1p}$ (kW/m^2) (f)	$q"_{2p}$ (kW/m^2) (g)	Ratio (f)/(g)
1.594E+02	11976.2	10047.5	10047.5	1.192	1.192	0	0	0	0	0	0
2.817E+02	12837.7	10205.8	10205.8	1.258	1.258	0	0	0	0	0	0
4.485E+02	13404.8	10471.0	10471.0	1.280	1.280	0	0	0	0	0	0
6.611E+02	14096.1	10783.4	10783.4	1.307	1.307	0	0	0	0	0	0
9.220E+02	14955.2	11223.1	8807.3	1.333	1.698	918.0418	3.9283	233.7024	0	0	0
1.241E+03	16118.6	13498.9	11867.8	1.194	1.358	1062.205	178.569	5.9484	889.0692	351.7052	2.5279
1.618E+03	17554.0	16758.1	15583.0	1.047	1.126	1162.103	455.7906	2.5496	1108.844	509.0489	2.1783
2.029E+03	25154.2	20439.8	19747.3	1.231	1.274	1246.337	782.9759	1.5918	1012.291	1017.022	0.9953
2.461E+03	31871.8	24459.1	24318.4	1.303	1.311	1311.199	1150.049	1.1401	1005.802	1455.447	0.6911
2.927E+03	35207.2	28880.5	29501.0	1.219	1.193	1375.396	1551.146	0.8867	1127.808	1798.735	0.627
3.460E+03	38748.6	34140.1	35776.2	1.135	1.083	1436.528	2023.213	0.71	1265.204	2194.537	0.5765
3.823E+03	43013.8	37947.3	40497.9	1.134	1.062	1477.91	2345.164	0.6302	1303.35	2519.724	0.5173
4.069E+03	46876.0	40697.3	43927.3	1.152	1.067	1495.746	2573.496	0.5812	1298.163	2771.079	0.4685
4.196E+03	49254.3	42157.7	45771.4	1.168	1.076	1503.555	2692.285	0.5585	1286.496	2909.344	0.4422
4.317E+03	51496.9	43532.5	47526.6	1.183	1.084	1511.403	2805.485	0.5387	1277.231	3039.657	0.4202
4.440E+03	53757.5	44902.8	49293.6	1.197	1.091	1520.696	2918.915	0.521	1269.797	3169.815	0.4006
4.578E+03	56487.5	46373.9	51202.6	1.218	1.103	1535.315	3043.052	0.5045	1260.016	3318.351	0.3797
4.713E+03	59279.4	47911.2	53238.2	1.237	1.113	1547.593	3165.352	0.4889	1250.399	3462.547	0.3611
4.840E+03	61944.9	49358.4	55181.9	1.255	1.123	1557.465	3282.672	0.4745	1240.601	3599.535	0.3447
4.974E+03	64997.7	50822.9	57156.2	1.279	1.137	1567.768	3406.539	0.4602	1225.468	3748.839	0.3269
5.104E+03	67525.1	52237.3	59086.8	1.293	1.143	1577.482	3526.193	0.4474	1219.942	3883.733	0.3141
5.249E+03	69647.9	53919.4	61357.1	1.292	1.135	1587.263	3661.752	0.4335	1228.452	4020.563	0.3055
5.383E+03	69199.1	55604.4	63682.0	1.244	1.087	1592.507	3790.915	0.4201	1279.272	4104.15	0.3117
5.525E+03	75490.5	57337.6	66071.6	1.317	1.143	1600.364	3924.876	0.4077	1215.176	4310.064	0.2819

5.688E+03	82671.5	59115.9	68526.1	1.398	1.206	1615.098	4073.31	0.3965	1154.572	4533.836	0.2547
5.835E+03	89018.7	60734.5	70792.4	1.466	1.257	1623.676	4210.968	0.3856	1107.458	4727.186	0.2343
5.973E+03	95821.2	62558.4	73443.9	1.532	1.305	1630.771	4342.586	0.3755	1064.366	4908.991	0.2168
6.074E+03	102905.4	64071.9	75681.2	1.606	1.360	1629.34	4445.11	0.3665	1014.18	5060.271	0.2004
6.159E+03	109297.7	65305.5	77519.1	1.674	1.410	1628.081	4531.24	0.3593	972.4984	5186.822	0.1875
6.257E+03	116087.3	66407.4	79132.1	1.748	1.467	1634.476	4622.165	0.3536	934.7256	5321.915	0.1756
6.346E+03	127140.4	67528.4	80802.0	1.883	1.573	1638.725	4707.274	0.3481	870.1277	5475.871	0.1589
6.431E+03	136452.7	68599.3	82409.2	1.989	1.656	1639.886	4791.243	0.3423	824.1865	5606.942	0.147
6.538E+03	136263.4	70031.5	84647.2	1.946	1.610	1645.551	4892.414	0.3363	845.473	5692.492	0.1485
6.633E+03	124546.6	71297.4	86637.1	1.747	1.438	1649.345	4983.218	0.331	943.9278	5688.636	0.1659
6.748E+03	110919.1	72731.6	88884.8	1.525	1.248	1660.856	5086.862	0.3265	1088.767	5658.951	0.1924
6.846E+03	102345.9	74279.6	91375.5	1.378	1.120	1657.547	5187.988	0.3195	1202.68	5642.854	0.2131
6.975E+03	120405.1	76106.5	94190.8	1.582	1.278	1658.692	5315.951	0.312	1048.162	5926.481	0.1769
7.088E+03	154338.3	77614.9	96461.1	1.989	1.600	1658.535	5429.544	0.3055	833.838	6254.241	0.1333
7.253E+03	198968.6	79803.0	99886.1	2.493	1.992	1664.531	5588.548	0.2978	667.4403	6585.638	0.1013
7.420E+03	197125.0	81613.2	102775.1	2.415	1.918	1682.607	5737.867	0.2932	696.4471	6724.027	0.1036

Table F-26 Test _ZN_pt_001v_05_G_2500_12_13_2007

Experiment	Experiment	Chen's prediction	Klimenko's prediction	Exp/Pred	Exp/Pred	Chen's prediction			Experiment		
q'' (kW/m^2)	h_{eff} (W/m^2·K) (a)	h_{eff} (W/m^2·K) (b)	h_{eff} (W/m^2·K) (c)	Ratio (a)/(b)	Ratio (a)/(c)	q''_{1p} (kW/m^2) (d)	q''_{2p} (kW/m^2) (e)	Ratio (d)/(e)	q''_{1p} (kW/m^2) (f)	q''_{2p} (kW/m^2) (g)	Ratio (f)/(g)
1.601E+02	13251	10433	10433	1.270	1.270	0	0	0	0	0	0
2.841E+02	13891	10587	10587	1.312	1.312	0	0	0	0	0	0
4.480E+02	14244	10799	10799	1.319	1.319	0	0	0	0	0	0
6.544E+02	14897	11080	11080	1.344	1.344	0	0	0	0	0	0
9.050E+02	15487	11385	8793	1.360	1.761	903.9001	1.1233	804.6814	0	0	0
1.204E+03	16464	13413	11680	1.227	1.410	1050.898	153.6006	6.8418	0	0	0
1.554E+03	17596	16375	15103	1.075	1.165	1149.759	404.1565	2.8448	1069.433	484.4824	2.2074
1.952E+03	19550	19880	19111	0.983	1.023	1229.511	722.2067	1.7024	1249.65	702.0681	1.78
2.372E+03	25785	23702	23467	1.088	1.099	1292.573	1079.073	1.1979	1187.628	1184.018	1.003
2.838E+03	29967	27984	28477	1.071	1.052	1363.13	1475.322	0.924	1272.457	1565.994	0.8126
3.337E+03	37070	32727	34068	1.133	1.088	1422.218	1915.178	0.7426	1255.122	2082.275	0.6028
3.661E+03	41685	35897	37925	1.161	1.099	1458.837	2202.554	0.6623	1255.817	2405.573	0.522

3.887E+03	44857	38136	40711	1.176	1.102	1484.651	2402.354	0.618	1261.782	2625.223	0.4806
4.006E+03	46441	39381	42239	1.179	1.099	1497.829	2508.072	0.5972	1269.701	2736.2	0.464
4.125E+03	48518	40600	43747	1.195	1.109	1509.933	2615.135	0.5774	1263.109	2861.958	0.4413
4.243E+03	50524	41804	45249	1.209	1.117	1519.035	2723.938	0.5577	1256.464	2986.509	0.4207
4.365E+03	52718	43047	46813	1.225	1.126	1529.088	2835.733	0.5392	1248.196	3116.626	0.4005
4.486E+03	54941	44286	48385	1.241	1.135	1539.39	2946.666	0.5224	1240.442	3245.613	0.3822
4.610E+03	57352	45550	50005	1.259	1.147	1550.089	3060.09	0.5066	1230.714	3379.465	0.3642
4.736E+03	60024	46904	51769	1.280	1.159	1553.698	3182.072	0.4883	1213.684	3522.087	0.3446
4.858E+03	62767	48172	53432	1.303	1.175	1561.546	3296.092	0.4738	1198.067	3659.571	0.3274
4.985E+03	65692	49493	55180	1.327	1.191	1573.118	3411.676	0.4611	1184.826	3799.968	0.3118
5.120E+03	69127	50909	57077	1.358	1.211	1585.116	3534.397	0.4485	1166.991	3952.521	0.2953
5.249E+03	72653	52297	58933	1.389	1.233	1595.728	3653.181	0.4368	1148.304	4100.605	0.28
5.385E+03	76711	53773	60879	1.427	1.260	1604.149	3781.179	0.4242	1124.161	4261.168	0.2638
5.521E+03	80884	55211	62790	1.465	1.288	1616.302	3904.851	0.4139	1102.966	4418.187	0.2496
5.664E+03	84699	56793	64928	1.491	1.304	1625.382	4039.069	0.4024	1089.556	4574.896	0.2382
5.806E+03	88896	58390	67118	1.522	1.324	1633.551	4172.162	0.3915	1072.667	4733.046	0.2266
5.916E+03	91153	59665	68894	1.528	1.323	1640.33	4276.058	0.3836	1073.392	4842.995	0.2216
6.033E+03	94742	60952	70689	1.554	1.340	1646.201	4387.293	0.3752	1058.786	4974.707	0.2128

Table F-27 Test _ZN_pt_001v_06_G_2500_12_14_2007

Experiment	Experiment	Chen's prediction	Klimenko's prediction	Exp/Pred	Exp/Pred	Chen's prediction			Experiment		
q'' (kW/m^2)	h_{eff} (W/m^2·K) (a)	h_{eff} (W/m^2·K) (b)	h_{eff} (W/m^2·K) (c)	Ratio (a)/(b)	Ratio (a)/(c)	q''_{1p} (kW/m^2) (d)	q''_{2p} (kW/m^2) (e)	Ratio (d)/(e)	q''_{1p} (kW/m^2) (f)	q''_{2p} (kW/m^2) (g)	Ratio (f)/(g)
1.641E+02	13583	10338	10338	1.314	1.314	0	0	0	0	0	0
2.922E+02	14377	10514	10514	1.367	1.367	0	0	0	0	0	0
4.607E+02	15024	10728	10728	1.400	1.400	0	0	0	0	0	0
6.720E+02	15584	11006	11006	1.416	1.416	0	0	0	0	0	0
9.286E+02	16230	11388	8983	1.425	1.807	921.6264	6.9857	131.93	0	0	0
1.234E+03	16969	13573	11915	1.250	1.424	1057.755	176.2797	6.0004	0	0	0
1.589E+03	17776	16591	15382	1.071	1.156	1153.466	435.6624	2.6476	1076.022	513.1063	2.0971
1.994E+03	19476	20143	19429	0.967	1.002	1239.123	754.719	1.6418	1280.93	712.9119	1.7968
2.422E+03	25416	24028	23845	1.058	1.066	1305.655	1116.627	1.1693	1233.833	1188.45	1.0382
2.891E+03	30847	28320	28859	1.089	1.069	1374.752	1516.569	0.9065	1261.648	1629.673	0.7742

3.400E+03	37618	33114	34524	1.136	1.090	1435.346	1964.774	0.7305	1263.054	2137.066	0.591
3.727E+03	42536	36327	38451	1.171	1.106	1465.96	2260.572	0.6485	1251.516	2475.016	0.5057
3.958E+03	45958	38642	41321	1.189	1.112	1488.329	2469.474	0.6027	1251.013	2706.79	0.4622
4.075E+03	47772	39867	42827	1.198	1.115	1501.183	2573.489	0.5833	1252.353	2822.318	0.4437
4.195E+03	50029	41092	44346	1.217	1.128	1513.021	2681.915	0.5642	1242.326	2952.611	0.4208
4.311E+03	52350	42273	45820	1.238	1.143	1522.205	2789.267	0.5457	1228.798	3082.674	0.3986
4.435E+03	54756	43522	47393	1.258	1.155	1532.437	2902.219	0.528	1217.64	3217.016	0.3785
4.561E+03	57349	44804	49024	1.280	1.170	1542.924	3017.696	0.5113	1205.023	3355.597	0.3591
4.685E+03	60037	46087	50673	1.303	1.185	1553.626	3131.829	0.4961	1192.263	3493.192	0.3413
4.819E+03	63318	47461	52455	1.334	1.207	1564.974	3254.262	0.4809	1172.669	3646.567	0.3216
4.936E+03	66282	48672	54044	1.362	1.226	1575.263	3361.191	0.4687	1156.372	3780.082	0.3059
5.068E+03	69865	50031	55847	1.396	1.251	1586.967	3481.104	0.4559	1136.092	3931.979	0.2889
5.203E+03	73738	51439	57738	1.434	1.277	1599.358	3603.21	0.4439	1115.353	4087.216	0.2729
5.344E+03	77763	52976	59765	1.468	1.301	1610.832	3733.478	0.4315	1097.07	4247.24	0.2583
5.485E+03	81916	54610	61944	1.500	1.322	1610.639	3874.274	0.4157	1073.434	4411.478	0.2433
5.627E+03	85614	56206	64092	1.523	1.336	1616.021	4011.086	0.4029	1060.628	4566.478	0.2323
5.776E+03	89570	57851	66330	1.548	1.350	1623.952	4151.842	0.3911	1048.579	4727.214	0.2218
5.928E+03	93726	59498	68590	1.575	1.366	1633.799	4294.462	0.3804	1036.853	4891.407	0.212
6.080E+03	98325	61197	70963	1.607	1.386	1643.369	4436.184	0.3704	1022.529	5057.024	0.2022
6.237E+03	103717	62975	73481	1.647	1.411	1652.514	4584.781	0.3604	1003.103	5234.192	0.1916
6.396E+03	109672	64775	76070	1.693	1.442	1662.835	4733.343	0.3513	981.8364	5414.342	0.1813
6.552E+03	116364	66550	78657	1.749	1.479	1672.535	4879.815	0.3427	956.2739	5596.076	0.1709
6.711E+03	123838	68384	81352	1.811	1.522	1679.604	5031.342	0.3338	927.2242	5783.721	0.1603
6.859E+03	132003	70115	83856	1.883	1.574	1684.169	5174.451	0.3255	894.3329	5964.287	0.1499

Table F-28 Test _ZN_pt_01v_03_G_2500_12_05_2007

Experiment	Experiment	Chen's prediction	Klimenko's prediction	Exp/Pred	Exp/Pred	Chen's prediction			Experiment		
q'' (kW/m^2)	h_{eff} (W/m^2·K) (a)	h_{eff} (W/m^2·K) (b)	h_{eff} (W/m^2·K) (c)	Ratio (a)/(b)	Ratio (a)/(c)	q''_{1p} (kW/m^2) (d)	q''_{2p} (kW/m^2) (e)	Ratio (d)/(e)	q''_{1p} (kW/m^2) (f)	q''_{2p} (kW/m^2) (g)	Ratio (f)/(g)
1.610E+02	14274	10456	10456	1.365	1.365	0	0	0	0	0	0
2.862E+02	15154	10620	10620	1.427	1.427	0	0	0	0	0	0
4.514E+02	15990	10824	10824	1.477	1.477	0	0	0	0	0	0
6.591E+02	16554	11106	11106	1.490	1.490	0	0	0	0	0	0

9.108E+02	17147	11414	8870	1.502	1.933	908.2781	2.5117	361.6223	0	0	0
1.210E+03	17811	13486	11756	1.321	1.515	1052.074	157.8292	6.6659	0	0	0
1.559E+03	19176	16451	15184	1.166	1.263	1149.11	409.9911	2.8028	985.2956	573.8055	1.7171
1.954E+03	21568	19935	19152	1.082	1.126	1232.644	721.1072	1.7094	1138.718	815.0338	1.3971
2.387E+03	25810	23870	23639	1.081	1.092	1303.154	1084.11	1.202	1204.676	1182.588	1.0187
2.860E+03	31132	28207	28716	1.104	1.084	1373.375	1486.472	0.9239	1243.856	1615.992	0.7697
3.365E+03	37942	32990	34368	1.150	1.104	1433.128	1931.431	0.742	1245.642	2118.917	0.5879
3.689E+03	42574	36174	38253	1.177	1.113	1469.646	2219.626	0.6621	1248.278	2440.993	0.5114
3.916E+03	45872	38428	41055	1.194	1.117	1495.312	2421.023	0.6176	1252.238	2664.097	0.47
4.032E+03	47776	39718	42664	1.203	1.120	1495.832	2535.731	0.5899	1243.13	2788.432	0.4458
4.149E+03	49754	40921	44158	1.216	1.127	1504.049	2644.79	0.5687	1236.637	2912.201	0.4246
4.269E+03	51709	42141	45681	1.227	1.132	1514.579	2754.097	0.5499	1233.926	3034.75	0.4066
4.391E+03	53708	43387	47252	1.238	1.137	1524.989	2866.262	0.532	1231.515	3159.736	0.3898
4.515E+03	55987	44634	48836	1.254	1.146	1537.484	2977.1	0.5164	1225.298	3289.286	0.3725
4.640E+03	58390	45915	50482	1.272	1.157	1549.654	3090.059	0.5015	1218.182	3421.531	0.356
4.765E+03	60885	47237	52204	1.289	1.166	1559.803	3205.289	0.4866	1209.778	3555.314	0.3403
4.891E+03	63651	48552	53933	1.311	1.180	1570.442	3321.002	0.4729	1197.522	3693.922	0.3242
5.024E+03	66634	49931	55767	1.335	1.195	1581.959	3442.062	0.4596	1185.039	3838.981	0.3087
5.150E+03	69768	51264	57561	1.361	1.212	1592.653	3557.738	0.4477	1169.875	3980.516	0.2939
5.284E+03	73520	52693	59456	1.395	1.237	1603.056	3681.135	0.4355	1148.605	4135.586	0.2777
5.422E+03	78519	54209	61462	1.448	1.278	1611.223	3810.973	0.4228	1112.056	4310.14	0.258
5.562E+03	84237	55764	63546	1.511	1.326	1619.198	3942.517	0.4107	1071.597	4490.119	0.2387
5.702E+03	89722	57326	65664	1.565	1.366	1627.765	4073.87	0.3996	1039.732	4661.903	0.223
5.843E+03	94588	58903	67832	1.606	1.394	1636.577	4206.131	0.3891	1018.857	4823.851	0.2112
5.961E+03	97863	60226	69675	1.625	1.405	1643.988	4316.712	0.3808	1011.448	4949.253	0.2044
6.090E+03	100577	61666	71704	1.631	1.403	1652.462	4437.302	0.3724	1012.876	5076.888	0.1995
6.194E+03	102986	62858	73406	1.638	1.403	1659.002	4535.162	0.3658	1012.285	5181.88	0.1954
6.322E+03	105669	64296	75480	1.643	1.400	1667.295	4655.147	0.3582	1014.218	5308.224	0.1911
6.445E+03	108565	65689	77516	1.653	1.401	1675.206	4769.323	0.3512	1013.323	5431.205	0.1866
6.572E+03	111902	67156	79666	1.666	1.405	1680.817	4890.823	0.3437	1008.428	5563.212	0.1813
6.701E+03	116491	68827	82161	1.693	1.418	1677.857	5022.859	0.334	991.0586	5709.657	0.1736
6.835E+03	121539	70608	84779	1.721	1.434	1673.248	5161.881	0.3242	971.8177	5863.311	0.1657
6.963E+03	126581	72207	87139	1.753	1.453	1676.619	5286.797	0.3171	956.165	6007.251	0.1592
7.064E+03	129584	72748	87863	1.781	1.475	1712.351	5351.412	0.32	961.0658	6102.698	0.1575

Table F-29 Test _ZN_pt_01v_04_G_2500_12_10_2007

Experiment	Experiment	Chen's prediction	Klimenko's prediction	Exp/Pred	Exp/Pred	Chen's prediction			Experiment		
q'' (kW/m^2)	h_{eff} (W/m^2·K) (a)	h_{eff} (W/m^2·K) (b)	h_{eff} (W/m^2·K) (c)	Ratio (a)/(b)	Ratio (a)/(c)	q''_{1p} (kW/m^2) (d)	q''_{2p} (kW/m^2) (e)	Ratio (d)/(e)	q''_{1p} (kW/m^2) (f)	q''_{2p} (kW/m^2) (g)	Ratio (f)/(g)
1.611E+02	13492	10515	10515	1.283	1.283	0	0	0	0	0	0
2.861E+02	14373	10677	10677	1.346	1.346	0	0	0	0	0	0
4.513E+02	14978	10890	10890	1.375	1.375	0	0	0	0	0	0
6.588E+02	15558	11173	11173	1.393	1.393	0	0	0	0	0	0
9.107E+02	16197	11466	8894	1.413	1.821	908.416	2.2697	400.2422	0	0	0
1.211E+03	16921	13535	11796	1.250	1.435	1052.799	157.7046	6.6758	0	0	0
1.561E+03	17764	16522	15249	1.075	1.165	1151.917	409.5278	2.8128	1070.805	490.6399	2.1825
1.954E+03	21647	19988	19196	1.083	1.128	1235.66	718.2474	1.7204	1140.395	813.5124	1.4018
2.379E+03	27511	23856	23608	1.153	1.165	1302.99	1076.445	1.2105	1129.366	1250.069	0.9034
2.845E+03	32746	28128	28608	1.164	1.145	1375.262	1470.06	0.9355	1180.86	1664.462	0.7095
3.353E+03	38574	32955	34320	1.171	1.124	1433.17	1919.92	0.7465	1223.946	2129.145	0.5749
3.679E+03	43876	36186	38272	1.213	1.146	1464.352	2214.457	0.6613	1207.256	2471.553	0.4885
3.904E+03	47997	38434	41066	1.249	1.169	1490.691	2412.893	0.6178	1193.284	2710.3	0.4403
4.019E+03	50697	39651	42562	1.279	1.191	1503.833	2515.062	0.5979	1175.789	2843.106	0.4136
4.140E+03	53421	40884	44087	1.307	1.212	1515.038	2624.604	0.5772	1159.105	2980.537	0.3889
4.262E+03	56067	42139	45655	1.331	1.228	1525.313	2736.47	0.5574	1146.009	3115.774	0.3678
4.383E+03	58761	43377	47216	1.355	1.245	1535.612	2847.126	0.5394	1133.214	3249.524	0.3487
4.503E+03	61714	44677	48884	1.381	1.262	1537.876	2965.378	0.5186	1112.966	3390.288	0.3283
4.630E+03	64795	45995	50584	1.409	1.281	1545.455	3084.125	0.5011	1096.697	3532.884	0.3104
4.754E+03	67859	47296	52277	1.435	1.298	1556.044	3198.343	0.4865	1084.187	3670.201	0.2954
4.884E+03	71017	48648	54056	1.460	1.314	1567.579	3316.415	0.4727	1073.484	3810.51	0.2817
5.011E+03	74356	49976	55824	1.488	1.332	1578.482	3432.554	0.4599	1060.591	3950.445	0.2685
5.138E+03	77619	51308	57617	1.513	1.347	1589.944	3548.348	0.4481	1050.65	4087.643	0.257
5.263E+03	80588	52658	59415	1.530	1.356	1599.027	3663.861	0.4364	1044.535	4218.353	0.2476
5.409E+03	84005	54254	61535	1.548	1.365	1607.358	3801.249	0.4228	1037.817	4370.79	0.2374
5.544E+03	87504	55775	63581	1.569	1.376	1615.9	3928.44	0.4113	1029.667	4514.673	0.2281
5.695E+03	91162	57463	65883	1.586	1.384	1624.267	4070.757	0.399	1023.562	4671.462	0.2191
5.839E+03	93416	59105	68157	1.581	1.371	1632.514	4206.576	0.3881	1032.61	4806.48	0.2148
5.962E+03	93685	60522	70154	1.548	1.335	1640.194	4322.098	0.3795	1059.299	4902.993	0.2161
6.092E+03	92729	61977	72227	1.496	1.284	1649.267	4442.467	0.3713	1102.009	4989.726	0.2209

6.220E+03	90310	63441	74348	1.424	1.215	1657.617	4562.624	0.3633	1164.12	5056.121	0.2302
6.348E+03	88206	64917	76519	1.359	1.153	1666.39	4682.096	0.3559	1226.07	5122.416	0.2394
6.481E+03	87954	66444	78766	1.324	1.117	1672.87	4807.9	0.3479	1263.395	5217.375	0.2422
6.611E+03	90331	67981	81047	1.329	1.115	1678.936	4932.54	0.3404	1263.17	5348.306	0.2362
6.747E+03	94138	69597	83452	1.353	1.128	1685.337	5062.084	0.3329	1245.664	5501.758	0.2264
6.883E+03	99334	71390	86099	1.391	1.154	1683.993	5198.639	0.3239	1209.953	5672.679	0.2133
7.018E+03	105285	73192	88792	1.438	1.186	1682.336	5335.427	0.3153	1169.235	5848.528	0.1999
7.152E+03	112129	74906	91374	1.497	1.227	1684.904	5467.519	0.3082	1125.288	6027.135	0.1867
7.281E+03	120182	76637	94027	1.568	1.278	1684.442	5596.406	0.301	1073.846	6207.002	0.173
7.472E+03	131641	79180	97989	1.663	1.343	1685.549	5786.345	0.2913	1013.574	6458.32	0.1569

Table F-30 Test _ZN_pt_1v_01_G_2500_11_28_2007

Experiment	Experiment	Chen's prediction	Klimenko's prediction	Exp/Pred	Exp/Pred	Chen's prediction			Experiment		
q" (kW/m^2)	h_{eff} (W/m^2·K) (a)	h_{eff} (W/m^2·K) (b)	h_{eff} (W/m^2·K) (c)	Ratio (a)/(b)	Ratio (a)/(c)	$q"_{1p}$ (kW/m^2) (d)	$q"_{2p}$ (kW/m^2) (e)	Ratio (d)/(e)	$q"_{1p}$ (kW/m^2) (f)	$q"_{2p}$ (kW/m^2) (g)	Ratio (f)/(g)
1.749E+02	16137	10459	10459	1.543	1.543	0	0	0	0	0	0
3.154E+02	17051	10632	10632	1.604	1.604	0	0	0	0	0	0
4.942E+02	17513	10886	10886	1.609	1.609	0	0	0	0	0	0
7.111E+02	17986	11242	11242	1.600	1.600	0	0	0	0	0	0
9.695E+02	18071	11686	9436	1.546	1.915	946.9359	22.551	41.9908	0	0	0
1.275E+03	18529	13980	12370	1.325	1.498	1069.641	205.3293	5.2094	0	0	0
1.625E+03	20901	16989	15804	1.230	1.323	1161.841	462.9484	2.5097	943.8647	680.9244	1.3862
2.009E+03	26200	20392	19678	1.285	1.331	1240.498	768.0058	1.6152	965.0371	1043.467	0.9248
2.444E+03	28427	24338	24188	1.168	1.175	1306.688	1136.887	1.1494	1118.237	1325.339	0.8437
2.923E+03	31859	28747	29353	1.108	1.085	1378.011	1544.796	0.892	1242.933	1679.874	0.7399
3.434E+03	39116	33605	35119	1.164	1.114	1435.402	1998.287	0.7183	1232.706	2200.982	0.5601
3.761E+03	44127	36805	39037	1.199	1.130	1473.707	2287.266	0.6443	1228.742	2532.231	0.4852
3.983E+03	48026	39038	41798	1.230	1.149	1499.201	2484.113	0.6035	1218.233	2765.08	0.4406
4.099E+03	50009	40254	43299	1.242	1.155	1512.823	2585.929	0.585	1217.33	2881.422	0.4225
4.216E+03	52156	41443	44774	1.259	1.165	1524.498	2691.535	0.5664	1210.966	3005.067	0.403
4.325E+03	54174	42547	46154	1.273	1.174	1536.624	2788.537	0.5511	1206.428	3118.732	0.3868
4.447E+03	56615	43805	47746	1.292	1.186	1547.859	2898.935	0.5339	1197.253	3249.542	0.3684
4.569E+03	58941	45009	49283	1.310	1.196	1555.024	3013.603	0.516	1187.087	3381.539	0.351

4.693E+03	61477	46328	50989	1.327	1.206	1565.854	3126.81	0.5008	1179.641	3513.023	0.3358
4.821E+03	64198	47722	52821	1.345	1.215	1564.795	3256.011	0.4806	1162.824	3657.982	0.3179
4.945E+03	67023	48979	54475	1.368	1.230	1575.323	3370.015	0.4675	1150.845	3794.493	0.3033
5.076E+03	69941	50311	56247	1.390	1.243	1587.772	3488.59	0.4551	1141.793	3934.569	0.2902
5.212E+03	73005	51680	58081	1.413	1.257	1607.13	3604.39	0.4459	1137.357	4074.163	0.2792
5.326E+03	75767	53012	59853	1.429	1.266	1610.654	3714.864	0.4336	1126.606	4198.912	0.2683
5.478E+03	79081	54672	62061	1.446	1.274	1619.408	3858.551	0.4197	1119.246	4358.714	0.2568
5.621E+03	81712	56183	64089	1.454	1.275	1630.585	3990.368	0.4086	1120.836	4500.116	0.2491
5.715E+03	82574	57256	65562	1.442	1.259	1639.65	4075.221	0.4023	1136.599	4578.272	0.2483
5.805E+03	81848	58315	67033	1.404	1.221	1639.321	4165.455	0.3936	1167.659	4637.117	0.2518
5.900E+03	79899	59358	68486	1.346	1.167	1642.98	4257.379	0.3859	1220.251	4680.108	0.2607
5.990E+03	80607	60367	69901	1.335	1.153	1647.608	4342.277	0.3794	1233.56	4756.324	0.2594
6.079E+03	83862	61352	71283	1.367	1.176	1654.971	4423.641	0.3741	1210.422	4868.191	0.2486
6.166E+03	87094	62342	72691	1.397	1.198	1664.9	4501.345	0.3699	1191.4	4974.846	0.2395
6.254E+03	90641	63412	74226	1.429	1.221	1665.553	4588.551	0.363	1164.885	5089.219	0.2289
6.341E+03	93510	64397	75644	1.452	1.236	1668.899	4672.543	0.3572	1149.001	5192.441	0.2213
6.431E+03	96276	65408	77115	1.472	1.248	1674.996	4756.057	0.3522	1137.638	5293.415	0.2149
6.451E+03	95454	65588	77390	1.455	1.233	1683.68	4767.337	0.3532	1156.561	5294.456	0.2184
6.524E+03	98468	66509	78743	1.481	1.251	1682.657	4841.096	0.3476	1136.209	5387.544	0.2109
6.619E+03	102473	67391	79994	1.521	1.281	1689.477	4929.141	0.3428	1110.782	5507.836	0.2017
6.718E+03	105319	68521	81662	1.537	1.290	1692.84	5024.838	0.3369	1101.065	5616.612	0.196
6.799E+03	109576	69531	83133	1.576	1.318	1692.871	5106.235	0.3315	1073.929	5725.177	0.1876
6.897E+03	114577	70659	84760	1.622	1.352	1696.848	5199.654	0.3263	1046.182	5850.321	0.1788
6.985E+03	120471	71745	86346	1.679	1.395	1699.012	5285.959	0.3214	1011.576	5973.395	0.1693
7.103E+03	132678	73068	88274	1.816	1.503	1709.481	5393.634	0.3169	941.201	6161.914	0.1527
7.221E+03	144374	74708	90744	1.933	1.591	1705.65	5515.177	0.3093	882.3896	6338.437	0.1392
7.348E+03	152009	76196	92988	1.995	1.635	1713.188	5635.033	0.304	858.5413	6489.679	0.1323
7.474E+03	158239	77772	95428	2.035	1.658	1719.593	5753.98	0.2989	844.9471	6628.626	0.1275
7.605E+03	170777	79742	98547	2.142	1.733	1713.998	5891.149	0.2909	800.1303	6805.017	0.1176

Table F-31 Test _ZN_pt_1v_02_G_2500_12_03_2007

Experiment	Experiment	Chen's prediction	Klimenko's prediction	Exp/Pred	Exp/Pred	Chen's prediction			Experiment		
q" (kW/m^2)	h_{eff} (W/m^2·K) (a)	h_{eff} (W/m^2·K) (b)	h_{eff} (W/m^2·K) (c)	Ratio (a)/(b)	Ratio (a)/(c)	$q"_{1p}$ (kW/m^2) (d)	$q"_{2p}$ (kW/m^2) (e)	Ratio (d)/(e)	$q"_{1p}$ (kW/m^2) (f)	$q"_{2p}$ (kW/m^2) (g)	Ratio (f)/(g)
176.8	14629	10535	10535	1.389	1.389	0	0	0	0	0	0
315.9	15933	10679	10679	1.492	1.492	0	0	0	0	0	0
500.5	16892	10916	10916	1.547	1.547	0	0	0	0	0	0
723.7	17381	11200	11200	1.552	1.552	0	0	0	0	0	0
987.6	17839	11857	9651	1.505	1.848	957.0909	30.4683	31.4126	0	0	0
1296.8	18393	14266	12667	1.289	1.452	1076.762	220.0702	4.8928	0	0	0
1652.4	19154	17369	16208	1.103	1.182	1168.707	483.7265	2.416	1059.264	593.1697	1.7858
2058.2	20822	20985	20349	0.992	1.023	1247.143	811.0407	1.5377	1256.326	801.8576	1.5668
2487.9	26851	24935	24864	1.077	1.080	1317.028	1170.92	1.1248	1222.51	1265.439	0.9661
2955.5	31860	29294	29983	1.088	1.063	1384.473	1571.064	0.8812	1272.482	1683.055	0.7561
3478.2	38843	34292	35949	1.133	1.080	1445.494	2032.702	0.7111	1275.669	2202.527	0.5792
3816.6	44020	37657	40108	1.169	1.098	1484.239	2332.348	0.6364	1269.218	2547.369	0.4982
4042.0	47973	40011	43028	1.199	1.115	1504.777	2537.213	0.5931	1254.614	2787.376	0.4501
4158.4	50037	41287	44627	1.212	1.121	1509.164	2649.214	0.5697	1244.864	2913.513	0.4273
4280.8	52113	42522	46174	1.226	1.129	1520.869	2759.891	0.5511	1240.555	3040.205	0.408
4403.6	54262	43763	47745	1.240	1.136	1530.883	2872.731	0.5329	1234.281	3169.333	0.3894
4521.4	56314	44942	49250	1.253	1.143	1541.994	2979.448	0.5175	1230.213	3291.23	0.3738
4656.9	58901	46299	50999	1.272	1.155	1552.81	3104.129	0.5002	1220.172	3436.767	0.355
4782.8	61417	47567	52650	1.291	1.167	1564.972	3217.87	0.4863	1211.672	3571.17	0.3393
4903.3	63482	48792	54266	1.301	1.170	1575.238	3328.02	0.4733	1210.342	3692.916	0.3277
5044.3	66245	50207	56147	1.319	1.180	1587.84	3456.442	0.4594	1203.037	3841.246	0.3132
5178.1	68905	51581	58001	1.336	1.188	1600.116	3577.938	0.4472	1197.44	3980.614	0.3008
5298.3	70704	52874	59711	1.337	1.184	1608.868	3689.458	0.4361	1202.793	4095.533	0.2937
5449.4	72936	54496	61868	1.338	1.179	1618.044	3831.383	0.4223	1208.614	4240.813	0.285
5589.3	75814	56029	63931	1.353	1.186	1625.815	3963.472	0.4102	1201.182	4388.105	0.2737
5741.2	77707	57675	66175	1.347	1.174	1635.912	4105.269	0.3985	1213.847	4527.334	0.2681
5890.1	77428	59352	68509	1.305	1.130	1643.328	4246.821	0.387	1259.327	4630.823	0.2719
6040.8	79700	61019	70846	1.306	1.125	1653.354	4387.468	0.3768	1265.467	4775.356	0.265
6162.7	84993	62446	72872	1.361	1.166	1661.161	4501.534	0.369	1220.142	4942.553	0.2469
6282.5	89082	63860	74913	1.395	1.189	1668.478	4614.017	0.3616	1195.755	5086.741	0.2351

6400.2	92824	65229	76912	1.423	1.207	1676.48	4723.77	0.3549	1177.77	5222.48	0.2255
6513.1	96689	66633	78976	1.451	1.224	1677.595	4835.507	0.3469	1155.789	5357.314	0.2157
6649.5	101079	68265	81396	1.481	1.242	1682.057	4967.43	0.3386	1135.676	5513.811	0.206
6774.1	105067	69741	83572	1.507	1.257	1686.242	5087.854	0.3314	1119.006	5655.09	0.1979
6888.9	110416	71167	85664	1.552	1.289	1690.795	5198.135	0.3253	1089.499	5799.431	0.1879
7008.0	119899	72688	87915	1.649	1.364	1693.501	5314.472	0.3187	1026.42	5981.553	0.1716
7144.0	126904	74291	90299	1.708	1.405	1699.894	5444.134	0.3122	994.8877	6149.14	0.1618

Table F-32 Test _C_pt_001v_01_G_2500_2_4_2008

Experiment	Experiment	Chen's prediction	Klimenko's prediction	Exp/Pred	Exp/Pred	Chen's prediction			Experiment		
q" (kW/m^2)	h_{eff} (W/m^2·K) (a)	h_{eff} (W/m^2·K) (b)	h_{eff} (W/m^2·K) (c)	Ratio (a)/(b)	Ratio (a)/(c)	$q"_{1p}$ (kW/m^2) (d)	$q"_{2p}$ (kW/m^2) (e)	Ratio (d)/(e)	$q"_{1p}$ (kW/m^2) (f)	$q"_{2p}$ (kW/m^2) (g)	Ratio (f)/(g)
152.7	13938	10458	10458	1.333	1.333	0	0	0	0	0	0
271.2	14680	10618	10618	1.383	1.383	0	0	0	0	0	0
427.3	15289	10818	10818	1.413	1.413	0	0	0	0	0	0
622.8	15984	11082	11082	1.442	1.442	0	0	0	0	0	0
859.3	16664	11351	11351	1.468	1.468	0	0	0	0	0	0
1139.4	17196	12929	11077	1.330	1.552	1028	111.4211	9.2263	0	0	0
1466.3	17952	15645	14270	1.147	1.258	1128.426	337.8293	3.3402	982.9274	483.3276	2.0337
1832.4	22412	18879	17920	1.187	1.251	1212.708	619.6923	1.957	1020.992	811.4084	1.2583
2240.2	25322	22538	22101	1.124	1.146	1282.157	958.0201	1.3383	1140.691	1099.486	1.0375
2683.5	28569	26602	26830	1.074	1.065	1345.733	1337.801	1.0059	1252.531	1431.004	0.8753
3161.2	34640	31121	32153	1.113	1.077	1401.062	1760.117	0.796	1258.267	1902.912	0.6612
3472.1	38378	34153	35797	1.124	1.072	1436.071	2036.062	0.7053	1277.507	2194.626	0.5821
3687.2	41207	36271	38396	1.136	1.073	1460.403	2226.789	0.6558	1285.009	2402.182	0.5349
3798.9	42577	37396	39796	1.139	1.070	1473.913	2324.947	0.634	1294.074	2504.785	0.5166
3911.8	44259	38518	41191	1.149	1.074	1486.879	2424.875	0.6132	1293.594	2618.16	0.4941
4025.9	45838	39669	42606	1.156	1.076	1499.543	2526.339	0.5936	1297.31	2728.572	0.4755
4140.6	47565	40836	44052	1.165	1.080	1510.142	2630.505	0.5741	1296.076	2844.57	0.4556
4258.8	49416	42029	45542	1.176	1.085	1520.202	2738.646	0.5551	1292.54	2966.307	0.4357
4378.4	51341	43251	47083	1.187	1.090	1529.785	2848.569	0.537	1288.299	3090.056	0.4169
4497.5	53498	44471	48635	1.203	1.100	1540.034	2957.452	0.5207	1279.768	3217.718	0.3977
4619.8	55861	45718	50236	1.222	1.112	1550.532	3069.247	0.5052	1268.592	3351.188	0.3785

4748.1	58290	47028	51935	1.239	1.122	1561.763	3186.361	0.4901	1259.624	3488.501	0.3611
4875.5	60694	48344	53663	1.255	1.131	1572.67	3302.853	0.4762	1252.268	3623.255	0.3456
5003.3	63421	49647	55388	1.277	1.145	1584.163	3419.175	0.4633	1239.717	3763.621	0.3294
5132.2	66462	51003	57210	1.303	1.162	1593.315	3538.916	0.4502	1222.334	3909.897	0.3126
5260.7	70059	52366	59025	1.338	1.187	1602.737	3657.94	0.4382	1197.631	4063.046	0.2948
5397.4	75164	53830	60950	1.396	1.233	1610.564	3786.809	0.4253	1153.099	4244.274	0.2717
5539.9	80977	55376	63007	1.462	1.285	1618.888	3921.026	0.4129	1106.759	4433.155	0.2497
5666.4	85468	56786	64912	1.505	1.317	1624.91	4041.505	0.4021	1079.312	4587.104	0.2353
5812.0	89550	58391	67106	1.534	1.334	1634.33	4177.682	0.3912	1065.369	4746.644	0.2244
5959.6	92660	60042	69400	1.543	1.335	1643.923	4315.723	0.3809	1064.938	4894.708	0.2176
6097.3	95479	61692	71736	1.548	1.331	1646.771	4450.52	0.37	1063.741	5033.549	0.2113
6249.6	99460	63489	74309	1.567	1.338	1651.506	4598.139	0.3592	1053.917	5195.729	0.2028
6391.9	102890	65118	76676	1.580	1.342	1660.932	4730.984	0.3511	1050.892	5341.024	0.1968
6537.3	106853	66801	79135	1.600	1.350	1667.107	4870.182	0.3423	1041.933	5495.357	0.1896
6692.3	111498	68582	81769	1.626	1.364	1675.424	5016.896	0.334	1030.262	5662.058	0.182
6849.9	117200	70502	84583	1.662	1.386	1680.842	5169.07	0.3252	1010.857	5839.056	0.1731
7002.8	124251	72394	87367	1.716	1.422	1684.391	5318.362	0.3167	981.1567	6021.596	0.1629

Table F-33 Test _C_pt_001v_02_G_2500_2_6_2008

Experiment	Experiment	Chen's prediction	Klimenko's prediction	Exp/Pred	Exp/Pred	Chen's prediction			Experiment		
q'' (kW/m^2)	h_{eff} (W/m^2·K) (a)	h_{eff} (W/m^2·K) (b)	h_{eff} (W/m^2·K) (c)	Ratio (a)/(b)	Ratio (a)/(c)	q''_{1p} (kW/m^2) (d)	q''_{2p} (kW/m^2) (e)	Ratio (d)/(e)	q''_{1p} (kW/m^2) (f)	q''_{2p} (kW/m^2) (g)	Ratio (f)/(g)
158.7	15183	10312	10312	1.472	1.472	0	0	0	0	0	0
282.4	15714	10481	10481	1.499	1.499	0	0	0	0	0	0
444.4	16042	10706	10706	1.498	1.498	0	0	0	0	0	0
651.9	16746	10963	10963	1.528	1.528	0	0	0	0	0	0
903.2	18074	11268	8728	1.604	2.071	901.8674	1.331	677.5867	0	0	0
1190.1	18345	13206	11482	1.389	1.598	1042.912	147.2152	7.0843	0	0	0
1523.3	19493	16006	14722	1.218	1.324	1137.904	385.4064	2.9525	933.8702	589.4398	1.5843
1900.6	21260	19323	18473	1.100	1.151	1222.402	678.2081	1.8024	1110.44	790.1702	1.4053
2308.7	24849	22988	22650	1.081	1.097	1287.757	1020.951	1.2613	1190.828	1117.88	1.0653
2754.0	29452	27040	27364	1.089	1.076	1353.929	1400.1	0.967	1242.498	1511.531	0.822
3232.8	36160	31535	32634	1.147	1.108	1415.547	1817.3	0.7789	1234.04	1998.808	0.6174

3531.7	39858	34438	36127	1.157	1.103	1448.708	2083.009	0.6955	1251.253	2280.464	0.5487
3746.3	42574	36545	38719	1.165	1.100	1470.797	2275.502	0.6464	1262.045	2484.254	0.508
3856.6	44438	37650	40095	1.180	1.108	1482.923	2373.679	0.6247	1255.952	2600.649	0.4829
3966.8	46297	38748	41443	1.195	1.117	1495.139	2471.701	0.6049	1250.938	2715.902	0.4606
4076.6	47940	39862	42815	1.203	1.120	1504.581	2572.009	0.585	1250.646	2825.945	0.4426
4189.9	49818	41009	44240	1.215	1.126	1514.4	2675.477	0.566	1246.214	2943.663	0.4234
4308.2	51821	42215	45747	1.228	1.133	1522.917	2785.255	0.5468	1240.208	3067.964	0.4042
4425.4	53579	43383	47214	1.235	1.135	1535.106	2890.269	0.5311	1242.559	3182.815	0.3904
4543.8	55362	44593	48755	1.242	1.136	1544.216	2999.587	0.5148	1243.422	3300.381	0.3768
4663.8	57183	45830	50346	1.248	1.136	1551.898	3111.869	0.4987	1243.38	3420.387	0.3635
4784.3	58594	47036	51909	1.246	1.129	1563.742	3220.554	0.4856	1254.895	3529.401	0.3556
4905.5	52339	48246	53529	1.085	0.978	1574.285	3331.262	0.4726	1450.699	3454.848	0.4199

Table F-34 Test _C_pt_001v_03_G_2500_2_8_2008

Experiment	Experiment	Chen's prediction	Klimenko's prediction	Exp/Pred	Exp/Pred	Chen's prediction			Experiment		
q" (kW/m^2)	h_{eff} (W/m^2·K) (a)	h_{eff} (W/m^2·K) (b)	h_{eff} (W/m^2·K) (c)	Ratio (a)/(b)	Ratio (a)/(c)	$q"_{1p}$ (kW/m^2) (d)	$q"_{2p}$ (kW/m^2) (e)	Ratio (d)/(e)	$q"_{1p}$ (kW/m^2) (f)	$q"_{2p}$ (kW/m^2) (g)	Ratio (f)/(g)
161.8	14284	10652	10652	1.341	1.341	0	0	0	0	0	0
287.6	14922	10829	10829	1.378	1.378	0	0	0	0	0	0
453.8	15564	11066	11066	1.407	1.407	0	0	0	0	0	0
662.0	16127	11309	11309	1.426	1.426	0	0	0	0	0	0
914.2	16676	11633	9037	1.433	1.845	910.7093	3.4837	261.4188	0	0	0
1213.4	17337	13745	11971	1.261	1.448	1053.51	159.8956	6.5887	0	0	0
1559.6	18255	16732	15439	1.091	1.182	1149.508	410.0982	2.803	1053.042	506.5644	2.0788
1950.2	21000	20226	19440	1.038	1.080	1230.637	719.595	1.7102	1184.691	765.5412	1.5475
2375.9	25150	24157	23944	1.041	1.050	1298.237	1077.676	1.2047	1246.437	1129.475	1.1036
2842.6	29546	28492	29042	1.037	1.017	1370.704	1471.859	0.9313	1321.289	1521.274	0.8685
3340.8	36537	33330	34797	1.096	1.050	1423.917	1916.924	0.7428	1298.459	2042.382	0.6358
3663.1	40956	36626	38866	1.118	1.054	1450.599	2212.463	0.6556	1296.752	2366.31	0.548
3889.5	44293	38928	41743	1.138	1.061	1478.719	2410.802	0.6134	1299.177	2590.344	0.5015
4003.8	46448	40172	43283	1.156	1.073	1488.206	2515.547	0.5916	1286.702	2717.051	0.4736
4118.8	48535	41386	44799	1.173	1.083	1498.362	2620.449	0.5718	1277.233	2841.579	0.4495
4235.0	50633	42607	46338	1.188	1.093	1507.958	2727.025	0.553	1268.494	2966.489	0.4276

4353.9	52701	43837	47903	1.202	1.100	1517.974	2835.96	0.5353	1262.238	3091.696	0.4083
4476.7	54897	45112	49540	1.217	1.108	1528.451	2948.274	0.5184	1255.597	3221.128	0.3898
4598.9	57358	46381	51186	1.237	1.121	1539.883	3058.986	0.5034	1244.789	3354.079	0.3711
4719.2	59519	47649	52852	1.249	1.126	1550.279	3168.89	0.4892	1240.721	3478.448	0.3567
4845.0	60022	48972	54616	1.226	1.099	1561.791	3283.216	0.4757	1273.854	3571.153	0.3567
4968.7	62907	50290	56386	1.251	1.116	1573.225	3395.507	0.4633	1257.291	3711.441	0.3388
5093.0	66499	51517	58028	1.291	1.146	1582.539	3510.421	0.4508	1225.623	3867.336	0.3169
5223.2	73030	52891	59849	1.381	1.220	1590.96	3632.287	0.438	1151.906	4071.341	0.2829
5352.8	78471	54331	61762	1.444	1.271	1597.932	3754.916	0.4256	1106.038	4246.811	0.2604
5482.0	82694	55763	63689	1.483	1.298	1605.488	3876.561	0.4142	1082.306	4399.744	0.246
5618.8	87450	57297	65780	1.526	1.329	1613.641	4005.154	0.4029	1056.951	4561.845	0.2317
5753.2	91326	58811	67873	1.553	1.346	1621.877	4131.298	0.3926	1044.148	4709.026	0.2217
5895.6	95299	60381	70062	1.578	1.360	1630.882	4264.728	0.3824	1033.03	4862.58	0.2124

Table F-35 Test _C_pt_001v_04_G_2500_2_11_2008

Experiment	Experiment	Chen's prediction	Klimenko's prediction	Exp/Pred	Exp/Pred	Chen's prediction			Experiment		
q'' (kW/m^2)	h_{eff} (W/m^2·K) (a)	h_{eff} (W/m^2·K) (b)	h_{eff} (W/m^2·K) (c)	Ratio (a)/(b)	Ratio (a)/(c)	q''_{1p} (kW/m^2) (d)	q''_{2p} (kW/m^2) (e)	Ratio (d)/(e)	q''_{1p} (kW/m^2) (f)	q''_{2p} (kW/m^2) (g)	Ratio (f)/(g)
160.4	13596	10638	10638	1.278	1.278	0	0	0	0	0	0
284.7	14369	10820	10820	1.328	1.328	0	0	0	0	0	0
447.5	14938	11037	11037	1.353	1.353	0	0	0	0	0	0
651.4	15462	11280	11280	1.371	1.371	0	0	0	0	0	0
898.7	16020	11561	8876	1.386	1.805	897.8175	0.8615	1042.201	0	0	0
1193.9	16708	13559	11760	1.232	1.421	1046.771	147.1332	7.1144	0	0	0
1538.3	17569	16495	15179	1.065	1.157	1145.949	392.3083	2.921	1075.362	462.8945	2.3231
1921.6	21973	19899	19068	1.104	1.152	1226.019	695.6298	1.7625	1109.717	811.9321	1.3668
2344.7	25364	23766	23500	1.067	1.079	1293.084	1051.591	1.2296	1211.083	1133.592	1.0684
2808.2	29971	28040	28517	1.069	1.051	1366.56	1441.678	0.9479	1278.04	1530.198	0.8352
3311.0	37330	32854	34214	1.136	1.091	1420.976	1890.007	0.7518	1250.119	2060.864	0.6066
3637.8	41787	36096	38182	1.158	1.094	1454.861	2182.901	0.6665	1256.241	2381.522	0.5275
3866.7	44820	38362	41013	1.168	1.093	1483.081	2383.614	0.6222	1268.962	2597.733	0.4885
3984.8	46261	39617	42565	1.168	1.087	1492.518	2492.288	0.5989	1277.736	2707.071	0.472
4107.2	47839	40874	44128	1.170	1.084	1501.674	2605.548	0.5763	1282.614	2824.608	0.4541

4227.0	49639	42106	45673	1.179	1.087	1510.604	2716.418	0.5561	1280.943	2946.08	0.4348
4346.9	51437	43337	47230	1.187	1.089	1520.46	2826.448	0.5379	1280.619	3066.29	0.4176
4471.3	53875	44615	48859	1.208	1.103	1531.564	2939.712	0.521	1267.892	3203.384	0.3958
4598.3	56533	45926	50548	1.231	1.118	1542.519	3055.748	0.5048	1252.709	3345.558	0.3744
4725.4	58890	47241	52262	1.247	1.127	1553.99	3171.45	0.49	1246.204	3479.236	0.3582
4866.9	60752	48682	54163	1.248	1.122	1566.384	3300.499	0.4746	1254.796	3612.087	0.3474
5013.2	49406	50153	56196	0.985	0.879	1579.248	3433.922	0.4599	1602.623	3410.547	0.4699

Table F-36 Test _C_pt_01v_05_G_2500_2_12_2008

Experiment	Experiment	Chen's prediction	Klimenko's prediction	Exp/Pred	Exp/Pred	Chen's prediction			Experiment		
q" (kW/m^2)	h_{eff} (W/m^2·K) (a)	h_{eff} (W/m^2·K) (b)	h_{eff} (W/m^2·K) (c)	Ratio (a)/(b)	Ratio (a)/(c)	$q"_{1p}$ (kW/m^2) (d)	$q"_{2p}$ (kW/m^2) (e)	Ratio (d)/(e)	$q"_{1p}$ (kW/m^2) (f)	$q"_{2p}$ (kW/m^2) (g)	Ratio (f)/(g)
154.1	13242	10522	10522	1.258	1.258	0	0	0	0	0	0
273.7	14116	10721	10721	1.317	1.317	0	0	0	0	0	0
431.0	14737	10929	10929	1.349	1.349	0	0	0	0	0	0
629.0	15308	11196	11196	1.367	1.367	0	0	0	0	0	0
869.3	15839	11419	11419	1.387	1.387	0	0	0	0	0	0
1155.3	16612	13119	11290	1.266	1.471	1032.169	123.1317	8.3826	0	0	0
1488.4	18472	15914	14558	1.161	1.269	1132.425	355.9335	3.1816	975.1334	513.2248	1.9
1850.7	23079	19113	18182	1.207	1.269	1213.494	637.2554	1.9042	1004.479	846.2696	1.1869
2269.0	25041	22882	22505	1.094	1.113	1279.758	989.2167	1.2937	1168.892	1100.084	1.0625
2725.8	28532	27071	27391	1.054	1.042	1348.121	1377.664	0.9786	1278.519	1447.266	0.8834
3214.1	34705	31677	32811	1.096	1.058	1409.516	1804.592	0.7811	1286.03	1928.078	0.667
3525.6	39216	34719	36481	1.130	1.075	1444.974	2080.632	0.6945	1278.8	2246.806	0.5692
3739.5	42545	36842	39101	1.155	1.088	1468.349	2271.14	0.6465	1271.076	2468.413	0.5149
3846.2	44152	37992	40558	1.162	1.089	1471.288	2374.957	0.6195	1265.547	2580.698	0.4904
3974.2	46313	39276	42137	1.179	1.099	1485.495	2488.747	0.5969	1259.392	2714.851	0.4639
4098.0	48466	40541	43699	1.195	1.109	1496.916	2601.095	0.5755	1251.722	2846.29	0.4398
4211.9	50283	41689	45129	1.206	1.114	1506.873	2705.022	0.5571	1248.927	2962.967	0.4215
4329.6	52372	42891	46640	1.221	1.123	1516.894	2812.681	0.5393	1241.867	3087.708	0.4022
4448.1	54471	44101	48175	1.235	1.131	1527.068	2921.04	0.5228	1235.931	3212.176	0.3848
4569.9	56857	45368	49799	1.253	1.142	1537.497	3032.444	0.507	1226.417	3343.524	0.3668
4694.5	59306	46664	51478	1.271	1.152	1547.983	3146.469	0.492	1217.605	3476.847	0.3502

4815.3	61856	47893	53082	1.292	1.165	1558.5	3256.832	0.4785	1206.298	3609.034	0.3342
4940.6	64711	49177	54778	1.316	1.181	1569.122	3371.432	0.4654	1192.069	3748.486	0.318
5067.9	67768	50469	56500	1.343	1.199	1581.83	3486.086	0.4538	1177.68	3890.235	0.3027
5197.4	71690	51894	58427	1.381	1.227	1590.909	3606.495	0.4411	1151.278	4046.125	0.2845
5327.8	76651	53345	60338	1.437	1.270	1596.613	3731.187	0.4279	1110.852	4216.948	0.2634
5456.6	82020	54746	62196	1.498	1.319	1606.033	3850.524	0.4171	1071.68	4384.877	0.2444
5592.2	87570	56242	64204	1.557	1.364	1613.98	3978.174	0.4057	1036.279	4555.875	0.2275
5729.4	92440	57766	66278	1.600	1.395	1621.75	4107.633	0.3948	1013.138	4716.245	0.2148
5868.2	97133	59301	68393	1.638	1.420	1630.845	4237.327	0.3849	995.3717	4872.8	0.2043
6005.9	101267	60837	70539	1.665	1.436	1639.756	4366.176	0.3756	984.8314	5021.1	0.1961
6152.6	105706	62484	72869	1.692	1.451	1648.84	4503.761	0.3661	974.3658	5178.235	0.1882
6295.5	110072	64095	75183	1.717	1.464	1658.332	4637.148	0.3576	965.3727	5330.107	0.1811
6442.1	115592	65868	77775	1.755	1.486	1663.312	4778.774	0.3481	947.5405	5494.545	0.1725
6586.1	120522	67579	80292	1.783	1.501	1668.209	4917.882	0.3392	935.1322	5650.959	0.1655
6727.3	126785	69226	82736	1.831	1.532	1674.041	5053.275	0.3313	913.799	5813.516	0.1572

Table F-37 Test _C_pt_01v_06_G_2500_2_14_2008

Experiment	Experiment	Chen's prediction	Klimenko's prediction	Exp/Pred	Exp/Pred	Chen's prediction			Experiment		
q'' (kW/m^2)	h_{eff} (W/m^2·K) (a)	h_{eff} (W/m^2·K) (b)	h_{eff} (W/m^2·K) (c)	Ratio (a)/(b)	Ratio (a)/(c)	q''_{1p} (kW/m^2) (d)	q''_{2p} (kW/m^2) (e)	Ratio (d)/(e)	q''_{1p} (kW/m^2) (f)	q''_{2p} (kW/m^2) (g)	Ratio (f)/(g)
162.0	14415	10579	10579	1.363	1.363	0	0	0	0	0	0
289.2	15127	10706	10706	1.413	1.413	0	0	0	0	0	0
455.6	15781	10905	10905	1.447	1.447	0	0	0	0	0	0
664.5	16366	11154	11154	1.467	1.467	0	0	0	0	0	0
918.0	16982	11470	8980	1.481	1.891	912.9361	5.0311	181.4601	0	0	0
1219.4	17662	13598	11892	1.299	1.485	1051.987	167.3836	6.2849	0	0	0
1570.4	18634	16586	15337	1.124	1.215	1149.343	421.0092	2.73	1022.44	547.9123	1.8661
1967.3	20632	20079	19328	1.028	1.067	1232.012	735.2492	1.6756	1198.374	768.8878	1.5586
2395.4	25523	23963	23756	1.065	1.074	1300.349	1095.084	1.1874	1220.343	1175.09	1.0385
2856.9	31208	28189	28699	1.107	1.087	1370.348	1486.548	0.9218	1237.312	1619.584	0.764
3354.6	38593	32918	34291	1.172	1.125	1424.749	1929.83	0.7383	1214.786	2139.792	0.5677
3676.9	43787	36088	38152	1.213	1.148	1461.755	2215.153	0.6599	1204.312	2472.596	0.4871
3904.6	48024	38450	41104	1.249	1.168	1477.941	2426.652	0.609	1182.907	2721.686	0.4346

4016.9	50256	39671	42608	1.267	1.180	1489.832	2527.049	0.5896	1175.64	2841.242	0.4138
4135.1	52592	40906	44138	1.286	1.192	1500.203	2634.912	0.5694	1166.462	2968.652	0.3929
4251.2	54852	42105	45637	1.303	1.202	1510.199	2741.004	0.551	1158.859	3092.344	0.3748
4371.5	57322	43342	47196	1.323	1.215	1520.309	2851.151	0.5332	1149.158	3222.301	0.3566
4489.7	59731	44556	48742	1.341	1.225	1530.641	2959.013	0.5173	1141.406	3348.248	0.3409
4614.1	62413	45834	50385	1.362	1.239	1541.294	3072.767	0.5016	1131.517	3482.544	0.3249
4734.3	65040	47082	52005	1.381	1.251	1552.512	3181.832	0.4879	1123.495	3610.85	0.3111
4862.2	68164	48408	53746	1.408	1.268	1563.304	3298.864	0.4739	1109.871	3752.297	0.2958
4985.5	71342	49695	55453	1.436	1.287	1574.127	3411.339	0.4614	1096.132	3889.333	0.2818
5113.9	74696	51021	57232	1.464	1.305	1586.01	3527.848	0.4496	1082.981	4030.877	0.2687
5246.6	78605	52444	59132	1.499	1.329	1596.313	3650.274	0.4373	1064.714	4181.874	0.2546
5377.1	83438	53866	61010	1.549	1.368	1604.045	3773.036	0.4251	1035.251	4341.83	0.2384
5513.5	89433	55430	63104	1.613	1.417	1605.585	3907.903	0.4109	994.8409	4518.647	0.2202
5648.7	95187	56929	65128	1.672	1.462	1612.383	4036.286	0.3995	964.055	4684.614	0.2058
5790.7	100629	58504	67282	1.720	1.496	1621.194	4169.473	0.3888	942.262	4848.405	0.1943
5933.4	105307	60074	69456	1.753	1.516	1630.656	4302.759	0.379	929.969	5003.446	0.1859
6081.7	109594	61723	71774	1.776	1.527	1640.276	4441.385	0.3693	923.5409	5158.119	0.179
6229.3	113932	63395	74161	1.797	1.536	1649.912	4579.415	0.3603	917.7958	5311.532	0.1728
6378.0	118542	65100	76635	1.821	1.547	1659.384	4718.6	0.3517	911.0313	5466.953	0.1666
6529.7	124437	66858	79203	1.861	1.571	1666.482	4863.227	0.3427	895.1255	5634.584	0.1589
6681.4	129412	68643	81848	1.885	1.581	1672.787	5008.623	0.334	887.0293	5794.381	0.1531
6837.0	139117	70489	84537	1.974	1.646	1677.651	5159.378	0.3252	849.8306	5987.198	0.1419

Table F-38 Test _C_pt_01v_07_G_2500_2_21_2008

Experiment	Experiment	Chen's prediction	Klimenko's prediction	Exp/Pred	Exp/Pred	Chen's prediction			Experiment		
q" (kW/m^2)	h_{eff} (W/m^2·K) (a)	h_{eff} (W/m^2·K) (b)	h_{eff} (W/m^2·K) (c)	Ratio (a)/(b)	Ratio (a)/(c)	$q"_{1p}$ (kW/m^2) (d)	$q"_{2p}$ (kW/m^2) (e)	Ratio (d)/(e)	$q"_{1p}$ (kW/m^2) (f)	$q"_{2p}$ (kW/m^2) (g)	Ratio (f)/(g)
167.0	13917	10545	10545	1.320	1.320	0	0	0	0	0	0
296.4	14673	10696	10696	1.372	1.372	0	0	0	0	0	0
467.8	15330	10920	10920	1.404	1.404	0	0	0	0	0	0
682.4	15933	11191	11191	1.424	1.424	0	0	0	0	0	0
943.2	16467	11613	9229	1.418	1.784	931.0698	12.1725	76.4896	0	0	0
1253.5	17154	13907	12242	1.233	1.401	1064.281	189.2565	5.6235	0	0	0

1612.7	18205	17001	15793	1.071	1.153	1160.884	451.8434	2.5692	1083.533	529.1943	2.0475
2010.7	23466	20515	19809	1.144	1.185	1241.123	769.5885	1.6127	1084.552	926.1588	1.171
2462.0	25603	24605	24495	1.041	1.045	1311.599	1150.379	1.1401	1259.899	1202.079	1.0481
2945.6	31227	29064	29728	1.074	1.050	1378.949	1566.665	0.8802	1282.922	1662.692	0.7716
3466.0	38253	33985	35589	1.126	1.075	1436.724	2029.303	0.708	1275.964	2190.064	0.5826
3803.5	43125	37269	39629	1.157	1.088	1474.911	2328.56	0.6334	1274.162	2529.309	0.5038
4034.8	47086	39584	42484	1.190	1.108	1500.131	2534.628	0.5919	1260.712	2774.047	0.4545
4151.7	49320	40806	44002	1.209	1.121	1508.305	2643.349	0.5706	1247.53	2904.124	0.4296
4271.2	51384	41987	45472	1.224	1.130	1518.201	2753.032	0.5515	1240.151	3031.082	0.4091
4392.5	53757	43191	46984	1.245	1.144	1529.021	2863.454	0.534	1228.114	3164.361	0.3881
4513.1	56173	44394	48507	1.265	1.158	1539.515	2973.632	0.5177	1216.303	3296.844	0.3689
4637.8	58950	45743	50249	1.289	1.173	1541.953	3095.809	0.4981	1196.118	3441.645	0.3475
4764.8	61503	47068	51967	1.307	1.183	1552.558	3212.21	0.4833	1187.781	3576.987	0.3321
4892.3	64152	48399	53712	1.325	1.194	1566.114	3326.223	0.4708	1181.164	3711.173	0.3183
5024.8	66842	49765	55523	1.343	1.204	1578.799	3445.993	0.4582	1175.06	3849.733	0.3052
5154.5	69059	51109	57328	1.351	1.205	1591.126	3563.412	0.4465	1177.185	3977.352	0.296
5285.6	71574	52511	59193	1.363	1.209	1601.854	3683.796	0.4348	1174.875	4110.775	0.2858
5426.2	74979	54045	61223	1.387	1.225	1610.169	3816.043	0.4219	1160.281	4265.932	0.272
5562.8	80270	55547	63227	1.445	1.270	1618.848	3943.951	0.4105	1119.931	4442.868	0.2521
5701.5	86148	57094	65317	1.509	1.319	1627.195	4074.26	0.3994	1078.109	4623.346	0.2332
5848.1	92422	58858	67746	1.570	1.364	1625.564	4222.493	0.385	1034.932	4813.125	0.215
5993.7	98505	60464	69969	1.629	1.408	1635.35	4358.342	0.3752	1003.521	4990.171	0.2011
6143.5	103866	62148	72340	1.671	1.436	1644.199	4499.273	0.3654	983.5308	5159.941	0.1906
6294.3	109417	63839	74754	1.714	1.464	1654.671	4639.604	0.3566	965.133	5329.142	0.1811
6447.1	114668	65596	77311	1.748	1.483	1664.43	4782.698	0.348	951.8797	5495.249	0.1732
6606.3	119845	67441	80011	1.777	1.498	1671.194	4935.061	0.3386	940.1752	5666.08	0.1659
6771.4	125872	69360	82842	1.815	1.519	1679.209	5092.168	0.3298	925.0684	5846.308	0.1582
6939.3	131734	71401	85821	1.845	1.535	1684.691	5254.64	0.3206	912.8904	6026.441	0.1515

Table F-39 Test _C_pt_1v_08_G_2500_2_23_2008

Experiment	Experiment	Chen's prediction	Klimenko's prediction	Exp/Pred	Exp/Pred	Chen's prediction			Experiment		
q" (kW/m^2)	h_{eff} (W/m^2·K) (a)	h_{eff} (W/m^2·K) (b)	h_{eff} (W/m^2·K) (c)	Ratio (a)/(b)	Ratio (a)/(c)	$q"_{1p}$ (kW/m^2) (d)	$q"_{2p}$ (kW/m^2) (e)	Ratio (d)/(e)	$q"_{1p}$ (kW/m^2) (f)	$q"_{2p}$ (kW/m^2) (g)	Ratio (f)/(g)
163.0	12865	10347	10347	1.243	1.243	0	0	0	0	0	0
289.4	13666	10503	10503	1.301	1.301	0	0	0	0	0	0
456.1	14237	10702	10702	1.330	1.330	0	0	0	0	0	0
665.8	14804	10974	10974	1.349	1.349	0	0	0	0	0	0
920.7	15492	11339	8892	1.366	1.742	916.1804	4.5297	202.2608	0	0	0
1224.8	16291	13479	11809	1.209	1.380	1055.559	169.2744	6.2358	0	0	0
1577.6	17675	16474	15255	1.073	1.159	1150.514	427.0762	2.6939	1071.731	505.8592	2.1186
1971.9	21693	19940	19197	1.088	1.130	1231.877	739.9939	1.6647	1131.746	840.1251	1.3471
2408.9	25426	23905	23710	1.064	1.072	1300.532	1108.356	1.1734	1222.184	1186.703	1.0299
2876.3	32077	28219	28741	1.137	1.116	1369.922	1506.404	0.9094	1204.684	1671.643	0.7207
3392.1	39993	33178	34613	1.205	1.155	1422.204	1969.906	0.722	1179.415	2212.695	0.533
3719.6	45616	36427	38579	1.252	1.182	1458.707	2260.862	0.6452	1164.458	2555.112	0.4557
3949.0	49593	38754	41460	1.280	1.196	1484.741	2464.273	0.6025	1159.858	2789.156	0.4158
4067.5	51567	40013	43012	1.289	1.199	1498.721	2568.763	0.5834	1162.552	2904.932	0.4002
4190.4	53502	41265	44564	1.297	1.201	1510.934	2679.456	0.5639	1164.959	3025.431	0.3851
4314.7	55845	42536	46156	1.313	1.210	1522.427	2792.317	0.5452	1159.229	3155.515	0.3674
4439.7	58303	43871	47853	1.329	1.218	1527.936	2911.772	0.5247	1149.345	3290.364	0.3493
4567.6	60973	45214	49575	1.349	1.230	1535.121	3032.449	0.5062	1138	3429.569	0.3318
4693.9	63741	46561	51321	1.369	1.242	1541.872	3152.014	0.4892	1125.918	3567.968	0.3156
4824.2	66542	47870	53024	1.390	1.255	1557.399	3266.848	0.4767	1120.033	3704.213	0.3024
4954.9	69637	49233	54824	1.414	1.270	1568.386	3386.493	0.4631	1108.479	3846.4	0.2882
5088.6	72993	50645	56714	1.441	1.287	1580.259	3508.345	0.4504	1096.091	3992.513	0.2745
5222.0	76464	52075	58636	1.468	1.304	1592.234	3629.788	0.4387	1084.054	4137.968	0.262
5359.1	80168	53574	60615	1.496	1.323	1601.049	3758.048	0.426	1069.643	4289.454	0.2494
5496.4	83966	55050	62580	1.525	1.342	1611.816	3884.563	0.4149	1056.443	4439.936	0.2379
5639.4	88369	56659	64752	1.560	1.365	1616.453	4022.967	0.4018	1036.103	4603.317	0.2251
5787.4	93162	58311	67008	1.598	1.390	1621.711	4165.731	0.3893	1014.755	4772.687	0.2126
5937.8	98205	59949	69268	1.638	1.418	1631.792	4306.039	0.379	995.8428	4941.988	0.2015
6089.1	104025	61656	71663	1.687	1.452	1640.656	4448.476	0.3688	972.1549	5116.977	0.19
6240.0	109957	63435	74207	1.733	1.482	1647.849	4592.177	0.3588	950.3861	5289.639	0.1797

6393.0	115846	65183	76741	1.777	1.510	1658.741	4734.265	0.3504	933.0614	5459.945	0.1709
6550.4	122609	66997	79387	1.830	1.544	1666.039	4884.373	0.3411	910.1216	5640.29	0.1614
6718.9	130626	68964	82296	1.894	1.587	1673.01	5045.868	0.3316	883.0259	5835.852	0.1513
6886.8	139338	71009	85277	1.962	1.634	1678.943	5207.86	0.3224	855.4003	6031.403	0.1418
6996.7	145055	72331	87220	2.005	1.663	1683.412	5313.275	0.3168	839.2096	6157.478	0.1363

Table F-40 Test _C_pt_1v_09_G_2500_3_6_2008

Experiment	Experiment	Chen's prediction	Klimenko's prediction	Exp/Pred	Exp/Pred	Chen's prediction			Experiment		
q" (kW/m^2)	h_{eff} (W/m^2·K) (a)	h_{eff} (W/m^2·K) (b)	h_{eff} (W/m^2·K) (c)	Ratio (a)/(b)	Ratio (a)/(c)	$q"_{1p}$ (kW/m^2) (d)	$q"_{2p}$ (kW/m^2) (e)	Ratio (d)/(e)	$q"_{1p}$ (kW/m^2) (f)	$q"_{2p}$ (kW/m^2) (g)	Ratio (f)/(g)
166.9	14060	10544	10544	1.333	1.333	0	0	0	0	0	0
296.1	14715	10703	10703	1.375	1.375	0	0	0	0	0	0
466.5	15292	10915	10915	1.401	1.401	0	0	0	0	0	0
680.8	15858	11182	11182	1.418	1.418	0	0	0	0	0	0
941.4	16477	11600	9214	1.420	1.788	929.5738	11.8235	78.621	0	0	0
1252.7	17313	13904	12241	1.245	1.414	1062.907	189.7608	5.6013	0	0	0
1614.4	18453	17027	15822	1.084	1.166	1160.321	454.0521	2.5555	1070.113	544.2606	1.9662
2020.6	21989	20627	19944	1.066	1.103	1240.251	780.3041	1.5894	1162.916	857.6394	1.3559
2464.2	25976	24695	24597	1.052	1.056	1310.279	1153.93	1.1355	1245.119	1219.09	1.0214
2944.9	31698	29177	29861	1.086	1.062	1376.419	1568.442	0.8776	1266.48	1678.38	0.7546
3462.7	38856	34133	35771	1.138	1.086	1434.521	2028.169	0.7073	1259.69	2203	0.5718
3793.3	43863	37392	39785	1.173	1.102	1474.585	2318.76	0.6359	1256.577	2536.768	0.4953
4025.0	48725	39800	42772	1.224	1.139	1493.855	2531.107	0.5902	1219.798	2805.164	0.4348
4143.5	50847	41109	44410	1.237	1.145	1497.55	2645.922	0.566	1210.354	2933.118	0.4127
4265.9	52634	42353	45971	1.243	1.145	1505.727	2760.167	0.5455	1211.223	3054.671	0.3965
4389.1	54398	43662	47635	1.246	1.142	1512.755	2876.335	0.5259	1213.803	3175.287	0.3823
4515.6	56768	44978	49317	1.262	1.151	1524.344	2991.296	0.5096	1207.376	3308.263	0.365
4637.1	59264	46237	50942	1.282	1.163	1534.473	3102.644	0.4946	1196.8	3440.318	0.3479
4765.7	61869	47576	52689	1.300	1.174	1545.683	3220.042	0.48	1188.204	3577.521	0.3321
4895.5	64524	48925	54469	1.319	1.185	1557.025	3338.435	0.4664	1180.217	3715.243	0.3177
5028.0	67148	50270	56261	1.336	1.193	1570.966	3457.081	0.4544	1175.729	3852.318	0.3052
5159.4	70464	51613	58071	1.365	1.213	1583.522	3575.923	0.4428	1159.535	3999.91	0.2899
5293.0	73885	53107	60050	1.391	1.230	1588.462	3704.509	0.4288	1141.425	4151.546	0.2749

5427.3	77563	54575	62001	1.421	1.251	1596.619	3830.728	0.4168	1123.102	4304.245	0.2609
5558.9	80722	56011	63931	1.441	1.263	1604.529	3954.411	0.4058	1113.03	4445.91	0.2503
5699.7	86899	57598	66087	1.509	1.315	1613.696	4086.012	0.3949	1069.263	4630.446	0.2309
5845.5	92427	59279	68412	1.559	1.351	1622.416	4223.054	0.3842	1040.265	4805.205	0.2165
5993.8	97689	60913	70694	1.604	1.382	1636.792	4356.966	0.3757	1020.314	4973.445	0.2052
6143.2	102696	62686	73223	1.638	1.403	1642.812	4500.352	0.365	1002.498	5140.666	0.195
6295.8	107882	64537	75916	1.672	1.421	1651.115	4644.671	0.3555	987.4449	5308.341	0.186
6447.3	113674	66374	78608	1.713	1.446	1657.55	4789.731	0.3461	967.5759	5479.705	0.1766
6603.5	120138	68260	81407	1.760	1.476	1664.27	4939.198	0.337	945.3383	5658.13	0.1671
6763.2	126635	70192	84277	1.804	1.503	1670.67	5092.552	0.3281	925.8019	5837.42	0.1586
6917.2	133757	71999	86920	1.858	1.539	1677.721	5239.484	0.3202	902.865	6014.34	0.1501

Table F-41 Test _C_pt_1v_10_G_2500_3_18_2008

Experiment	Experiment	Chen's prediction	Klimenko's prediction	Exp/Pred	Exp/Pred	Chen's prediction			Experiment		
q" (kW/m^2)	h_{eff} ($W/m^2 \cdot K$) (a)	h_{eff} ($W/m^2 \cdot K$) (b)	h_{eff} ($W/m^2 \cdot K$) (c)	Ratio (a)/(b)	Ratio (a)/(c)	$q"_{1p}$ (kW/m^2) (d)	$q"_{2p}$ (kW/m^2) (e)	Ratio (d)/(e)	$q"_{1p}$ (kW/m^2) (f)	$q"_{2p}$ (kW/m^2) (g)	Ratio (f)/(g)
148.2	13706	10404	10404	1.317	1.317	0	0	0	0	0	0
262.7	14305	10522	10522	1.359	1.359	0	0	0	0	0	0
413.5	14874	10715	10715	1.388	1.388	0	0	0	0	0	0
602.9	15447	10974	10974	1.408	1.408	0	0	0	0	0	0
832.4	16124	11259	11259	1.432	1.432	0	0	0	0	0	0
1106.1	17265	12613	10722	1.369	1.610	1014.074	92.0009	11.0224	0	0	0
1424.6	18462	15230	13821	1.212	1.336	1115.667	308.969	3.6109	919.8315	504.8049	1.8222
1784.6	22018	18392	17403	1.197	1.265	1194.084	590.5189	2.0221	996.9396	787.6632	1.2657
2182.8	25948	21954	21463	1.182	1.209	1263.631	919.2012	1.3747	1068.636	1114.196	0.9591
2617.3	29914	25921	26042	1.154	1.149	1329.306	1287.968	1.0321	1151.364	1465.91	0.7854
3082.0	36572	30258	31117	1.209	1.175	1395.249	1686.749	0.8272	1153.916	1928.083	0.5985
3375.8	41704	33105	34506	1.260	1.209	1427.497	1948.307	0.7327	1132.732	2243.071	0.505
3581.9	45432	35147	36993	1.293	1.228	1445.918	2135.942	0.6769	1118.187	2463.673	0.4539
3690.0	47229	36220	38308	1.304	1.233	1461.114	2228.859	0.6555	1120.124	2569.849	0.4359
3797.8	49234	37285	39634	1.320	1.242	1471.01	2326.813	0.6322	1113.606	2684.217	0.4149
3906.4	51292	38371	40986	1.337	1.251	1481.055	2425.344	0.6107	1107.607	2798.792	0.3957
4016.3	53355	39482	42348	1.351	1.260	1492.243	2524.033	0.5912	1103.874	2912.402	0.379

4129.4	55364	40602	43728	1.364	1.266	1505.538	2623.838	0.5738	1103.746	3025.63	0.3648
4240.8	57156	41744	45153	1.369	1.266	1513.319	2727.49	0.5548	1104.898	3135.911	0.3523
4355.9	58741	42954	46684	1.368	1.258	1517.335	2838.529	0.5345	1109.195	3246.67	0.3416
4475.0	60563	44214	48289	1.370	1.254	1524.532	2950.477	0.5167	1112.635	3362.374	0.3309
4594.8	62894	45432	49845	1.384	1.262	1536.825	3058.023	0.5026	1109.78	3485.068	0.3184
4713.9	65319	46620	51374	1.401	1.271	1550.925	3162.928	0.4903	1106.586	3607.266	0.3068
4837.2	68080	47913	53065	1.421	1.283	1559.649	3277.559	0.4759	1097.286	3739.921	0.2934
4963.9	70991	49248	54831	1.442	1.295	1569.349	3394.594	0.4623	1088.334	3875.609	0.2808
5090.7	73828	50519	56521	1.461	1.306	1584.108	3506.615	0.4517	1083.616	4007.107	0.2704
5219.7	76957	51846	58301	1.484	1.320	1598.164	3621.584	0.4413	1076.392	4143.357	0.2598
5349.0	80413	53292	60214	1.509	1.335	1603.547	3745.428	0.4281	1062.415	4286.56	0.2478
5473.2	83808	54636	61997	1.534	1.352	1612.216	3860.981	0.4176	1050.723	4422.474	0.2376
5607.9	87672	56058	63900	1.564	1.372	1622.948	3984.981	0.4073	1037.436	4570.493	0.227
5743.9	91949	57586	65979	1.597	1.394	1628.645	4115.289	0.3958	1019.711	4724.223	0.2158
5885.1	96142	59141	68114	1.626	1.411	1637.536	4247.547	0.3855	1007.024	4878.059	0.2064
6026.2	100307	60734	70336	1.652	1.426	1644.932	4381.228	0.3755	995.6908	5030.469	0.1979
6168.4	105428	62562	72943	1.685	1.445	1638.932	4529.447	0.3618	972.2783	5196.101	0.1871
6312.4	109384	64228	75341	1.703	1.452	1647.182	4665.195	0.3531	966.9253	5345.451	0.1809
6457.5	112149	65846	77698	1.703	1.443	1659.289	4798.196	0.3458	973.9386	5483.547	0.1776
6604.7	117399	67572	80226	1.737	1.463	1664.178	4940.479	0.3368	957.5872	5647.069	0.1696

Table F-42 Test _C_pt_1v_11_G_2500_3_23_2008

Experiment	Experiment	Chen's prediction	Klimenko's prediction	Exp/Pred	Exp/Pred	Chen's prediction			Experiment		
q'' (kW/m^2)	h_{eff} (W/m^2·K) (a)	h_{eff} (W/m^2·K) (b)	h_{eff} (W/m^2·K) (c)	Ratio (a)/(b)	Ratio (a)/(c)	q''_{1p} (kW/m^2) (d)	q''_{2p} (kW/m^2) (e)	Ratio (d)/(e)	q''_{1p} (kW/m^2) (f)	q''_{2p} (kW/m^2) (g)	Ratio (f)/(g)
171.5	15085	10424	10424	1.447	1.447	0	0	0	0	0	0
304.8	16165	10607	10607	1.524	1.524	0	0	0	0	0	0
480.1	16815	10835	10835	1.552	1.552	0	0	0	0	0	0
701.4	17362	11133	11133	1.560	1.560	0	0	0	0	0	0
970.5	17921	11678	9416	1.535	1.903	949.313	21.1523	44.8799	0	0	0
1293.1	18400	14129	12532	1.302	1.468	1078.252	214.8396	5.0189	0	0	0
1672.0	18729	17392	16270	1.077	1.151	1171.898	500.1362	2.3432	1087.644	584.3903	1.8612
2088.6	22320	21086	20481	1.059	1.090	1252.071	836.5446	1.4967	1182.326	906.2894	1.3046

2540.3	27127	25195	25193	1.077	1.077	1321.695	1218.592	1.0846	1227.031	1313.257	0.9343
3022.7	34015	29666	30422	1.147	1.118	1391.862	1630.88	0.8534	1213.455	1809.287	0.6707
3549.3	42345	34679	36419	1.221	1.163	1446.871	2102.446	0.6882	1184.499	2364.818	0.5009
3888.6	48329	38077	40633	1.269	1.189	1476.328	2412.284	0.612	1162.79	2725.822	0.4266
4121.6	52198	40481	43590	1.289	1.197	1500.503	2621.07	0.5725	1163.291	2958.282	0.3932
4242.1	53529	41759	45189	1.282	1.185	1509.825	2732.283	0.5526	1177.472	3064.636	0.3842
4366.9	55577	43024	46775	1.292	1.188	1523.303	2843.637	0.5357	1178.86	3188.08	0.3698
4494.0	57998	44318	48415	1.309	1.198	1535.417	2958.546	0.519	1172.877	3321.086	0.3532
4621.5	60451	45594	50046	1.326	1.208	1548.242	3073.305	0.5038	1167.359	3454.188	0.338
4752.2	63333	46980	51849	1.348	1.221	1553.302	3198.922	0.4856	1151.874	3600.35	0.3199
4882.2	66293	48375	53685	1.370	1.235	1558.123	3324.091	0.4687	1136.627	3745.587	0.3035
5013.3	69219	49745	55502	1.391	1.247	1568.598	3444.669	0.4554	1126.93	3886.337	0.29
5149.6	72313	51125	57348	1.414	1.261	1583.363	3566.204	0.444	1119.073	4030.495	0.2777
5286.6	75728	52591	59295	1.440	1.277	1595.73	3690.913	0.4323	1107.874	4178.769	0.2651
5417.3	79517	54110	61316	1.470	1.297	1597.48	3819.855	0.4182	1086.752	4330.583	0.2509
5559.1	83805	55773	63555	1.503	1.319	1599.891	3959.174	0.4041	1064.431	4494.634	0.2368
5698.3	88590	57303	65626	1.546	1.350	1610.709	4087.63	0.394	1041.565	4656.774	0.2237
5844.6	93261	58895	67806	1.584	1.375	1622.911	4221.659	0.3844	1024.592	4819.978	0.2126
5992.9	98242	60519	70060	1.623	1.402	1634.961	4357.942	0.3752	1006.886	4986.017	0.2019
6141.7	104248	62256	72514	1.675	1.438	1641.037	4500.623	0.3646	979.7393	5161.921	0.1898
6296.1	109785	64043	75076	1.714	1.462	1648.898	4647.202	0.3548	961.6053	5334.494	0.1803
6452.3	115688	65849	77704	1.757	1.489	1657.668	4794.669	0.3457	943.2772	5509.06	0.1712
6594.9	120273	67469	80078	1.783	1.502	1667.072	4927.788	0.3383	934.9062	5659.954	0.1652
6757.4	127564	69364	82880	1.839	1.539	1675.559	5081.857	0.3297	910.8762	5846.54	0.1558